

DYNAFLOW USER'S GUIDE

By

J.H. Prevost, Princeton University,
and R. Slyh, J. Ferritto and K. Hager,
Naval Civil Engineering Laboratory



DTIC
ELECTE
MAR 10 1989
S H D

Sponsored by:
Naval Facilities Engineering Command

Naval Civil Engineering Laboratory
Port Hueneme, California 93043

89 3 09 020

CONTENT

	<u>Page</u>
INTRODUCTION	1
TECHNICAL BACKGROUND	5
THE PRINCETON UNIVERSITY EFFECTIVE STRESS FINITE ELEMENT PROCEDURE	7
Governing Equations	7
Balance of Mass	7
Balance of Linear Momentum	7
Equations of State	9
Constitutive Assumptions	9
Field Equations	11
Weak Form - Semi-Discrete Finite Element Equations	12
Time Integration	14
Implementation	16
Program DYNAFLOW	22
Post-Dynamic Event Simulation	24
DESCRIPTION OF STORAGE TECHNIQUES	25
Compacted Column Storage Scheme	27
Crout Elimination	29
Forward Reduction and Back Substitution	29
Storage in Blank Common	30
INSTALLATION INSTRUCTIONS	33
CONCLUDING REMARKS	33
USER'S MANUAL	35
Storage of Element Group Data	35
1.0 TITLE CARD	37
2.0 CONTROL CARDS	39
3.0 PLOTTING REQUESTS	49
4.0 COORDINATE DATA	53
5.0 BOUNDARY CONDITION DATA	63
6.0 INITIAL DISPLACEMENT/VELOCITY DATA	69
7.0 APPLIED NODAL FORCES AND PRESCRIBED DISPLACEMENTS/ VELOCITY/ACCELERATIONS	75

	<u>Page</u>
8.0 LOAD-TIME FUNCTIONS	81
9.0 ELEMENT DATA	85
9.1.0 Two-Dimensional and Axisymmetric Element	85
9.2.0 Three-Dimensional Element	110
9.3.0 Contact Element	134
9.4.0 Slide-line Element	141
9.5.0 Slide-line Element with Coulomb Friction	147
9.6.0 Nodal Mass/Damping Element	152
9.7.0 Two- and Three-Dimensional Truss Element	156
9.8.0 Two- and Three-Dimensional Beam Element	163
9.9.0 Two- and Three-Dimensional Plate and Shell Elements	186
9.10.0 Three-Dimensional Membrane Element	193
9.11.0 Boundary Element	199
9.12.0 Link Element	203
9.13.0 Nodal Penalty Element	207
10.0 MATERIAL MODELS	211
10.1.0 Description of Princeton Effective Stress Soil Model	211
10.2.0 Linear Isotropic ELasticity Model	230
10.3.0 Elasto-Plastic Constitutive Models	232
10.4.0 Drucker-Prager Elasto-Plastic Model	249
10.5.0 Von Mises Elasto-Plastic Model	253
10.6.0 Thermo-Elastic Model	257
10.7.0 Newtonian Fluid Model	263
10.8.0 Heat Conduction Model	264
ANALYSIS RESTART	269
1.0 TITLE CARD	271
2.0 CONTROL CARDS	272
3.0 BOUNDARY CONDITION DATA	278
4.0 APPLIED NODAL FORCES AND PRESCRIBED DISPLACEMENTS/ ACCELERATIONS	280
5.0 LOAD-TIME FUNCTION	285
REFERENCES	287
REFERENCES/BIBLIOGRAPHY	291

	<u>Page</u>
INTRODUCTION TO APPENDIXES	295

APPENDIXES

A - Monterey Soil Column	A-1
B - Brass Footing Test	B-2
C - Dry Retaining Wall Test	C-1
D - Storage Tank Consolidation Test	D-1
E - Blast induced Liquefaction	E-1
F - Caltech Centrifuge Tests	F-1
G - Soil Data	G-1

Accession For	
NTIS GRA&I	<input checked="" type="checkbox"/>
DTIC TAB	<input type="checkbox"/>
Unannounced	<input type="checkbox"/>
Justification	
By	
Date	
Available	
Dist	
A-1	

INTRODUCTION

The Navy has \$25 billion worth of facilities in seismically active regions. Each year \$200 million of new facilities are added to those in seismically active areas. The Navy, because of its mission, must locate at the waterfront with a high watertable and often on marginal land. Seismically induced liquefaction is a major threat to the Navy. Presently, procedures do not exist to analyze the effect of liquefaction on structures. Developing an effective stress soil model will provide a tool for such analysis of waterfront structures.

To understand the significance of liquefaction, it is important to note the damage caused in recent earthquakes. The following summarizes recent experiences during major earthquakes.

1960 Chilean Earthquake (Magnitude 6-8.3)

Most spectacular damage occurred in Puerto Montt, to quay walls, steel sheet piles, and sea walls. Liquefaction of the loose fine sandy soils was the primary cause of the failures.

1964 Alaska Earthquake (Magnitude 8.4)

Severe damage at Anchorage, Cordova, Homer, Kodiak, Seldovia, Seward, Valdez, Klawock, and Whittier. Large-scale land slides and liquefaction induced most of the extremely heavy damage and total destruction.

1964 Niigata Earthquake (Magnitude 7.5)

Severe damage in Niigata Port (West Harbor). Areas affected were Additional Harbor, Yamanoshita Wharf, North Wharf, East Wharf, Central Wharf, South Wharf, Kurinoki River Landings, Bandai Island Wharf, Shinano River Left Bank Bulkhead, and West Coast Bulkheads. Liquefaction caused most of the heavy damage.

1968 Tokachi-Oki Earthquake (Magnitude 7.8)

Ports affected were Hachinohe, Aomori, Hakodate, and Muroran. Damage was relatively light compared to that caused by Niigata Earthquake. Most of the damage occurred to structures of smaller scale. Liquefaction was not the primary cause of damage even though spouting sand sediments were seen at several waterfront areas near the damaged structures.

1973 Nemuro-Hanto-Okii Earthquake (Magnitude 7.4)

Severe damage occurred mainly in Hanasaki and Kiritappu Ports. Nemuro Port situated only 6 km away from Hanasaki Port sustained very slight damage. The damage was attributed to soil liquefaction.

1978 Miyagi-Ken-Okii Earthquake (Magnitude 7.4)

Areas affected were Shiogama, Sendai, and Ishinomaki Ports, and Ishinomaki and Yuriage Fishing Ports. The damage in Ishinomaki Port accounted for approximately 90 percent of the total damage costs at port and harbor facilities caused by this earthquake. Gravity quay walls and piers suffered various degrees of damage. Sheet pile quay wall damage was primarily due to liquefaction of fill materials. Liquefaction again played a significant role in this earthquake. At sites where liquefaction did occur, the damage to the port and harbor structures was very severe. Conversely, the damage to port and harbor structures was small at sites where no liquefaction occurred.

As can be seen, liquefaction played a major role in waterfront damage, most of the time being the single cause of widespread losses. Fortunately the United States has not suffered a devastating earthquake in recent years. However, the seismic risk is great, particularly in the West where it is estimated that there is a 5 percent annual probability of a major event in Southern California that could affect a number of Naval bases. This problem has been noted in an ONR sponsored study evaluating the Navy's seismic vulnerability. The experience noted in recent earthquakes is that liquefaction greatly increased the amount of damage observed in waterfront facilities. Particular problems exist with sheet piles, quay walls, wharfs, and embedded structures. Conventional buildings also suffer severe damage.

The Navy's experience has been limited to damage inflicted in the 1964 Alaskan earthquake, where heavy damage was noted in the seawall at the Kodiak Naval Station. One foot of differential settlement was noted beneath aircraft hangars. Compaction of fill occurred under asphalt aircraft ramps. It is significant to note that these facilities were constructed on 15 to 20 feet of engineered fill where seismically induced pore pressure increases would be expected to reduce soil stiffness and shear strength. The damage noted was caused by soil failure, and in addition, substantial damage was caused by the seismic sea wave. The United States has not had a large number of events exposing Navy facilities to damage. However, the Japanese have had a number of events and their experience illustrates that seismic liquefaction was responsible for most waterfront damage.

The conclusions from this are:

- (1) Seismic liquefaction causes severe damage to waterfront structures.

(2) The Navy, located in seismically active areas having numerous waterfront structures on marginal land, is vulnerable to substantial damage.

(3) Techniques presently do not exist to accurately analyze the response of a large complex waterfront structure on soil in which seismically induced pore pressures cause loss of soil stiffness and shear strength (liquefaction).

The most promising solution to this problem is developing a constitutive soil relationship that is capable of accurately predicting soil behavior under generalized loading conditions. Implementing this effective stress soil model into a finite element computer program would allow analysis of soil and structure together.

TECHNICAL BACKGROUND

The analysis of dynamic transient phenomena in fluid-saturated porous media is of great interest in geophysics and geotechnical engineering. Fluid saturation of an otherwise inviscid porous solid skeleton introduces a time dependence into the response to applied loads. Biot (Ref 1) first considered the propagation of harmonic waves in a fluid-saturated porous medium. Since then, his theory and results have been the standard reference and basis for most of the investigations in acoustics, geophysics, and geomechanics. Many one-dimensional wave propagation theories have since been proposed (see Ref 2 and 3 for recent surveys of western and Russian literature), and one-dimensional wave propagation numerical results were first presented in References 4 and 5. The need for a general multidimensional formulation and solution technique has become important in recent years because of the increased concern with the dynamic behavior of saturated soil deposits and associated liquefaction of saturated sand deposits (see Ref 6 and 7) under seismic loading conditions. Also concern in marine foundation engineering with water wave induced dynamic pore pressures in saturated marine deposits has spurred interest in the subject matter (see Ref 8 and 9 for related analytical solutions). Most of the solution procedures reported in the literature are restricted to linear systems. Ghaboussi and Wilson (Ref 10) first proposed a multidimensional finite element numerical scheme to solve the linear coupled governing equations. Despite the extensive literature published in soil dynamics (see Ref 11 for extensive references), no general technique capable of accounting for all present nonlinear effects (large deformations/strains; nonlinear material behavior) has yet been fully developed and implemented, although attempts at presenting a suitable general framework have been reported (see Ref 12 through 17).

Professor J.H. Prevost of Princeton University (Ref 13) has developed an efficient finite element numerical procedure to analyze transient phenomena in fluid saturated porous media. The saturated porous medium is modeled as a two-phase system consisting of a solid and a fluid phase. The solid skeleton may be linear, or nonlinear and hysteretic. Large deformations may also be included. The fluid may be compressible or incompressible depending upon the intended applications (e.g., seismic, blast loading). Time integration of the resulting semi-discrete finite element equations is performed by using an implicit-explicit algorithm (Refs 18 and 19). In order to remove the time step size restriction associated with the presence of the stiff fluid in the mixture, the fluid contribution is always treated implicitly.

This study is directed toward examining the predictive capabilities of the numerical procedure proposed in Reference 20. Of particular interest is the validity of the proposed numerical model in adequately capturing the generation and dissipation of excess pore-water pressures in saturated sand deposits during (and after) earthquakes, and its performance in dynamic soil-structure interaction problems. The most appropriate method for such a validation study would be to utilize field data from instrumented prototype situations. However, such a study is preempted by the paucity and scarcity of the field data. In the absence

of actual prototype earthquake field data, an alternate method of validation is provided by analyzing centrifuge soil model test data. Although imperfect in many respects, it is felt that dynamic centrifuge soil model tests can still provide a data base for calibration of numerical procedures. A number of dynamic centrifuge soil model tests have been reported. The particular tests selected for this calibration study have been reported in References 21 through 24. The basic plan developed to achieve the research objective can be summarized as follows:

1. Select a particular constitutive model which most appropriately fits observed soil behavior in conventional triaxial soil tests.
2. Determine the soil model parameters for each particular soil utilizing the results of conventional triaxial soil tests.
3. Analyze the boundary value problems corresponding to centrifuge soil-structure interaction tests, and compare predicted and measured behavior.

THE PRINCETON UNIVERSITY EFFECTIVE STRESS FINITE ELEMENT PROCEDURE

Governing Equations

The saturated porous medium is viewed in this report as a two-phase system consisting of a solid and a fluid phase, each of which is regarded as a continuum, and each following its own motion. Early in the 1950s, Biot (Ref 1) extended the work of Terzaghi (Ref 25) on soil consolidation, and formulated linear governing equations for the interaction of two of these phases. The required formalism for the development of general nonlinear equations was later introduced through the theory of mixtures (Ref 26, 27, and 28). General mixture results can be shown through formal linearization of the field and constitutive equations, to reduce to Biot linear poroelastic model (see Ref 29). The balance laws for the two-phase mixture are summarized in this report.

Balance of Mass

$$\frac{Dn^\alpha}{Dt} + n^\alpha \underline{v} \cdot \underline{v}^\alpha = - \frac{n^\alpha}{\rho_\alpha} \frac{D}{Dt} (\rho_\alpha) \quad (\alpha = s, w) \quad (1)$$

Balance of Linear Momentum

$$\underline{v} \cdot \underline{g}^\alpha + \hat{\underline{p}}^\alpha + \rho^\alpha \underline{b} = \rho^\alpha \underline{a}^\alpha \quad (\alpha = s, w) \quad (2)$$

where: $\frac{D}{Dt}$ = material derivative following the motion of the α -phase

$\rho^\alpha = n^\alpha \rho_\alpha$ = macroscopic average mass density

ρ_α = microscopic mass density

n^α = fraction of elemental volume, dV , occupied by α -phase
(i.e., $n^\alpha = dV^\alpha/dV$).

Clearly, $\sum n^\alpha = n^s + n^w = 1$,

where: s and w = solid and fluid phases, respectively

n^w = porosity

\underline{v}^α = velocity (spatial) of α -phase

\underline{a}^α = acceleration of α -phase

\underline{b} = body force per unit mass

$\hat{\underline{p}}^\alpha$ = momentum supply to the α -phase from the other phase,
subject to $\sum_{\alpha} \hat{\underline{p}}^\alpha = \hat{\underline{p}}^s + \hat{\underline{p}}^w = 0$.

In the following, momentum interaction consists of diffusive and dilatational contributions, viz.,

$$\hat{\underline{p}}^s = \hat{\underline{p}}^w = - \underline{\xi} \cdot (\underline{v}^s - \underline{v}^w) - p_w \underline{\nabla} n^w \quad (3)$$

where: $\underline{\xi}$ = symmetric, positive definite second-order tensor

p_w = fluid pressure

The first term is sometimes called the "Stokes drag" (see Ref 26).

In Equation 2, $\underline{\sigma}^\alpha$ = partial (Cauchy) stress tensor corresponding to the α -phase. The partial stress tensor $\underline{\sigma}^w$ corresponding to the fluid phase is equal to n^w times the pore fluid stress $\underline{\sigma}_w$, i.e.,

$$\underline{\sigma}^w = n^w \underline{\sigma}_w \quad (4)$$

However, the partial stress tensor $\underline{\sigma}^s$ corresponding to the solid phase is not the effective stress $\underline{\sigma}'^s$ of classical soil mechanics (Ref 25), but rather is

$$\underline{\sigma}^s = \underline{\sigma}'^s + n^s \underline{\sigma}_w \quad (5)$$

where $n^s \underline{\sigma}_w$ accounts for the effects of the pore fluid stress on the individual solid grains which constitute the solid skeleton. The global stress, $\underline{\sigma}$, is the sum of the partial stresses, and is equal to (from Equations 4 and 5)

$$\underline{\sigma} = \underline{\sigma}^s + \underline{\sigma}^w + \underline{\sigma}'^s + \underline{\sigma}_w \quad (6)$$

as postulated in classical soil mechanics (Ref 25).

Equations of State

For all practical applications of interest in soil dynamics, the soil grains may always be assumed to be incompressible, and in the following ρ_s constant. Equation 1 for the solid phase then simplifies to,

$$\frac{Dn^w}{Dt} = (1 - n^w) \underline{v} \cdot \underline{v}^s \quad (7)$$

and Equations 1 and 7 may be combined to yield the so called "storage equation." viz.,

$$\underline{v} \cdot [n^w \underline{v}^w] + \underline{v} \cdot [(1 - n^w) \underline{v}^s] = - \frac{n^w}{\rho_w} \frac{D}{Dt} (\rho_w) \quad (8)$$

Constitutive Assumptions

A rate-type constitutive equation describes the behavior of the porous solid skeleton, of the following form:

$$\frac{D}{Dt} (\underline{\sigma}'^s) = \underline{D}^s : \underline{v}_{(}^s) + \underline{D}^G : \underline{v}_{[}^s] - (\underline{\sigma}'^s \underline{x} \delta'^s) : \underline{v}_{(}^s) \quad (9a)$$

where: $\underline{v}_{(}^s$ = symmetric parts of the solid velocity gradient

$\underline{v}_{[}^s$ = skew-symmetric parts of the solid velocity gradient

\underline{D}^S = material constitutive tensor, an objective tensor
valued function of possible \underline{g}^S and the solid
deformation gradient

\underline{D}^G = contribution from the rotational component of the
stress rate.

Namely,

$$\underline{D}_{ijkl}^G = \frac{1}{2}[\sigma_{il}^S \delta_{jk} + \sigma_{jl}^S \delta_{ik} - \sigma_{ik}^S \delta_{jl} - \sigma_{jk}^S \delta_{il}] \quad (9b)$$

The last term on the right-hand side in Equation 9a is introduced to ensure that the tangent stiffness operator obtained through linearization of the momentum equations possesses the major symmetry as the \underline{D}^S tensor. Many nonlinear material models of interest can be put in the above form (e.g., all nonlinear elastic and many elastic-plastic material models). The particular form of the constitutive equation (Equation 13) adopted here was first proposed by Hill (Ref 30) within the context of plasticity theory. Appropriate expressions for the effective modulus tensor, \underline{D}^S , for soil media are given in References 31 and 32. For a linear isotropic elastic porous skeleton:

$$\underline{D}_{ijkl}^S = \lambda^S \delta_{ij} \delta_{kl} + v^S (\delta_{ik} \delta_{jl} + \delta_{il} \delta_{jk}) \quad (10)$$

where: λ^S, v^S = effective Lamé's moduli

δ_{ij} = Kronecker delta

The following constitutive equation is assumed to describe the behavior of the fluid phase

$$\underline{g}_w = -p_w \underline{\delta} \quad (11)$$

where: p = pore-fluid pressure

We assumed that the fluid has no average shear viscosity. Further, the fluid flow is assumed barotropic so that the fluid kinetic equation of state is independent of the temperature, viz.,

$$F(p_w, \rho_w) = 0 \quad (12)$$

for which it follows that

$$\frac{1}{p_w} \frac{D}{Dt} (p_w) = \frac{1}{\lambda^w} \frac{D}{Dt} (p_w) \quad (13)$$

where: $\lambda^w = \rho_w \delta p_w / \partial \rho_w =$ bulk modulus of the fluid phase.

The fluid pressure can thus be determined from Equation 8, which now writes:

$$\frac{D}{Dt} (p_w) = \frac{\lambda^w}{v^w} \{ \underline{v} \cdot (n^w \underline{v}^w) + \underline{v} \cdot [(1 - n^w) \underline{v}^s] \} \quad (14)$$

For soil media, the compressibility of the fluid phase is often no smaller than the compressibility of the solid skeleton. Therefore, the fluid phase may, in some soil dynamics applications, be regarded as incompressible, and Equation 8 reduces to:

$$\underline{v} \cdot [n^w \underline{v}^w] + \underline{v} \cdot [(1 - n^w) \underline{v}^s] = 0 \quad (15)$$

Field Equations

Under the assumptions described above, the linear momentum equations (Equation 2) simplify to:

$$\rho^s \underline{a}^s = \underline{v} \cdot \underline{g}'^s - n^s \underline{v} p_w - \xi \cdot (\underline{v}^s - \underline{v}^w) + \rho^s \underline{b} \quad (16a)$$

$$\begin{aligned} \rho^w \frac{D}{Dt} (\underline{v}^w) &= \rho^w (\underline{v}^w - \underline{v}^w) \cdot \underline{v} \underline{v}^w - n \underline{v} p_w \\ &+ \xi \cdot (\underline{v}^s - \underline{v}^w) + \rho^w \underline{b} \end{aligned} \quad (16b)$$

when the movement of the solid phase is used as the reference motion. When inertia and convective terms are neglected, Equation 16b reduces to Darcy's law as:

$$n^w (\underline{v}^w - \underline{v}^s) = -(n^w)^2 \xi^{-1} \cdot (\underline{v} p - \rho \underline{b}) \quad (17)$$

and thus $\underline{k} = (n^w)^2 \underline{\gamma}_w \xi^1 =$ Darcy permeability tensor (symmetric, positive definite), (units. L/T), $\underline{\gamma}_w = g \rho_w \approx$ unit weight of the fluid; $g =$ acceleration of gravity.

Weak Form - Semi-Discrete Finite Element Equations

The initial boundary value problem consists of finding the solid displacement, \underline{v}^s , the fluid velocity, \underline{v}^w , and the fluid pressure, p_w (all functions of position and time satisfying the field equations (Equations 16a and 16b) together with the constitutive relations and continuity conditions subject to appropriate initial and boundary conditions). In order to reduce the number of unknowns, the fluid pressure is eliminated from the formulation, thereby producing a most efficient scheme. In the case of a compressible fluid, the fluid pressure is determined from the computed velocities through time integration of Equation 14. In the case of an incompressible fluid, a penalty-function formulation of the continuity constraint expressed by the storage equation (Equation 15) is used to compute the fluid pressure as:

$$p_w = - \frac{\lambda^w}{n} \{ \underline{\nabla} \cdot [n^w \underline{v}^w] + \underline{\nabla} \cdot [(1 - n^w) \underline{v}^s] \} \quad (18)$$

where $\lambda^w > 0$ is a penalty parameter, not the effective bulk modulus appearing in Equation 14. The penalty parameter is selected as a large number. This parameter is further discussed later.

The weak formulation associated with the initial boundary value problem is obtained by proceeding along standard lines (see Ref 33). The associated matrix problem is obtained by discretizing the domain occupied by the porous medium into nonoverlapping finite elements. Associated with this discretization are nodal points at which shape functions are prescribed. Two sets of shape functions will be required for the solid displacement and the fluid velocity fields, respectively. However, since attention in the following is restricted to low order (i.e., four-node plane, eight-node brick) finite elements, which are the most efficient in nonlinear analysis, the same shape functions are used

for both the solid and the fluid. The shape functions for the solid displacement and fluid velocity associated with node A are denoted by N^A . They satisfy the relations $N^A(\underline{x}^B) = \delta_{AB}$ in which \underline{x}^B denotes the position vector of node B, δ_{AB} = Kronecker delta. The solution of the Galerkin counterpart of the weak formulation is then expressed in terms of the shape functions and gives rise to the following system of equations:

$$\begin{bmatrix} \underline{\underline{M}}^s & \underline{\underline{0}} \\ \underline{\underline{0}} & \underline{\underline{M}}^w \end{bmatrix} \begin{bmatrix} \underline{\underline{a}}^s \\ \underline{\underline{a}}^w \end{bmatrix} = \begin{bmatrix} \underline{\underline{F}}^s \\ \underline{\underline{F}}^w \end{bmatrix} - \begin{bmatrix} \underline{\underline{Z}} & -\underline{\underline{Z}} \\ -\underline{\underline{Z}}^T & \underline{\underline{Z}} \end{bmatrix} \begin{bmatrix} \underline{\underline{v}}^s \\ \underline{\underline{v}}^w \end{bmatrix} \quad (19)$$

where: $\underline{\underline{M}}^\alpha$ = mass matrix

$\underline{\underline{a}}^\alpha$ = acceleration vector

$\underline{\underline{v}}^\alpha$ = velocity vector

$\underline{\underline{F}}^\alpha$ = force vector

Several computational simplifications result in using a diagonal mass matrix, and a "lumped" mass matrix is used throughout. For the two-dimensional (three-dimensional), and four- (eight-) node bilinear (tri-linear) isoparametric element,

$$(\underline{\underline{M}}_{ij}^{AB})^\alpha = \delta_{ij} \delta^{AB} \int_{\Omega^e} \rho^\alpha N^A d\Omega \quad (\text{no sum on A}) \quad (20)$$

where $\underline{\underline{M}}_{ij}^{AB}$ = the elemental mass contribution to node a from node b for directions i and j to the global mass matrix Ω^e = spatial domain occupied by element e.

In Equation 19, $\underline{\underline{Z}}$ is a damping matrix arising from the momentum transfer terms in Equations 16 and 17 as:

$$Z_{ij}^{AB} = \int_{\Omega^e} N_{ij}^A \xi \quad N^B \, d\Omega \quad (21)$$

The solid force vector \tilde{F}^s is:

$$\tilde{F}^s = (\tilde{F}^{ext})^s - \tilde{N}^s \quad (22)$$

where: $(F^{ext})^s$ = vector of external solid forces (i.e., body force, surface transactions)

\tilde{N}^s = vector of solid stress forces, viz.,

$$N_1^A \quad s = \int_{\Omega^e} N_{,j}^A (\sigma_{ij}^s - n^s p_w \delta_{ij}) \, d\Omega \quad (23)$$

The fluid force vector \tilde{F}^w (24)

where: $(\tilde{F}^{ext})^w$ = vector of external fluid forces

\tilde{N}^w = vector of convective and fluid stress forces, viz.,

$$N_1^A \quad w = \int_{\Omega^e} \rho^w N^A (v_j^w - v_j^s) v_{1,j}^w \, d\Omega - \int_{\Omega^e} N_{,i}^A n^w p_w \, d\Omega \quad (25)$$

Time Integration

Time integration of the semidiscrete finite element equations (Equation 19) is performed by using a finite difference time stepping algorithm. Many types of time stepping algorithms and algorithmic strategies are presently available (see Ref 34 for a description of the most widely used computational transient analysis methodologies). Broadly speaking, implicit or explicit procedures are available. Explicit procedures are the most computationally efficient procedures since they do not require (for a diagonal mass matrix) equation solving to advance

the solution. However, stability restricts the size of the allowable time step. On the other hand, unconditional stability can usually be achieved in implicit procedures but they do require solution of a system of equations at each time step. First and foremost, it must be pointed out that a purely explicit procedure is not appropriate for the problem at hand because of the unreasonably stringent time step restriction resulting from the presence of the overly stiff fluid in the mixture (even for highly nonlinear solid material models). Methods that combine the attractive features of explicit and implicit integrations have recently been developed. The methods used here fall under the category of "split operator methods." In operator splitting methods an implicit integrator is selected as the starting point and the integrand (right-hand side in Equation 19) is split so that the system of equations solved is reduced. The specific choice made is obviously problem dependent as discussed further.

Symbolically, the discretized equations of motion (Equation 19) can be written as:

$$\underline{M} \underline{\ddot{a}} + \underline{C} \underline{\dot{v}} + \underline{N}(\underline{d}, \underline{v}) = \underline{F}^{\text{ext}} \quad (26)$$

where \underline{M} , \underline{C} , \underline{N} , \underline{a} , and \underline{d} are defined by Equation 19 in an obvious manner. Time integration is performed by using the implicit-explicit algorithm of References 35, 18, and 19, which consists of satisfying the following equations:

$$\underline{M} \underline{\ddot{a}}_{n+1} + \underline{C}^I \underline{\dot{v}}_{n+1} + \underline{C}^E \underline{\tilde{v}}_{n+1} + \underline{N}^I(\underline{d}_{n+1}, \underline{v}_{n+1}) \quad (27)$$

$$+ \underline{N}^E(\underline{\tilde{d}}_{n+1}, \underline{\tilde{v}}_{n+1}) = \underline{F}_{n+1}^{\text{ext}}$$

$$\underline{d}_{n+1} = \underline{d}_{n+1} + \alpha \Delta t^2 \underline{\ddot{a}}_{n+1}$$

$$\underline{v}_{n+1} = \underline{\tilde{v}}_{n+1} + \beta \Delta t \underline{\ddot{a}}_{n+1}$$

$$\text{where: } \tilde{d}_{n+1} = d_n + \Delta t \, v_n + (1 - 2\beta) \frac{\Delta t^2}{2} a_n$$

$$\tilde{v}_{n+1} = v_n + (1 - \alpha) \Delta t \, a_n$$

and the superscript I and E refer to the parts of \underline{C} and \underline{a} that are treated as implicit or explicit, respectively. The notation is: Δt = time step; $\underline{F}^{\text{ext}} = \underline{F}^{\text{ext}}(t_n; \underline{d}_n, \underline{v}_n, \underline{v}_n, \text{ and } \underline{a}_n$ are the approximations to $\underline{d}(t_n)$, $\underline{v}(t_n)$, and $\underline{a}(t_n)$; α and β = algorithmic parameters that control accuracy and stability of the method. It may be recognized that Equations 27 and 28 correspond to the Newmark formulas (Ref 36). The quantities, \tilde{d}_{n+1} and \tilde{v}_{n+1} , are referred to as "predictor" values, while \underline{d}_{n+1} and \underline{v}_{n+1} are referred to as "corrector" values. From Equations 26 through 28, it is apparent that the calculations are rendered partly explicit by evaluating part of the viscous contribution $\underline{C}^E \tilde{v}_{n+1}$, and the force, \underline{N}^E , in terms of data known from the previous step.

Calculations commence with the given initial data (i.e., \underline{d}_0 and \underline{v}_0) and \underline{a}_0 , which is defined by.

$$\underline{M} \underline{a}_0 = \underline{F}_0^{\text{ext}} - \underline{C}_0 \underline{v}_0 - \underline{N}(\underline{d}_0, \underline{v}_0) \quad (28)$$

since \underline{M} is diagonal, the solution of Equation 28 is rendered trivial.

Implementation

At each time step, Equations 26 through 28 constitute a nonlinear algebraic problem that is solved by a Newton-Raphson type iterative procedure. The most useful and versatile implementation is to form an "effective static problem" from Equations 26 through 28 in terms of the unknown \underline{a}_{n+1} , which is in turn linearized. Within each time step, the calculations are performed as summarized in Table 1 in which \underline{C}^I and \underline{K}^I denote the parts of the damping and tangent stiffness operations, respectively, to be treated implicitly.

The following choices have been found most appropriate:

Incompressible Fluid (Penalty Formulation). In this case, \underline{C}^I is selected to contain both the momentum transfer and the penalty term

$$\underline{C}^I = \begin{bmatrix} \underline{Z} + \underline{C}^{ss} & -\underline{Z} + \underline{C}^{sw} \\ -\underline{Z} + \underline{C}^{ws} & \underline{Z} + \underline{C}^{ww} \end{bmatrix} \quad (29)$$

where: $\underline{C}^{\alpha\beta}(\alpha, \beta = s, w) =$ damping matrices arising from the penalty treatment of the fluid contribution as:

$$C_{ij}^{AB \alpha\beta} = \int_{\Omega^e} \lambda^w \frac{n^\alpha n^\beta}{n^w} N_{,i}^A N_{,j}^B d\Omega \quad (30)$$

The convective fluid force (see Equation 24) is usually small and is treated explicitly with no resulting computational difficulty. Note that since $\underline{C}^{sw} = (\underline{C}^{ws})^T$ the resulting \underline{C}^I is symmetric for the choice adopted here.

As for the solid stress force (Equation 23) contribution to the equations of motion, three options are possible: "implicit," "explicit," or "implicit-explicit" treatment. The choice is made as follows:

Wave Propagation Type Calculations. Very short time scale (and high frequency) solutions are sought and an explicit treatment of the solid effective stress contribution is usually found most appropriate in this case. The time step size restriction resulting from stability considerations is of the same order as the one resulting from accuracy considerations for nonlinear material models. Further, the specific implicit treatment adopted for the fluid contribution allows the calculations to be carried out at a time step usually close to the time step corresponding to the propagation of the solid compressional wave through the solid phase of the critical element.

Vibration Type Calculations. Since the frequencies captured are usually much higher than above, an implicit treatment of the solid effective stress contribution is usually convenient in this case since it

allows the time step to be selected following accuracy considerations only. Unconditional stability is achieved by selecting the proper algorithmic parameters (discussed later). However, for nonlinear analyses, a purely implicit treatment requires a matrix reform/factorize at each time step (and for every iteration to be performed, in general), thus producing a considerable computational burden. It is therefore convenient, in the nonlinear case, to adopt an implicit-explicit treatment of the effective stress contribution as follows: The linear part of the stiffness is treated implicitly while the remaining nonlinear part is treated explicitly. For that purpose, a solid stiffness operator is defined from Equations 9 and 23 through linearization as:

$$\tilde{K}_s = \begin{bmatrix} \tilde{K}^s + \tilde{K}^G & \underline{0} \\ \underline{0} & \underline{0} \end{bmatrix} \quad (31)$$

where: \tilde{K}^s = material tangent part

\tilde{K}^G = "initial stress" or geometric part, formed from the tensors \underline{D}^s and \underline{D}^G (Equation 9) in the usual manner (see Ref 16).

Table 1. Flow Chart

1. Initialization:

$$i = 0$$

$$Q1 = Q2 = 0$$

2. Predictor Phase:

$$\tilde{d}_{n+1}^{(1)} = \tilde{d}_{n+1}$$

$$\tilde{v}_{n+1}^{(1)} = \tilde{v}_{n+1}$$

$$\tilde{a}_{n+1}^{(1)} = \tilde{0}_{n+1}$$

Table 1. Continued

3. Form Effective Mass: (Reform and factorize only if required)

$$\underline{M}^* = \underline{M} + \Delta t \alpha \underline{C}^I + \Delta t^2 \beta \underline{K}^I$$

4. Form Residual Force:

$$\Delta \underline{F}_{n+1}^{(i)} = \underline{F}_{n+1}^{\text{ext}} - \underline{M} \underline{a}_{n+1}^{(i)} - \underline{C} \underline{v}_{n+1}^{(i)} - \underline{N}(\underline{d}_{n+1}^{(i)}, \underline{v}_{n+1}^{(i)})$$

5. Solution Phase:

$$\underline{M}^* \Delta \underline{a}^{(i)} = \Delta \underline{F}^{(i)}$$

6. Corrector Phase:

$$\underline{a}_{n+1}^{(i+1)} = \underline{a}_{n+1}^{(i)} + \Delta \underline{a}^{(i)}$$

$$\underline{v}_{n+1}^{(i+1)} = \underline{\tilde{v}}_{n+1} + \Delta t \alpha \underline{a}_{n+1}^{(i+1)}$$

$$\underline{d}_{n+1}^{(i+1)} = \underline{\tilde{d}}_{n+1} + \Delta t^2 \beta \underline{a}_{n+1}^{(i+1)}$$

7. Convergence Check: (only if 1 > 0)

$$Q2 = Q1$$

$$Q1 = \left\| \underline{\Delta a}^{(i)} \right\| / \left\| \underline{a} \Delta^{(i-1)} \right\|$$

$$Q = \text{AMAX}(Q1, Q2)$$

$$\text{If } \left\| \underline{\Delta F}^{(i)} \right\| / \left\| \underline{\Delta F}^{(0)} \right\| \leq \text{TOL}^* \text{ .AND.}$$

$$Q \left\| \underline{\Delta a}^{(i)} \right\| / \left\| \underline{\Delta a}^{(0)} \right\| \leq (1-Q)\text{TOL}^* \text{) GOTO 9}$$

Otherwise; continue

8. $i \leftarrow i + 1$; GOTO 3

9. $n \leftarrow n + 1$; GOTO 1

*Typically, $\text{TOL} = 10^{-3}$.

In the implicit-explicit procedure:

$$\mathbf{K}^I = \begin{bmatrix} \mathbf{K}_E^s & \mathbf{0} \\ \mathbf{0} & \mathbf{0} \end{bmatrix} \quad (32)$$

where: \mathbf{K}_E^s = linear elastic contribution to the material tangent stiffness (from Equation 10).

Such a choice does not always lead to unconditional stability. The difficulty is not usually associated with the explicit treatment of \mathbf{K}^G (which contains terms of the stress order and therefore usually has a negligible impact on stability), but rather from the explicit treatment of the nonlinear term $(\mathbf{K}^s \quad \mathbf{K}_E^s)$ for materials with a locking tendency. In that case, care must be exercised in selecting a time step smaller than the one associated with the fastest expected wave speed corresponding to the subsequent stress histories to be followed by the material elements.

Diffusion Type Calculations. It is sometimes desirable to capture the purely diffusive part ("consolidation" part) of the solution "dynamically." Such a necessity arises in situations in which both short and long time solutions to a dynamical problem are sought (such as in seismic or blast induced liquefaction simulations). As shown in References 14 and 16; by switching to an appropriate choice of the Newmark parameters, $\alpha = 3/2$ and $\beta = 1$, and by using the implicit-explicit option described above all dynamic transients can be damped out, and purely diffusive (consolidation) solutions can be obtained "dynamically" by solving the dynamic equations.

The penalty treatment of the storage equation constraint requires that λ^w be selected as a "large number" capable of predominating the other moduli. It should be picked according to the relation:

$$\lambda^w = C \text{ Max } \left[\frac{n^w{}^2 \gamma_w}{k}, \frac{1}{2} \Delta t (\lambda^s + 2 v^s) \right] \quad (33)$$

where: C = a constant that depends only on the computer word length. Numerical studies reveal that for floating-point word lengths of 60 to 64 bits, $C \sim 10^7$.

It has been determined, on the basis of numerical experiments, that it is better to use reduced integration of the penalty terms and of the solid volumetric stiffness ($\text{div } \underline{v}^s$ contribution) to alleviate potential mesh locking phenomena.

Compressible Fluid. In this case, \underline{C}^I contains the momentum transfer term contribution to the equations of motion, viz.,

$$\underline{C}^I = \begin{bmatrix} \underline{Z} & -\underline{Z} \\ -\underline{Z}^T & -\underline{Z} \end{bmatrix} \quad (34)$$

and the convective fluid force is treated explicitly.

Again, the fluid pressure contribution is treated implicitly. For this purpose, a fluid stiffness operator is defined from Equations 14 and 19 through linearization as,

$$\underline{K}_w = \begin{bmatrix} \underline{C} & \underline{C} \\ \underline{C}^{ws} & \underline{C}^{ww} \end{bmatrix} \quad (35)$$

Where $\underline{C}^{\alpha\beta}$ ($\alpha, \beta = s, w$) are the same matrices as previously defined in Equation 31. However, note that in this case, the matrices contribute to the stiffness matrix rather than to the damping matrix.

The same options as described previously for the solid stress force contribution to the equations are used. Note that in the implicit-explicit procedures,

$$\underline{K}^I = \begin{bmatrix} \underline{K}_E^s + \underline{C}^{ss} & \underline{C}^{sw} \\ \underline{C}^{ws} & \underline{C}^{ww} \end{bmatrix} \quad (36)$$

which again is a symmetric matrix.

Stability. The resulting stability conditions (Ref 35) are summarized: In all cases $\alpha \geq 1/2$:

1. **Implicit Treatment:** Unconditional stability is achieved if $\beta \geq \alpha/2$ and it is recommended that (Ref 37):

$$\beta = \frac{\left(\alpha + \frac{1}{2}\right)^2}{4} \quad (37a)$$

2. **Implicit-Explicit Treatment:** The time step restriction is

$$\omega \Delta t < \frac{2}{\left(\alpha + \frac{1}{2}\right)} \quad (37b)$$

to maximize high-frequency numerical dissipation; ω = highest natural frequency associated with the explicit part of the stiffness operator. The maximum expected frequency may be bounded by the frequency of the smallest element, viz., for a rectangular four node bilinear element,

$$\omega = 2 \frac{C}{L} \quad (37c)$$

where: L = smallest dimension of the element

C = wave speed ($= \sqrt{(\lambda^s + 2 \mu^s)/\rho^s}$ for the linear model).

Program DYNAFLOW

Equations 19 through 37 have been incorporated into the finite element computer program DYNAFLOW (Ref 38). Numerical results that illustrate the performance of the proposed numerical schemes in analyzing the propagation of plane progressive waves (Refs 40, 1, 29, 26, 41, and 42) in fluid saturated porous soil media have been reported in Reference 13. In Reference 13 both compressible and incompressible fluid cases are considered. In the following, attention is restricted to vibration calculations in soil-structure interacting systems associated with seismic events in which the pore fluid may be assumed to be incompressible (compared to the compressibility of the soil skeleton).

In the calculation reported the four-node bilinear isoparametric element (see Refs 43 and 33 for a detailed description) is used with the standard selective integrations scheme (Ref 43). Also, the Newark algorithmic parameters are always selected such that $\alpha \geq 1/2$ and $\beta = (\alpha + 1/2)^2/4$ to maximum high-frequency numerical dissipation (Ref 37).

Time integration of the semidiscrete finite element equations is performed by using the implicit-explicit, predictor-(multi) corrector option. The structural domains and the fluid phase are always treated implicitly, whereas the solid skeleton phase is treated partly implicitly, partly explicitly. Specifically, the "elastic" part of the solid stiffness is treated implicitly, whereas the elastic-plastic part of the stiffness is treated explicitly. Such a choice allows time integration to be performed most efficiently for cases where many load/unload cycles occur, such as during dynamic events.

In order to simulate realistic initial conditions for the stresses and strains in the soil deposits before input of the earthquake-like ground motions, numerical simulations are carried in at least two sequential steps:

1. **Installation of Soil Deposit:** This step in the numerical simulation is designed to simulate realistic initial conditions. The computed gravitational stresses/displacements/pore-water pressures are used as initial conditions for the ground motion calculations.

2. **Ground Motion Simulation:** The computed gravitational stresses/displacements/pore-water pressures computed in the first sequence are used as initial conditions for the ground motion calculations. In order to avoid the initial propagations of any spurious noises, the acceleration array is first cleared before activating the ground motion. Also, the algorithmic parameters are reset to $\alpha = 0.65$, $\beta = 0.33$ (slightly diffusive), the time to zero, and the time step, Δt , selected to properly follow the details of the stresses (and pore-water pressures) "at rest" before input of the ground shaking. For this purpose, small initial stresses are first input in the soil deposit and gravity is turned on.

A number of steps (and iterations) are used to apply gravity with a large enough time step, Δt , to ensure: (1) that no excess pore-water pressures (over steady state conditions) can build up; (2) that there is full development of effective stresses in the foundation soil; and (3) that no transients occur. For that purpose, a backward scheme with high numerical dissipation was used to damp out all transients setting $\alpha = 1.50$ and $\beta = 1.00$. Iterations (Newton-Raphson or modified Newton-Raphson) are used to ensure proper convergence of the solution at each time step.

Post-Dynamic Event Simulation

In saturated soil deposits, excess pore-water pressures usually build up and do not have time to fully dissipate within the time frame of the earthquake. Subsequent redistribution and diffusion of these excess pore-water pressures following the dynamic event are often of interest since they may lead to failure (e.g., in earth dams where failures have been recorded in the field several minutes to several hours following the earthquake). It is, however, usually inefficient (cost wise) to numerically capture the post-event behavior with a time step designed to follow the details of an earthquake motion. Therefore, post-dynamic events are calculated by resetting $\alpha = 1.5$ and $\beta = 1.00$ (highly diffusive backward) and by selecting the appropriate time step, Δt , for capturing the post-event diffusion part of the solution.

DESCRIPTION OF STORAGE TECHNIQUES

In DYNAFLOW all data may be stored in core (central memory) in blank common. The basic features of the data structure are:

- compacted column architecture:

This feature is engendered by the method of equation solving employed. The solver is called variously a "profile," "skyline" or "active column" solver. Since, in large problems, the dominant portion of storage is that devoted to the stiffness matrix, K , the storage scheme for K is the most important feature of the storage.

- dynamic storage allocation:

Because of the variable sizes of the arrays needed in different problems, it would be very inefficient to "fix" the dimensioning. In the dynamic storage allocation concept the dimensions of arrays are set in the program at the time of execution. If insufficient storage is allocated, a message is printed out.

- element groups:

Many features of finite element computer programs are the same even though the intended applications may be quite different. To some extent this is also true of the individual finite element subroutines. However, the data structure and options available may vary considerably from one element to another. To accommodate these differences, the elements are read in, stored and operated upon in groups. The data structure for the group is set up via dynamic storage allocation in individual element subroutines.

For certain models, a non-symmetric stiffness is necessary. In this case, additional storage is required for the lower part of the stiffness. It is a property of the connectivity of the finite element mesh that although the stiffness is non-symmetric, its profile is symmetric. An example is shown below.

$$K = [K_{ij}] =$$

X	X	0	0	0	0	0	X
X	X	X	0	X	0	0	0
0	X	X	X	X	0	0	0
0	0	X	X	0	X	0	X
0	X	0	X	X	X	0	0
0	0	0	X	X	X	X	0
0	0	0	0	0	X	X	X
X	X	X	0	X	X	X	X

The upper part of K is stored in the array AUPPER as described above for the symmetric case. The array IDIAG is also the same as for the symmetric case. The lower part of K is stored in the one-dimensional array ALOWER row-wise beginning with the first nonzero element in each row and ending with the diagonal term. The scheme is similar to the storage of the upper-triangular part of K in AUPPER. Thus, the length of ALOWER is also NA and the explicit definition of ALOWER for the example is given as follows:

AUPPER(1) = K11 col. 1

AUPPER(2) = K12
AUPPER(3) = K22 col. 2

AUPPER(4) = K23
AUPPER(5) = K33 col. 3

AUPPER(6) = K34
AUPPER(7) = K44 col. 4

AUPPER(8) = K25
AUPPER(9) = K35
AUPPER(10) = K45 col. 5
AUPPER(11) = K55
AUPPER(12) = K46
AUPPER(13) = K56 col. 6
AUPPER(14) = K66

AUPPER(15) = K67
AUPPER(16) = K77 col. 7

AUPPER(17) = K18
AUPPER(18) = K28
AUPPER(19) = K38
AUPPER(20) = K48
AUPPER(21) = K58 col. 8
AUPPER(22) = K68
AUPPER(23) = K78
AUPPER(24) = K88

IDIAG(1) = 1
IDIAG(2) = 3
IDIAG(3) = 5
IDIAG(4) = 7
IDIAG(5) = 11
IDIAG(6) = 14
IDIAG(7) = 16
IDIAG(8) = 24

The zero terms beneath the skyline must be stored because they become nonzero during the solution process. All information in the original matrix K is now contained in the arrays AUPPER and IDIAG in compact fashion.

Compacted Column Storage Scheme

Assume the symmetric stiffness matrix K has dimension 8×8 and has zero and nonzero elements indicated by 0 and X, respectively, in the figure below.

$$K = [K_{ij}] = \begin{array}{cccccccc} \text{---} & & & & & & & \text{---} \\ \begin{array}{c} X \\ \\ \\ \\ \\ \\ \\ \end{array} & \begin{array}{c} X \\ \\ \\ \\ \\ \\ \\ \end{array} & \begin{array}{c} 0 \\ X \\ X \\ \\ \\ \\ \\ \end{array} & \begin{array}{c} 0 \\ 0 \\ X \\ X \\ 0 \\ 0 \\ 0 \end{array} & \begin{array}{c} 0 \\ X \\ X \\ 0 \\ X \\ X \\ X \end{array} & \begin{array}{c} 0 \\ 0 \\ 0 \\ 0 \\ 0 \\ 0 \\ 0 \end{array} & \begin{array}{c} X \\ 0 \\ 0 \\ X \\ 0 \\ X \\ X \end{array} \\ \text{Symm.} & & & & & & & \end{array}$$

The dashed line enveloping the nonzero terms is sometimes called the "profile" or "skyline."

K is stored in a one-dimensional array, AUPPER, column-wise beginning with the first nonzero element in each column and ending with the diagonal term. The locations of the diagonal terms in AUPPER are stored in a one-dimensional integer array IDIAG. The dimension of IDIAG is NEQ, the number of equations (e.g., for K above NEQ = 8). The dimension of AUPPER is NA, the sum of the "column heights." The column height is the number of terms in a column beginning with the first nonzero term and ending with the diagonal term (e.g., for the above matrix K , column 1 has height 1, column 4 has height 2, column 6 has height 3, etc.) NA for K is 24. The arrays AUPPER and IDIAG corresponding to K are given explicitly as follows:

ALOWER(1) = K11	row 1
ALOWER(2) = K21	row 2
ALOWER(3) = K22	
ALOWER(4) = K32	row 3
ALOWER(5) = K33	
ALOWER(6) = K43	row 4
ALOWER(7) = K44	
ALOWER(8) = K52	
ALOWER(9) = K53	row 5
ALOWER(10) = K54	
ALOWER(11) = K55	
ALOWER(12) = K64	
ALOWER(13) = K65	row 6
ALOWER(14) = K66	
ALOWER(15) = K76	row 7
ALOWER(16) = K77	
ALOWER(17) = K81	
ALOWER(18) = K82	
ALOWER(19) = K83	
ALOWER(20) = K84	row 8
ALOWER(21) = K85	
ALOWER(22) = K86	
ALOWER(23) = K87	
ALOWER(24) = K88	

We note that diagonal entries of K are stored in both AUPPER and ALOWER. This is compensated for by the logical simplicity of the storage scheme. All information in the original matrix is now contained in the arrays AUPPER, ALOWER, and IDIAG.

For large finite element stiffness matrices the saving of storage is considerable.

The heights of the columns in K are determined by subroutine COLHT from the node numbers on element data cards. The column heights are initially stored in IDIAG. When the calculation of column heights is completed, subroutine IDIAG determines the diagonal addresses and "overwrites" them in IDIAG.

The right-hand side vector in

$$K d = F$$

is stored in an array B, of dimension NEQ in the obvious way:

$$B(1) = F1$$

$$B(2) = F2$$

$$\begin{matrix} \cdot & \cdot \\ \cdot & \cdot \\ \cdot & \cdot \end{matrix}$$

$$B(8) = F8$$

The solution of the matrix equations is facilitated by a factorization of K , into an upper triangular matrix U , a lower triangular matrix L , and a diagonal matrix D such that

$$K = L D U$$

Both L and U have unit diagonal entries. In the symmetric case, $L = U$ transpose, and consequently L is not needed.

The matrices U and L have the same profile as K . Since U and L have unit diagonal entries, storage is saved by placing the diagonal entries of D in the array AUPPER. Thus, after factorization the nonzero entries of L , U , and D are stored in the arrays AUPPER and ALOWER. During the factorization procedure storage is required.

During the evolution of the analysis, the pivots (diagonal entries of D) are scanned. If any zero or negative values are encountered, messages are printed out summarizing the situation.

Crout Elimination

The procedure used for performing the factorization is called Crout elimination, a convenient variant of Gauss elimination. In the Crout algorithm one column at a time is completely factorized, beginning with the first column and not involving subsequent columns. (This feature proves convenient in nonlinear analysis in which only a small zone of the entire effective stiffness is nonlinear. The linear portion can be located in the first columns and factorized once and for all.)

For further information on the Crout elimination algorithm employed see R. L. Taylor, "Computer Procedures for Finite Element Analysis," Chapter 24, in O.C. Zienkiewicz, The Finite Element Method, Third Edition, McGraw-Hill, London, 1977.

Forward Reduction and Back Substitution

After factorization the solution is carried out in three steps:

$$L x = F \quad (\text{forward reduction})$$

$$D y = x$$

$$U d = y \quad (\text{back substitution})$$

In each step the solution is an explicit process, the coefficient matrix being triangular or diagonal. The intermediate vectors x and y are in turn stored in the array B. Thus again no additional storage besides that for AUPPER, ALOWER and B (and IDIAG) is needed to carry out the factorization and solution process.

Storage in Blank Common

All of the main arrays in DYNFLOW are stored in blank common. This includes both integer and floating point data. In the main program and the driver subprogram (i.e., subroutine DRIVER), the blank common is denoted by the one-dimensional array A.

The locations and lengths of arrays in blank common are as follows:

First Word	Array
N0 = 1	TIME(NTS+1)
N1 = N0 + (NTS+1)	IH(2,NOUT)
N2 = N1 + NDOUT*2	ID(NDOF,NUMNP)
N3 = N2 + NUMNP*NDOF	X(NSD,NUMNP)
N4 = N3 + NUMNP*NSD*IPREC	D(NDOF,NUMNP)
N4A = N4 + NUMNP*NDOF*IPREC	V(NDOF,NUMNP)
N4B = N4A + NUMNP*NDOF*IPREC	A(NDOF,NUMNP)
N11 = N4B + NUMNP*NDOF*IPREC	DINC(NDOF,NUMNP)
N11A = N11 + NUMNP*NDOF*IPREC	DT(NDOF,NUMNP)
N12 = N11A + NUMNP*NDOF*IPREC	DOUT(NDOUT,NTS+1)
N12A = N12 + (NTS+1)*NDOUT	VOUT(NDOUT,NTS+1)
N12B = N12A + (NTS+1)*NDOUT	AOUT(NDOUT,NTS+1)
N5 = N12B + (NTS+1)*NDOUT	F(NDOF,NUMNP,NLC)
N6 = N5 + NLC*NUMNP*NDOF*IPREC	G(NLS+1,2,NLC)
N7 = N6 + NLC*2*(NLS+1)*IPREC	IDIAG(NEQ)
N8 = N7 + NEQ	E(MAX)
N9 = N8 + MAX	B(NEQ)

N10 = N9 + NEQ*IPREC

AUPPER(NA)

$$N10A = \left\{ \begin{array}{ll} N10 & \text{if ISYMM.EQ.0} \\ N10 + NA*IPREC & \text{if ISYMM.EQ.1} \end{array} \right\} \quad \text{ALOWER(NA)}$$

N13 = N10A + NA*IPREC - 1

total required storage
for in-core solution

N13 must be .LT.MTOT for in-core execution

where

TIME(M) = time at time step M-1

IH(1,M) = node number for nodal output history M

IH(2,M) = degree of freedom number for nodal output history M

ID(L,M) = equation number for degree of freedom L, node M

X(L,M) = Lth coordinate of node M

D(L,M) = Lth displacement of node M

V(L,M) = Lth velocity of node M

A(L,M) = Lth acceleration of node M

DINC(L,M) = Lth displacement increment component of node M

DT(L,M) = Lth predictor displacement component of node M

DOUT(L,M) = nodal displacement output history L at time step M-1

VOUT(L,M) = nodal velocity output history L at time step M-1

AOUT(L,M) = nodal acceleration output history L at time step M-1

F(L,M,N) = Lth prescribed force/displacement/acceleration of
node M for load case N

G(L,1,N) = time L for load case N

G(L,2,N) = load multiplier at time L for load case N

IDIAG(L) = location of Lth diagonal element in coefficient
arrays AUPPER and ALOWER

E(L) = Lth (single-precision) word of element
group data

B(L) = Lth out-of-balance force component

AUPPER(L) = Lth element of upper triangular coefficient matrix
 stored in compacted column form

ALOWER(L) = Lth element of lower triangular coefficient matrix

INSTALLATION INSTRUCTIONS

DYNAFLOW is written in standard FORTRAN IV and has been developed on an IBM 370/3081 computer.

For installation of DYNAFLOW on machines other than the IBM series, it must be remembered that arithmetic calculations must be performed with a precision of about 14 hexadecimal digits (approximately 17 decimal digits). This means that on IBM, UNIVAC, PRIME and VAX type machines, for instance, double precision must be used. However, on CRAY and CYBER type machines, single precision can be used. The requirement of double precision on IBM-like machines is applicable to both linear and nonlinear analysis. If DYNAFLOW is used in single precision on IBM-like machines, the results may be doubtful, and in some cases, the analysis will not be possible.

All system-dependent subroutines (plotting routines, interactive routines, etc....) are gathered in the DESSIN module, and are clearly marked so that modifications for other systems can be done easily.

For installation of DYNAFLOW on your machine, the following steps should be taken:

- (1) Read the tape provided.
- (2) Edit the main program following the instructions contained on the comment statements.
- (3) Review the source code contained in the program module DESSIN, and check for compatibility of system routines. Make appropriate changes if necessary.
- (4) Compile all program modules. They should compile with no FORTRAN errors.
- (5) Load the program.
- (6) Run the data set of test problems provided on the tape and compare your answers with the results contained on the tape. They should be identical.

CONCLUDING REMARKS

DYNAFLOW is a general purpose finite element analysis program for linear and nonlinear, two- and three-dimensional, elliptic, parabolic and hyperbolic initial boundary value problems in structural, solid and fluid mechanics. Although DYNAFLOW can be a very powerful analysis tool, it should be emphasized that its use requires a thorough understanding of the underlying field theories used, and of the integration techniques employed.

USER'S MANUAL

NDOUT	= number of nodal output histories
NDOF	= number of degrees of freedom
NUMNP	= number of nodal points
NSD	= number of space dimensions
NLC	= number of load cases
NLS	= number of load steps
NEQ	= number of equations
MAX	= total (or largest) number of single-precision words in element group data
NA	= number of terms in AUPPER and ALOWER
ISYMM	= symmetry parameter: EQ.0 symmetric coefficient matrix EQ.1 non-symmetric coefficient matrix
NTS	= maximum number of time steps
IPREC* =	1, single precision used 2, double precision used
MTOT*	= total length of blank common available

The above names are the ones most commonly used in individual sub-routines for the arrays in question.

Storage of Element Group Data

The storage for element group data is described in the individual element routines.

(*) Set in the main program.

1.0 TITLE CARD (20A4)

Note	Columns	Variable	Description
(1)	1-80	TITLE(20)	Job title for heading the output

Notes:

- (1) Each data set must begin with a title card.

2.0 CONTROL CARDS

2.1 Card 1 (16I5)

Note	Columns	Variable	Description
	1-5	NUMNP	Number of nodes; GE.0 If EQ.0, program stops
(1)	6-10	NSD	Number of spatial dimensions; GE.1 and LE.3
(2)	11-15	NDOF	Number of degrees of freedom at each node; GE.1 and LE.6
(3)	16-20	NUMEG	Number of element groups; GE.1
(4)	21-25	NTS	Maximum number of time steps; GE.0
(5)	26-30	NLC	Number of load cases; GE.1
(6)	31-35	NLS	Number of load steps; GE.0
(7)	36-40	NSB	Number of time steps between spatial printout; GE.0
(8)	41-45	IMESH	Equation optimization option; GE.0 EQ.0, no optimization EQ.1, optimization
(9)	46-50	MODE	Execution mode; GE.0 EQ.0, direct step-by-step integration, data check EQ.1, direct step-by-step integration, execution EQ.2, eigenvalue/vector, data check EQ.3, eigenvalue/vector, solution
(10)	51-55	ISYMM	Symmetry parameter; GE.0 EQ.0, symmetric stiffness EQ.1, non-symmetric stiffness 0
(11)	56-60	NSLAV	Number of slaved nodes; GE.0

(Cont'd)

2.1 Card 1 (16I5) (Cont'd)

Note	Columns	Variable	Description
	61-65	MODES	Analysis Type; GE.0 and LE.2 EQ.0, Elliptic BVP EQ.1, Hyperbolic initial BVP EQ.2, Parabolic initial BVP
(12)	66-70	NITER	Maximum number of iterations; GE.0
(13)	71-75	NFAC	Effective Stiffness Reform/Factorize Code; GE.0 GT.0, every NFAC time step
	76-80	ACCBC	Nodal boundary condition code; GE.0 EQ.0, Displacement BC EQ.1, Acceleration BC EQ.2, Velocity BC

Notes:

(1) Consult individual element routines in Section 9 for requirements. Either two- or three-dimensional analysis.

(2) In problems where there are different numbers of degrees of freedom at different nodes, NDOF should be set equal to the maximum number. Consult individual element routines in Section 9 for requirements. Superfluous degrees of freedom can be eliminated by employing boundary condition codes (see Section 5.0). For example, two-phase soil elements used in conjunction with single-phase elements. The two-phase elements require 3 (parabolic boundary) or 4 (hyperbolic boundary) degrees of freedom. The single-phase element requires only two degrees of freedom. The single-phase element should then have degrees of freedom 3, or 3 and 4 fixed to avoid unnecessary (and error causing) equations added to the system.

(3) The elements are read in groups. Consult individual element routines in Section 9.

(4) A sufficient number of steps must be taken to accurately characterize nonlinear behavior. Refer to time step length considerations in Section 2.2, note 4, and the length of time through which the dynamic behavior or consolidation takes place.

(5) The applied nodal forces and prescribed displacement (acceleration) histories are synthesized by NLC vectors and corresponding load-time functions. Details are presented in Sections 7 and 8. Note that the proper boundary conditions ACCBC must be set to achieve displacement or acceleration.

(6) The load-time functions are discretized into up to NLS load steps. See Section 8 for details.

(7) Printed spatial output (i.e., displacements, velocities, accelerations and element stresses) will occur only after each multiple of NSB steps. If NSB.EQ.0 or NSB.GT.NTS, there will be no spatial output.

(8) The equation numbering may be optimized by activating that option, resulting in smaller effective stiffness profile. This option should not be invoked without first analyzing preliminary results without optimization, and will be automatically employed to some degree when nodal slaving is invoked.

(9) In the data check modes, input data are printed out and storage requirements are indicated. Also, a tape is created for restart and execution. This mode should be employed prior to making expensive executions.

(10) For certain problems, a non-symmetric stiffness is required. See element data input in Section 9 and material data input in Section 10 for details. Non-symmetric matrices are used primarily in parabolic boundary value problems and for problems involving lightly anisotropic soils. For the case of anisotropic soils, that type of triaxial data is required for input to the constitutive model, Section 10.

(11) Nodes may be slaved to share the same equation number for any selected degree of freedom. Such an option is useful for modeling cyclic symmetry in structures, and for modeling free-field conditions in seismic calculations. Details and figures are presented in Section 5.

(12) Up to NITER iterations will be performed, unless convergence is detected earlier. The convergence tolerance TOL is set in DRIVER to TOL = 1.0E-03 (default), or read on next card. The number of iterations effects the accuracy of solutions. Generally NITER should be between 5 and 10. NFAC is a control on how many time steps will be completed before the stiffness matrix will be reformed (Modified Newton-Raphson only). It is a good idea to reform at every step when rapid changes in the stiffness of the material are taking place. Examples of this are initiation of element stresses (gravity loading for model 8) and liquefaction simulations. Stated another way, if effective stress magnitudes are changing rapidly, the mean effective stress, and therefore the material stiffness, change rapidly. This effect will require more stiffness matrix reformations to obtain accurate solutions.

(13) Only applicable to implicit nonlinear calculations.

2.2 Card 2 (2I5, 7F10.0) (only required if MODE.LE.1)

Note	Columns	Variable	Description
(1)	1-5	NTSS	Number of time steps; GE.0 and LE.NTS
(2)	6-10	IBFGS	Iterations procedure; GE.0 EQ.0, Modified Newton-Raphson EQ.1, Newton-Raphson EQ.2, quasi-Newton (BFGS update) EQ.3, quasi-Newton (Broyden update) EQ.4, quasi-Newton (STRANG update)
(3)	11-20	ALPHA	Algorithm parameter alpha; GE.0.0
(4)	21-30	DT1	Time step; GT.0.0
(5)	31-40	DTMULT	Time step multiplier; GE.0.0 If EQ.0.0, set internally EQ.1.0
	41-50	DTMAX	Maximum allowable time step; GE.0.0 If EQ.0.0, set internally EQ.DT1
(6)	51-60	BETA	Algorithm parameter beta; GE.0.0
(7)	61-70	TIME	Convergence tolerance; GE.0.0 If EQ.0.0 set internally EQ.1.0E-3
	71-90	TO	Time at start of analysis; GE.0.0

Notes:

(1) If NTSS.LT.NTS, a tape is created after NTSS time steps for restart. NTSS is the number of time steps required to initialize the problem in the case of dynamic models (i.e., gravity initialization). In elastoplastic, nonpressure-dependent material models, one step may be adequate. In elastic contact problems one step may be adequate. Elastic solutions require only one step.

(2) Modified Newton-Raphson and Newton-Raphson iterations are recommended. Modified Newton-Raphson with a stiffness matrix reformation at every time step (NFAC, Section 2.1) generally coverages in gravity loading simulations. It may be necessary to use Newton Raphson (stiffness reformation at each iteration) in models which exhibit rapid changes in the stiffness matrix. The BFGS, Broyden, and Strang updates may be useful in some instances involving stiffening systems. The Strang update employs a "line search" algorithm.

(3) For elliptic boundary value problems ALHPA.EQ1.0. Parabolic and hyperbolic boundary value problems require alpha to be adjusted between 0.5 and 1.5, depending on the amount of numerical dumping required. Generally, in the diffusive computations, such as gravity loading and reconsolidation, alpha should be set to 1.5. In dynamic simulations, alpha should be set to 0.65. Alpha and Beta are Newmarks integration constants and more information on those parameters may be found in References 1 and 2.

(4) The time step must be sufficiently small to accurately characterize the nonlinear behavior. Time steps are the most frustrating and difficult part of nonlinear analysis. In elastic or elastoplastic, single-phase analyses, time steps are not important, and generally set equal to a nondimensional 1. In effective stress (two-phase) dynamic analysis, time steps are critical. Contact boundaries may also complicate problems. The following are general guidelines for appropriate time step selection:

(A) Gravity initialization: Consideration must be given to mesh dimension (real), permeability, and boundary conditions. The primary concern in gravity initialization is to develop the in situ effective stress states in the soil model without inducing unnecessary distribution of pore fluid (i.e., consolidation behavior). This may require somewhat of a trial and error process, such that the effective vertical stress and the internal fluid pressure are forced to increase linearly with increasing gravity. These factors may be readily checked in one or two time steps by examining results at several points in the finite element mesh for predicted versus computed fluid and effective stresses at the specific gravity level. Contact boundaries may complicate this process, particularly with long time steps, and large changes in displacement. Permeability variations have a nonlinear relationship with the time step size, (i.e., a decrease in the permeability by one order of magnitude will need to be offset by an increase of two orders of magnitude in the time step).

(B) Dynamic Considerations: The time step size in dynamic simulations is governed by two factors; adequate tracking of load-time functions, and relationships between minimum element dimensions and wavespeed. To insure proper tracking of the load-time function time step size should not exceed the largest Δt in the function and ideally would be set to approximately 1/3 of the minimum Δt . Cost and time consideration may play an important part in that decision. The stability restrictions for time step size are as follows:

(1) Implicit-Explicit Treatment:

$$\omega \Delta t < \frac{2}{\left(\alpha + \frac{1}{2}\right)} \quad \text{or} \quad \Delta t < \frac{2}{\omega \left(\alpha + \frac{1}{2}\right)}$$

where: $\omega = 2 \frac{C}{L}$

L = smallest element dimension

C = wave speed

C may be computed from the equation:

$$C = (\lambda + 2\mu)/\rho$$

where: λ, μ = Lamé's parameters for the material solid phase
(Elastic)

ρ = mass density of the solid.

(2) Implicit Treatment:

$$\beta = \left(\alpha + \frac{1}{2} \right)^2 \text{ yields unconditional stability.}$$

In cases 1 & 2, α is always greater than 0.5.

Example of time step size selection for shear wave propagation:

Material Properties-

G = elastic shear modulus

B = elastic Bulk modulus

$$= \frac{2G}{3}$$

W = natural frequency of material

C_d = wave speed (dilatational)

Δt = time step size

α, β = Newmark's integration parameters

ρ = mass density of material

L = smallest element dimension

$$G = 2000 \text{ kg/m}^2 \quad L = 0.02\text{m}$$

$$K = 1250 \text{ kg/m}^2$$

$$\rho = 1500 \text{ kg/m}^3$$

$$\begin{aligned} \lambda + 2\mu &= B - \frac{2\mu}{3} + \frac{6\mu}{3} \\ &= \frac{2\mu}{3} - \frac{2\mu}{3} + \frac{6\mu}{3} = 2\mu = 2G \end{aligned}$$

$$C_d = \left(\frac{(2000 \text{ k/m}^2)}{1500 \text{ kg/m}^3} \right)^{1/2} = 1.155 \text{ m/sec}$$

$$\alpha = 0.65 \text{ (slightly damped)}$$

$$\omega = 2 \frac{(1.155 \text{ m/sec})}{0.02 \text{ m}} = 115.5$$

$$\Delta t < \frac{2}{115.5(0.65 + 0.5)} = 0.0151 \text{ sec}$$

for proper tracking of the shear wave propagation through the element. Consideration should also be given to the pressure wave propagation in this case.

$$\lambda + 2\mu = 2G \text{ (see above)}$$

$$C = \left(\frac{2(2000)}{1500} \right)^{1/2} = 1.633$$

$$\omega = \left(\frac{2(1.633 \text{ m/sec})}{0.02 \text{ m}} \right) = 163.3$$

$$\Delta t < \frac{2}{163.31 \text{ sec} (1.15)} = 0.106 \text{ sec}$$

It is important that both the algorithm parameters (α , β) and maximum time step considerations both be met, as each plays a significant role. This is due to the implicit-explicit time domain integration requirements. Appendix B contains some excerpts from Zinkewiz on the effects of repair α and β and their dependence on the time step size.

(5) DTMULT allows variable time steps. In what case,

$$DT(N+1) = DTMULT * DT(N)$$

$$T(N) = T_0 + DT(1) * (1. - (DTMULT**N)) / (1. - DTMULT)$$

and

$$DT(N+1) = DT(1) * (DTMULT**N)$$

The maximum allowable time step amplitude is set by MTMAX. DTMULT invokes a geometric progression in the time step size. This feature is very useful in transitioning between loading-reconsolidation behavior. DTMULT = 2.0 will double the time step size, up to DTMAX

(6) If BETA = 0, set internally to $BETA = (\alpha + 1/2)(\alpha + 1/2)/4$.

Do not set BETA, the code will assign the appropriate value. The tolerance (TOL) may be selected to any value, however results will tend to decay in accuracy with $TOL > 10^{-3}$, which is the default value. TOL may be decreased or increased to help improve contact element behavior.

2.3 Card 3 (2I5) (only required if MODE.GE.2)

Note	Columns	Variable	Description
	1-5	NEIGEN	Number of eigenvalues required; GE.1
	6-10	IOPT	Solution algorithm; GE.0 If EQ.0, set internally EQ.2 IOPT = 1, Determinant search IOPT = 2, Subspace iterations

3.0 PLOTTING REQUESTS

3.1 CARD 1 - MESH PLOTTING REQUESTS - (815)

NOTE	Columns	Variable	Description
	1-5	IP1	Undeformed mesh plot coded NE.0, plot undeformed mesh
(1)	6-10	IP2	Deformed mesh plot code NE.0, plot every IP2 time steps
	11-15	IP3	Displacement vectors plot code NE.0, plot every IP3 steps
(2)	16-20	IP4	Velocity vectors plot code (with respect to undeformed mesh) NE.0, plot every IP4 steps
(2)	21-25	IP5	Velocity vectors plot code (with respect to deformed mesh) NE.0, plot every IP5 steps
	26-30	IP6	Nodal time histories plot code NE.0, plot every IP6 steps
(3)	31-35	IP7	Contour data dump NE.0, dump every IP7 steps
(4)	36-40	IP8	Mesh data dump NE.0, dump every IP8 steps

Notes:

(1) For eigenvalue solutions, the deformed mesh is the eigenshape for every IP2 eigenmode.

(2) For elliptic boundary value problems the velocity vectors are actually the displacement increments computed over the last time step.

(3) For post-processing with CONTOUR.

(4) For post-processing with DYNAMESH and/or COIFES.

General:

For noneigenvalue solutions, disregard IP1-IP6, IP7 and IP8 will set the number of time steps between contour and mesh data outputs. In general, one data dump at the end of gravity initialization is sufficient. In dynamic cases, more contouring and deformed mesh information is useful in determining the quality of the solution.

3.2 Card(s) 2 - Nodal History Output Data - ((1 + NDOF)*I5)

"On-line" and Calcomp plots of nodal histories (displacement, velocity, and acceleration) may be obtained. Each component requested is plotted versus time. Plots of this type are useful in providing quick information concerning the time history of important components.

Note	Columns	Variable	Description
(1)	1-5	N	Node number; GE.1 and LE.NUMNP
(2)	6-10	ITEMP(1)	Degree of freedom 1 output code
	11-15	ITEMP(2)	Degree of freedom 2 output code
	etc.	.	.
		.	.
		.	.
		ITEMP(NDOF)	Degree of freedom NDOF output code

Notes:

(1) Nodal history output data must be input for each node at which the time history of one or more degrees of freedom is to be plotted on-line. Cards need not be read in order. Terminate with a blank card.

(2) Output codes may be assigned the following values:

ITEMP(I) = 0, no plot of degree of freedom I, node N

ITEMP(I) = 1, plot degree of freedom I, node N

where I = 1, 2, ..., NDOF. The total number of degrees of freedom to be plotted for all nodes equals NDOUT.

The node numbers and degrees of freedom to be plotted are stored in the first and second rows, respectively, of IH(2,NDOUT).

General:

Nodal displacement, velocity, and acceleration time histories record specific nodal behavior. This output is very useful in analyzing the quality of results. Tremendous amounts of data can be produced by inclusion of unnecessary nodes.

4.0 COORDINATE DATA

4.1 Nodal Coordinate Cards (2I5,NSD*F10.0)

Note	Columns	Variable	Description
(1)	1-5	N	Node number; GE.1 and LE.NUMNP
(2)	6-10	NUMGP	Number of generation points EQ.0, no generation GT.0, generate data
(3)	11-20	X(1,N)	x1-coordinate of node N
	21-30	X(2,N)	x2-coordinate of node N
	31-40	x(3,N)	x3-coordinate of node N

Notes:

(1) The coordinates of each node must be defined, but need not be read in order. Terminate with a blank card.

(2) If NUMGP is greater than zero, this card initiates an isoparametric data generation sequence. Cards 2 to NUMGP of the sequence define the coordinates of the additional generation points (see Section 4.2). The final card of the sequence defines the nodal increment information (see Section 4.3). After the generation sequence is completed, additional nodal coordinate cards, or generation sequences, may follow.

The generation may be performed along a line, over a surface, or over a volume. A description of each of these options is given below.

Generation along a line

The line may be defined by 2, or 3, generation points (see Figure 4.1), and the physical space may be one-, two-, or three-dimensional.

In the case NUMGP = 2, linear interpolation takes place resulting in equally spaced nodal points.

In the case NUMGP = 3, quadratic interpolation is employed and graded nodal spacing may be achieved by placing the third generation point (J = 3) off center. Note that the third generation point does not generally coincide with any nodal point. The spacing in this case may be determined from the following mapping:

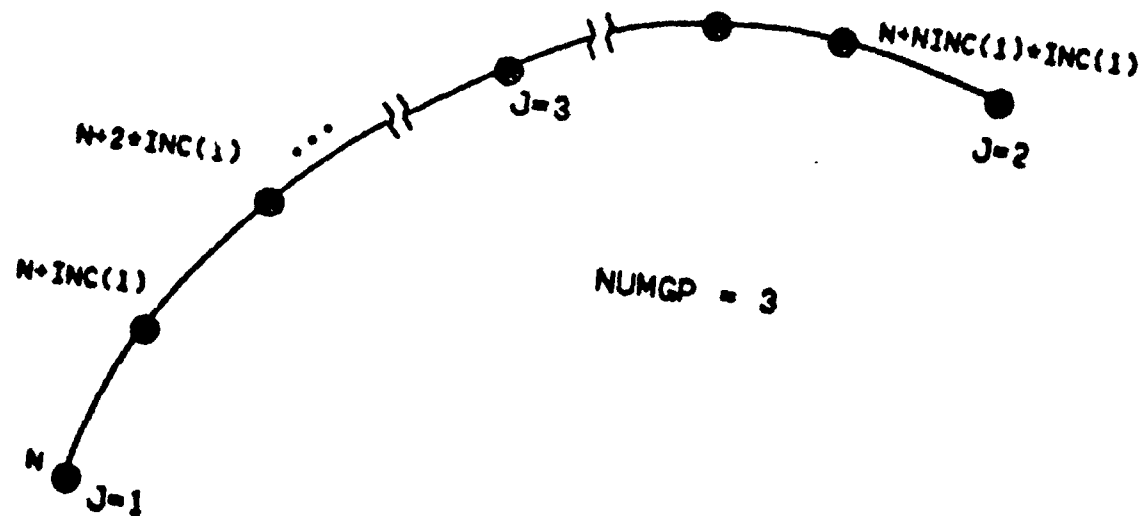
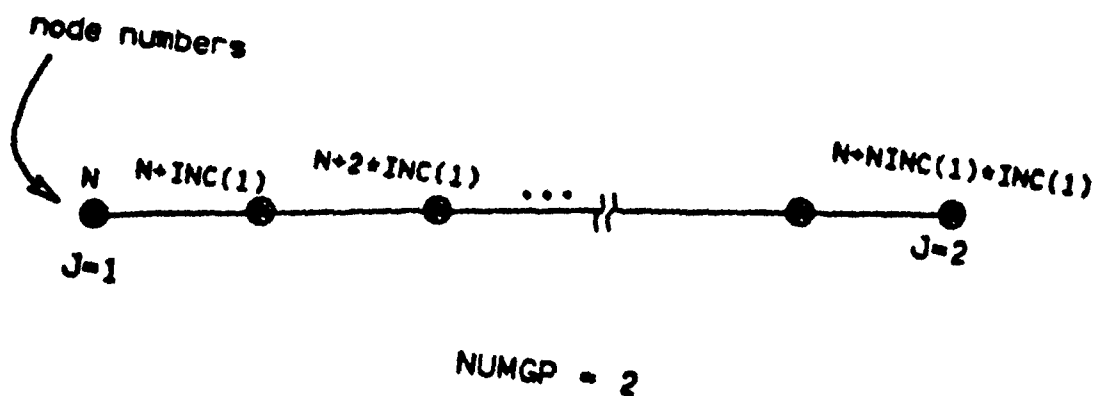


Figure 4.1 Line generation along a line (2 points)

$$X_A = X(z_A) = 1/2z_A(z_A-1)X_1 + 1/2z_A(z_A+1)X_2 + (1-z_A)(1+z_A)X_3$$

where z_A is the location of node number A in z space (the nodes are placed at equal intervals in z-space); X_1 , X_2 and X_3 are the coordinates of the three generation points in x-space; and X_A denotes the coordinates of the Ath node in x-space (see Figure 4.2).

Generation over a surface

The surface may be defined by 4, or 8, generation points (see Figure 4.3) and the physical space may be two-, or three-dimensional. In the three-dimensional case, the surfaces may be curved.

In the case NUMGP = 4, bilinear interpolation is employed, resulting in equally spaced nodal points along generation lines.

In the case NUMGP = 8, biquadratic "serendipity" interpolation is employed and graded nodal spacing may be achieved by placing generation points 5-8 off center. Note that generation points 5-8 do not generally coincide with any nodal points. The spacing of the nodal points may be determined from the serendipity mapping.

Generation over a volume

The volume is brick shaped and may be defined by 8, or 20, generation points (see Figure 4.4). In this case the physical space must be three-dimensional.

If NUMGP = 8, trilinear interpolation is employed, resulting in equally spaced nodal points along generating lines.

If NUMGP = 20, triquadratic serendipity interpolation is employed and graded nodal spacing may be achieved by placing generation points 9-20 off center. Note that generation points 9-20 do not generally coincide with any nodal points. The spacing of the nodal points may be determined by the serendipity mapping.

(3) If the coordinates of node N are input and/or generated more than one time, the last values take priority.

General:

Nodal generation can best be explained through the use of examples. Table 4.1 shows a portion of a DYNFLOW data set. The groups of numbers denoted by brackets are each a set of nodal coordinates which generate the mesh shown in Figure 4.5. Note the "zooming" of the mesh around the structure. This is accomplished by selecting the appropriate midside coordinates highlighted by the X in Figure 4.5.

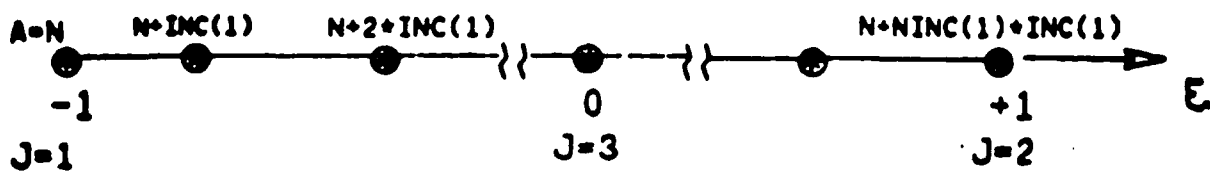
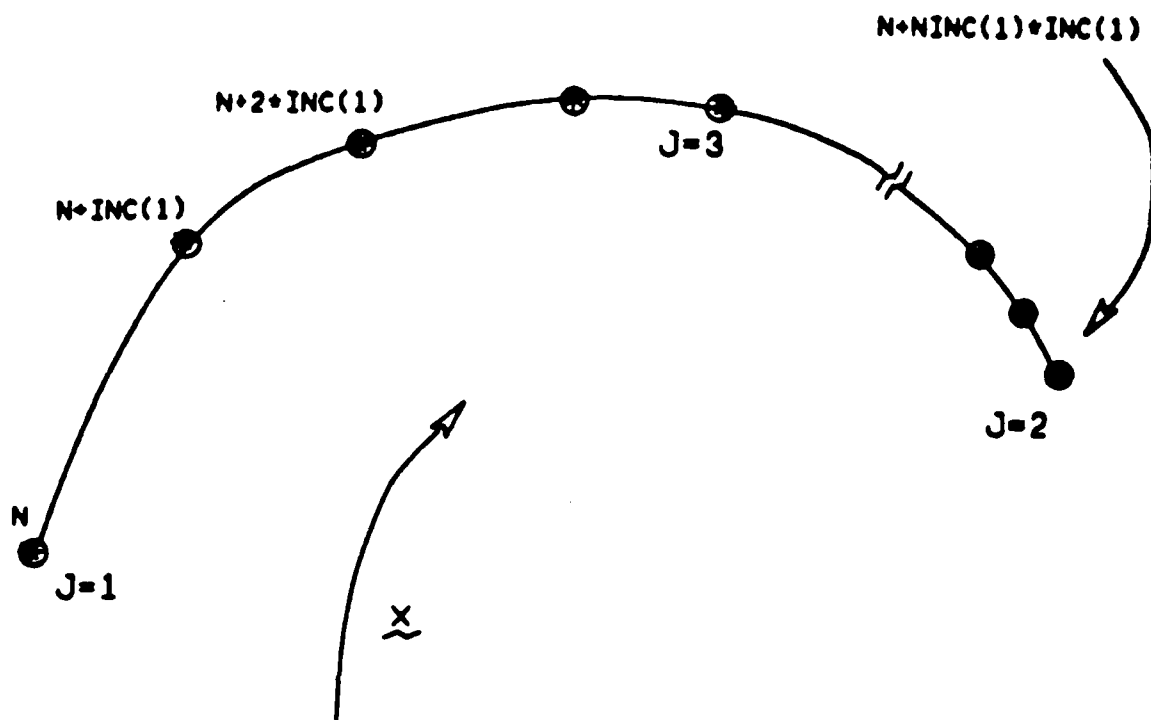


Figure 4.2 Line generation in curved coordinates
(3 points)

$$N1 = NINC(1) * INC(1)$$

$$N2 = NINC(2) * INC(2)$$

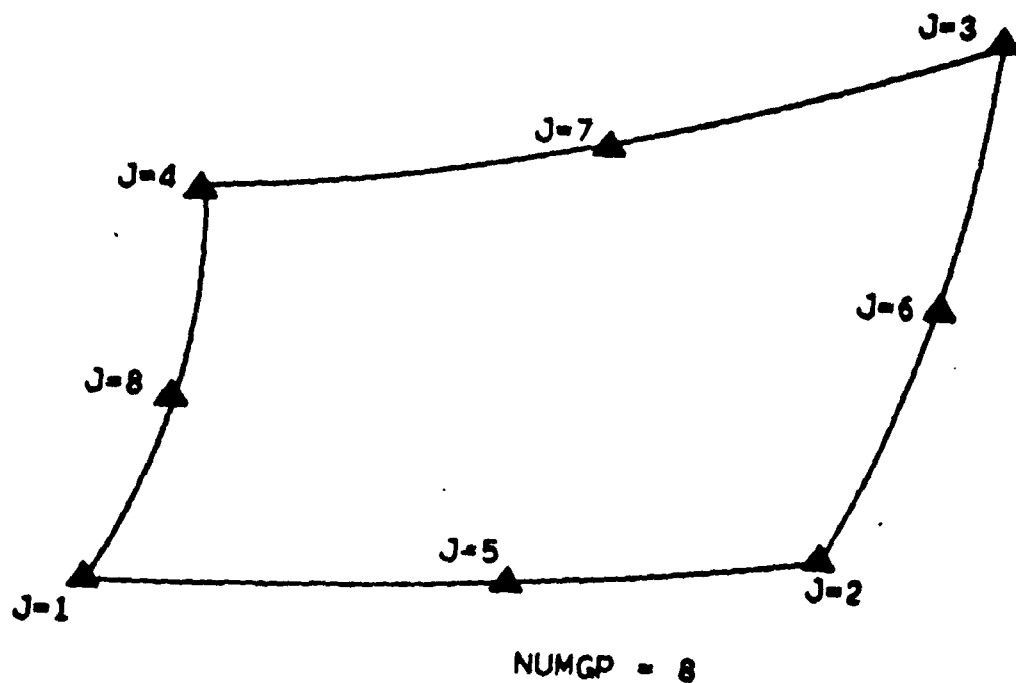
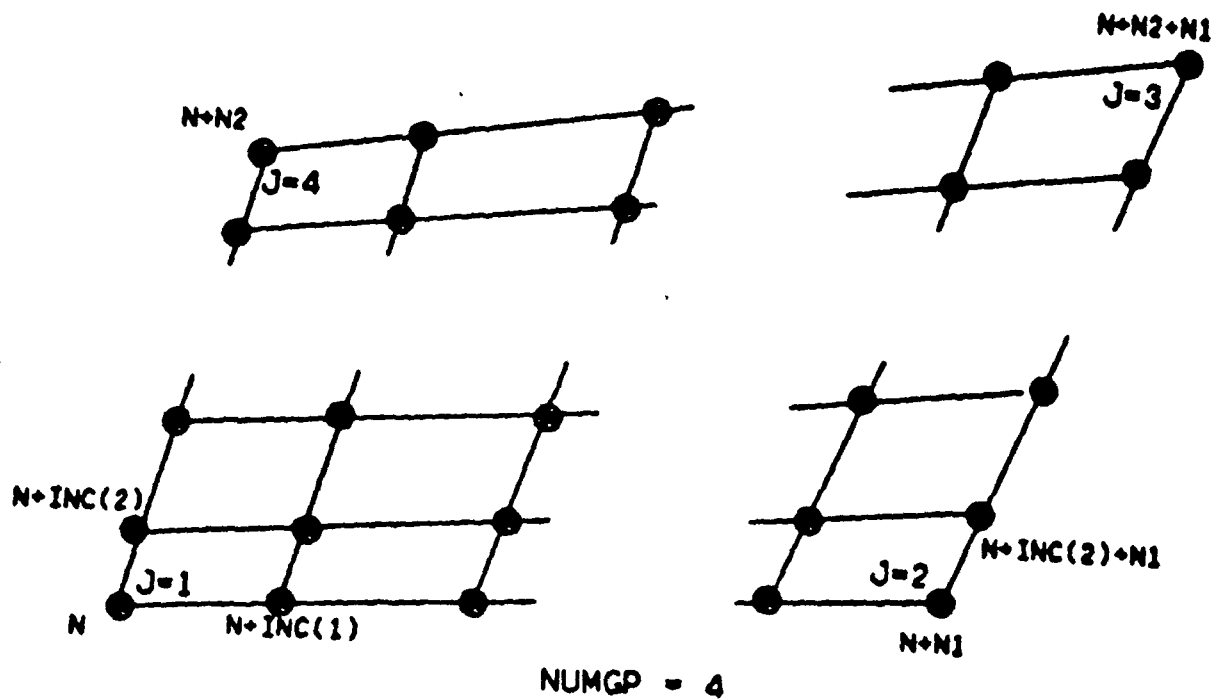


Figure 4.3 Nodal generation on a surface

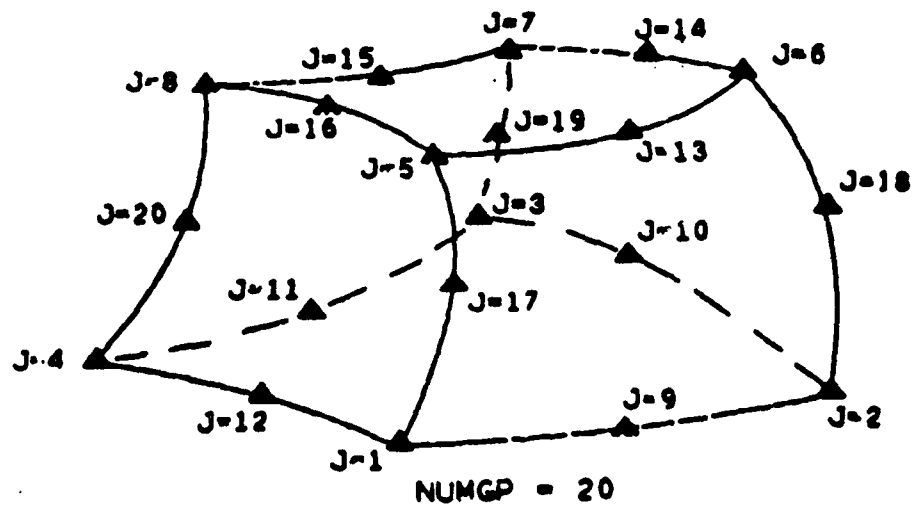
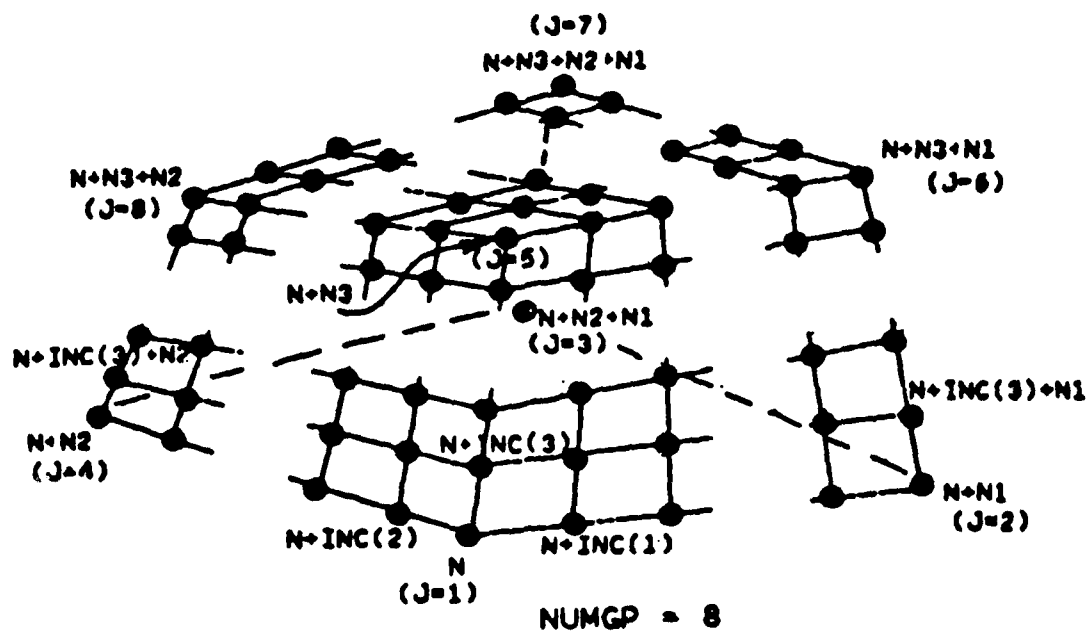


Figure 4.4 Nodal generation on a volume

Zone 2*



Figure 4.5 Node generation mesh

1	8	0.000	0.00	
2		0.000	-8.00	
3		6.00	-8.00	Zone 1, nodes 1-72
4		6.00	0.00	
5		0.00	-3.00	Zoom effect, typical for each zone.
6		4.00	-8.00	
7		6.00	-3.00	
8		4.00	0.00	
8	1	7	9	
73	8	6.50	0.00	
2		6.50	-8.00	
3		7.50	-8.00	
4		7.50	0.00	
5		6.50	-3.00	Zone 2*, nodes 73-99
6		7.00	-8.00	Note: nodes 78-81, 88-90, and 97-99 are
7		7.50	-3.00	fixed out of solution.
8		7.00	0.00	
8	1	2	9	
100	8	8.00	0.00	
2		8.00	-8.00	
3		14.00	-8.00	
4		14.00	0.00	Zone 3, nodes 100-171
5		8.00	-3.00	
6		10.00	-8.00	
7		14.00	-3.00	
8		10.00	0.00	
8	1	7	9	
172	4	6.00	0.750	
2		6.00	-0.600	
3		8.00	-0.600	Structure, nodes 172-196
4		8.00	0.750	
3	1	4	4	

Table 4.1 Node generation input

Zone 1 on the right of Figure 4.5 is generated by the cards shown in "zone 1", Table 4.1. The zoom is based on 3/8 vertical and 2/3 (4.0/6.0) horizontal scales.

Zone 2 uses the same 8 point generation scheme. The zoom in the base is in the vertical direction only. Note that nodes 78-81, 88-90, and 97-99 are not connected in the elements. They are actually "dummy" nodes which are "fixed out" of the solution. That procedure allows for an easier generation of nodes (and elements) without extensive "node-by-node" input.

Zone 3 uses a mirror image of the zone 1 generation. The structure, nodes 172-196, employs a four point generation. Note that the structure is defined "over" the existing soil nodes which were fixed out. Element generation, Section 9.1.4, uses only the nodes specified to define the specific elements.

4.2 Generation Point Coordinate Cards (2I5,NSD*F10.0)

The coordinates of each generation point are defined by a generation point coordinate card. The cards must be read in order ($J = 2, 3, \dots, \text{NUMGP}$) following the nodal coordinate card which initiated the generation sequence ($J = 1$). A nodal card (see Section 4.3), which completes the sequence, follows the last generation point card ($J = \text{NUMGP}$).

Note	Columns	Variable	Description
	1-5	M	Node number
	6-10	MGEN	Generation parameter EQ.0, coordinates of the Jth generation point are input on this card; M is ignored EQ.1, coordinates of the Jth generation point are set equal to coordinates of Mth node which were previously defined; coordinates on this card are ignored
	11-20	TEMP(1,J)	x1-coordinate of generation point J
	21-30	TEMP(2,J)	x2-coordinate of generation point J
	31-40	TEMP(3,J)	x3-coordinate of generation point J 0

(See Table 4.1)

4.3 Nodal Increments Cards (6I5)

Note	Columns	Variable	Description
	1-5	NINC(1)	Number of nodal increments for direction 1;GE.0
	6-10	INC(1)	Node number increment for direction 1
(1)	11-15	NINC(2)	Number of nodal increments for direction 2;GE.0
	16-20	INC(2)	Node number increment for increment 2
(1)	21-25	NINC(3)	Number of nodal increments for direction 3;GE.0
	26-30	INC(3)	Node number increment for direction 3

Notes:

(1) Each option is assigned an option code (IOPT) as follows:

IOPT	Option
1	generation along a line
2	generation over a surface
3	generation over a volume

IOPT is determined by the following logic:

IOPT = 3 0

IF(NINC(3).EQ.0) IOPT = 2

IF(NINC(2).EQ.0) IOPT = 1

(See Table 4.1)

5.0 BOUNDARY CONDITION DATA

5.1 Prescribed Nodal Boundary Conditions ((2+NDOF)*I5)

Note	Columns	Variable	Description
(1)	1-5	N	Node number; GE.1 and LE.NUMNP
(2)	6-10	NG	Generation increment
(3)	11-15	ID(1,N)	Degree of freedom 1 boundary code
	16-20	ID(2,N)	Degree of freedom 2 boundary code
	etc.	.	.
		.	.
		.	.
		ID(NDOF,N)	Degree of freedom NDOF boundary code

Notes:

(1) Boundary condition data must be input for each node which has one or more specified displacements. Cards need not be input in order.
Terminate with a blank card.

(2) Boundary condition data can be generated by employing a two card sequence as follows:

Card 1: L, LG, ID(1,L), ..., ID(NDOF,L)

Card 2: N, NG, ID(1,N), ..., ID(NDOF,N)

The boundary codes of all nodes

$L+LG, L+2*LG, \dots, N-MOD(N-L, LG)$

(i.e., less than N) are set equal to those of node L. If LG is blank or zero, no generation takes place between L and N.

(3) Boundary condition codes may be assigned the following values:

ID(I,N) = 0 , unspecified displacement

IL(I,N) = 1 , specified displacement

where $I = 1, 2, \dots, \text{NDOF}$. Specified displacements are assumed to be fixed (i.e., have the value 0.0) unless assigned a nonzero value as described in Section 7.0. If more than one boundary condition data card for node N is input, the last one read takes priority.

General:

Boundary conditions are explained reasonably well. It is important to see the included example, Table 5.1, because of the different generation procedures employed. Always remember to "fix out" any superfluous degrees of freedom and/or nodes which may have been generated.

Note also that to prescribe displacement or acceleration it is necessary to fix the associated degree of freedom, otherwise the loading will be treated as a force.

9	9	1	1	1	1
171		1	1	1	1
73		1	1	1	1
74		1	1	1	1
82		1	1	1	1
83		1	1	1	1
91		1	1	1	1
92		1	1	1	1
6				1	1
75				1	1
84				1	1
93				1	1
172	1			1	1
191				1	1

Table 5.1 Nodal fixity conditions

The first two cards of the sequence denoted by the bracket invoke the generated fixed conditions for nodes 1, 10, 19...., through 163, along the base of the mesh shown in Figure 3.5. The next six cards in the group invoke the generation of fixed conditions for nodes 79-81, 88-90, and 97-99. The final two cards generate the fixed conditions for degrees of freedom three and four in the "single-phase" structural nodes, 172-196.

5.2 Slaved nodes ((3+NDOF)*I5) (only if required, i.e., if NSLAV.NE.0)

Note	Columns	Variable	Description
(1)	1-5	N1	Node number 1
	6-10	N2	Node number 2
(2)	10-15	NG	Generation increment
(3)	16-20	IS(1,N)	Degree of freedom 1
	21-25	IS(2,N)	Degree of freedom 2
		.	.
		.	.
		.	.
		IS(MDOF,N)	Degree of freedom NDOF

Notes:

(1) Nodes N1 and N2 are assigned to share the equation numbers for the specific degrees of freedom listed on that card. Terminate with a blank card.

(2) Slaved condition data can be generated by employing a two card sequence as follows:

Card 1: L1,L2,LG,ID(1,L),...,ID(NDOF,L)

Card 2: N1,N2,NG,ID(1,N),...,ID(NDOF,N)

The slaved conditions codes of all nodes

L1+LG, L1+2*LG, ..., N1-MOD(N1-L1,LG)

L2+LG, L2+2*LG, ..., N2-MOD(N2-L2,LG)

(i.e., less than N1) are set equal to those of node L1. If LG is blank or zero, no generation takes place between L and N.

(3) Degrees of freedom codes may be assigned the following values:

IS(I,N) = 0, do not share the same equation number

IS(I,N) = 1, do share the same equation number

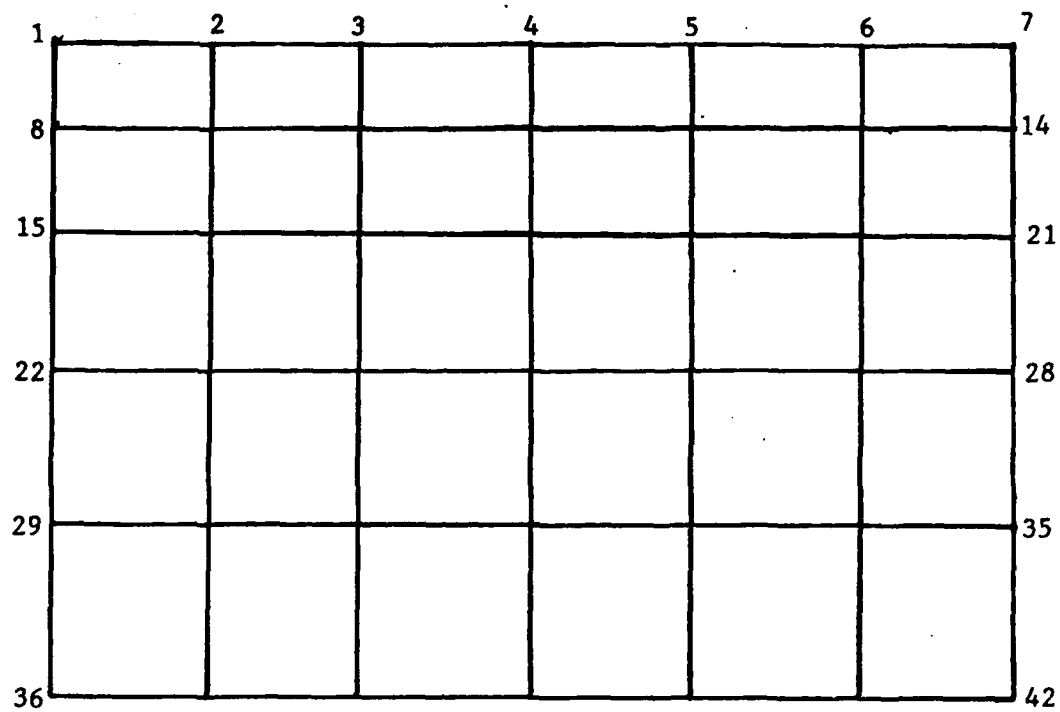
where I = 1,2,...,NDOF.

General:

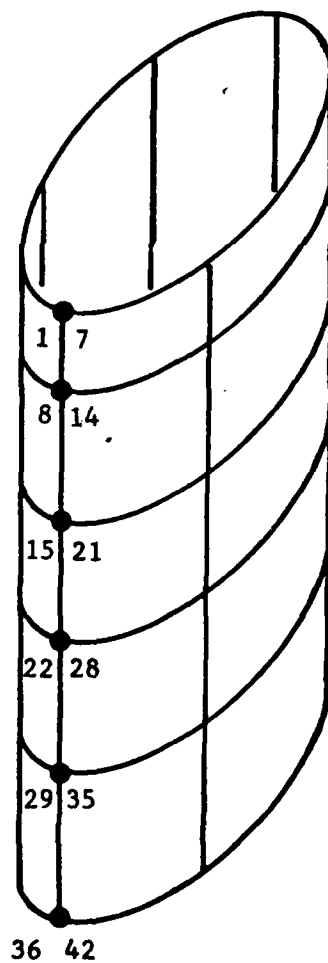
Nodal slaving provides an indispensable means of simulating "free-field" boundaries. By this method, shear waves can be initiated at the base of a mesh and allowed to propagate upward without concern of fixed boundary reflection. Figures 5.1 A and B show a finite element mesh and slaved idealization, respectively. In the slaved configuration (Figure 5.1 B) the mesh is free to deform in the horizontal (torsional) direction. In addition, the fluid degrees are also free to translate without creating any horizontal boundary reflections. This technique has many applications in soil mechanics problems, or structural problems involving analysis of a section out of a continuum. The generation scheme used in the modal slaving is shown in Table 5.2. The result of the scheme is nodes 2 - 164, 3 - 165, 4 - 166,..., 9 - 171 being defined as having the same equal numbers.

2	164	1	1	1	1	1
9	171		1	1	1	1

Table 5.2 Slaved node generation



A



B

Figure 5.1 Nodal slaving meshes

6.0 INITIAL DISPLACEMENT/VELOCITY DATA

6.1 Nodal Initial Displacement Cards (2I5, NDOF*F10.0)

Note	Column	Variable	Description
(1)	1-5	N	Node number; GE.1 and LE.NUMNP
(2)	6-10	NUMGP	Number of generation points EQ.0, no generation NE.0, generate data
(3)	11-20	D(1,N)	Degree of freedom 1 initial displacement
	21-30	D(2,N)	Degree of freedom 2 initial displacement
	etc.	.	.
		.	.
		.	.
		D(NDOF,N)	Degree of freedom NDOF initial displacement

Notes:

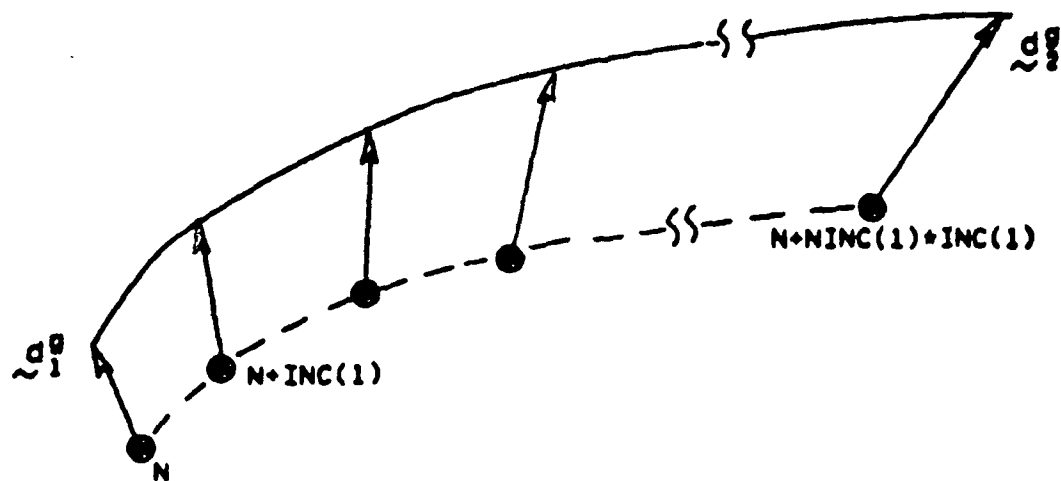
(1) Initial displacement data must be included for each node subjected to nonzero initial displacement. Cards need not be read in order. Terminate with a blank card.

(2) If NUMGP is greater than zero, this card initiates an isoparametric data generation sequence. The scheme used is the same as the one used for coordinate generation described previously in Section 4. Cards 2 to NUMGP of the sequence define the initial displacements of the additional generation points (see Section 6.2). The final card of the sequence defines the nodal increment information, and is identical to the one used for coordinate generation (see Section 4.3). After the generation sequence is completed, additional nodal initial displacement cards, or generation sequences, may follow.

The generation may be performed along a line, over a surface, or over a volume. A description of these options is given below.

Generation along a line

Generation of data (initial displacement, applied force, prescribed displacement, etc.) along a line may be performed using 2, or 3 generation points (see Figure 6.1), and the physical space (X-space) may be one-, two-, or three-dimensional.



Data generated in x -space

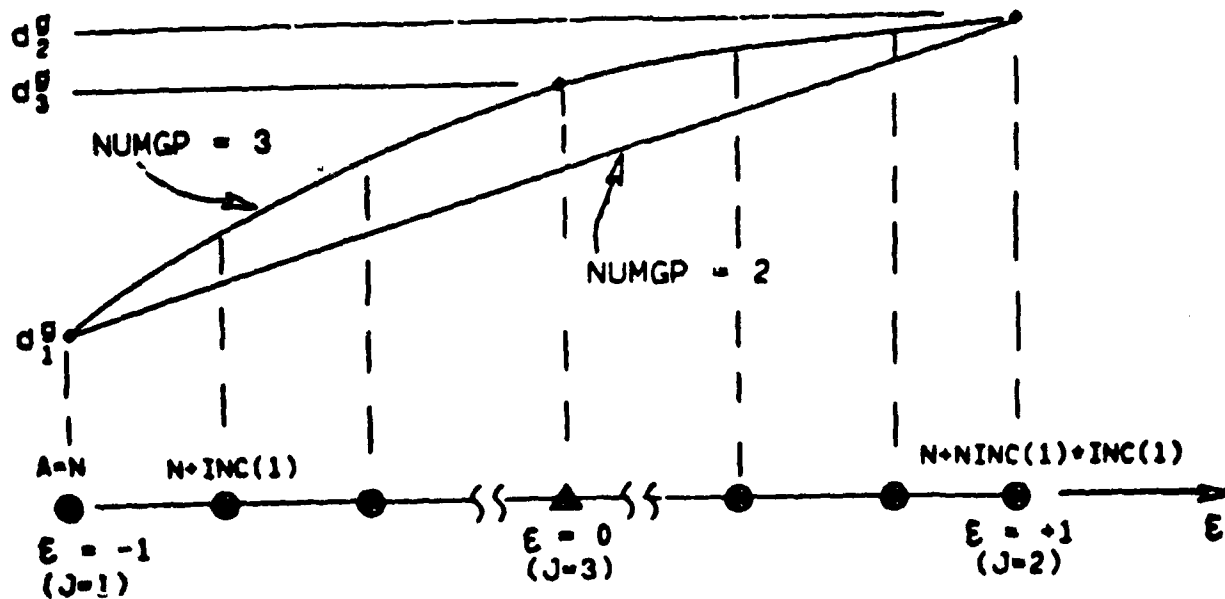


Figure 6.1 Single component of data generation in e -space

If NUMGP = 2, linear interpolation takes place with respect to z-space. If the nodes are equally spaced in X-space, then the variation will also be linear in X-space. Otherwise a nonlinear variation will be induced by the unequal nodal spacing.

If NUMGP = 3, quadratic interpolation is performed with respect to space. Note that the third generation point does not generally coincide with a nodal point. The variation of data may be determined from the following mapping:

$$D_A = D(z_A) = 1/2z_A(z_A - 1)D_1 + 1/2z_A(z_A + 1)D_2 + (1 - z_A^2)D_3$$

where z_A is the location of node number A in z-space (recall that the nodes are assumed to be placed at equal intervals in z-space); D_1 , D_2 , and D_3 are the data assigned to the three generation points (i.e., $z = -1, +1$, and 0 , respectively); and D_A is the generated data at node A. The data D may be taken to represent the initial displacements, applied forces, or prescribed displacements.

The case in which NUMGP = 2, may be deduced from the case NUMGP = 3 by setting $D_3 = (D_1 + D_2)/2$

Generation over a surface

Generation of data may be performed using 4, or 8, generation points. The generation points and nodal patterns are the same as in co-ordinate generation (see Figure 4.3).

In the case NUMGP = 4, bilinear interpolation is performed; for NUMGP = 8, biquadratic "serendipity" interpolation is performed. Note that generation points 5-8 do not in general coincide with nodal points.

Generation over a volume

Generation of data over a brick-shaped volume may be performed using 8, or 20, generation points. The generation points and nodal patterns are the same as for coordinate generation (see Figure 4.4).

If NUMGP = 8, trilinear interpolation is employed; if NUMGP = 20, triquadratic "serendipity" interpolation is employed. Note that generation points 9-20 do not in general coincide with nodal points.

(3) The elements of the array $D(NDOF, NUMNP)$ are initialized to zero. If the initial displacements of node N are input and/or generated more than one time, the last values take priority.

6.2 Generation Point Initial Displacement Cards (2I5, NDOF*F10.0)

The initial displacements of each generation point are defined by a generation point initial displacement card. The cards must be read in order ($J = 2, 3, \dots, \text{NUMGP}$) following the nodal initial displacement card which initiated the generation sequence ($J = 1$). A nodal increments card (see Section 4.3), which completes the sequence, follows the last generation point card ($J = \text{NUMGP}$).

Note	Columns	Variable	Description
	1-5	M	Node number
	6-10	MGEN	Generation parameter EQ.0, initial displacements of the Jth generation point are input on this card; M is ignored EQ.1, initial displacements of the Jth generation point are set equal to initial displacements of the Mth node which were previously defined; initial displacements on this card are ignored
	11-20	TEMP(1,J)	Degree of freedom 1 initial displacement of generation point J
	21-30	TEMP(2,J)	Degree of freedom 2 initial displacement of generation point J
etc.	.	.	.
	.	.	.
	.	.	.
		Temp(NDOF,J)	Degree of freedom NDOF initial displacement of generation point J 0

6.3 Nodal Increments Cards (6I5)

Note	Columns	Variable	Description
	1-5	NINC(1)	Number of nodal increments for direction 1;GE.0
	6-10	INC(1)	Node number increment for direction 1
(1)	11-15	NINC(2)	Number of nodal increments for direction 2;GE.0
	16-20	INC(2)	Node number increment for increment 2
(1)	21-25	NINC(3)	Number of nodal increments for direction 3;GE.0
	26-30	INC(3)	Node number increment for direction 3

Notes:

(1) Each option is assigned an option code (IOPT) as follows:

IOPT	Option
1	generation along a line
2	generation over a surface
3	generation over a volume

IOPT is determined by the following logic:

IOPT = 3

IF(NINC(3).EQ.0) IOPT = 2 0

IF(NINC(2).EQ.0) IOPT = 1

6.4 Nodal Initial Velocity Data Cards

Only required for MODES=1 (Section 2.1). Use same sequence of cards as for nodal initial displacement data.

7.0 APPLIED NODAL FORCES AND PRESCRIBED DISPLACEMENTS/ACCELERATIONS

Applied nodal forces and prescribed displacements/accelerations are defined by an expansion of the form:

$$F(X,t) = G(I,t) * F(I,X) \quad (\text{Sum } I = 1, \text{NLC})$$

where $F(X,t)$ is the resultant force, displacement, or acceleration acting at node A at time t ; G is the load time function of the i th load condition; F is the "mode shape" of the i th load condition; and NLC is the total number of load conditions defined on the first control card (see Section 2.1). The data preparation for the load-time functions is described in Section 8.0. In this section, the data preparation for the F 's is described.

The mode shapes must be read in the order $F_1, F_2, \dots, F_{\text{NLC}}$. There must be at least one mode shape. Data cards for a typical mode shape are described below.

7.1 Nodal applied force and prescribed displacement/acceleration cards (2I5,NDOF*F10.0)

Note	Columns	Variable	Description
(1)	1-5	N	Node number; GE.1 and LE.NUMNP 0
(2)	6-10	NUMGP	Number of generation points EQ.0, no generation NE.0, generate data
(3)	11-20	F(1,N)	Degree of freedom 1 force or displacement/acceleration
	21-30	F(2,N)	Degree of freedom 2 force or displacement/acceleration
	etc.	.	.
		.	.
		.	.
		F(NDOF,N)	Degree of freedom NDOF force or displacement/ acceleration

Notes:

(1) Applied nodal force/prescribed displacement or acceleration data must be included for each node subjected to a nonzero applied force or nonzero prescribed displacement/acceleration. Cards need not be read in order. Terminate with a blank card.

(2) If NUMGP is greater than zero, this card initiates an isoparametric data generation sequence. The scheme used is the same as the one for coordinate and initial displacement/velocity generation (see Section 4 and 6, respectively). Cards 2 to NUMGP of the sequence define the applied forces/prescribed displacements of the additional generation points (see Section 7.2). The final card of the sequence defines the nodal increment information and is identical to the one used for coordinate generation (see Section 4.3). After the generation sequence is completed, additional nodal applied force/prescribed displacement/acceleration cards, or generation sequences, may follow.

The generation may be performed along a line, over a surface, or over a volume. For additional information concerning these options see Note (2) of Section 6.1.

(3) The elements of the array F(NDOF,NUMNP,NLC) are initialized to zero. If the applied forces/prescribed displacement of node N are input and/or generated more than one time, the last value takes priority.

General:

Nodal forces and displacements/accelerations provide a means of applying point loadings and variable distributed loadings; and prescribed displacements or accelerations. To apply acceleration or displacements, the nodal degree freedom must be initially fixed. If it is not, the program assumes the value to be a force.

Program DYNFLOW incorporates a simple uniform pressure load algorithm in the element data, Section 10. That algorithm is somewhat restrictive, however, when generating complex variable loads as would be encountered in some problems. A standard finite element procedure using point loads as a function of element area can be employed to generate more complex loadings. This involves simply integrating the applied pressure over the tributary area of a given node (Figure 7.1),

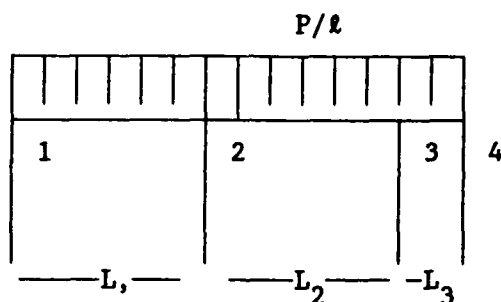


Figure 7.1. Equivalent Nodal Loads

Node 1

Applied nodal force

$$F_{N_1} = \frac{L_1}{2} \left(\frac{2P_1 + P_2}{3} \right)$$

Node 2

$$F_{N_2} = \frac{L_1}{2} \left(\frac{2P_2 + P_1}{3} \right) + \frac{L_2}{2} \left(\frac{2P_2 + P_3}{3} \right)$$

Node 3

$$F_{N_3} = \frac{L_2}{2} \left(\frac{2P_3 + P_2}{3} \right) + \frac{L_3}{3} \left(\frac{2P_3 + P_4}{3} \right)$$

Node 4

$$F_{N_4} = \frac{L_3}{2} \left(\frac{2P_4 + P_3}{3} \right)$$

where: P_i = Pressure at node i

L_i = Length of side for element i

F_{N_i} = Equivalent nodal force

These equations are valid for any linearly, varying load as well. Once F_{N_i} is calculated, it may be applied with any load time function to generate the loading desired. In two-phase applications, it is also important to apply loadings to solid and fluid phase as the physical problem requires. This is accomplished through multiplication of the equivalent nodal force as in the following:

$$F_{N_i}^S = F_{N_i} (1.0 - n)$$

$$F_{N_i}^F = F_{N_i} (n)$$

where: n = material Porosity

$F_{N_i}^S$ = equivalent nodal force on soil phase

$F_{N_i}^F$ = equivalent nodal force on fluid phase

F_{N_i} = equivalent nodal force due to distributed load

7.2 Generation Point Applied Force or Prescribed Displacement/ Acceleration Cards (2I5,NDOF*10.0)

The applied forces/prescribed displacements of each generation point are defined by a generation point applied force/initial displacement card. The cards must be read in order ($J = 2, 3, \dots, \text{NUMGP}$) following the nodal applied force/prescribed displacement card which initiated the generation sequence ($J = 1$). A nodal increments card (see Section 4.3) follows the last generation point card ($J = \text{NUMGP}$) and completes the sequence...

Note	Columns	Variable	Description
	1-5	M	Node number
	6-10	MGEN	Generation parameter EQ.0, applied forces/prescribed displacements of the Jth generation points are input on this card; M is ignored EQ.1, applied forces/prescribed displacements of the Jth generation point are set equal to applied forces/prescribed displacements of the Mth node which were previously defined; applied forces/prescribed displacements on this card are ignored.
	11-20	TEMP(1,J)	Degree of freedom 1 force or displacement of generation point J
	21-30	TEMP(2,J)	Degree of freedom 2 force or displacement of generation point J 0
	etc.	.	.
		.	.
		.	.
		TEMP(NDOF,J)	Degree of freedom NDOF force or displacement of generation point J

7.3 Nodal Increments Cards (6I5)

Note	Columns	Variable	Description
	1-5	NINC(1)	Number of nodal increments for direction 1;GE.0
	6-10	INC(1)	Node number increment for direction 1
(1)	11-15	NINC(2)	Number of nodal increments for direction 2;GE.0
	16-20	INC(2)	Node number increment for increment 2
(1)	21-25	NINC(3)	Number of nodal increments for direction 3;GE.0
	26-30	INC(3)	Node number increment for direction 3

Notes:

(1) Each option is assigned an option code (IOPT) as follows:

IOPT	Option
1	generation along a line
2	generation over a surface
3	generation over a volume

IOPT is determined by the following logic:

```

IOPT = 3
IF(NINC(3).EQ.0)  IOPT = 2
IF(NINC(2).EQ.0)  IOPT = 1

```


8.0 LOAD-TIME FUNCTIONS

There must be at least one load-time function. Each load-time function is defined by $(NLS + 1)$ pairs of time instants and function values, where NLS is the number of load steps defined on the first control card (see Section 2.1). A schematic of typical load-time function is shown in Figure 8.1. The time instants must be in ascending order (i.e., $t(j+1).GE.t(j)$, $1.LE.j.LE.NLS$). Load step intervals need not be equal and need not be the same from one load case to another. However, there must be the same number of load steps (i.e., NLS) for each load-time function. As may be seen from Figure 8.1, the load-time function is assumed to behave in a piecewise linear fashion between data points. For values of t outside the interval $[t(1), t(NLS)]$ we define the G 's by constant extrapolation (i.e. $G[t] = G[t(1)]$ for all $t.LE.t(1)$; and $G[t] = G[t(NLS+1)]$ for all $t.GE.t(NLS+1)$). As an example of the use of this feature, we may take the case in which $NLC = 1$, and the load-time function is constant throughout the duration of the analysis. In this case, we may set $NLS = 0$ on the first control card and simply read in one data point to define $G(t)$.

The load for time step NS is defined to be:

$$F(X) = G[t(NS), I] * F(X, I) \quad (\text{Sum } I=1, NLC)$$

where $t(NS) = NS * DT$ (see Section 2.0). The quantity in square brackets is called the load factor (FAC).

Element consistent loads (e.g., pressure, gravity, etc.) are also multiplied by load-time functions. The load case number is defined in the element group data (see Section 9).

The load-time functions must be read in order G_1, G_2, \dots, G_{NLC} . Data cards for a typical load-time function are described below.

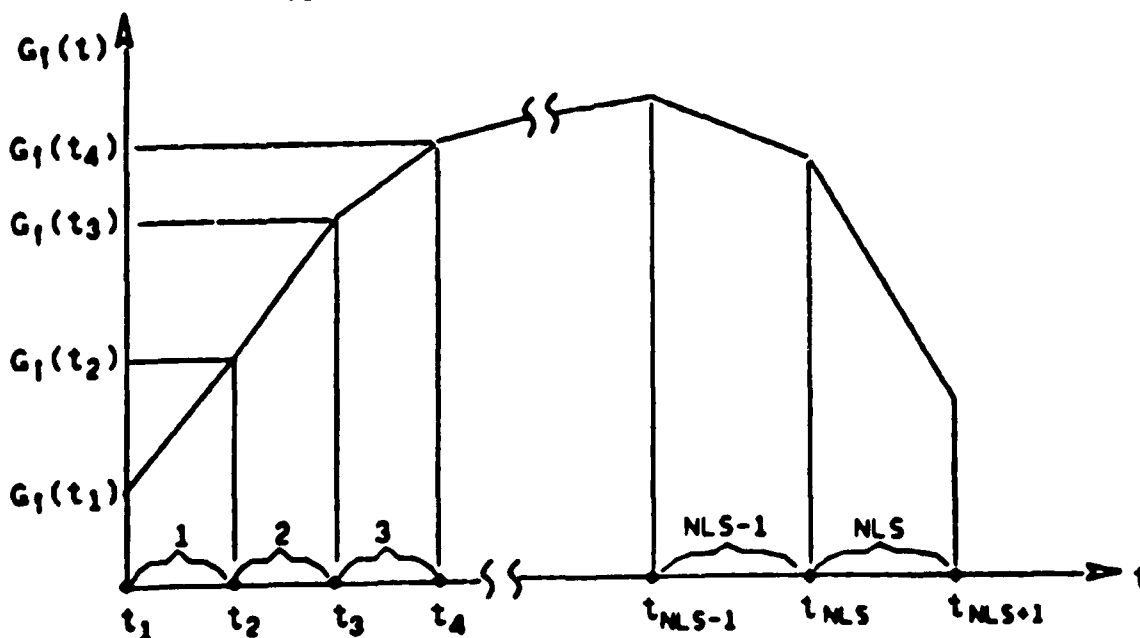


Figure 8.1 Schematic of load time function for load case i

8.1 Load-Time Function Card (2I5,2F10.0)

Note	Columns	Variable	Description
(1)	1-5	N	Load-time function number
	5-10	NLSN	Number of load steps .LE.NLS
	11-20	G(1,1)	Time instant 1 (t(1))
	21-30	G(2,2)	Value of load-time function at t(1)

Notes:

(1) Load-time functions must be input in the order 1, 2, ..., NLC.
Terminate each load-time function with a blank card.

8.2 Load-Time Function Cards (10X,2F10.0)*NLSN

Note	Columns	Variable	Description
	11-20	G(J,1)	Time instant J (t(j))
	21-30	G(J,2)	Value of load-time function at t(j)

General:

The load-time function cards are the means of inputting to the finite element model, the particular load/displacement/acceleration - time history for each element/nodal loading to be considered. Depending on the number of element/nodal loadings, the load-time functions may be best set up as normalized histories, i.e., sinusoidal varying between 1.0 and -1.0. Then by varying only the magnitudes of the applied nodal forces, pressure loads, etc., parametric analysis can be achieved quite readily. To clarify, the load-time function is a set of multipliers, through a time span, through which all input perturbation can be modified (Table 8.1).

1	2	0.0	0.0]	1
		5000.0	1.0		
		6000.0	1.0		
2	2	0.0	0.0]	2
		5000.0	0.0		
		6000.0	1.0		
3	2	0.0	0.0]	3
		5000.0	0.0		
		6000.0	0.0		

Load time functions 1-3. Function 1 implies the load at 5000 seconds will be equal to 1.0. Function 2 implies 0.0 load at 5000 seconds and full load at 6000 seconds.

Table 8.1 Load time functions

9.0 ELEMENT DATA

9.1.0 Two-Dimensional and Axisymmetric Element

The present element may be used in triangular (three-node) or quadrilateral (four-node) form for plane and axisymmetric analysis. The plane of analysis is assumed to be the x_1 , x_2 plane, and the element is assumed to have unit thickness in the plane option. In axisymmetric analysis the radial direction is specified as the x_1 axis. Two displacement degrees of freedom, in the x_1 and x_2 directions, are assigned to each node. Incompatible modes and selective numerical integration may be employed to improve element behavior in various situations. These options should be activated only by users fully knowledgeable in their use. The nodes of the element must be input in counterclockwise order.

The various analysis options together with required variables are summarized in Tables 9.1 and 9.2. On the master control card (see Section 2.0) NSD must EQ.2, and NDOF must be GE.NED.

For two-phase porous media applications, two solid displacement degrees of freedom, in the x_1 and x_2 directions, are assigned to each node. In the parabolic mode (diffusion analysis), the third degree of freedom is assigned to the fluid pressure. In the hyperbolic mode (dynamic analysis), the third and fourth degrees of freedom are assigned to the fluid displacement, in the x_1 and x_2 directions, respectively.

Stresses/strains in the global coordinate system, principal stresses/strains, maximum shear stress/strain and angle of inclination, in degrees, of principal states are output at the element centroid, which is generally the point of optimal accuracy. All shear strains are reported according to the "engineering" convention (i.e., twice the value of the tensor components).

Table 9.1, as stated above, gives the relationships between various numerical model types (options) and the specific "Flag" settings necessary to make each specific model function. For example, a saturated soil column analysis would require:

NTYPE = 4 Element type flag, two-phase plane strain

MODES = 1 Hyperbolic boundary value problem

NED = 4 4 degrees of freedom per node

ISYMM = 0 Symmetric stiffness matrix

MATYP = 2 Elasto-plastic constitutive model

Table 9.1. Two-Dimensional Element

Options	Analysis Mode	NTYPE	MODES	NED LE.NDOF	ISYMM	MATYP
		Sec. 9.1	Sec. 2.1	Sec. 2.1	Sec. 2.1	Sec. 10.
One-Phase Solid Continuum	Elliptic	1	0	2	0,1	1,2
	Hyperbolic	1	1	2	0,1	1,2
	Parabolic	1	2	2	0,1	1,2
One-Phase Fluid Continuum	Elliptic	16	0	2	0,1	4
	Parabolic	16	1,2	2	0,1	4
Euler-Lagrange Fluid Continuum	Hyperbolic	17	1	2	0,1	4
Two-Phase Porous Continuum	Parabolic	4	2	3	1	1,2
	Hyperbolic	4	1	4	0,1	1,2

Table 9.2. Axisymmetric Element

Options	Analysis Mode	NTYPE	MODES	NED	ISYMM LE.NDOF	MATYP
		Sec. 9.1	Sec. 2.1	Sec. 2.1	Sec. 2.1	Sec. 10.
One-Phase Solid Continuum	Elliptic	12	0	2	0,1	1,2
	Hyperbolic	12	1	2	0,1	1,2
	Parabolic	12	2	2	0,1	1,2
Two-Phase Porous Continuum	Parabolic	13	2	3	1	1,2
	Hyperbolic	13	1	4	0,1	1,2

The following sequence of cards is used to describe the elements:

9.1.1a Element Group Control Card (15I5) - One-Phase Continuum

Note	Columns	Variable	Description
(1)	1-5	NPAR (1) (=NTYPE)	The number 1,12 or 16 (See Tables 9.1 and 9.2)
	6-10	NPAR (2) (=NUMEL)	Number of elements in this group; GE.1
	11-15	NPAR (3) (=IOPT)	Analysis option EQ.0, plane strain EQ.1, plane stress EQ.3, axisymmetric
(2)	16-20	NPAR (4) (=IFD)	Finite deformation code EQ.0, finite deformation effects neglected EQ.1, finite deformation effects included
	21-25	NPAR (5) (=IT)	Force vector numerical integration code EQ.0, two-by-two Gaussian quadrature EQ.1, one-point Gaussian quadrature
(3)	26-30	NPAR (6) (=IL)	Volumetric stiffness numerical integration code EQ.0, two-by-two Gaussian quadrature EQ.1, one-point Gaussian quadrature
(4)	31-35	NPAR (7) (=IM)	Deviatoric stiffness numerical integration code EQ.0, two-by-two Gaussian quadrature EQ.1, one-point Gaussian quadrature

(Cont'd)

9.1.1a Element Group Control Card (15I5) (Cont'd)

Note	Columns	Variable	Description
(5)	36-40	NPAR (8) (=INC)	Incompatible modes code EQ.0, incompatible modes neglected EQ.1, incompatible modes added
	41-45	NPAR (9) (=NUMPR)	Number of element pressure load cards
	46-50	NPAR (10) (=NOUT)	Number of stress-strain output histories
	51-55	NPAR (11) (=IST)	Spatial stress/strain output code EQ.0, Include spatial stress/strain output for group EQ.1, Omit spatial stress/strain output for group
(6)	56-60	NPAR (12) (=LCASP)	Pressure load case number; GE.0; if EQ.0, set internally to 1
(6)	61-65	NPAR (13) (=LCASG)	Gravity load case number; GE.0; if EQ.0, set internally to 1
(7)	66-70	NPAR (14) (=IEXPLT)	Implicit/explicit code; GE.0; EQ.0, Implicit element EQ.1, Explicit element EQ.2, Implicit-Explicit element
(8)	71-75	NPAR (15) (=NSPTS)	Number of stress points; GE.0; EQ.0, One stress point EQ.4, Four stress points

Notes:

(1) 1, Elastic one-phase continuum, plane stress/strain; 12, Elastic one-phase continuum axisymmetric; and 16, Elastic fluid continuum. If IFD = 0, the initial stress stiffness matrix is omitted and output strain are "infinitesimal." If IFD = 1, the initial stress stiffness matrix is included and output strains are Lagrangian. Including finite deformation effects increase the run time significantly.

(2) In problems involving nearly incompressible materials an effective approach is to use one-point Gaussian quadrature on the volume term, and two-by-two Gaussian quadrature on the deviatoric term (see T.J.R. Hughes, "Equivalence of finite Elements for Nearly-Incompressible Elasticity," Journal of Applied Mechanics, Vol. 44, Series E, No. 1, p. 181, March 1977). The use of under integration on the volume term is explained in Zinkeiwicz, "Finite Element Method". The use of 2X2 quadrature on the deviatoric stiffness prevents problems associated with zero energy modes.

(3) The "standard" four-node quadrilateral employs two-by-two Gaussian quadrature on both the volume and deviatoric terms. However, it is ineffective in application to nearly-incompressible materials (see above note) and also in application to "bending" situations. One-point Gaussian quadrature on both terms produces a more accurate, but dangerous element. The danger is that zero energy modes of deformation, so-called hourglass or keystone modes, may be present resulting in a singular stiffness matrix. If enough displacement boundary conditions are present, these modes may be eliminated. However, one-point Gaussian quadrature on both terms should only be used if you know exactly what you are doing.

(4) The presence of incompatible modes produces an element effective in bending and in application to incompressible materials. Two-by-two Gaussian quadrature on both the volume and deviatoric terms should be employed when using incompatible modes. Much pro and con has been written about incompatible modes. The present implementation is based upon R.L. Taylor, P.J. Beresford and E.L. Wilson, "A Non-Conforming Element for Stress Analysis," International Journal for Numerical Methods in Engineering, 10 (6) p. 1211, 1976.

(5) The load case number corresponds to the load-time function input in Section 8.0.

(6) Applicable to transient analysis only. Implicit-Explicit treatment is recommended for most dynamic two-phase models. By treating the stiffness of the fluid and solid in this manner, optimum time step size may be achieved, see Section 22, note 3.

(7) Applicable to nonlinear material models only. Using four stress points increases the size of blank common required to solve a particular problem. The four stress points do offer more definition of the internal stress state of the element.

9.1.1b Element Group Control Card (16I5) - Two-Phase Porous Continuum

Note	Columns	Variable	Description
	1-5	NPAR (1) (=NTYPE)	The number 4 or 13 (See Tables 9.1 and 9.2)
	6-10	NPAR (2) (=NUMEL)	Number of elements in this group; GE.1
	11-15	NPAR (3) (=IOPT)	Analysis option EQ.0, plane strain EQ.1, plane stress EQ.3, axisymmetric
(1)	16-20	NPAR (4) (=IFD)	Finite deformation code EQ.0, finite deformation effects neglected EQ.1, finite deformation effects included
	21-25	NPAR (5) (=IT)	Force vector numerical integration code EQ.0, two-by-two Gaussian quadrature EQ.1, one-point Gaussian quadrature
(2)	26-30	NPAR (6) (=IL)	Volumetric stiffness numerical integration code EQ.0, two-by-two Gaussian quadrature EQ.1, one-point Gaussian quadrature
(3)	31-35	NPAR (7) (=IM)	Deviatoric stiffness numerical integration code EQ.0, two-by-two Gaussian quadrature EQ.1, one-point Gaussian quadrature
	36-40	NPAR (8) (=IC)	Damping stiffness numerical intergration code EQ.0, two-by-two Gaussian quadrature EQ.1, one-point Gaussian quadrature

(Cont'd)

9.1.1b Element Group Control Card (15I5) (Cont'd)

Note	Columns	Variable	Description
	41-45	NPAR (9) (=NUMPR)	Number of element pressure load cards (see Section 9.1.5)
	46-50	NPAR (10) (=NOUT)	Number of stress-strain output histories (see Section 9.1.6)
	51-55	NPAR (11) (=IST)	Spatial stress/strain output code EQ.0, Include spatial stress/strain output for group EQ.1, Omit spatial stress/strain output for group
(4)	56-60	NPAR (12) (=LCASP)	Pressure load case number; GE.0; if EQ.0, set internally to 1
(4)	61-65	NPAR (13) (=LCASG)	Gravity load case number; GE.0; if EQ.0, set internally to 1
(5)	66-70	NPAR (14) (=IEXPLT)	Implicit/explicit code; GE.0; EQ.0, Implicit element EQ.1, Explicit element EQ.2, Implicit-Explicit element
(6)	71-75	NPAR (15) (=NSPTS)	Number of stress points; GE.0; EQ.0, One stress point EQ.4, Four stress points
(7)	76-80	NPAR (16) (=ISC)	Fluid treatment code; GE.0; EQ.0, Incompressible EQ.1, Compressible

Notes:

(1) If IFD = 0, the initial stress stiffness matrix is omitted and output strains are "infinitesimal." If IFD = 1, the initial stress stiffness matrix is included and output strains are Lagrangian.

(2) In problems involving nearly incompressible materials an effective approach is to use one-point Gaussian quadrature on the volume term, and two-by-two Gaussian quadrature on the deviatoric term.

(3) The "standard" four-node quadrilateral employs two-by-two Gaussian quadrature on both the volume and deviatoric terms. However, it is ineffective in application to nearly-incompressible materials (see above note). One-point Gaussian quadrature on both terms produces a more accurate, but dangerous element. The danger is that zero energy modes of deformation, so-called hourglass or keystone modes, may be present, resulting in a singular stiffness matrix. If enough displacement boundary conditions are present, these modes may be eliminated. However, one-point Gaussian quadrature on both terms should only be used if you know exactly what you are doing.

(4) The load case number corresponds to the load-time function input in Section 8.0.

(5) Applicable to transient analysis only.

(6) Applicable to nonlinear material models only.

(7) Applicable to hyperbolic option only.

General:

Notes from Section 9.1.1a apply here as well.

The best selection of parameters for the stable operation with the two-phase soil elements are as follows:

NTYPE = 4, two-phase quadrilateral element

NUMEL = problem dependent

IOPT = 0, plane strain

IFD = 0, no Lagrangian strains. This factor may be important in some analysis where geometric changes effect the element stiffness.

IT = 0, two-by-two quadrature on the force terms.

IL = 1, single-point integration on the volumetric stiffness to avoid locking in the stiffness matrix.

IM = 0, two-by-two quadrature to avoid keystone nodes.

IL = 0, two-by-two quadrature on the damping terms, may be reduced if the material response seems over damped.

LCASP = 2, it is useful when using multiple load cases to maintain a convention on the assignment of pressure and gravity load time functions.

LCASG = 1, as above

IEXPLOT = 2, implicit-explicit treatment is generally the best choice to optimize the time step size. (Section 2.2, note 4).

NSPTS = 4, use of four stress points gives very good element definition.

ISC = 0, incompressible treatment of the fluid in seismic analysis, compressible treatment of fluid for blast loading.

9.1.1c.1 Element Group Control Card (15I5) - One-Phase Fluid Continuum

Note	Columns	Variable	Description
	1-5	NPAR (1) (=NTYPE)	The number 16 or 17 (See Table 9.1)
	6-10	NPAR (2) (=NUMEL)	Number of elements in this group; GE.1
	11-15	NPAR (3) (=IOPT)	Analysis option (Set internally EQ.0)
	16-20	NPAR (4) (=IFD)	Finite deformation code (Set internally EQ.0)
	21-25	NPAR (5) (=IL)	Force vector numerical integration code EQ.0, two-by-two Gaussian quadrature EQ.1, one-point Gaussian quadrature
(1)	26-30	NPAR (6) (=IL)	Volumetric stiffness numerical integration code EQ.0, two-by-two Gaussian quadrature EQ.1, one-point Gaussian quadrature
(2)	31-35	NPAR (7) (=IM)	Deviatoric stiffness numerical integration code EQ.0, two-by-two Gaussian quadrature EQ.1, one-point Gaussian quadrature
	36-40	NPAR (8) (=INC)	Incompatible modes (Set internally EQ.0) EQ.0, two-by-two Gaussian quadrature EQ.1, one-point Gaussian quadrature
	41-45	NPAR (9) (=NUMPR)	Number of element pressure load cards

(Cont'd)

9.1.1c.1 Element Group Control Card (1515) (Cont'd)

Note	Columns	Variable	Description
	46-50	NPAR (10) (=NOUT)	Number of stress-strain output histories
	51-55	NPAR (11) (=IST)	Spatial stress/strain output code EQ.0, Include spatial stress/strain output for group EQ.1, Omit spatial stress/strain output for group
(3)	56-60	NPAR (12) (=LCASP)	Pressure load case number; GE.0; if EQ.0, set internally to 1
(3)	61-65	NPAR (13) (=LCASG)	Gravity load case number; GE.0; if EQ.0, set internally to 1
(4)	66-70	NPAR (14) (=IEXPLT)	Reform code; GE.0; EQ.0, No reform EQ.1, Reform at every time step
(4)	71-75	NPAR (15) (=LNODE)	Number of nodes; GE.0 and LE.NUMNP

Notes:

(1) In problems involving nearly incompressible fluids an effective approach is to use one-point Gaussian quadrature on the volume term, and two-by-two Gaussian quadrature on the deviatoric term.

(2) The "standard" four-node quadrilateral employs two-by-two Gaussian quadrature on both the volume and deviatoric terms. However, it is ineffective in application to nearly-incompressible materials (see above note). One-point Gaussian quadrature on both terms produces a more accurate, but dangerous element. The danger is that zero energy modes of deformation, so-called hourglass or keystone modes, may be present, resulting in a singular stiffness matrix. If enough displacement boundary conditions are present, these modes may be eliminated. However, one-point Gaussian quadrature on both terms should only be used if you know exactly what you are doing.

(3) The load case number corresponds to the load-time function input in Section 8.0.

(4) Applicable to NTYPE = 17 only.

9.1.1c.2 Euler-Lagrange Array ((2+NSD)*15)
Only Applicable to NTYPE = 17

Note	Columns	Variable	Description
(1)	1-5	N	Node number; GE.1 and LE.NUMNP
(2)	6-10	NG	Generation increment
(3)	11-15	ID(1,N)	Degree of freedom 1 Euler-Lagrange code
	16-20	ID(2,N)	Degree of freedom 2 Euler-Lagrange code
		ID(NSD,N)	Degree of freedom NSD Euler-Lagrange code

Notes:

(1) Euler-Lagrange condition data must be input for each node which is not Eulerian in one or more directions. Cards need not be input in order. Terminate with a blank card.

(2) Euler-Lagrange condition data can be generated by employing a two card sequence as follows:

Card 1: L, LG, ID(1,L), ..., ID(NSD,L)

Card 2: N, NG, ID(1,N), ..., ID(NSD,N)

Euler-Lagrange codes of all nodes

$L+LG, L+2*LG, \dots, N-MOD(N-L, LG)$

(i.e., less than N) are set equal to those of node L. If LG is blank or zero, no generation takes place between L and N.

(3) Euler-Lagrange condition codes may be assigned the following values:

ID(I,N) = 0 , Euler degree of freedom

ID(I,N) = 1 , Lagrange degree of freedom

where I = 1,2,...,NSD. If more than one Euler-Lagrange condition data card for node N is input, the last one read takes priority.

An example problem involving fluid elements is included in the appendixes. This problem has not been run at NCEL.

9.1.2 Material Properties Cards

The data cards for material properties follow the element group control card. Consult Section 10 for the required input of the individual material models.

9.1.3 Mass density and Gravity Load Multiplier Cards (4F10.0)

Note	Columns	Variable	Description
	1-10	WS	Mass density (solid phase) per unit volume.
(1)	11-20	GRAV (1)	Multiplier of gravity load in the x1 direction
(1)	21-30	GRAV (2)	Multiplier of gravity load in the x2 direction
(2)	31-40	WF	Mass density (fluid phase) per unit volume.

Notes:

(1) Gravity load multipliers are used to define the components of the gravity vector with respect to the global x1, x2 system.

(2) Applicable to porous media only.

General:

DYNAFLOW uses the mass density of the solid (on the order of 2.7 times the fluid mass density) and the material porosity to compute a bouyant unit weight for the two-phase materials.

Gravity load multipliers are used in conjunction with the load time functions (Section 8) to assign body forces to the elements, and induce the initial states of stress.

9.1.4 Element Data Cards

Nodal Data Cards (7I5)

Note	Columns	Variable	Description
(1)	1-5	N	Element number
	11-15	IEN(1,N)	Number of 1st node
	16-20	IEN(2,N)	Number of 2nd node
	21-25	IEN(3,N)	Number of 3rd node
(2)	26-30	IEN(4,N)	Number of 4th node
(3)	31-35	NG	Generation parameter EQ.0, no generation EQ.1, generate data

Notes:

(1) All elements must be input on a nodal data card or generated.
Terminate with a blank card.

(2) For triangular elements, set node number IEN(4,N) equal to IEN(3,N).

(3) If the generation parameter is set to 1, a generation data card must be input next.

General:

Node numbers must be read in a counterclockwise order. Do not use triangular elements unless absolutely necessary. They are actually highly deformed quadrilateral elements with a rigid point in place of one element side. Methods to avoid triangular elements are shown in Figures 9.1 and 9.2. Table 9.3 shows the proper card sequence for element generation. Figure 9.3 shows the resulting mesh. The following is a description of Table 9.3:

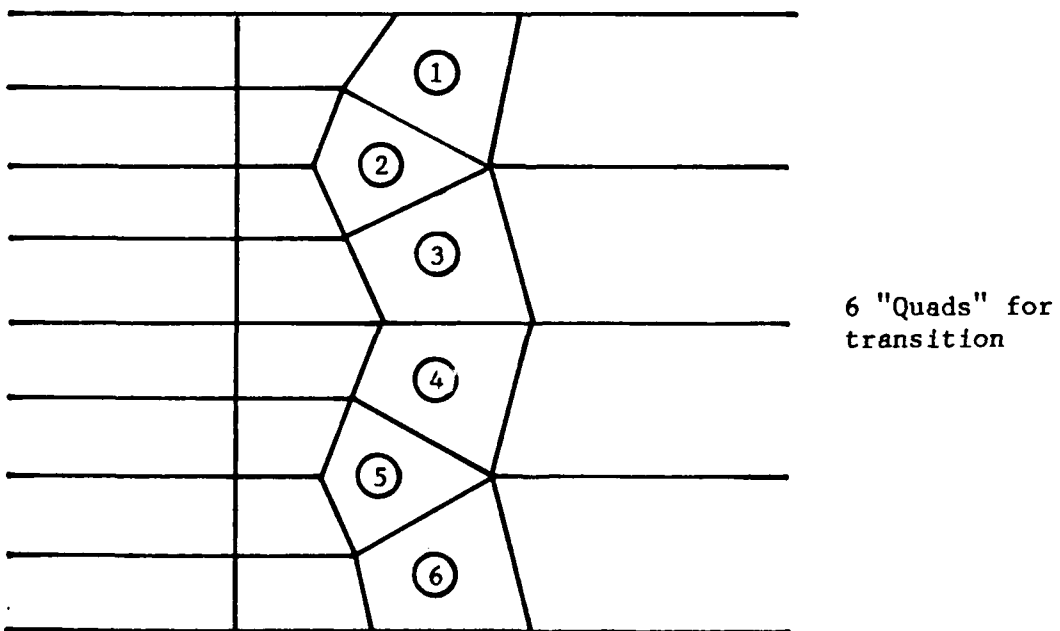
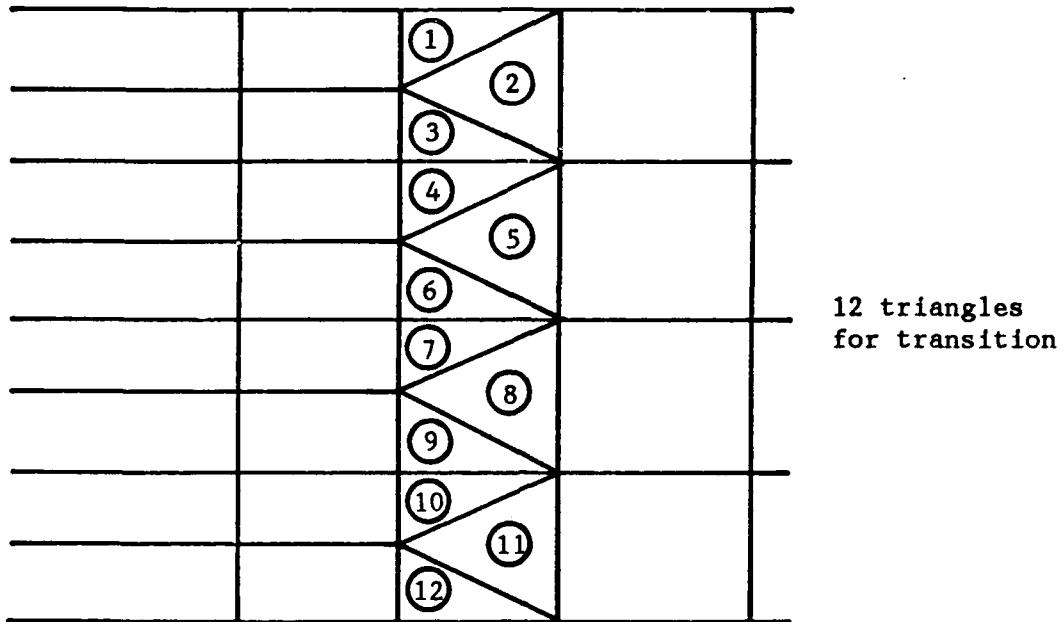
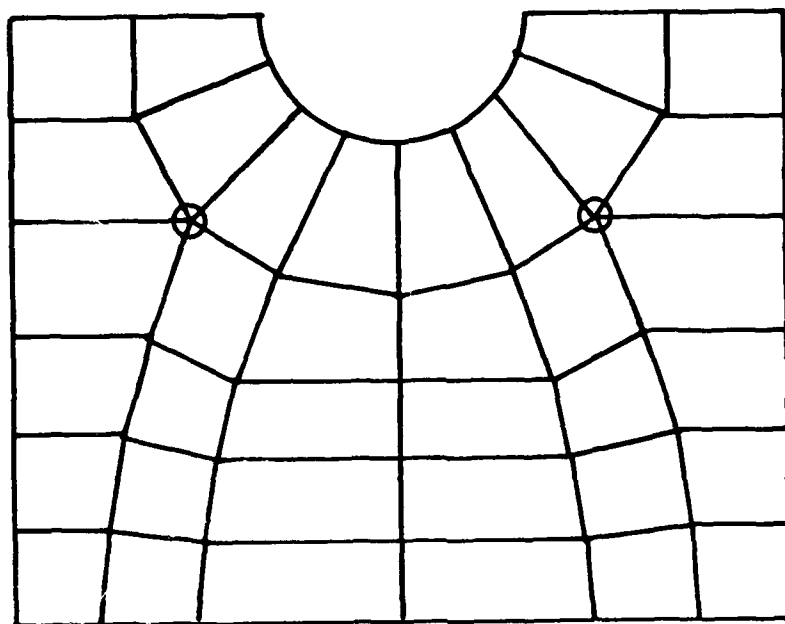


Figure 9.1 Four node "quad" transition elements



5 Quads joining
at one node

Figure 9.2 Four node "quad" transition around a hole

1	1	1	2	11	10	1
7	8	9	8	1	1	
57	1	66	67	76	75	1
1	1	9	6	1	1	
63	1	75	76	85	84	1
1	1	9	6	1	1	
69	1	84	85	94	93	1
1	1	9	6	1	1	
75	1	93	94	103	102	1
1	1	9	6	1	1	
81	1	100	101	110	109	1
7	8	9	8	1	1	

Table 9.3 Element generation

SOIL STRUCTURE TEST, NEVADA SAND, ELAS MODEL, ACCELERATION BC

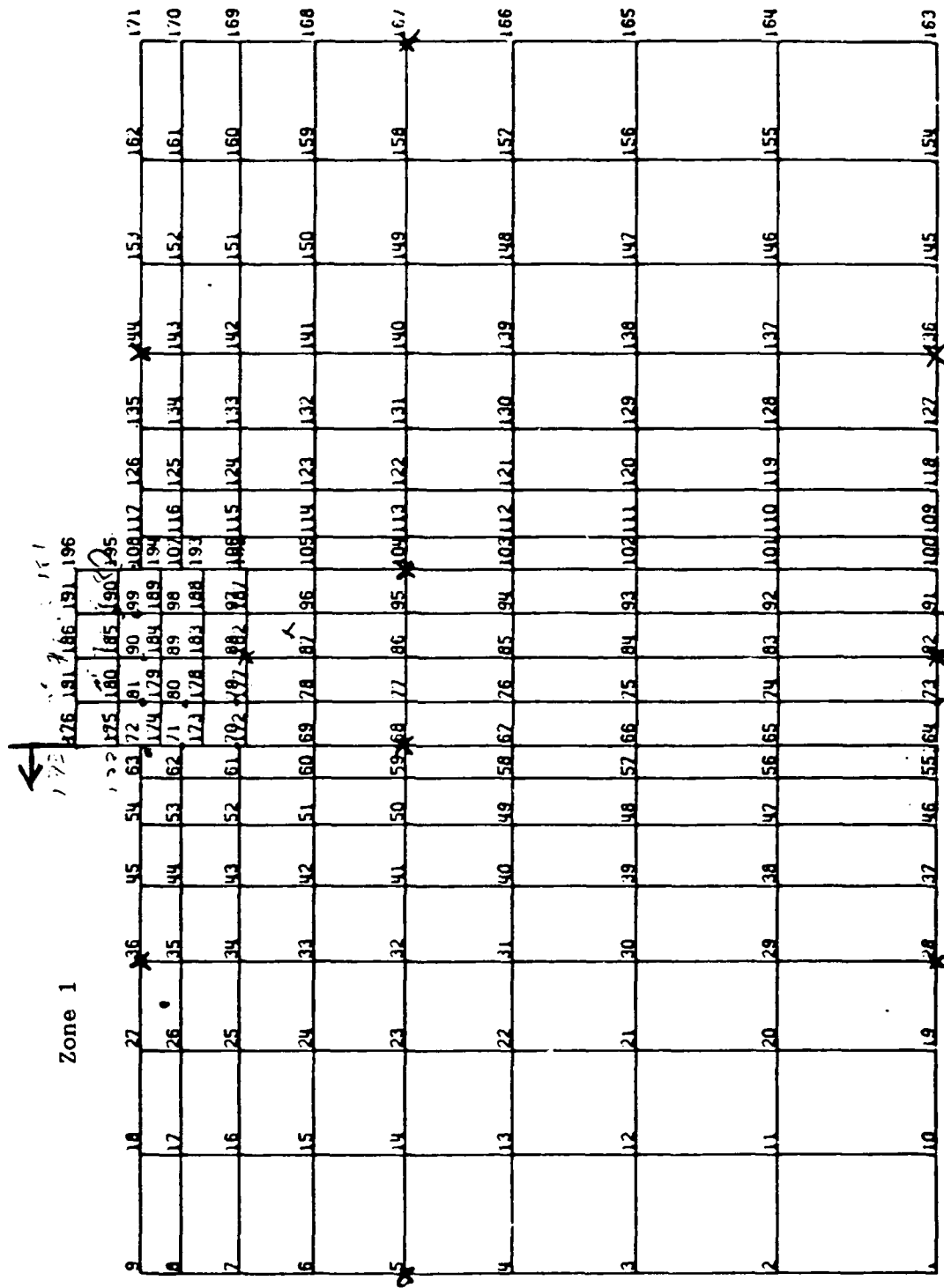


Figure 9.3 Element generation

The first card in the groups denoted by the bracket gives the nodal connectivity (1,10,11,2) for element #1. Note the order of connectivity is counterclockwise. The second card in the group is interpreted as follows:

- 7 elements in direction 1, zone 1.
- 8 is the element number increment for direction 1 zone 1.
- 9 is the nodal number increment for direction 1.
- 8 is the number of elements in direction 2, zone 1.
- 1 is the element number increase first inspection 2.
- 1 is the nodal number increment for direction 2.

Figure 9.4 illustrates a general case of element generation. This two card sequence generates the portion of the mesh denoted as zone 1 in Figure 9.3. Similar generations are used to generate the remainder of the mesh. Note the four columns of elements beneath the structure are generated individually.

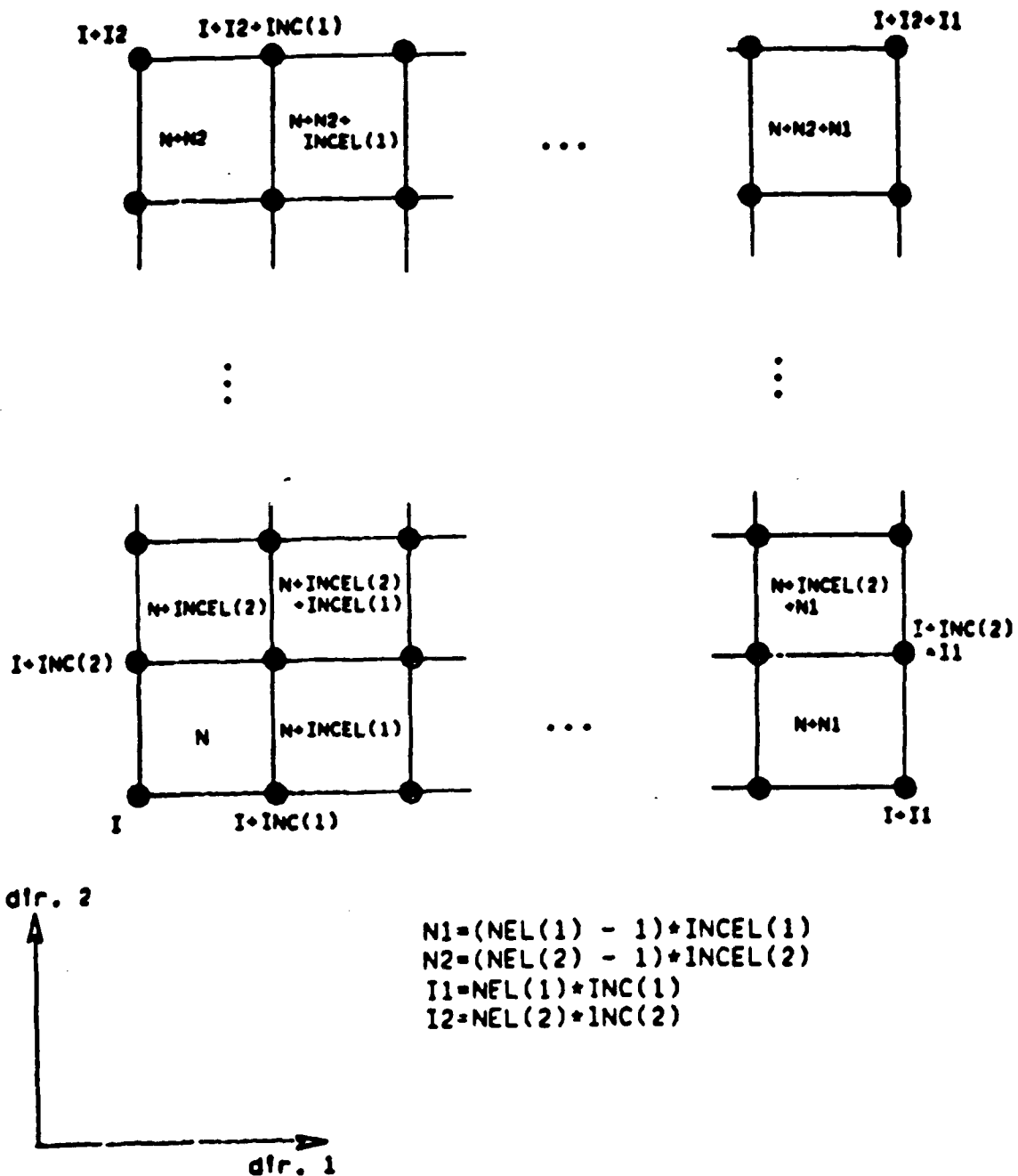


Figure 9.4 Element generation in two dimensions

Generation Data Cards (6I5)

See Figure 9.3 for a schematic representation of the generation scheme.

Note	Columns	Variable	Description
	1-5	NEL (1)	Number of elements in direction 1; GE.0; if EQ.0, set internally to 1
	6-10	INCEL (1)	Element number increment for direc- tion 1; if EQ.0, set internally to 1
	11-15	INC (1)	Node number increment for direction 1; if EQ.0, set internally to 1
	16-20	NEL (2)	Number of elements in direction 2; GE.0; if EQ.0, set internally to 1
	21-25	INCEL (2)	Element number increment for direc- tion 2; if EQ.0, set internally to NEL(1)
	26-30	INC (2)	Node number increment for direc- tion 2; if EQ.0, set internally to $(1 + \text{NEL}(1)) * \text{INC}(1)$

9.1.5 Element Pressure Load (2I5,F10.0)

Note	Columns	Variable	Description
(1)	1-5	IELNO(I)	Element number 1.LE.IELNO(I).LE.NUMEL
(2)	6-10	ISIDE(I)	Element side number 1.LE.ISIDE(I).LE.4
(3)	21-30	PRES(I)	Pressure (force/unit area)

Notes:

(1) Each element subjected to a pressure load must be input on an element pressure load card. If more than one side of the element is loaded, one card for each loaded side must be input. The total number of element pressure load cards must equal NUMPR read in on the element group control card (see Section 9.1.1). The index I in the arrays IELNO, ISIDE, and PRES corresponds to the order read in; 1.LE.I.LE.NUMPR. The cards need not be read in any particular order; terminate with a blank card.

(2) The element side number is deduced as follows:

<u>Side number</u>	<u>Nodes defining side</u>
1	1, 2
2	2, 3
3	3, 4
4	4, 1

(3) The pressure is assumed to be constant over the surface. A positive pressure is assumed to be pointing inward.

General:

Pressure loads were discussed briefly in Section 7.0. The pressure load cards are a quick and simple means of applying a constant pressure loading over a series of elements. The pressure load is a multiplier used in conjunction with the load-time function assigned on the element groups control card, Sections 9.1.1a and 9.1.1b.

9.1.6 Element Output History Cards (17I5)

"On-line" and Calcomp plots of various element response components may be obtained. Each component required is plotted versus time. Plots of this type are useful in providing quick information concerning the time history behavior of important data. The total number of components to be plotted must equal NOUT, which is defined on the element group control card (see Section 9.1.1).

For each element, two (2) data cards are required.

Card 1 (16I5)

Note	Columns	Variable	Description
(1)	1-5	N	Element number
	6-10	ITEMP(1)	Direct stress S11 plot code EQ.0, no plot EQ.1, plot
	11-15	ITEMP(2)	Direct stress S22 plot code EQ.0, no plot EQ.1, plot
	16-20	ITEMP(3)	Shear stress S12 plot code EQ.0, no plot EQ.1, plot
	21-25	ITEMP(4)	Direct stress S33 plot code EQ.0, no plot EQ.1, plot
	26-30	ITEMP(5)	Principal stress PS1 plot code EQ.0, no plot EQ.1, plot
	31-35	ITEMP(6)	Principal stress PS2 plot code EQ.0, no plot EQ.1, plot

(Cont'd)

9.1.6 Element Output History Cards (17I5) (Cont'd)

Note	Columns	Variable	Description
36-40	ITEMP(7)	Principal shear stress PTAU plot code EQ.0, no plot EQ.1, plot	
41-45	ITEMP(8)	Principal stress angle SANG plot code EQ.0, no plot EQ.1, plot	
46-50	ITEMP(9)	Direct strain E11 plot code EQ.0, no plot EQ.1, plot	
51-55	ITEMP(10)	Direct strain E22 plot code EQ.0, no plot EQ.1,plot	
56-60	ITEMP(11)	Shear strain G12 plot code EQ.0, no plot EQ.1, plot	
61-65	ITEMP(12)	Principal strain PE1 plot code EQ.0, no plot EQ.1, plot	
66-70	ITEMP(13)	Principal strain PE2 plot code EQ.0, no plot EQ.1, plot	
71-75	ITEMP(14)	Principal shear strain PGAM plot code EQ.0, no plot EQ.1, plot	
76-80	ITEMP(15)	Principal strain angle EANG plot code EQ.0, no plot EQ.1, plot	

Notes:

(1) Output history information is stored in the array IHS in element group data. The dimension of IHS is 2 x NOUT. The first row of IHS contains element numbers and the second row contains output history component numbers. Fifteen different component numbers may be plotted as described above. The corresponding component numbers and output labels are:

<u>Component Number</u>	<u>Output Label</u>
1	S11
2	S22
3	S12
4	S33
5	PS1
6	PS2
7	PTAN
8	SANG
9	E11
10	E22
11	G12
12	PE1
13	PE2
14	PGAM
15	EANG
16	PF

Card 2 (I5)

Note	Columns	Variable	Description
	1 - 5	ITEMP(16)	Fluid pressure PF plot code EQ.0, no plot EQ.1, plot 0

General:

Output histories for specific elements may be selected by listing the element number and the series of stress (or strain) time histories desired. These output histories are written to a post processing file labeled TAPE 88 at the end of execution for a number of time steps, selected in either Section 2.2, page 8 (NTSS) or in the RESTART manual. Storage requirements are dependent on the number of histories requested. The number of histories, not the number of elements at which histories are requested, should be input on the element control card, Sections 9.1.1 A and B. Note also, that the specific element history requires two cards with the second card containing only the pore fluid history flag.

9.1.7 Storage Requirements for Two-Dimensional and Axisymmetric Element (NTYPE=1,4,7,12,13)

<u>First Word</u>	<u>Array</u>
N101 = NF*	NPAR(16)
N102 = N101 + 16	IEN(4,NUMEL)
N103 = N102 + NUMEL*4	LM(NED,4,NUMEL)
N104 = N103 + NUMEL*4*NED**	WS
N105 = N104 + IPREC	WF
N106 = N105 + IPREC	GRAV(2)
N107 = N106 + 2*IPREC	IELNO(NUMPR)
N108 = N107 + NUMPR	ISIDE(NUMPR)
N109 = N108 + NUMPR	PRES(NUMPR)
N110 = N109 + NUMR*IPREC	IHS(2,NOUT)
N111 = N110 + NOUT*2	SOUT(NOUT,NTS + 1)
MF = N111 + (NTS+1)*NOUT	material data array
NL = ML***	

(NL - NF + 1 = total required storage for element group)

*NF is the address of the first word in blank common for the element group.

**NED is the number of degrees of freedom per node.

***ML depends upon the particular material model (see Section 10).

9.2.0 Three-Dimensional Element

The present element may be used in wedge (6 node) or brick (8 node) form. Three displacement degrees of freedom in the x1, x2, and x3 directions are assigned to each node. Incompatible modes and selective numerical integration may be employed to improve element behavior in various situations. These options should be activated only by users fully knowledgeable in their use. The nodes of the element must be input in the order shown in Figure 9.5. In a case of a wedge-shaped element, the fourth node number must be the same as the third, and the eighth must be the same as the seventh. On the master control card, (see Section 2.0), NSD must equal EQ.3, and NDOF must be GE.3.0.

The various analysis options together with required variables are summarized in Table 9.4. Stresses/strains in the global coordinate system and principal stresses/strains are output at the element center, which is generally the point of optimal accuracy. All shear strains are reported according to the "engineering" convention (i.e., twice the value of the tensor components).

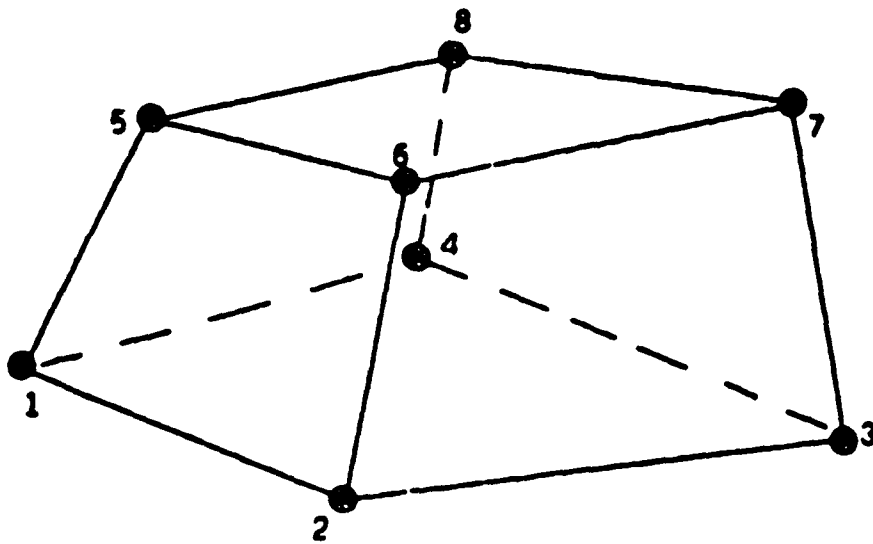
Note:

Three-dimensional elements have not been greatly tested at NCEL. The work done in this area has shown that extreme care is necessary in nodal generation and element definition. Difficulties arise from improper definition and nonpositive definite stiffness matrixes.

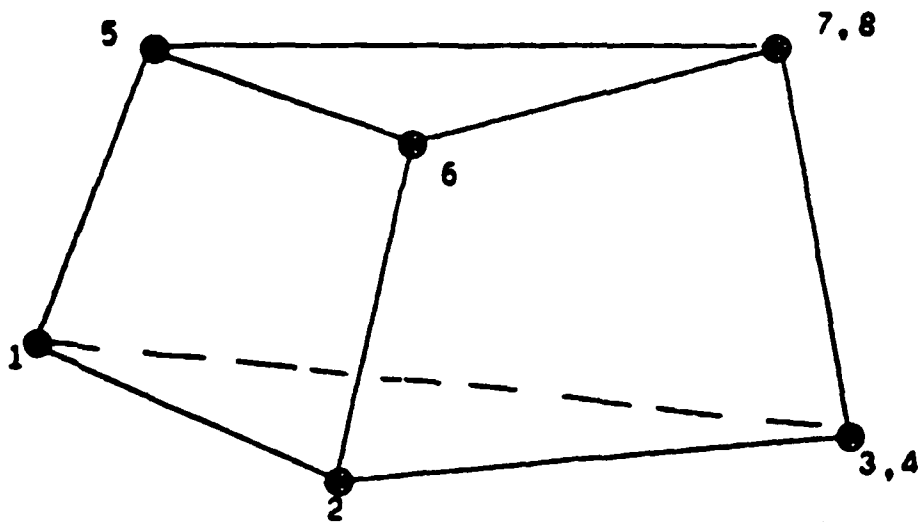
Element control parameter selection is the same as discussed in previous sections for two-dimensional elements.

Table 9.4. Three-Dimensional Element

Options	Analysis Mode	NTYPE	MODES	NED LE.NDOF	ISYMM	MATYP
		Sec. 9.1	Sec. 2.1	Sec. 2.1	Sec. 2.1	Sec. 10.
One-Phase Solid Continuum	Elliptic	2	0	3	0,1	1,2
	Hyperbolic	2	1	3	0,1	1,2
	Parabolic	2	2	3	0,1	1,2
Two-Phase Porous Continuum	Parabolic	5	2	4	1	1,2
	Hyperbolic	5	1	6	0,1	1,2



8-node brick element



6-node wedge element

Figure 9.5 Three dimensional elements

The following sequence of cards is used to describe the elements:

9.2.1a Element Group Control Card (15I5) - One-Phase Continuum

Note	Columns	Variable	Description
	1-5	NPAR (1) (=NTYPE)	The number 2 (see Table 9.4)
	6-10	NPAR (2) (=NUMEL)	Number of elements in this group; GE.1
	11-15	NPAR (3) (=IOPT)	Analysis option (set internally to 3)
(1)	16-20	NPAR (4) (=IFD)	Finite deformation code EQ.0, finite deformation effects neglected EQ.1, finite deformation effects included
	21-25	NPAR (5) (=IT)	Force vector numerical integration code EQ.0, 2 x 2 x 2 Gaussian quadrature EQ.1, one-point Gaussian quadrature
(2)	26-30	NPAR (6) (=IL)	Volumetric stiffness numerical integration code EQ.0, 2 x 2 x 2 Gaussian quadrature EQ.1, one-point Gaussian quadrature
(3)	31-35	NPAR (7) (=IM)	Deviatoric stiffness numerical integration code EQ.0, 2 x 2 x 2 Gaussian quadrature EQ.1, one-point Gaussian quadrature
(4)	36-40	NPAR (8) (=INC)	Incompatible modes code EQ.0, incompatible modes neglected EQ.1, incompatible modes added

(Cont'd)

9.2.1a Element Group Control Card (15I5) (Cont'd)

Note	Columns	Variable	Description
	41-45	NPAR (9) (=NUMPR)	Number of element pressure load cards
	46-50	NPAR(10) (=NOUT)	Number of stress/strain output histories
	51-55	NPAR (11) (=IST)	Spatial stress/strain output code EQ.0, Include spatial stress/strain output for group EQ.1, Omit spatial stress/strain output for group
(5)	56-60	NPAR (12) (=LCASP)	Pressure load case number; GE.0 if EQ.0, set internally to 1
(5)	61-65	NPAR (13) (=LCASG)	Gravity load case number; GE.0; if EQ.0, set internally to 1
(6)	66-70	NPAR (14) (=IEXPLT)	Implicit-Explicit code; GE.0; EQ.0, Implicit Element EQ.1, Explicit Element EQ.2, Implicit-Explicit Element
(7)	71-75	NPAR (15) (=NSPTS)	Number of stress points; GE.0; EQ.0, One stress point EQ.8, Eight stress points 0

Notes:

(1) If IFD = 0, the initial stress stiffness matrix is omitted and output strains are "infinitesimal." If IFD = 1, the initial stress stiffness matrix is included and output strains are Lagrangian.

(2) In problems involving nearly incompressible materials an effective approach is to use one-point Gaussian quadrature on the volume term, and 2 x 2 x 2 Gaussian quadrature on the deviatoric term (see T.J.R. Hughes, "Equivalence of Finite Elements for Nearly-Incompressible Elasticity," Journal of Applied Mechanics, Vol. 44, Series E, No. 1, p. 181, March 1977.)

(3) The "standard" eight-node brick employs $2 \times 2 \times 2$ Gaussian quadrature on both the volume and deviatoric terms. However, it is ineffective in application to nearly-incompressible materials (see above note) and also in application to "bending" situations. One-point Gaussian quadrature on both terms produces a more accurate, but dangerous element. The danger is that zero energy modes of deformation may be present, resulting in a singular stiffness matrix. If enough displacement boundary conditions are present, these modes may be eliminated. However, one-point Gaussian quadrature on both terms should only be used if you know exactly what you are doing.

(4) The presence of incompatible modes produces an element effective in bending and in application to incompressible materials. Two-by-two Gaussian quadrature on both the volume and deviatoric terms should be employed when using incompatible modes. Much pro and con has been written about incompatible modes. The present implementation is based upon R.L. Taylor, P.J. Beresford, and E.L. Wilson, "A non-Conforming Element for Stress Analysis," International Journal for Numerical Methods in Engineering, 10 (6) p.1211, 1976.

(5) The pressure load option has not been implemented for the three-dimensional element.

(6) The load case number corresponds to the load-time function input in Section 8.0.

(7) Applicable to transient analysis only.

9.2.1b Element Group Control Card (1615) - Two-Phase Porous Continuum

Note	Columns	Variable	Description
	1-5	NPAR (1) (=NTYPE)	The number 5 (see Table 9.4)
	6-10	NPAR (2) (=NUMEL)	Number of elements in this group; GE.1
	11-15	NPAR (3) (=IOPT)	Analysis option (set internally to 3)
(1)	16-20	NPAR (4) (=IFD)	Finite deformation code EQ.0, finite deformation effects neglected EQ.1, finite deformation effects included
	21-25	NPAR (5) (=IT)	Force vector numerical integration code EQ.0, 2 x 2 x 2 Gaussian quadrature EQ.1, one-point Gaussian quadrature
(2)	26-30	NPAR (6) (=IL)	Volumetric stiffness numerical integration code EQ.0, 2 x 2 x 2 Gaussian quadrature EQ.1, one-point Gaussian quadrature
(3)	31-35	NPAR (7) (=IM)	Deviatoric stiffness numerical integration code EQ.0, 2 x 2 x 2 Gaussian quadrature EQ.1, one-point Gaussian quadrature

(Cont'd)

9.2.1b Element Group Control Card (1615) (Cont'd)

Note	Columns	Variable	Description
	36-40	NPAR (8) (=IC)	Damping stiffness numerical intergration code EQ.0, 2 x 2 x 2 Gaussian quadrature EQ.1, one-point Gaussian quadrature
	41-45	NPAR (9) (=NUMPR)	Number of element pressure load cards
	46-50	NPAR(10) (=NOUT)	Number of stress/strain output histories
	51-55	NPAR (11) (=IST)	Spatial stress/strain output code EQ.0, Include spatial stress/ strain output for groups EQ.1, Omit spatial stress/ strain output for group
(4)	56-60	NPAR (12) (=LCASP)	Pressure load case number; GE.0 if EQ.0, set internally to 1
(4)	61-65	NPAR (13) (=LCASG)	Gravity load case number; GE.0; if EQ.0, set internally to 1
(5)	66-70	NPAR (14) (=IEXPLT)	Implicit-Explicit code; GE.0; EQ.0, Implicit Element EQ.1, Explicit Element EQ.2, Implicit-Explicit Element
(6)	71-75	NPAR (15) (=NSPTS)	Number of stress point; GE.0; EQ.0, One stress point EQ.8, Eight stress points
(7)	75-80	NPAR (16) (=ISC)	Fluid treatment code; GE.0; EQ.0, Incompressible EQ.1, Compressible

Notes:

- (1) If IFD = 0, the initial stress stiffness matrix is omitted and output strains are "infinitesimal." If IFD = 1, the initial stress stiffness matrix is included and output strains are Lagrangian.
- (2) In problems involving nearly incompressible materials an effective approach is to use one-point Gaussian quadrature on the volume term, and 2 x 2 x 2 Gaussian quadrature on the deviatoric term (see T.J.R. Hughes, "Equivalence of Finite Elements for Nearly-Incompressible Elasticity," Journal of Applied Mechanics, Vol. 44, Series E, No. 1, p. 181, March 1977.)
- (3) The "standard" eight-node brick employs 2 x 2 x 2 Gaussian quadrature on both the volume and deviatoric terms. However, it is ineffective in application to nearly-incompressible materials (see above note) and also in application to "bending" situations. One-point Gaussian quadrature on both terms produces a more accurate, but dangerous element. The danger is that zero energy modes of deformation may be present, resulting in a singular stiffness, these modes may be eliminated. However, one-point Gaussian quadrature on both terms should be used if you know exactly what you are doing.
- (4) The load case number corresponds to the load-time function input in Section 8.0.
- (5) Applicable to transient analysis only.
- (6) Applicable to nonlinear material models only.
- (7) Applicable to hyperbolic option only.

9.2.2 Material Properties Cards

The data cards for material properties follow the element group control card. Consult Section 10 for the input required of the individual material models.

9.2.3 Mass Density and Gravity Load Multiplier Cards (5F10.0)

Note	Columns	Variable	Description
	1-10	WS	Mass density (solid phase) per unit volume
(1)	11-20	GRAV (1)	Multiplier of gravity load in the x1 direction
(1)	21-30	GRAV (2)	Multiplier of gravity load in the x2 direction
(1)	31-40	GRAV (3)	Multiplier of gravity load in the x3 direction
(2)	41-50	WS	Mass density (fluid phase) per unit volume

Notes:

(1) Gravity load multipliers are used to define the components of the gravity vector with respect to the global x1, x2, x3 system.

(2) Applicable to porous media only.

9.2.4 Element Data Cards

Nodal Data Cards (11I5)

Note	Columns	Variable	Description
(1)	1-5	N	Element number
	5-1	MAT(N)	Material set number, GE.0
	11-15	IEN(1,N)	Number of 1st node
	16-20	IEN(2,N)	Number of 2nd node
	21-25	IEN(3,N)	Number of 3rd node
(2)	26-30	IEN(4,N)	Number of 4th node
	31-35	IEN(5,N)	Number of 5th node
	36-40	IEN(6,N)	Number of 6th node
	41-45	IEN(7,N)	Number of 7th node
(3)	46-50	IEN(8,N)	Number of 8th node
(4)	51-55	NG	Generation parameter

Notes:

(1) All elements must be input on a nodal data card or generated.
Terminate with a blank card.

(2) For wedge elements, set node number IEN (4,N) equal to IEN (3,N).

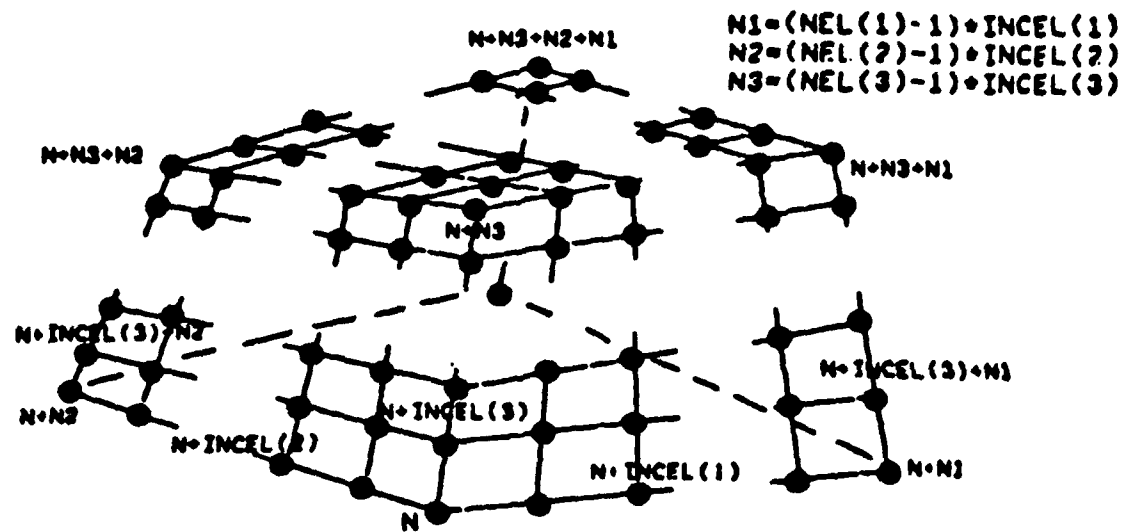
(3) For wedge elements, set node number IEN (8,N) equal to IEN (7,N).

(4) If the generation parameter is set to 1, a generation data card must be input next.

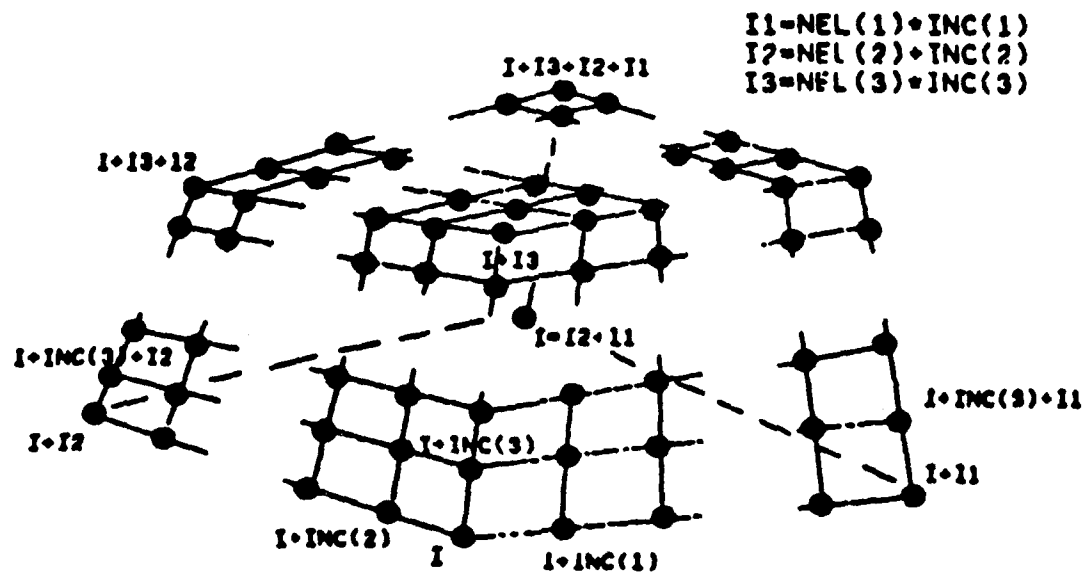
Generation Data Cards (9I5)

See Figure 9.6 for a schematic representation of the generation scheme.

Note	Columns	Variable	Description
	1-5	NEL (1)	Number of elements in direction 1; GE.0; if EQ.0, set internally to 1
	6-10	INCEL (1)	Element number increment for direc- tion; if EQ.0, set internally to 1
	11-15	INC (1)	Node number increment for direction 1; if EQ.0, set internally to 1
	16-20	NEL (2)	Number of elements in direction 2; GE.0; if EQ.0, set internally to 1
	21-25	INCEL (2)	Element number increment for direction 2; if EQ.0, set internally to NEL (1)
	26-30	INC (2)	Node number increment for direc- tion 2; if EQ.0, set internally to $(1 + \text{NEL (1)}) * \text{INC (1)}$
	31-35	NEL (3)	Number of elements in direction 3; GE.0, if EQ.0, set internally to 1
	36-40	INCEL (3)	Element number increment for direction 3; if EQ.0, set internally to $\text{NEL (1)} * \text{NEL (2)}$
	41-45	INC (3)	Node number increment for direc- tion 3; if EQ.0, set internally to $(1 + \text{NEL (2)}) * \text{INC (2)}$



element numbers



node numbers

Figure 9.6 Element generation in three dimensions

9.2.5 Element Pressure Load Cards (2I5,10X,2F10.0)

Note	Columns	Variable	Description
(1)	1-5	IELNO (I)	Element number 1.LE.IELNO (I).LE.NUMEL
(2)	6-10	ISIDE (I)	Element side number 1.LE.ISIDE (I).LE.6
(3)	21-30	PRES (I)	Pressure (force/unit area)

Notes:

(1) Each element subjected to a pressure load must be input on an element pressure load card. If more than one surface of the element is loaded, one card for each loaded surface must be input. The total number of element pressure load cards must equal NUMPR read in on the element group control card (see 9.2.1). The index I in the arrays IELNO, ISIDE and PRES corresponds to the order read in; 1.LE.I.LE.NUMPR. The cards need not be read in any particular order; terminate with a blank card.

(2) The element surface numbers are defined as follows:

<u>Surface number</u>	<u>Nodes defining surface</u>
1	1, 2, 3, 4
2	5, 6, 7, 8
3	1, 2, 6, 5
4	2, 3, 7, 6
5	3, 4, 8, 7
6	4, 1, 5, 8

(3) The pressure is assumed to be constant over the surface. A positive pressure is assumed to be pointing inward.

9.2.6 Element Output History Cards (20I5)

"On-line" and Calcomp plots of various element response components may be obtained. Each component required is plotted versus time. Plots of this type are useful in providing quick information concerning the time history behavior of important data. The total number of components to be plotted must equal NOUT, which is defined on the element group control card (see Section 9.2.1).

For each element, two (2) data cards are required.

Card 1: (16I5)

Note	Columns	Variable	Description
(1)	1-5	N	Element number
	6-10	ITEMP (1)	Direct stress S11 plot code EQ.0, no plot EQ.1, plot
	11-15	ITEMP (2)	Direct stress S22 plot code EQ.0, no plot EQ.1, plot
	16-20	ITEMP (3)	Direct stress S33 plot code EQ.0, no plot EQ.1, plot
	21-25	ITEMP (4)	Shear stress S12 plot code EQ.0, no plot EQ.1, plot
	26-30	ITEMP (5)	Shear stress S23 plot code EQ.0, no plot EQ.1, plot
	31-35	ITEMP (6)	Shear stress S31 plot code EQ.0, no plot EQ.1, plot
	36-40	ITEMP (7)	Principal stress PS1 plot code EQ.0, no plot EQ.1, plot
	41-45	ITEMP (8)	Principal stress PS2 plot code EQ.0, no plot EQ.1, plot

(Cont'd)

Card 1: (16I5) (Cont'd)

Note	Columns	Variable	Description
	46-50	ITEMP (9)	Principal stress PS3 plot code EQ.0, no plot EQ.1, plot
	51-55	ITEMP (10)	Direct strain E11 plot code EQ.0, no plot EQ.1, plot
	56-60	ITEMP (11)	Direct strain E22 plot code EQ.0, no plot EQ.1, plot
	61-65	ITEMP (12)	Direct strain E33 plot code EQ.0, no plot EQ.1, plot
	66-70	ITEMP (13)	Shear strain G12 plot code EQ.1, plot EQ.0, no plot
	71-75	ITEMP (14)	Shear strain G23 plot code EQ.0, no plot EQ.1, plot
	76-80	ITEMP (15)	Shear strain G31 plot code EQ.0, no plot EQ.1, plot
(1)	1-5	ITEMP (16)	Principal strain PE1 plot code EQ.0, no plot EQ.1, plot
	6-10	ITEMP (17)	Principal strain PE2 plot code EQ.1, plot EQ.0, no plot
	11-15	ITEMP (18)	Principal strain PE3 plot code EQ.0, no plot EQ.1, plot
	16-20	ITEMP (19)	Fluid pressure PF plot code EQ.0, no plot EQ.1, plot

Note:

(1) Output history information is stored in the array IHS in the element group data. The dimension of IHS is 2 x NOUT. The first row of IHS contains element numbers and the second row contains output history component numbers. Nineteen different component numbers may be plotted as described above. The corresponding component numbers and output labels are:

<u>Component Number</u>	<u>Output</u>
1	S11
2	S22
3	S33
4	S12
5	S23
6	S31
7	PS1
8	PS2
9	PS3
10	E11
11	E22
12	E33
13	G12
14	G23
15	G31
16	PE1
17	PE2
18	PE3
19	PF

9.2.7 Storage Requirements for Three-Dimensional Element (NTYPE=2,5,10)

<u>First Word</u>	<u>Array</u>
N101 = NF*	NPAR(16)
N102 = N101 + 16	IEN(8,NUMEL)
N103 = N102 + NUMEL*8	LM(NED,8,NUMEL)
N104 = N103 + NUMEL*8*NED**	WS
N105 = N104 + IPREC	WF
N106 = N105 + IPREC	GRAV(3)
N107 = N106 + 3*IPREC	IELNO(NUMPR)
N108 = N107 + NUMPR	ISIDE(NUMPR)
N109 = N108 + NUMPR	PRES(NUMPR)
N110 = N109 + NUMPR*IPREC	IHS(2,NOUT)
N111 = N110 + NOUT*2	SOUT(NOUT,NTS + 1)
MF = N111 + (NTS+1)*NOUT	material data array
NL = ML**	

(NL - NF + 1 = total required storage for element group.)

* NF is the address of the first word in blank common for the element group.

** NED is the number of degrees of freedom per node.

** ML depends upon the particular material model (see Section 10).

DYANFLOW incorporates three different "contract" elements:

- (1) Section 9.3.0 Contact
- (2) Section 9.4.0 Slide Line
- (3) Section 9.5.0 Frictional Slideline

There is "physically" not much difference in the way each of the elements behaves, other than the frictional capabilities in Section 9.5.0.

The contact element, Section 9.3.0, does allow for element output histories for displacement and contact force, and requires only two nodes and a direction vector \underline{n} , to define the contact plane (Figure 9.7a).

The slide line elements define the contact plane by two nodes, connected by a "rigid beam" or "rigid solid" element. The contactor node is defined by a node in the "deformable" material, Figures 9.8 and 9.9. The gaps in both cases are imaginary under static conditions, but may open when dynamic excitation occurs.

The frictional slide line element employs a Coulomb friction algorithm to define the contact slippage behavior. Selection of the frictional constant should be based on physical data. Selection of spring constants is best achieved through the following:

- (1) Select a reasonable stiffness, three orders of magnitude greater than the stiffness of the contacting materials.
- (2) Choose several critical variables in the solution to monitor, such as displacement at the interface.
- (3) Run a short simulation of three or four time steps.
- (4) Check the behavior of the selected variables (displacements).
- (5) Increase the stiffness of the contact element by one order of magnitude, and repeat step 3.
- (6) Plot the behavior of the selected variables and reduce or increase the stiffness of the contact elements to achieve the behavior similar to that shown below (Figure 9.7b). Node D should remain in the horizontal space defined by nodes C and E (Figure 9.7c). The idealized gap formed by D-F-E is an important inclusion to the contact interface. This gap is necessary to eliminate "locking behavior" exhibited in Figure 9.10.

The process becomes simpler with experience, and is valid with any "penalty" parameter, such as the incompressible fluid options (Section 9.1.1b, Element Control Card and Section 10, Material Models, where a fluid bulk (penalty) modulus is selected). To avoid symmetry problems, the spring constants for tangential and normal components in Section 9.5.0, Frictional Slideline, should be selected as the same number.

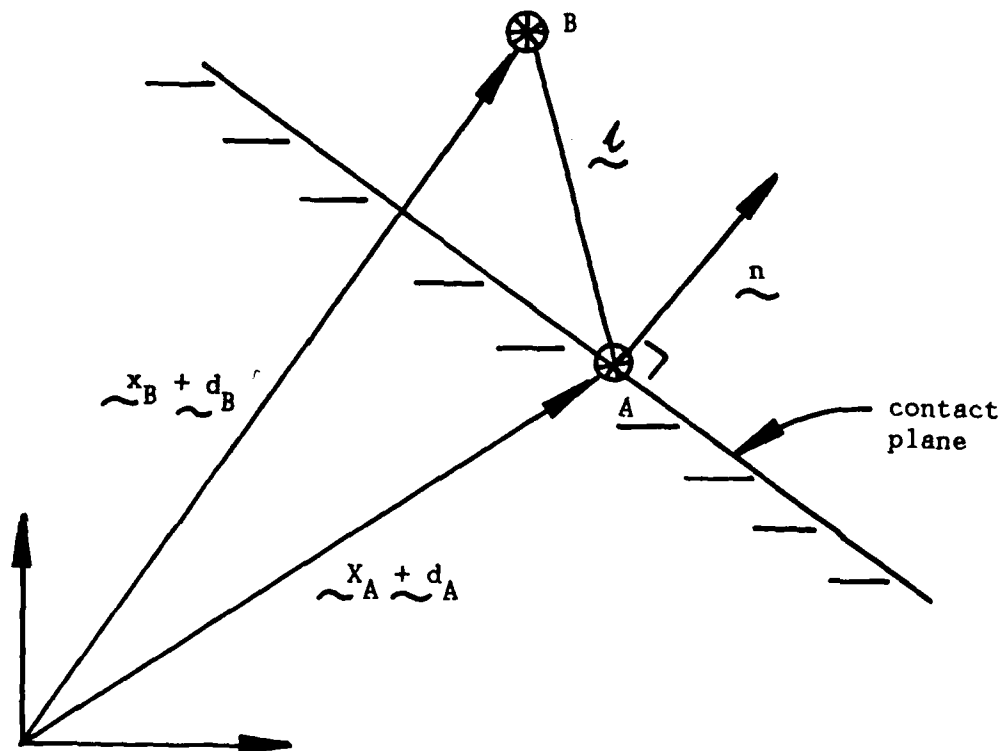


Figure 9.7a . Idealized contact element .

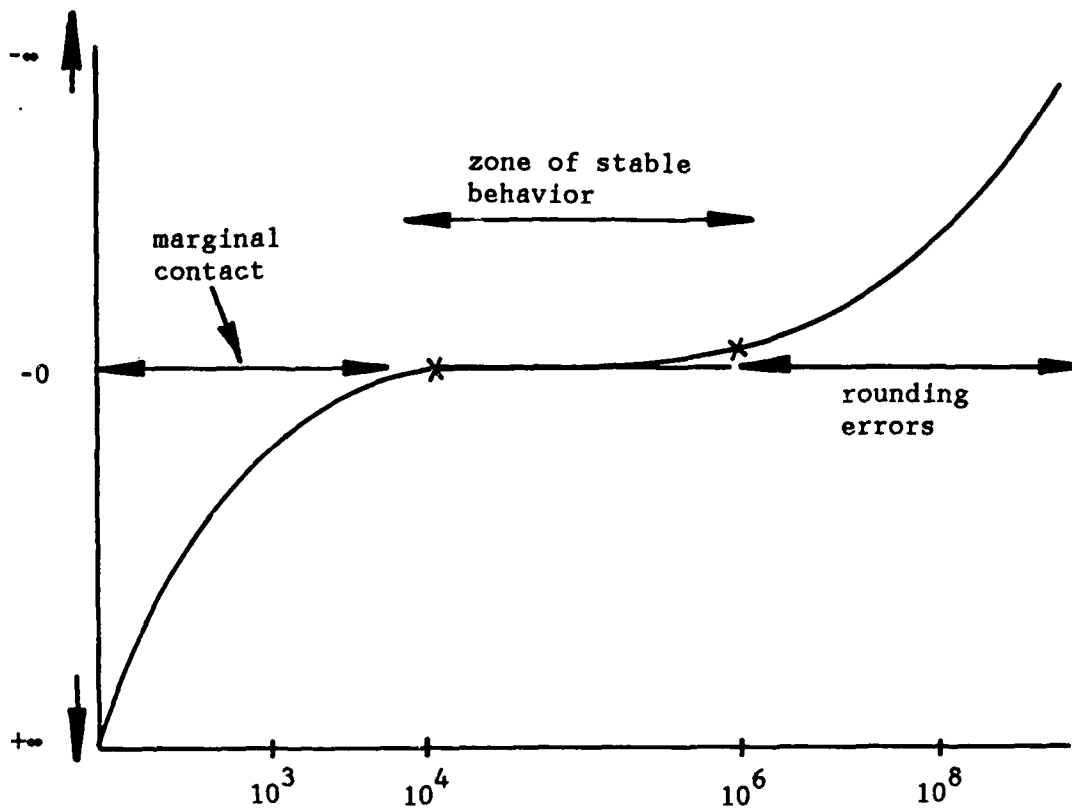
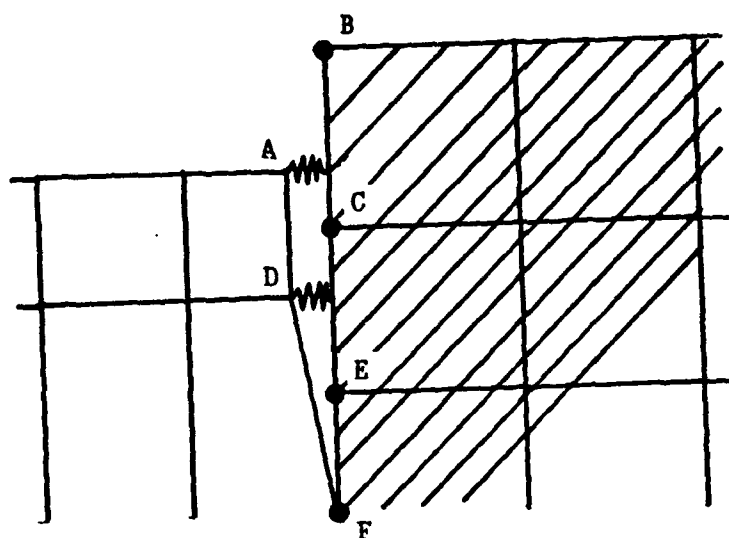
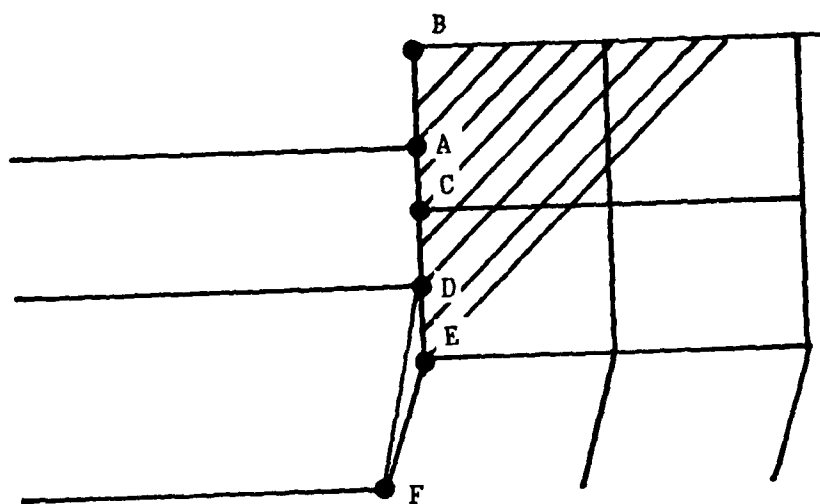


Figure 9.7b Contact penalty parameter behavior



idealized element
configuration



typical contact in
dynamically deformed
mesh

Figure 9.7c Contact element configuration

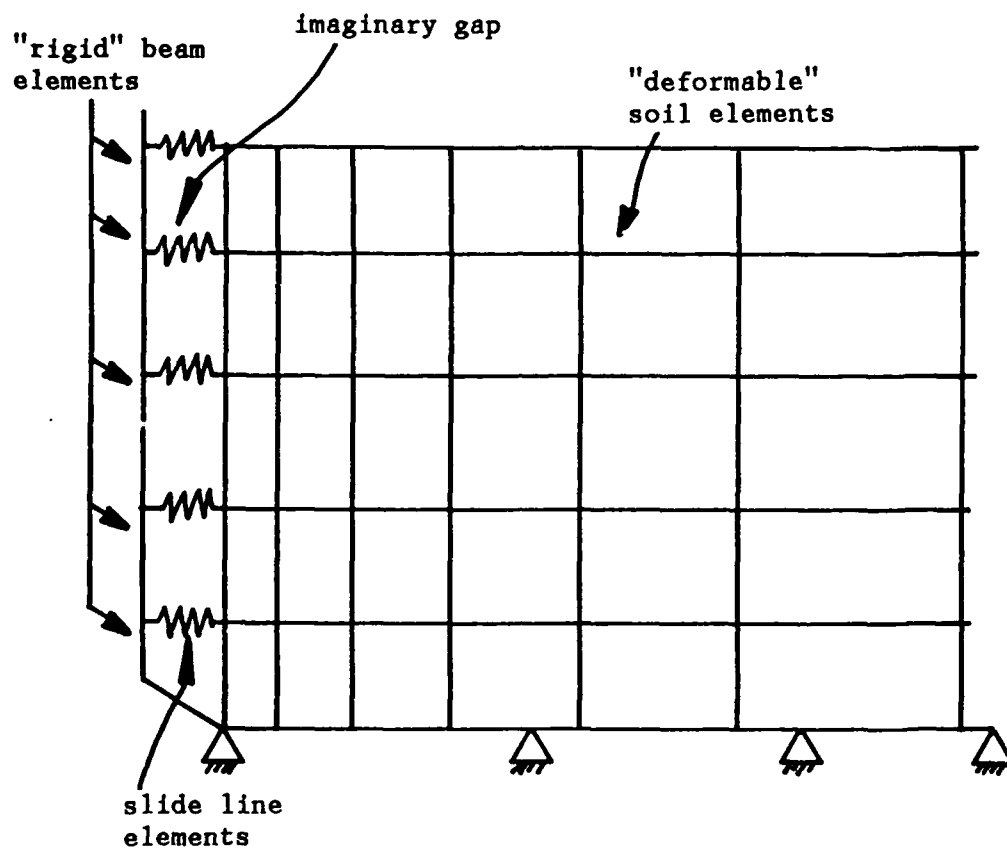


Figure 9.8 Idealized contact condition for slideline element, retaining wall

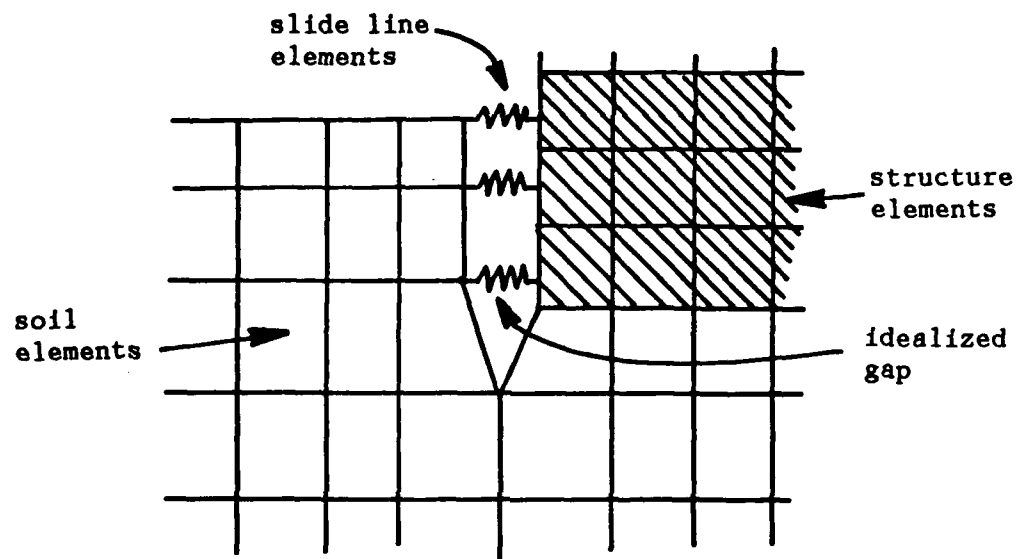


Figure 9.9 Idealized contact condition for slideline element, embedded structure

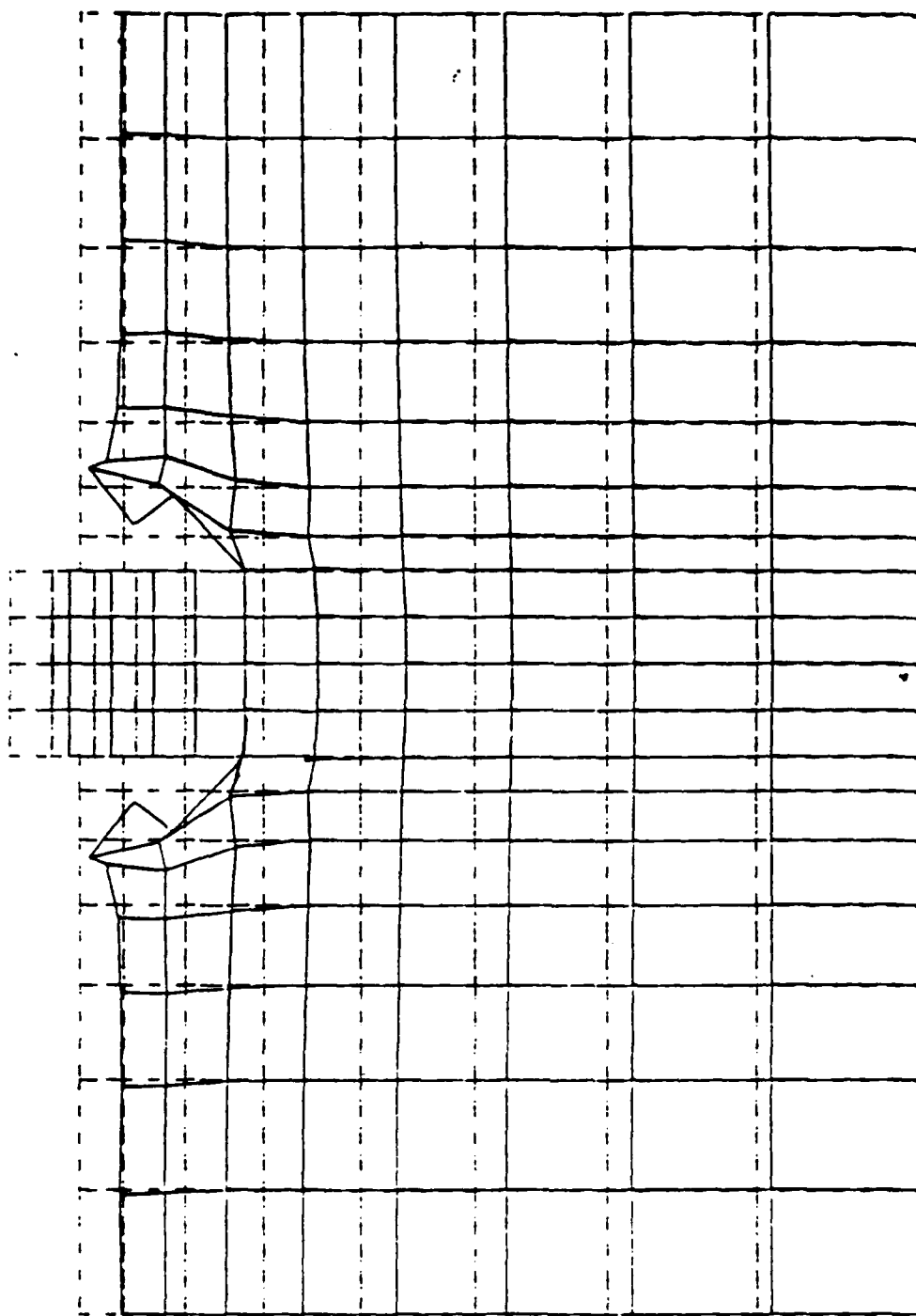


Figure 9.10 Mesh locking behavior

9.3.0 Contact Element

The contact element may be used to impose inequality constraints between nodes. Either perfect friction (i.e., "stick") or frictionless (i.e., "slip") conditions may be achieved.

A contact element is defined by two nodes, a spring constant, or "penalty parameter," k ; and a fixed direction vector, N . The present location of node A ($A = 1, 2$) is given by $X(A) + D(A)$, where $X(A)$ is the initial position vector and $D(A)$ is the displacement vector. The contact plane passes through the point $X(A) + D(A)$ and is perpendicular to N (Figure 9.7a).

The contact/release condition is defined as follows:

d.GT.0 release

d.LE.0 contact

where: $d = L \cdot N$

$$L = X(B) + D(B) - X(A) - D(A)$$

The quantity d is a measure of the distance between $X(B) + D(B)$ and the contact plane. When contact is noted, a contact element stiffness and out-of-balance force are added to the global equations. These arrays are defined as follows:

Stiffness matrices

(two-dimensional case)

$$K(\text{stick}) = k \begin{vmatrix} 1 & 0 & -1 & 0 \\ & 1 & 0 & -1 \\ \text{symm.} & & 1 & 0 \\ & & & 1 \end{vmatrix}$$

$$K(\text{slip}) = k \begin{vmatrix} n1n1 & n1n2 & -n1n1 & -n1n2 \\ & n2n2 & -n1n2 & -n2n2 \\ \text{symm.} & & n1n1 & n1n2 \\ & & & n2n2 \end{vmatrix} = k \begin{vmatrix} N & N \\ -N & -N \\ 0 & 0 \end{vmatrix}^T$$

(three-dimensional case)

$$K(\text{stick}) = k \begin{vmatrix} 1 & 0 & 0 & -1 & 0 & 0 \\ & 1 & 0 & 0 & -1 & 0 \\ & & 1 & 0 & 0 & -1 \\ & & & 1 & 0 & 0 \\ \text{symm.} & & & & 1 & 0 \\ & & & & & 1 \end{vmatrix}$$

$$K(\text{slip}) = k \begin{vmatrix} n1n1 & n1n2 & n1n3 & -n1n1 & -n1n2 & -n1n3 \\ & n2n2 & n2n3 & -n1n2 & -n2n2 & -n2n3 \\ & & n3n3 & -n1n3 & -n2n3 & -n3n3 \\ & & & n1n1 & n1n2 & n1n3 \\ \text{symm.} & & & & n2n2 & n2n3 \\ & & & & & n3n3 \end{vmatrix}$$

out-of-balance force

$$f = -K(\text{slip}) \begin{vmatrix} X(A) + D(A) \\ \\ X(B) + D(B) \end{vmatrix} = kd \begin{vmatrix} N \\ \\ -N \end{vmatrix}$$

If $k.GT.0$ is sufficiently large, the point $X(B) + D(B)$ will be forced to lie (approximately) on the contact plane. In subsequent steps, only the contact stiffness is assembled and the decision to remain in contact, or release, is made on the basis of the sign of d , as above.

For purposes of interpreting output, the contact element "displacement" is defined to be d , and the "force" is given by:

kd if $d.LT.0$

0 if $d.GE.0$

9.3.1 Element Group Control Card (6I5)

Note	Columns	Variable	Description
	1-5	NPAR(1)	The number 3 (=NTYPE)
	6-10	NPAR(2) (=NUMEL)	Number of elements in this group; GE.1
	11-15	NPAR(3) (=NUMAT)	Number of geometric/ material properties sets
(1)	16-20	NPAR(4) (=ISTIK)	Contact condition code EQ.0 "stick" option EQ.1 "slip" option
	21-25	NPAR(5) (=NOUT)	Number of force/displacement output histories
	26-30	NPAR(6) (=IST)	Spatial force/displacement output code EQ.0, Include spatial force/ displacement output for group EQ.1, Omit spatial force/ displacement output for group

Notes:

(1) The contact condition may be either perfect friction (i.e., "stick") or frictionless (i.e., "slip"). In the stick case, no relative motion is allowed between nodes when in contact. In the slip case, frictionless sliding is allowed in the contact plane. (The contact plane is defined to be perpendicular to a direction defined by the user. See Section 9.3.2, Geometric/Material Properties Cards.)

9.3.2 Geometric/Material Properties Cards (I5,5X,4F10.0)

Note	Columns	Variable	Description
	1-5	M	Geometric/material set number
	11-20	STIFF(M)	Spring constant k (i.e., "penalty parameter")
	21-30	AN(1,M)	Component 1 of direction vector N
	31-40	AN(2,M)	Component 2 of direction vector N
	41-50	AN(3,M)	Component 3 of direction vector N

9.3.3 Element Data Cards (5I5)

Note	Columns	Variable	Description
(1)	1-5	N	Element number
	6-10	MAT(N)	Geometric/material properties set number
	11-15	IEN(1,N)	Number of 1st node
	16-20	IEN(2,N)	Number of 2nd node
(2)	21-25	NG	Generation increment

Notes:

(1) All elements must be read in on an element data card or generated.
Terminate with a blank card.

(2) Element data cards may be generated by employing a two card sequence as follows:

Card 1: L,MAT(L),IEN(1,L),IEN(2,L),LG

Card 2: N,MAT(N),IEN(1,N),IEN(2,N)

N must be greater than L. The geometric/material set number for all

L, L+1, L+2, ..., N

is set to MAT(L) and the node numbers are incremented by LG.

9.3.4 Element Output History Cards (3I5)

"On-line" and Calcomp plots of contact element displacement and force may be obtained. Each component required is plotted versus time. Plots of this type are useful in providing quick information concerning the behavior of a contact element. The total number of components to be plotted must equal NOUT, which is defined on the element group control card (see Section 9.3.1).

Note	Columns	Variable	Description
(1)	1-5	N	Element number
	6-10	ITEMP (1)	Displacement (DELT) plot code EQ.0, no plot EQ.1, plot
	11-15	ITEMP (2)	Contact force (FORC) plot code EQ.0, no plot EQ.1, plot

Notes:

(1) Output history information is stored in the array IHS in element group data. The dimension of IHS is 2 x NOUT. The first row of IHS contains element numbers and the second row contains component numbers. Two components may be plotted as described above. Component numbers 1 and 2 correspond to DELT and FORC, respectively.

9.3.5 Storage Requirements for Two/Three-Dimensional Stick/Slip Contact Element (NTYPE = 3)

<u>First Word</u>	<u>Variable Array</u>
N101 = NF*	NPAR(16)
N102 = N101 + 16	IEN(2, NUMEL)
N103 = N102 + NUMEL*2	LM(NSD, 2, NUMEL)
N104 = N103 + NUMEL*2*NSD	IHS(2, NOUT)
N105 = N104 + NOUT*2	SOUT(NOUT, NTS + 1)
N106 = N105 + (NTS + 1)*NOUT	MAT(NUMEL)
N107 = N106 + NUMEL	STIFF(NUMAT)
N108 = N107 + NUMAT*IPREC	AN(NSD, NUMAT)
NL = N108 + NUMAT*NSD*IPREC	

(NL - NF + 1 = total required storage for element group.)

*NF is the address of the first word in blank common for the element group.

9.4.0 Slide-line Element

The slide-line element may be used to impose inequality constraints between nodes. Either perfect friction (i.e., "stick") or frictionless (i.e., "slip") conditions may be achieved.

A slide-line element is defined by three nodes and a spring constant or "penalty parameter," k . The connection from node A to node B defines the "slide-line" direction, and node C is the contact node (see Figure 9.11).

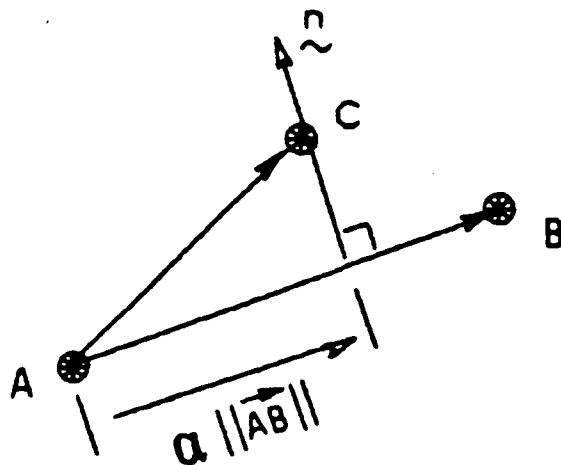


Figure 9.11 Slideline element

The projected distance of node C to node A onto the slide-line direction is denoted by a , and is given by:

$$a = \mathbf{AB} \cdot \mathbf{AC} / (\mathbf{AB} \cdot \mathbf{AB}) \quad 0.LE.a.LE.1$$

where "." denotes the dot product of two vectors. The direction of the unit vector \mathbf{N} normal to the slide-line direction is given by:

$$\mathbf{N} = (\mathbf{AB} \times \mathbf{AC}) \times \mathbf{AB} / || (\mathbf{AB} \times \mathbf{AC}) \times \mathbf{AB} ||$$

where "x" denotes the cross product of two vectors. The local contact stiffness matrix \mathbf{K} is given by

$$\mathbf{K} = k \begin{vmatrix} (1-a)(1-a) & a(1-a) & -(1-a) \\ & aa & -a \\ \text{symm.} & & 1 \end{vmatrix}$$

where the rows and columns are arranged such that the first, second and third rows (columns) correspond to nodes A, B and C, respectively. The contact/release condition is defined as follows:

0.LE.a.LE.1 contact

otherwise, release.

When contact is noted, a contact element stiffness and out-of-balance force are added to the global equations. These arrays are defined as follows:

Stiffness Matrix: (three-dimensional case)

$$K(\text{stick}) = \begin{array}{c} \begin{array}{cccccccccc} (1-a)(1-a) & 0 & 0 & a(1-a) & 0 & 0 & -(1-a) & 0 & 0 \\ & (1-a)(1-a) & 0 & 0 & a(1-a) & 0 & 0 & -(1-a) & 0 \\ & & (1-a)(1-a) & 0 & 0 & a(1-a) & 0 & 0 & -(1-a) \\ \text{symm.} & & & aa & 0 & 0 & -a & 0 & 0 \\ & & & & aa & 0 & 0 & -a & 0 \\ & & & & & aa & 0 & 0 & -a \\ & & & & & & 1 & 0 & 0 \\ & & & & & & & 1 & 0 \\ & & & & & & & & 1 \end{array} \end{array}$$

$$K(\text{slip}) = R^T K R$$

where

$$R = \begin{array}{c} \begin{array}{ccc} \begin{array}{c} T \\ N \end{array} & 0 & 0 \\ 0 & \begin{array}{c} T \\ N \end{array} & 0 \\ 0 & 0 & \begin{array}{c} T \\ N \end{array} \end{array} \end{array}$$

and

$$0 = \begin{array}{c} \begin{array}{ccc} 0 & 0 & 0 \end{array} \end{array}$$

Out-of-Balance Force

$$f = -K(\text{slip}) \begin{vmatrix} X(A) + D(A) \\ X(B) + D(B) \\ X(C) + D(C) \end{vmatrix}$$

If $k.GT.0$ is sufficiently large, the point C will be forced to lie (approximately) on the slide-line AB. In subsequent steps, only the contact stiffness is assembled and the decision to remain in contact, or not, is made as described above.

9.4.1 Element Group Control Card (4I5)

Note	Columns	Variable	Description
	1-5	NPAR(1) (=NTYPE)	The number 6
	6-10	NPAR(2) (=NUMEL)	Number of elements in this group; GE.1
	11-15	NPAR(3) (=NUMAT)	Number of geometric/material properties sets
(1)	16-20	NPAR(4) (=ISTIK)	Contact condition code EQ.0 EQ.0, "stick" option EQ.1, "slip" option

Notes:

(1) The contact condition may be either perfect friction (i.e., "stick") or frictionless (i.e., "slip"). In the stick case, no relative motion is allowed between nodes when in contact. In the slip case, frictionless sliding is allowed on the slide-line.

9.4.2 Geometric/Material Properties Cards (I5,5X,F10.0)

Note	Columns	Variable	Description
	1-5	M	Geometric/material set number
	11-20	STIFF(M)	Spring constant k (i.e., "penalty parameter") 0

9.4.3 Element Data Cards (6I5)

Note	Columns	Variable	Description
(1)	1-5	N	Element number
	6-10	MAT(N)	Geometric/material properties set number
	11-15	IEN(1,N)	Number of 1st node (A)
	6-20	IEN(2,N)	Number of 2nd node (B)
	21-25	IEN(3,N)	Number of 3rd node (C)
(2)	26-30	NG	Generation increment 0

Notes:

(1) All elements must be read in on an element data card or generated.
Terminate with a blank card.

(2) Element data cards may be generated by employing a two card sequence as follows:

Card 1: L,MAT(L),IEN(1,L),IEN(2,L),IEN(3,L),LG

Card 2: N,MAT(N),IEN(1,N),IEN(2,N),IEN(3,N)

N must be greater than L. The geometric/material set number for all

L, L + 1, L + 2, ..., N

is set to MAT(L) and the node numbers are incremented by LG.

9.4.4 Storage Requirements for Two/Three-Dimensional Stick/Slip Slide-line Element (NTYPE = 6)

<u>First Word</u>	<u>Variable Array</u>
N101 = NF*	NPAR(16)
N102 = N101 + 16	IEN(3, NUMEL)
N103 = N102 + NUMEL*3	LM(NSD, 3, NUMEL)
N104 = N103 + NUMEL*3*NSD	MAT(NUMEL)
N105 = N104 + NUMEL	STIFF(NUMAT)
NL = N105 + NUMAT*IPREC	

(NL - NF + 1 = total required storage for element group.)

*NF is the address of the first word in blank common for the element group.

9.5.0 Slide-line Element with Coulomb Friction

The slide-line element is defined by three nodes and two spring constants or "penalty parameters," K_1 and K_2 , in the tangential and normal directions, respectively. The connection from node A to node B defines the "slide-line" direction, and node C is the contact node (see Figure 9.12)

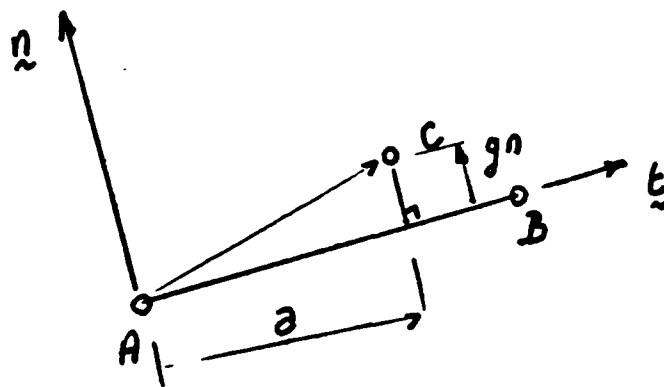


Figure 9.12 Frictional slideline element

The projected distance of node C to node A onto the slide-line direction is denoted by a , and is given by

$$a = \mathbf{AB} \cdot \mathbf{AC} / (\mathbf{AB} \cdot \mathbf{AB}) \quad 0.LE.a.LE.1$$

where "." denotes the dot product of two vectors. The tangent vector is defined as: $\mathbf{t} = \mathbf{AB} / |\mathbf{AB}|$. The direction of the unit vector \mathbf{n} normal to the slide-line direction is given by:

in 2D: by rotating the tangent vector 90 degrees counterclockwise,

$$\text{in 3D : } \mathbf{n} = -(\mathbf{AB} \times \mathbf{AC}) \times \mathbf{AB} / |(\mathbf{AB} \times \mathbf{AC}) \times \mathbf{AB}|$$

where "x" denotes the cross product of two vectors.

The relative normal displacement, or gap, is computed as:

$$g_n = |\mathbf{AB} \times \mathbf{AC}| / |\mathbf{AB} \cdot \mathbf{AB}|$$

and the relative slip as:

$$g_t = a - a(0)$$

where $a(0)$ is the relative position at which node C first contacted the line AB. The normal and tangential stresses are computed as:

$$SN = k_2 * gn \quad \text{and} \quad ST = k_1 * gt$$

There normal stress must be compressive, i.e.,

$$SN \leq 0$$

and the tangential stress such that

$$|ST| \leq -\tan(\phi) * SN (*)$$

where ϕ = friction angle. The Coulomb friction law is associated with a nonslip condition which states that

$$gt = 0 \text{ if the inequality } (*) \text{ is met}$$

and a directional constraint that requires the friction force to always act opposite to the direction of the relative slip of node C with respect to nodes A and B. A return procedure is used to enforce inequality (*) when violated.

The local contact stiffness matrix K is given by

$$K = k \begin{vmatrix} (1-a)(1-a) & a(1-a) & -(1-a) \\ & aa & -a \\ \text{symm.} & & 1 \end{vmatrix}$$

where $k = k_1$ and k_2 for the tangential and normal directions, respectively, and where the rows and columns are arranged such that the first, second and third rows (columns) correspond to nodes A, B, and C, respectively. The contact/release condition is defined as follows:

$$0 \leq SN \leq 1 \quad \text{and} \quad SN \leq 0 \quad \text{contact}$$

otherwise, release.

When contact is noted, a contact element stiffness and out-of-balance force are added to the global equations, by rotating the local stiffness and force to the global axes.

9.5.1 Element Group Control Card (3I5)

Note	Columns	Variable	Description
	1-5	NPAR(1) (=NTYPE)	The number 8 for nodal damping
	6-10	NPAR(2) (=NUMEL)	Number of elements in this group; GE.1
	11-15	NPAR(3) (=NUMAT)	Number of material properties sets properties sets

9.5.2 Geometric/Material Properties Cards (I5,5X,3F10.0)*NUMAT

Note	Columns	Variable	Description
	1-5	M	Geometric/material set number
	11-20	STIFF(1,M)	Spring constant k1
	21-30	STIFF(2,M)	Spring constant K2
	31-40	STIFF(3,M)	Friction angle (degrees)

9.5.3 Element Data Cards (6I5)

Note	Columns	Variable	Description
(1)	1-5	N	Element number
	6-10	MAT(N)	Geometric/material properties set number
	11-15	IEN(1,N)	Number of 1st node (A)
	16-20	IEN(2,N)	Number of 2nd node (B)
	21-25	IEN(3,N)	Number of 3rd node (C)
(2)	26-30	NG	Generation increment

Notes:

(1) All elements must be read in on an element data card or generated.
Terminate with a blank card.

(2) Element data cards may be generated by employing a two card sequence as follows:

Card 1 : L, MAT(L), IEN(1,L), LG

Card 2 : N, MAT(N), IEN(1,N)

N must be greater than L. The material set number for all

L + 1, L + 2, ..., N

is set equal to MAT(L) and the node numbers are incremented by LG.

9.5.4 Storage Requirements for Two/Three-Dimensional Nodal Damping/Mass Elements (NTYPE = 8 and 9)

<u>First Word</u>	<u>Variable Array</u>
N101 = NF*	NPAR(16)
N102 = N101 + 16	IEN(3, NUMEL)
N103 = N102 + NUMEL*3	LM(NDOF, 3, NUMEL)
N104 = N103 + NUMEL*3*NSD	MAT(NUMEL)
N105 = N104 + NUMEL	STIFF(NUMAT,3)
N106 = N105 + NUMAT*IPREC*3	ICON(NUMEL)
N107 = N106 + NUMEL	GLIDE(NUMEL)
NL = N107 + NUMEL*IPREC	

(NL - NF + 1 = total required storage for element groups.)

*NF is the address of first word in blank common for the element group.

9.6.0 Nodal Mass/Damping Element

9.6.1 Element Group Control Card (3I5)

Note	Columns	Variable	Description
	1-5	NPAR(1) (=NTYPE)	The number 8 for nodal damping The number 9 for nodal mass
	6-10	NPAR(2) (=NUMEL)	Number of elements in this group: GE.1
	11-15	NPAR(3) (=NUMAT)	Number of material properties sets

9.6.2 Material Properties Cards (I5,5X,ND0F*F10.0)*NUMAT

Note	Columns	Variable	Description
	1-5	M	Material set number
	11-20	DAMPG(1)/ MASS(1)	Nodal value DOF component 1
	21-30	DAMPG(2)/ MASS(2)	Nodal value DOF component 2
	31-40	DAMPG(3)/ MASS(3)	Nodal value DOF component 3
	:	:	:
	:	:	:

General:

Nodal mass/damping element may be used in conjunction with any elements to achieve various physical restraints at the boundaries. Mass element use is self explanatory, with only a caution given to proper identification of units.

Sizing of damping elements is achieved for elastic material through the following equation:

$$C = \rho \cdot c_d \frac{h}{2}$$

where: C = damping constant

ρ = mass density of material

h = height (or width) of the element being damped..

$$c_d = \sqrt{D/\rho}, \text{ D represents the shear or bulk modulus depending on the type of wave being damped (i.e., shear or compression)}$$

C_d therefore represents the wave speed through the elastic portion of the material.

Selection of damping constants for elasto-plastic materials can best be done with the equations given above. The plastic moduli will generally be somewhat softer than the elastic, thereby reducing the wave speed, and boundary effects in a "self damping" manner.

Note that damping elements applied to fixed nodes will have no effect on the finite element model.

9.6.3 Element Data

Note	Columns	Variable	Description
(1)	1-5	N	Element number
	6-10	MAT(N)	Material Properties set number
	11-15	IEN(1,N)	Node number
(2)	16-20	NG	Generation increment

Note:

(1) All elements must be read in on an element data card or generated.
Terminate with a blank card.

(2) Element data cards may be generated by employing a two card sequence as follows:

Card 1 : L, MAT(L), IEN(1,L), LG

Card 2 : N, MAT(N), IEM(1,N)

N must be greater than L. The material set number for all

L + 1, L + 2,, N

is set equal to MAT(L) and the node numbers are incremented by LG.

9.6.4 Storage Requirements for Two/Three-Dimensional Nodal Damping/Mass Elements (NYPE = 8 and 9)

<u>First Word</u>	<u>Variable Array</u>
N101 = NF*	NPAR(16)
N102 = N101 + 16	IEN(1,NUMEL)
N103 = N102 + NUMEL	LM(NDOF, 1, NUMEL)
N104 = N103 + NUMEL*NDOF	MAT(NUMEL)
N105 = N104 + NUMEL	DAMPG(NDOF, NUMAT)/ MASS (NDOF, NUMAT)
NL = N105 + NUMAT*NDOF*IPREC	
(NL - NF + 1 = total required storage for element groups)	

*NF is the address of the first word in blank common for the element group.

9.7.0 Two- and Three-Dimensional Truss Element

Truss elements connect two points in space and transmit axial force only. There are three possible degrees of freedom at each of the two nodes (i.e., the x1, x2, and x3 translations). When employing truss elements, NSD must be GE.2 and NDOF must be GE.NSD on the master control card (see Section 2.0). The following sequence of cards is used to describe truss elements:

9.7.1 Element Group Control Card (815)

Note	Columns	Variable	Description
	1-5	NPAR(1) (=NTYPE)	The number 14
	6-10	NPAR(2) (=NUMEL)	Number of elements in this group; GE.1
(1)	11-15	NPAR(3) (=NUMAT)	Number of geometric/material sets in this group; GE.0 if EQ.0, set internally to 1 0
	16-20	NPAR(4) (=IFD)	Finite deformation code EQ.0, finite deformation effects neglected; EQ.1, finite deformation effects included
(2)	21-25	NPAR(5) (=NOUT)	Number of stress/force output histories
	26-30	NPAR(6) (=IST)	Spatial stress/force output code EQ.0, Include spatial output for group EQ.1, Omit spatial output for group
(3)	31-35	NPAR(7) (LCASG)	Gravity load case number; GE.0 if EQ.0, set internally to 1 0
	36-40	NPAR(8) (=AXIAL)	Geometric Stiffness Code; GE.0 EQ.1, Included

Notes:

- (1) Defines number of geometric/material properties cards to be input in Section 9.7.2.
- (2) Not implemented (set internally EQ.0)
- (3) The load case number corresponds to the load-time function input in Section 8.0.

9.7.2 Geometric/Material Properties Cards (I5,5X,3F10.0)

Note	Columns	Variable	Description
(1)	1-5	N	Material identification number
	11-20	E(N)	Young's modulus
	21-30	AREA(N)	Cross-section area
(2)	31-40	WT(N)	Mass density per unit length

Notes:

- (1) One card is required for each set of elements possessing the same cross-section and material properties.
- (2) The product of weight per unit length and length defines gravity loads for the truss element.

9.7.3 Gravity Load Multiplier Card (3F10.0)

Note	Columns	Variable	Description
(1)	1-10	GRAV(1)	Multiplier of gravity load in the x1 direction
	11-20	GRAV(2)	Multiplier of gravity load in the x2 direction
	21-30	GRAV(3)	Multiplier of gravity load in the x3 direction

Notes:

(1) Gravity load multipliers may be used to define the components of the gravity vector with respect to the global x1, x2, x3 system. For example, if the gravity load multipliers are

0.0, 0.0, -1.0,

then the entire gravitational load acts in the -x3 direction.

9.7.4 Element Data Cards (5I5)

Note	Columns	Variable	Description
(1)	1-5	N	Element number
	6-10	MAT(N)	Geometric/material properties set number
	11-15	IEN(1,N)	Number of 1st node
	16-20	IEN(2,N)	Number of 2nd node
(2)	21-25	NG	Generation increment

Notes:

(1) All elements must be input on an element data card or generated.
Terminate with a blank card.

(2) Element data cards may be generated by employing a two card sequence as follows:

Card 1: L,MAT(L),IEN(1,L),IEN(2,L),LG

Card 2: N,MAT(N),IEN(1,N),IEN(2,N)

N must be greater than L. The geometric/material set number for all elements

L + 1, L + 2, ..., N

is set to MAT(L), and the node numbers are incremented by LG.

9.7.5 Element Output History Cards (3I5)

"On-line" and Calcomp plots of truss element axial stress and force may be obtained. Each component required is plotted versus time. The total number of components to be plotted must be equal to NOUT, which is defined on the element group control card (see Section 9.7.1).

Note	Columns	Variable	Description
(1)	1-5	N	Element number
	6-10	ITEMP(1)	Axial stress plot code (STRS) EQ.0, no plot EQ.1, plot
	11-15	ITEMP(2)	Axial force plot code (FORC) EQ.0, no plot EQ.1, plot 0

Notes:

(1) Output history information is stored in the array IHS in element group data. The dimension of IHS is 2 x NOUT. The first row of IHS contains element numbers and the second row contains component numbers. Two components may be plotted as described above. Component numbers 1 and 2 correspond to STRS and FORC, respectively.

9.7.6 Storage Requirements for Two/Three-Dimensional Truss Element (NTYPE = 14)

<u>First Word</u>	<u>Variable Array</u>
N101 = NF*	NPAR(16)
N102 = N101 + 16	IEN(2,NUMEL)
N103 = N102 + NUMEL*2	LM(NSD,2,NUMEL)
N104 = N103 + NUMEL*2*NSD	IHS(2,NOUT)
N105 = N104 + NOUT*2	SOUT(NOUT,NTS+1)
N106 = N105 + (NTS+1)*NOUT	MAT(NUMEL)
N107 = N106 + NUMEL	E(NUMAT)
N108 = N107 + NUMAT*IPREC	AREA(NUMAT)
N109 = N108 + NUMAT*IPREC	WT(NUMAT)
N110 = N109 + NUMAT*IPREC	GRAV(3)
NL = N110 + 3*IPREC	
(NL - NF + 1 = total required storage for element group)	

*NF is the address of the first word in blank common for the element group.

9.8.0 Two- and Three-Dimensional Beam Element

Beam elements connect two points in space and transmit forces (axial and shear) and moments (torsion and bending). In 2D analysis there are three possible degrees of freedom at each of the two nodes (i.e., two translations and one rotation). In 3D analysis there are six possible degrees of freedom at each of the two nodes (i.e., three translations and three rotations). The local sign convention for the beam element is shown in Figure 9.13. When employing beam elements, NSD must be GE.2 and NDOF must be GE.3 if NSD.EQ.2, and NDOF must be GE.6 if NSD.EQ.3. The sequence of cards used to describe beam elements is given in the next sections.

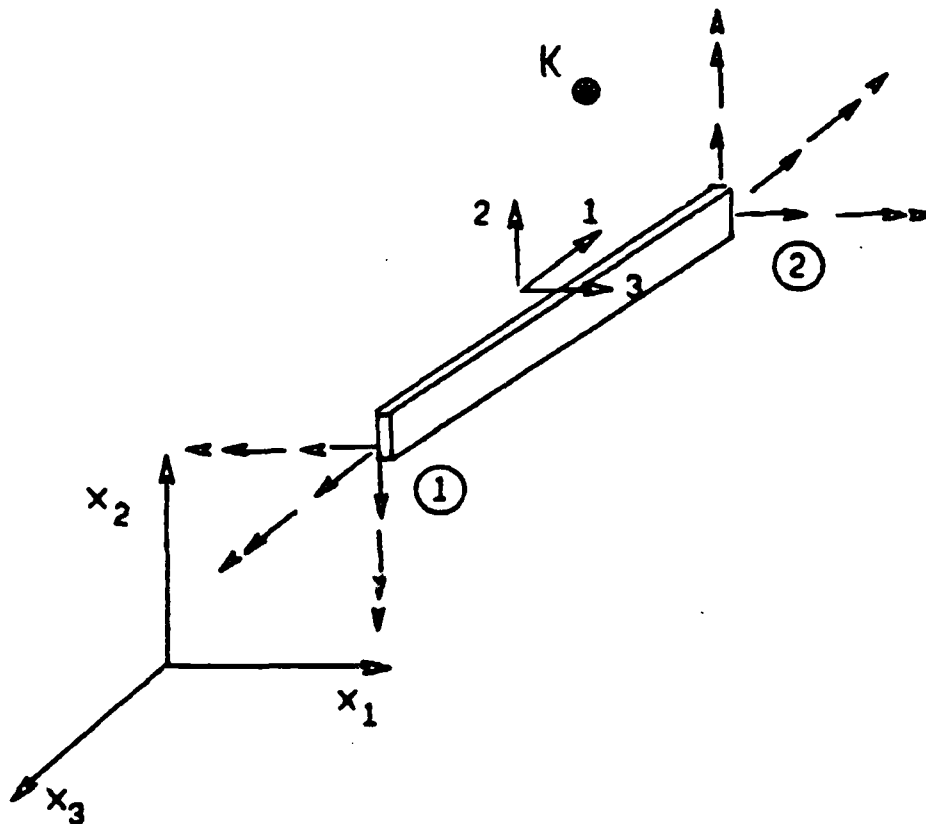


Figure 9.13 Local coordinate system for beam element

General:

DYNAFLOW incorporates both elastic and elasto-plastic beam elements, Sections 9.8.1 and 9.8.2, respectively. The elastic beam element is reasonably well explained. The inclusion of a point k coordinate for the two-dimensional model is shown in Figure 9.14, and allows the moment computation.

The elasto-plastic beam element detailed in Section 9.8.2 allows incorporation of nonlinear behavior for modeling of concrete, composite, or steel beams beyond initial yield. Again, the explanations for the element data are complete.

Section 9.3.7.3.2 describes the elasto-plastic constitutive model. The model uses a variation of the other multisurface models listed in Section 10. Figure 9.15 shows a typical nonlinear stress-strain curve. The horizontal dashed lines represent the bold surfaces. In this case there is no offset "a" and the behavior would be symmetric in compression and tension.

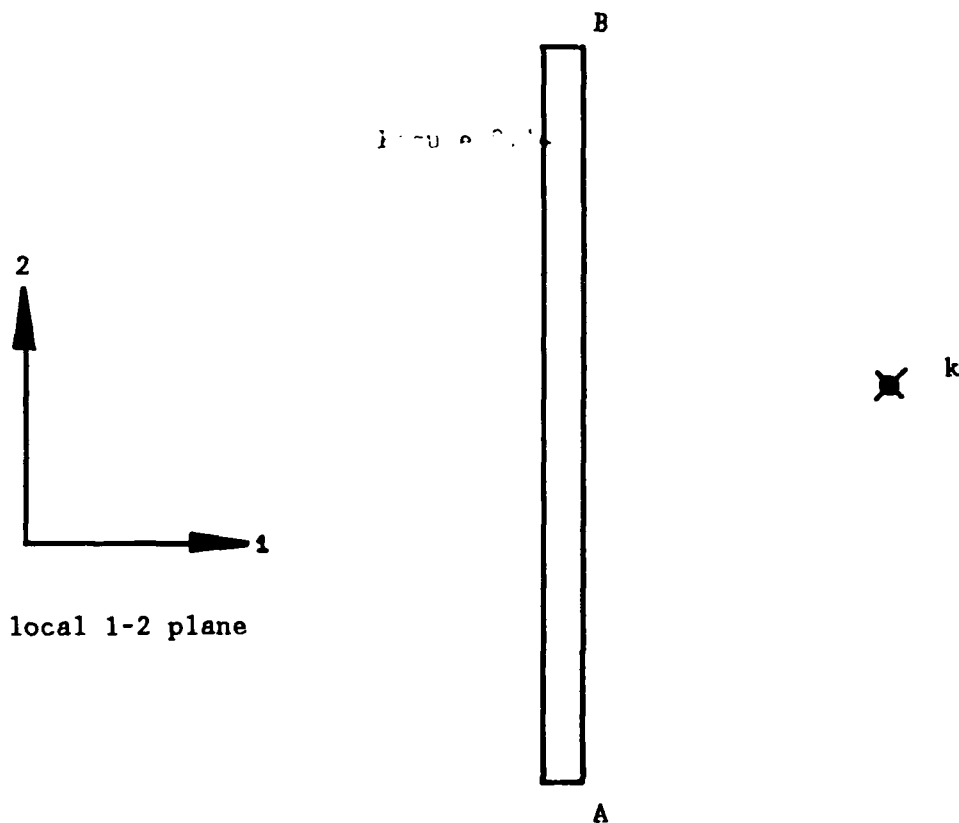


Figure 9.14 Beam element in 1-2 plane

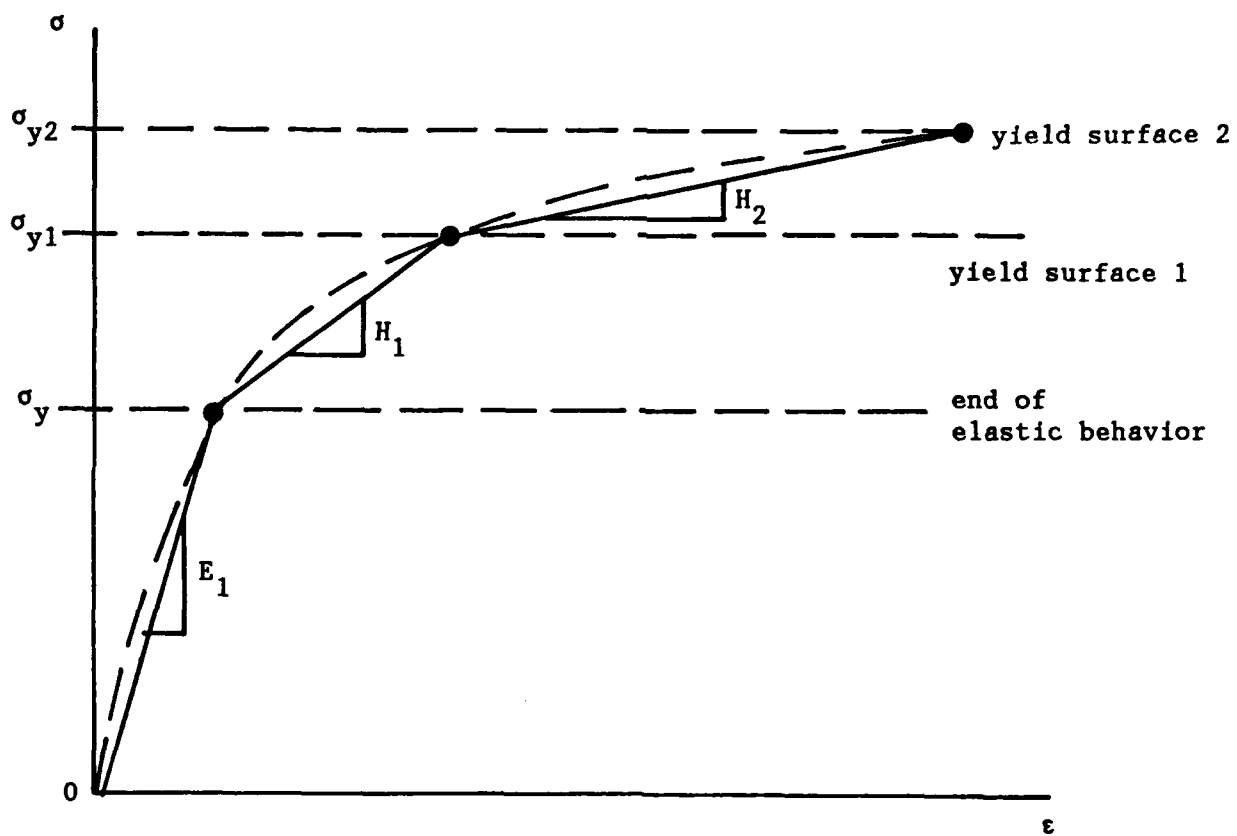


Figure 9.15 Non-linear material model description for beam element

9.8.1.1 Element Group Control Card (8I5)

Note	Columns	Variable	Description
	1-5	NPAR(1) (=NTYPE)	The number 15
	6-10	NPAR(2) (=NUMEL)	Number of elements in this group; GE.1
(1)	11-15	NPAR(3) (=NUMAT)	Number of geometric/material sets in this group; GE.0 if EQ.0, set internally to 1
	16-20	NPAR(4) (=IFD)	Finite Deformation Code EQ.0, Finite deformation Effects neglected EQ.1, Finite deformation Effects included
(2)	21-25	NPAR(5) (=NOUT)	Number of force/moment output histories
	26-30	NPAR(6) (=IST)	Spatial force/moment output code EQ.0, Include spatial output for group EQ.1, Omit spatial output for group
	31-35	NPAR(7) (=LCASG)	Gravity load case number; GE.0 if EQ.0, set internally to 1
	36-40	NPAR(8) (=AXIAL)	Geometric Stiffness Code; GE.0 EQ.1, Included

Notes:

(1) Defines number of geometric/material properties to be input in Section 9.8.1.2.

(2) Not implemented (set internally EQ.0)

(3) The load case number corresponds to the load-time function input in Section 8.0.

9.8.1.2 Geometric/Material Properties Cards (NUMAT sets of 2 cards)

9.8.1.2.1 Card 1 (I5,5X,7F10.0)

Note	Columns	Variable	Description
(1)	1-5	N	Material identification number
	11-20	E(N)	Young's Modulus
	21-30	G(N)	Shear Modulus
	31-40	AREA(N)	Cross-section area
	41-50	XI1(N)	Moment of inertia, I(11) (Torsional)
	51-60	XI2(N)	Moment of inertia, I(22) (Transverse)
	61-70	XI3(N)	Moment of inertia, I(33) (Bending)
(2)	71-80	WT(N)	Mass density per unit length

Notes:

- (1) One set of two cards is required for each material set.
- (2) The product of weight per unit length and length defines gravity loads for the beam element.

9.8.1.2.2 Card 2 (3F10.0)

Note	Columns	Variable	Description
(3)	1-10	XK(1)	Point K; coordinate x1
	11-20	XK(2)	Point K; coordinate x2
	21-30	XK(3)	Point K; coordinate x3

Notes:

(1) K is any point which lies in the local 1-2 plane (not on the 1-axis). See Figure 9.13.

9.8.1.3 Gravity Load Multiplier Card (3F10.0)

Note	Columns	Variable	Description
(1)	1-10	GRAV(1)	Multiplier of gravity load in the x1-direction
	11-20	GRAV(2)	Multiplier of gravity load in the x2-direction
	21-30	GRAV(3)	Multiplier of gravity load in the x3-direction

Notes:

(1) Gravity load multipliers may be used to define the components of the gravity vector with respect to the global x1, x2, x3 system.

9.8.1.4 Element Data Cards (5I5)

Note	Columns	Variable	Description
(1)	1-5	N	Element number
	6-10	MAT(N)	Geometric/material properties set number
	11-15	IEN(1,N)	Number of 1st node
	16-20	IEN(2,N)	Number of 2nd node
(2)	21-25	NG	Generation increment

Notes:

(1) All elements must be input on an element data card or generated.
Terminate with a blank card.

(2) Element data cards may be generated by employing a two card
sequence as follows:

Card 1: L,MAT(L),IEN(1,L),IEN(2,L),LG

Card 2: N,MAT(N),IEN(1,N),IEN(2,N)

N must be greater than L. The geometric/material set number for
all elements

L + 1, L + 2, ..., N

is set to MAT(L), and the node numbers are incremented by LG.

9.8.1.5 Storage Requirements for Two/Three-Dimensional Beam Element (NTYPE=15)

<u>First Word</u>	<u>Variable Array</u>
N101 = NF*	NPAR(16)
N102 = N101 + 16	IEN(2,NUMEL)
N103 = N102 + NUMEL*2	LM(NED,2,NUMEL)
N104 = N103 + NUMEL*2*NED**	IHS(2,NOUT)
N105 = N104 + NOUT*2	SOUT(NOUT,NTS+1)
N106 = N105 + (NTS+1)*NOUT	MAT(NUMEL)
N107 = N106 + NUMEL	E(NUMAT)
N108 = N107 + NUMAT*IPREC	G(NUMAT)
N109 = N108 + NUMAT*IPREC	AREA(NUMAT)
N110 = N109 + NUMAT*IPREC	XI1(NUMAT)
N111 = N110 + NUMAT*IPREC	XI2(NUMAT)
N112 = N111 + NUMAT*IPREC	XI3(NUMAT)
N113 = N112 + NUMAT*IPREC	WT(NUMAT)
N114 = N113 + NUMAT*IPREC	XK(3,NUMAT)
N115 = N114 + 3*NUMAT*IPREC	GRAV(3)
NL = N115 + 3*IPREC	

(NL-NF+1 = total required storage for element group)

*NF is the address of the first word in blank common for the element group.

**NED is the number of degrees of freedom per node:

if NSD.EQ.2, NED.EQ.3
if NSD.EQ.3, NED.EQ.6

9.8.2.0 Two- and Three-Dimensional Linear/Nonlinear Beam Element

Beam elements connect two points in space and transmit forces (axial and shear) and moments (torsion and bending). In 2D analysis there are three possible degrees of freedom at each of the two nodes (i.e., two translations and one rotation). In 3D analysis there are six possible degrees of freedom at each of the two nodes (i.e., three translations and three rotations). The local sign convention for the beam element is shown in Figure 9.13. When employing beam elements, NDOF must be GE.3 if NSD.EQ.2, and NDOF must be GE.6 if NSD,EQ.3. The sequence of cards used to describe beam elements is given in the next sections.

9.8.2.1 Element Group Control Card (815)

Note	Columns	Variable	Description
	1-5	NPAR(1) (=NTYPE)	The number 25
	6-10	NPAR(2) (=NUMEL)	Number of elements in this group; GE.1
(1)	11-15	NPAR(3) (=NUMAT)	Number of geometric sets in this group; GE.0 if EQ.0, set internally to 1
	16-20	NPAR(4) (=IFD)	Finite Deformation Code EQ.0, Finite deformation Effects neglected EQ.1, Finite deformation Effects included
(2)	21-25	NPAR(5) (=NOUT)	Number of force/moment output histories
	26-30	NPAR(6) (=IST)	Spatial force/moment output code EQ.0, Include spatial output for group EQ.1, Omit spatial output for group
(3)	31-35	NPAR(7) (=LCASG)	Gravity load case number; GE.0 if EQ.0, set internally to 1
(4)	36-40	NPAR(8) (=AXIAL)	Geometric Stiffness Code; GE.0 EQ.1, Included

Note:

(1) Defines number of geometric properties to be input in Section 9.8.2.3. Geometric sets refers to the number of different beam cross-sections to be input, Section 9.8.2.3.

Inclusion of deformation effects will invoke a total Lagrangian algorithm, and deformation effects will be included in the stiffness for the beam elements.

- (2) Not implemented (set internally EQ.0)
- (3) The load case number corresponds to the load-time function input in Section 8.0.
- (4) Inclusion of geometric stiffness is used in conjunction with Finite Deformation Code.

9.8.2.2. Material Properties Cards

The data cards for material properties follow the element group control card. Consult Section 9.8.3 for the required input of the individual material models.

9.8.2.3 Geometric Properties Cards (I5,5X,7F10.0)*NUMAT

Note	Columns	Variable	Description
	1-5	N	Geometric identification number
	11-20	AREA(N)	Cross-section area
	21-30	XI1(N)	Torsional moment of inertia, I11
	31-40	XI3(N)	Bending moment of inertia, I33
	41-50	WT(N)	Mass density per unit length
(1)	51-60	XK(1,N)	Point K; coordinate x1
	61-70	XK(2,N)	Point K; coordinate x2
	71-80	XK(3,N)	Point K; coordinate x3

Notes:

(1) K is any point which lies in the local 1-2 plane (not on the 1-axis) (see Figure 9.14).

9.8.2.4 Gravity Load Multiplier Card (3F10.0)

Note	Columns	Variable	Description
(1)	1-10	GRAV(1)	Multiplier of gravity load in the x1-direction
	11-20	GRAV(2)	Multiplier of gravity load in the x2-direction
	21-30	GRAV(3)	Multiplier of gravity load in the x3-direction

Notes:

(1) Gravity load multipliers may be used to define the components of the gravity vector with respect to the global x1, x2, x3 system.

9.8.2.5 Element Data Cards (5I5)

Note	Columns	Variable	Description
(1)	1-5	N	Element number
	6-10	MAT(N)	Geometric properties set number, LE. NUMAT
	11-15	IEN(1,N)	Number of 1st node
	16-20	IEN(2,N)	Number of 2nd node
(2)	21-25	NG	Generation increment

Notes:

(1) All elements must be input on an element data card or generated.
Terminate with a blank card.

(2) Element data cards may be generated by employing a two card sequence as follows:

Card 1: L,MAT(L),IEN(1,L),IEN(2,L),LG

Card 2: N,MAT(N),IEN(1,N),IEN(2,N)

N must be greater than L. The geometric set number for all elements

L + 1, L + 2, , N

is set to MAT(L), and the node numbers are incremented by LG.

9.8.2.6 Storage Requirements for Beam Element (NTYPE=25)

<u>First Word</u>	<u>Variable Array</u>
N101 = NF*	NPAR(16)
N102 = N101 + 16	IEN(2,NUMEL)
N103 = N102 + NUMEL*2	LM(NED,2,NUMEL)
N104 = N103 + NUMEL*2*NED**	IHS(2,NOUT)
N105 = N104 + NOUT*2	SOUT(NOUT,NTS+1)
N106 = N105 + (NTS+1)*NOUT	MAT(NUMEL)
N107 = N106 + NUMEL	XHH(NUMAT)
N108 = N107 + NUMAT*IPREC	XWW(NUMAT)
N109 = N108 + NUMAT*IPREC	WT(NUMAT)
N110 = N109 + NUMAT*IPREC	GRAV(NSD)
N111 = N110 + NDS*IPREC	XI1(NUMAT)
N112 = N111 + NUMAT*IPREC	XK(3,NUMAT)
MF = N112 + NUMAT*3*IPREC	Material data array
NL = ML***	

(NL-NF+1 total required storage for element group)

*NF is the address of the first word in blank common for the element group.

**NED is the number of degrees of freedom per node:

if NSD.EQ.2, NED.EQ.3
if NSD.EQ.3, NED.EQ.6

***ML depends upon the particular material model (see Section 9.8.3)

9.8.3 MATERIAL DATA

9.8.3.1.0 Linear Elasticity Model

9.8.3.1.1 Material Control Card (15)

Note	Columns	Variable	Description
	1-5	MATYP	The number 1

9.8.3.1.2 Material Properties Card (2F10.0)

Note	Columns	Variable	Description
	1-10	E	Young's modulus
	11-20	POIS	Poisson's ratio

9.8.3.1.3 Storage Requirements

<u>First Word</u>	<u>Variable Array</u>
MF	MATYP
M1 = MF + 1	E
ML = M1 + IPREC	POIS

(ML - MF + 1 = total required storage for material in element group data).

9.8.3.2.0 Elasto-Plastic Constitutive Models

The yield function in this case is of the following type

$$f = (s - a)(s - a) - k*k = 0$$

where s is the stress, a is the offset of the yield surface, and K , the yield stress, is the size of the yield surface.

The relationship between the elastic modulus E , the plastic modulus H' , and the elasto-plastic modulus H is given by

$$1/H = 1/E + 1/H'$$

A collection of nested yield surfaces may be used. This allows for the adjustment of the plastic hardening rule to any experimental hardening data; for example, data obtained from axial tests. It is assumed that the yield surfaces are all similar, and that a plastic modulus is associated with each one (Figure 9.16).

Several different plastic hardening rules may be selected by specifying the value of PLTYP, as indicated below:

PLTYP = 0 Isotropic hardening rule

The yield surfaces in this case do not change position, but merely increase in size as loading proceeds. The elasto-plastic moduli must be selected such that each H.GE.0 (Figure 9.17).

PLTYP = 1 Kinematic hardening rule

In this case, the yield surfaces do not change size, but are translated in stress space by the stress point. The elasto-plastic moduli must be selected such that each H.GE.0 (Figure 9.18).

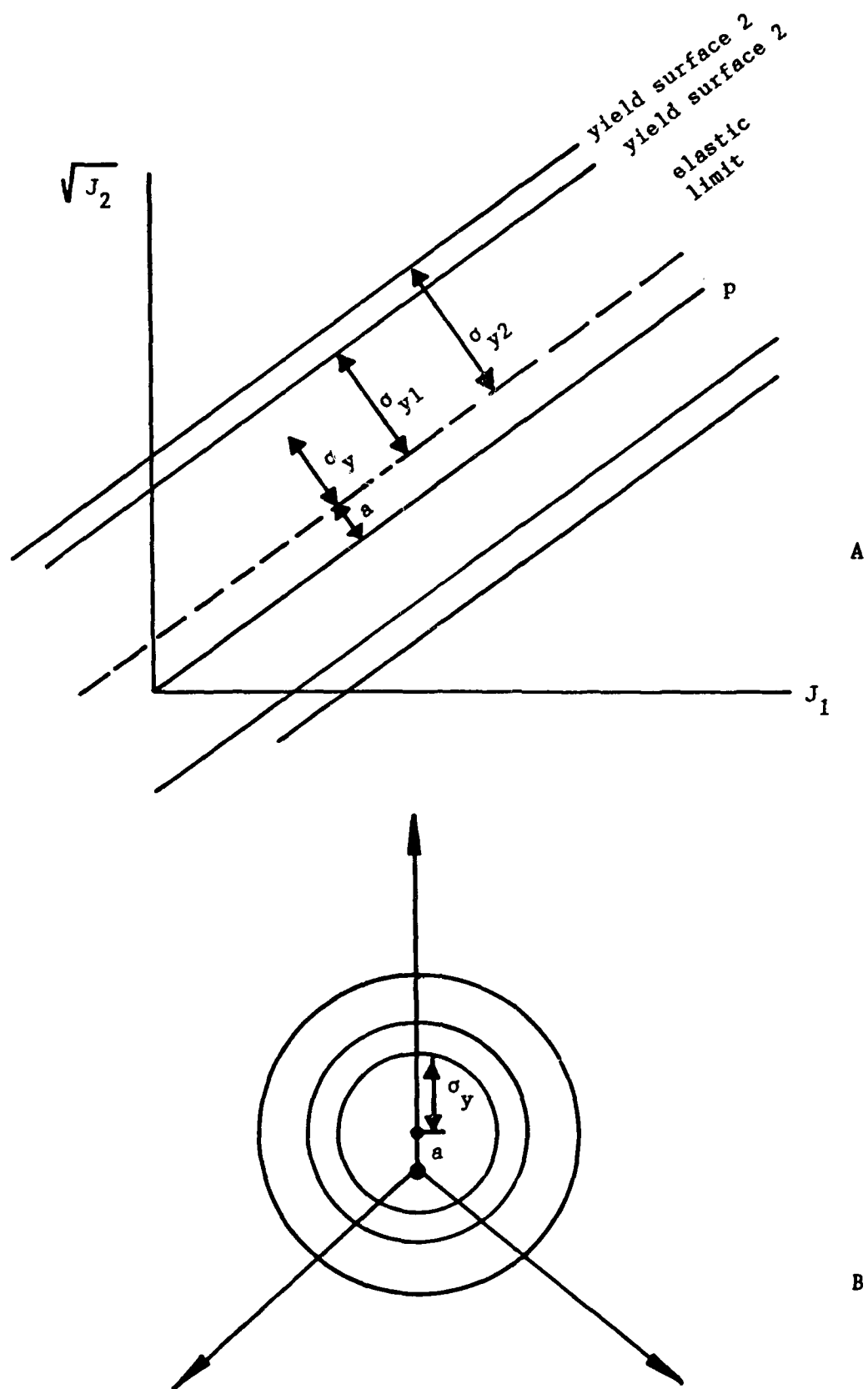


Figure 9.16 Non-linear beam element yield surfaces

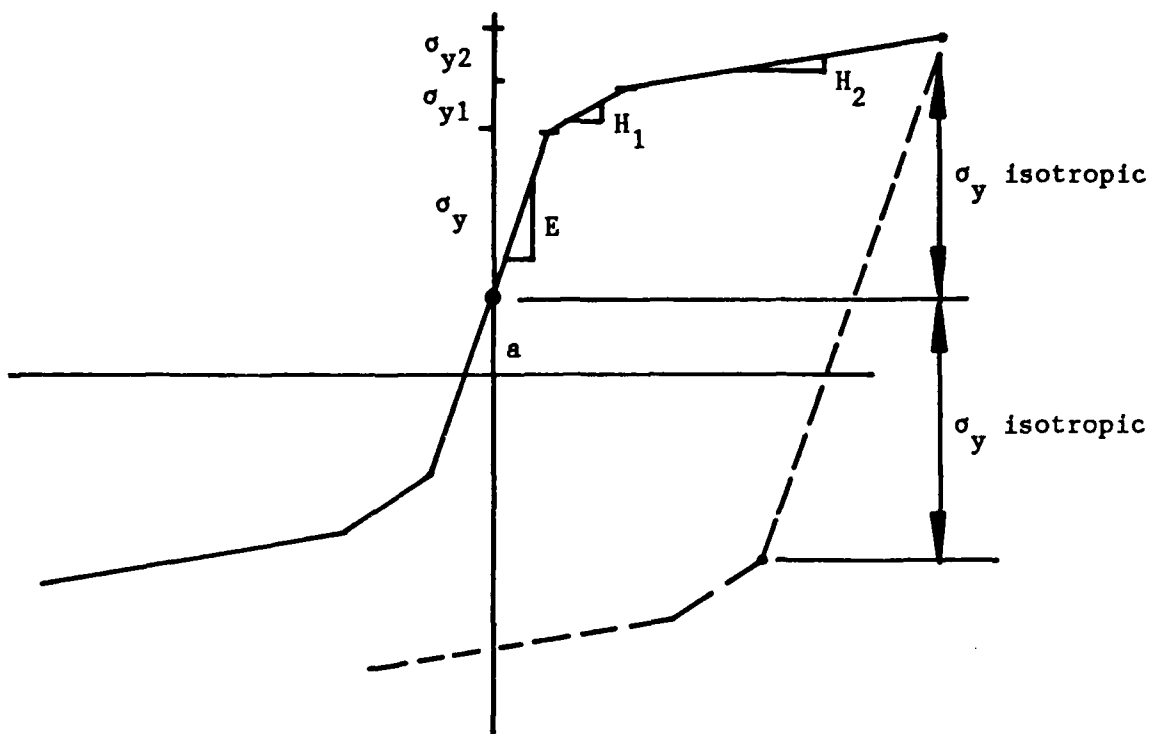


Figure 9.17 Isotropic hardening

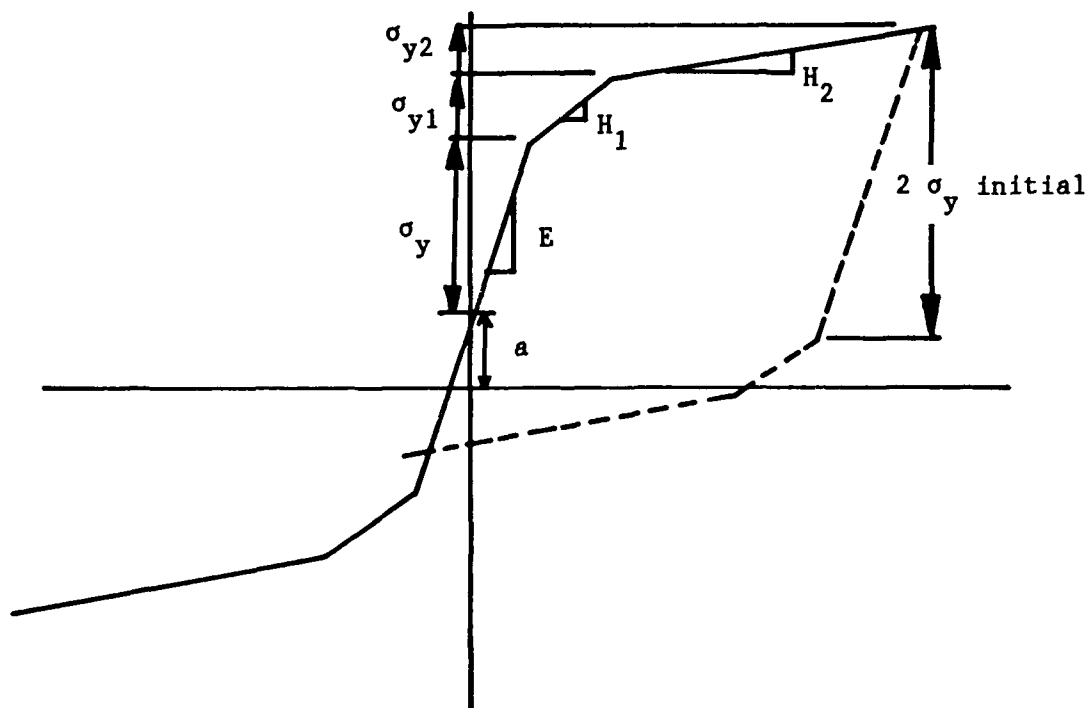


Figure 9.18 Kinematic hardening

Subsequent Card, Yield Surface Data

One card is required for each yield surface. The number of yield surfaces equals NYS. (NYS is defined on the material control card; see Section 9.8.3.2.1)

Note	Columns	Variable	Description
	1-5	M1	Yield surface number; 1.LE.M1.LE.NYS
(1)	11-20	FM(ND+1,M,1)	Yield stress ($k= s-a $)
(2)	21-30	FM(ND+2,M,1)	Elasto-plastic modulus (H)
(3)	31-40	FM(ND+3,M,1)	Initial offset (a)

Notes:

(1) The yield stress for each surface can be computed from axial stress strain information as shown in Figures 9.17 and 9.18. Note that T_y , and T_{yz} are measured from the offset point "a," and not from the origin.

(2) The elasto-plastic moduli can be readily computed from axial data as shown in Figure 9.17 and 9.18. Note the elasto-plastic modulus incorporates elastic and plastic behavior into the single value.

(3) The offset "a" may be set to any value as needed to generate the non-symmetric behavior between compression and extension for the material.

9.8.3.2.3 Storage Requirements

<u>First Word</u>	<u>Variable Array</u>
MF.	MATYP
MF + 1	PLTYP
MF + 2	NYS
M1 = MF + 3	IND(NSPTS*)
M2 = M1 + NSPTS*3	FM(3,NYS+1,NSPTS)
ML = M2 + NSPTS*3*NYS*IPREC	
(ML - MF + 1 = total required storage for material in element group data.)	

*NSPTS = Number of stress points

9.8.3.2.1 Material Control Card (3I5)

Note	Columns	Variable	Description
	1-5	MATYP	The number 2
(1)	6-10	PLTYP	Plasticity material sub-type; EQ.0; Isotropic plasticity EQ.1; Kinematic plasticity
	11-15	NYS	Number of yield surfaces; GE.0; if EQ.0, set internally EQ.1

Note:

(1) The isotropic and kinematic hardening rules are demonstrated in Figures 9.17 and 9.18. The isotropic hardening rule will work well in modeling materials that exhibit work hardening. Kinematic hardening should be employed for materials which degrade significantly as cyclic loading takes place.

9.8.3.2.2 Material Properties Cards

Card 1 (2F10.0)

Note	Columns	Variable	Description
	1-10	E	Young's modulus
	11-20	POIS	Poisson's ratio

Card 2 Initial Stress (10.0)

Note	Columns	Variable	Description
(1)	11-20	S(1)	Component 11 (SIGMA11)

Note:

(1) The initial stress, sigma (11), is used to determine the point in stress space where the material originates. A choice of sigma (11) greater than "a" will yield a smaller change in sigma (11) before plasticity is encountered.

9.9.0 Two- and Three-Dimensional Plate and Shell Elements

The element may be used in triangular or quadrilateral form for 2D plate (flat) and 3D plate/shell analysis. In 2D analysis there are three possible degree of freedom at each nodes (i.e., one vertical translation and two rotations). In 3D analysis there are six possible degrees of freedom at each nodes (i.e., three translations and three rotations). The local sign convention for the plate/shell element is shown in Figure 9.19. When employing plate/shell elements, NSD must be GE.2 and NDOF must be GT.NSD (recall NED=3 in 2D, NED=6 in 3D). The sequence of cards used to describe plate/shell elements is given in the next sections.

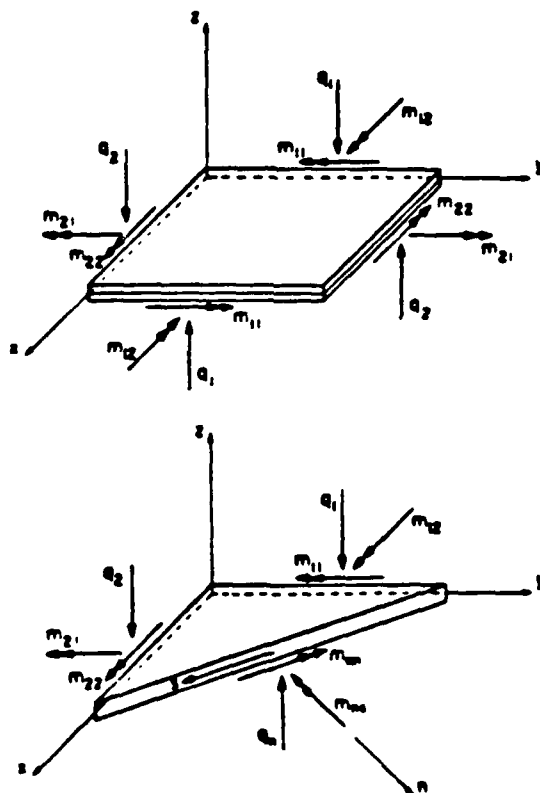


Figure 9.19 Local coordinates for plate and shell elements

9.9.1 Element Group Control Card (815)

Note	Columns	Variable	Description
	1-5	NPAR(1) (=NTYPE)	The number 20
	6-10	NPAR(2) (=NUMEL)	Number of elements in this group; GE.1
(1)	11-15	NPAR(3) (=NUMAT)	Number of geometric/material sets in this group; GE.0 if EQ.0, set internally to 1 0
	16-20	NPAR(4) (=IB)	Bending stiffness numerical integration code EQ.0, 2x2 Gaussian quadrature EQ.1, 1-pt Gaussian quadrature 0
	21-25	NPAR(5) (=IS)	Shear stiffness numerical integration code EQ.0, 2x2 Gaussian quadrature EQ.1, 1-pt Gaussian quadrature 0
	26-30	NPAR(6) (=INC)	Incompatible modes code EQ.0, neglected EQ.1, added
	31-35	NPAR(7) (=IST)	Spatial stress/force/moment output code EQ.0, Include spatial output for group EQ.1, Omit spatial output for group
(2)	36-40	NPAR(8) (=LCASP)	Pressure load case number; GE.0 if EQ.0, set internally to 1
(2)	41-45	NPAR(9) (=LCASG)	Gravity load case number; GE.0 if EQ.0, set internally to 1

Notes:

(1) Defines number of geometric/material properties to be input in Section 9.9.2.

(2) The load case number corresponds to the load-time function input in Section 8.0.

9.9.2 Geometric/Material Properties Cards (I5,5X,4F10.0)

Note	Columns	Variable	Description
	1-5	N	Material identification number
	11-20	E(N)	Young's Modulus
	21-30	POIS(N)	Poisson's Ratio
	31-40	TH(N)	Thickness
	41-50	WT(N)	Mass density per unit volume

9.9.3 Pressure Load Multiplier Card - For NSD=2, only - (3F10.0)

Note	Columns	Variable	Description
	1-10	GRAV(1)	Multiplier of distributed shear in the transverse x3-direction
	11-20	GRAV(2)	Multiplier of distributed couple1 in the x1-direction
	21-30	GRAV(3)	Multiplier of distributed couple2 in the x2-direction

9.9.3 Gravity Load Multiplier Card - For NSD=3, only - (3F10.0)

Note	Columns	Variable	Description
(1)	1-10	GRAV(1)	Multiplier of gravity load in the x1-direction
	11-20	GRAV(2)	Multiplier of gravity load in the x2-direction
	21-30	GRAV(3)	Multiplier of gravity load in the x3-direction

Notes:

(1) Gravity load multipliers may be used to define the components of the gravity vector with respect to the global x1, x2, x3 system.

9.9.4 Element Data Cards

Nodal Data Cards (715)

Note	Columns	Variable	Description
(1)	1-5	N	Element number
	6-10	MAT(N)	Geometric/material properties set number
	11-15	IEN(1,N)	Number of 1st node
	16-20	IEN(2,N)	Number of 2nd node
	21-25	IEN(3,N)	Number of 3rd node
(2)	26-30	IEN(4,N)	Number of 4th node
(3)	31-35	NG	Generation parameter EQ.0, no generation EQ.1, generate data

Notes:

(1) All elements must be input on a nodal data card or generated.
Terminate with a blank card.

(2) For triangular elements, set node number IEN(4,N) equal to IEN(3,N).

(3) If the generation parameter is set to 1, a generation data card must be input next.

Generation Data Cards (6I5)

See Figure 9.3 for a schematic representation of the generation scheme.

Note	Columns	Variable	Description
	1-5	NEL (1)	Number of elements in direction 1; GE.0; if EQ.0, set internally to 1
	6-10	INCEL (1)	Element number increment for direc- tion 1; if EQ.0, set internally to 1
	11-15	INC (1)	Node number increment for direction 1; if EQ.0, set internally to 1
	16-20	NEL (2)	Number of elements in direction 2; GE.0; if EQ.0, set internally to 1
	21-25	INCEL (2)	Element number increment for direc- tion 2; if EQ.0, set internally to NEL(1)
	26-30	INC (2)	Node number increment for direc- tion 2; if EQ.0, set internally to $(1 + NEL(1)) * INC(1)$

9.9.5 Storage Requirements for Two/Three-Dimensional Plate/Shell Elements (NTYPE=20)

<u>First Word</u>	<u>Variable Array</u>
N101 = NF*	NPAR(16)
N102 = N101 + 16	IEN(4,NUMEL)
N103 = N102 + NUMEL*2	LM(NED,2,NUMEL)
N104 = N103 + NUMEL*2*NED**	MAT(NUMEL)
N105 = N104 + NUMEL	E(NUMAT)
N106 = N105 + NUMAT*IPREC	POIS(NUMAT)
N107 = N106 + NUMAT*IPREC	TH(NUMAT)
N108 = N107 + NUMAT*IPREC	WT(NUMAT)
N109 = N108 + NUMAT*IPREC	GRAV(3)
NL = N109 + 3*IPREC	
(NL-NF+1 = total required storage for element group)	

*NF is the address of the first word in blank common for the element group.

**NED is the number of degrees of freedom per node:

if NSD.EQ.2, NED.EQ.3
if NSD.EQ.3, NED.EQ.6

9.10.0 Three-Dimensional Membrane Element

The element may be used in triangular or quadrilateral form. There are three possible degrees of freedom at each node (i.e., three translations). When employing membrane elements, NSD must be EQ.3 and NDOF must be GE.3. The sequence of cards used to describe membrane elements is given in the next sections.

9.10.1 Element Group Control Card (14I5)

Note	Columns	Variable	Description
	1-5	NPAR (1) (=NTYPE)	The number 7
	6-10	NPAR (2) (=NUMEL)	Number of elements in this group; GE.1
(1)	11-15	NPAR (3) (=IOPT)	Number of geometric/material sets in this group; GE.0 if EQ.0, set internally to 1
	16-20	NPAR (4) (=IFD)	Finite deformation code EQ.0, neglected EQ.1, included
	21-25	NPAR (5) (=IB)	Lambda stiffness numerical integration code EQ.0, 2x2 Gaussian quadrature EQ.1, 1-pt Gaussian quadrature
	26-30	NPAR (6) (=IS)	Shear stiffness numerical integration code EQ.0, 2x2 Gaussian quadrature EQ.1, 1-pt Gaussian quadrature
	31-35	NPAR (7) (=IST)	Spatial stress/force/moment output code EQ.0, Include spatial output for group EQ.1, Omit spatail output for group
(2)	36-40	NPAR(8) (=LCASG)	Gravity load case number; GE.0 if EQ.0, set internally to 1

Notes:

(1) Defines number of geometric/material properties to be input in Section 9.10.2.

(2) The load case number corresponds to the load-time function input in Section 8.0.

9.10.2 Geometric/Material Properties Cards (I5,5X,4F10.0)*NUMAT

Note	Columns	Variable	Description
	1-5	N	Material identification number
	11-5	E(N)	Young's Modulus
	21-30	POS(N)	Poisson's Ratio
	31-40	TH(N)	Thickness
	41-50	WT(N)	Mass density per unit volume

9.10.3 Gravity Load Multiplier Card (3F10.0)

Note	Columns	Variable	Description
(1)	1-10	GRAV(1)	Multiplier of gravity load in the x1-direction
	11-20	GRAV(2)	Multiplier of gravity load in the x2-direction
	21-30	GRAV(3)	Multiplier of gravity load in the x3-direction

Notes:

(1) Gravity load multipliers may be used to define the components of the gravity vector with respect to the global x1, x2, x3 system.

**9.10.4 Element Data Cards
Nodal Data Cards (7I5)**

Note	Columns	Variable	Description
(1)	1-5	N	Element number
	6-10	MAT(N)	Geometric/material properties set number
	11-15	IEN(1,N)	Number of 1st node
	16-20	IEN(2,N)	Number of 2nd node
	21-25	IEN(3,N)	Number of 3rd node
(2)	26-30	IEN(4,N)	Number of 4th node
(3)	31-35	NG	Generation parameter EQ.0, no generation EQ.1, generate data

Notes:

(1) All elements must be input on a nodal data card or generated.
Terminate with a blank card.

(2) For triangular elements, set node number IEN(4,N) equal to IEN(3,N).

(3) If the generation parameter is set to 1, a generation data card must be input next.

Generation Data Cards (6I5)

See Figure 9.3 for a schematic representation of the generation scheme.

Note	Columns	Variable	Description
	1-5	NEL (1)	Number of elements in direction 1; GE.0; if EQ.0, set internally to 1
	6-10	INCEL (1)	Element number increment for direc- tion 1; if EQ.0, set internally to 1
	11-15	INC (1)	Node number increment for direction 1; if EQ.0, set internally to 1
	16-20	NEL (2)	Number of elements in direction 2; GE.0; if EQ.0, set internally to 1
	21-25	INCEL (2)	Element number increment for direc- tion 2; if EQ.0, set internally to NEL(1)
	26-30	INC (2)	Node number increment for direc- tion 2; if EQ.0, set internally to $(1 + NEL(1)) * INC(1)$

9.10.5 Storage Requirements for Three-Dimensional Membrane Elements (NTYPE=21)

<u>First Word</u>	<u>Variable Array</u>
N101 = NF*	NPAR(16)
N102 = N101 + 16	IEN(4,NUMEL)
N103 = N102 + NUMEL*4	LM(3,4,NUMEL)
N104 = N103 + NUMEL*12	MAT(NUMEL)
N105 = N104 + NUMEL	E(NUMAT)
N106 = N105 + NUMAT*IPREC	POIS(MUMAT)
N107 = N106 + NUMAT*IPREC	TH(NUMAT)
N108 = N107 + NUMAT*IPREC	WT(NUMAT)
N109 = N108 + NUMAT*IPREC	GRAV(3)
NL = N109 + 3*IPREC	
(NL - NF + 1 = total required storage for element group.)	

*NF is the address of the first word in blank common for the element group.

9.11.0 Boundary Element

The boundary element is used to constrain nodal displacement/rotations in any direction to specified values, to compute support reactions, and to provide elastic supports to nodes. The element is defined by a single directed axis through a specified nodal point, by a linear extensional stiffness along the axis, or by a linear rotational stiffness about the axis. The element is essentially a spring that can have axial displacement stiffness and rotational stiffness. There is no limit to the number of boundary elements that can be applied to any nodal point to produce the desired effects. Boundary elements have no effect on the size of the stiffness matrix.

9.11.1 Element Group Control Card (6I5)

Note	Columns	Variable	Description
	1-5	NPAR(1) (=NTYPE)	The number 22
	6-10	NPAR(2) (=NUMEL)	Number of elements in this group; GE.1
	11-15	NPAR(3) (=NUMAT)	Number of geometric/ material properties sets
	16-20	NPAR(4) (=ISTIK)	Boundary condition code EQ.0 displacement EQ.1 rotation
	22-25	NPAR(5) (=NOUT)	Number of force/displacement output histories
	26-30	NPAR(6) (=IST)	Spatial force/displacement output code EQ.0, Include spatial force/ displacement output for group EQ.1, Omit spatial force/ displacement output for group

9.11.2 Geometric/Material Properties Cards (I5,5X,4F10.0)*NUMAT

Note	Columns	Variable	Description
	1-5	M	Geometric/material set number
	11-20	STIFF(M)	Spring constant k
	21-30	AN(1,M)	Component 1 of direction vector N
	31-40	AN(2,M)	Component 2 of direction vector N

9.11.3 Element Data Cards (4I5)

Note	Columns	Variable	Description
(1)	1-5	N	Element number
	6-10	MAT(N)	Geometric/material properties set number
	11-15	IEN(1,N)	Node number
(2)	16-20	NG	Generation increment

Notes:

(1) All elements must be read in on an element data card or generated. Terminate with a blank card.

(2) Element data cards may be generated by employing a two card sequence as follows:

Card 1: L,MAT(L),IEN(1,L),LG

Card 2: N,MAT(N),IEN(1,N)

N must be greater than L. The geometric/material set number for all

L, L+1, L+2, ..., N

is set to MAT(L) and the node numbers are incremented by LG.

9.11.4 Element Output History Card (3I5)

"On-line" and Calcomp plots of contact element displacement and force may be obtained. Each component required is plotted versus time. The total number of components to be plotted must equal NOUT, which is defined on the element group control card (see Section 9.11.1).

Note	Columns	Variable	Description
(1)	1-5	N	Element number
	6-10	ITEMP (1)	Displacement (DELT) plot code EQ.0, no plot EQ.1, plot
	11-15	ITEMP (2)	Contact force (FORC) plot code EQ.0, no plot EQ.1, plot

Note:

(1) Output history information is stored in the array IHS in element group data. The dimension of IHS is 2 x NOUT. The first row of IHS contains element numbers and the second row contains component numbers. Two components may be plotted as described above. Component numbers 1 and 2 correspond to DELT and FORC, respectively.

9.11.5 Storage Requirements Boundary Element (NTYPE = 22)

<u>First Word</u>	<u>Variable Array</u>
N101 = NF*	NPAR(16)
N102 = N101 + 16	IEN(1, NUMEL)
N103 = N102 + NUMEL	LM(NDOF, 1, NUMEL)
N104 = N103 + NUMEL*NDOF	IHS(2, NOUT)
N105 = N104 + NOUT*2	SOUT(NOUT, NTS +1)
N106 = N105 + (NTS + 1)*NOUT	MAT(NUMEL)
N107 = N106 + NUMEL	STIFF(NUMAT)
N108 = N107 + NUMAT*IPREC	AN(3, NUMAT)
NL = N108 + NUMAT*3*IPREC	
(NL - NF + 1 = total required storage for element group.)	

*NF is the address of the first word in blank common for the element group.

9.12.0 Link Element

The link element is used to connect two nodal displacements/rotations in any direction. The element is defined by two nodes and a single directed axis, by a linear extensional stiffness along the axis, or by a linear rotational stiffness about the axis. The element is essentially a spring that can have either axial stiffness or rotational stiffness. There is no limit to the number of links that can be established between two nodal points to produce the desired effects.

9.12.1 Element Group Control Card (4I5)

Note	Columns	Variable	Description
	1-5	NPAR(1) (=NTYPE)	The number 23
	6-10	NPAR(2) (=NUMEL)	Number of elements in this group; GE.1
	11-15	NPAR(3) (=NUMAT)	Number of geometric/ material properties sets
	16-20	NPAR(4) (=ISTIK)	Link condition code EQ.0 displacement EQ.1 rotation

9.12.2 Geometric/Material Properties Cards (I5,5X,4F10.0)*NUMAT

Note	Columns	Variable	Description
	1-5	M	Geometric/material set number
	11-20	STIFF(M)	Spring constant k
	21-30	AN(1,M)	Component 1 of direction vector N
	31-40	AN(2,M)	Component 2 of direction vector
	41-50	AN(3,M)	Component 3 of direction vector N

9.12.3 Element Data Cards (5I5)

Note	Columns	Variable	Description
(1)	1-5	N	Element number
	6-10	MAT(N)	Geometric/material properties set number
	11-15	IEN(1,N)	Node number 1
	16-20	IEN92,N)	Node number 2
(2)	21-25	NG	Generation increment

Notes:

(1) All elements must be read in on an element data card or generated.
Terminate with a blank card.

(2) Element data cards may be generated by employing a two card sequence as follows:

Card 1: L,MAT(L),IEN(1,1),IEN(2,L),LG
Card 2: N,MAT(N),IEN(1,N),IEN(2,N)

N must be greater than L. The geometric/material set number for all

L, L+1, L+2,..., N

is set to MAT(L) and the node numbers are incremented by LG.

9.12.4 Storage Requirements Link Element (NTYPE = 23)

<u>First Word</u>	<u>Variable Array</u>
N10 = NF*	NPAR(16)
N102 = N101 + 16	IEN(22, NUMEL)
N103 = N102 + 2*NUMEL	LM(NDOF, 2, NUMEL)
N104 = N103 + NUMEL*NDOF	MAT(NUMEL)
N105 = N104 + NUMEL	STIFF(NUMAT)
N106 = N105 + NUMAT*IPREC	AN(3, NUMAT)
NL = N106 + NUMAT*3*IPREC	
(NL - NF + 1 = total required storage for element group.)	

*NF is the address of the first word in blank common for the element group.

9.13.0 Nodal Penalty Element

9.13.1 Element Group Control Card (3I5)

Note	Columns	Variable	Description
	1-5	NPAR(1) (=NTYPE)	The number 24
	6-10	NPAR(2) (=NUMEL)	Number of elements in this group; GE.1
	11-15	NPAR(3) (=NUMAT)	Number of material properties sets

9.13.2 Material Properties Cards (I5,5X,NDOF*F10.0)*NUMAT

Note	Columns	Variable	Description
	1-5	M	Material set number
	11-20	PENALT(1)/	Nodal value DOF component 1
	21-30	PENALT(2)/	Nodal value DOF component 2
	31-40	PENALT(3)/	Nodal value DOF component 3

9.13.3 Element Data Cards (4I5)

Note	Columns	Variable	Description
(1)	1-5	N	Element number
	6-10	MAT(N)	Material Properties set number
	11-15	IEN(1,N)	Node number
(2)	16-20	NG	Generation increment

Notes:

(1) All elements must be read in on an element data card or generated.
Terminate with a blank card.

(2) Element data cards may be generated by employing a two card sequence as follows:

Card 1 : L, MAT(L), IEN(1,L), LG

Card 2 : N, MAT(N), IEN(1,N)

N must be greater than L. The material set number for all

L + 1, L + 2,, N

is set equal to MAT(L) and the node numbers are incremented by LG.

9.13.4 Storage Requirements for Nodal Penalty Elements (NTYPE = 24)

<u>First Word</u>	<u>Variable Array</u>
N101 = NF*	NPAR(16)
N102 = N101 + 16	IEN(1,NUMEL)
N103 = N102 + NUMEL	LM(NDOF, 1, NUMEL)
N104 = N103 + NUMEL*NDOF	MAT(NUMEL)
N105 = N104 + NUMEL	PENALT(NDOF, NUMAT)
NL = N105 + NUMAT*NDOF*IPREC	
(NL - NF + 1 = total required storage for element group)	

*NF is the address of the first word in blank common for the element group.

10.0 MATERIAL MODELS

10.1.0 Description of Princeton Effective Stress Soil Model

DYNFLOW incorporates elastic, and a variety of elasto-plastic constitutive models, for both total (single phase) and effective (two phase) stress analysis. The majority of the work conducted at NCEL involved PLTYP = 8, which employs a purely kinematic hardening. The model, when properly derived, exhibits good stability PLTYP = 8. The Princeton Effective Stress Soil Model (PESSM) has been used to model both sands and clays. PESSM demonstrates excellent predictive capabilities in simulation of monotonic triaxial test results. Cyclic triaxial and simple shear simulations using PESSM degree data, very well with measured PLTYP 1-5 have not been extensively tested at NCEL. The variations offered by these models should be evaluated by the user prior to detailed computation PLTYP=6 has been used with little success. The material model is difficult to derive, and without extensive manipulation, exhibits unstable behavior.

1	2	8	8	1					
2	1.118E+02	2.235E+02	7.451E+01	5.000E-01					
3	1	-1.000E+00	-1.000E+00	-1.000E+00	0.0	0.0	0.0		
4	1.300E+00	6.000E-01	0.0	-1.000E+00	0.0	0.43	0.0	0.0	
5	1	8.937E-02	1.181E+03	1.581E+03	0.0	0.0	0.0		
6	-2.979E-02	5.958E-02	-2.979E-02	0.0	0.0	0.0			
7	2	1.861E-01	5.244E+02	8.136E+02	0.0	0.0	0.0		
8	-6.203E-02	1.241E-01	-6.203E-02	0.0	0.0	0.0			
9	3	4.080E-01	1.169E+02	2.105E+02	3.398E-01	0.0	0.0		
10	-4.739E-02	9.478E-02	-4.739E-02	0.0	0.0				
11	4	4.977E-01	6.915E+01	1.424E+02	5.958E-01	0.0	0.0		
12	-6.665E-02	1.333E-01	-6.665E-02	0.0	0.0	0.0			
13	5	6.371E-01	2.346E+01	5.776E+01	8.589E-01	0.0	0.0		
14	-8.814E-02	1.763E-01	-8.814E-02	0.0	0.0	0.0			
15	6	8.152E-01	3.137E+00	1.008E+01	1.158E+00	5.913E-01	0.0		
16	-1.219E-01	2.438E-01	-1.219E-01	0.0	0.0	0.0			
17	7	9.091E-01	1.110E+00	4.209E+00	1.270E+00	5.324E-01	0.0		
18	-1.302E-01	2.604E-01	-1.302E-01	0.0	0.0	0.0			
19	8	9.699E-01	5.242E-01	2.174E+00	1.294E+00	5.988E-01	0.0		
20	-1.251E-01	2.502E-01	-1.251E-01	0.0	0.0	0.0			

Table 10.1 Typical material model

Card #1 (Section 10.3.1)

MATYP = 2
PLTYP = 8
NYS = 8
NUMAT = 1

Card #2 (Section 10.3.2, card 1)

Elastic Shear Modules = 1.118 E + 02
Initial Elasto-Plastic Shear Modulus = 2.235 E + 02
Elastic Bulk Modulus = 7.451 E + 01
Bulk Exponent = 5.000 E - 01

Card #3 (Section 10.3.3, card 2)

Material set number = 1
Sigma 11 = -1.000 E + 00
Sigma 22 = -1.000 E + 00
Sigma 33 = -1.000 E + 00
Sigma 12 = 0.0
Sigma 23 = 0.0
Sigma 31 = 0.0

Card #4 (Section 10.3.2, card 3, PLTYP = 8)

Critical Stress Ratio (Comp) = 1.300 E + 00
Critical Stress Ratio (Exten) = 6.000 E - 01
Attraction (cohesion) = 0.000 E - 01
Reference Mean Stress = 1.000 E + 00
Pore Fluid Bulk Modulus =
Initial Porosity = 4.300 E - 01
Initial Pore Fluid Pressure = 0.000 E - 01

Card 5 (Section 10.3.2, subsequent cards yield surface data, PLTYP = 8)

Yield surface number = 1
Yield surface size = 8.937 E - 02
Plastic Modulus H_1 = 1.181 E + 03
Plastic Modulus H_2 = 1.581 E + 03
Stress Ratio Compression = 0.000 E - 01
Stress Ratio Extension = 0.000 E - 01

Card 6 (continuation of card 5, yield surface data, initial yield surface position)

Component 11 = - 2.979 E - 02
Component 22 = 5.958 E - 02
Component 33 = - 2.979 E - 02
Component 12,23,31 = 0.000 E - 01

Cards 7 and F, 9 and 10, ..., 19 and 20 are set as cards 5 and 6.

The soil model (PESSM) has extensive capabilities in modeling granular soil behavior. It is important to understand, however, the behavior that is being modeled. Figure 10.1, A-D show "qualitative" drained triaxial response for both dense and loose samples. Figure 10.1A shows sample response in terms of deviatoric stress (q) and axial strain (E). Note the very regular "softening" of the loose sample as it approaches its ultimate strength. The dense specimen, in contrast, yields significantly different behavior by developing an instability at peak strength. The material then degenerates to approximately the same deviatoric strength exhibited in the loose samples. Figure 10.1B shows the same behavior described above as deviatoric stress versus confining stress. Note that both "tests" are at the same confining stress. Figure 10.1C shows the change in void ratio (e) as a function of the axial strain. The change in void ratio, or volume strain response is that most significant cause of the behavioral differences shown. The loose sample densifies in a very regular manner, up to the point of ultimate strength. The dense sample compacts initially, and then dilates. The dilation ends once the "steady state" for the soil has been reached. The theory for "steady state" (Casagrande Poulos, et al.) postulates that a soil will deform as shown above until it reaches the state line, at which point it will continue to deform, or flow, without any increase in the applied stresses, or volume changes. It is important to realize that the strain levels necessary to achieve steady state are much larger than those commonly encountered in standard soil mechanics tests. Commonly, the major concern is the behavior within the first 15 percent axial strain. Figure 10.2, A-D shows a qualitative assessment of undrained triaxial behavior for two sands at the same relative density, but with different initial confining pressures. In this case it is important to recall the volume strain tendencies of the qualitative drained tests. Figure 10.2A shows dense and loose behavior, from a change in confining stress, not a change in density. The loose behavior arises from the samples tendency to compact at that confining stress. The dense behavior shows that samples tend to compact, then dilate at the lower confining pressure (Figures 10.2B and 10.2C). Interpretation of this general behavior from steady-state theory is summarized in Figure 10.2D. Note that once the initial compaction ends, the state point moves toward the steady state line. Figure 10.3D, A-D shows the qualitative results for dense and loose specimens at the same initial confining stress. The differences in behavior are again, strongly dependent on the volume strain behavior.

PESSM is capable of capturing the majority of behavior shown in Figures 10.2 and 10.3. This is demonstrated in the following sections detailing parameter variation. The behavioral changes regarding change in confining stress may be modeled by simply changing the "confining" stress in the soil model. This is a result of the soil moduli being pressure dependent. Figure 10.4 shows variations of moduli according to a power of $n = 0.4$ and 0.5 . The behavior shown in Figure 10.3 can be modeled by simply adjusting the critical stress ratio.

PESSM is not capable of accurately capturing the large strain (>15 percent) behavior shown in Figure 10.1. PESSM has no capability in handling the instability shown in Figure 10.1 at this time.

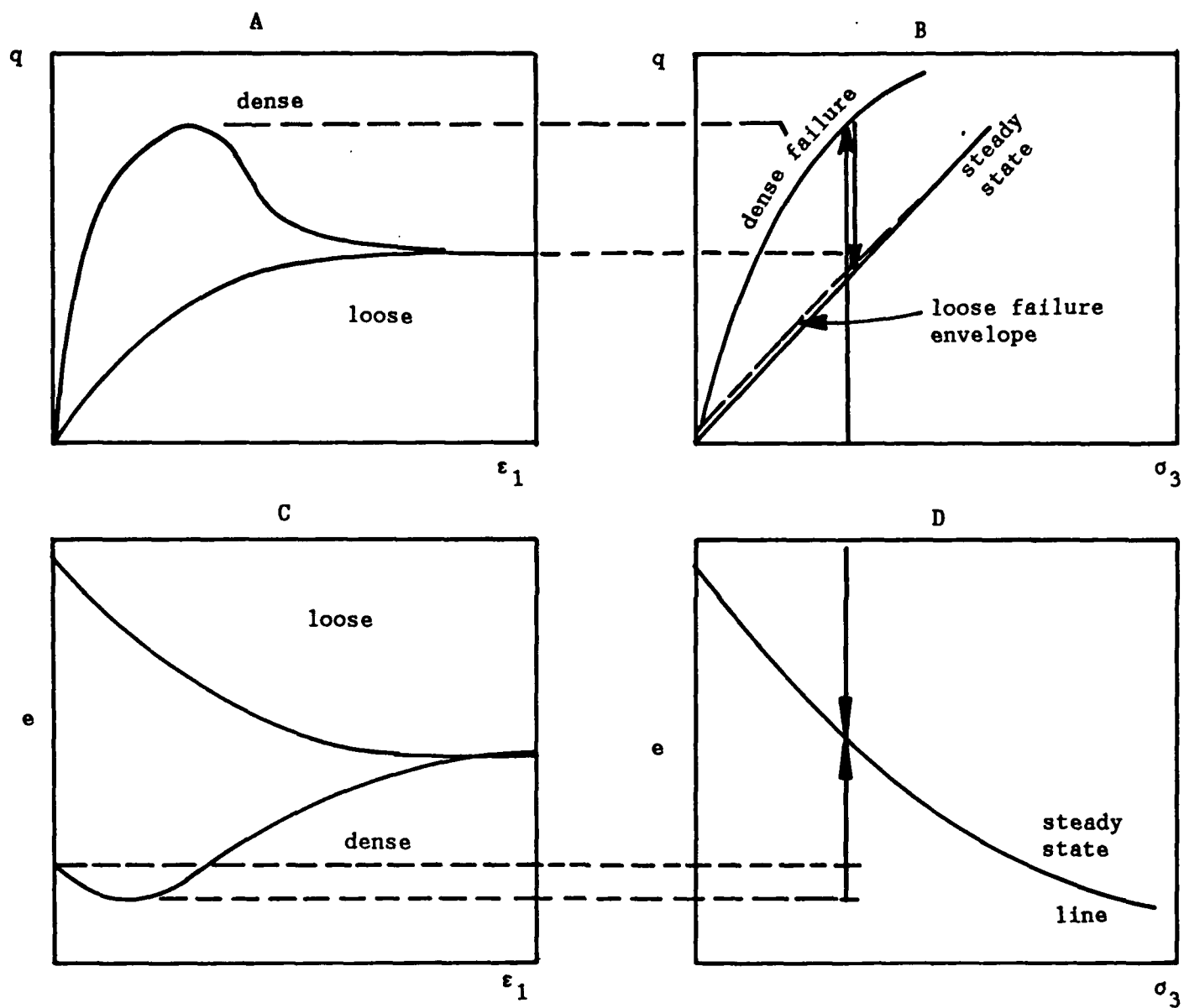


Figure 10.1 Drained triaxial compression, dense and loose sand

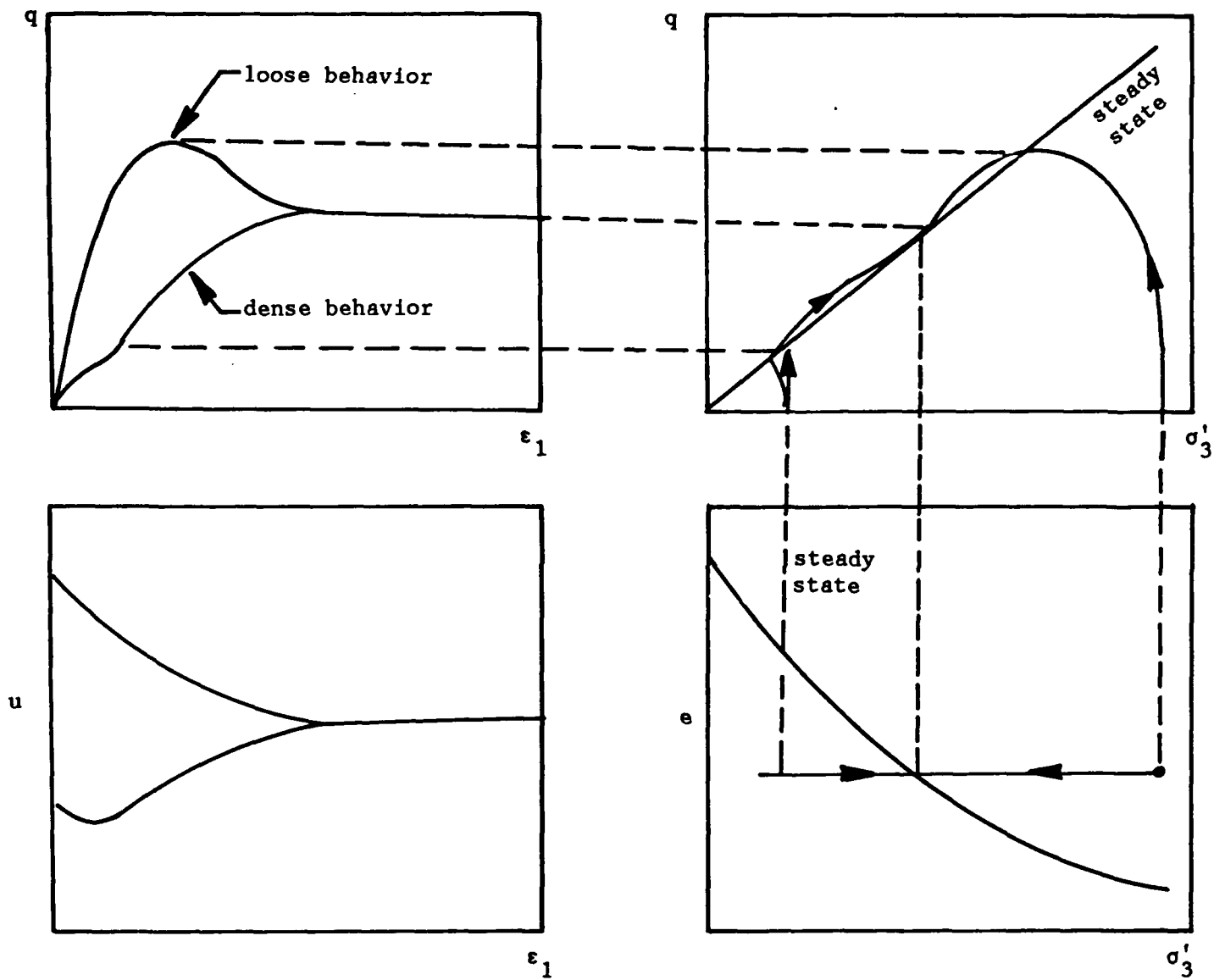


Figure 10.2 Undrained triaxial compression and steady state soil behavior, void ratio constant

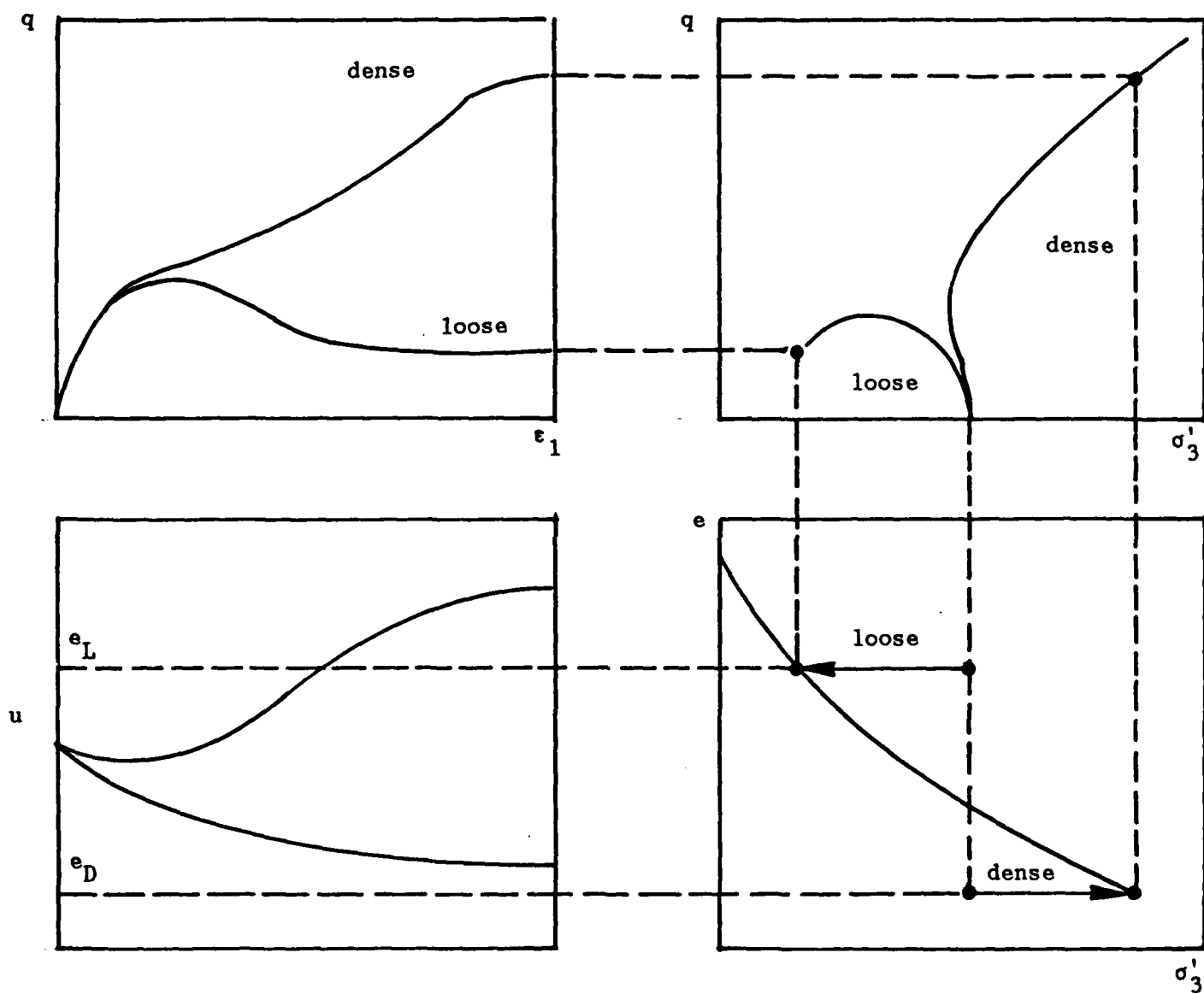


Figure 10.3 Undrained triaxial compression and steady state soil behavior, σ_3 constant

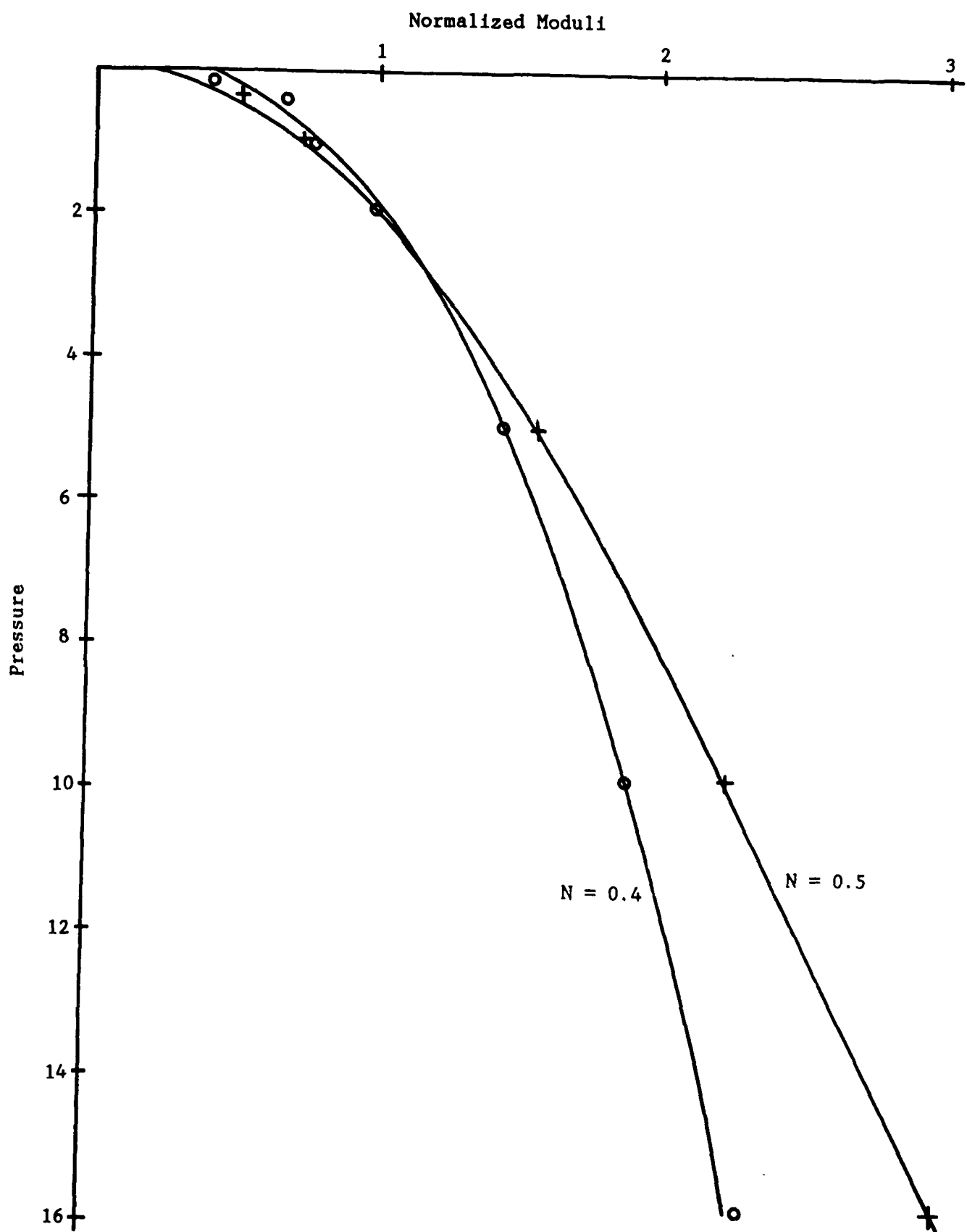


Figure 10.4 Effects on moduli with depth

10.1.1 Critical Stress Ratio

The critical ratio (CSR) is the parameter in extension or compression that determines the stress state where there is a change between compactive and dilative volume strains. Adjustment of this parameter has little effect on the shear stress-strain curves in the drained simulation, but does make significant changes in the amount of volume strain generated by the model. An example of varying the critical stress ratio ± 6 percent is presented for a drained test using the silica sand model (Figure 10.5).

Figure 10.6 presents the results of the same modification in the critical stress ratio during an undrained simulation. Note the significant changes in strength caused by the 10 percent increase in critical stress ratio leading to a prediction of near total loss of strength. Decreasing the value of the stress ratio by 6 percent more than doubles the amount of shear strength developed. Figure 10.6 (b) presents the stress paths associated with each of the modifications. Note that each of the models follows essentially the same path up to the point of contacting the critical state line. At this point, if the sample has not begun to dilate, it then loses strength by moving toward zero effective stress.

10.1.2 Elastic Moduli

Figure 10.7 demonstrates the effects of varying the elastic moduli for all surfaces in the drained material model by ± 25 percent. The effects on the shear stress-strain curves are minimal; however, there is a more significant change in the degree of compactive volume strain generated. Note that the changes in volume strain are not equivalent for both cases. This is caused by an increase in plasticity associated with the decreased elastic stiffness, necessary to reach the same load level. The increased elastic stiffness, in turn, allows the given load to be reached at a smaller strain level, but does not decrease the strain to the same degree. Figure 10.8 presents the effects of the same variation on the undrained simulation.

10.1.3 Plastic Moduli

Varying the plastic moduli for all surfaces has significant effects on both the drained and undrained simulations (Figures 10.9 and 10.10). A greater change appears as a result of increasing the plastic moduli for each yield surface. The effect is two-fold in that it not only increases the overall stiffness of the system in the drained simulation (Figure 10.9 (a)), but decreases the overall compactive volumetric strain as well (Figure 10.9 (b)). The factors contribute to the greatly enhanced stiffness in the undrained simulation (Figure 10.10 (a)) by improving the skeletal response while at the same time decreasing the excess pore water pressure generation.

Reducing the plastic moduli has less effects on both drained and undrained simulations causing a slightly larger amount of compaction before dilation begins. This produces a moderately softer system in both the drained and undrained environments.

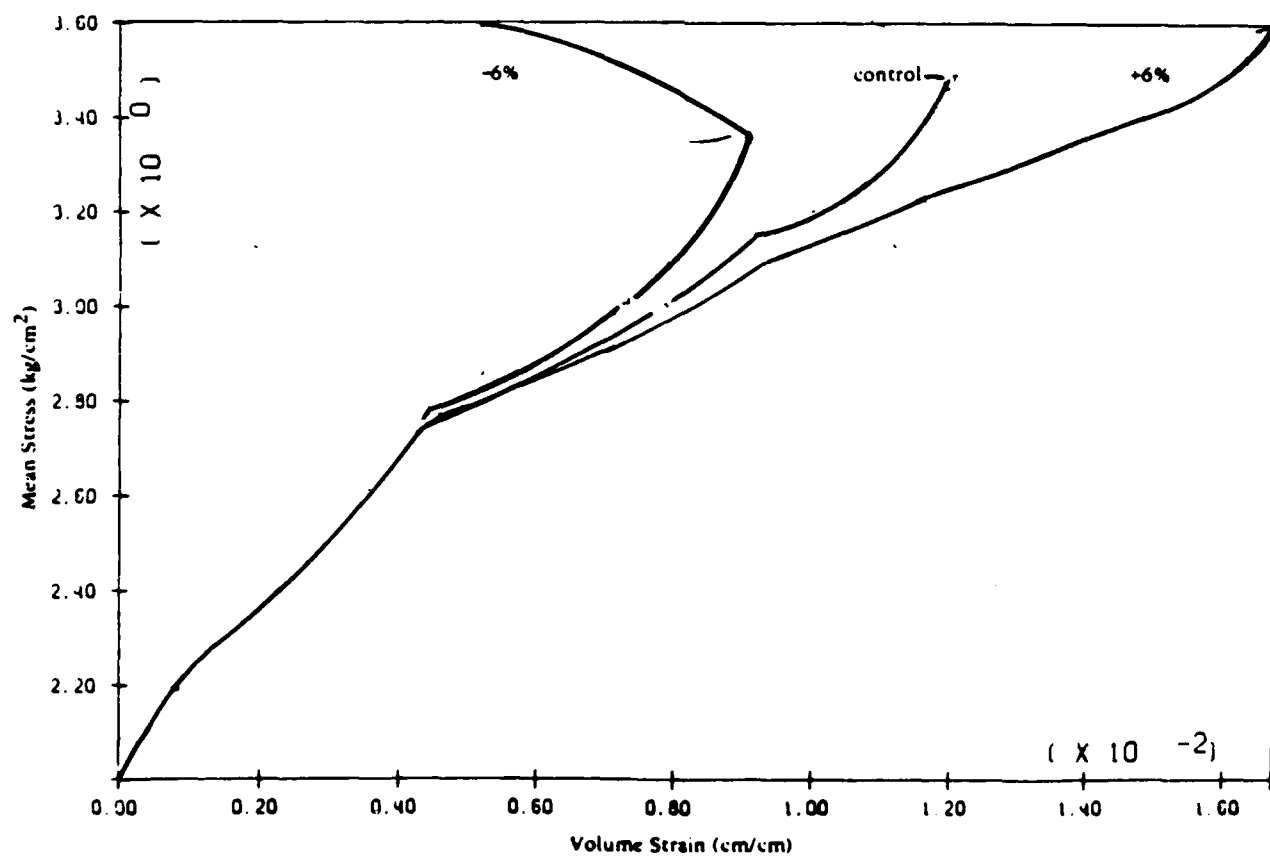
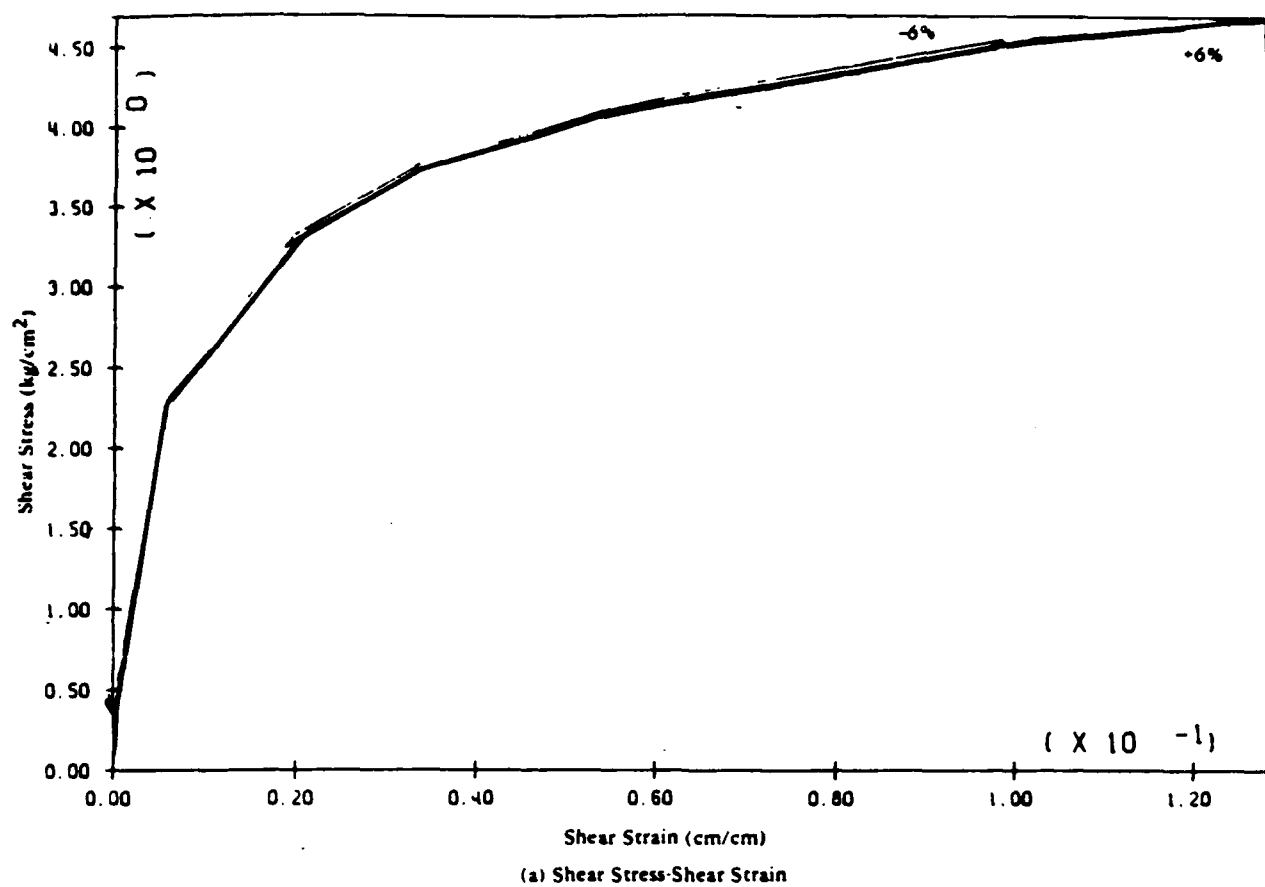
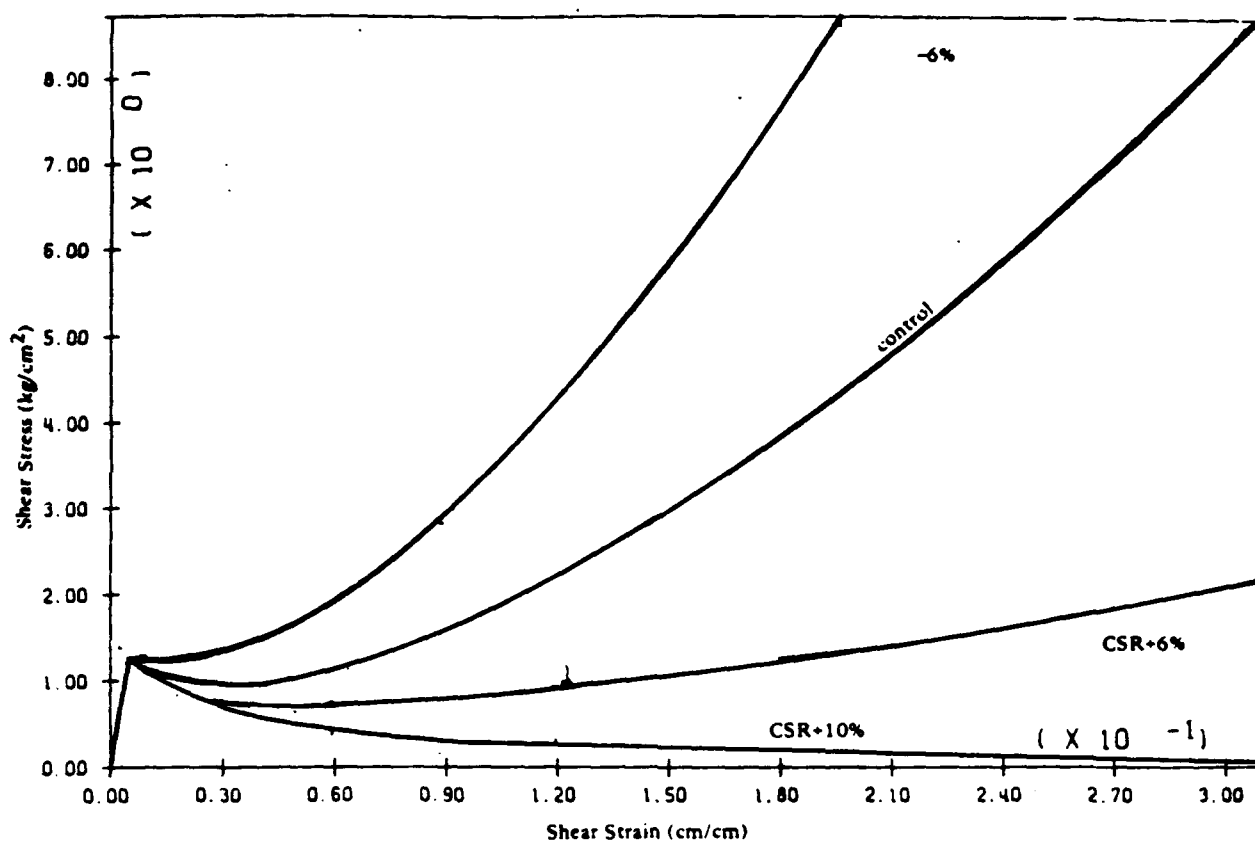
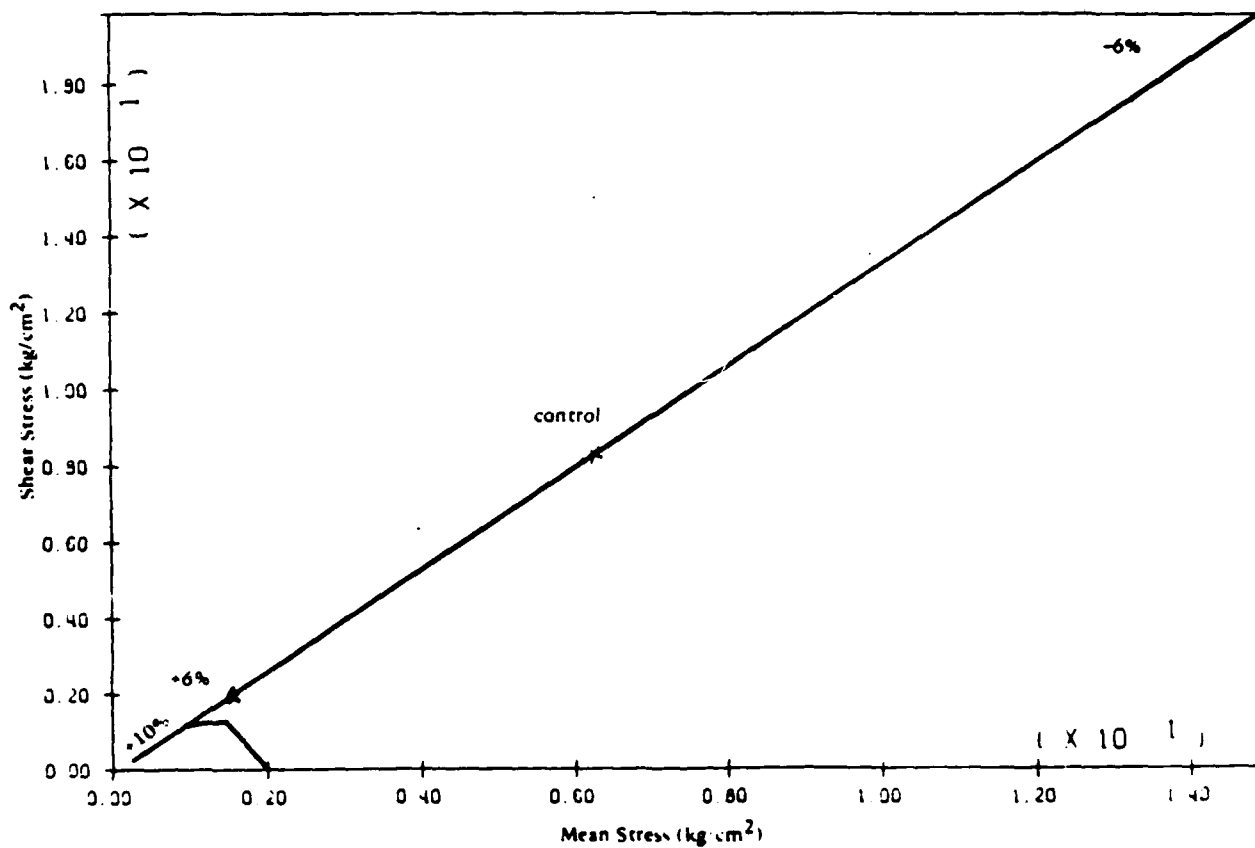


Figure 10.5. Critical stress ratio variation 6% drained compression shear stress-strain, mean-volume strain



(a) Shear Stress-Shear Strain



(b) Stress Path

Figure 10.6. Critical stress ratio variation 6%, 10%, undrained compression shear stress-strain, stress path

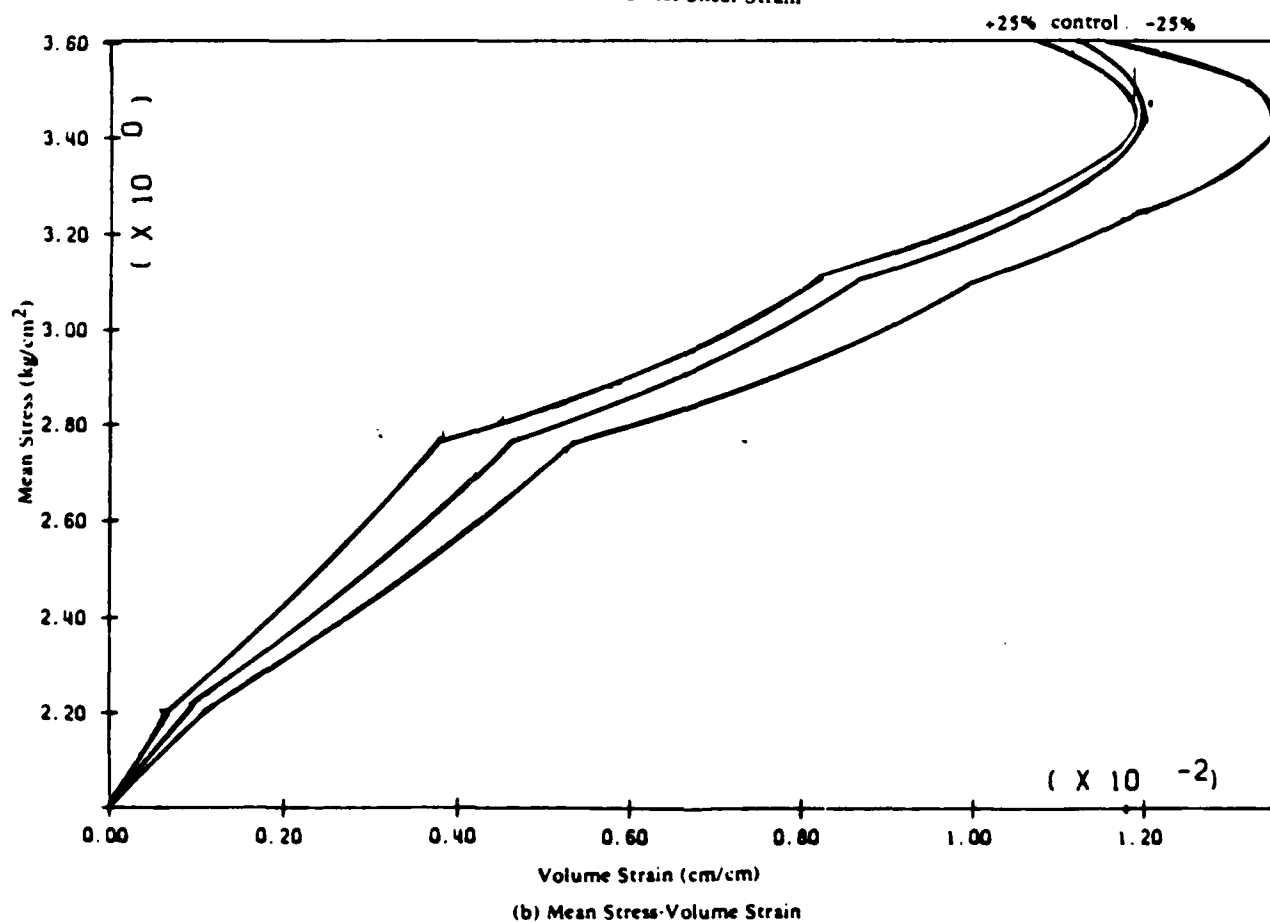
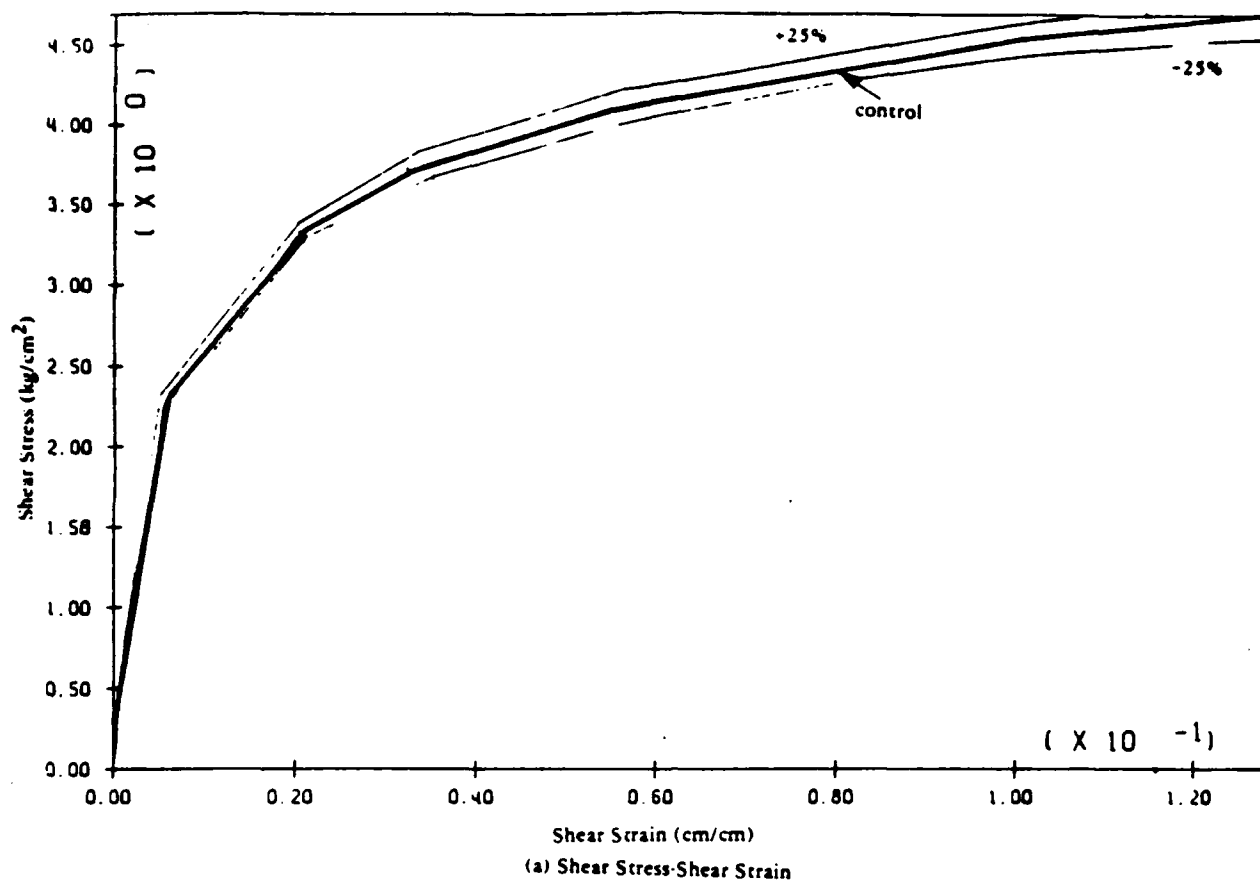


Figure 10.7. Elastic moduli variation 25% drained compression
shear stress-strain, mean stress-volume strain

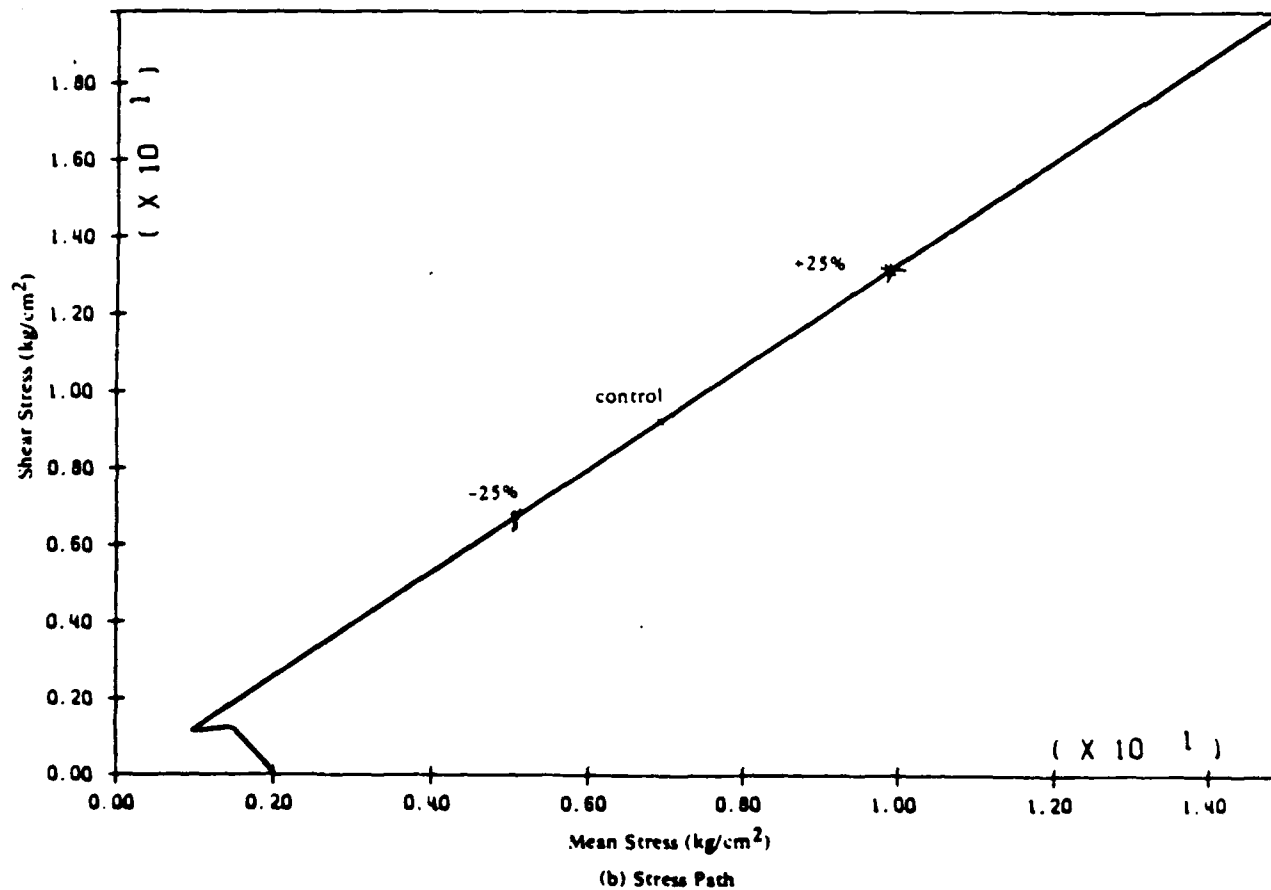
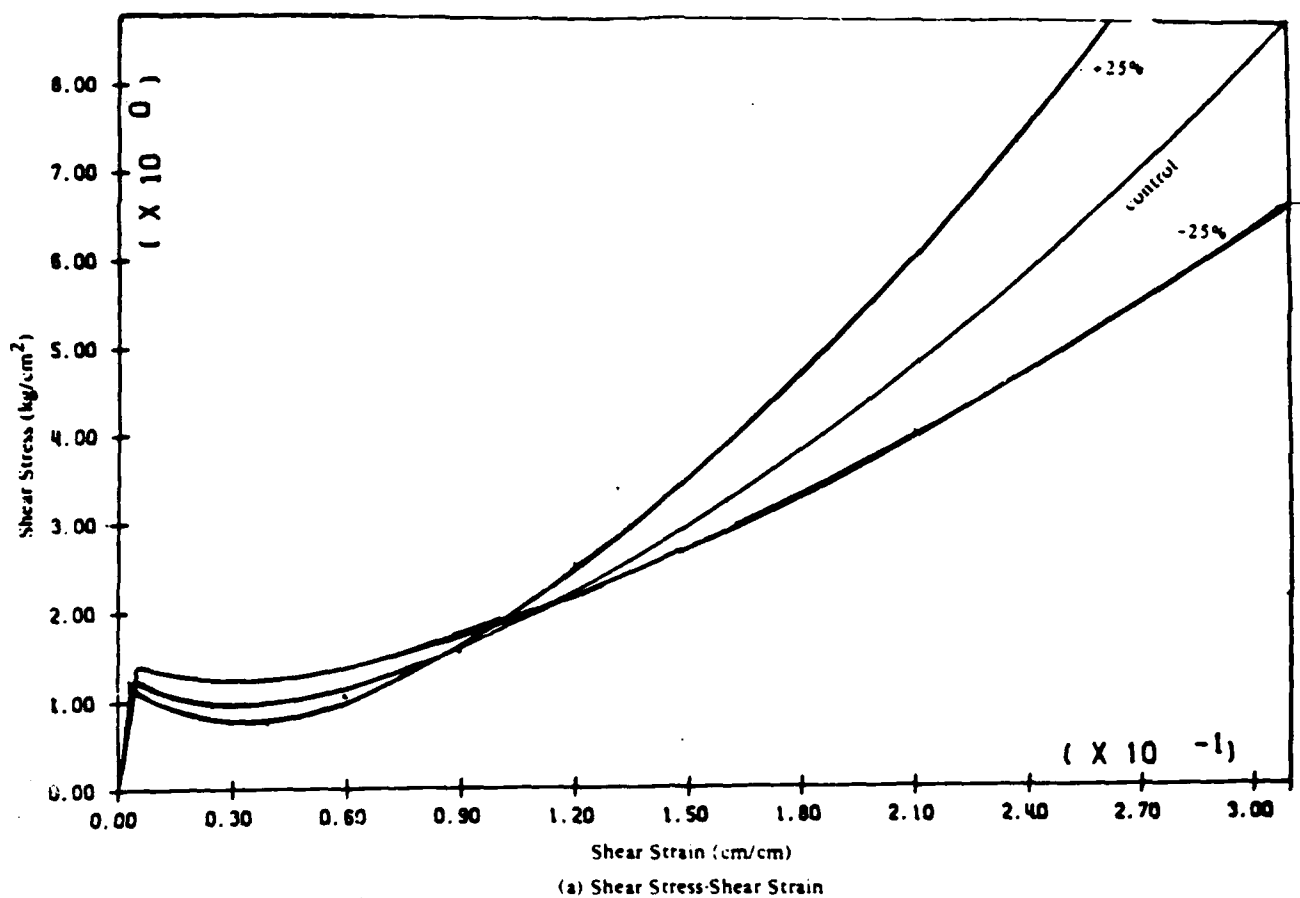
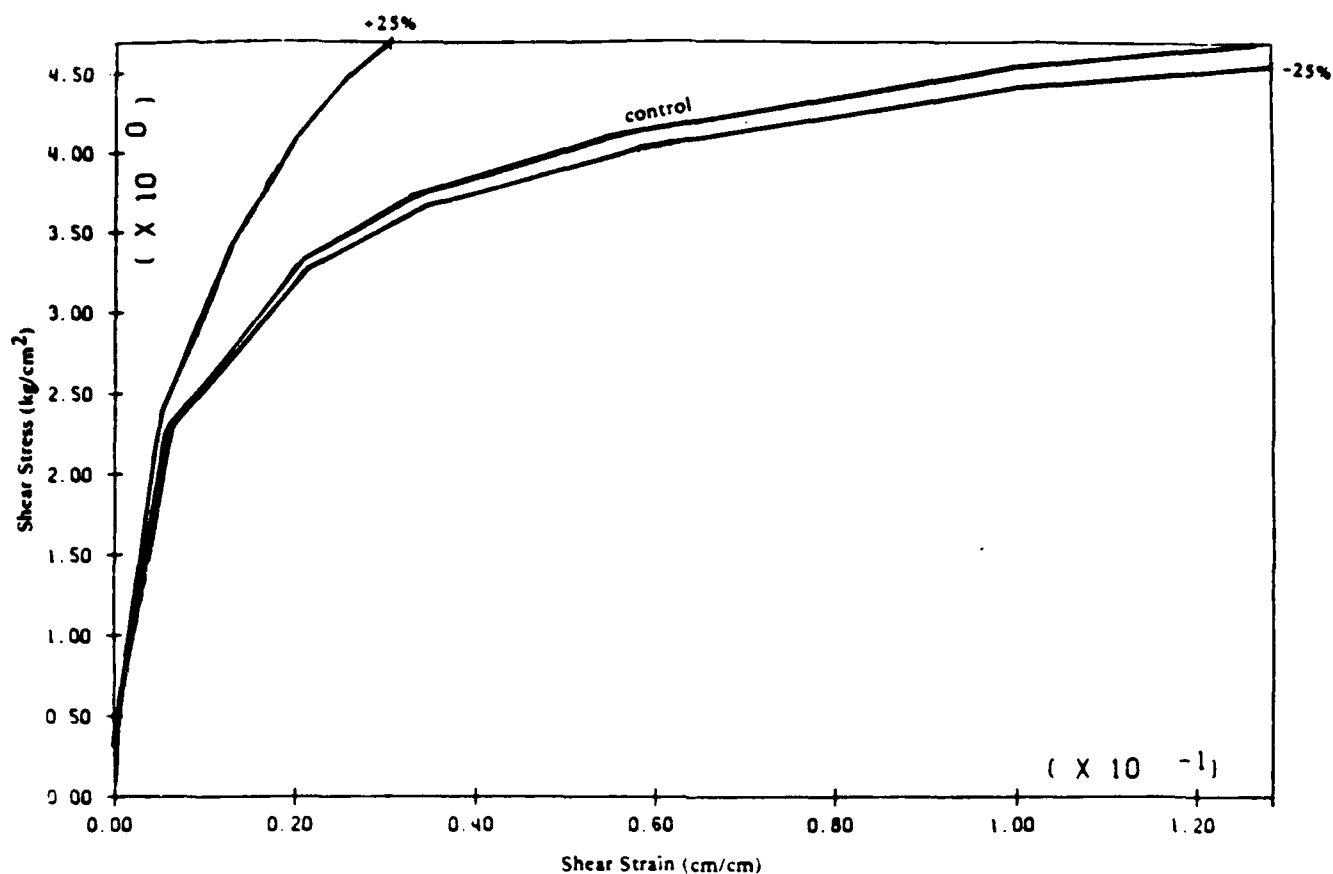
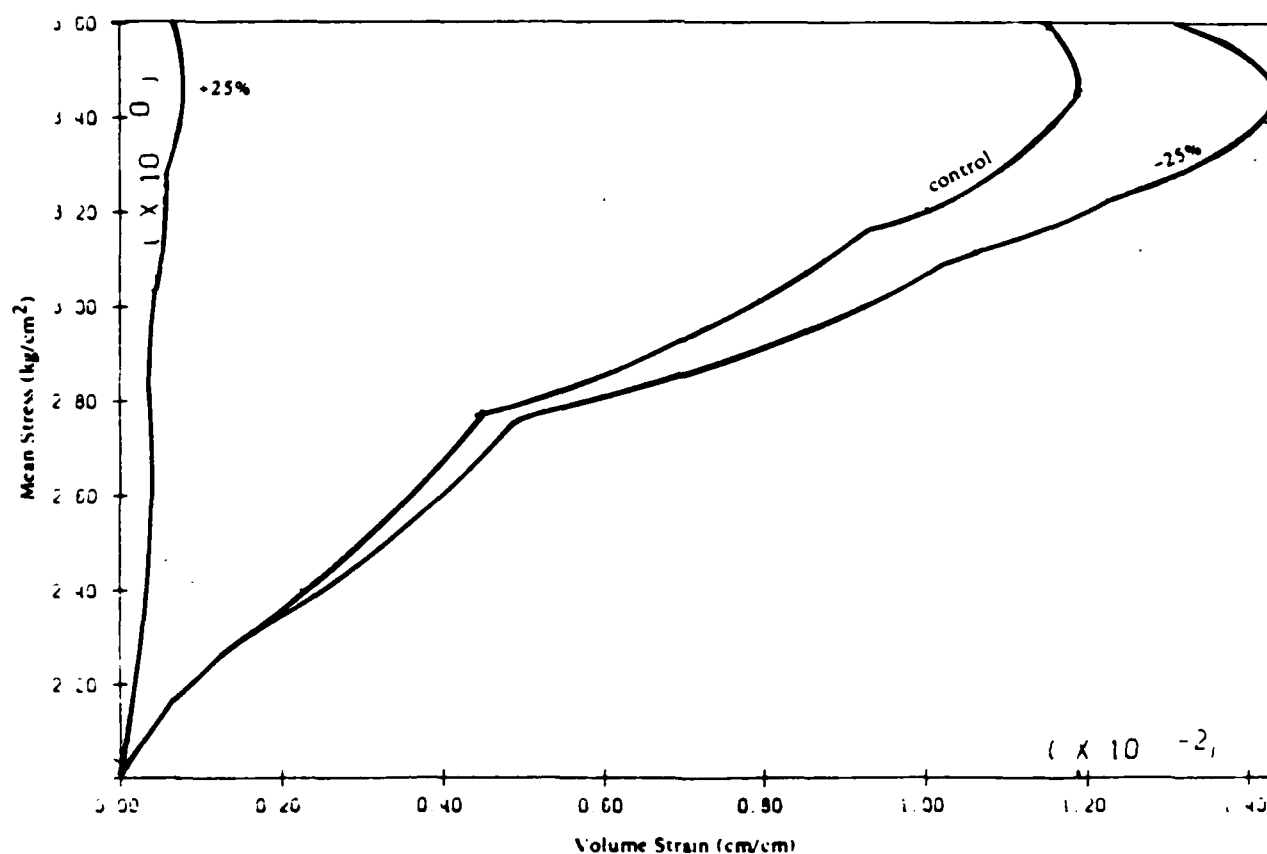


Figure 10.8. Elastic moduli variation 25% undrained compression shear stress-strain, stress path

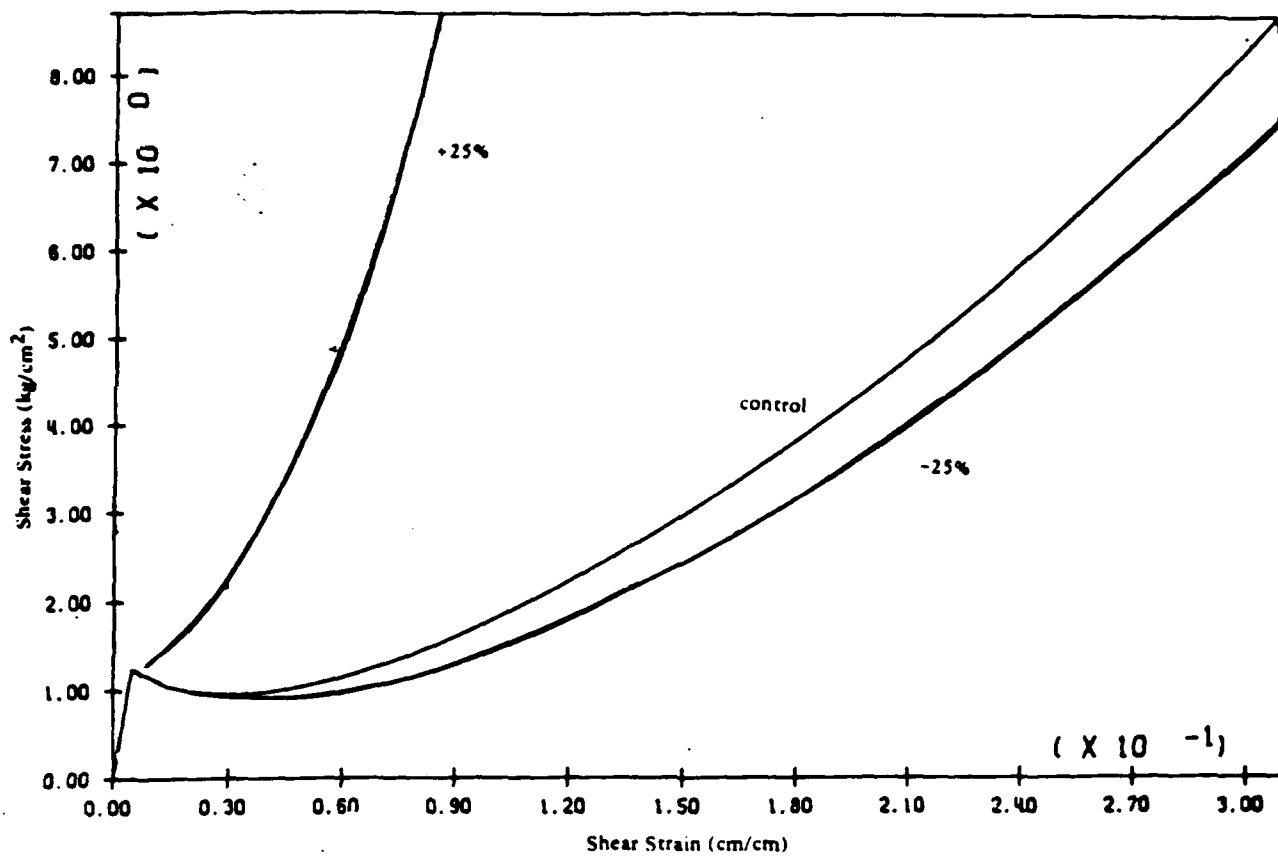


(a) Shear Stress-Shear Strain

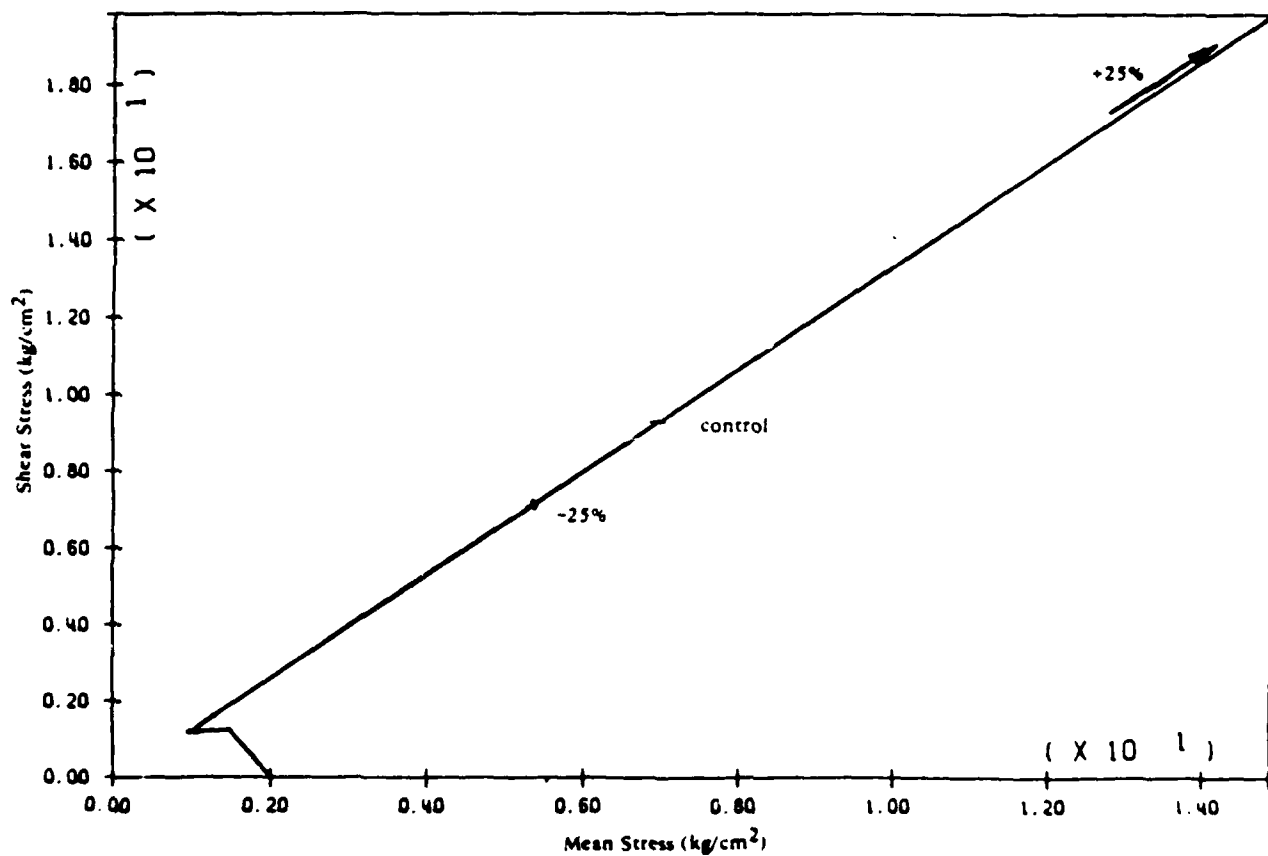


(b) Mean Stress-Volume Strain

Figure 10.9. Plastic moduli variation 25% drained compression shear stress-strain, mean stress-volume strain



(a) Shear Stress-Shear Strain



(b) Stress Path

Figure 10.10. Plastic moduli variation 25% undrained compression shear stress-strain, mean stress-volume strain

10.1.4 Yield Surface Size

Changing the yield surface size changes the shear strength values which may be achieved at a particular strain level. Figures 10.11 and 10.12 clearly demonstrate this property of the model.

In the drained (Figure 10.11), increasing the yield surface size decreases the shear strain at a particular level of shear stress, and reduces volumetric strain not by a change in moduli values, but rather as a result of changing the position of compactive-dilate interchange in relation to the original critical surface position. Reducing the yield surface size results in reaching the various surfaces earlier, at reduced stress levels, and induces greater amounts of plasticity. At the same time, the reduction also moves the compactive-dilative point outside the outermost surface, allowing large compactive volumetric strains to occur (Figure 10.11 (b)).

In the undrained simulation (Figure 10.12) the two-fold effect of a stiffer skeleton and reduced volumetric strains is present. The increase in yield surface size produces a stiffer system with a reduction in positive pore water pressure generation before dilation begins. The reduction in size causes an early generation of volume strains and positive pore water pressures, coupled with a softer system resulting in the zero effective stress condition.

10.1.5 Yield Surface Position

Variation of yield surface position has equal effects in both drained and undrained simulations (Figures 10.13 and 10.14). By moving the surfaces in a positive direction, the system is stiffened by changing the points at which the load path intercepts a particular surface, i.e., the path achieves greater stress levels with less plasticity before impacting the next surface, thereby remaining at a given stiffness through a larger strain increment. By moving the surface position in a negative direction, the load path then intercepts a particular surface at a smaller stress increment, and induces greater amounts of plasticity, effectively softening the system.

Effects on the undrained simulation are presented in Figure 10.14. Qualitatively, the changes produce the same response as demonstrated in the drained simulation.

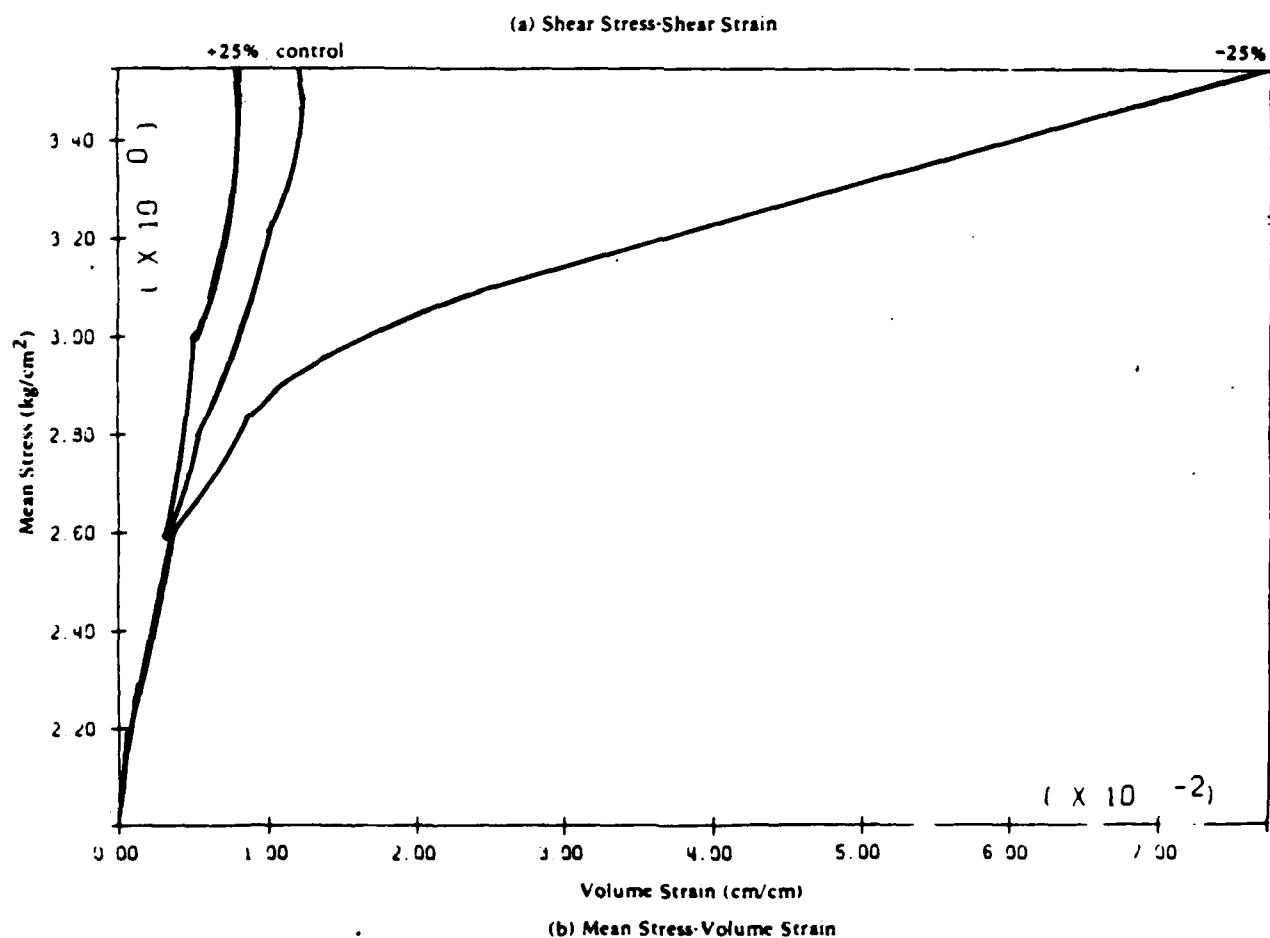
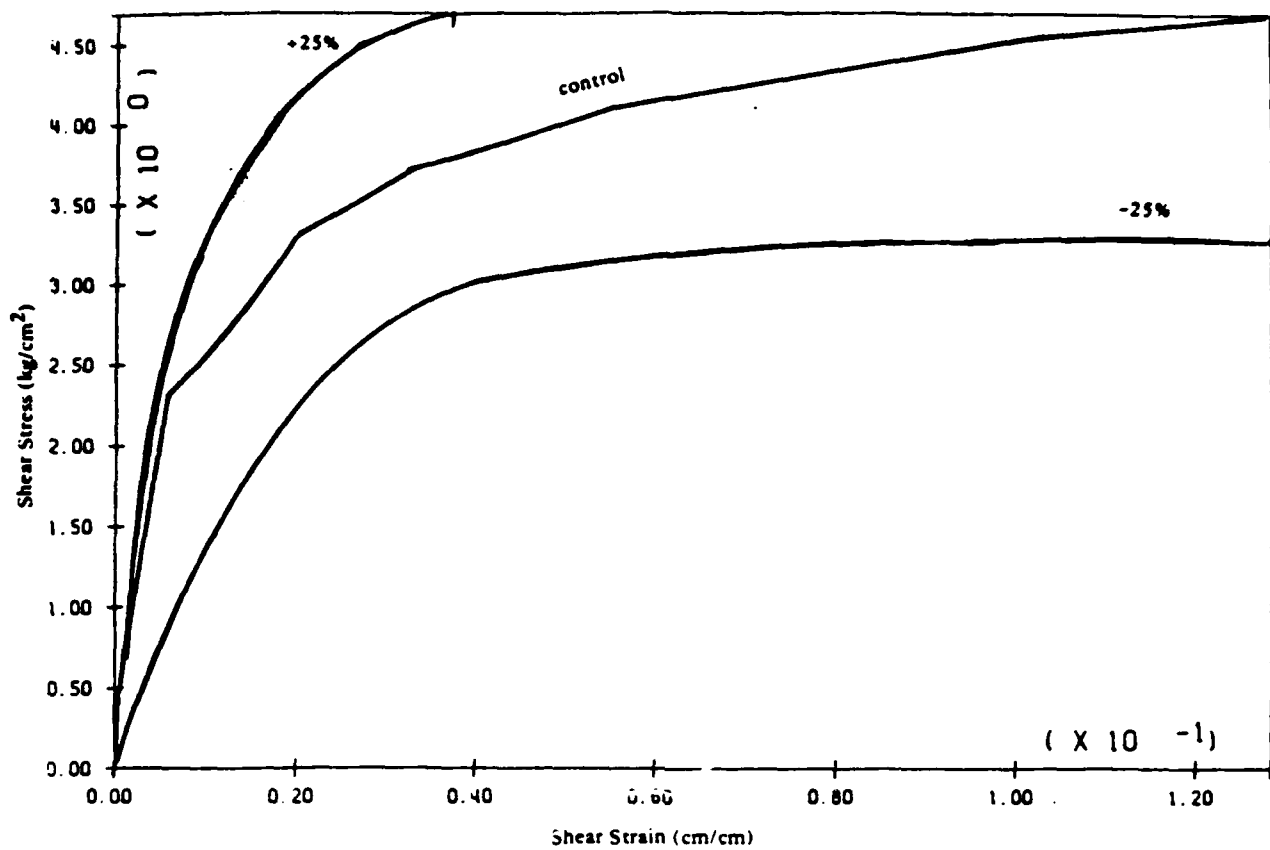


Figure 10.11. Yield surface size variation 25% drained compression shear stress-strain, mean stress-volme strain

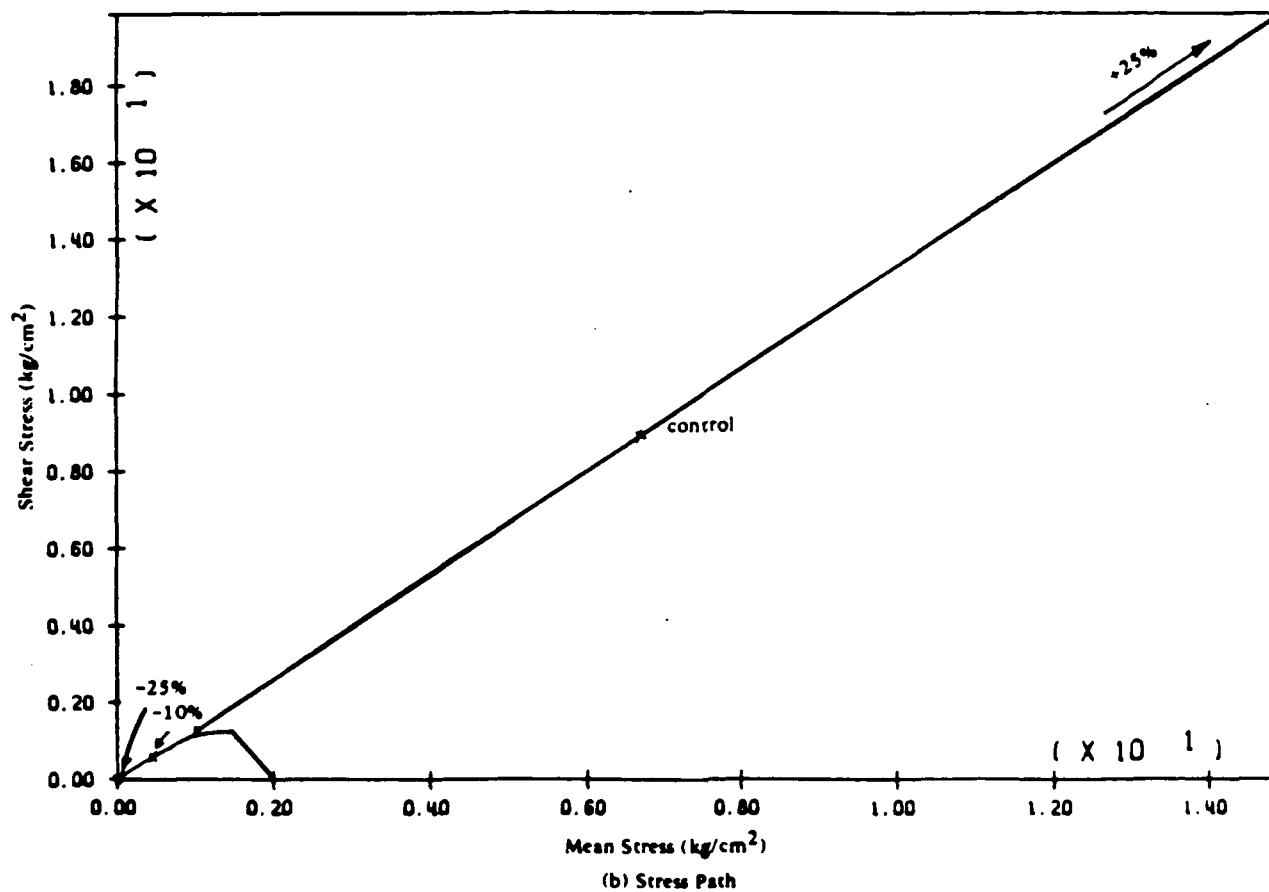
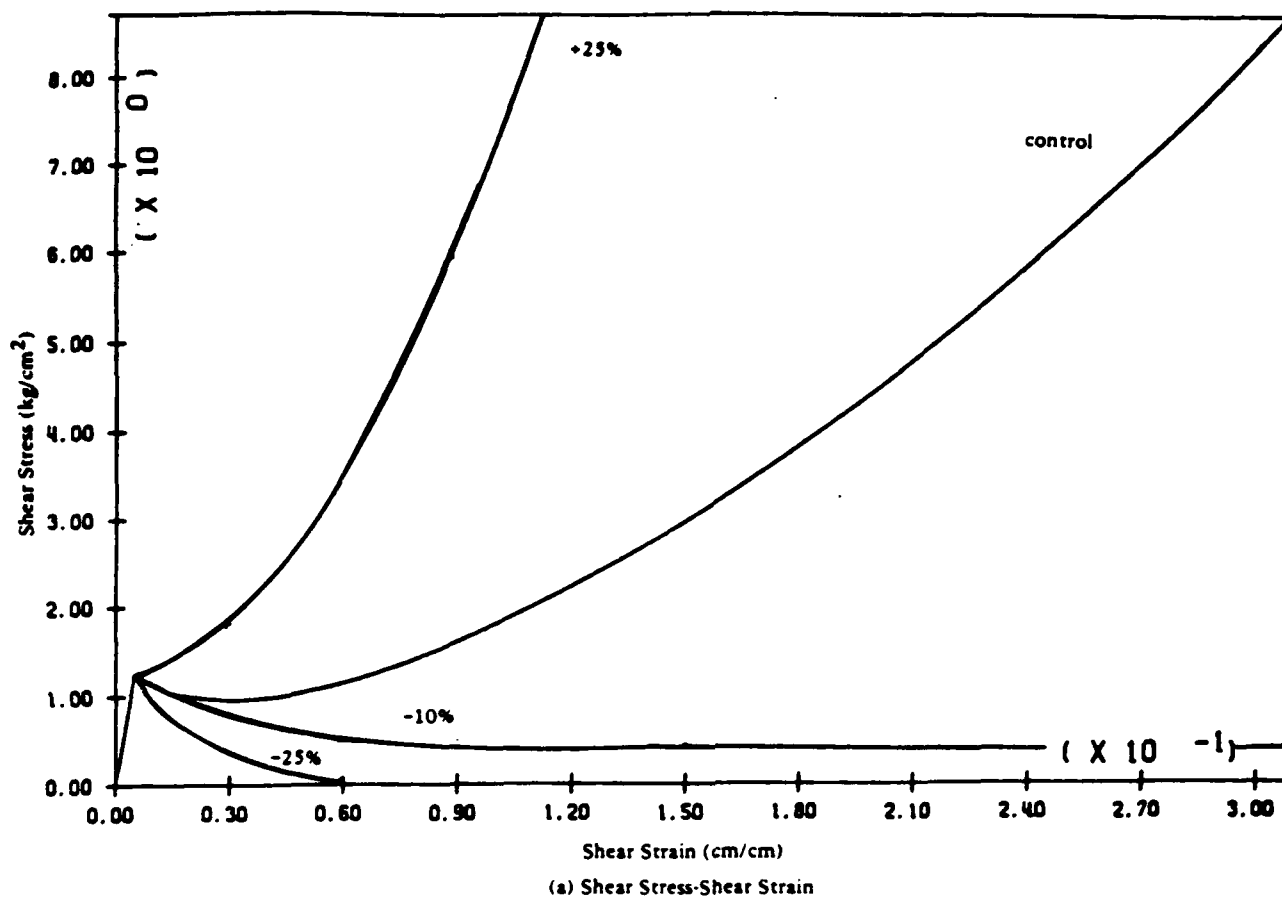


Figure 10.12. Yield surface size variation 25%, 10% undrained compression shear stress-strain, mean stress-volme strain

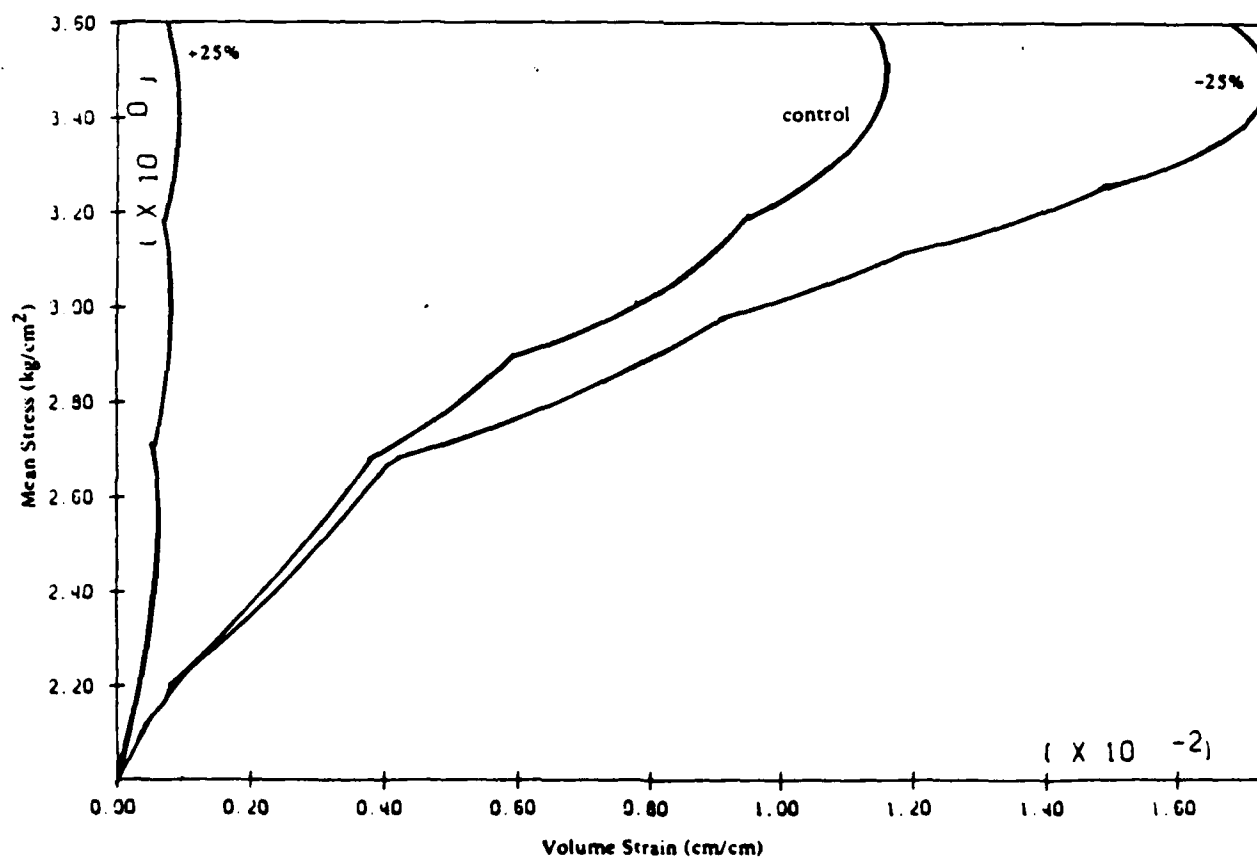
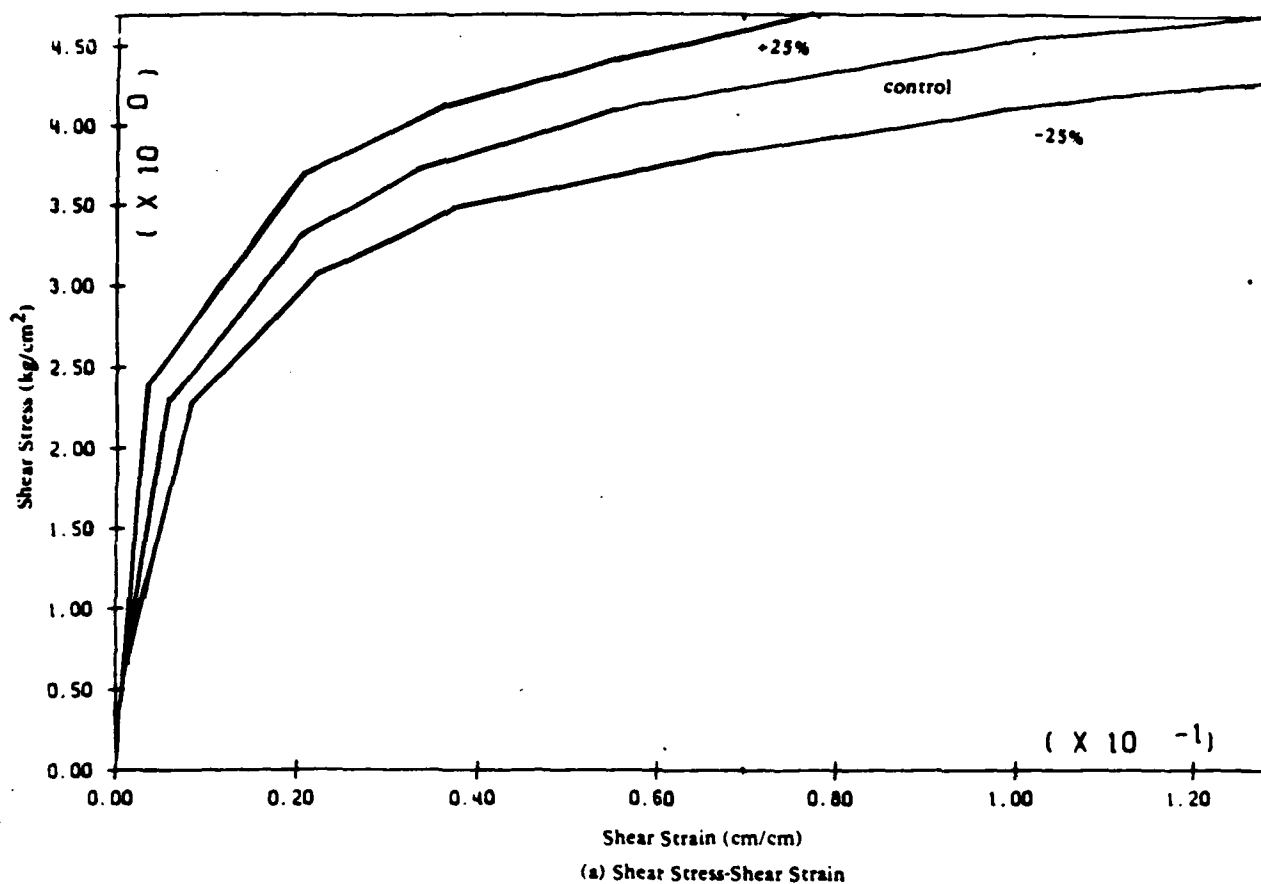
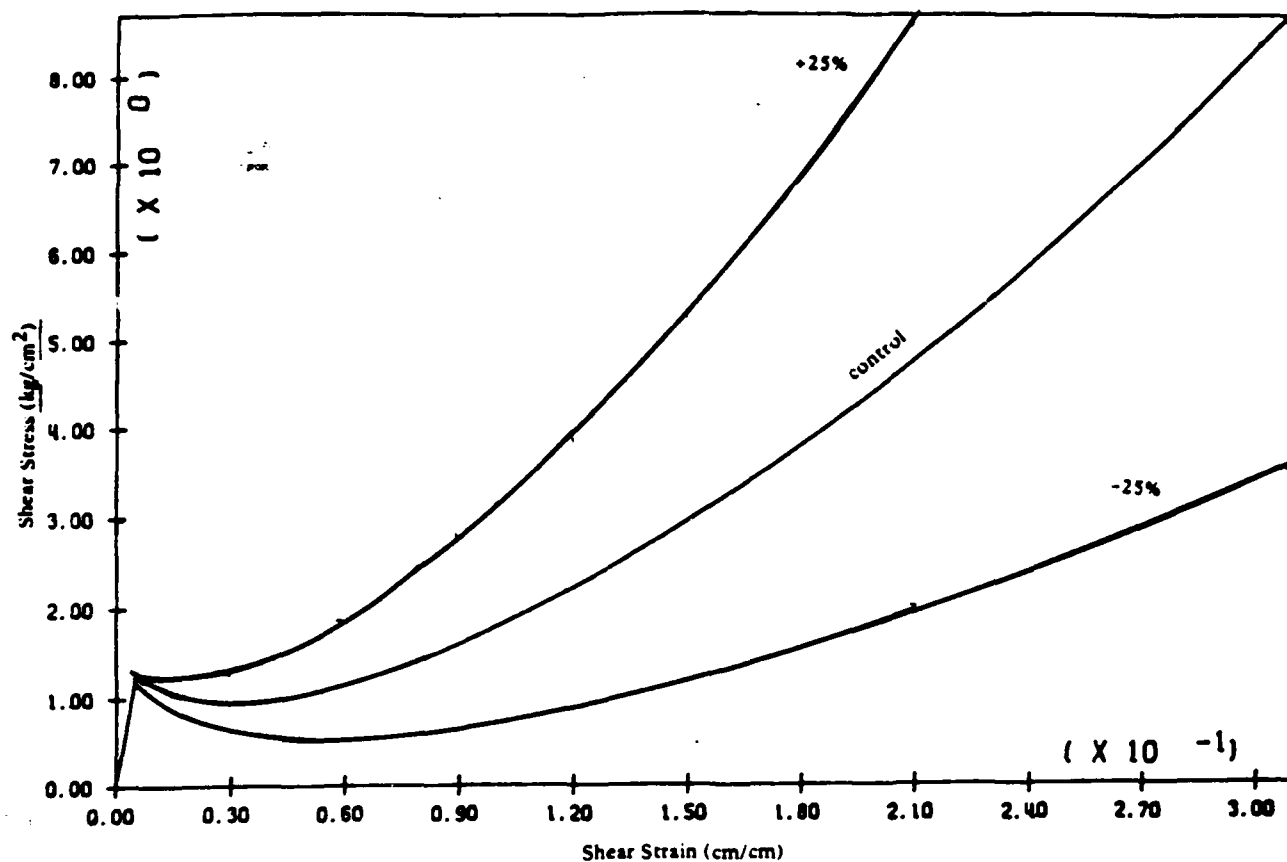
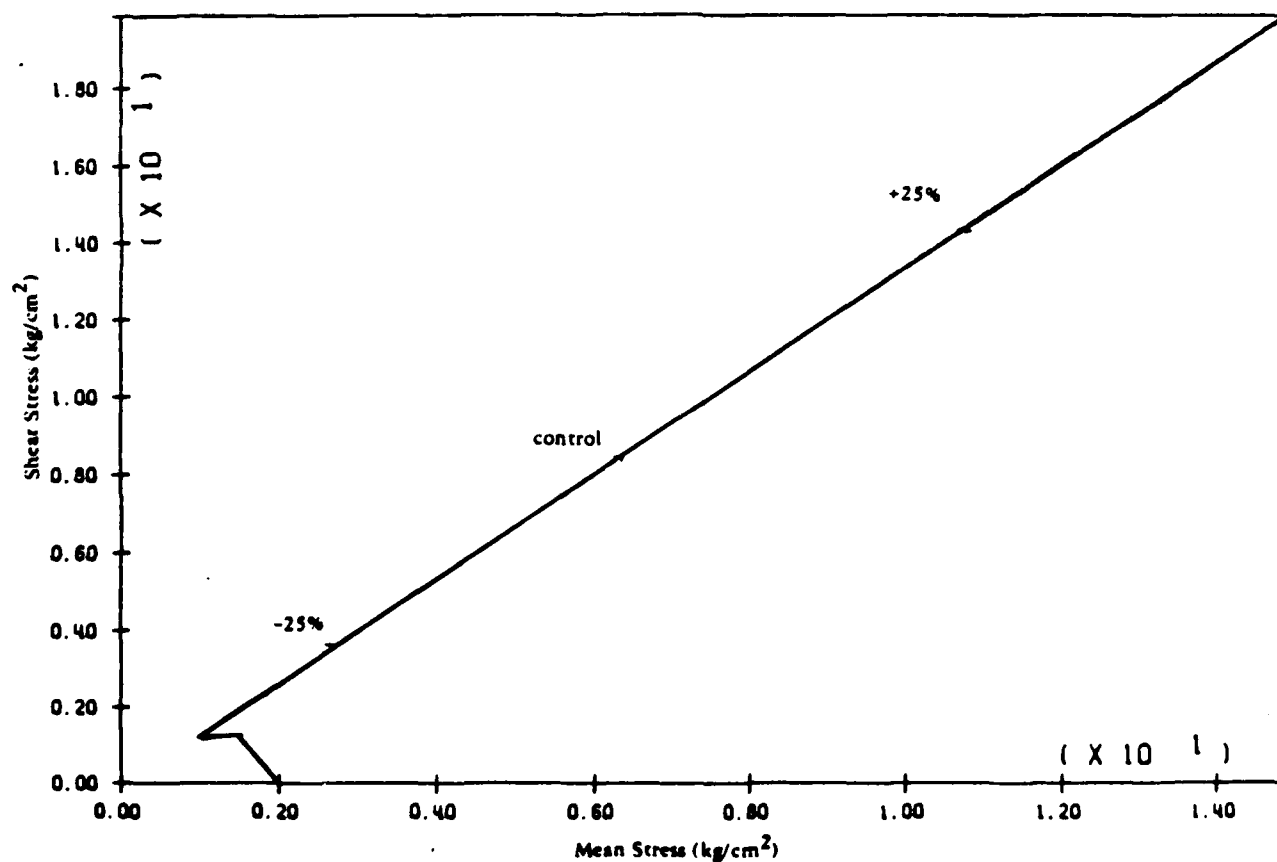


Figure 10.13. Yield surface position variation 25% drained compression shear stress-strain, mean stress-volume strain



(a) Shear Stress-Shear Strain



(b) Stress Path

Figure 10.14. Yield surface position variation 25% un drained compression shear stress-strain, mean stress-volume strain 229

10.2.0 Linear Isotropic Elasticity Model

The linear isotropic elasticity model may be used with plane strain, plane stress, and three-dimensional options. Finite deformation effects are not accounted for by this model.

10.2.1 Material Control Card (15)

Note	Columns	Variable	Description
	1-5	MATYP	The number 1

10.2.2 Material Properties Card (4F10.0)

Note	Columns	Variable	Description
	1-10	E	Young's modulus (solid phase)
(1)	11-20	POIS	Poisson's ratio (solid phase)
(2)	21-30	BF	Bulk modulus (fluid phase)
(2)	31-40	XNF	Porosity

Notes:

(1) Poisson's ratio cannot be set equal to $1/2$ since it results in division by zero. A value close to $1/2$, say .4999, can be employed for incompressible applications.

(2) Only applicable to porous media models.

10.2.3 Diffusion Properties (6F10.0) (only if required)

Note	Columns	Variable	Description
(1)	1-10	XK(1)	Permeability 11
	11-20	XK(2)	Permeability 12
	21-30	XK(3)	Permeability 22
(2)	31-40	XK(4)	Permeability 13
(2)	41-50	XK(5)	Permeability 23
(2)	51-60	XK(6)	Permeability 33

Notes:

- (1) Only applicable to NTYPE = 4, 5 and 13 (see Section 9.0).
- (2) Only applicable to three-dimensional problems.

10.2.4 Storage Requirements

If IOPT equals 3, NRC = 21; otherwise NRC = 6.

<u>First Word</u>	<u>Variable Array</u>
MF	MATYP
M1 = MF + 1	ALL
M2 = M1 + IPREC	ALLF
M3 = M2 + IPREC	XNF
M4 = M3 + IPREC	CC(NRC)
ML = M4 + NRC*IPREC	
(ML - MF + 1 = total required storage for material in element group data).	

10.3.0 Elasto-Plastic Constitutive Models (Geomechanics)

The elasto-plastic models may be used only with the plane strain and three-dimensional options. The form of the \mathbf{K} is given as follows

$$\mathbf{K} = \mathbf{E} - (\mathbf{E} : \mathbf{P})(\mathbf{Q} : \mathbf{E}) / (\mathbf{H}' + \mathbf{Q} : \mathbf{E} : \mathbf{P})$$

in which \mathbf{H}' = plastic modulus; \mathbf{P} and \mathbf{Q} = symmetric second-order tensors such that \mathbf{P} gives the direction of plastic deformations, \mathbf{Q} is the outer normal to the active yield surface, \mathbf{E} = fourth-order tensor of elastic moduli, assumed isotropic for the particular class of material models implemented.

The plastic potential is always selected such that

$$\mathbf{P} - 1/3 (\text{trace } \mathbf{P}) \mathbf{1} = \mathbf{Q} - 1/3 (\text{trace } \mathbf{Q}) \mathbf{1} = \mathbf{Q}'$$

Several material models have been incorporated in the program and may be selected by specifying the value of the control parameter PLTYP as follows:

- (1) PLTYP = 1 to 5: pressure non-sensitive materials.

The yield function in these cases is of the Von Mises type with

$$f = 3/2 (\mathbf{s} - \mathbf{a}) : (\mathbf{s} - \mathbf{a}) - k^*k = 0$$

where \mathbf{s} is the deviatoric stress tensor, i.e.,

$$\mathbf{s} = \mathbf{SIGMA} - p' \mathbf{1} \quad p' = 1/3 \text{ trace}(\mathbf{SIGMA})$$

\mathbf{a} is the coordinate of the center of the yield surface in the deviatoric stress space; and k is the size of the yield surface.

The relationship between the elastic shear modulus G , the plastic modulus \mathbf{H}' , and the elasto-plastic shear modulus \mathbf{H} is given by

$$1/\mathbf{H} = 1/2G + 1/\mathbf{H}'$$

- (2) PLTYP = 6: pressure sensitive materials.

The yield function in that case is of the following form

$$f = 3/2 (\mathbf{s} - \mathbf{a}) : (\mathbf{s} - \mathbf{a}) + c^*c(p' - b)^*(p' - b) - k^*k = 0$$

in which b is the coordinate of the center of the yield surface along the hydrostatic axis; and c is a material parameter called the yield surface axis ratio. The plastic potential is selected as follows:

$$\text{trace } \mathbf{P} = 1/3 \text{ trace } \mathbf{Q} + A J'(3) / \mathbf{Q}' : \mathbf{Q}'$$

where: $Q':Q' = \text{trace}(Q'.Q')$

$$J'(3) = 3 \det(Q') = \text{trace}(Q'.Q'.Q')$$

and A is a material parameter which measures the departure from an associative flow rule. When $A = 0$, $P = Q$ and consequently K possesses the major symmetry.

(3) PLTYP = 8: pressure sensitive materials.

The yield function in that case is of the following form

$$f = 3/2 (s - p' a):(s - p' a) - (k p')*(k p') = 0$$

where $p = (p' - a)$, and $a = \text{attraction (GE.0.0)}$. The plastic potential is selected as follows:

$$\text{trace } P = (M^*M - 1.)/(M^*M + 1.)$$

in which $M = \text{normalized stress ratio}$.

A collection of nested yield surfaces may be used. This allows for the adjustment of the plastic hardening rule to any experimental hardening data; for example, data obtained from axial or simple shear tests. It is assumed that the yield surfaces are all similar, and that a plastic modulus (H') is associated with each one.

Several different plastic hardening rules may be selected by specifying the value of PLTYP, as indicated below:

PLTYP = 1 Isotropic hardening rule

The yield surfaces in this case do not change position, but merely increase in size as loading proceeds. The elasto-plastic shear moduli, H' 's, must be selected so that each $H.GE.0$ 0.

PLTYP = 2 Isotropic hardening/softening rule

This case is a generalization of the previous model in which softening starts to occur when the outermost yield surface is reached. At this point, the elasto-plastic shear modulus is set to be $H = d(1)G$, and remains constant until $k.LE.d(2)$. Thereafter $H = 0$.

PLTYP = 3 Kinematic hardening rule

In this case, the yield surfaces do not change size, but are translated in stress space by the stress point. Each $H.GE.0$.

PLTYP = 4 Kinematic hardening/softening rule

In this case, the yield surfaces do not change size, but are translated in stress space until the outermost yield surface is reached. Isotropic softening then occurs with $H = d(1)G$ until $k.LE.d(2)$. Thereafter, $H = 0$ on the outermost yield surface and kinematic hardening takes place.

PLTYP = 5 Combination of isotropic and kinematic hardening/softening rules

The particular material model implemented in that option assumes cyclic degradation of the material properties according to the rule:

$$d(\tau)/\tau = - d1*(\gamma^{d2})*d(\log N)$$

as observed in cyclic strain-controlled simple shear tests. τ = Shear stress; γ = Shear strain; N = Number of cycles.

PLTYP = 6 Hardening rule for pressure-sensitive materials

A combination of isotropic and kinematic hardening rules is used for that model. The dependence of the model parameters upon the effective mean normal stress and plastic volumetric strain are assumed of the following forms:

$$x = x1 (p'/p1')^{**n}$$

and

$$y = y1 \exp (\lambda * e(v))$$

respectively, where $x = B, G, H'$, and $y = a, b, k$. λ and n are experimental constants; $p1'$ = initial effective mean normal stress (i.e., at $e(v) = 0$); p' = effective mean normal stress; $e(v) = [(v1-v)/v]$ where v = current volume and $v1$ = initial volume (i.e., at $p' = p1'$) of the material specimen.

PLTYP = 8 Kinematic hardening rule

A purely kinematic hardening is adopted for that model. The dependence of the moduli on the effective mean normal stress is assumed of the following form:

$$x = x1 (p'/p1')^{**n} 0$$

where $x = G, B, H'$. For cohesionless soils $n = 1/2$.

10.3.1 Material Control Card (3I5)

Note	Columns	Variable	Description
(1)	1-5	MATYP	The number 2
	6-10	PLTYP	Plasticity material subtype; GE.1 and LE.8
	11-15	NYS	Number of yield surfaces; GE.0; if EQ.0, set internally EQ.1

Notes:

(1) If PLTYP = 1,2,...,5, the stiffness matrix is symmetric. If PLTYP.GE.6, the stiffness is nonsymmetric, and ISYMM must be set equal to 1 on Control Card 1 (see Section 2.1) for implicit calculations.

This card and those following necessary for material model definition are generated by Program MUD.

10.3.2 Material Properties Cards

Card 1 (4F10.0)

Note	Columns	Variable	Description
(1)	1-10 1-20	FM(ND+1,1,1)	Elastic shear modulus (G1) Initial elasto-plastic shear modulus ($H1 = 2G1$)
(2)	21-30	FM(ND+2,1,1)	Elastic bulk modulus (B1)
(3)	31-40	FM(ND+3,1,1)	Bulk exponent (n)

Notes:

(1) The shear modulus, G, is the same as the Lamé parameter, MU.

(2) The elastic bulk modulus may be defined in terms of the Lamé parameters by

$$B = (\text{LAMBDA} + 2 \text{ MU}) / 3$$

For PLTYP.GE.6, G1 and B1 is the reference elastic shear and bulk moduli at initial mean stress $p1'$.

(3) Only applicable to PLTYP.GE.6

Card 2 Initial Stress (I5,5X,6F10.0)*NUMAT)

Note	Columns	Variable	Description
	1-5	N	Material set number; LE. NUMAT
	11-20	S(1,N)	Component 11 (SIGMA11)
	21-30	S(2,N)	Component 22 (SIGMA22)
	31-40	S(3,N)	Component 33 (SIGMA33)
	41-50	S(4,N)	Component 12 (SIGMA12)
	51-60	S(5,N)	Component 23 (SIGMA23)
	61-70	S(6,N)	Component 31 (SIGMA31)

Card 3 Yield Parameters - PLTYP = 1,...,5 (5F10.0) +

Note	Columns	Variable	Description
	1-10	XLAM(3,1)	Delta 1 (d1)
	11-20	XLAM(4,1)	Delta 2 (d2)
(1)	21-30	ALF	Pore fluid bulk modulus
(1)	31-40	XNF(1)	Initial porosity
(1)	41-50	PF(1)	Initial pore fluid pressure

Notes:

(1) Only applicable to porous media models

Card 3 Yield Parameters - PLTYP = 6 (8F10.0)

Note	Columns	Variable	Description
	1-10	XLAM(3,1)	Delta 1 (d1)
	11-20	XLAM(4,1)	Delta 2 (d2)
	21-30	XLAM(5,1)	Yield surface axis ratio (c)
	31-40	XLAM(6,1)	Reference pressure (LE.0.)
	41-50	XLAM(7,1)	Volumetric exponent (Lambda)
(1)	51-60	ALF	Pore fluid bulk modulus
(1)	61-70	XNF(1)	Initial porosity
(1)	71-80	PF(1)	Initial pore fluid pressure

(1) Only applicable to porous media models

Card 3 Yield Parameters - PLTYP = 8 (7F10.0)

Note	Columns	Variable	Description
(1)	1-10	XLAM(3,1)	Critical stress ratio (Comp.)
(2)	11-20	XLAM(4,1)	Critical stress ratio (Ext.)
(3)	21-30	XLAM(5,1)	Attraction (GE.0.0)
(4)	31-40	XLAM(6,1)	Reference pressure (LE.0.)
(5)	41-50	ALF	Pore fluid bulk modulus
(6)	51-60	XNF(1)	Initial porosity
(7)	61-70	PF(1)	Initial pore fluid pressure

Notes:

(1) The critical stress ratio (CSR) is the point defined by the ratio of deviatoric stress to mean effective stress where the material begins to exhibit dilative (expansive) behavior. The effects of varying this value are detailed, for monotonic triaxial simulations, in Appendix A.

(2) Same as (1) above defined in extension.

(3) Attraction is qualitatively the same as cohesion.

(4) The reference mean stress is defined in the following:

$$G = G_1 \left(\frac{p}{p_1} \right)^n \quad B = B_1 \left(\frac{p}{p_1} \right)^n \quad H' = H'_1 \left(\frac{p}{p_1} \right)^n \quad (1)$$

where: G = elastic shear modulus

B = elastic bulk modulus

H' = plastic modulus

n = experimental parameter ($n = 0.5$ for most cohesionless soils)

G_1, B_1, H'_1 = moduli at reference effective mean normal stress p_1 .

The proper selection of the effective mean confining stress will allow conversion to any set of consistant units for analysis.

Example 1:

Conversion: Kilograms per square centimeter to pounds per square inch.

$$P_r = \frac{P}{(G/G_r)^{1/n}} \quad (2)$$

where Equation 2 is defined in the same manner as Equation 1.

Using initial values of

$$G = 400 \text{ kg/cm}^2$$

$$P = 2 \text{ kg/cm}^2 = 28.4 \text{ lb/in}^2$$

$$n = 0.5 \text{ (Experimental)}$$

$$G_r = 5678 \text{ lb/in}^2$$

$$P_r = \left(\frac{28.4 \text{ lb/in}^2}{5678 \text{ lb/in}^2 / 400 \text{ kg/cm}^2} \right)^{1/0.5}$$

$$P_r = 0.141$$

The moduli at any pressure can be computed using P_r as the reference, and the units from the original material model unchanged. The same operations may be used to adapt any other units, such as pounds per square inch to pounds per square foot by repeating the procedure above.

The need for the reference mean effective stress is a result of the soil moduli being pressure dependent. Variations in the moduli with depth and experimental parameter n from Equation 1 are shown in Figure 10.4. The value for n may be computed directly from a curve fitting procedure if enough triaxial data is available. A large number of granular soils have shown $n = 0.5$ to be an acceptable choice. Shear wave velocity data may also be used.

(5) The pore fluid bulk modulus is a penalty number. Selection of penalty values is discussed in Section 9.3, Contact Elements. In general, the fluid bulk modulus should be 10^6 the bulk modulus of the solid phase. Again the procedure outlined in Section 9.3 is recommended for final selection.

(6) Porosity values can be readily computed from the equations:

$$n = \frac{V_v}{V}$$

or

$$n = \frac{e}{1 + e}$$

where: n = porosity

V_v = volume of voids in material

V = volume of sample

e = void ratio

(7) Initial pore fluid pressure may be input to provide a simulated "back pressure" to the material model.

Subsequent Cards, Yield Surface Data PLTYP = 6

Two cards are required for each yield surface. The number of yield surfaces equals NYS. (NYS is defined on the material control card; see Section 10.3.1.)

Card 1 (I5, 5X, 7F10.0)

Note	Columns	Variable	Description
	1-5	M1	Additional yield surface number; 1.LE.M1.LE.NYS
(1)	11-20	FM(ND+1,M,1)	Size of yield surface (k)
(2)	21-30	FM(ND+2,M,1)	Plastic modulus (one) (h1)
(3)	31-40	FM(ND+3,M,1)	Plastic modulus (two) (h2)
(4)	41-50	FM(ND+4,M,1)	Coefficient (one)
(4)	51-60	FM(ND+5,M,1)	Degree of non-associativity (one)
(4)	61-70	FM(ND+6,M,1)	Degree of non-associativity (two)

Notes:

- (1) $ND = 2 \cdot NSD$ and $M = M1 + 1$
- (2) If $PLTYP = 1, \dots, 5$ $H = H' / (1. + (H' / 2G))$
- (3) Only applicable to $PLTYP .GE. 6$
- (4) Only applicable to $PLTYP .EQ. 6$

Card 2 Initial Positions of Yield Surface (6F10.0)

Note	Columns	Variable	Description
(1)	1-10	FM(1,M,1)	Component 11
	11-20	FM(2,M,1)	Component 22
	21-30	FM(3,M,1)	Component 33
	31-40	FM(4,M,1)	Component 12
(2)	41-50	FM(5,M,1)	Component 23
(2)	51-60	FM(6,M,1)	Component 31

Notes:

(1) The components are the coordinates of the center of the yield surface in stress space (Figure 10.15).

(2) Only applicable to three-dimensional problems.

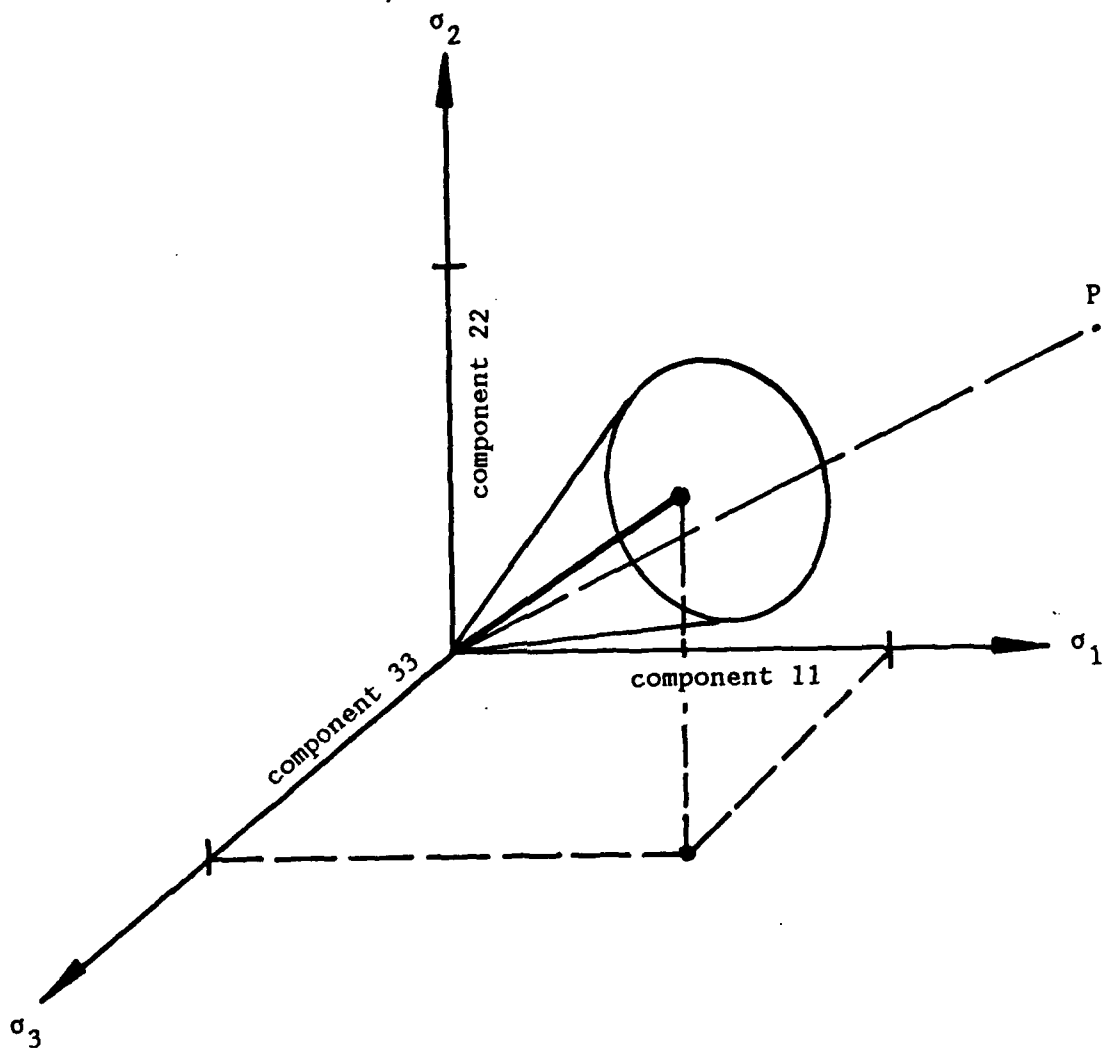


Figure 10.15. Yield surface location

Subsequent Cards, Yield Surface Data (PLTYP) = 8)

Two cards are required for each yield surface. The number of yield surface equals NYS. (NYS is defined on the material control card; see Section 10.3.1)

Card 1 (I5,5X,7F10.0)

Note	Columns	Variable	Description
	1-5	M1	Additional yield surface number; 1.LE.M1.LE.NYS
(1)	11-20	FM(ND+1,M,1)	Size of yield surface (k)
(2)	21-30	FM(ND+2,M,1)	Plastic modulus (one) (h1)
(2)	31-40	FM(ND+3,M,1)	Plastic modulus (two) (h2)
(3)	41-50	FM(ND+4,M,1)	Stress Ratio in compression
(3)	51-60	FM(ND+5,M,1)	Stress Ratio in extension

Notes:

(1) $ND = 2 * NSD$ and $M = M1 + 1$

The yield surface size is shown in Figure 10.16. Note that this value is dependent on the effective confining pressure, $k = f(p)$.

(2) If $PLTYP = 1, \dots, 5$ $H = H' / (1. + (H' / 2G))$

The plastic moduli H_1 and H_2 are the moduli associated with the compression and extension data for that surface, and are also pressure dependent.

(3) The stress ratio is detailed in Reference 39. The stress ratio is computed for each surface but is ignored in the computations. The values here may be averaged to determine a value for the critical stress ratio.

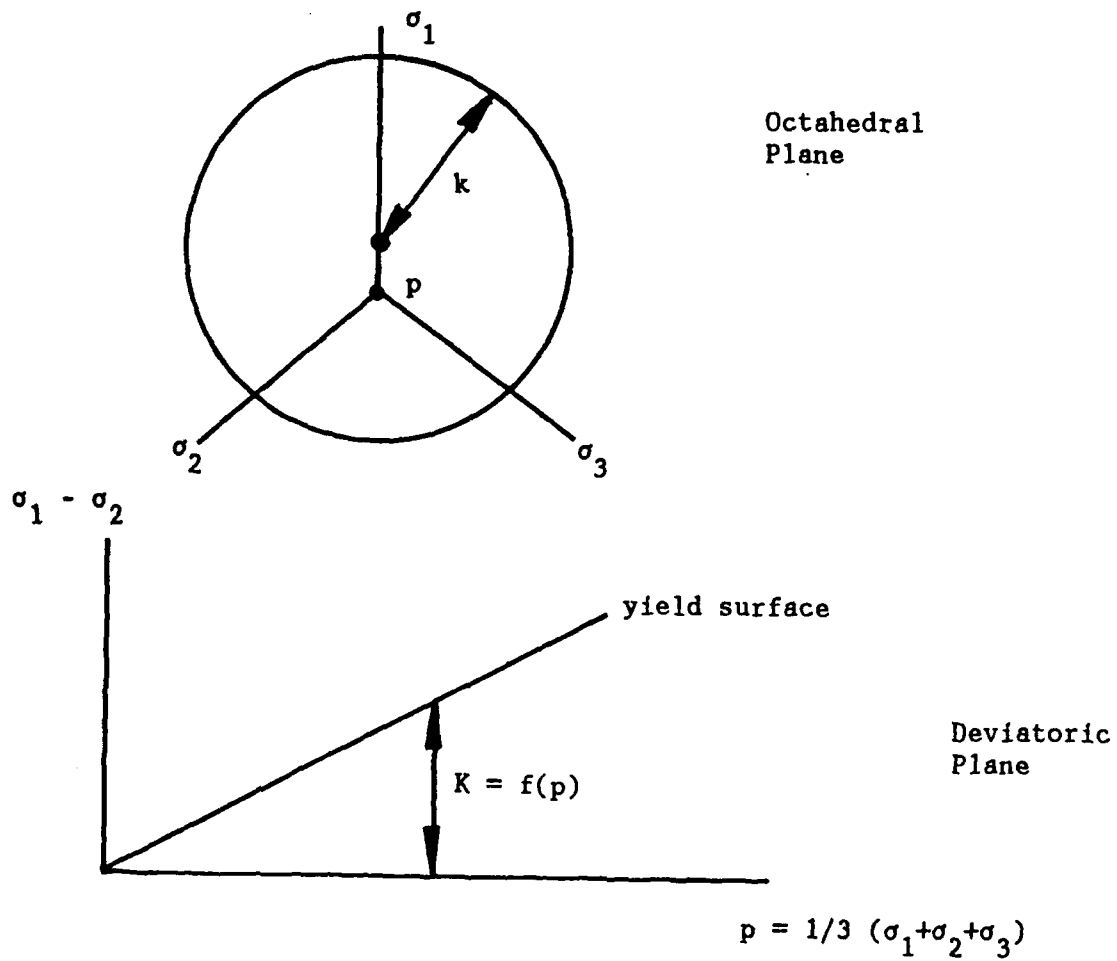


Figure 10.16. Yield surface size, K

10.3.3 Diffusion Properties (6F10.0) (only if required)

Note	Columns	Variable	Description
(1)	1-10	XK(1)	Permeability 11
	11-20	XK(2)	Permeability 12
	21-30	XK(3)	Permeability 22
(2)	31-40	XK(4)	Permeability 13
(2)	41-50	XK(5)	Permeability 23
(2)	51-60	XK(6)	Permeability 33

Notes:

(1) Only applicable to NTYPE = 4, 5 and 13 (see Section 9.0)

(2) Only applicable to three-dimensional problems.

The permeability is input as a measured material property, either from laboratory tests or field pumping tests. Permeability 12 should not be input other than 0.0. The algorithm in DYNAFLOW also changes the input permeability by whatever the input gravity field is. To model the actual material permeability in gravity fields other than the 1_g (i.e., 9.81 M/s² or 32.2 ft/s²) is necessary to increase the input value by the product of the load time function and the gravity multiplier (Sections 8.0 and 9.0).

10.3.4 Storage Requirements

In two-dimensional applications, if PLTYP equals 6, then NRFM = 10, otherwise NRFM = 6. In three-dimensional applications, if PLTYP equals 6, then NRFM = 12, otherwise NRFM = 8 (NRXLAM = 7 always).

<u>First Word</u>	<u>Variable Array</u>
MF	MATYP
MF + 1	PLTYP
MF + 2	NYS
M1 = MF + 3	IND(3, NSPTS*)
M2 = M1 + NSPTS*3	FM(NRFM, NYS+1, NSPTS)
M3 = M2 + NSPTS*NYS*NRFM*IPREC	XLAM(NRXLAM, NSPTS)
ML = M3 + NSPTS*NRXLAM*IPREC	
(ML - MF + 1 = total required storage for material in element group data.)	
*NSPTS = Number of stress points (= NUMEL for the linear plane and brick elements).	

10.4.0 Drucker-Prager Elasto-Plastic Model

The Drucker-Prager elasto-plastic model may be used with plane strain, and three-dimensional options. Finite deformation effects are not accounted for by this model.

The yield function is of the following type :

$$f = \text{ALPHA} * p + \text{Tau} - c = 0$$

where: $\text{Tau} = \text{SQRT}(J2)$

$$p = \text{tr}(\text{SIGMA}) / 3$$

ALPHA and c are material constants, SIGMA = Solid effective stress,

$$J2 = \text{tr}(s.s) / 2 \quad s = \text{SIGMA} - p \mathbf{1}$$

If BETA=ALPHA an associative flow rule is used. Otherwise a non-associative flow rule is used.

10.4.1 Material Control Card (2I5)

Note	Columns	Variable	Description
	1-5	MATYP	The number 6
	6-10	NUMAT	Number of initial stresses; GE.0; if EQ.0, set internally EQ.1

10.4.2 Material Properties Card

Card 1 (7F10.0)

Note	Columns	Variable	Description
	1-10	G	Elastic shear modulus (solid phase)
	11-20	B	Elastic bulk modulus (solid phase)
	21-30	ALPHA	Frictional coefficient
	31-40	C	Cohesive coefficient
	41-50	BETA	Non-associativity coefficient
(1)	51-60	ALF	Pore fluid bulk modulus
(1)	61-70	XNF	Porosity

Notes:

(1) Only applicable to porous media models.

Card 2 Initial Stress (I5,5X,6F10.0)*NUMAT)

Note	Columns	Variable	Description
	1-5	N	Initial stress set number LE.NUMAT
	11-20	S(1,N)	Component 11 (SIGMA11)
	21-30	S(2,N)	Component 22 (SIGMA22)
	31-40	S(3,N)	Component 33 (SIGMA33)
	41-50	S(4,N)	Component 12 (SIGMA12)
	51-60	S(5,N)	Component 23 (SIGMA23)
	61-70	S(6,N)	Component 31 (SIGMA31)

10.4.3 Diffusion Properties (6F10.0) (only if required)

Note	Columns	Variable	Description
(1)	1-10	XK(1)	Permeability 11
	11-20	XK(2)	Permeability 12
	21-30	XK(3)	Permeability 22
(2)	31-40	XK(4)	Permeability 13
(2)	41-50	XK(5)	Permeability 23
(2)	51-60	XK(6)	Permeability 33

Notes:

- (1) Only applicable to NTYPE = 4, 5 and 13 (see Section 9.0)
- (2) Only applicable to three-dimensional problems

10.4.4 Storage Requirements

<u>First Word</u>	<u>Variable Array</u>
MF	MATYP
M1 = MF + 1	S(2*NSD, NSPTS)
M2 = M1 + NSPTS*NSD*2*IPREC	IND(NSPTS)
M3 = M2 + NSPTS	G
M4 = M3 + IPREC	B
M5 = M4 + IPREC	ALPHA
M6 = M5 + IPREC	C
M7 = M6 + IPREC	BETA
ML = M7 + IPREC	
(ML - MF + 1 = total required storage for material in element group data.)	

*NSPTS = Number of stress points

10.5.0 Von Mises Elasto-Plastic Model

The Von Mises elasto-plastic model may be used with plane strain, and three-dimensional options. Finite deformation effects are not accounted for by this model.

The yield function is of the following type :

$$f = \text{Tau} - c = 0$$

where c (= cohesion) is a material constant,

$$\text{Tau} = \text{SQRT}(J2) \quad p = \text{tr}(\text{SIGMA}) / 3$$

SIGMA = Soild effective stress,

$$J2 = \text{tr}(\mathbf{s} \cdot \mathbf{s}) / 2 \quad \mathbf{s} = \text{SIGMA} - p \mathbf{1}$$

10.5.1 Material Control Card (I5)

Note	Columns	Variable	Description
	1-5	MATYP	The number 7

10.5.2 Material Properties Card

Card 1 (5F10.0)

Note	Columns	Variable	Description
	1-10	G	Elastic shear modulus (solid phase)
	11-20	B	Elastic bulk modulus (solid phase)
	21-30	C	Cohesive coefficient
(1)	31-40	ALF	Pore fluid bulk modulus
(1)	41-50	XNF	Porosity

Notes:

(1) Only applicable to porous media models.

Card 2 Initial Stress (6F10.0)

Note	Columns	Variable	Description
	1-10	S(1,1)	Component 11 (SIGMA11)
	11-20	S(2,1)	Component 22 (SIGMA22)
	21-30	S(3,1)	Component 33 (SIGMA33)
	31-40	S(4,1)	Component 12 (SIGMA12)
	41-50	S(5,1)	Component 23 (SIGMA23)
	51-60	S(6,1)	Component 31 (SIGMA31)

10.5.3 Diffusion Properties (6F10.0) (only if required)

Note	Columns	Variable	Description
(1)	1-10	XK(1)	Permeability 11
	11-20	XK(2)	Permeability 12
	21-30	XK(3)	Permeability 22
(2)	31-40	XK(4)	Permeability 13
(2)	41-50	XK(5)	Permeability 23
(2)	51-60	XK(6)	Permeability 33

Notes:

- (1) Only applicable to NTYPE = 4, 5 and 13 (see Section 9.0)
- (2) Only applicable to three-dimensional problems

10.5.4 Storage Requirements

<u>First Word</u>	<u>Variable Array</u>
MF	MATYP
M1 = MF + 1	S(2*NSD, NSPTS)
M2 = M1 + NSPTS*NSD*2*IPREC	IND(NSPTS)
M3 = M2 + NSPTS	G
M4 = M3 + IPREC	B
M5 = M4 + IPREC	C
ML = M5 + IPREC	
(ML - MF + 1 = total required storage for material in element group data.)	

*NSPTS = Number of stress points

10.6.0 Thermo-Elastic Model

The linear/nonlinear generalized thermo-elastic model may be used with plane strain, plane stress, and three-dimensional options. Finite deformation effects are not accounted for by this model.

10.6.1 Material Control Card (I5)

Note	Columns	Variable	Description
	1-5	MATYP	The number 3

10.6.2 Material Properties Cards

10.6.2.1 General Properties (6F10.0)

Note	Columns	Variable	Description
	1-10	E	Young's Modulus
	11-20	POIS	Poisson's Ratio
	21-30	ROC	Specific Heat
	31-40	TZERO	Reference Temperature
	41-50	RT1	First Relaxation Time
	51-60	RT2	Second Relaxation Time

10.6.2.2 Nonlinear Young's Modulus Multipliers (2F10.0)

Note	Columns	Variable	Description
(1)	1-10	ENON(1)	Nonlinear Young's Modulus Multiplier 1
(1)	11-20	ENON(2)	Nonlinear Young's Modulus Multiplier 2

Notes:

(1) Nonlinear Young's Modulus EN is computed by the following equation

$$EN = E*(ENON(1)+ENON(2)*TETA)$$

where TETA = absolute temperature. For linear material, just leave this card blank.

10.6.2.3 Thermal Expansion Properties (6F10.0)

Note	Columns	Variable	Description
	1-10	BETA(1)	Thermal Expansion 11
	11-20	BETA(2)	Thermal Expansion 12
	21-30	BETA(3)	Thermal Expansion 22
(1)	31-40	BETA(4)	Thermal Expansion 13
(1)	41-50	BETA(5)	Thermal Expansion 23
(1)	51-60	BETA(6)	Thermal Expansion 33

Notes:

(1) Only applicable to three-dimensional problems

10.6.2.4 Nonlinear Thermal Expansion Multipliers (3F10.0)

Note	Columns	Variable	Description
(1)	1-10	BNON(1)	Nonlinear Thermal Expansion Multiplier 1
(1)	11-20	BNON(2)	Nonlinear Thermal Expansion Multiplier 2
(1)	21-30	BNON(3)	Nonlinear Thermal Expansion Multiplier 3

Notes:

(1) Nonlinear thermal moduli $B(I)$ are computed by the following equation

$$B(I) = BETA(I) * (BNON(1) + (BNON(2) + BNON(3) * TETA) * TETA) * EN,$$
$$I = 1, 2, \dots, 6,$$

where TETA = absolute temperature, EN is defined in Section 10.6.2.2.
For linear material, just leave this card blank.

10.6.2.5 Thermal Conductivity Properties (6F10.0)

Note	Columns	Variable	Description
	1-10	CD(1)	Conductivity 11
	11-20	CD(2)	Conductivity 12
	21-30	CD(3)	Conductivity 22
(1)	31-40	CD(4)	Conductivity 13
(1)	41-50	CD(5)	Conductivity 23
(1)	51-60	CD(6)	Conductivity 33

Notes:

(1) Only applicable to three-dimensional problems

10.6.2.6 Nonlinear Thermal Conductivity Multipliers (6F10.0)

Note	Columns	Variable	Description
(1)	1-10	CDNON(1)	Nonlinear Thermal Conductivity Multiplier 1
(1)	11-20	CDNON(2)	Nonlinear Thermal Conductivity Multiplier 2
(1)	21-30	CDNON(3)	Nonlinear Thermal Conductivity Multiplier 3
(1)	31-40	CDNON(4)	Nonlinear Thermal Conductivity Multiplier 4
(1)	41-50	CDNON(5)	Nonlinear Thermal Conductivity Multiplier 5
(1)	51-60	CDNON(6)	Nonlinear Thermal Conductivity Multiplier 6

Notes:

(1) Nonlinear thermal Conductivities XK(I) are computed by the following equation

$$XK(I) = CD(I) * (CDNON(1) + (CDNON(2) + (CDNON(3) + (CDNON(4) + (CDNON(5) + CDNON(6) * TETA) * TETA) * TETA) * TETA) * TETA), \quad I = 1, 2, \dots, 6,$$

where TETA = absolute temperature. For linear material, just leave this card blank.

10.6.2.7 Nonlinear Specific Heat Multipliers (6F10.0)

Note	Columns	Variable	Description
(1)	1-10	ROCNON(1)	Nonlinear Specific Heat Multiplier 1
(1)	11-20	ROCNON(2)	Nonlinear Specific Heat Multiplier 2
(1)	21-30	ROCNON(3)	Nonlinear Specific Heat Multiplier 3
(1)	31-40	ROCNON(4)	Nonlinear Specific Heat Multiplier 4
(1)	41-50	ROCNON(5)	Nonlinear Specific Heat Multiplier 5
(1)	51-60	ROCNON(6)	Nonlinear Specific Heat Multiplier 6

Notes:

(1) Nonlinear specific heat RC is computed by the following equation

$$RC = ROC * (ROCNON(1) * TETA + ROCNON(2) + (ROCNON(3) + (ROCNON(4) + (ROCNON(5) + ROCNON(6) / TETA) / TETA) / TETA) / TETA)$$

where TETA = absolute temperature. For linear material, just leave this card blank.

10.6.3 Initial Temperature (only applicable to elliptic option)

See Section 4.0

10.6.4 Storage Requirements

If IOPT equals 3, $N = 6$, otherwise $N = 3$.

<u>First Word</u>	<u>Variable Array</u>
MF	MATYP
$M1 = MF + 1$	E
$M2 = M1 + IPREC$	ENON(2)
$M3 = M2 + 2*IPREC$	POIS
$M4 = M3 + IPREC$	ROC
$M5 = M4 + IPREC$	TZERO
$M6 = M5 + IPREC$	RT1
$M7 = M6 + IPREC$	RT2
$M8 = M7 + IPREC$	BETA(N)
$M9 = M8 + N*IPREC$	BNON(3)
$M10 = M9 + 3*IPREC$	CD(N)
$M11 = M10 + N*IPREC$	CDNON(6)
$M12 = M11 + 6*IPREC$	ROCNON(6)
$ML = M12 + 6*IPREC$	
(ML - MF + 1 = total required storage for material in element group data)	

10.7.0 Newtonian Fluid Model

The Newtonian fluid model may be used with two- and three-dimensional options.

10.7.1 Material Control Card (I5)

Note	Columns	Variable	Description
	1-5	MATYP	The number 4

10.7.2 Material Properties Card (2F10.0)

Note	Columns	Variable	Description
(1)	1-10	ALL	Lambda
	11-20	MU	Shear Viscosity

Notes:

(1) For incompressible applications $ALL = C * MU$ where $C = 10^{**7}$ in machines with 60 to 64 bits floating point word lengths.

10.7.3 Storage Requirements

If IOPT = 3, NRC = 21; otherwise NRC = 6

<u>First Word</u>	<u>Variable Array</u>
MF	MATYP
M1 = MF + 1	ALL
M2 = M1 + IPREC	CC(NRC)
ML = M2 + NRC*IPREC	

(ML - MF + 1 = total required storage for material in element group data).

10.8.0 Heat Conduction Model

The linear/nonlinear heat conduction model may be used with plane and three-dimensional options.

10.8.1 Material Control Card (I5)

Note	Columns	Variable	Description
	1-5	MATYP	The number 5

10.8.2 Material Property Cards

10.8.2.1 Thermal Conductivity Properties (6F10.0)

Note	Columns	Variable	Description
	1-10	CD(1)	Conductivity 11
	11-20	CD(2)	Conductivity 12
	21-30	CD(3)	Conductivity 22
(1)	31-40	CD(4)	Conductivity 13
(1)	41-50	CD(5)	Conductivity 23
(1)	51-60	CD(6)	Conductivity 33

Notes:

(1) Only applicable to three-dimensional problems

10.8.2.2 Nonlinear Thermal Conductivity Multipliers (6F10.0)

Note	Columns	Variable	Description
(1)	1-10	CDNON(1)	Nonlinear Thermal Conductivity Multiplier 1
(1)	11-20	CDNON(2)	Nonlinear Thermal Conductivity Multiplier 2
(1)	21-30	CDNON(3)	Nonlinear Thermal Conductivity Multiplier 3
(1)	31-40	CDNON(4)	Nonlinear Thermal Conductivity Multiplier 4
(1)	41-50	CDNON(5)	Nonlinear Thermal Conductivity Multiplier 5
(1)	51-60	CDNON(6)	Nonlinear Thermal Conductivity Multiplier 6

Notes:

(1) Nonlinear thermal Conductivities XK(I) are computed by the following equation

$$XK(I) = CD(I) * (CDNON(1) + (CDNON(2) + (CDNON(3) + (CDNON(4) + (CDNON(5) + CDNON(6) * TETA) * TETA) * TETA) * TETA) * TETA), \quad I = 1, 2, \dots, 6,$$

where TETA = absolute temperature. For linear material, just leave this card blank.

10.8.2.3 Specific Heat and Reference Temperature (2F10.0)

Note	Columns	Variable	Description
	1-10	ROC	Specific Heat
	11-20	TZERO	Reference Temperature

10.8.2.4 Nonlinear Specific Heat Multipliers (6F10.0)

Note	Columns	Variable	Description
(1)	1-10	ROCNON(1)	Nonlinear Specific Heat Multiplier 1
(1)	11-20	ROCNON(2)	Nonlinear Specific Heat Multiplier 2
(1)	21-30	ROCNON(3)	Nonlinear Specific Heat Multiplier 3
(1)	31-40	ROCNON(4)	Nonlinear Specific Heat Multiplier 4
(1)	41-50	ROCNON(5)	Nonlinear Specific Heat Multiplier 5
(1)	51-60	ROCNON(6)	Nonlinear Specific Heat Multiplier 6

Notes:

(1) Nonlinear specific heat RC is computed by the following equation

$$RC = ROC * (ROCNON(1) * TETA + ROCNON(2) + (ROCNON(3) + (ROCNON(4) + (ROCNON(5) + ROCNON(6) / TETA) / TETA) / TETA) / TETA)$$

where TETA = absolute temperature. For linear material, just leave this card blank.

10.8.3 Storage Requirements

If NSD = 3, N = 6, otherwise N = 3.

<u>First Word</u>	<u>Variable Array</u>
MF	MATYP
M1 = MF + 1	CD(N)
M2 = M1 + N*IPREC	CDNON(6)
M3 = M2 + 6*IPREC	ROC
M4 = M3 + IPREC	ROCNON(6)
M5 = M4 + 6*IPREC	TZERO
ML = M5 + IPREC	
(ML - MF + 1 = total required storage for material in element group data)	

ANALYSIS RESTART

1.0 TITLE (20A4)

Note	Columns	Variable	Description
(1)	1-80	TITLE(20)	Job title for heading the output

Notes:

- (1) Data set must begin with a title card.

2.0 CONTROL CARDS

2.1 Card 1 (13I5)

Note	Columns	Variable	Description
(1)	1-5	NSB	Number of time steps between spatial printout; GE.0 If EQ.0, set internally EQ.(NTS+1)
(2)	6-10	NITER	Maximum number of iterations; GE.0
(3)	11-15	NFAC	Effective Stiffness Reform/ factorize code; GE.0 GT.0, every NFAC time step
(4)	16-20	MODE	Execution mode; GE.0 EQ.0, time integration, data check EQ.1, time integration, execution EQ.2, eigenvalue/vector, data check EQ.3, eigenvalue/vector, execution
(5)	21-25	ACCBC	Nodal boundary condition code; GE.0 EQ.0 Displacement BC EQ.1, Acceleration BC EQ.2, Velocity BC
(6)	26-30	IBC	Boundary condition code; GE.0 EQ.0, No new boundary conditions EQ.1, New boundary conditions
(7)	31-35	IFORCE	Nodal forces/displacements/ accelerations; GE.0 EQ.0, No new nodal conditions EQ.1, New nodal conditions
(8)	36-40	ILTIME	Load-time functions; GE.0 EQ.0, No new load-time functions EQ.1, New load-time functions

2.1 Card 1 (13I5) (Cont'd)

Note	Columns	Variable	Description
(9)	41-45	CLEAR0	Clear option; GE.0 EQ.0, no clear EQ.1, clear displacement array
(10)	46-50	CLEAR1	Clear option; GE.0 EQ.0, no clear EQ.1, clear velocity array
(11)	51-55	CLEAR2	Clear option, GE;0 EQ.0, no clear EQ.1, clear acceleration array
(12)	56-60	CLEAR3	Clear option; GE.0 EQ.0, no clear EQ.1, reset step number NS to 0
(13)	61-65	CLEAR4	Clear option; GE.0 EQ.0, no clear EQ.1, reset time T to 0.0

Notes:

(1) Spatial output is printed output, and generates significant amounts of paper.

(2) Maximum number of iterations performed. (Reference users Manual Sections 2.1, 2.2).

(3) See Section 2.1 2.2.

(4) The mode sets either data check or execution. Data checks are always useful.

(5) Boundary conditions code should be set as with the initial case.

(6) Flag for new boundary constraints. If this option is invoked, all boundaries need to be reset. This also invokes a reformation of the stiffness matrix. This option should not be invoked when nodal slaving or equation optimizing are invoked.

(7) Redefining nodal accelerations/displacements or forces is acceptable, if they were originally defined in the initial data set.

(8) Load-time functions can be modified with this flag on. Only functions that were present in the initial data set can be modified.

(9) Clearing the displacement array is a method to "save" a solution. This is generally not used.

(10) Same as (9).

(11) Clearing the acceleration array is a good option to employ when transitioning between dynamic and consolidation behavior.

(12) Resets timestep to zero, clears all time histories which may have been recorded up to that point.

(13) Used in conjunction with (12) to reset time step to zero. Re-initializes time step, but does not change the stiffness matrix.

2.2 Card 2 (2I5,6F10.0) (only required if Mode.LE.1)

Note	Columns	Variable	Description
(1)	1-5	NTSS	Number of time steps; GE.0 and LE.NTS
	6-10	IBFGS	Iterations procedure; GE.0 EQ.0, Modified Newton-Raphson EQ.1, Newton-Raphson EQ.2, quasi-Newton (BFGS update) EQ.3, quasi-Newton (Broyden update)
(2)	11-20	ALPHA	Algorithm parameter alpha; GE.0.0
(3)	21-30	DTI	Time step; GT.0.0
(4)	31-40	DTMULT	Time step multiplier; GE.0.0 If EQ.0.0, set internally EQ.1.0
(4)	41-50	DTMAX	Maximum allowable time step; GE.0.0 If EQ.0.0, set internally EQ.DT1
(5)	51-60	BETA	Algorithm parameter beta; GE.0.0
	61-70	TOL	Convergence tolerance; GE.0.0 If EQ.0.0 set internally EQ.1.OE-3

Notes:

- (1) If NTSS.LT.NTS a tape is created after NTSS time steps for restart.
- (2) For elliptic boundary value problems ALPHA.EQ.1.0.
- (3) The time step must be sufficiently small to accurately characterize the nonlinear behavior.
- (4) DTMULT allows variable time steps. In that case,

$$DT(N+1) = STMULT*DT(N)$$

$$T(N) = DT(1)*(1. - (DTMULT**N))/(1. - DTMULT)$$

and

$$DT(N+1) = DT(1) * (DTMULT ** N)$$

The maximum allowable time step amplitude is set by DTAMX.

(5) If BETA = 0, set internally to $BETA = (\alpha + 1/2)(\alpha + 1/2)/4$.

2.3 Card 3 (2I5) (only required if MODE.GE.2)

Note	Columns	Variable	Description
	1-5	NEIGEN	Number of eigenvalues required; GE.1
	6-10	IOPT	Solution algorithm; GE.0 If EQ.0, set internally EQ.2 IOPT = 1, Determinant search IOPT = 2, Subspace iterations

2.4 Card 4 - Plotting Requests - (815)

Note	Columns	Variable	Description
	1-5	IP1	Undeformed mesh plot code NE.0, plot undeformed mesh
(1)	6-10	IP2	Deformed mesh plot code NE.0, plot every IP2 steps
	11-15	IP3	Displacement vectors plot code NE.0, plot every IP3 steps
(2)	16-20	IP4	Velocity vectors plot code (with respect to undeformed mesh) NE.0, plot every IP4 steps
(2)	21-25	IP5	Velocity vectors plot code (with respect to deformed mesh) NE.0, plot every IP5 steps
	26-30	IP6	Nodal time histories plot code NE.0, plot every IP6 steps
(3)	31-35	IP7	Contour dump code NE.0, dump every IP7 steps
(4)	36-40	IP8	Mesh data dump NE.0, dump every IP8 steps

Notes:

- (1) For eigenvalue solutions, the deformed mesh is the eigenshape for every IP2 mode.
- (2) For elliptic boundary value problems the velocity vectors are actually the displacement increments computed over the last time step.
- (3) For post-processing with CONTUR.
- (4) For post-processing with DYNAMESH and/or COIFES.

3.0 BOUNDARY CONDITION DATA ((2+NDOF)*I5) (only required if IBC.EQ.1)

Note	Columns	Variable	Description
(1)	1-5	N	Node number; GE.1 and LE.NUMP
(2)	6-10	NG	Generation increment
(3)	11-15	ID(1,N)	Degree of freedom 1 boundary code
	16-20	ID(2,N)	Degree of freedom 2 boundary code
	etc.	.	.
		.	.
		.	.
		ID(NDOF,N)	Degree of freedom NDOF boundary code

Notes:

(1) Boundary condition data must be input for each node which has one or more specified displacements. Cards need not be input in order.
Terminate with a blank card.

(2) Boundary condition data can be generated by employing a two card sequence as follows:

Card 1: L,LG,ID(1,L),...,ID(NDOF,L)

Card 2: N,NG,ID(1,N),...,ID(NDOF,N)

The boundary codes of all nodes

$L+LG, L+2*LG, \dots, N-MOD(N-LG)$

(i.e., less than N) are set equal to those of node L. If LG is blank or zero, no generation takes place between L and N.

(3) Boundary condition codes may be assigned the following values:

ID(I,N) = 0, unspecified displacement

ID(I,N) = 1, specified displacement

Notes: (Cont'd)

where $I = 1, 2, \dots, \text{NDOF}$. Specified displacements are assumed to be fixed (i.e., have the value 0.0) unless assigned a nonzero value as described in Section 4.0. If more than one boundary condition data card for node N is input, the last one read takes priority.

4.0 APPLIED NODAL FORCES AND PRESCRIBED DISPLACEMENTS/ACCELERATIONS (only required if IFORCE.EQ.1)

Applied nodal forces and prescribed displacement/accelerations are defined by an expansion of the form:

$$F(X,t) = G(I,t) * F(I,X) \quad (\text{SUM } I = 1, \text{NLC})$$

where $F(X,t)$ is the resultant force, displacement, or acceleration acting at node A at time t; $G(I,t)$ is the load-time function of the i th load condition; F is the "mode shape" of the i th load condition; and NLC is the total number of load conditions defined on the first control card (see Section 2.1 of DYNAFLOW manual). The data preparation for the load-time functions is described in Section 5.0. In the section, the data preparation for the F 's is described.

The mode shapes must be read in the order $F_1, F_2, \dots, F_{\text{NLC}}$. There must be at least one mode shape. Data cards for a typical mode shape are described below.

4.1 Nodal Applied Force and Prescribed Displacement/Acceleration Cards (2I5,NDOF*F10.0)

Note	Columns	Variable	Description
(1)	1-5	N	Node number; GE.1 and LE.NUMNP
(2)	6-10	NUMGP	Number of generation points EQ.0, no generation EQ.1, generate data
(3)	11-20	F(1,N)	Degree of freedom 1 force or displacement/ acceleration
	21-30	F(2,N)	Degree of freedom 2 force or displacement/ acceleration
	etc.	.	.
		.	.
		.	.
		F(NDOF,N)	Degree of freedom NDOF force or displacement/ acceleration

Notes:

(1) Applied nodal force/prescribed displacement or acceleration data must be included for each node subjected to a nonzero applied force or nonzero prescribed displacement/acceleration. Cards need not be read in order. Terminate with a blank card.

(2) If NUMGP is greater than zero, this card initiates an isoparametric data generation sequence. The scheme used is the same as the one for coordinate and initial displacement/velocity generation (see Section 4 and 6, respectively of DYNAFLOW manual). Cards 2 to NUMGP of the sequence define the applied forces/prescribed displacements of the additional generation points. The final card of the sequence defines the nodal increment information and is identical to the one used for coordinate generation (see Section 4.3 of DYNAFLOW manual). After the generation sequence is completed, additional nodal applied force/prescribed displacement/acceleration cards, or generation sequences, may follow.

The generation may be performed along a line, over a surface, or over a volume. For additional information concerning these options see Note (2) of Section 6.1 of DYNAFLOW manual.

(3) The elements of the array $F(NDOF, NUMNP, NLC)$ are individualized to zero. If the applied forces/prescribed displacement of node N are input and/or generated more than one time, the last value takes priority.

4.2 Generation Point Applied Force or Prescribed Displacement/ Acceleration Cards (2I5,NDOF*10.0)

The applied forces/prescribed displacements of each generation point are defined by a generation point applied force/initial displacement card. The cards must be read in order ($J = 2, 3, \dots, \text{NUMGP}$) following the nodal applied force/prescribed displacement card which initiated the generation sequence ($J = 1$). A nodal increments card follows the last generation point card ($J = \text{NUMGP}$) and completes the sequence.

Note	Columns	Variable	Description
	1-5	M	Node number
	6-10	MGEN	Generation parameter EQ.0, applied forces/prescribed displacements of the jth generation points are input on this card; M is ignored EQ.1 applied forces/prescribed displacements of the Jth generation point are set equal to applied forces/prescribed displacements of the Mth node which were previously defined; applied forces/prescribed displacements on this card are ignored.
	11-20	TEMP(1,J)	Degree of freedom 1 force or displacement of generation point J
	21-30	TEMP(2,J)	Degree of freedom 2 force or displacement of generation point J
	etc.	.	.
		.	.
		.	.
		TEMP(NDOF,J)	Degree of freedom NDOF force or displacement of generation point J

4.3 Nodal Increments Cards (6I5)

Note	Columns	Variable	Description
	1-5	NINC(1)	Number of nodal increments for direction 1;GE.0
	6-10	INC(1)	Node number increment for direction 1
(1)	11-15	NINC(2)	Number of nodal increments for direction 2;GE.0
	16-20	INC(2)	Node number increment for increment 2
(1)	21-25	NINC(3)	Number of nodal increments for direction 3;GE.0
	26-30	INC(3)	Node number increment for direction 3

Notes:

(1) Each option is assigned an option code (IOPT) as follows:

IOPT	Option
1	generation along a line
2	generation over a surface
3	generation over a volume

IOPT is determined by the following logic:

IOPT = 3

IF(NINC(3).EQ.0) IOPT = 2

IF(NINC(2).EQ.0) IOPT = 1

5.0 LOAD-TIME FUNCTION (only required if ILTIME.EQ.1)

Each load-time function is defined by (NLSN + 1) pairs of time instants and function values, where NLSN is the number of load steps defined on the control card (see Section 5.1). Note that NLSN must be less or equal than NLS the maximum number of load steps defined on the first control card (see Section 2.1 of DYNAFLOW manual). The time instants must be in ascending order (i.e., $t(j+1) \geq t(j)$, $1 \leq j \leq \text{NLSN}$). Load step intervals need not be equal and need not be the same from one load case to another. The load-time function is assumed to behave in a piecewise linear fashion between data points. For values of t outside the interval $[t(1), t(\text{NLSN})]$ we define the G 's by constant extrapolation (i.e., $G[t] = G[t(1)]$ for all $t \leq t(1)$; and $G[t] = G[t(\text{NLSN}+1)]$ for all $t \geq t(\text{NLSN}+1)$). As an example of the use of this feature, we may take the case in which $\text{NLC} = 1$, and the load-time function is constant throughout the duration of the analysis. In this case, we may set $\text{NLS} = 0$ on the first control card and simply read in one data point to define $G(t)$.

The load for time step NS is defined to be

$$F(X) = G[t(\text{NS}), I] * F(X, I) \quad (\text{Sum } I=1, \text{NLC})$$

where $t(\text{NS}) = \text{NS} * \text{DT}$. The quantity in square brackets is called the load factor (FAC).

Element consistent loads (e.g., pressure, gravity, etc.) are also multiplied by load-time functions. The load case number is defined in the element group data.

The load-time functions must be read in order $G_1, G_2, \dots, G_{\text{NLC}}$. Data cards for a typical load-time function are described below.

5.1 Load-Time Function Card (2I5,2F10.0)

Note	Columns	Variable	Description
(1)	1-5	N	Load-time function number
	5-10	NLSN	Number of load steps .LE.NLS
	11-20	G(1,1)	Time instant 1 (t(1))
	21-30	G(2,2)	Value of load-time function at t(1)

Notes:

(1) Load-time functions must be input in the order 1,2,..., NLC.
Terminate each load-time function with a blank card.

5.2 Load function cards (10X,2F10.0)*NLSN

Note	Columns	Variable	Description
	11-20	G(J,1)	Time instant J (t(j))
	21-30	G(J,2)	Value of load-time function at t(j)

REFERENCES

1. M.A. Biot. "Theory of propagation of elastic waves in a fluid-saturated porous solid," Journal of Acoustical Society of America, vol 28, 1956, pp 168-191.
2. H. Van der Kogel. Wave propagation in saturated porous media, Ph D thesis, California Institute of Technology. Pasadena. CA, 1977.
3. V.N. Nikolaevskii, K.S. Vasniev, A.T. Gorbunov and G.A. Zotov. Mechanics of saturated porous media, Nedra, Moscow, 1970, 335 pages.
4. S.K. Garg, D.H. Brownell, J.W. Pritchett and R.G. Herrmann. "Shock-wave propagation in fluid-saturated porous media," Journal of Applied Physics vol 46, no. 2, 1975, pp 702-713.
5. S.K. Garg, A.H. Nayfeh and A.J. Good. "Compressional waves in fluid-saturated elastic porous media," Journal of Applied Physics, vol 45, no. 5, 1974, pp 1968-1974.
6. J. Ghaboussi and S.U. Dikmen. "Liquefaction analysis of horizontally layered sands," Journal of Geotechnical Engineering Division, American Society of Civil Engineers, vol 104, no. FT3, 1978, pp 341-356.
7. C.P. Liou, V.L. Specter and F.E. Richard. "Numerical model for liquefaction," Journal of Geotechnical Engineering Division, American Society of Civil Engineers, vol 103, no. GT6, 1977, pp 589-606.
8. R.M. Bowen and R.R. Lockett. "Inertial effects in poroelasticity," Journal of Applied Mechanics, American Society of Mechanical Engineering Transactions, vol 50, 1983, pp 334-342.
9. C.C. Mei and M.A. Foda. "Wave-induced responses in a fluid-filled poro-elastic solid with a free surface: A boundary layer theory," Geophysics Journal, Royal Astrological Society, vol 66, 1981, pp 597-631.
10. J. Ghaboussi and E.L. Wilson. "Variational formulation of dynamics of fluid-saturated porous elastic solids," Journal of Engineering Mechanics Division, American Society of Civil Engineers. Vol 98, no. EM4, 1972, pp 947-963.
11. J. Lysmer. "Analytical procedures in soil dynamics," in Proceedings of the American Society of Civil Engineers. Geotechnical Engineering Division, Specialty Conference on Earthquake Engineering and Soil Dynamics, Pasadena, CA., vol 3, Jun 1978, pp 1267-1316.
12. J.H. Prevost. "Effective stress analysis of seismic site response," International Journal for Numerical Analytical Methods in Geomechanics, Dec 1985.

13. J. H. Prevost. "Wave propagation in fluid-saturated porous media: An efficient finite element procedure," *International Journal of Soil Dynamics in Earthquake Engineering*, Nov 1985.
14. J.H. Prevost. "Nonlinear transient phenomena in soil media," in *Mechanics of Engineering Materials*, Chapter 26, Editors: C.S. Oesai and R.H. Gallagher. New York, NY, Wiley and Sons, 1984, pp 515-533.
15. J.H. Prevost. "Implicit-explicit schemes for nonlinear consolidation," *Computer Methods in Applied Mechanics Engineering*, vol 39, no. 2, 1983, pp 225-239.
16. J.H. Prevost. "Nonlinear transient phenomena in saturated porous media," *Computer Methods in Applied Mechanics Engineering*, vol 30, 1982, pp 3-18.
17. O.C. Zienkiewicz and T. Shiomi. "Dynamic behavior of saturated porous media; the generalized biot formulation and its numerical solution," *International Journal for Numerical Analytical Methods in Geomechanics*, vol 8, no. 1, 1984, pp 71-96.
18. T.J.R. Hughes and W.K. Liu. "Implicit-explicit finite elements in transient analysis: Stability theory," *Journal of Applied Mechanics*, *American Society of Mechanical Engineers Transactions*, vol 45, 1978, pp 371-374.
19. T.J.R. Hughes and W.K. Liu. "Implicit-explicit finite elements in transient analysis: Implementation and numerical examples," *Journal of Applied Mechanics*, *American Society of Mechanical Engineers Transactions*, vol 45, 1978, pp 395-398.
20. J.H. Prevost. "Study of the capabilities of a soil model to predict axial drained/undrained responses of two sands," Report to NCEL, Jun 1985.
21. K. Arulanandan, A. Anandarajah and A. Abghari. "Centrifugal modeling of soil liquefaction susceptibility," *Journal of Geotechnical Engineering*, *American Society of Civil Engineers*, vol 109, no. 3, Mar 1983, pp 281-300.
22. M.D. Bolton and R.S. Steedman. "Centrifugal testing of micro-concrete retaining walls subjected to base shaking," in *Proceedings of the Soil Dynamics and Earthquakes Engineering Conference*, Southampton, U.K., 1982, pp 311-329.
23. P.C. Lambe. *Dynamic centrifugal modelling of a horizontal sand stratum*, Sc. D. Thesis, MIT, Cambridge, MA., 1981.
24. R.V. Whitman and P.C. Lambe. "Liquefaction: Consequences for a structure," in *Proceedings of the Soil Dynamics and Earthquakes Engineering Conference*, Southampton, U.K., 1982, pp 941-949.

25. K. Terzaghi. Theoretical soil mechanics. New York, NY, Wiley and Sons, 1943.
26. R.M. Bowen. "Theory of mixtures," in Continuum Physics. vol III, edited by A.C. Eringen, Academic Press, 1976, pp 1-127.
27. A.C. Eringen and J.D. Ingram. "A continuum theory of chemically reacting media I and II," International Journal of Engineering Science, vol 3, 1955, pp 197-212, and vol 5, 1967, pp 289-322.
28. A.C. Green and P.M. Naghdi. "A dynamical theory of interacting continua," International Journal of Engineering Science, vol 3, 1965, pp 231-241.
29. R.M. Bowen. "Compressible porous media models by use of the theory of mixtures," International Journal of Engineering Science, vol 20, no. 6, 1982, pp 697-735.
30. R. Hill. "A general theory of uniqueness and stability in elastic-plastic solids," Journal of Mechanics and Physics of Solids, vol 6, 1958, pp 236-249.
31. J.H. Prevost. "A simple plasticity theory for frictional cohesionless soils," International Journal of Soil Dynamics in Earthquake Engineering, vol 4, no. 1, 1985, pp 9-17.
32. J.H. Prevost. "Plasticity theory for soil stress-strain behavior," Journal of Engineering Mechanics Division, American Society of Civil Engineers, vol 104, no. EM5, 1978, pp 1177-1194.
33. O.C. Zienkiewicz. The finite element method. Third Edition, London, McGraw-Hill, 1977.
34. T.J.R. Hughes and T. Belytschko. "A precis of developments in computational methods for transient analysis," Journal of Applied Mechanics, American Society of Mechanical Engineers Transactions, vol 50, no. 4b, 1983, pp 1033-1041.
35. T.J.R. Hughes, K.S. Pister and R.L. Taylor. "Implicit-explicit finite elements in nonlinear transient analysis," Computer Methods in Applied Mechanics Engineering, vol 17/18, 1979, pp 159-182.
36. N.M. Nemark. "A method of computation for structural dynamics," Journal of Engineering Mechanics Division, American Society of Civil Engineers, vol 85, no. EM3, 1959, pp 67-94.
37. University of California. Report No. EERC 76-29: Analysis and design of numerical intergration methods in structural dynamics, by H.M. Hilber. Earthquake Engineering Research Center, Berkeley, CA., Nov 1976.

38. Princeton University. DYNAFLOW: A nonlinear transient finite element analysis program, by J.H. Prevost. Department of Civil Engineering, Princeton, NJ, 1981. (Last revision Aug 1985)
39. Naval Civil Engineering Laboratory. Technical Report R-919: Evaluation and validation of the Princeton University effective stress soil model, by J.H. Prevost, J.M. Ferritto, and R.J. Slyh. Port Hueneme, CA., Dec 1985.
40. R.J. Atkin. "Completeness theorems for linearized theories of interacting continua," Quarterly Journal of Mechanics and Applied Mathematics, vol 21, 1968, pp 171-193.
41. R.M. Bowen and K.M. Reinicke. "Plane progressive waves in a binary mixture of linear elastic materials," Journal of Applied mechanics, American Society of Mechanical Engineers Transactions, vol 45, 1978, pp 493-499.
42. R.M. Bowen and P.J. Chen. "Waves in a binary mixture of linear elastic materials," Journal of Mecanique, vol 14, no. 2, 1975, pp 237-266.
- 43 K.J. Bathe and E.L. Wilson. Numerical methods in finite element analysis. Englewood Cliffs, N.J., Prentice-Hall, 1976.

REFERENCES/BIBLIOGRAPHY

(i) ALGORITHMS

1. Brodlie, K.W., Gourlay, A.R., and Greenstadt, J. (1973). "Rank-one and rank-two corrections to positive definite matrices expressed in product form," *Journal of Institute of Mathematics and Its Application*, vol 11, 1973, pp 73-82.
2. Dennis, J.E., and More, J.J. (1977). "Quasi-Newton methods, motivation and theory," *SIAM Review*, vol 19, no. 1, 1977, pp 46-89.
3. Hilber, H.M. (1976). "Analysis and design of numerical integration methods in structural dynamics, Report No. EERC 76.29, Earthquake Engineering Research Center, University of California, Berkeley, CA, 1976.
4. Hughes, T.J.R., Pister, K.S., and Taylor, R.L. (1979). "Implicit-explicit finite elements in nonlinear transient analysis," *Computer Methods in Applied Mechanics Engineering*, vol 17/18, 1979, pp 159-182.
5. Newmark, N.M. (1959). "A method of computation for structural dynamics," *Journal of Engineering Mechanics Division, American Society of Civil Engineers*, vol 85, no. EM3, 1959, pp 67-94.

(ii) FLUID/STRUCTURE/SOIL INTERACTION

1. Hughes, T.J.R., et al. (1982). "Lagrangian-Eulerian finite element formulation for incompressible flows," *Computer Methods in Applied Mechanics Engineering*, vol 31, 1982, pp 329-349.
2. Prevost, J.H., and Hughes, T.J.R. (1983). "Dynamic fluid-structure-soil interaction," *ASCE Publication on Geotechnical Practice in Offshore Engineering*, 1983, pp 133-143.

(iii) THERMOELASTICITY

1. Prevost, J.H., and Tao, D.J. (1983). "Finite element analysis of dynamic coupled thermoelastic problems with relaxation times," *Journal of Applied Mechanics, American Society of Mechanical Engineers*, vol 50, 1983, pp 817-822.
2. Tao, D.J., and Prevost, J.H. (1984). "Relaxation effects on generalized thermoelastic waves," *Journal of Thermal Stresses*, vol 7, 1984, pp 79-89.

3. Prevost, J.H., and Tao, D.J. (1983). "Finite element analysis of heat conduction problems with generalized heat transfer modes," *Journal of Applied Mechanics*, American Society of Mechanical Engineers, August 1983 (in process).
4. Tao, David D.J. (1984). Finite element analysis of thermo-elasticity problems, Ph D thesis, Department of Civil Engineering, Princeton University, Princeton, NJ, Jun 1984.

(iv) PLASTICITY

1. Prevost, J.H. (1978). "Plasticity theory for soil stress-strain behavior," *Journal of Engineering Mechanics Division*, American Society of Civil Engineers, vol 104, No. EM5, 1978, pp 1177-1194.
2. Prevost, J.H., and Hughes, T.J.R. (1981). "Finite element solution of elastic-plastic boundary value problems," *Journal of Applied Mechanics*, American Society of Civil Engineers, vol 48, no. 1, 1981, pp 69-74.
3. Prevost, J.H. (1982). "Nonlinear transient phenomena in elastic-plastic solids," *Journal of Engineering Mechanics Division*, American Society of Civil Engineers, vol 108, no. EM6, 1982, pp 1297-1311.
4. Prevost, J.H. (1984). "Localization of Deformations in elastic-plastic solids," *International Journal of Numerical Methods in Engineering*, vol 8, no. 2, 1984, pp 187-196.
5. Prevost, J.H. (1985). "A simple plasticity theory for frictional cohesionless soils," *International Journal of Soil Dynamics in Earthquake Engineering*, vol 4, no. 1, 1985, pp 9-17.

(v) POROUS MEDIA

1. Prevost, J. H. (1980). "Mechanics of continuous porous media," *International Journal of Engineering Science*, vol 18, no. 5, 1980, pp 787-800.
2. Prevost, J.H., et al. (1981). "Offshore gravity structures: Analysis," *Journal of Geotechnical Engineering Division*, American Society of Civil Engineers, vol 107, no. GT2, 1981, pp 143-165.
3. Prevost, J.H. (1982). "Nonlinear transient phenomena in saturated porous media," *Computer Methods in Applied Mechanics Engineering*, vol 30, no. 1, 1982, pp 3-18.

4. Prevost, J.H. (1983). "Implicit-explicit schemes for non-linear consolidation," *Computer Methods in Applied Mechanics Engineering*, vol 39, 1983, pp 225-239.
5. Prevost, J.H. (1984). "Nonlinear transient phenomena in soil media," Chap. 26 in *Mechanics of Engineering Materials*, Eds C.S. Desai and R.H. Gallagher, Wiley & Sons, 1984, pp 515-533.
6. Prevost, J.H. (1985). "Wave propagation in fluid-saturated porous media: An efficient finite element procedure," *International Journal of Soil Dynamics in Earthquake Engineering*, vol 4, no. 4, 1985, pp 183-202.

INTRODUCTION TO APPENDIXES

All of the problems listed in these appendixes involve essentially the same methodology for the analysis. The procedure is described in the following:

1. Material Model and Mesh Selection. DYNAFLOW incorporates a number of elastic and elasto-plastic material models. The Princeton University Effective Stress Soil Model is detailed in the following appendixes. Mesh selection is an important criteria and effects solution accuracy, and solution costs. The user must weigh carefully the trade offs between proper mesh definition and costs. Recognizing the various element behaviors ("modes") and the "acceptable" incompatibility between elements is important. Several examples are given in the following text.
2. Running the Solution. The solution, either static or dynamic, may have several different "phases" in its methodology.
 - A) Static Linear Elastic Problems. In general, static linear elastic problems require only a single "time" step to solve. An obvious exception to this is encountered in poro-elastic consolidation problems. These problems will be time dependent and will require several time steps.
 - B) Dynamic Linear Elastic Problems. Dynamic problems in the elastic domain require multiple time steps and/or eigenvalue solutions.
 - C) Quasi Static Nonlinear Elastic. The nonlinearity introduced by contact problems requires a single time step to apply the loading, however, multiple iterations will be required to achieve equilibrium.
 - D) Quasi-Static, Nonlinear Elasto-Plastic. The elasto-plastic nonlinear material requires both multiple time steps and interactions to achieve proper convergence.
 - E) Dynamic, Nonlinear Effective Stress Elasto-Plastic Pressure Sensitive. The class of problem requires three phases to the solution.
 - 1) Phase 1: Gravity Initialization. In pressure sensitive, effective stress models, the moduli for each element are dependent on the mean effective confining stress. The mean effective confining stress is controlled by the unit weight of the soil, K_0 , and the pore fluid pressure. The soil model, in general, starts with a single set of stiffness (moduli) and an isotropic confining stress for the whole of the material. The moduli, used in the

actual analysis the stiffness matrix, and the initial hydrostatic pore pressure conditions are computed through the gravity initialization. This allows the soil model to control the computation of K_0 and installs realistic soil stress conditions, similar to those occurring in nature. At this point the solution is stopped.

2) Phase 2: At the end of the gravity loading, the finite element model has a correct and stable set of initial conditions on which to base the dynamic calculation. The dynamic simulation can be controlled through the solution restart options. The restart allows for new load-time histories, boundary conditions, etc., to be input. It also allows for the clearing of acceleration, velocity, and displacement arrays (histories).

3) Phase 3: After the dynamic phase is complete, re-consolidation (stabilization) of the solution (providing liquefaction has not been completed) is the final step. Re-consolidation allows the computation of final settlements and the excess pore pressure diffusion. This procedure is again accomplished through the use of the restart option.

The methodology for running the solution and the use of the restart options is demonstrated in the example included in the appendices.

Appendix A
MONTEREY SOIL COLUMN

MONTEREY SOIL TEST

The test procedures and test results are reported in Reference A-1. The sand was pluviated in water in a stacked-ring apparatus. The model test was conducted on a centrifuge at a centrifugal acceleration of 100 gs, and was subjected to a sinusoidal base input acceleration. The corresponding prototype situation was analyzed in this report. The particular test selected for analysis is referred to as MODEL 1/TEST 1 in Reference A-1.

The centrifuge test intended to model free-field conditions by using a stacked-ring device simulating a horizontally layered soil deposit. For the finite element analysis, the soil column is modeled with one row of elements divided into a number of two-dimensional plane elements as shown in Figure A-1. Each node was assigned four translational degrees of freedom: two for the soil skeleton and two for the fluid phase (pore-water). In the free-field simulation, the nodal planes must remain horizontal and can only undergo parallel motions. As shown in Reference A-2, this is exactly specified by assigning the same equation number to each nodal degree of freedom on the same horizontal plane.

Figure A-1 shows the finite-element mesh. Twenty equally spaced elements are used to span the 20.32-meter height of the sand column. The water table is located at the ground surface. No drainage of the pore-fluid is allowed to take place through the rigid bottom boundary (nor the side boundaries) and the ground shaking is applied as a horizontal sinusoidal input acceleration at the bottom boundary nodes. The permeability (Table A-1) used in the simulation $k = 5 \times 10^{-7}$ m/sec in order to correct for the fact that in the centrifuge (at 100 gs) diffusion or pore-water takes place 100 times faster than in the corresponding prototype.

Figure A-2 shows the computed horizontal acceleration time histories at the bottom (Figure A-2(a)) and at the top (Figure A-2(b)) of the soil column for an input horizontal base acceleration with an amplitude 0.285 gs and a frequency of 5 Hz. The results for 25 cycles of loading (5 seconds of shaking) are reported in Figure A-2. Note the strong modification of the signal computed at the surface as a result of its passage through the saturated soil deposit. The computed maximum surface acceleration compares favorably with the recorded value in the test.

Figure A-3 shows the computed vertical motion at the surface. As a result of the shaking, excess pore-water pressure builds up and partly dissipates in the soil column. These in turn generalize vertical motions (via volumetric strain in the soil skeleton). Although small, the computed vertical acceleration (Figure A-3(b)) at the top (0.0377 g) is not negligible and is about one-half the horizontal peak acceleration. Figure A-3(a) shows the resulting settlement of the soil column that accumulated during and after the shaking as excess pore-water pressure is being dissipated from the column. The computed ultimate settlement = 24 cm.

Figure A-4 shows the computed excess pore-water pressure, vertical effective stress, and shear stress time histories at various depths. The plots have been normalized by dividing the quantities of interest by the initial vertical effective stress. In Figure A-4(a), $h = 0.51$ meter and in Figure A-4(b), $h = 10.66$ meters where h = distance from the bottom

boundary (close to points B and A in Reference A-1). Note the computed increase in pore-water pressures. In Figure A-4(a), $\Delta u/\sigma'_{vo} = 0.69$ and in Figure A-4(b), $\Delta u/\sigma'_{vo} = 0.85$ compares most favorably with recorded value in the test (0.74 and 0.86, respectively). Note the diffusion taking place after the base motion has stopped.

LEIGHTON-BUZZARD SOIL COLUMN TEST

The test procedures and test results are reported in Reference A-23. The sand was rained in water, in a stacked-ring apparatus. The model was tested on a centrifuge at a centrifugal acceleration of 35.5 gs, and subjected to a decaying sinusoidal base acceleration. The corresponding prototype situation is analyzed. The particular test selected for analysis is referred to as PL-3A in Reference A-3.

As in the previous section, the test is intended to simulate free-field conditions in a horizontally layered soil deposit, and the same analysis procedure was used. Ten equally spaced elements are used to simulate the 10.8 meters of the sand column (12-inch model at 35.5 gs). The water table is located at the ground surface. No drainage of the pore fluid is allowed to take.

MODELING ASSUMPTIONS

The boundary conditions for the Monterey Soil column (and other soil column tests) are very straight forward. The nodes at the base are fixed in both the vertical and horizontal degrees of freedom, for fluid and solid phases. Those two nodes are then the points of application for the input accelerations (or displacements). The remaining nodes are then "slaved" together on each degree of freedom (nodes 3 and 4, 5 and 6, etc.). Because of the slaving the elements can deform in shearing "modes" only and the horizontal planes remain horizontal. Vertical settlements are symmetric across the soil column. Therefore the soil column will not develop instabilities due to "tipping" or "rotation." The slaving theory: "What goes out on one side, comes in on the other," certainly has limitations. It does provide, however, a very good means of approximating free field or continuum conditions.

PROBLEMS AND FIXES

It was felt the elastic moduli derived in E^T Program MUD for the Monterey sand were too small. This led to the selection of the moduli from the equations of Hardin and Drenevich for elastic shear moduli:

$$G = \frac{2630 (2.17 - e)^2}{(1+e)} (\bar{\sigma}_0)^{0.5} \quad \text{(all units pounds (1) per square inch)}$$

where: e = void ratio

$\bar{\sigma}$ = mean effective confining stress

G^0 = shear modulus

The analysis was then carried out using the values listed in Table A-1 with the exception of the permeability.

The original permeability selected was that measured (0.085 cm/sec x 100g) in the tests and reported by Arulanadan et al. (Ref A-1). The simulated response showed unacceptably high pore pressure generations. The permeability was then increased by a factor of 10.0. The pore pressure generation was too low at this point, and permeability was decreased.

The final value selected and used was 0.05 m/sec (0.05 cm/sec x 100dg) which produced acceptable results. Similar behavior changes could be readily achieved by varying the plastic moduli in the material model, which dramatically effects the volume strain tendencies. An increase in the plastic moduli decreased the pore pressure generation.

POINTS OF INTEREST

1. Pore pressure generation.
2. Column response, acceleration.
3. Vertical displacement/settlements.

The displacement values are difficult to capture correctly in any computation, but particularly in the soil column. The boundary conditions specified by nodal slaving eliminate any nonuniform settlements and may reduce the total vertical column movement. (Rotation of the elements is eliminated.)

The following tables (data sets) and figures show the steps necessary to construct the material model and the DYNFLOW data set, for the Monterey Soil column. Figures 6A through P are supplemental, and are included to give the overall stress behavior of the soil.

REFERENCES

- A-1. K. Arulanandan, A.J. Anandaraja and A. Abghari. "Centrifugal of soil liquifaction susceptibility," Journal of Geotechnical Engineering, American Society of Civil Engineers, vol 109, no. 3, Mar 1983, pp 281-306.
- A-2. J.H. Prevost. "Effective stress analysis of seismic site response," International Journal for Numerical Analytical Methods in Geomechanics, Dec 1985.
- A-3. P.C. Lambe. Dynamic centrifugal modeling of a horizontal sand stratum, Sc D Thesis MIT, Cambridge, MA, 1981.

$\rho_s = 2.64 \times 10^3 \text{ kg/m}^3$ (mass density, solid grains)
 $\rho_w = 1.00 \times 10^3 \text{ kg/m}^3$ (mass density, fluid phase)
 $n^w = 0.43$ (porosity)
 $k = 5 \times 10^{-4} \text{ m/sec}$ (permeability)
 $\psi'_C = 34^\circ$ (friction angle; compression case)
 $\psi'_E = 17.6^\circ$ (friction angle; extension case)
 $g_1/p_1 = 800.00$ (elastic shear modulus)
 $B_1/p_1 = 533.33$ (elastic bulk modulus)
 $p_1 = 9.81 \times 10^4 \text{ N/m}^2$ (reference pressure)
 $\eta = 0.50$ (power exponent)
 $\eta_C = 1.20$
 $\eta_E = 0.60$

Yield Surface Number	α	m	$(H'_C)_1/p_1$	$(H'_E)_1/p_1$
1	0.08937	0.08937	1181.00	1581.00
2	0.18613	0.18610	524.40	813.60
3	0.14217	0.40800	116.90	210.50
4	0.19995	0.49770	69.15	142.40
5	0.26444	0.63710	23.46	57.76
6	0.36570	0.81520	3.14	10.08
7	0.39060	0.90910	1.11	4.21
8	0.37530	0.96990	0.52	2.17

Table A-1. Soil parameters

INPUT DATA FOR PROGRAM MUD

MONTEREY 0 SAND

MONTEREY 'O' SAND - DR=40% - SC3,SE3 - MODIFIED				
100	1	1	1	0 0 8
13	12	00		
0.0000	0.50	0.00	1.00	
1	0.	0.	1.	0.
2	0.19	0.00085	1.063	0.00019
3	0.425	0.00205	1.142	0.00049
4	0.674	0.00347	1.225	0.00094
5	0.907	0.00579	1.3	0.0015
6	1.153	0.0089	1.384	0.0022
7	1.397	0.0133	1.466	0.0029
8	1.639	0.0193	1.55	0.0037
9	1.816	0.0286	1.61	0.004
10	2.084	0.0431	1.695	0.0043
11	2.29	0.0682	1.762	0.0037
12	2.435	0.11	1.81	0.0011
13	2.544	0.1715	1.85	-0.0032
1	0.	0.	1.	0.
2	-0.059	-0.00035	0.98	0.00004
3	-0.132	-0.00080	0.956	0.00015
4	-0.19	-0.00120	0.936	0.0003
5	-0.25	-0.00145	0.917	0.0006
6	-0.294	-0.00195	0.902	0.001
7	-0.368	-0.00333	0.877	0.00384
8	-0.413	-0.0066	0.862	0.0048
9	-0.444	-0.0107	0.852	0.00485
10	-0.477	-0.0205	0.841	0.00485
11	-0.51	-0.0344	0.83	0.0048
12	-0.55	-0.0561	0.817	0.00475

Table A-2. Input for Program MUD

MONTEREY 0 SAND

[illegible]

Table A-3. Material model from Program MUD

Table A-4. DYNAFLOW data set for Monterey sand

CENTRIFUGE ANALYSIS,		MONTEREY O SAND,		PERM=0.05											
42	1	4	1	1000	2	1000	0	0	1	0	0	1	10	1	1
15	1		1.5	1800.0											
0	0	0	0	0	0	0	0								
1	1														
41	1	1													
1	4		0.0	-20.32											
2			1.0	-20.32											
42			1.0	0.0											
41			0.0	0.0											
1	1	20	2												
1	0	1	1	1	1										
2	0	1	1	1	1										
1	0		1.0	0.0	1.0	0.0									
2	0		1.0	0.0	1.0	0.0									
1	1		0.0	0.0											
		18000.0		1.0											
2	0		0.0	0.0											
4	20	0	0	0	1	0	1	0	60	0	0	0	2	04	0
2	8	8													
4.000E+02	1.600E+03	5.333E+02	5.000E-01												
-1.000E+00	-1.000E+00	-1.000E+00	0.0	0.0	0.0										
1.200E+00	6.000E-01	0.0	-1.019E-05	1.000E+12	4.300E-01	0.0							0.0		
1	8.937E-02	1.181E+03	1.581E+03	0.0	0.0	0.0									
-2.979E-02	5.958E-02	-2.979E-02	0.0	0.0	0.0	0.0									
2	1.861E-01	5.244E+02	8.136E+02	0.0	0.0	0.0									
-6.203E-02	1.241E-01	-6.203E-02	0.0	0.0	0.0	0.0									
3	4.080E-01	1.169E+02	2.105E+02	3.398E-01	0.0	0.0									
-4.739E-02	9.478E-02	-4.739E-02	0.0	0.0	0.0	0.0									
4	4.977E-01	6.915E+01	1.424E+02	5.958E-01	0.0	0.0									
-6.665E-02	1.333E-01	-6.665E-02	0.0	0.0	0.0	0.0									
5	6.371E-01	2.346E+01	5.776E+01	8.589E-01	0.0	0.0									
-8.814E-02	1.763E-01	-8.814E-02	0.0	0.0	0.0	0.0									
6	8.152E-01	3.137E+00	1.008E+01	1.158E+00	5.913E-01	0.0									
-1.219E-01	2.438E-01	-1.219E-01	0.0	0.0	0.0	0.0									
7	9.091E-01	1.110E+00	4.209E+00	1.270E+00	5.324E-01	0.0									
-1.302E-01	2.604E-01	-1.302E-01	0.0	0.0	0.0	0.0									
8	9.699E-01	5.242E-01	2.174E+00	1.294E+00	5.988E-01	0.0									
-1.251E-01	2.502E-01	-1.251E-01	0.0	0.0	0.0	0.0									
0.050			0.050												
2640.0		0.0	-9.81	1000.0											
1		1	2	4	3	1									
1	1	1	20	1	2										
1	0	1	1												
1															
2	0	1	1												

Table A-4. Continued

CENTRIFUGE ANALYSIS, MONTEREY O SAND,

PERM=0.05

1			
3	0	1	1
1			
4	0	1	1
1			
5	0	1	1
1			
6	0	1	1
1			
7	0	1	1
1			
8	0	1	1
1			
9	0	1	1
1			
10	0	1	1
1			
11	0	1	1
1			
12	0	1	1
1			
13	0	1	1
1			
14	0	1	1
1			
15	0	1	1
1			
16	0	1	1
1			
17	0	1	1
1			
18	0	1	1
1			
19	0	1	1
1			
20	0	1	1
1			

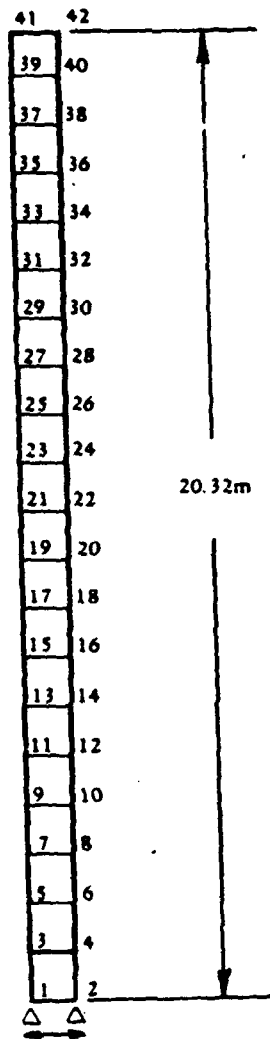
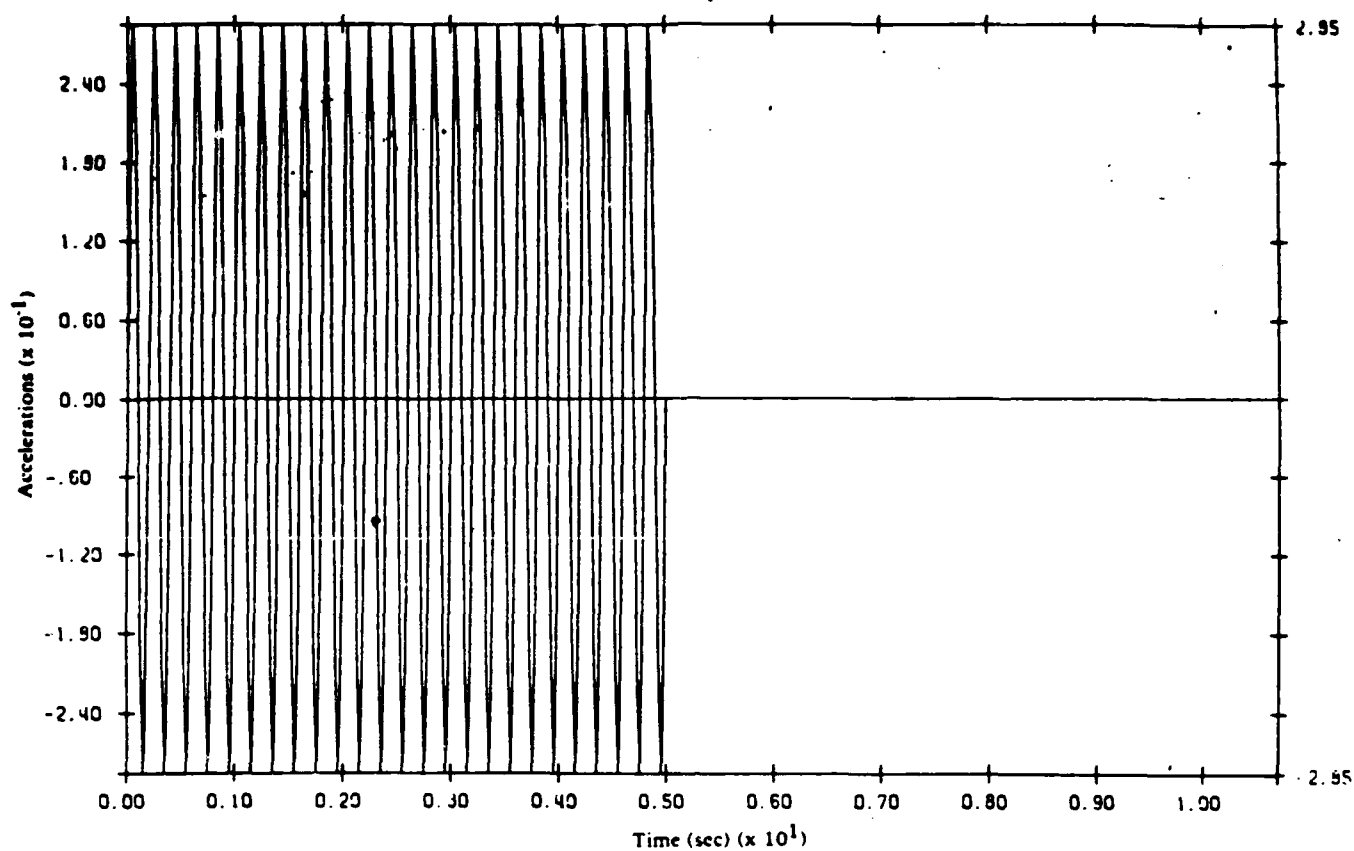
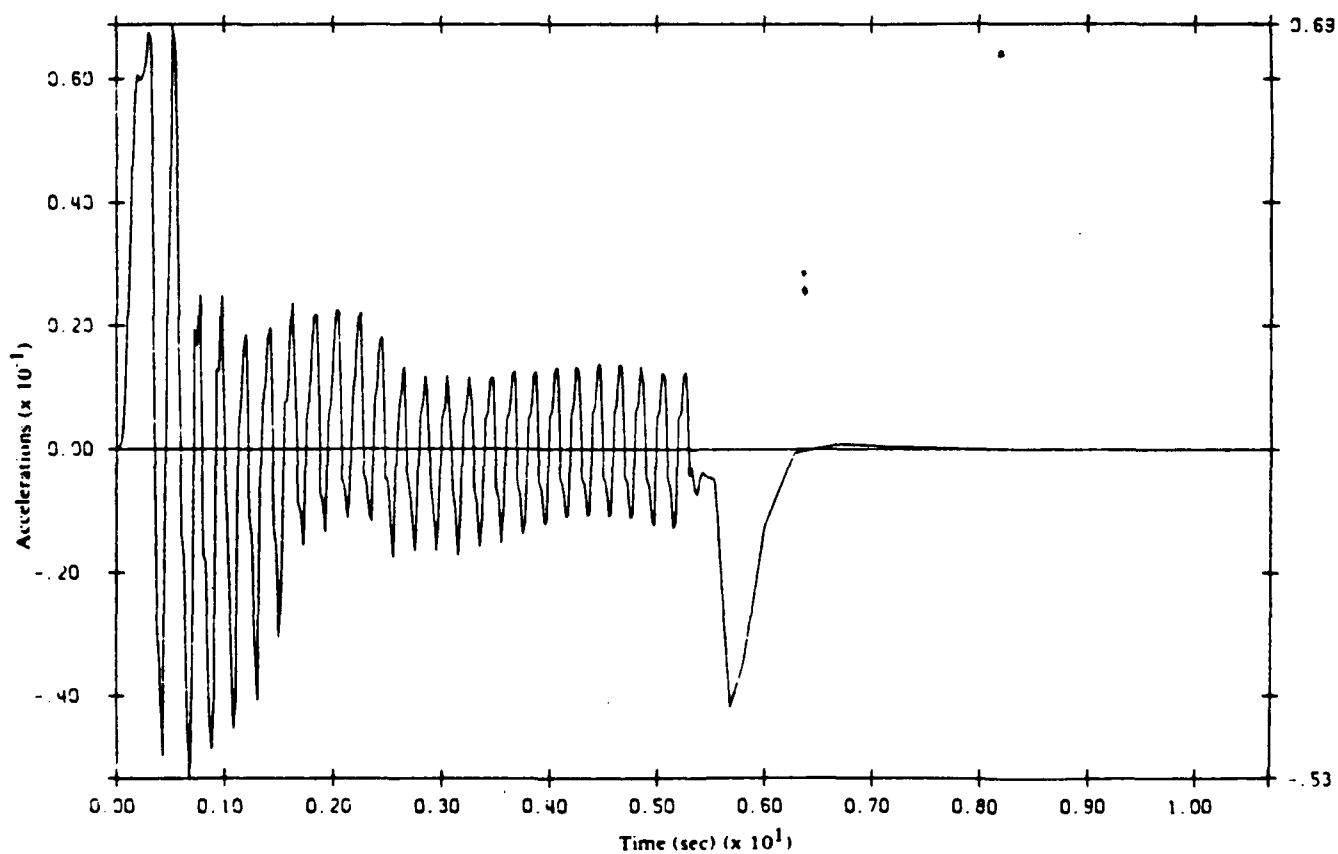


Figure A-1. Undeformed mesh soil column

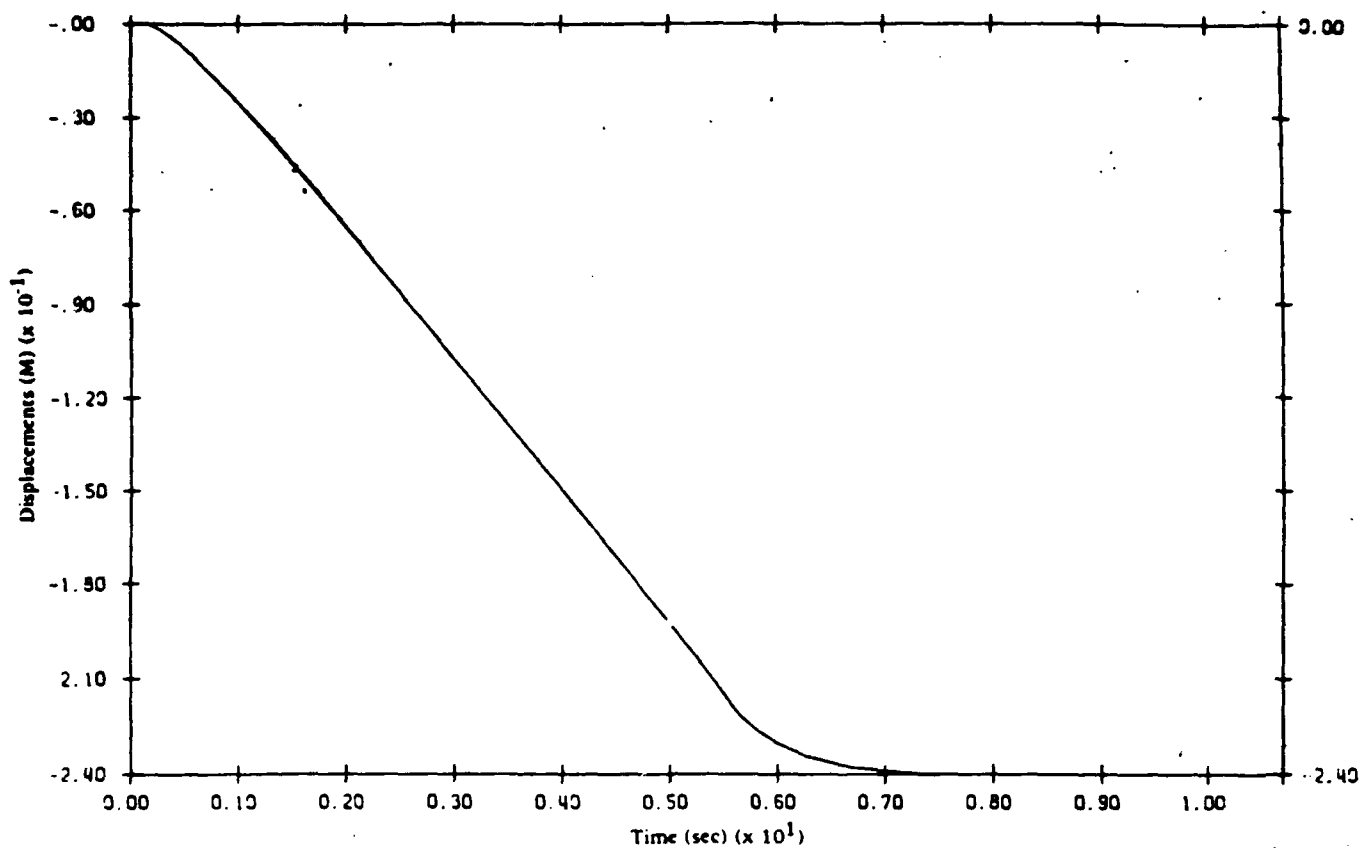


(a)

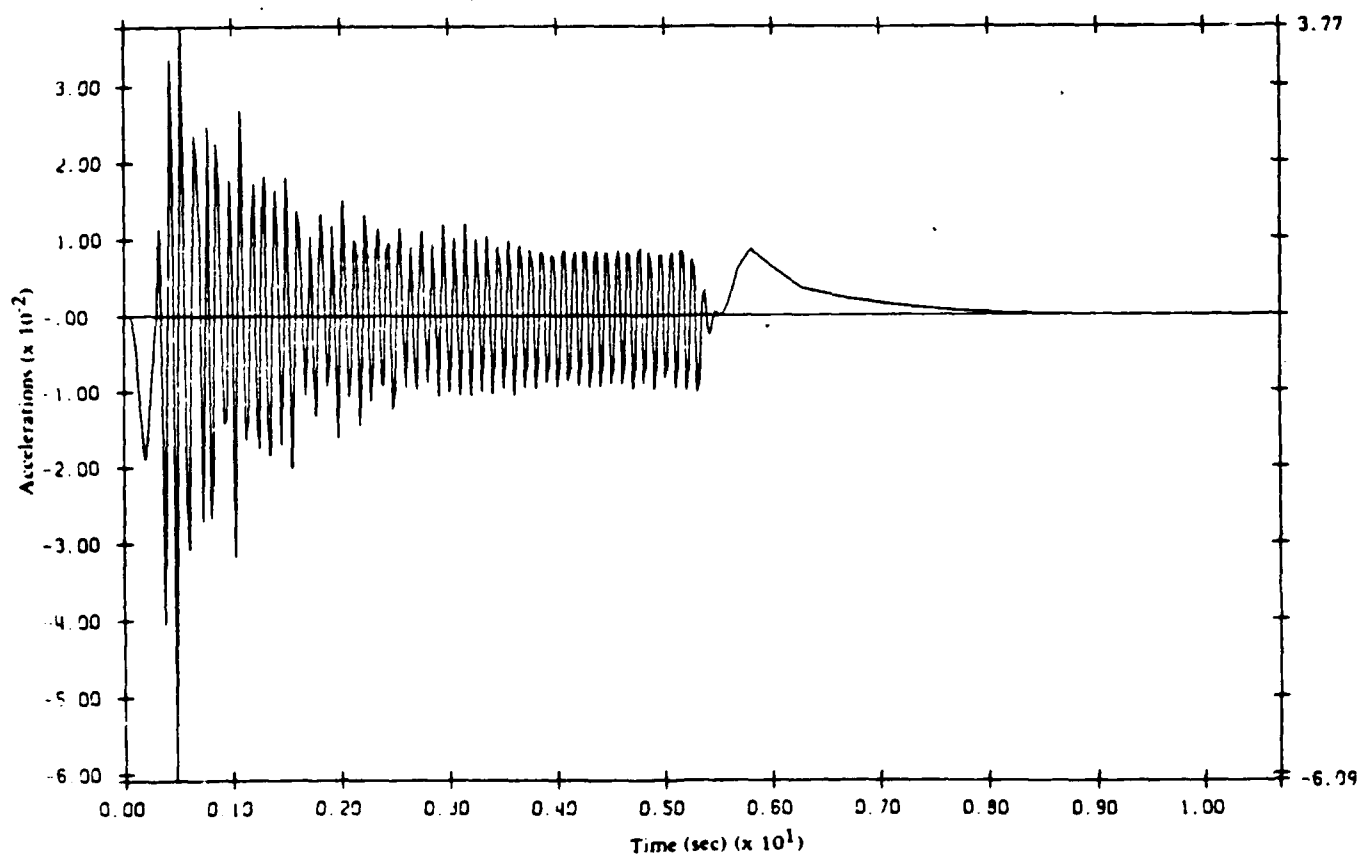


(b)

Figure A-2. Horizontal accelerations at bottom and top of column (Monterey "O" sand)



(a)



(b)

Figure A-3. Vertical displacements and accelerations at top of column (Monterey "O" sand)

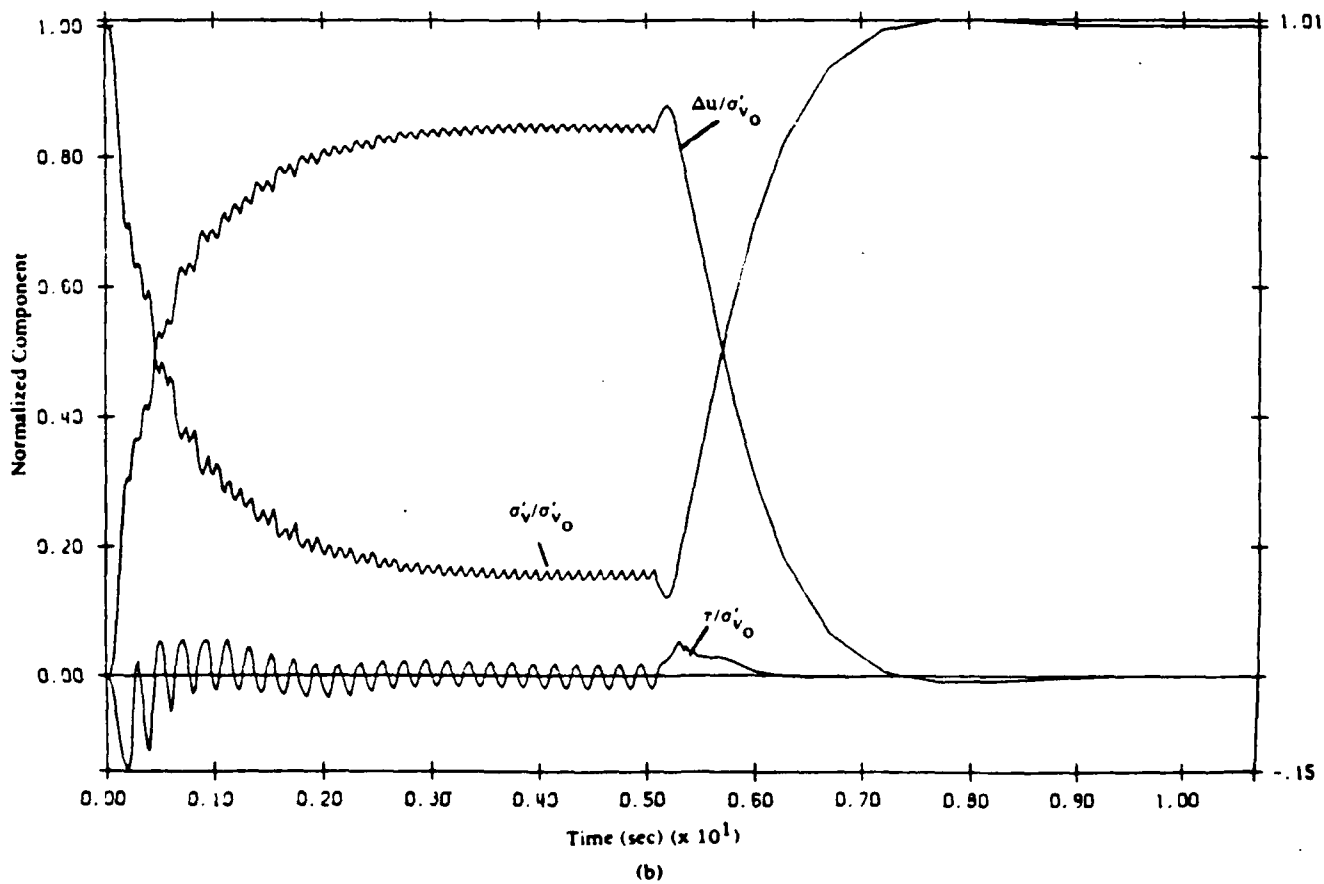
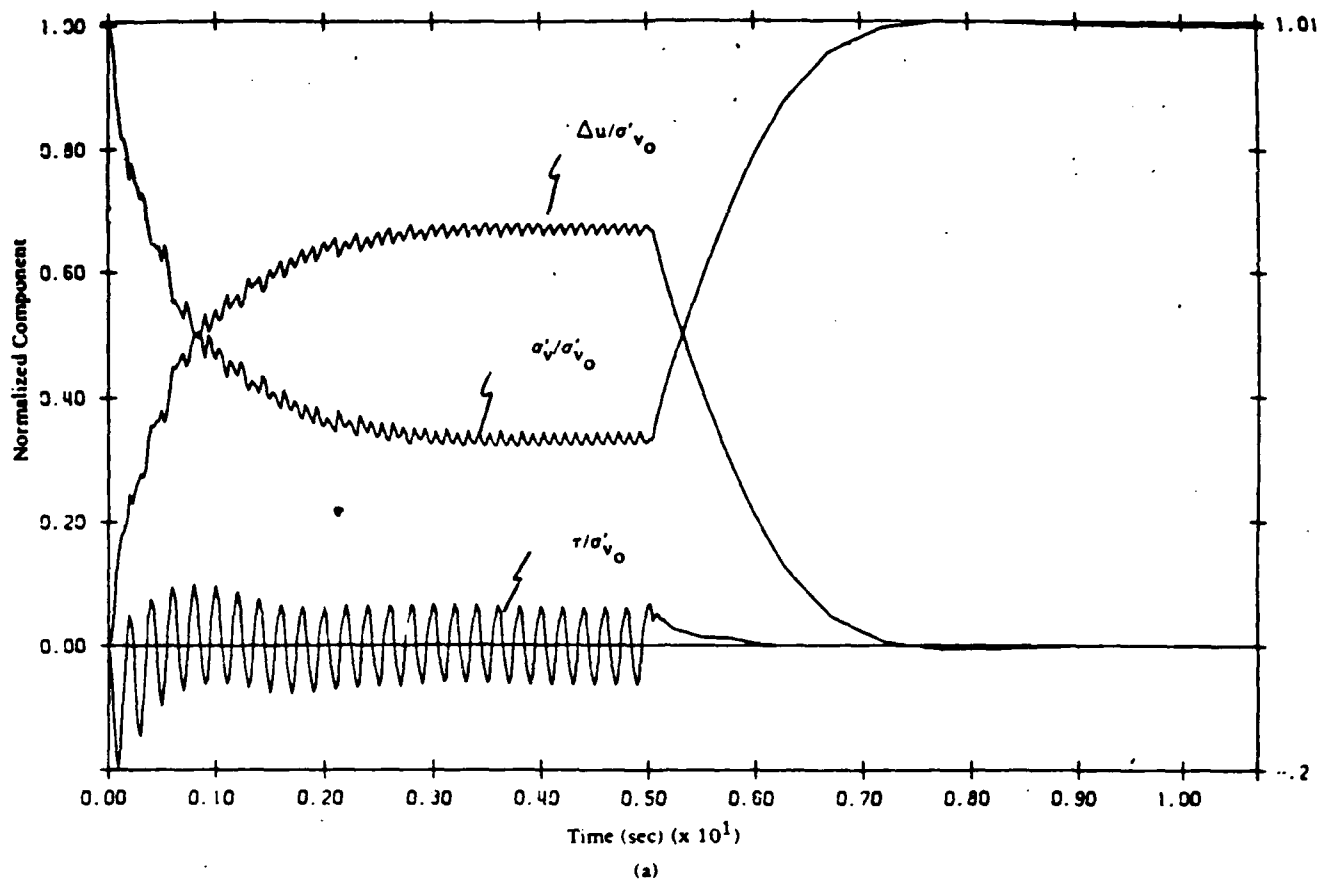
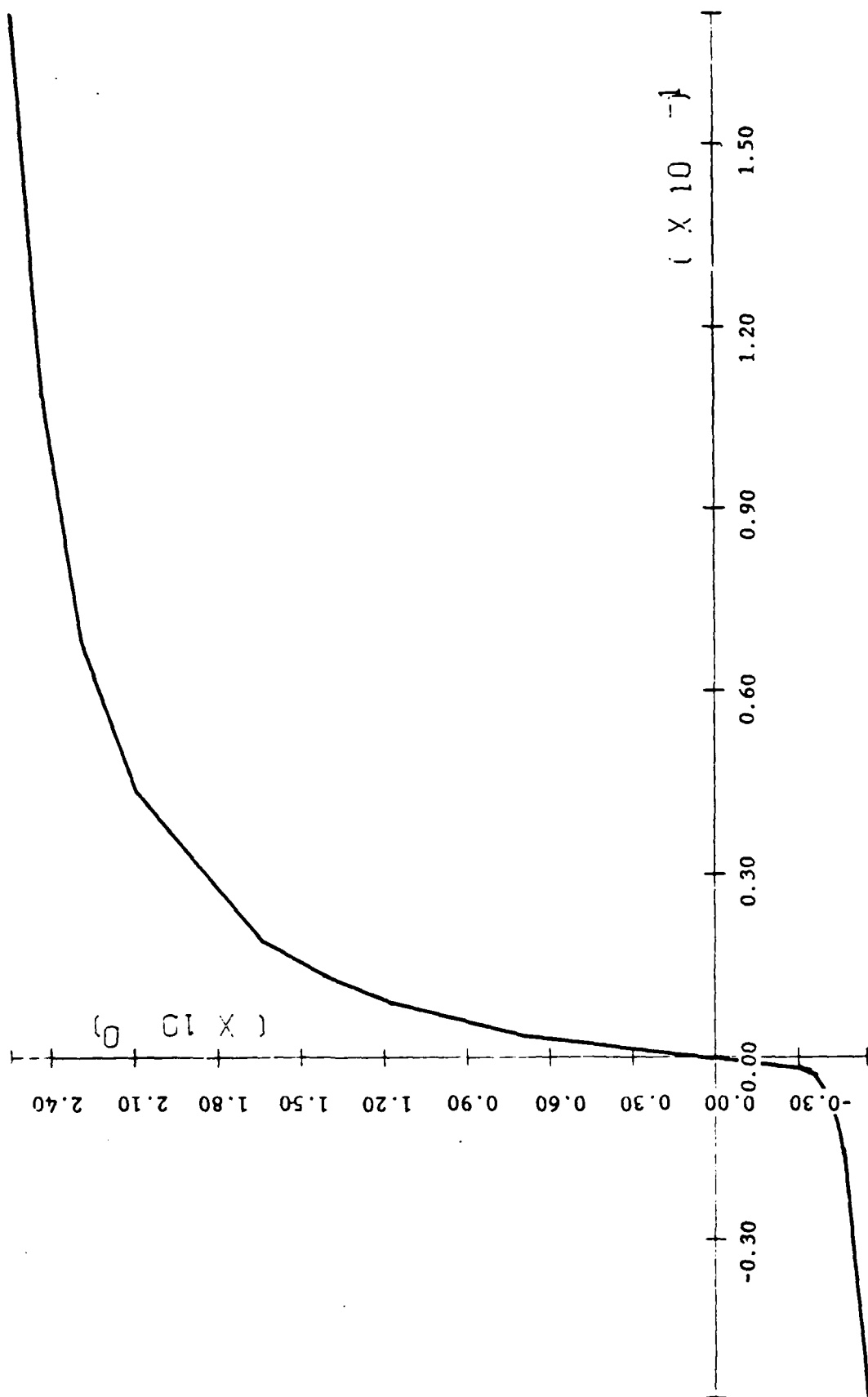
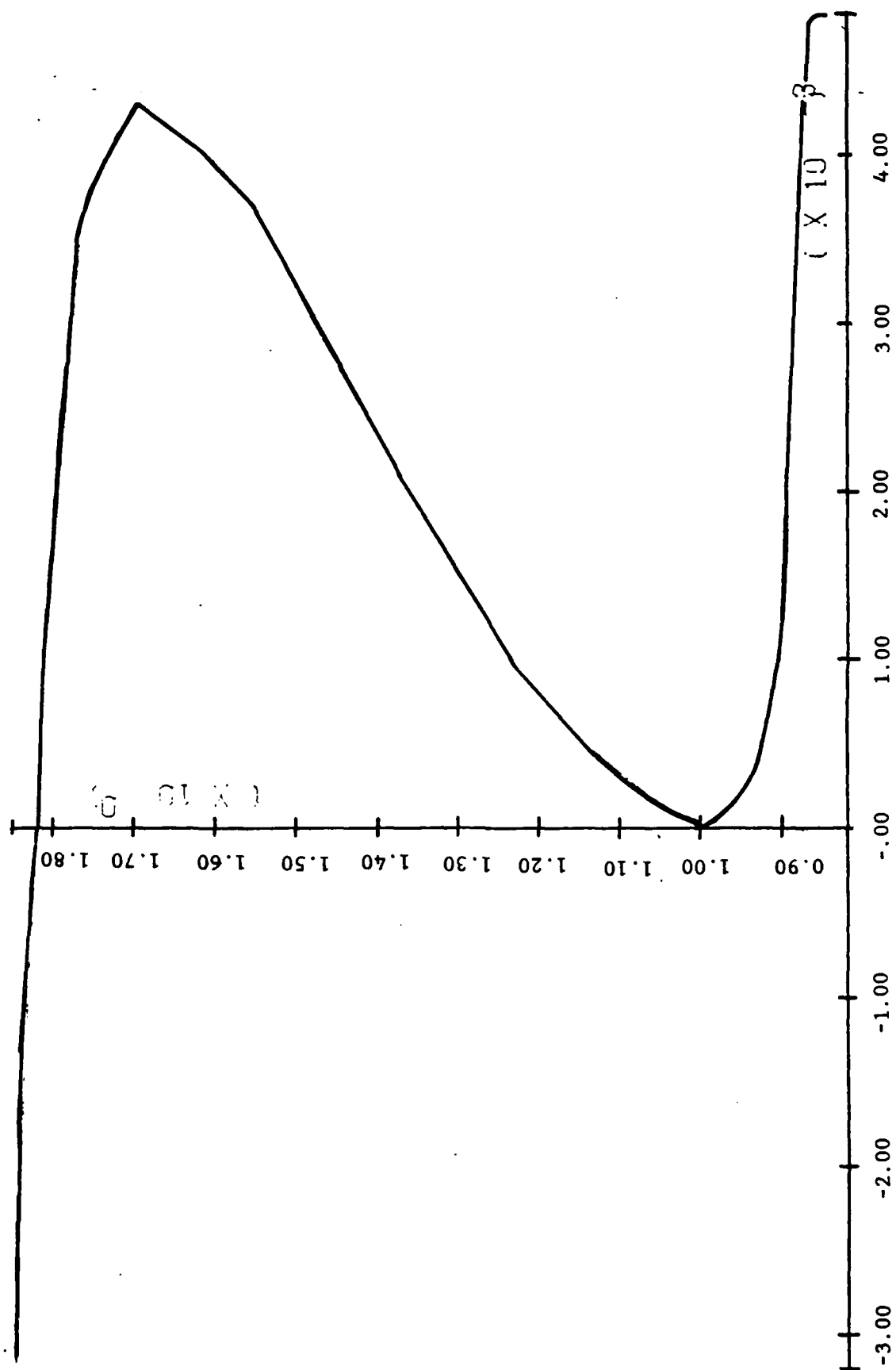


Figure A-4. Normalized pore pressure, vertical stress, and shear stress (Monterey "O" sand)



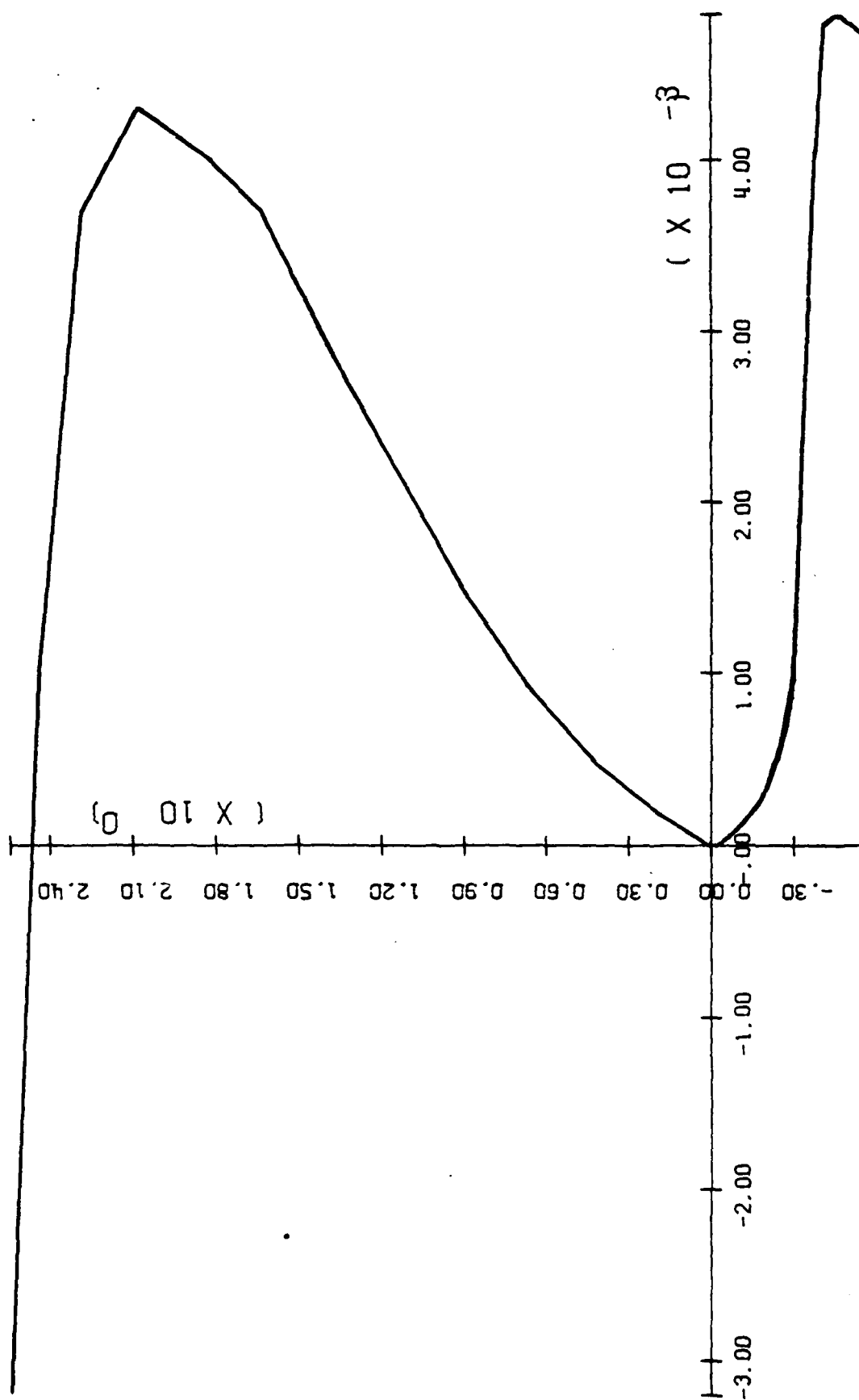
Deviatoric Stress vs. Deviatoric Strain

Figure A-5A. MUD input data



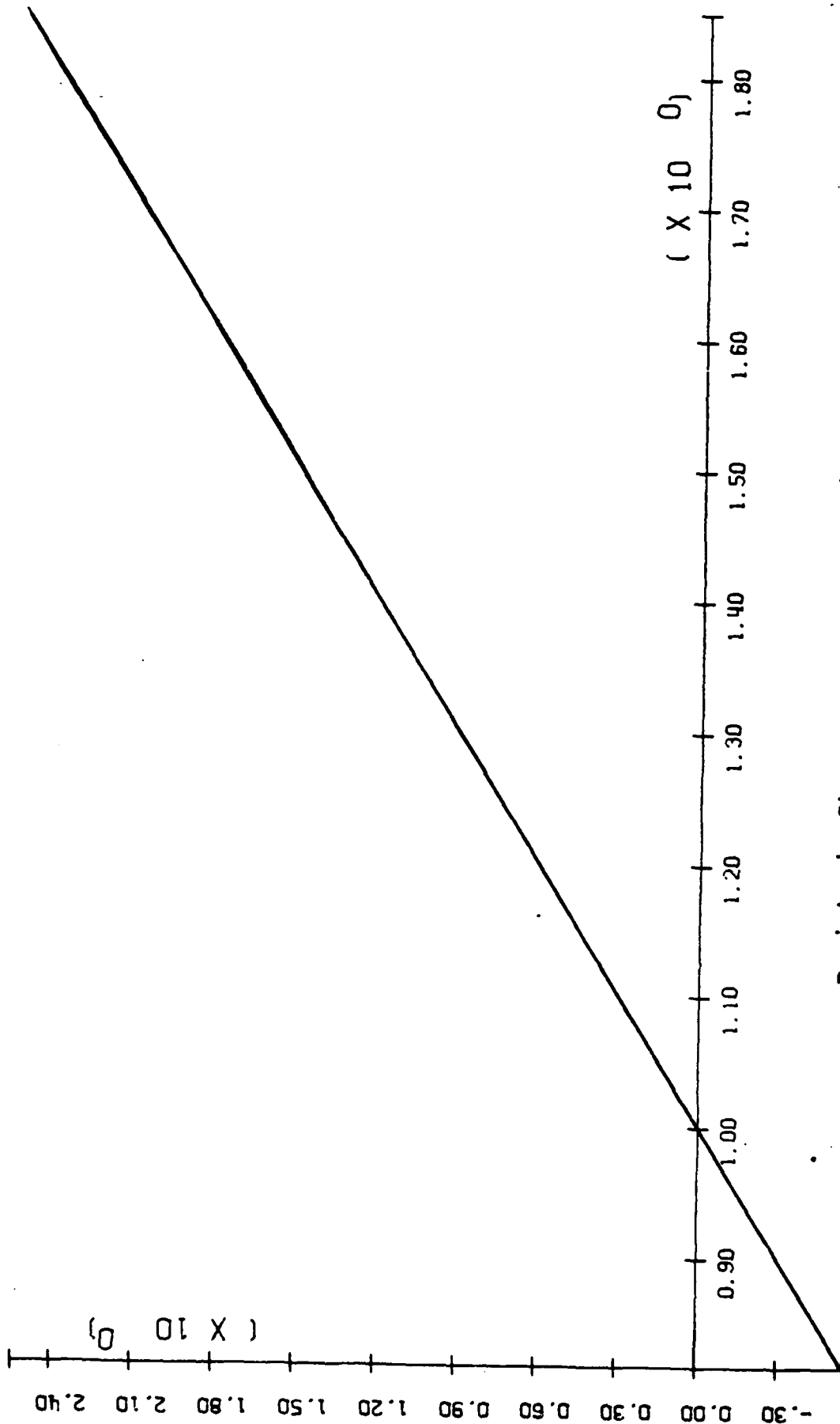
Mean Effective Stress vs. Volumetric Strain

Figure A-5B: MUD input data



Deviatoric Stress vs. Volumetric Strain

Figure A-5C. MUD input data



Deviatoric Stress vs. Mean Effective Stress

Figure A-5D. MUD input data

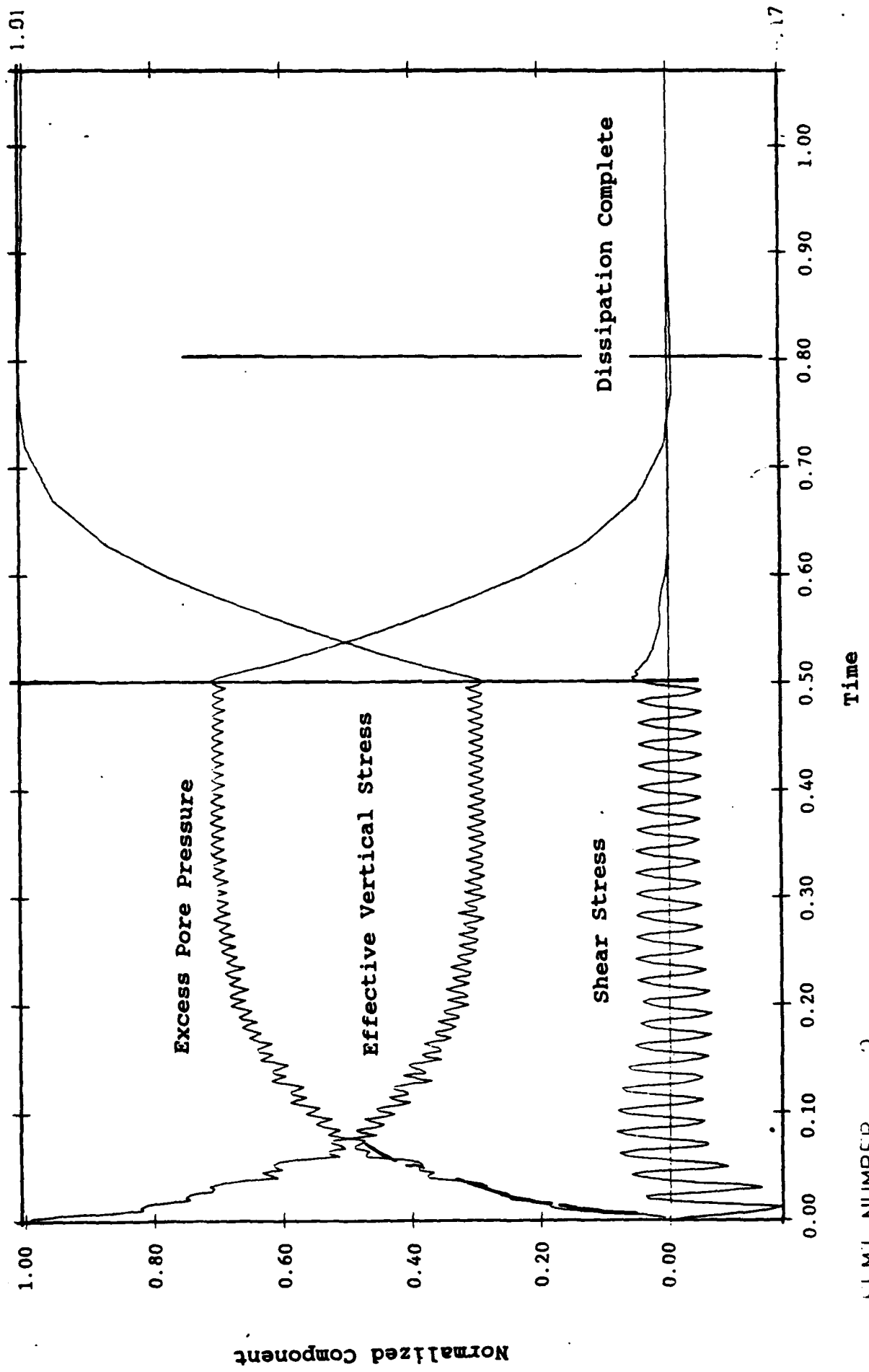


Figure A-6A. Overall stress behavior of soil

ELMI NUMBER 2

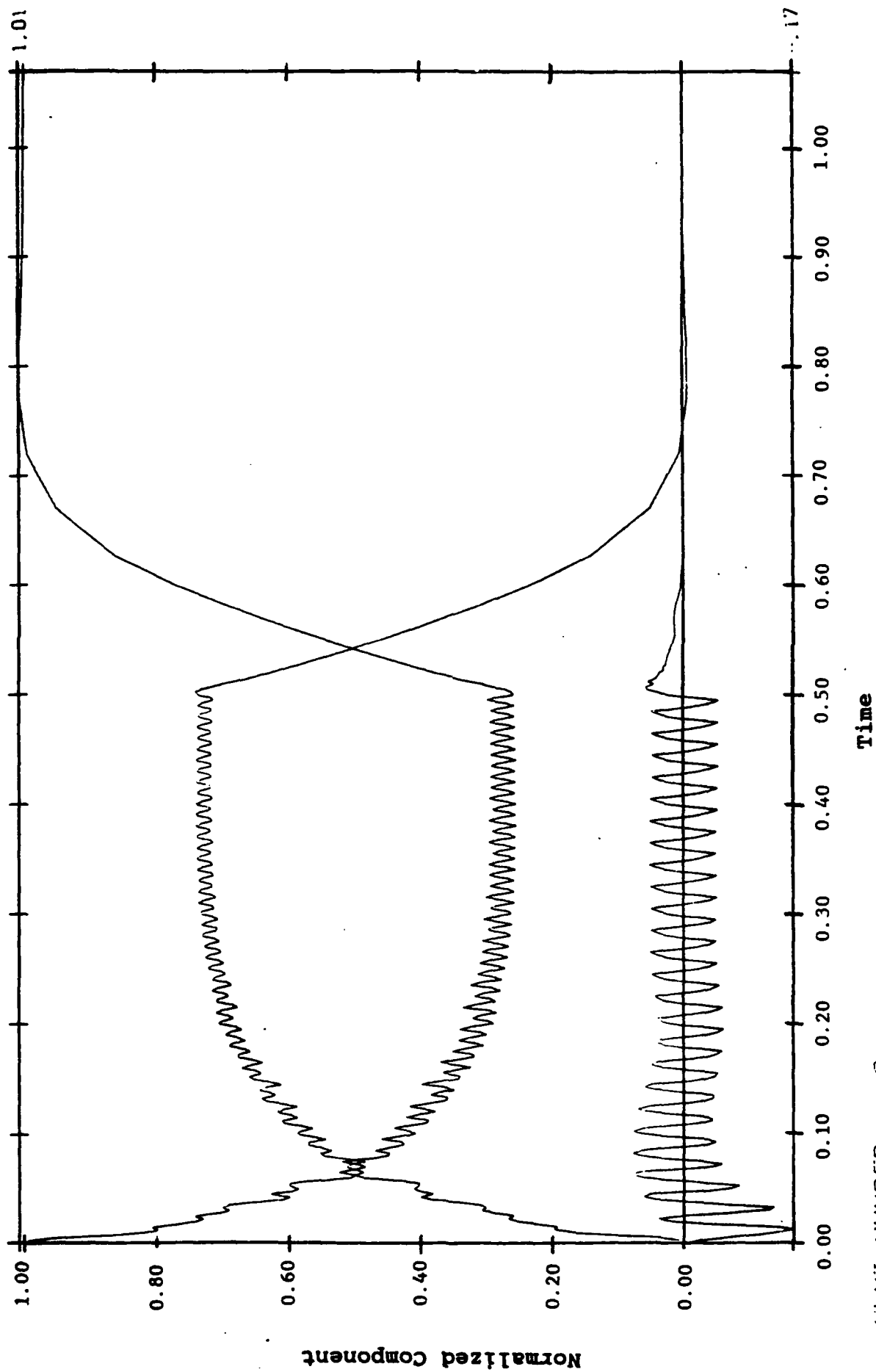


Figure A-6B. Overall stress behavior of soil

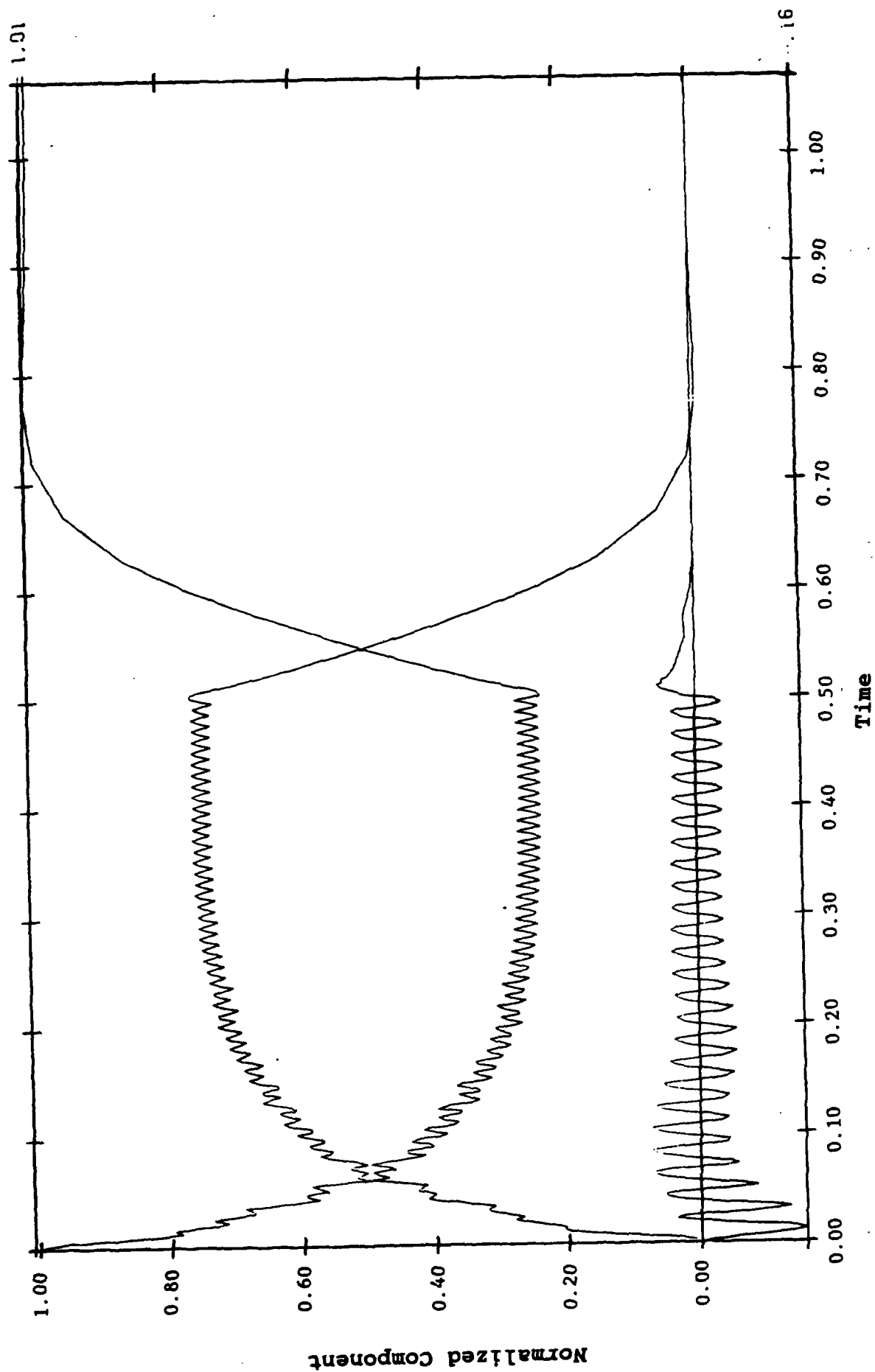


Figure A-6C. Overall stress behavior of soil

ELMT NUMBER 4

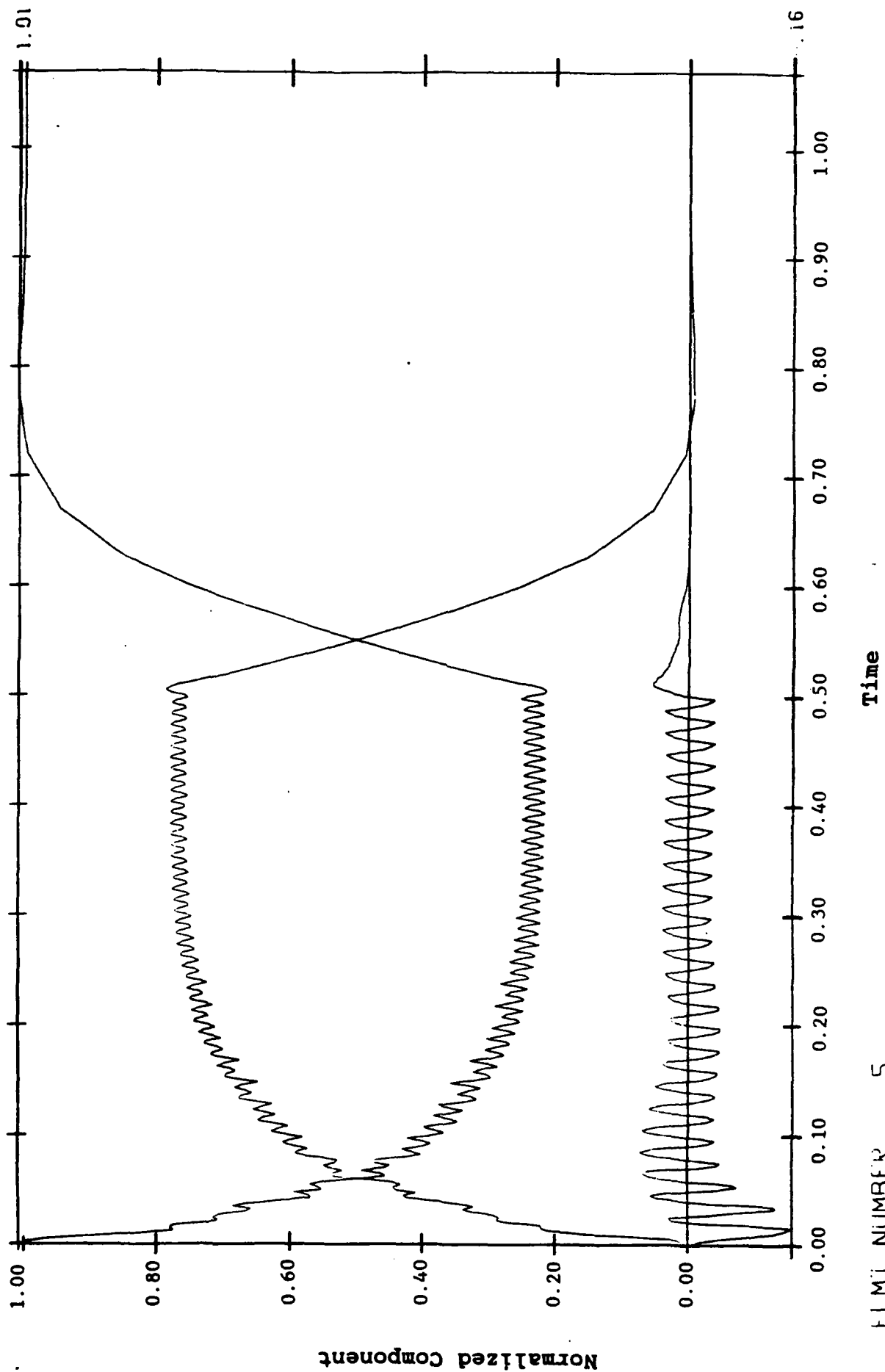


Figure A-6D. Overall stress behavior of soil

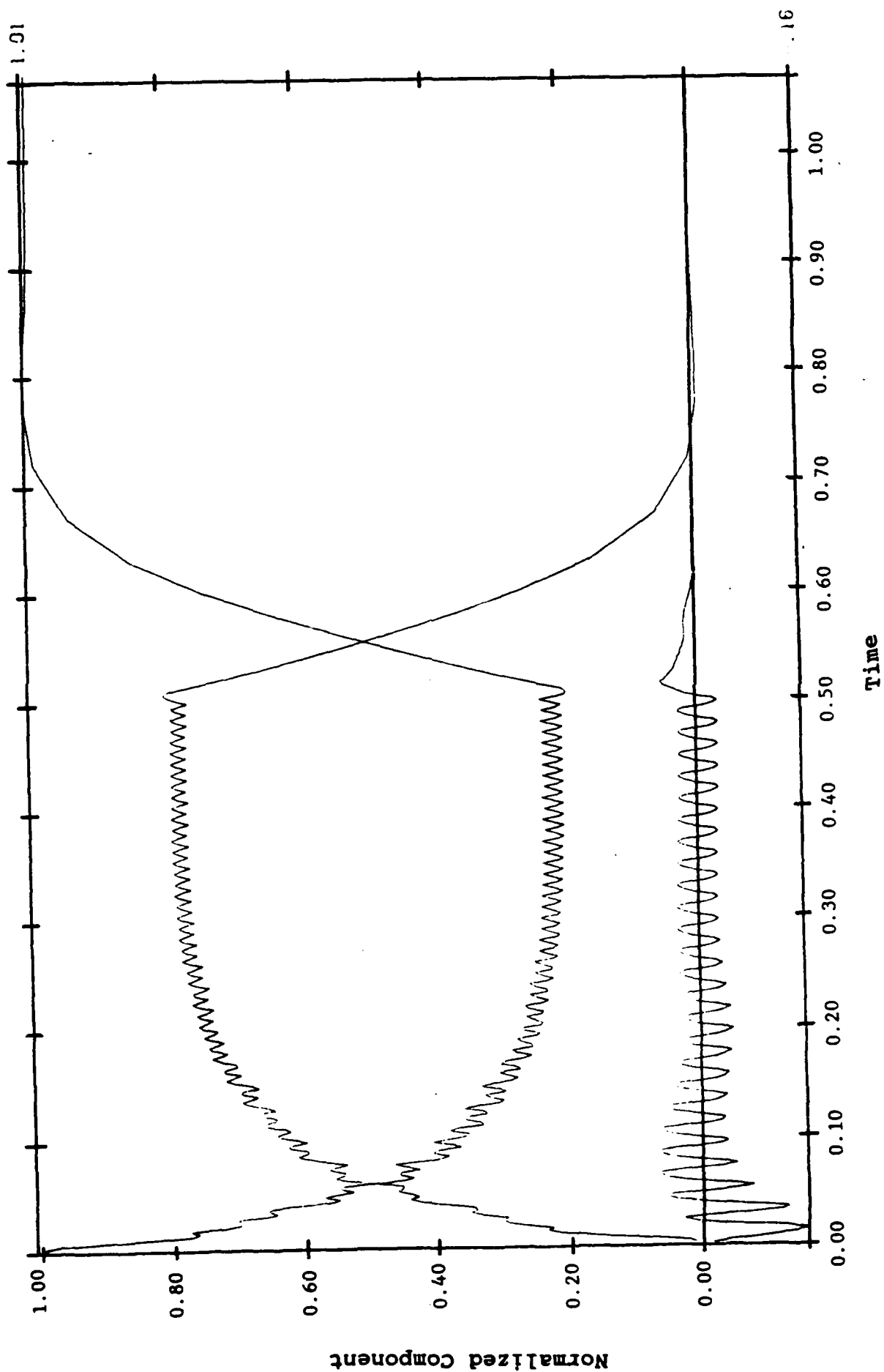


Figure A-6E. Overall stress behavior of soil

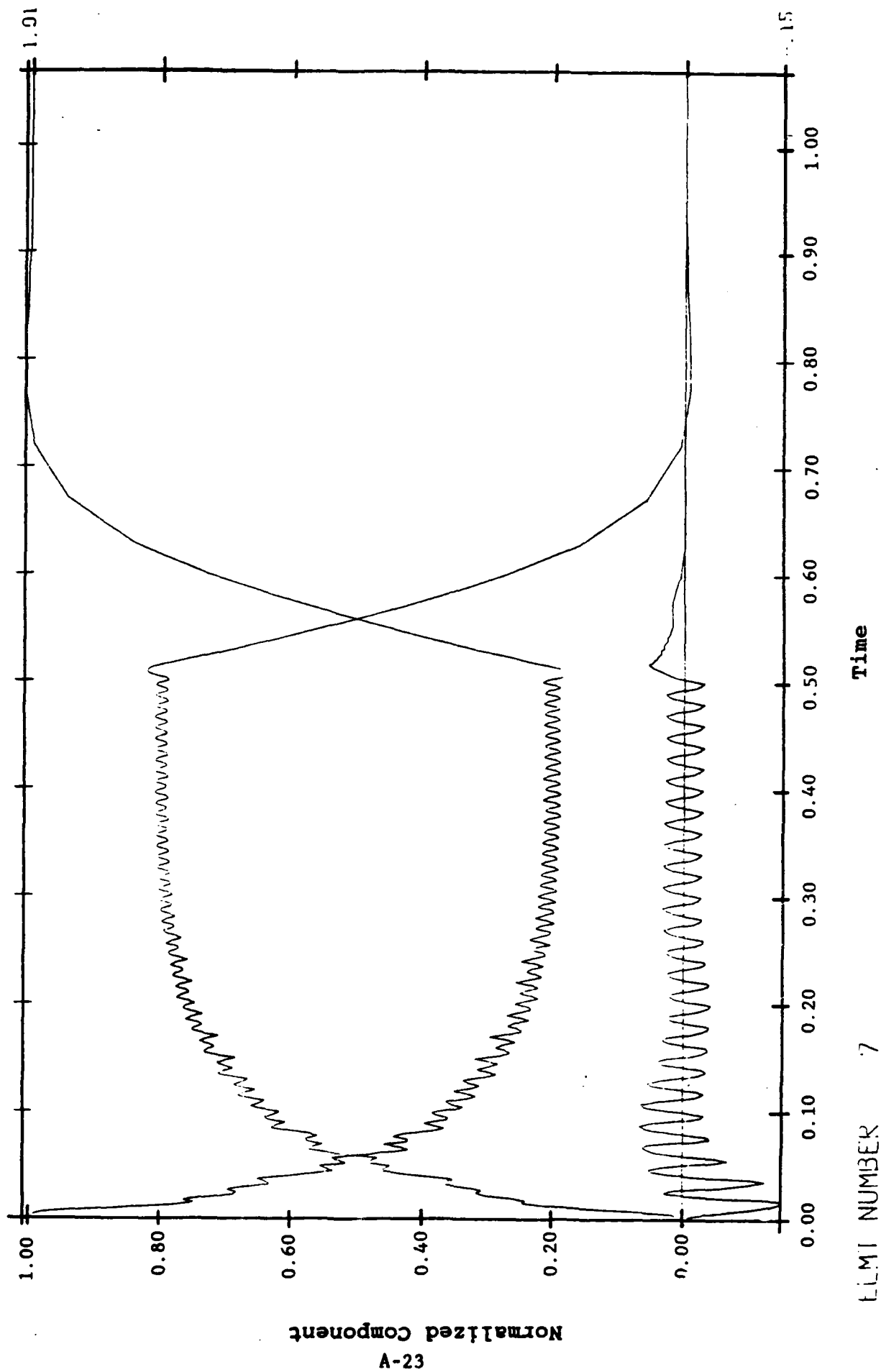


Figure A-6F. Overall stress behavior of soil

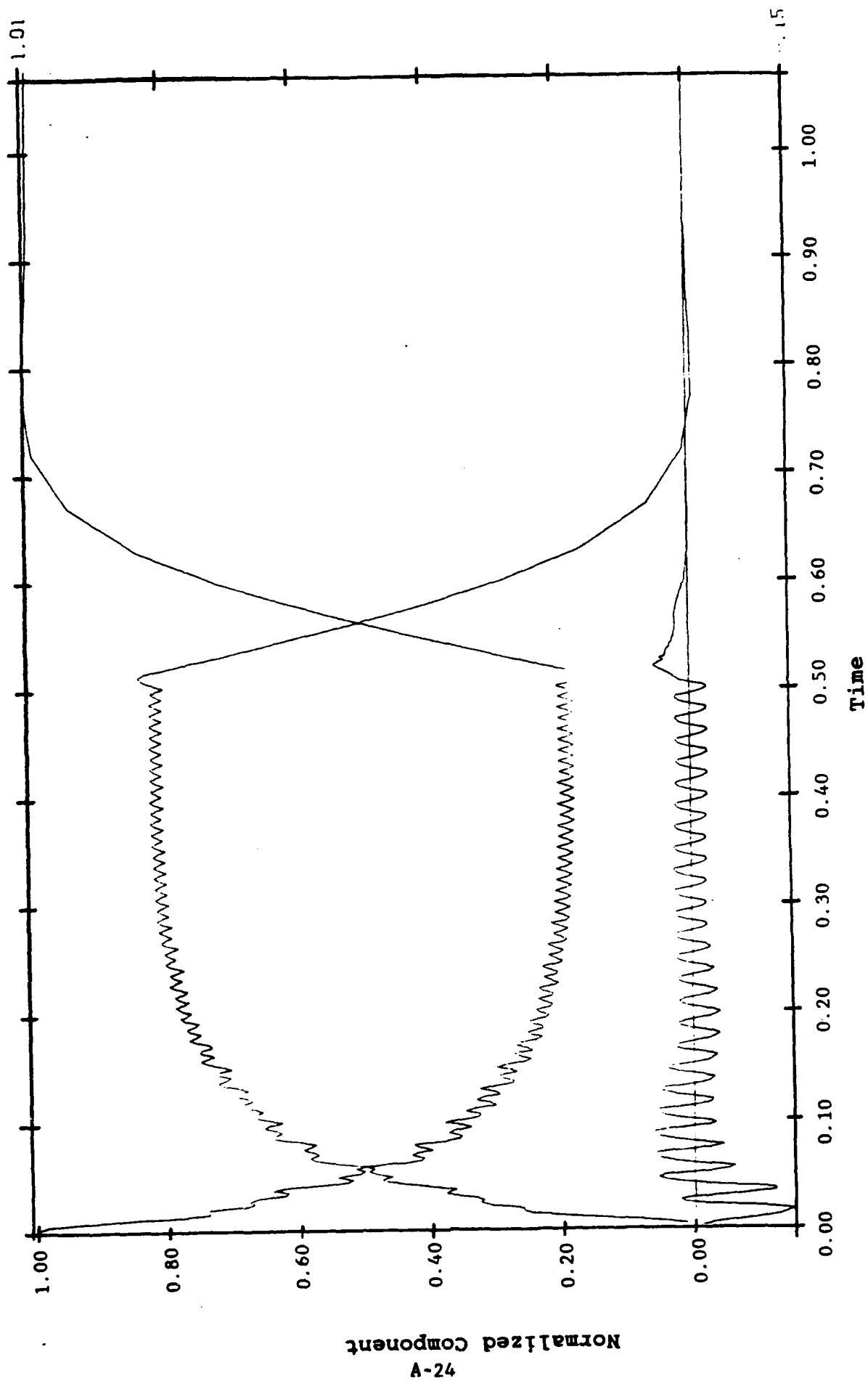


Figure A-6G. Overall stress behavior of soil

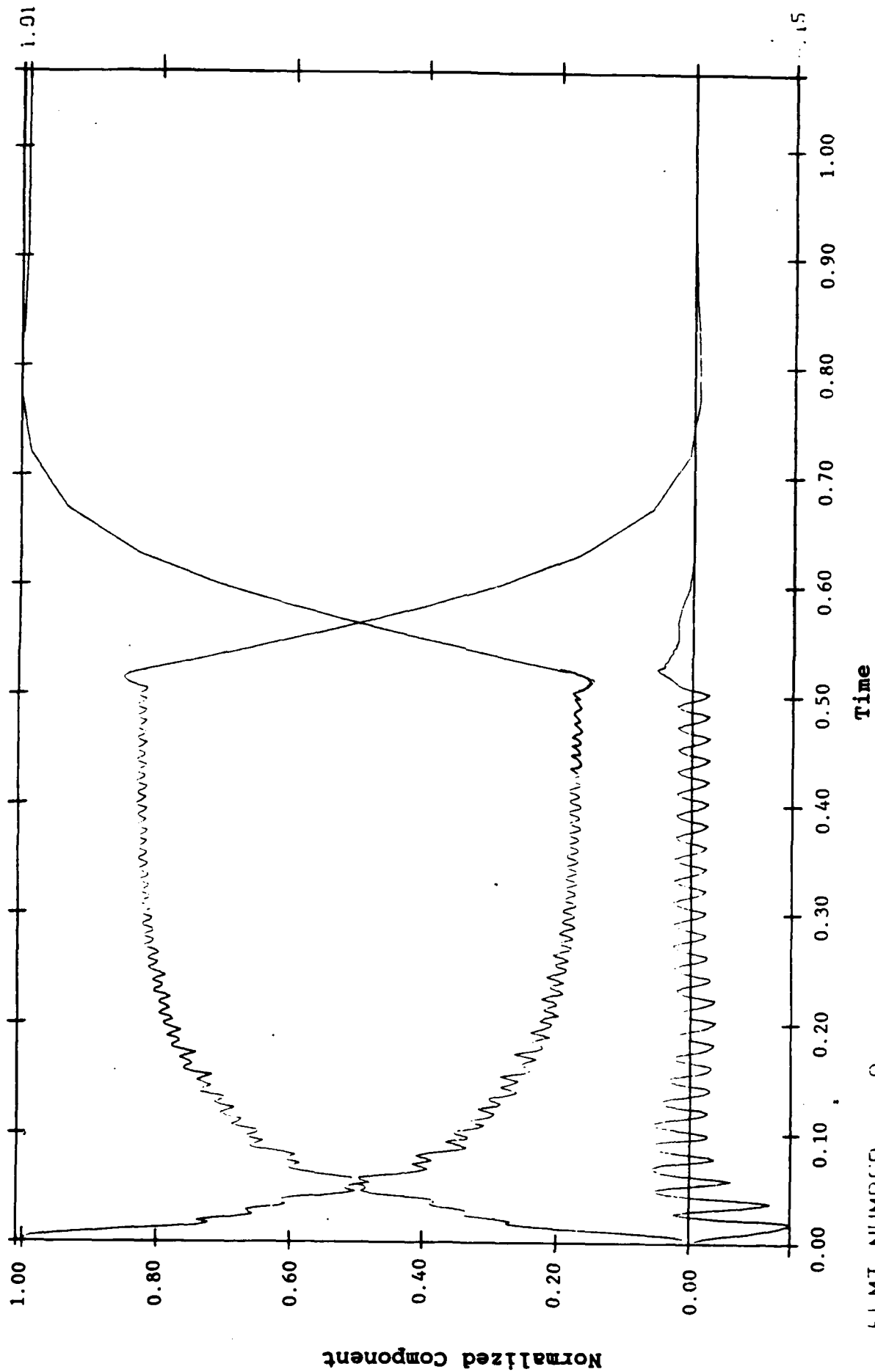
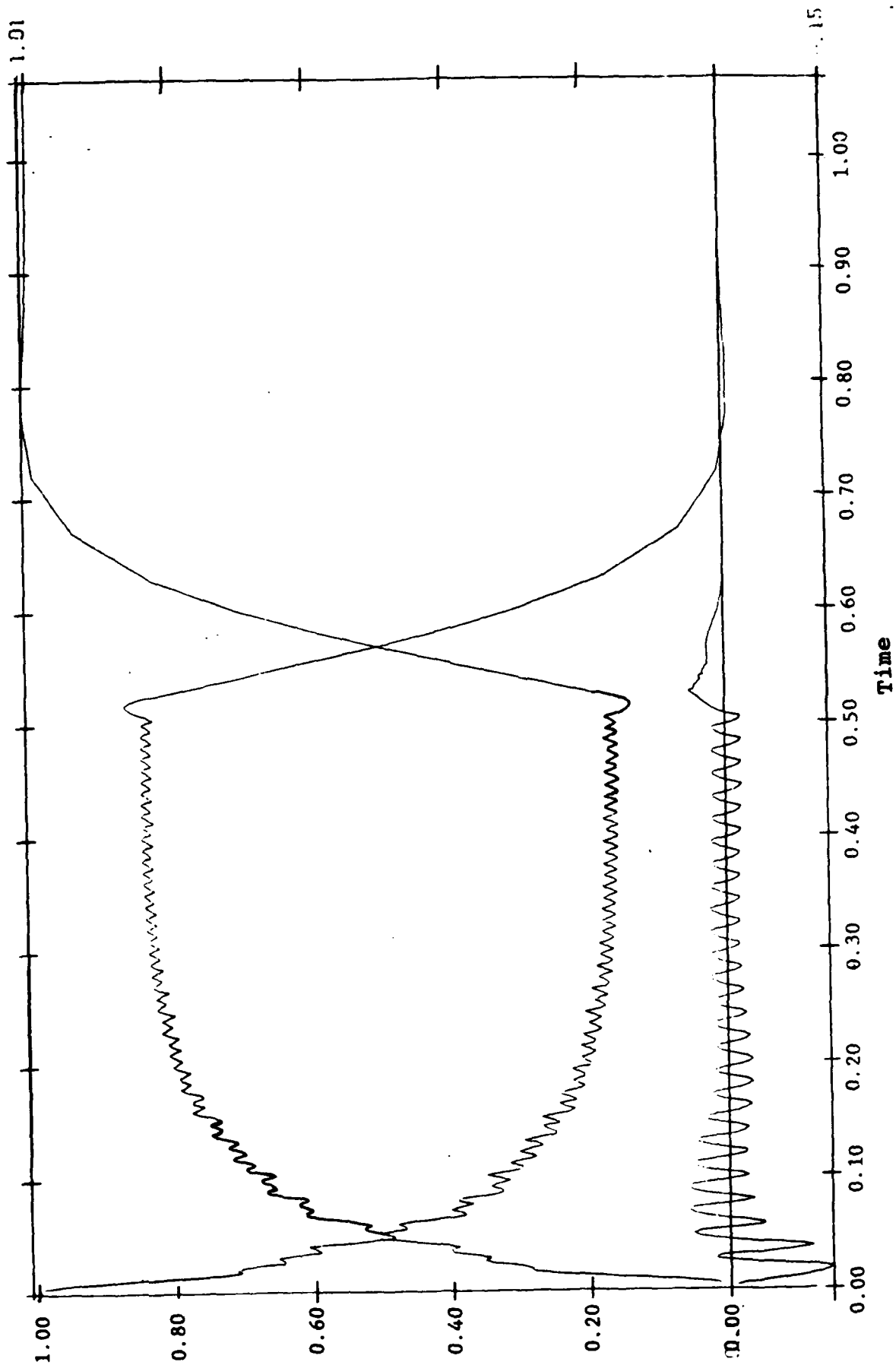


Figure A-6H. Overall stress behavior of soil

ELMT NUMBER 9



ELEM NUMBER 10

Figure A-6I. Overall stress behavior of soil

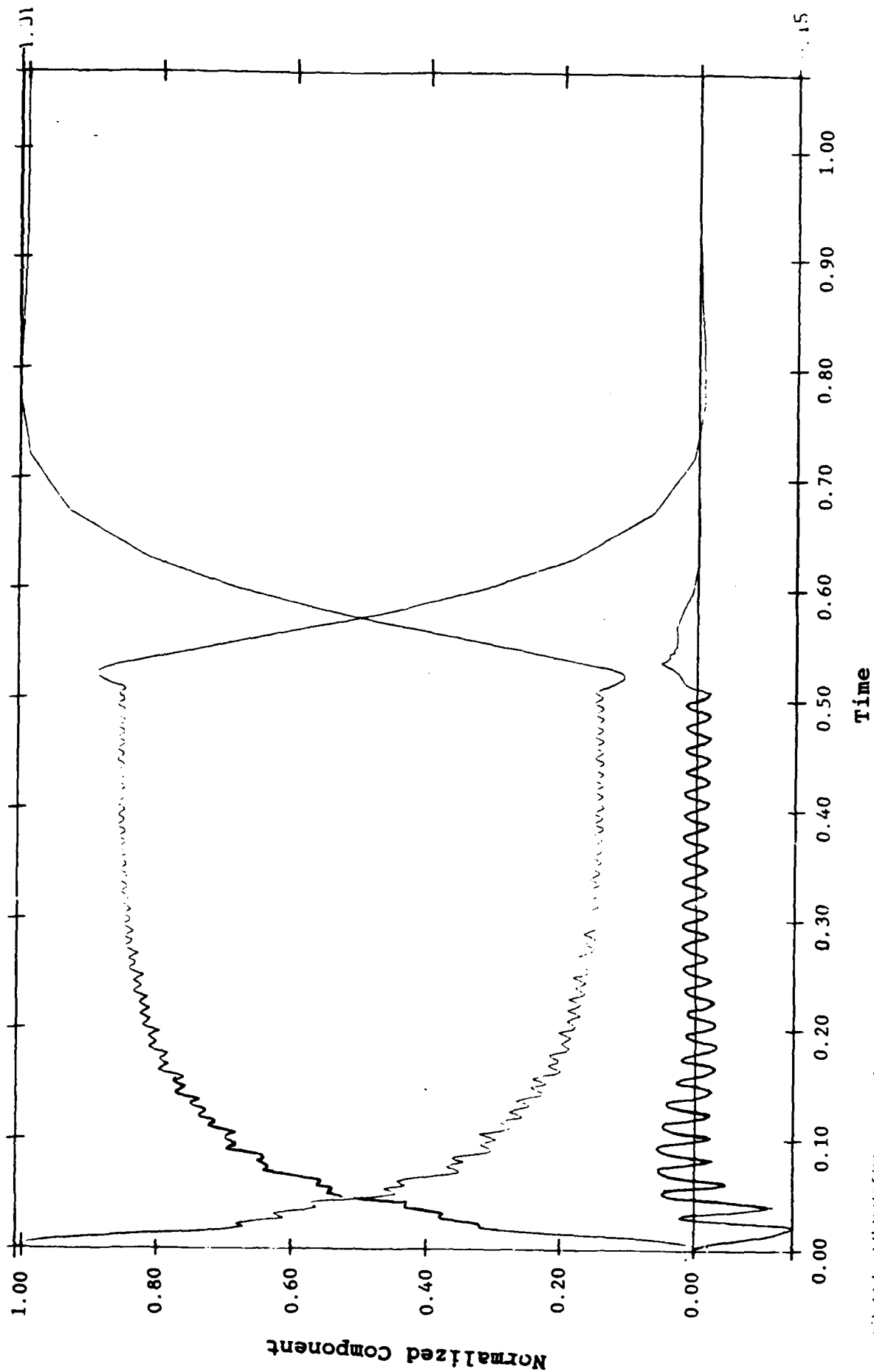
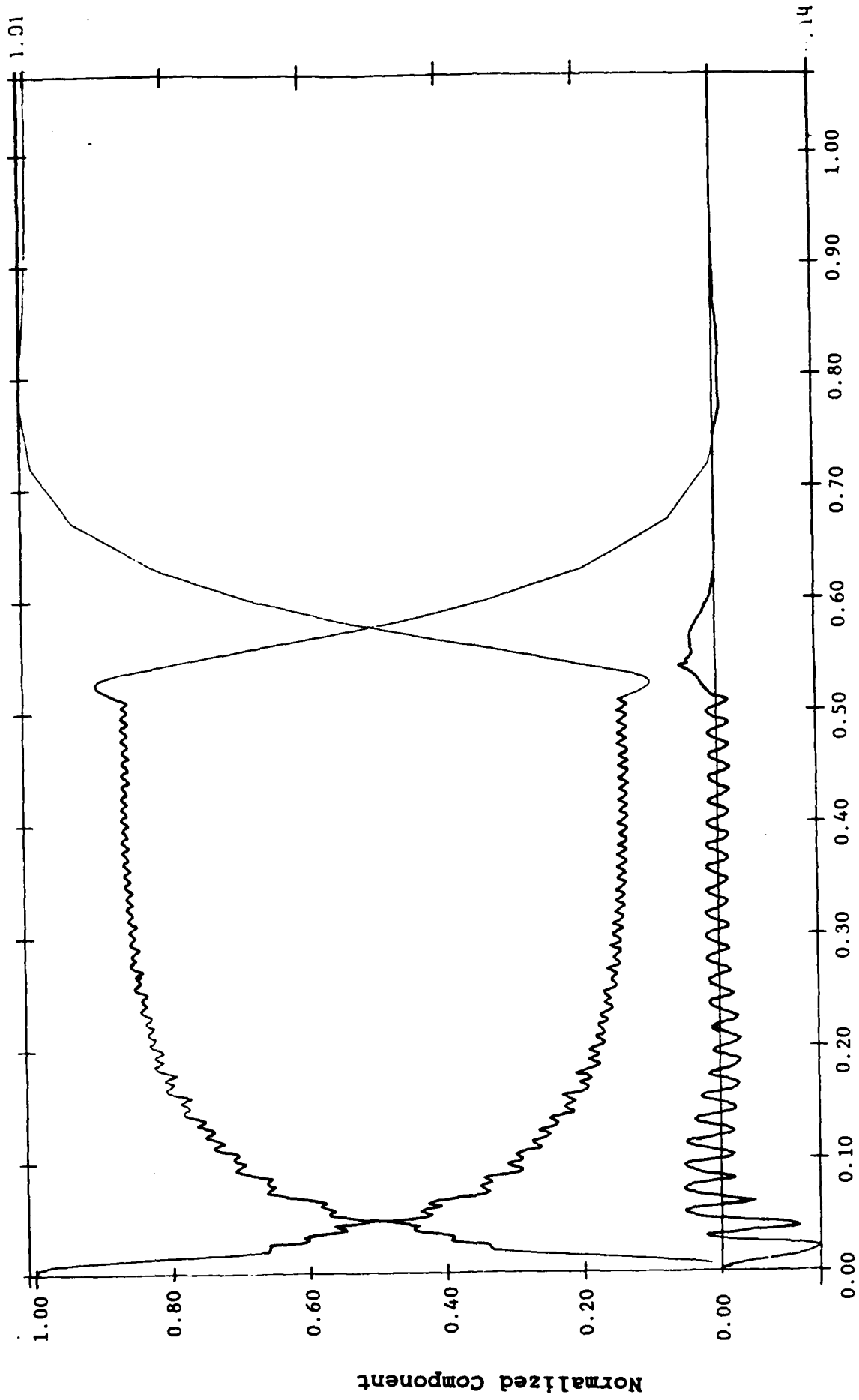


Figure A-6J. Overall stress behavior of soil



Time

Figure A-6K. Overall stress behavior of soil

ELMT NUMBER 13

Normalized Component

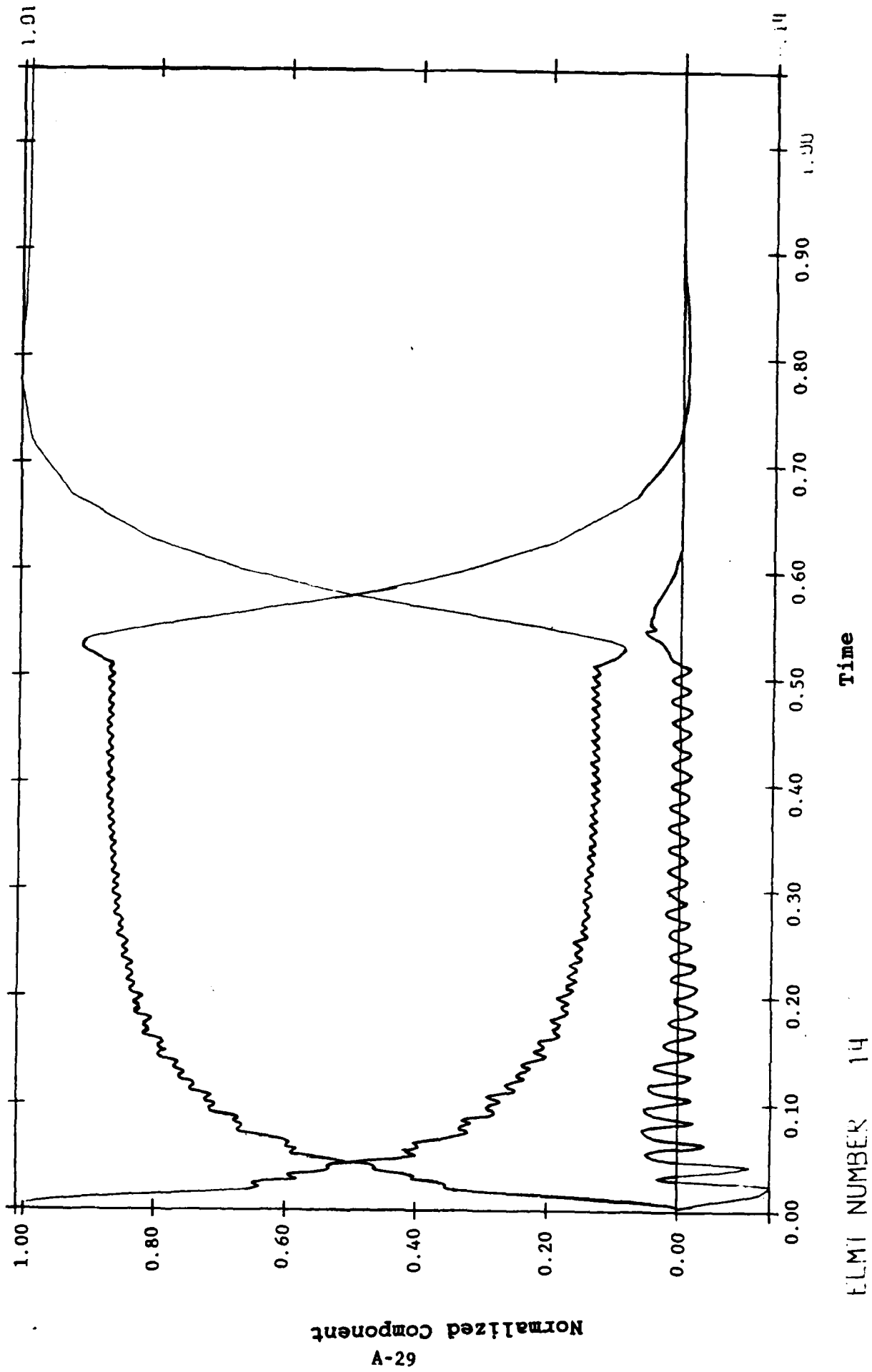
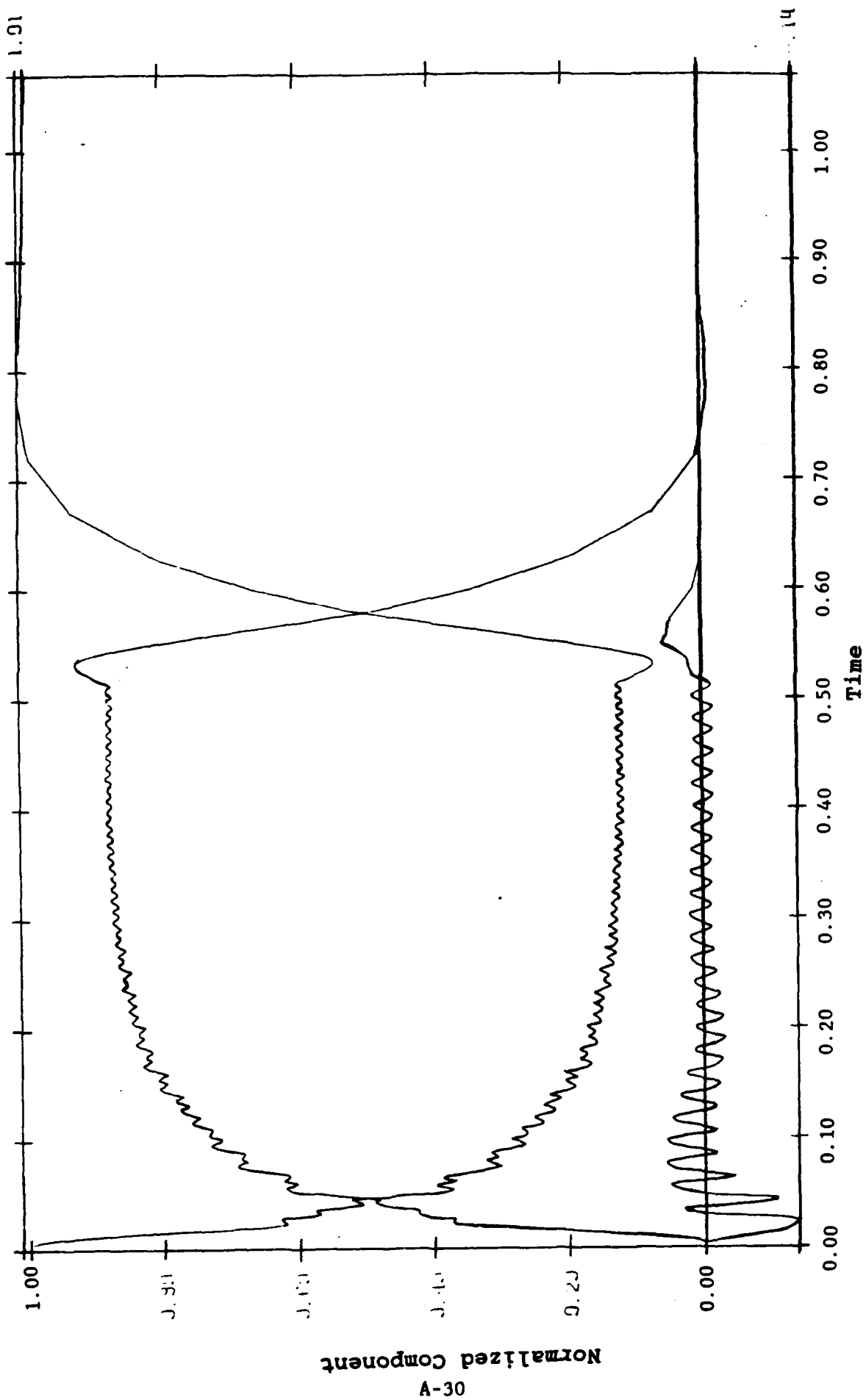


Figure A-6L. Overall stress behavior of soil



ELEM NUMBER 15

Figure A-6M. Overall stress behavior of soil

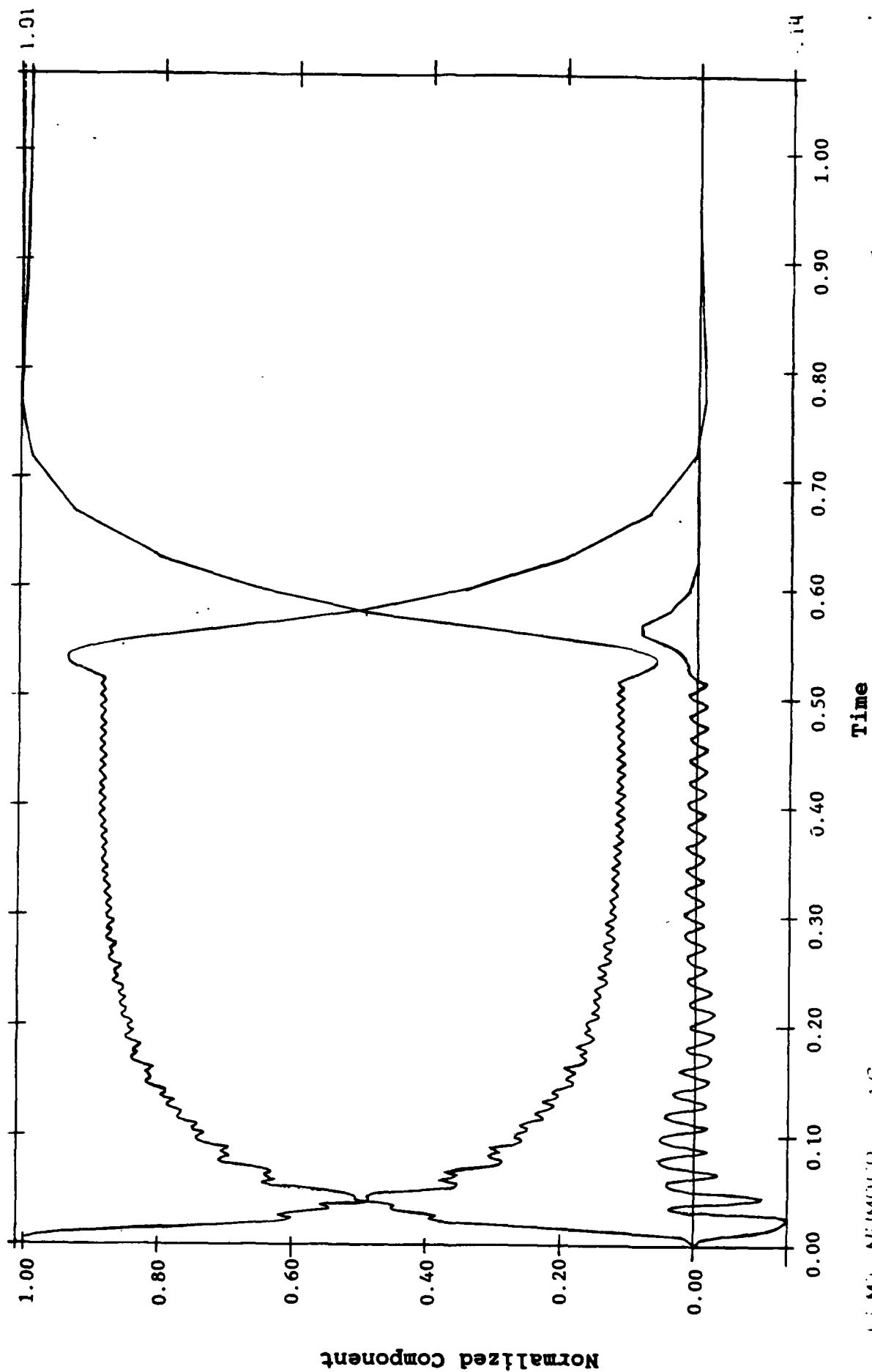


Figure A-6N. Overall stress behavior of soil

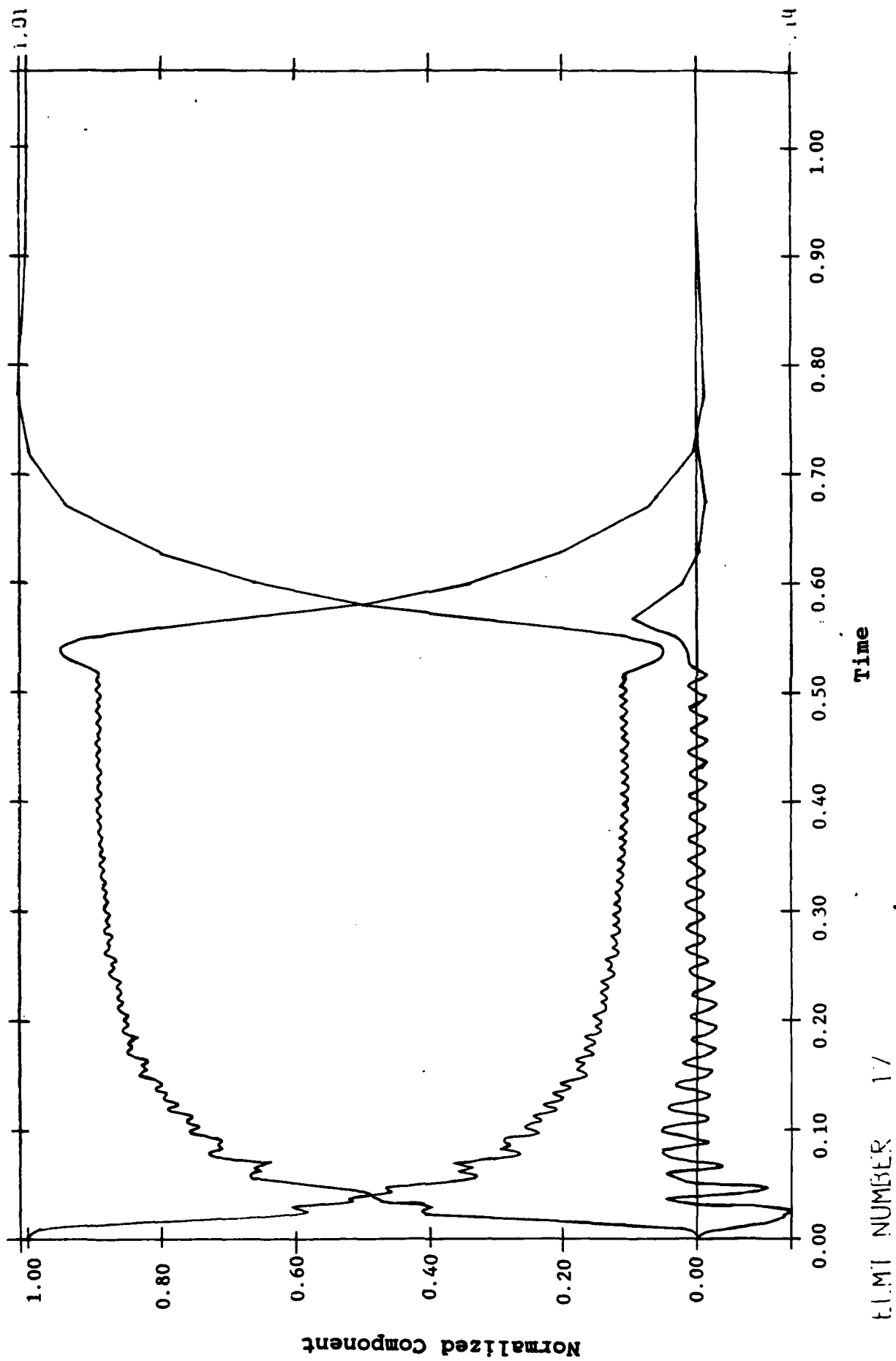


Figure A-60. Overall stress behavior of soil

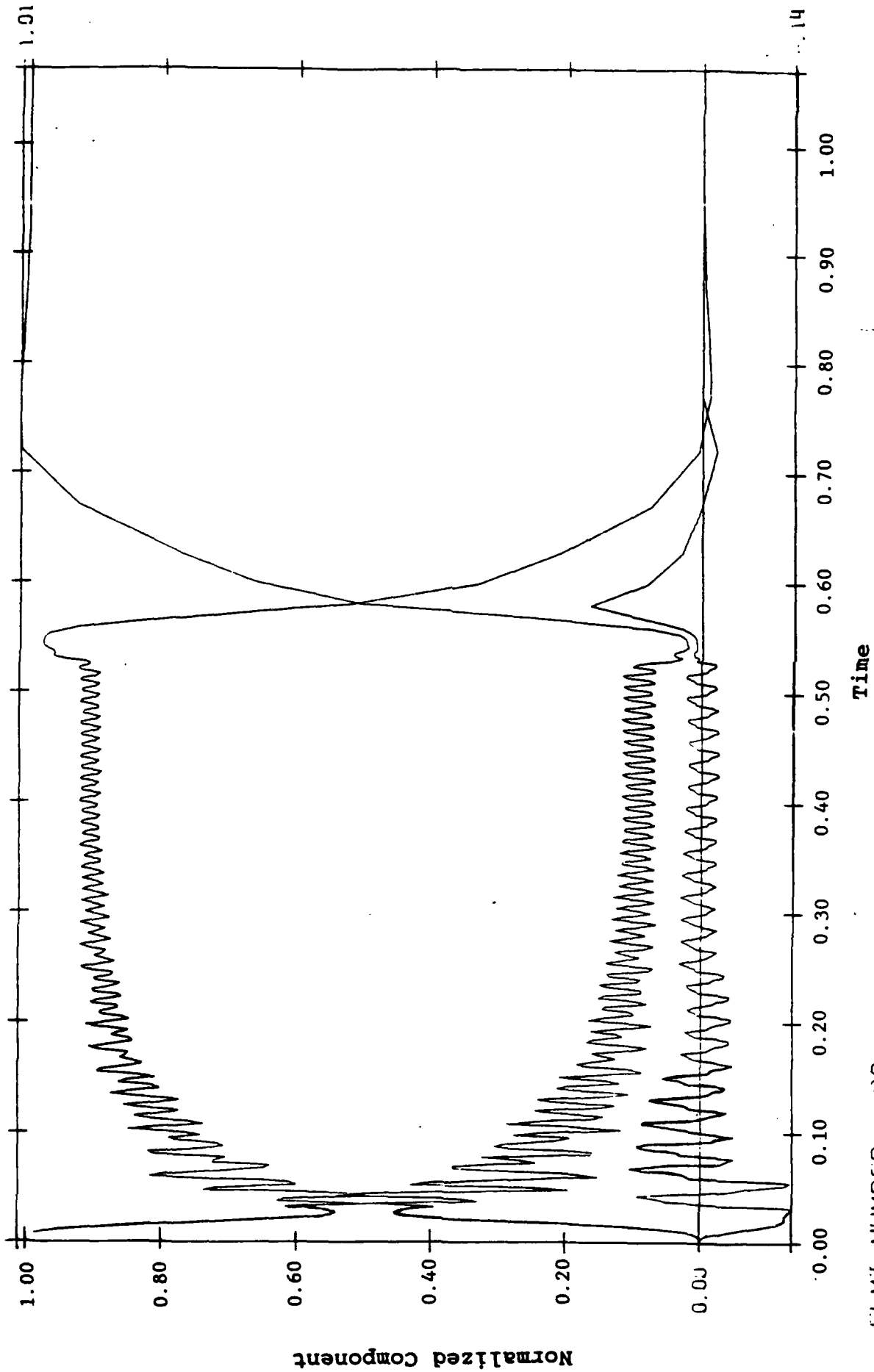


Figure A-6P. Overall stress behavior of soil

Appendix B
BRASS FOOTING TEST

INTRODUCTION

The test procedures and test results are reported in Reference B-1. The soil was Leighton-Buzzard 120/200 sand. The soil deposit was placed in a stacked-ring apparatus by pluviating the sand in layers into water and then rodding to achieve the desired density. A brass footing with a diameter of 113 mm was placed on top of the saturated sand deposit (height = 151 mm, diameter = 406 mm) and tested on a centrifuge at a centrifugal acceleration of 80 gs. The deposit was then subjected to sinusoidal base acceleration. The corresponding prototype situation was analyzed.

Figure B-1 shows the finite-element mesh used for analysis, pore-pressure, and vertical stresses at measured points and a comparison of measured and computed results. The soil is discretized by using 240 elements and the brass footing by using two rows of 10 elements each. The soil parameters are given in Table B-1, and in the analysis $k = 2.5 \times 10^3 \times 80 \text{ m/sec}$ to properly scale diffusion time. The brass footing is modeled as a one-phase elastic solid with $\rho = 8.5 \times 10^3 \text{ kg/m}^3$ (mass density); $E = 10^{12} \text{ N/m}^2$ (Young's modulus), and $\nu = 0.0$ (Poisson's ratio). A static pressure is applied to the top of the footing to achieve a static bearing pressure of $1.30 \times 10^5 \text{ N/m}^2$ in the test (at 80 gs).

The water is located at the ground surface. Drainage of the pore fluid is not allowed to take place through the rigid bottom boundary or the lateral side boundaries. A ground shaking is applied as a horizontal sinusoidal input acceleration at the bottom boundary nodes, with a maximum acceleration = 0.17 g and a frequency of 1 Hz for 10 seconds (10 cycles).

The stacked-ring apparatus was used to simulate free-field conditions in the test. Therefore, the same procedure as used previously in the soil column test simulations was used. Specifically, the same equation number was assigned to each nodal degree of freedom on the same horizontal plane for the two side boundaries.

Figure B-2 shows the computed horizontal acceleration time histories at the bottom (Figure B-2(a), node 131) of the soil deposit and at the top (Figure B-2(b), node 285) of the brass footing on the center line. Note that as a result of the dynamic soil-structure interaction the recorded motion on the footing is different from the input motion at the base.

Figure B-3 shows the computed vertical acceleration time histories at the left corner (Figure B-3(a), node 275), center (Figure B-3(b), node 285), and right corner (Figure B-3(c), node 295) of the footing. Note that as a result of the horizontal base shaking, rocking motions are imparted to the footing. Figure B-4 shows the corresponding footing vertical displacements at the left corner (Figure B-4(a)), center (Figure B-4(b)), and right corner (Figure B-4(c)). As recorded in the test, the settlement increased continuously and almost linearly while the shaking continued. Further, no additional settlements were noted after the shaking stopped (10 seconds) as observed in the test. However, the computed maximum settlement (1.8 meters) exceeded the amount that was measured experimentally (30 cm).

The Navy chose, at this point in the research, to use existing centrifuge test data. This choice required that laboratory triaxial tests be performed to derive the material model for input to program DYNAFLOW.

The specifications for the triaxial tests required the specimens be constructed at the same relative density as the soil used in the centrifuge tests. Unfortunately, this requirement, due to different preparation techniques, resulted in differences in void ratios for the respective soils. This factor effects the soils ultimate strength and moduli. The computed results showed stress levels on the relatively flat yield portion of the stress-strain diagram where small increases in loading result in large increases in displacement. The actual centrifuge loading conditions remained slightly below those which would generate "flow-type" strain and large displacements. In addition, the authors (Ref B-1) acknowledged difficulties in precisely controlling the properties of the centrifuge soil deposit.

The factors combined to generate the soil model (which, though only moderately weaker in ultimate strength, caused much larger strain and displacements to be generated).

Figure B-5 (a, b, and c) shows the deformed mesh at $t = 5$ seconds, 10 seconds, and 15 seconds.

Figure B-6 shows the contours of the pore-water pressure at $t = 0$ seconds, 10 seconds, and 15 seconds. Note that as observed in the test, in the "free-field" close to the sides, the pore-water pressure rises quickly (Figures B-6(b),(c)). Directly under the structure, the pore-water pressure increase is slower and always remains smaller than the pore-water pressure in the free-field at the same elevation (Figure B-6(b), (c)). Immediately following the shaking, the excess pore-water pressures dissipate rapidly and reach their steady state conditions 5 seconds after the end of shaking (Figure B-6(d)). This condition was further illustrated in Figure B-2, which shows time histories for the vertical effective stress and excess pore-water pressure for the points shown on the mesh (Figure B-1(a)).

MODELING ASSUMPTIONS

The brass footing analysis considers the soil-structure interaction for a simple structure founded on the surface of a saturated soil continuum. The interface between the soil and the structure was assumed to be in constant contact with no slippage allowed. The fluid degrees of freedom at the interface were unrestrained. No contact elements were used in the analysis. Fluid pressure on the base of the structure, as a result of the dynamic excitation, was assumed negligible and ignored. The horizontal boundaries for the solid-fluid continuum were restrained in the same manner as the soil column. The slaving in this case appears to be more valid, because it does not eliminate the shear and rotational element distortions (Figure B-5). This in turn allows for larger vertical accelerations, and more settlement in the soil mass.

PROBLEMS AND SOLUTIONS

The brass footing problem was based on the Leighton-Buzzard sand material model. The elastic moduli from the triaxial tests were considered to be low. Employing the equations of Hardin and Drenevich

(Appendix A) allowed for the computation of more realistic elastic shear moduli. The material permeability was manipulated to compute acceptable pore-pressure behavior. The initial value was selected from references and modified by the effects of a glycerin/water mixture (P.C. Lamber PhD Thesis) and by the centrifuge/acceleration of 80 gs. It is useful to note at this point that permeability may be computed if consolidation information is known. This is demonstrated in the following:

$$T = \frac{C_v t}{H^2} \quad (B-1)$$

where: T_{100} = time factor
 C_v = consolidation coefficient
 H^0 = height of drainage path
 t = time

further:

$$C_v = \kappa / \gamma_w M_v \quad (B-2)$$

where: κ = material permeability
 γ_w = unit weight of water
 M_v = Coefficient of volume change

substitution of Equation (B-2) for c_v yields

$$T = \frac{\left(\frac{\kappa}{\gamma_w M_v} \right) t}{H^2} \text{ or } K = \frac{TH^2 \gamma_w M_v}{t} \quad (B-3)$$

recognizing that $T_{100} = 1.0$

$$K = \frac{H^2 \gamma_w M_v}{t}$$

The following tables and figures are the data sets required for the material model derivation and DYNFLOW analysis. Figures B-8 through B-10 are included for additional reference to the existing analysis.

REFERENCE

B-1. R.V. Whitman and P.C. Lambe. "Liquefaction Consequences for a structure," in Proceedings of Soil Dynamics and Earthquake Engineering Conference, Southampton, U.K., 1982, pp 941-949.

Leighton-Buzzard 120/200 Sand - Dr = 55%

$\rho_s = 2.73 \times 10^3 \text{ kg/m}^3$	(mass density, solid grains)
$\rho_w = 1.00 \times 10^3 \text{ kg/m}^3$	(mass density, fluid phase)
$n^w = 0.47$	(porosity)
$k = 2.5 \times 10^{-3} \text{ m/sec}$	(permeability)
$\psi'_c = 34.35^\circ$	(friction angle; compression case)
$\psi'_E = 21.14^\circ$	(friction angle; extension case)
$g_1/p_1 = 500.$	(elastic shear modulus)
$B_1/p_1 = 333.33$	(elastic bulk modulus)
$p_1 = 9.81 \times 10^4 \text{ N/m}^2$	(reference pressure)
$\eta = 0.50$	(power exponent)
$\eta_c = 1.30$	
$\eta_E = 0.80$	

Yield Surface Number	α	m	$(H'_c)_1/p_1$	$(H'_E)_1/p_1$
1	0.03099	0.06582	966.80	1168.00
2	0.06261	0.14300	357.70	459.20
3	0.09681	0.26590	219.40	337.30
4	0.08969	0.32670	162.00	265.40
5	0.15857	0.50160	42.03	81.95
6	0.23864	0.63800	17.47	41.31
7	0.27796	0.76120	7.60	21.99
8	0.32030	0.9023	3.78	13.21
9	0.32580	0.9930	1.17	4.47

Table B-1. Soil parameters

LEIGHTON-BUZZARD 120/200 SAND - DR=55% - SC3,SE3 - MODIFIED				
100	1	3	1	1
13	12	00	0	6
..0000	0.50	0.00	1.00	
1	0.	0.	1.	0.
2	.1	.000519	1.033	.0001179
3	.22	.00125	1.07	.00026
4	.3	.001852	1.1	.0003722
5	.4	.002592	1.133	.0005143
6	.483	.0033	1.16	.00063
7	.847	.00678	1.283	.00156
8	1.236	.01435	1.41	.0029
9	1.59	.0263	1.53	.0052
10	2.06	.0544	1.685	.0074
11	2.17	.0649	1.73	.00778
12	2.44	.1072	1.81	.0074
13	2.59	.15	1.86	.0059
1	0.	0.	1.	0.
2	-.044	-.000237	.985	-.00007
3	-.088	-.000519	.97	-.00007
4	-.2197	-.00157	.927	-.000148
5	-.337	-.00298	.888	.000037
6	-.3815	-.00426	.873	.00048
7	-.41	-.00538	.86	.00082
8	-.44	-.00689	.85	.00123
9	-.51	-.0119	.83	.00245
10	-.565	-.0209	.81	.0051
11	-.6	-.0455	.8	.00587
12	-.643	-.0674	.786	.00623

Table B-2. MUD input data for leighton Buzzard sand

SOIL MODEL FOR LEIGHTON BUZZARD SAND

[illegible]

Table B-3. MUD output for Leighton Buzzard sand

CENTRIFUGE ANALYSIS, BRASS FOOTING MODEL, LBSAND - K = 0.0025*80G										
	2	4	2	1000	3	80	0	1	0	1
295	1	0	1.5	1000.0	0	05	05	10	5	1
20	0	0	0	0	0	05	05			
131	1	0								
260	1	1								
273	1	1								
275	1	1								
285	1	1								
295	1	1								
1	8		0.00		0.00					
2			11.75		0.00					
3			11.75		12.10					
4			0.00		12.10					
5			7.25		0.00					
6			11.75		6.05					
7			7.25		12.10					
8			0.00		6.05					
5	13	12	1							
66	4		11.75		0.00					
2			20.75		0.00					
3			20.75		12.10					
4			11.75		12.10					
10	13	12	1							
96	8		20.75		0.00					
2			32.50		0.00					
3			32.50		12.10					
4			20.75		12.10					

Table B-4. DYNAFLOW data for brass footing problem

5			25.25	0.00
6			32.50	6.05
7			25.25	12.10
8			20.75	6.05
5	13	12	1	
274	4	11.75		12.88
2		20.75		12.88
3		20.75		13.66
4		11.75		13.66
10	2	1	1	
1	13	1	1	1
261		1	1	1
274	1	0	0	1
295		0	0	1
1	2	1.6677	0.0	1.6677
261		1.6677	0.0	1.6677
20	13			
1	1	0.0	0.0	
		10000.0	1.0	
2	2	0.0	0.0	
		10000.0	0.0	
		20000.0	1.300E+05	
3	0	0.0	0.0	

0.0
0.0

Table B-4. Continued

	4	240	0	0	0	1	0	1	0	60	0	0	1	2	04	0
	2	8	9													
		5.000E+02	1.000E+02	3.333E+02	5.000E-01											
		-1.000E+00	-1.000E+00	-1.000E+00	0.0											
		1.300E+00	8.000E-01	0.0	-1.019E-05	1.000E+12	0.47								0.0	
	1	6.582E-02	9.668E+02	1.168E+03	0.0											
		-1.033E-02	2.066E-02	-1.033E-02	0.0											
	2	1.430E-01	3.577E+02	4.592E+02	0.0											
		-2.087E-02	4.174E-02	-2.087E-02	0.0											
	3	2.659E-01	2.194E+02	3.373E+02	0.0											
		-3.227E-02	6.454E-02	-3.227E-02	0.0											
	4	3.267E-01	1.620E+02	2.654E+02	2.113E-01	0.0										
		-2.990E-02	5.979E-02	-2.990E-02	0.0											
	5	5.016E-01	4.203E+01	8.195E+01	5.593E-01	6.955E-01	0.0									
		-5.287E-02	1.057E-01	-5.287E-02	0.0											
	6	5.380E-01	1.747E+01	4.131E+01	8.488E-01	8.864E-01	0.0									
		-7.954E-02	1.591E-01	-7.954E-02	0.0											
	7	7.612E-01	7.597E+00	2.199E+01	1.086E+00	7.604E-01	0.0									
		-9.266E-02	1.853E-01	-9.266E-02	0.0											
	8	9.023E-01	3.774E+00	1.321E+01	1.233E+00	7.872E-01	0.0									
		068E-01	2.135E-01	-1.068E-01	0.0											
	9	9.930E-01	1.169E+00	4.474E+00	1.295E+00	8.411E-01	0.0									
		-1.086E-01	2.172E-01	-1.086E-01	0.0											
		0.200		0.200												

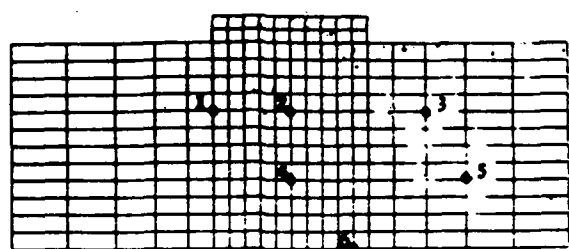
Table B-4. Continued

	2730.0	0.0	-9.81	1078.9
1	1	1	15	1
20	12	13	1	1
69	1	1	1	
125	1	1	1	
129	1	1	1	
169	1	1	1	
197	1	1	1	
200	1	1	1	
203	1	1	1	
207	1	1	1	
210	1	1	1	
213	1	1	1	
221	1	1	1	
223	1	1	1	
226	1	1	1	
228	1	1	1	
237	1	1	1	
1				

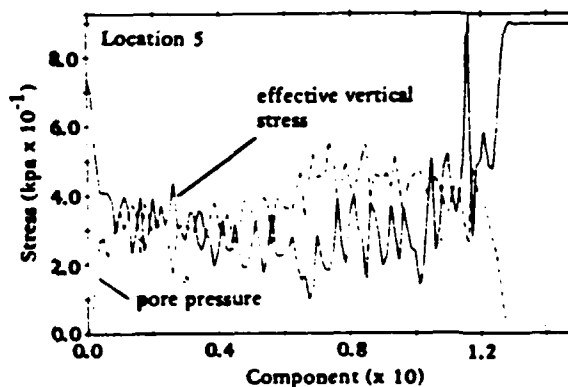
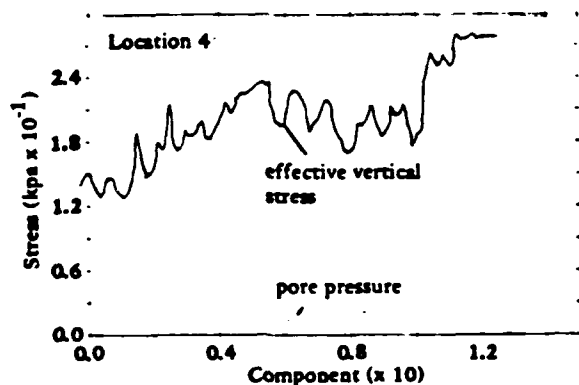
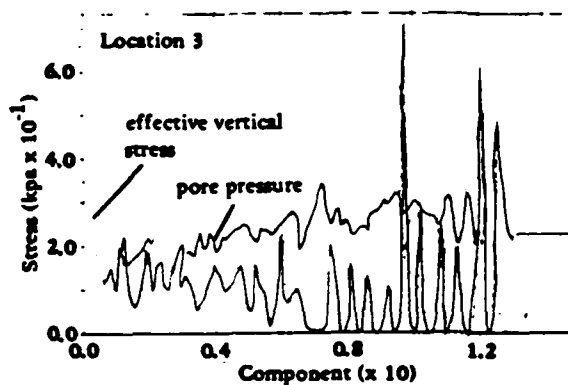
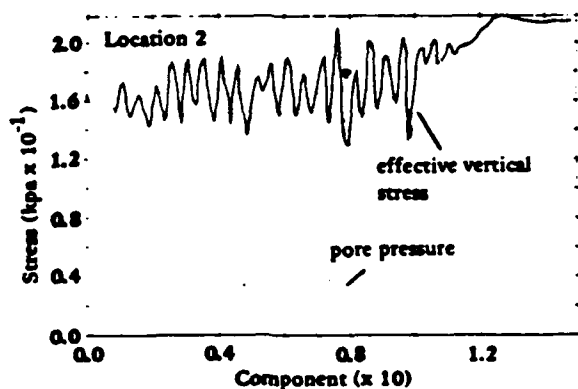
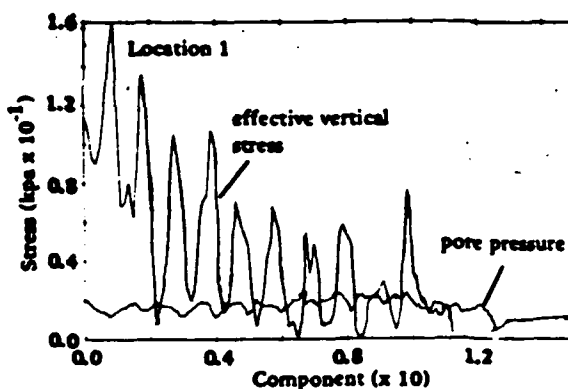
Table B-4. Continued

1	20	0	0	0	0	0	0	0	0	2	0
1											
1.000E+12			0.0								
8.500E+03			0.0								
1		78	91	276	0.0						
2		91	104	278	274						
3		104	117	280	276						
4		117	130	282	278						
5		130	143	284	280						
6		143	156	286	282						
7		156	169	288	284						
8		169	182	290	286						
9		182	195	292	288						
10		195	208	294	290						
11		274	276	277	292						
10	1	2	1	1	275	1					
11	3				1.0						
12	3				1.0						
13	3				1.0						
14	3				1.0						
15	3				1.0						
16	3				1.0						
17	3				1.0						
18	3				1.0						
19	3				1.0						
20	3				1.0						

Table B-4. Continued



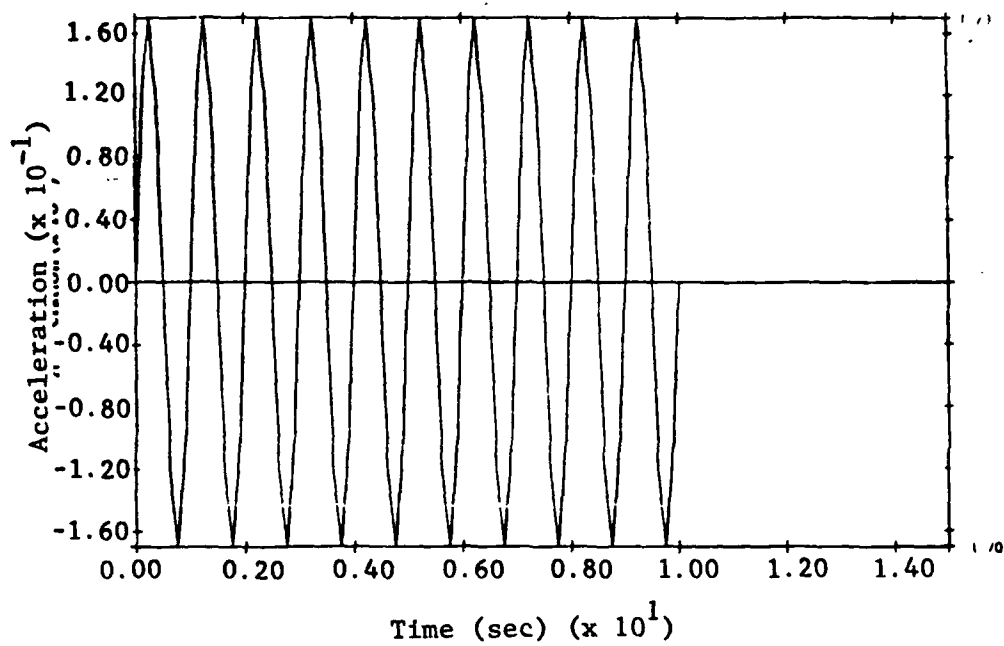
Finite Element Mesh



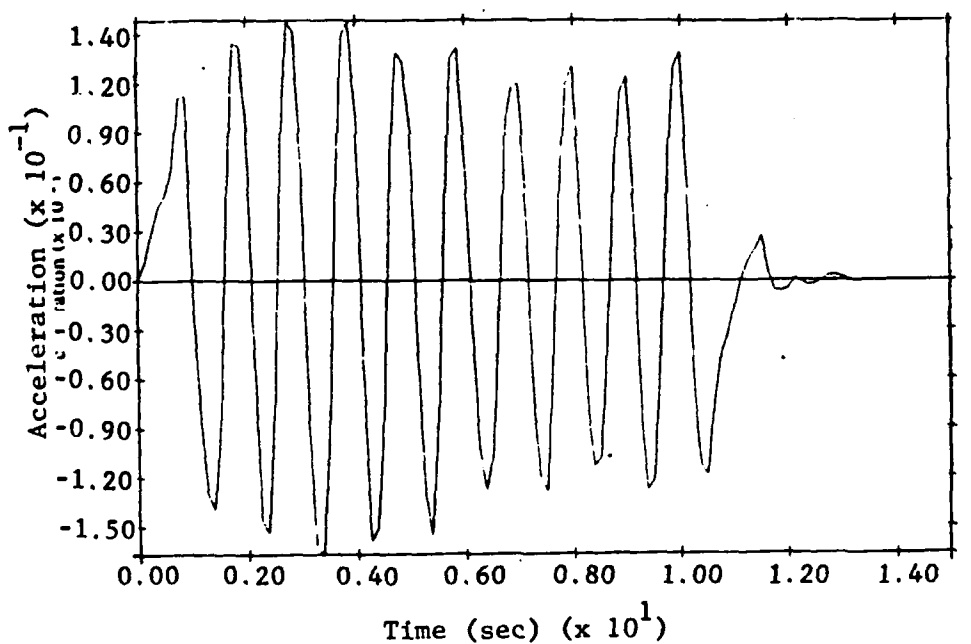
Peak Pore Pressure (kpa)

Location	Computer	Measured
1	20	20
2	30	30
3	30	25
4	15	12
5	50	65
6	40	60

Figure B-1. Undeformed mesh, brass footing, computed vertical stress, and pore pressure



(a) Node 131



(b) Node 285

Figure B-2. Input horizontal accelerations and resultant accelerations at center of the footing

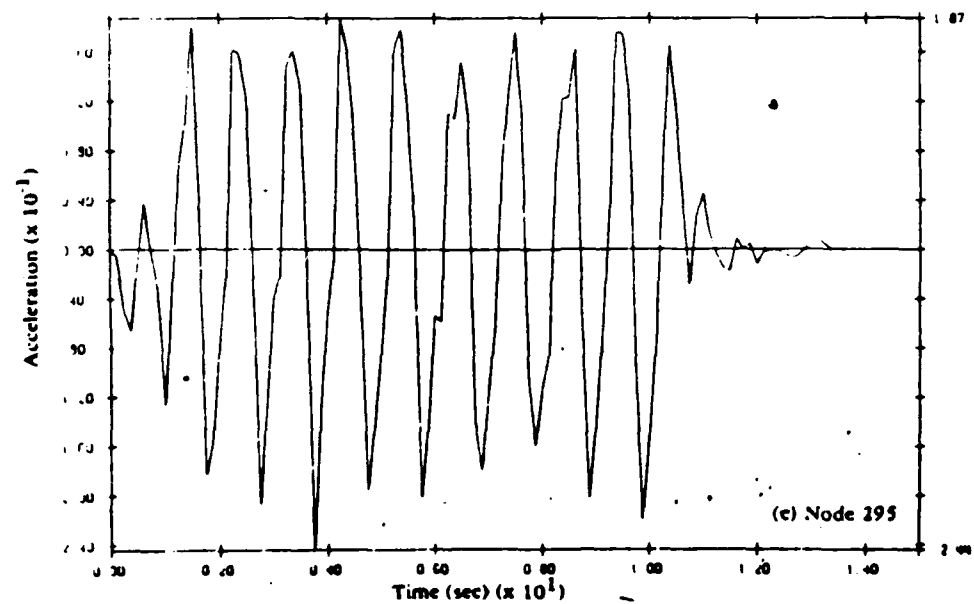
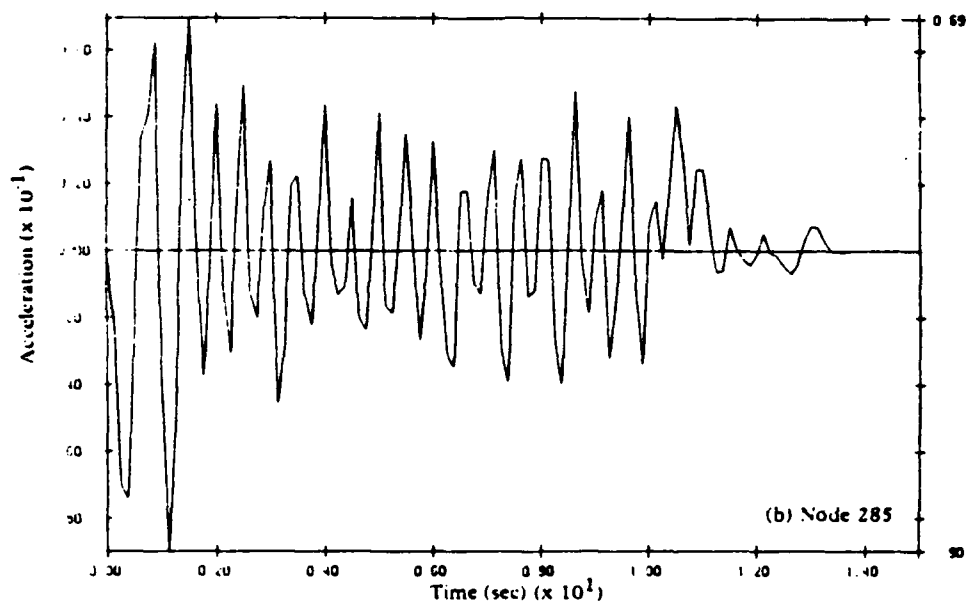
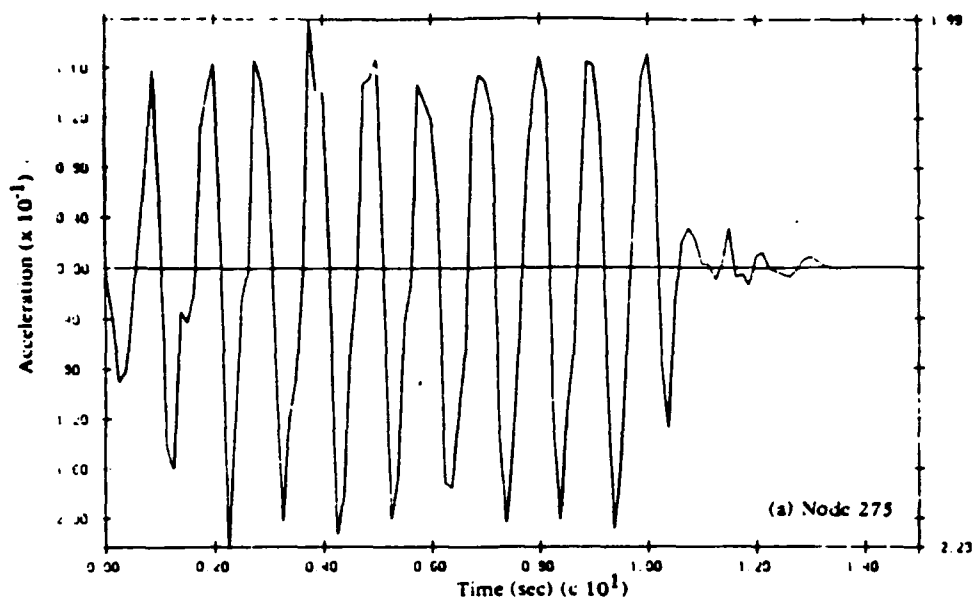


Figure B-3. Vertical footing accelerations
B-15

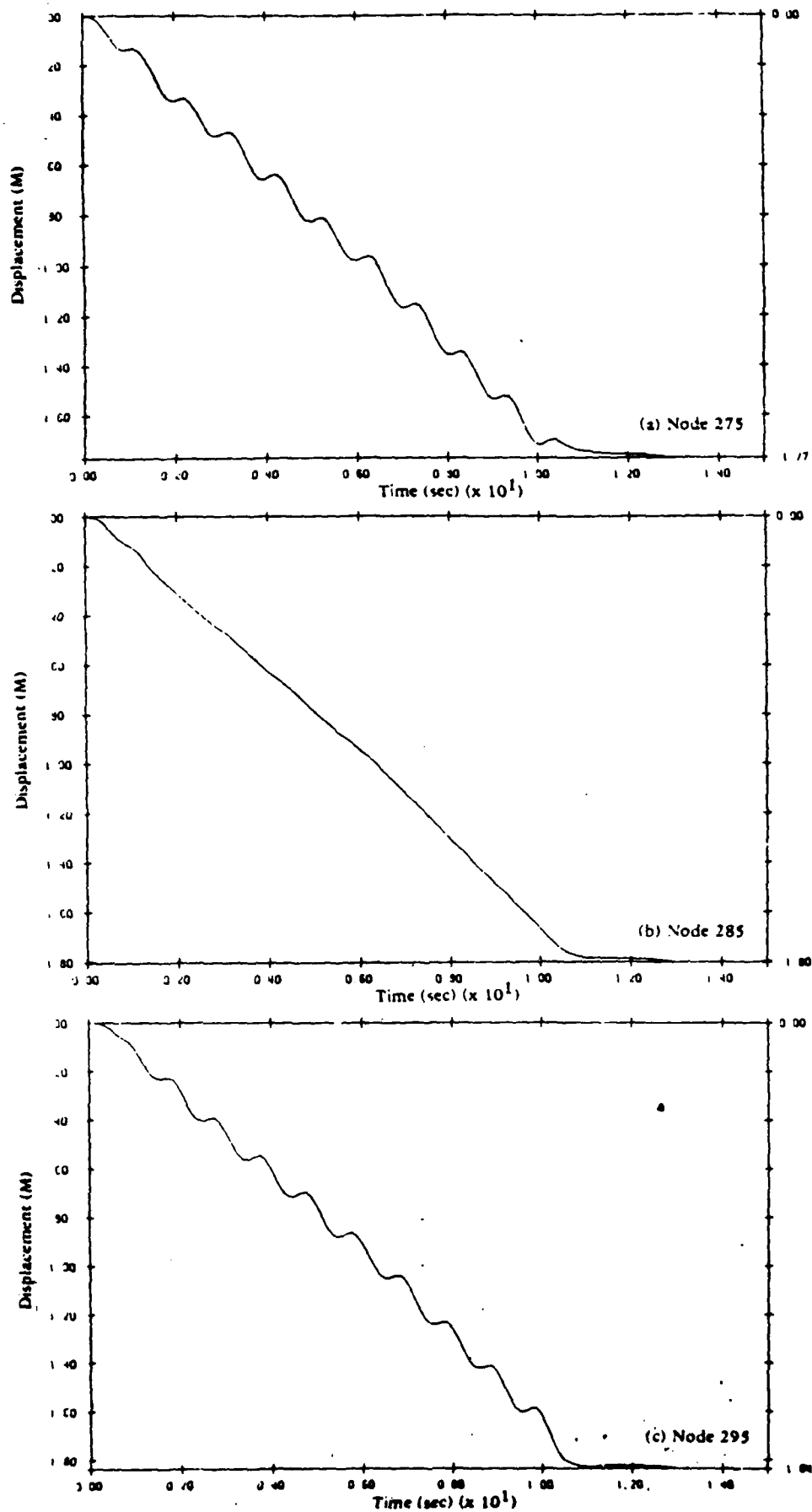
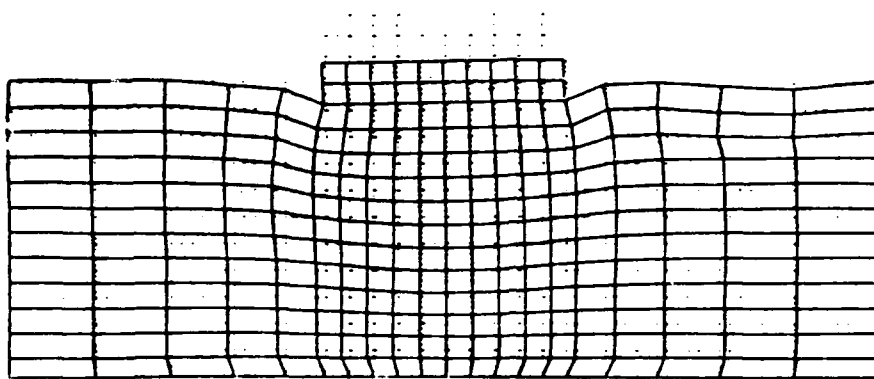
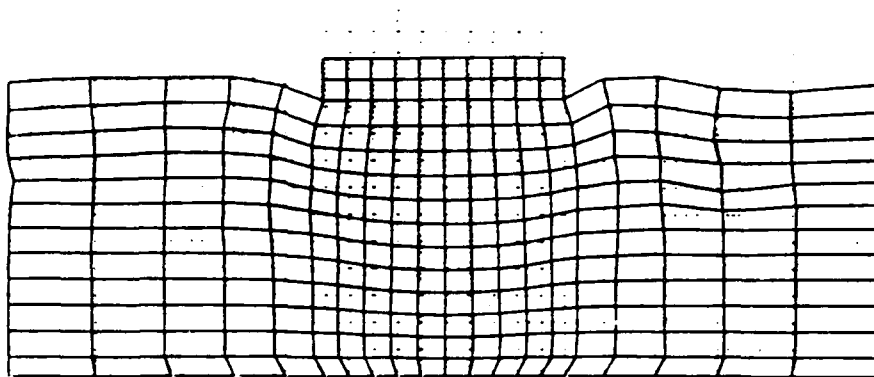


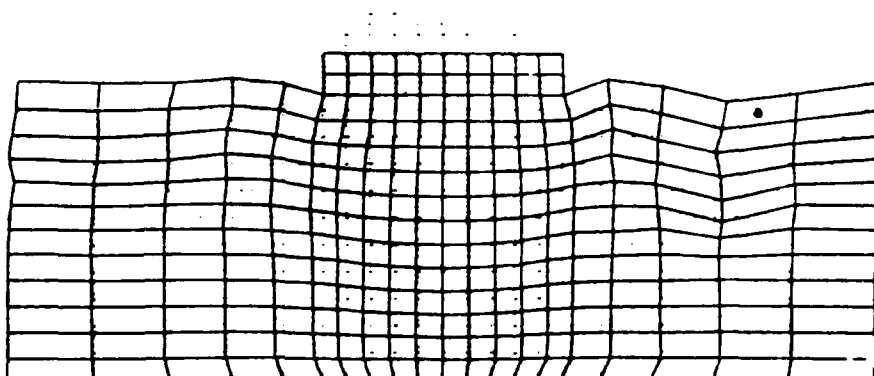
Figure B-4. Vertical footing displacements



(a) $t = 5$ seconds

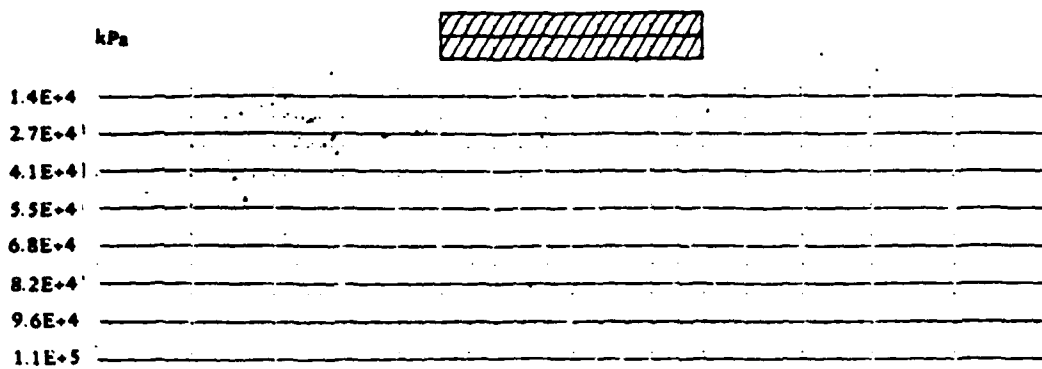


(b) $t = 10$ seconds

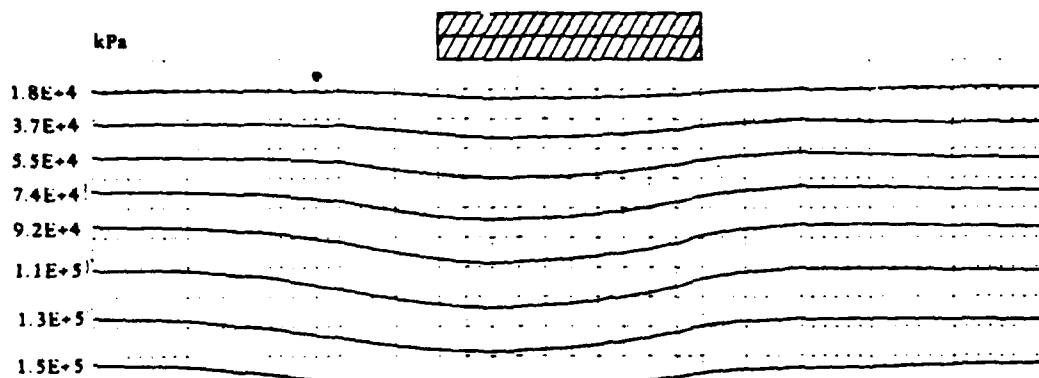


(c) $t = 15$ seconds

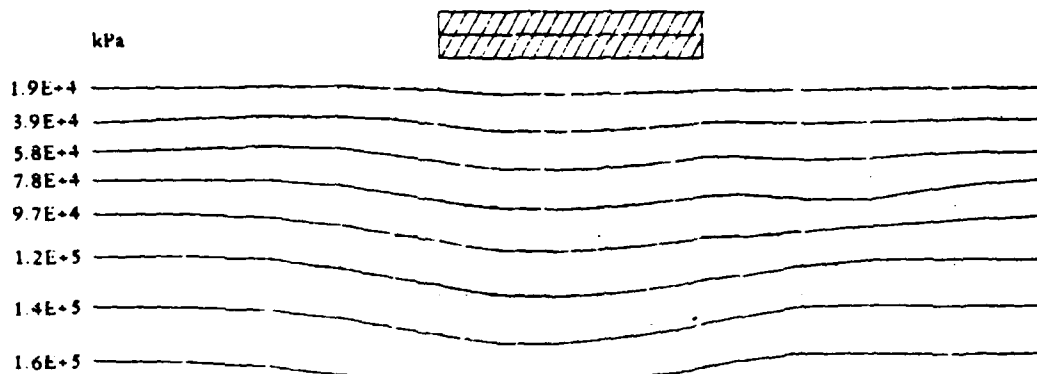
Figure B-5. Deformed mesh



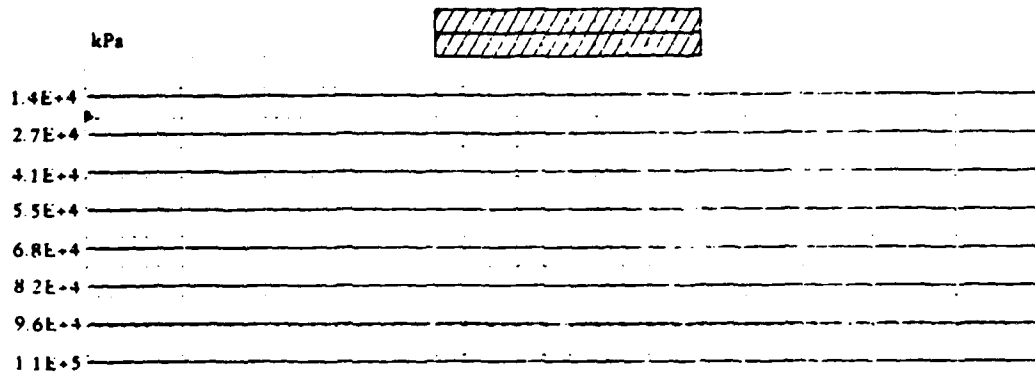
(a) $t = 0$ second



(b) $t = 5$ seconds

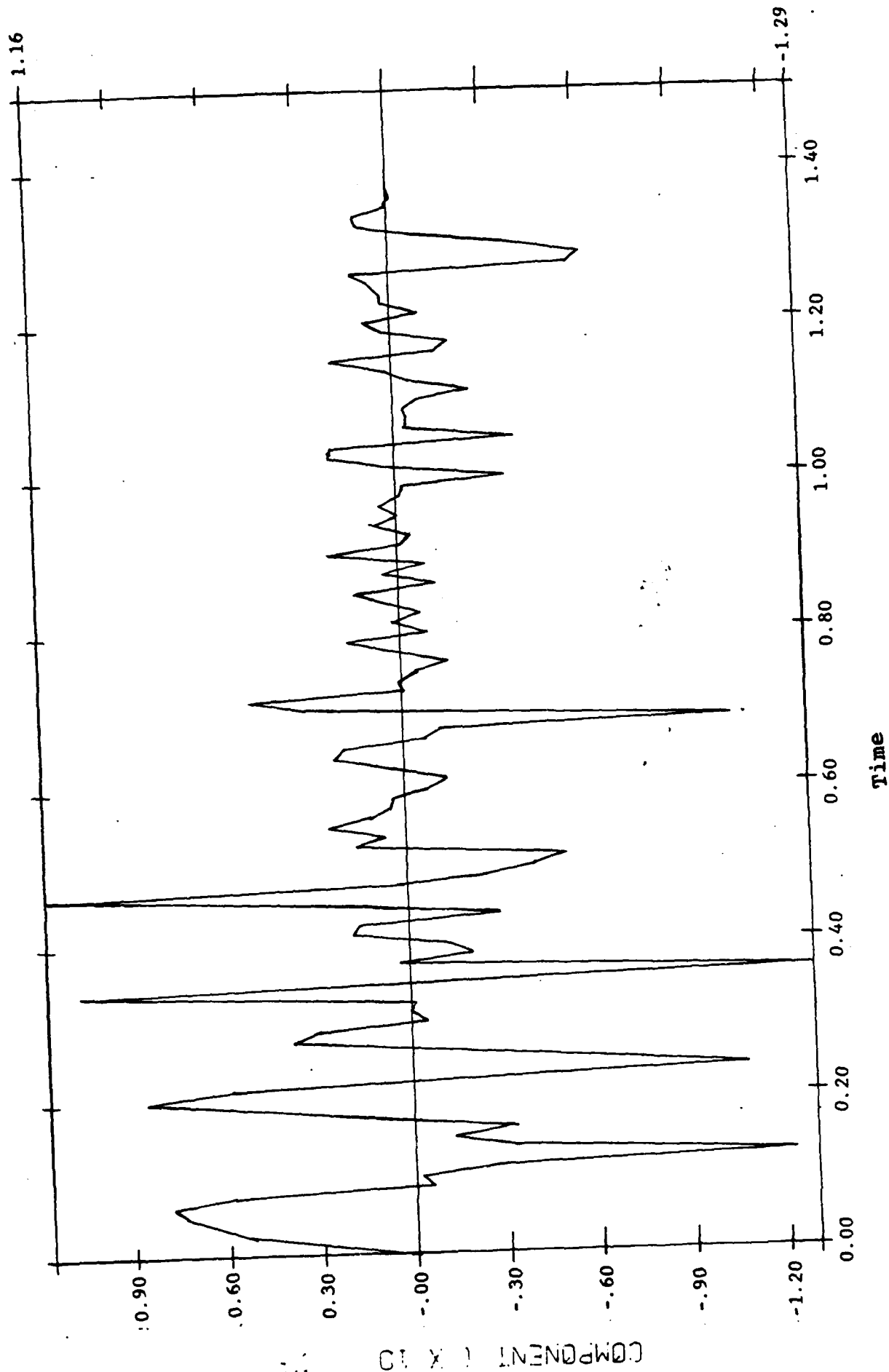


(c) $t = 10$ seconds

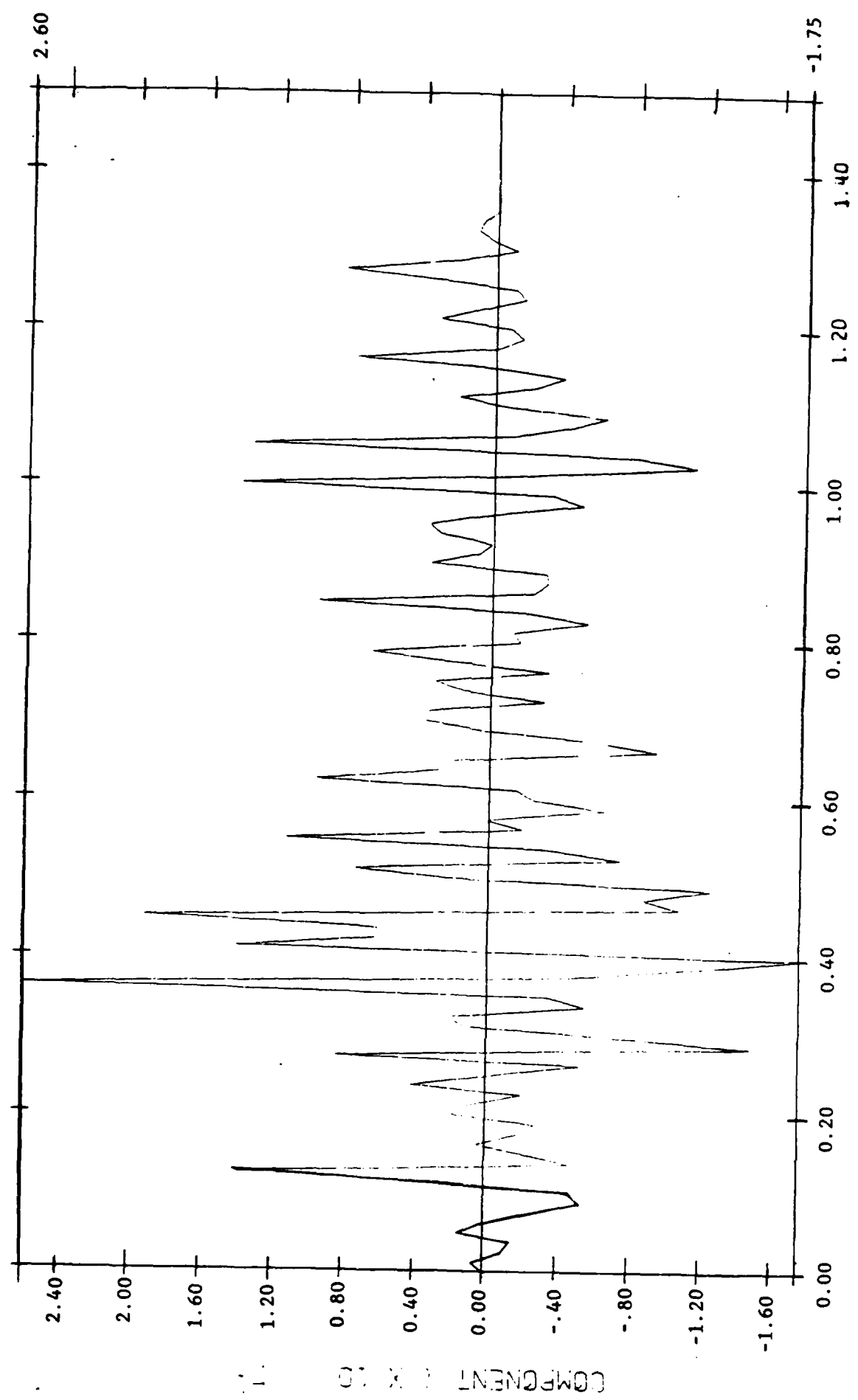


(d) $t = 15$ seconds

Figure B-6. Pore pressure contours



NODE NUMBER 200
ACCELERATION
Figure B-8A. Horizontal acceleration

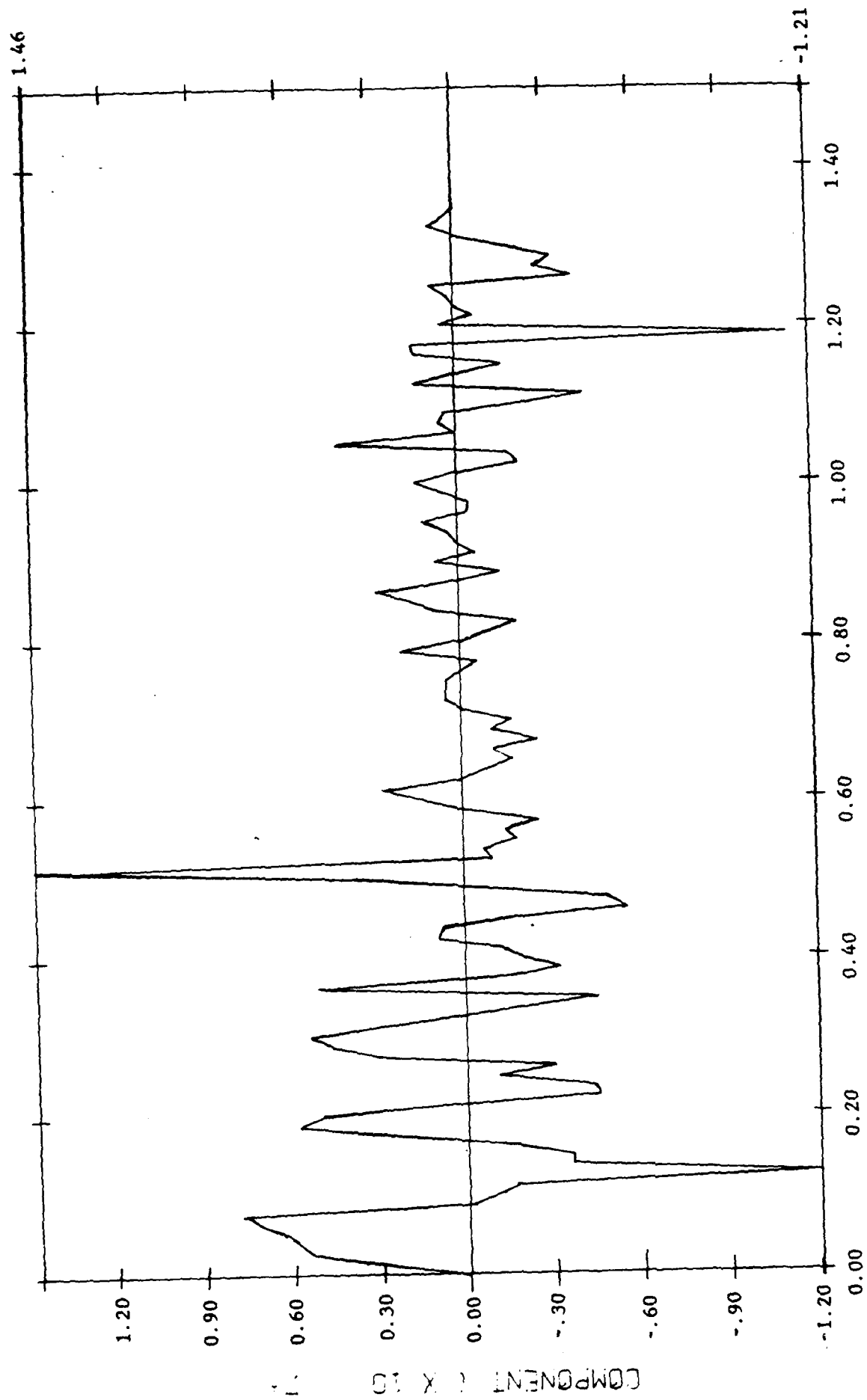


NODE NUMBER 260

ACCELERATION

Figure B-8B. Vertical acceleration

CENTRIFUGAL BRACE FOOTING, OBSERVED - K = 0.0025 * 300



NODE NUMBER 273
ACCELERATION

Time

Figure B-8C. Horizontal acceleration

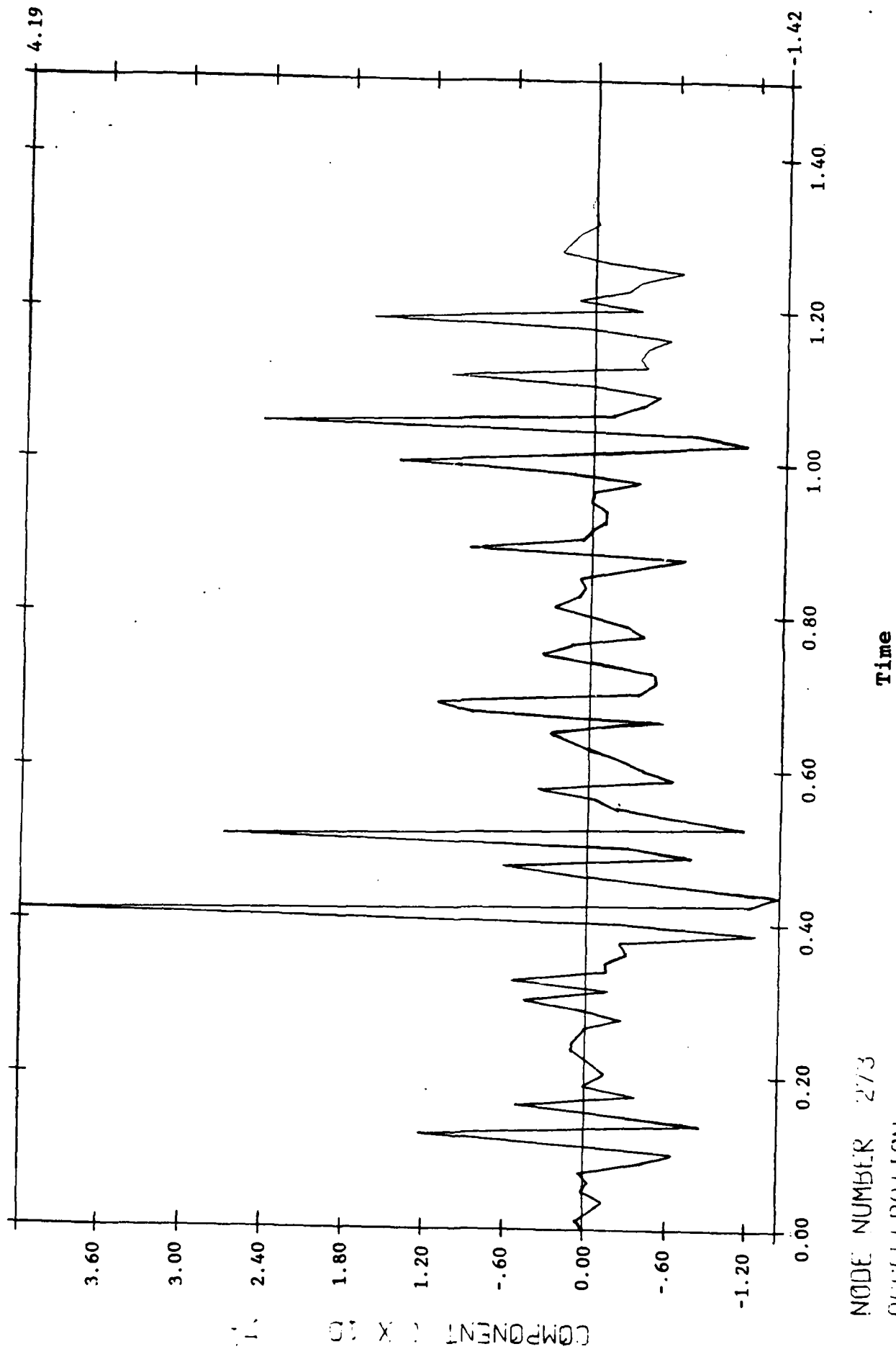


Figure B-8D. Vertical acceleration

GEN. REFUGE ANALYSIS, BRIDGE FOOTING, LB50ND - K - 070025-900

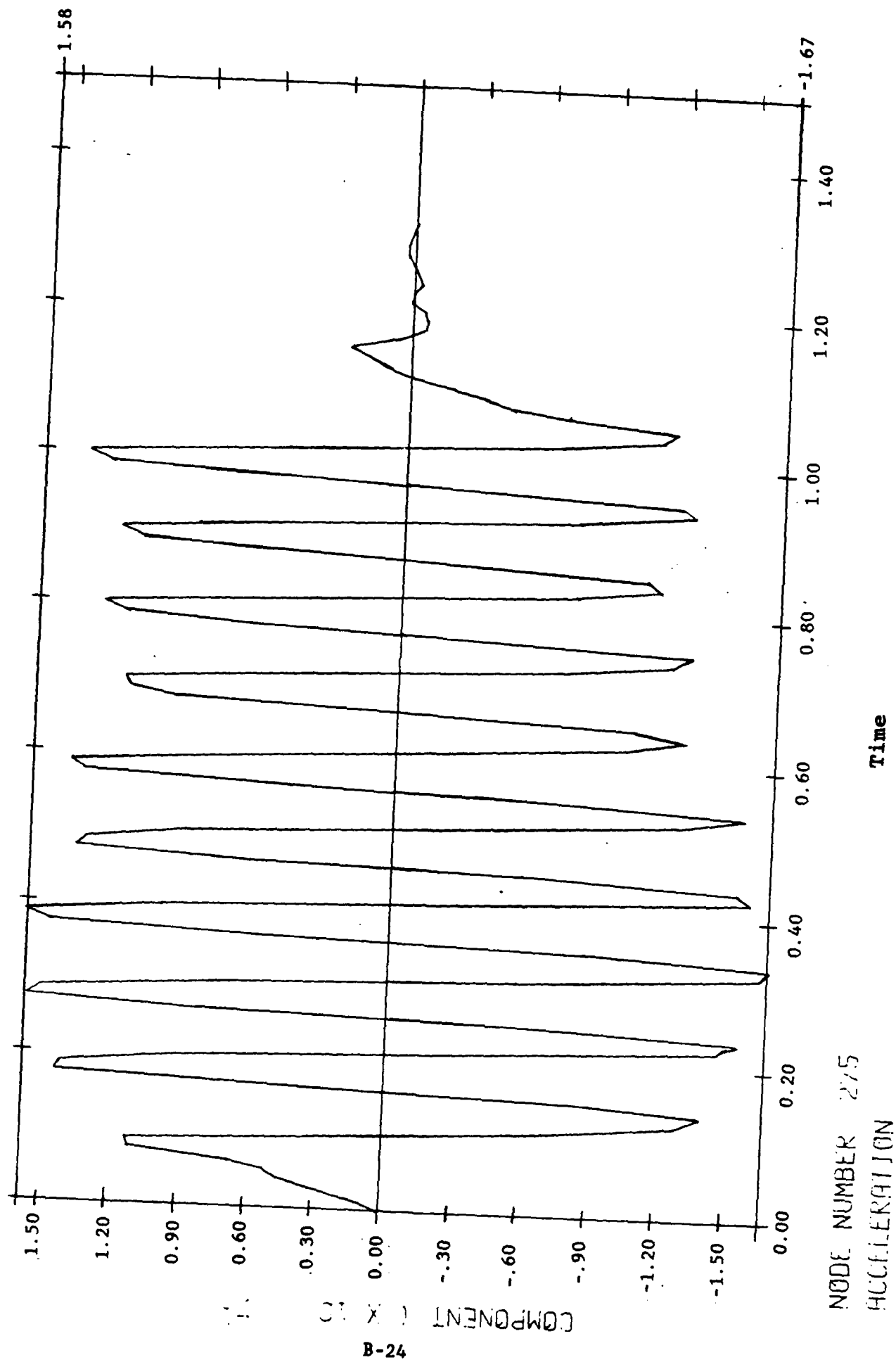


Figure B-8E. Horizontal acceleration

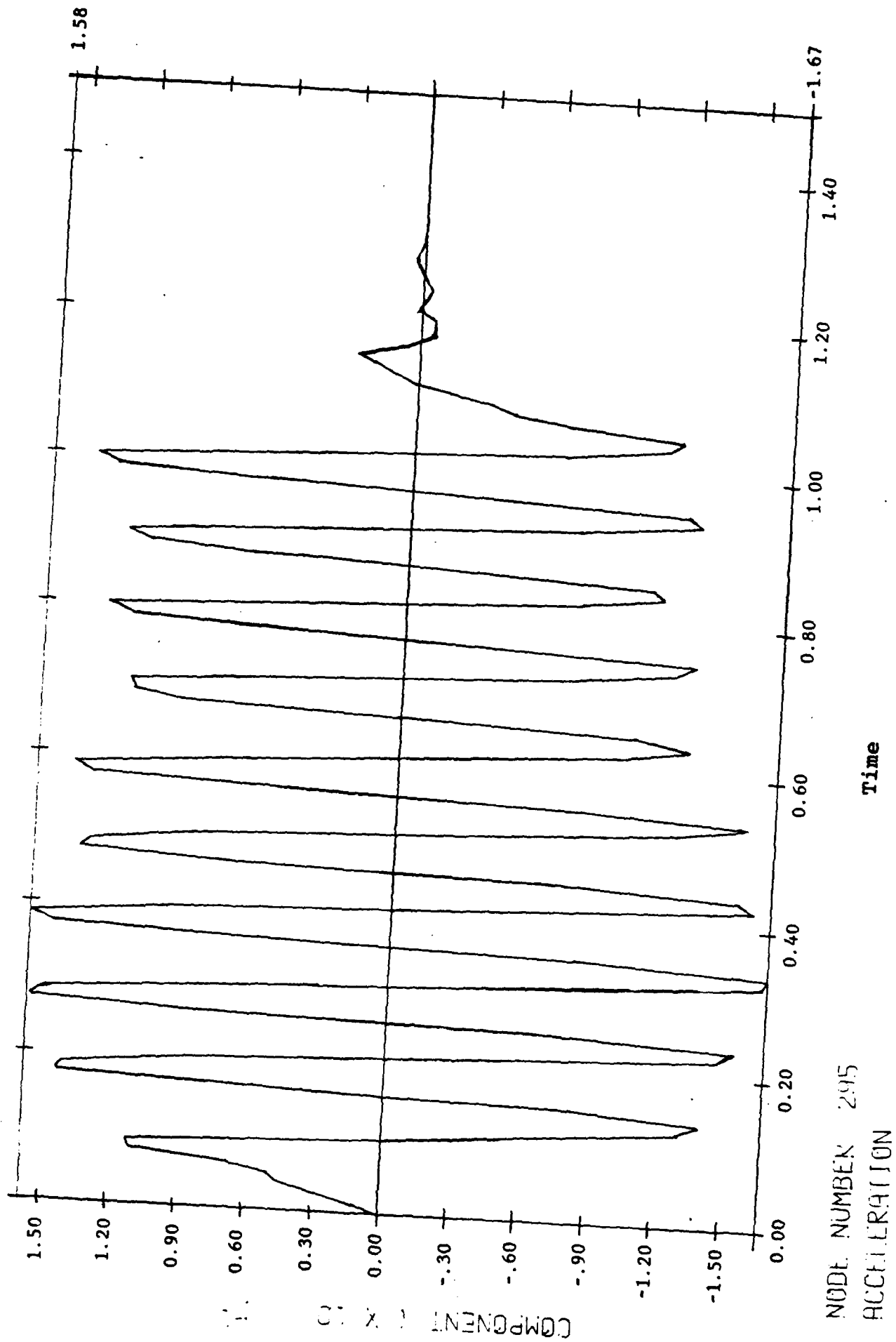


Figure B-8F. Horizontal acceleration

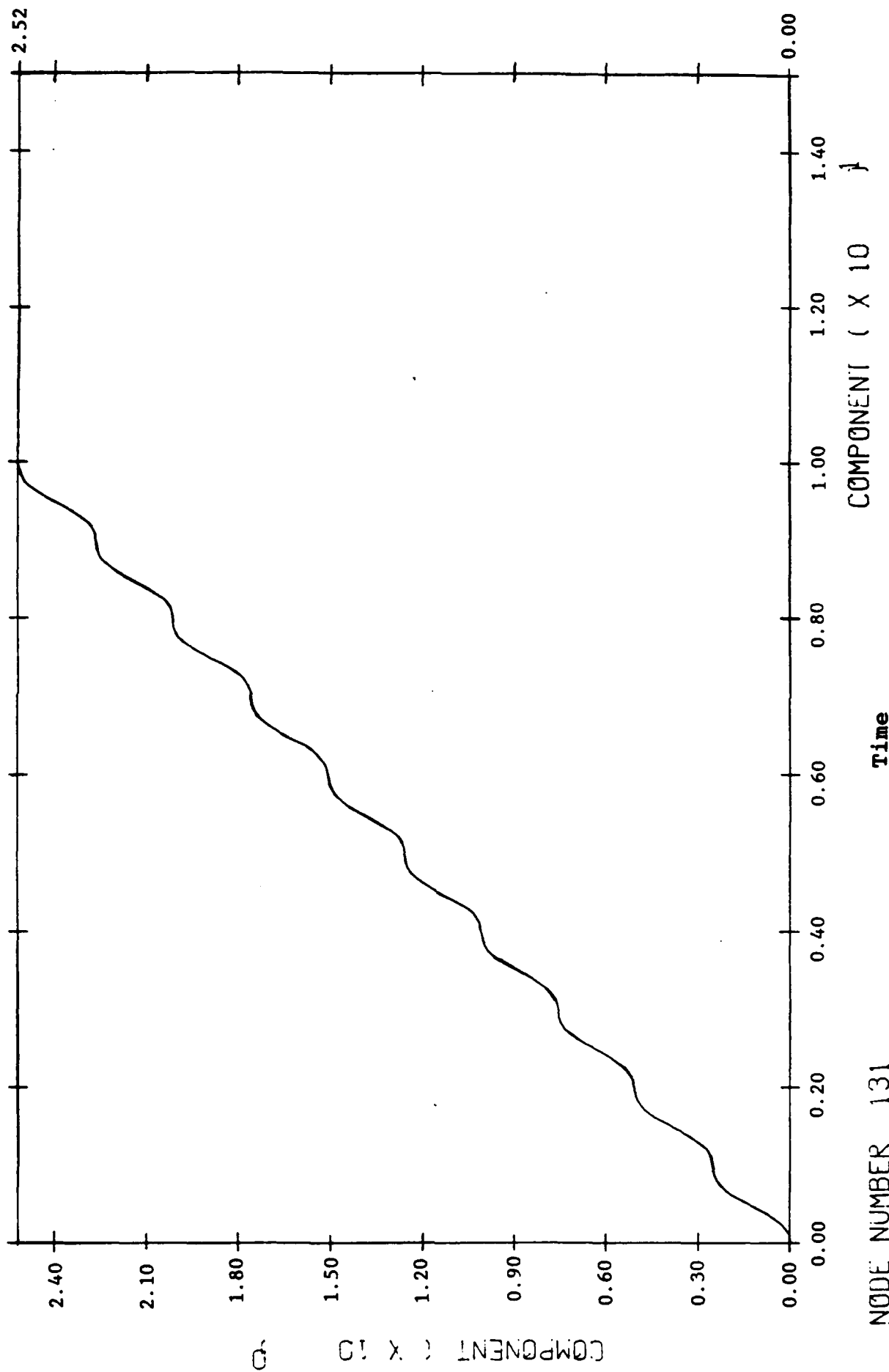


Figure B-9A. Horizontal displacement

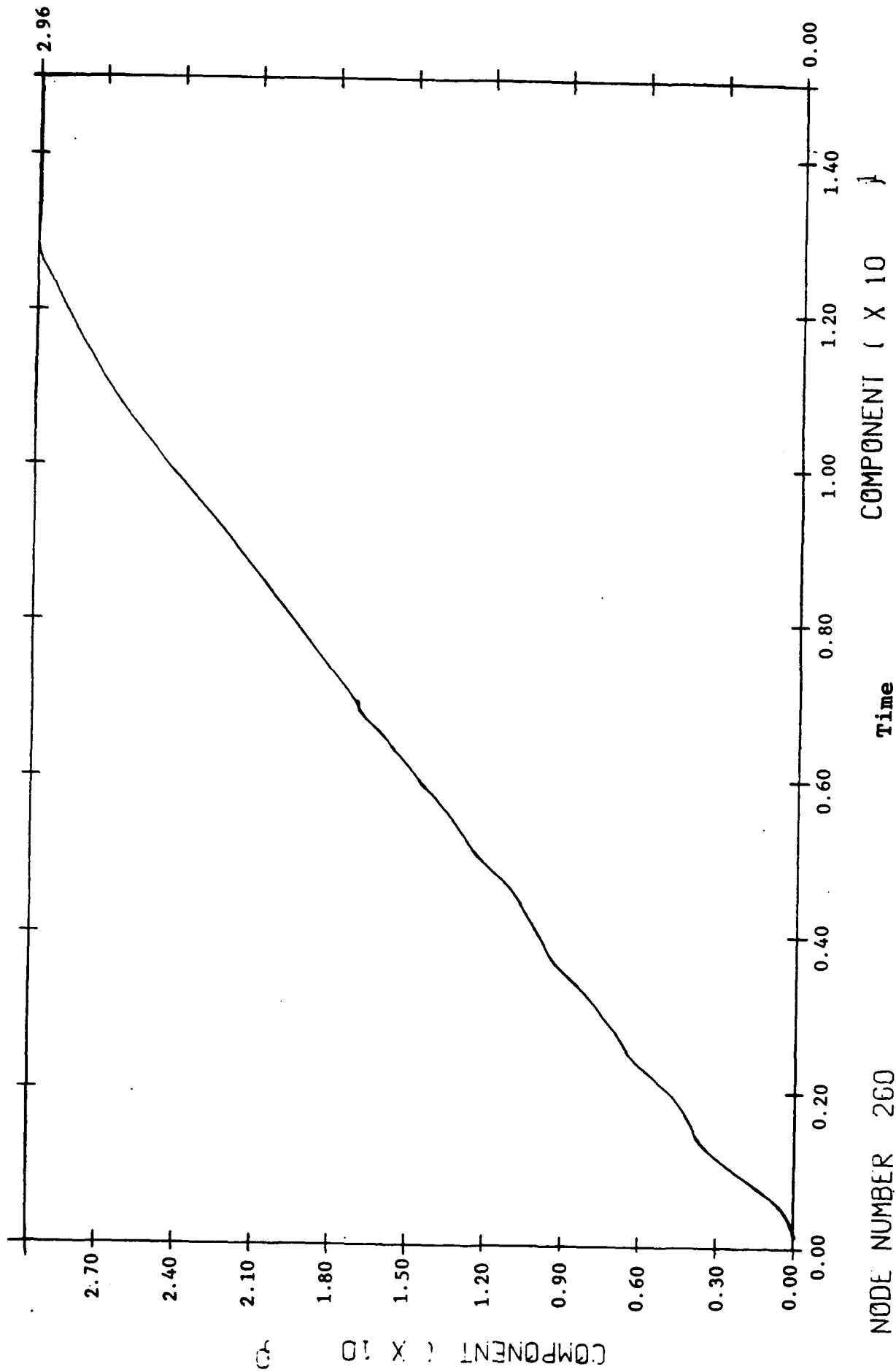
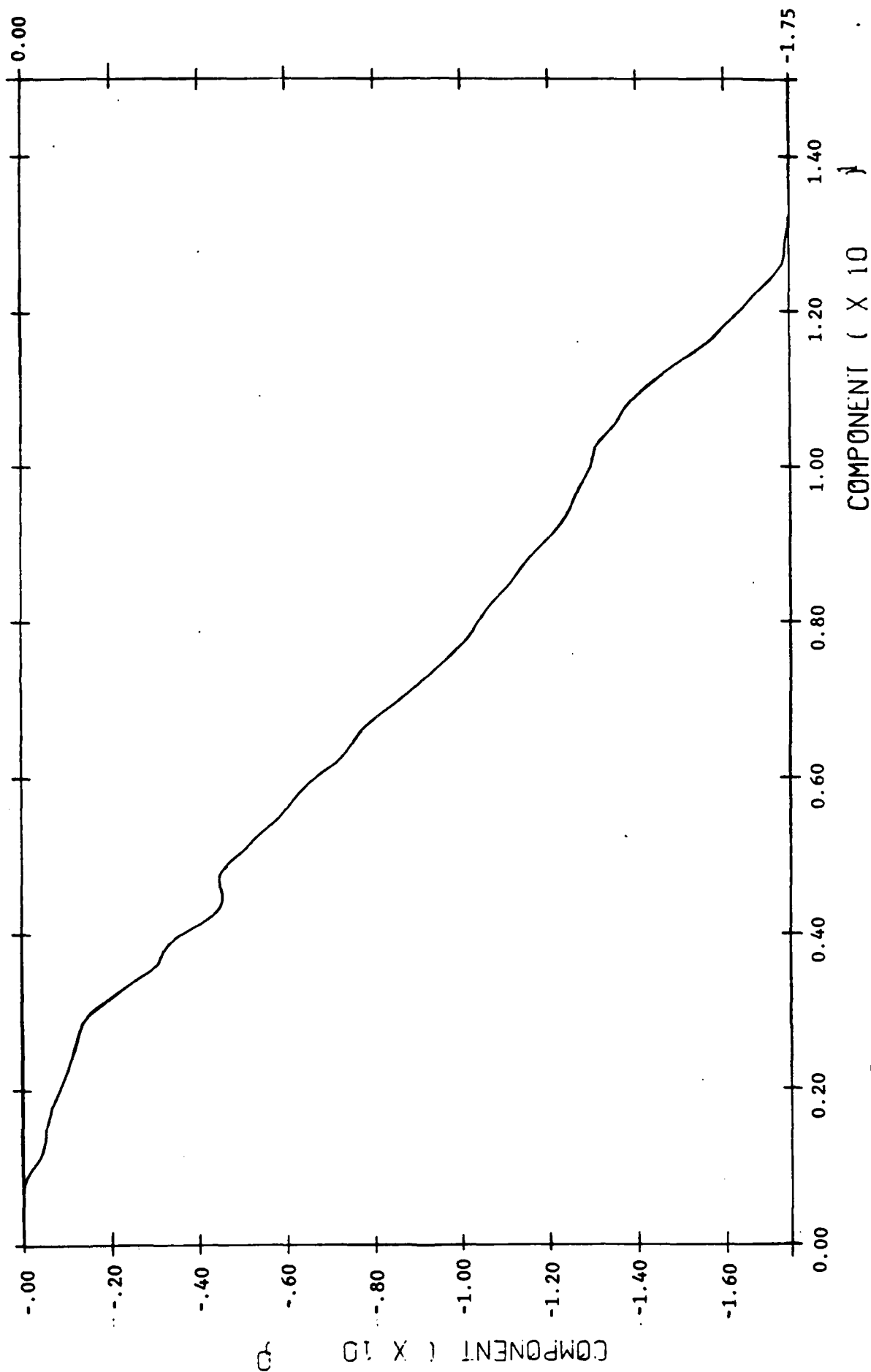


Figure B-9B. Horizontal displacement

CENTRIFUGE ANALYSIS, BRASS FOOTING, LBS/IN. $\alpha = 0.0025 \text{ sec}^2$



NODE NUMBER 200
DISPLACEMENT

Figure B-9C. Vertical displacement

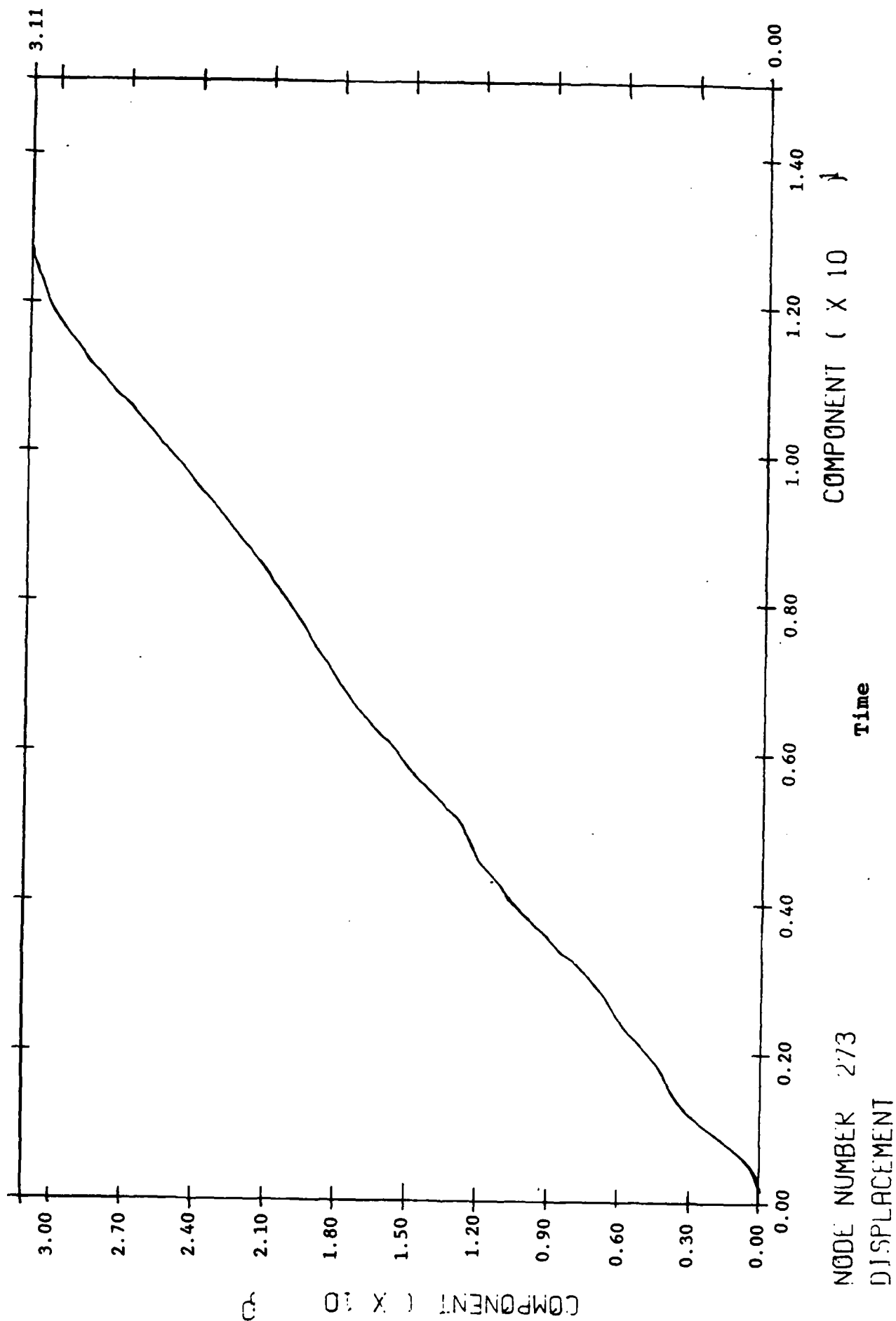
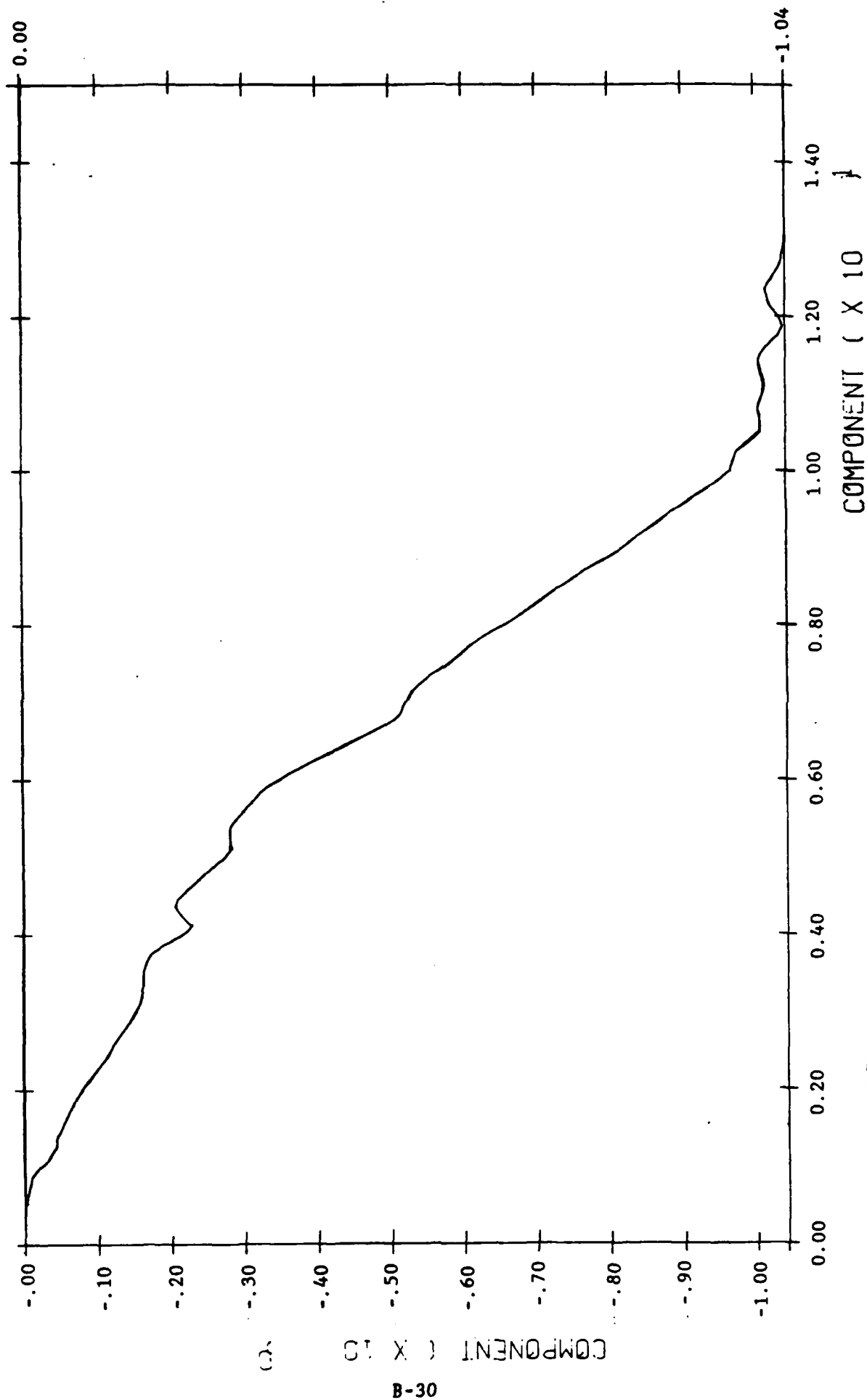


Figure B-9D. Horizontal displacement



NODE NUMBER 273

DISPLACEMENT

Figure B-9E. Vertical displacement

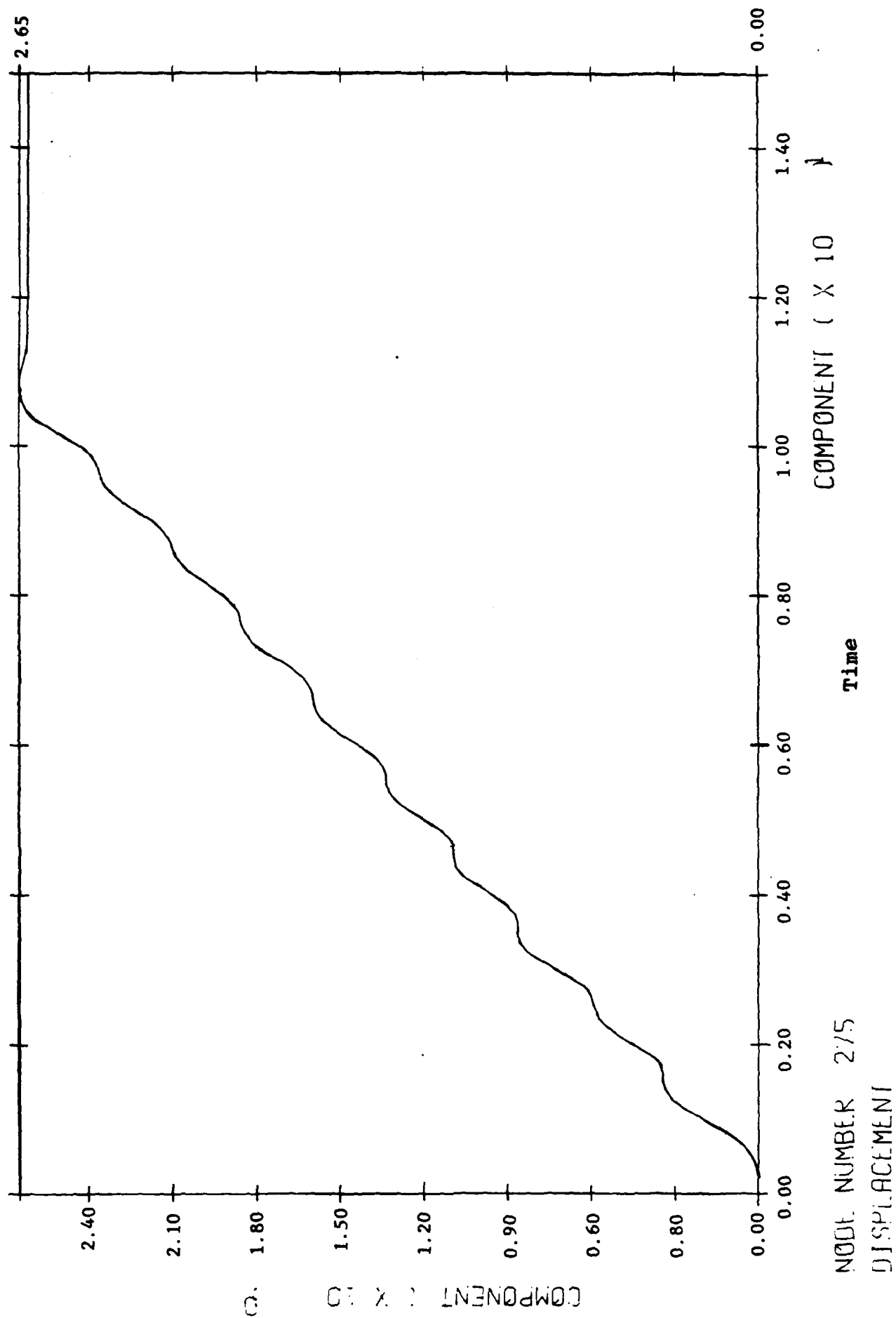
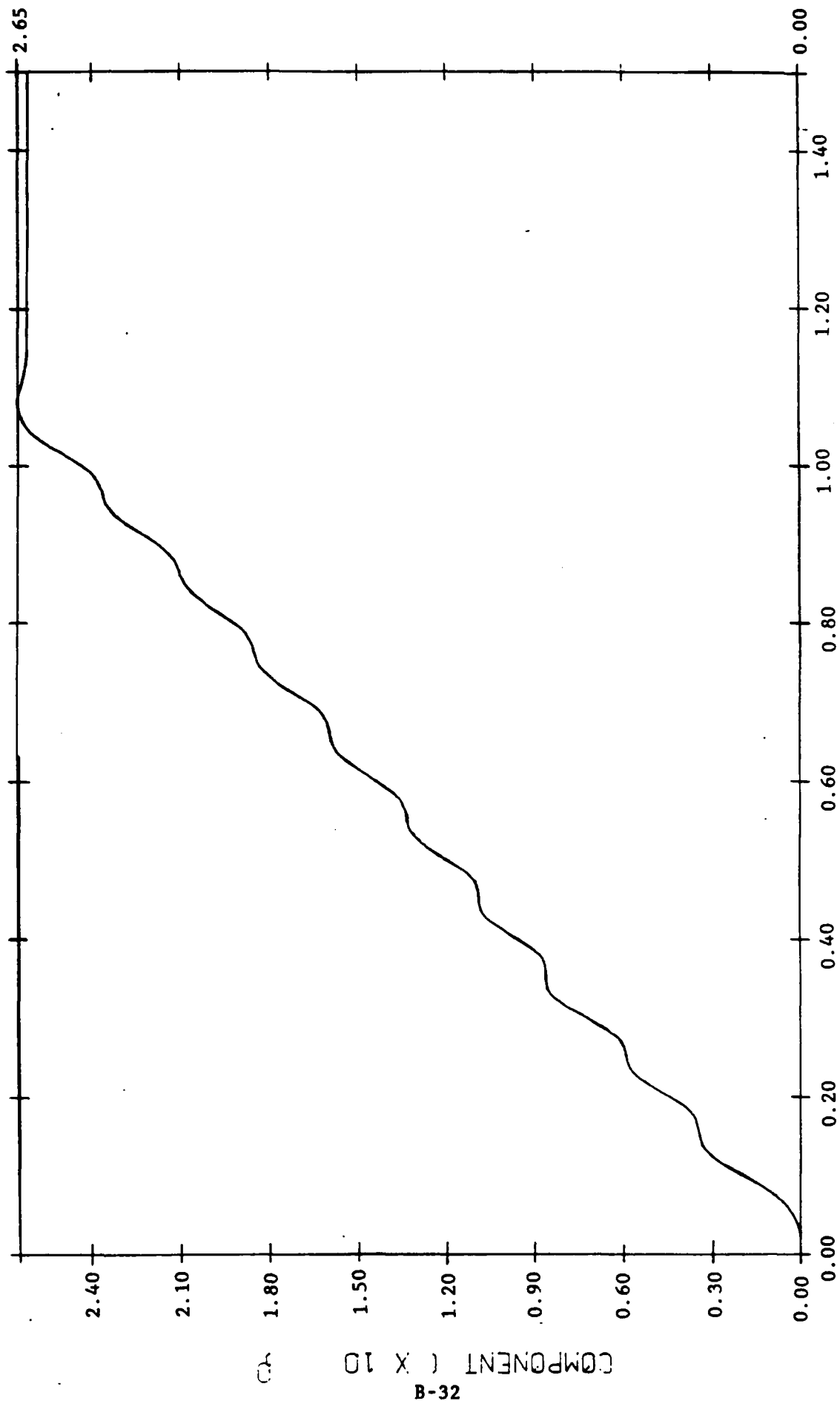


Figure B-9F. Horizontal displacement

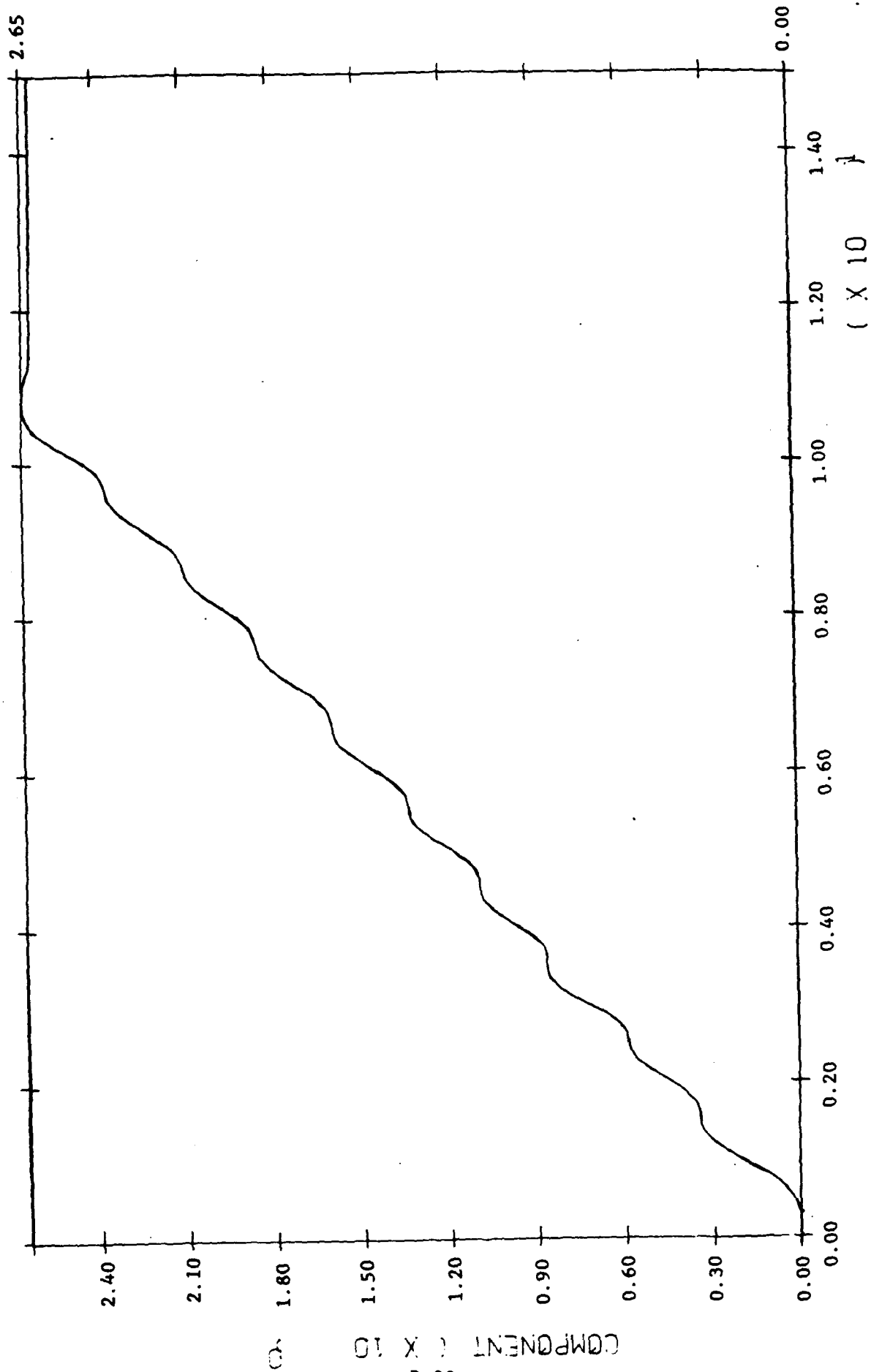


NODE NUMBER 285

DISPLACEMENT

Time

Figure B-9G. Horizontal displacement

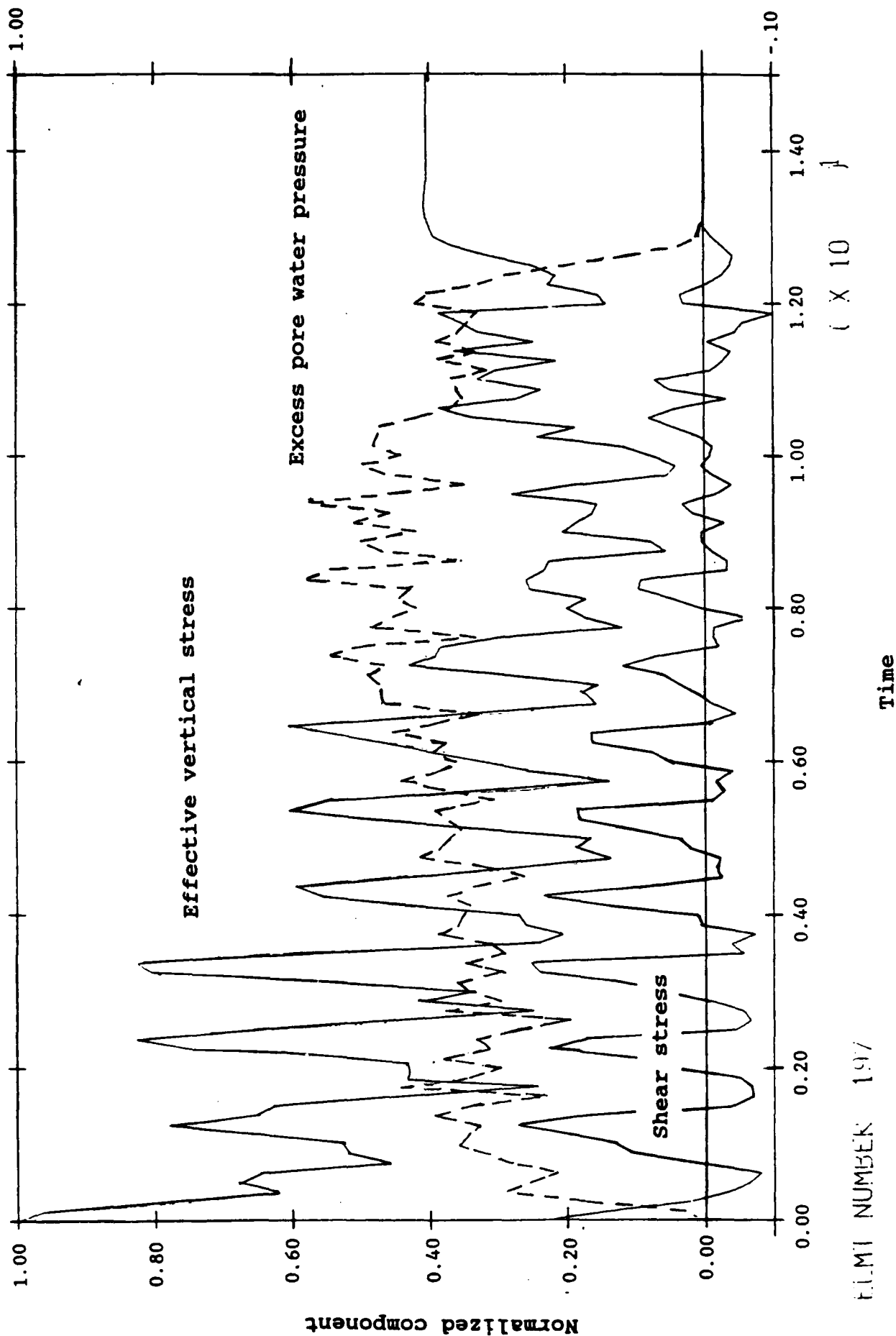


NODE NUMBER 295

DISPLACEMENT

Time

Figure B-9H. Horizontal displacement



FILM NUMBER 197

Figure B-10A. Overall stress behavior of soil

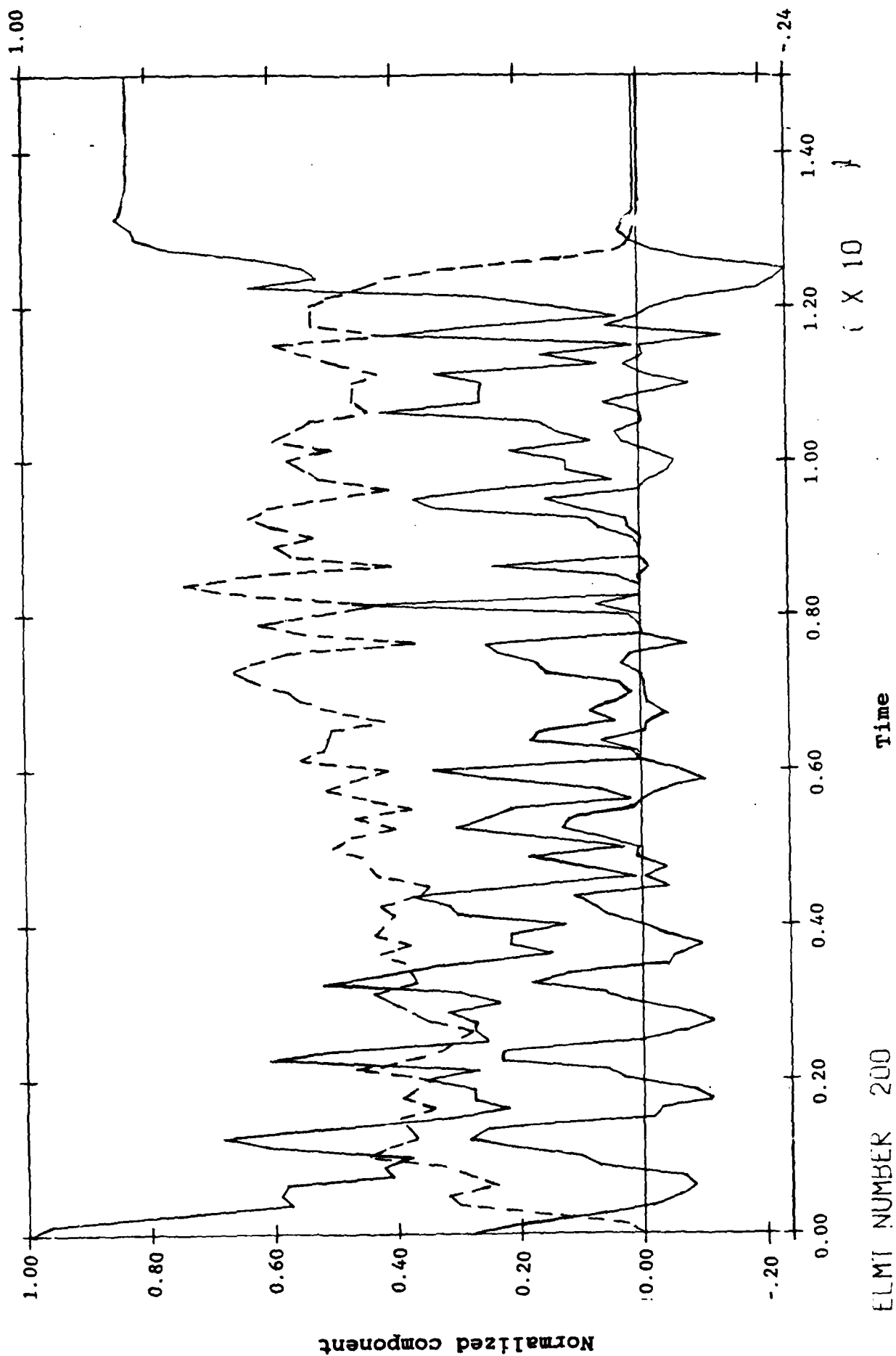


Figure B-10B. Overall stress behavior of soil

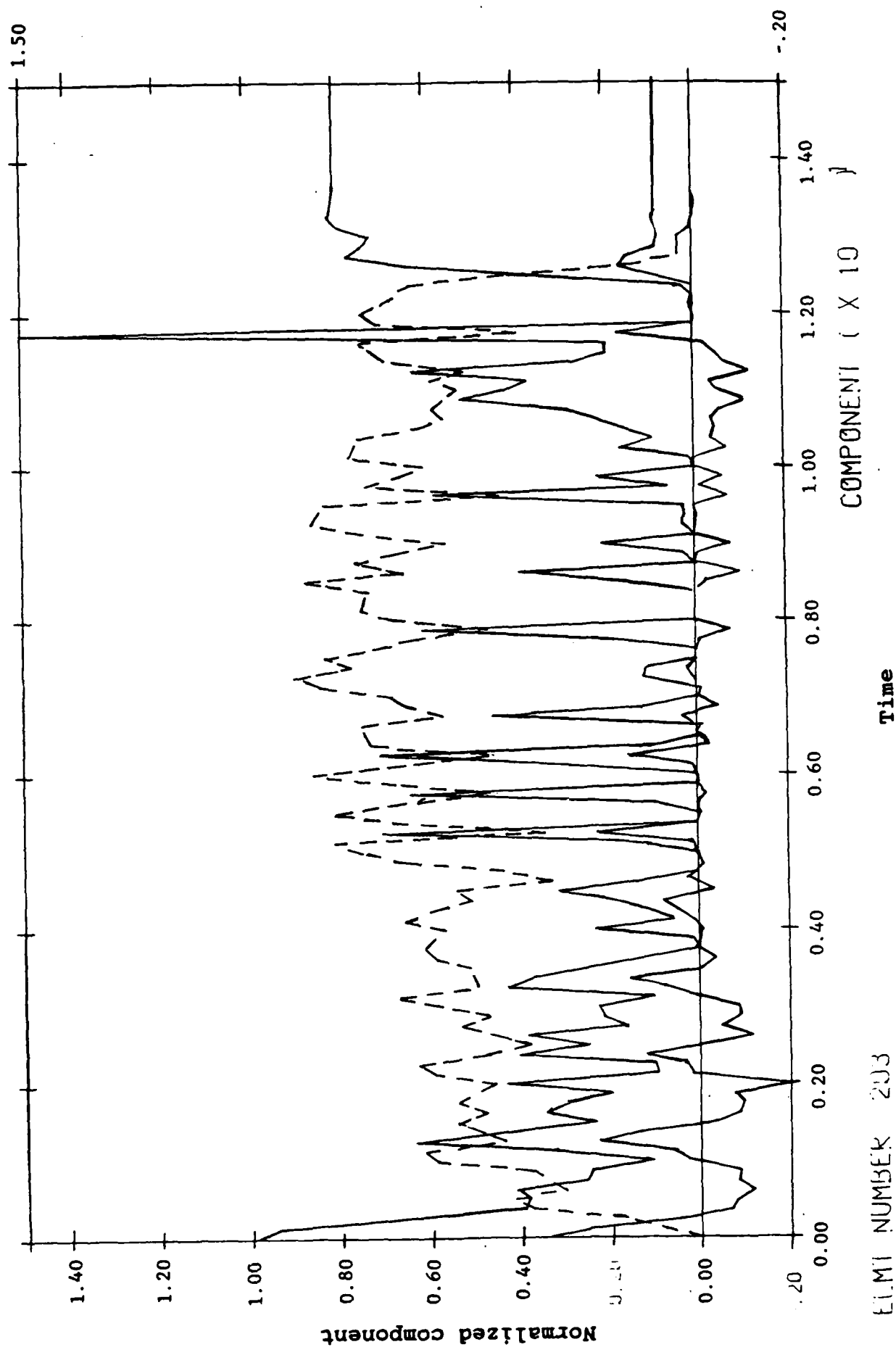


Figure B-10C. Overall stress behavior of soil

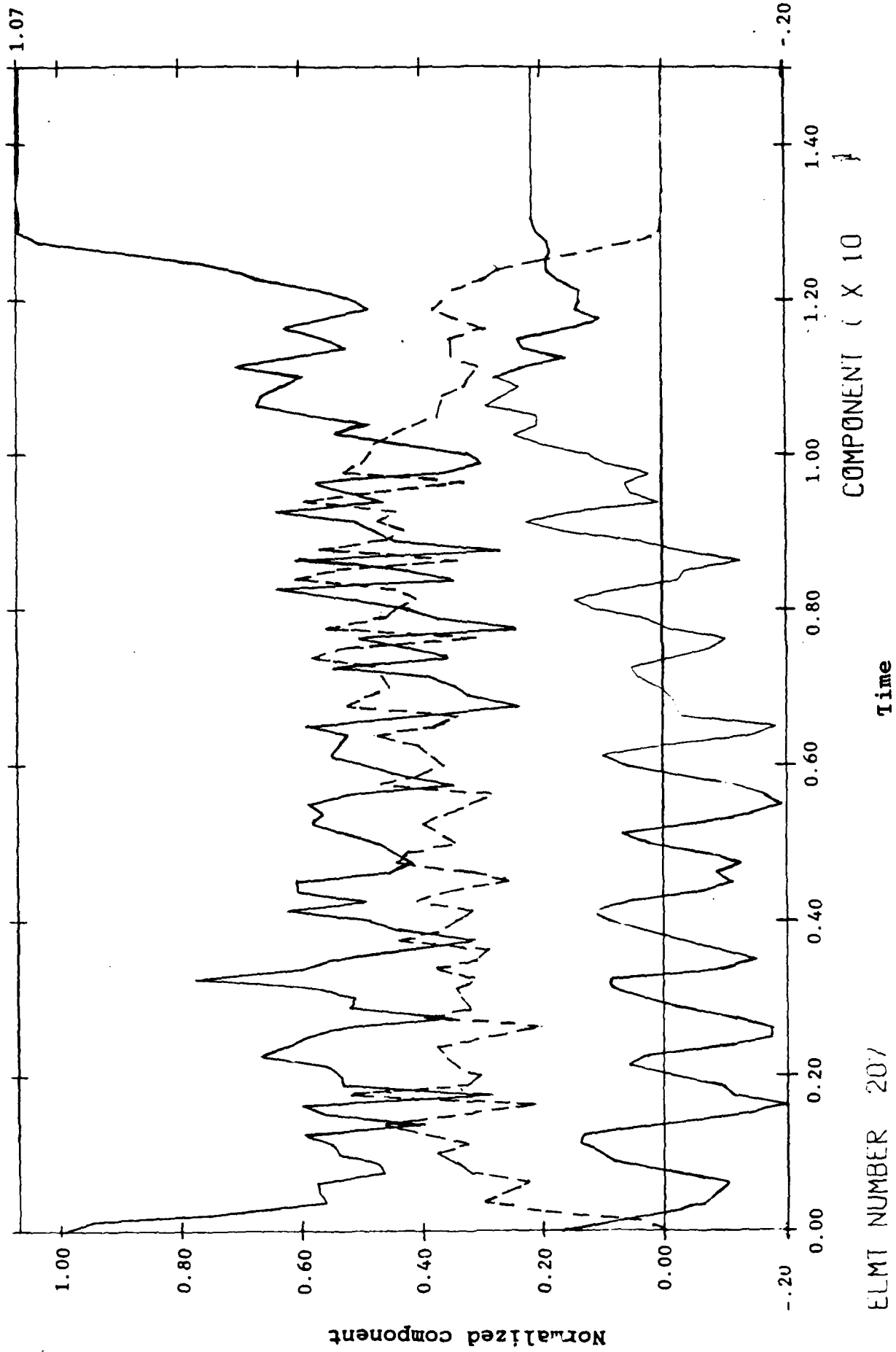


Figure B-10D. Overall stress behavior of soil

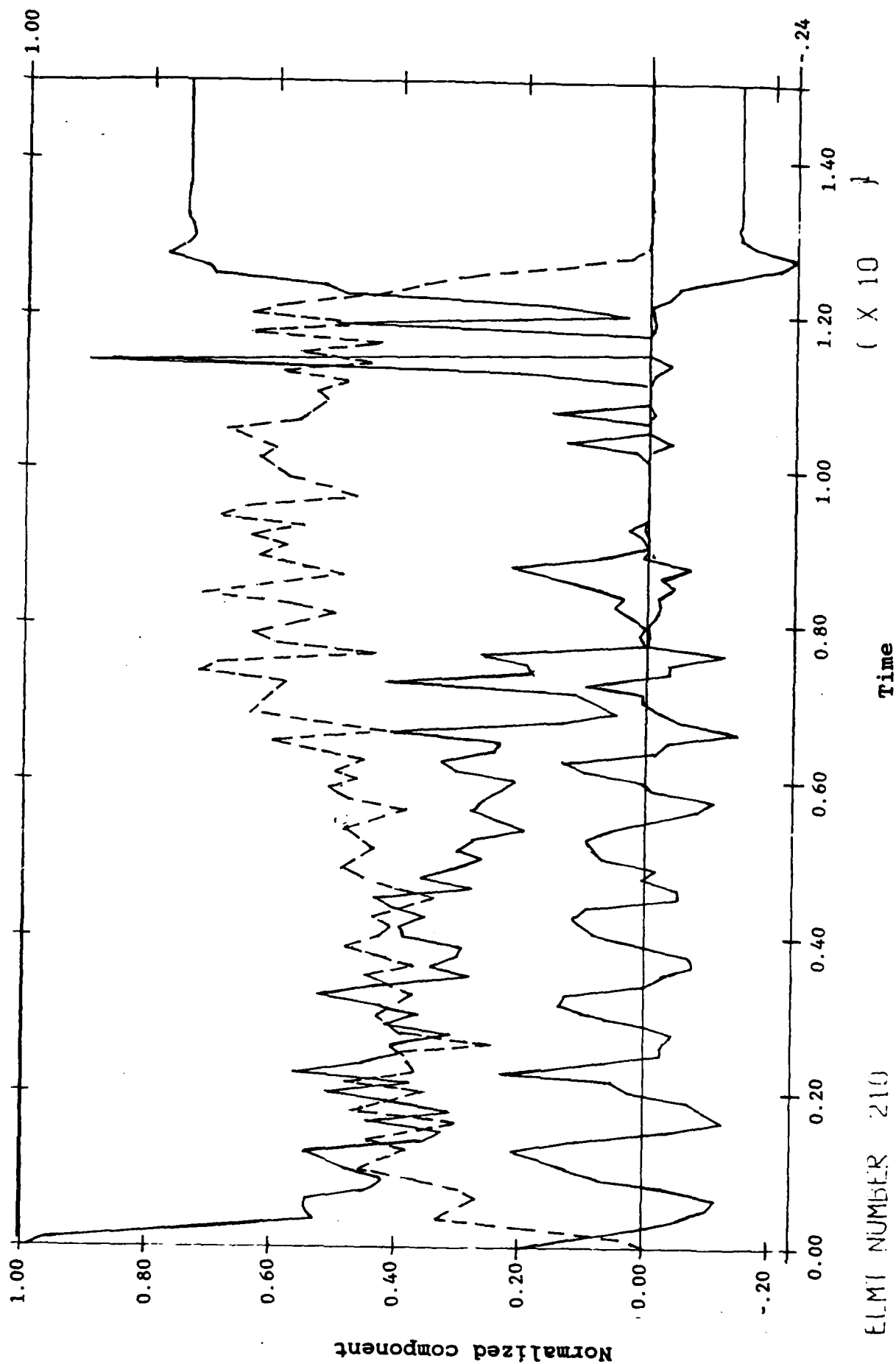
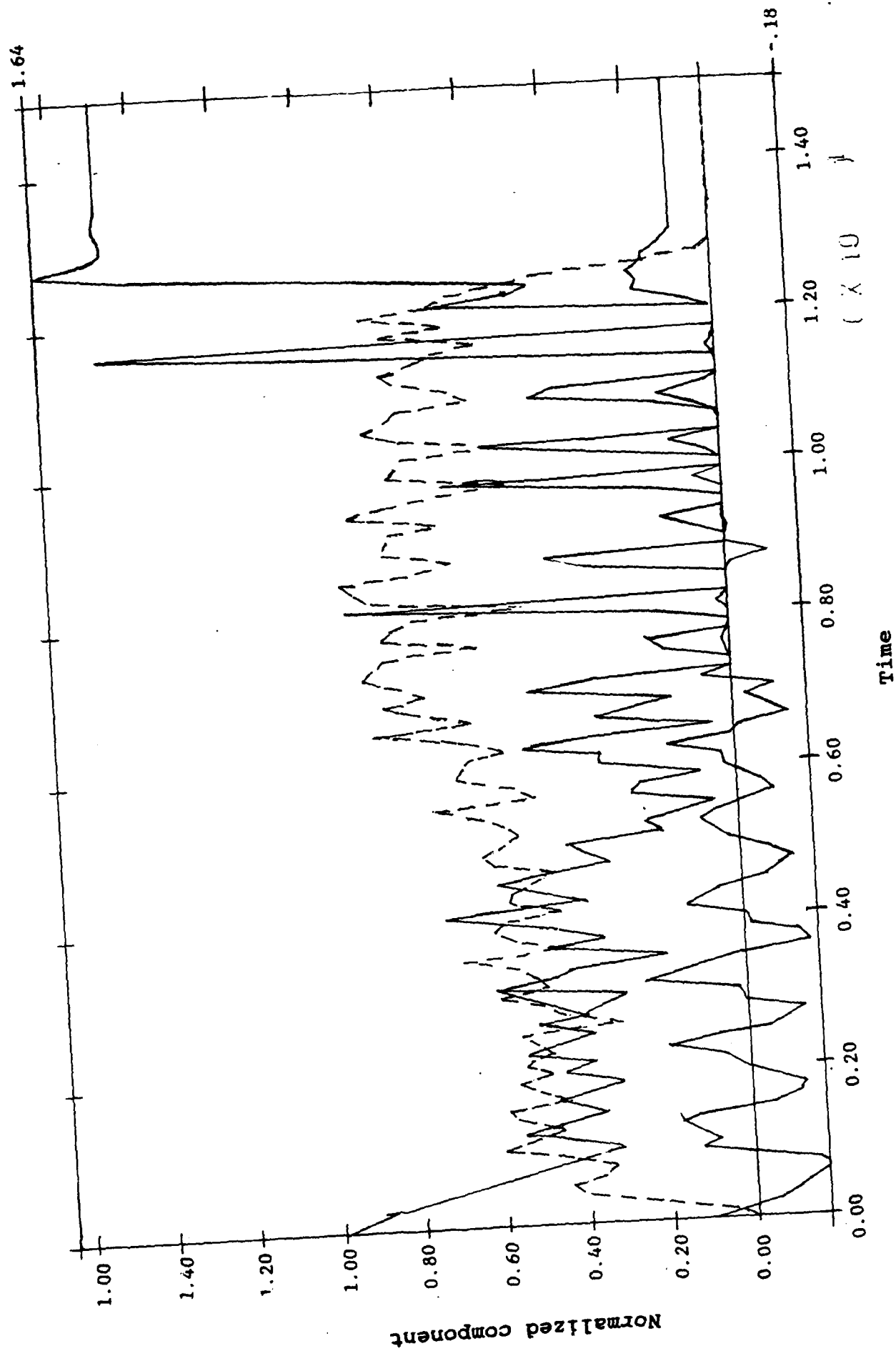


Figure B-10E. Overall stress behavior of soil



FILM NUMBER 2.3

Figure B-10F. Overall stress behavior of soil



Figure B-10G. Overall stress behavior of soil

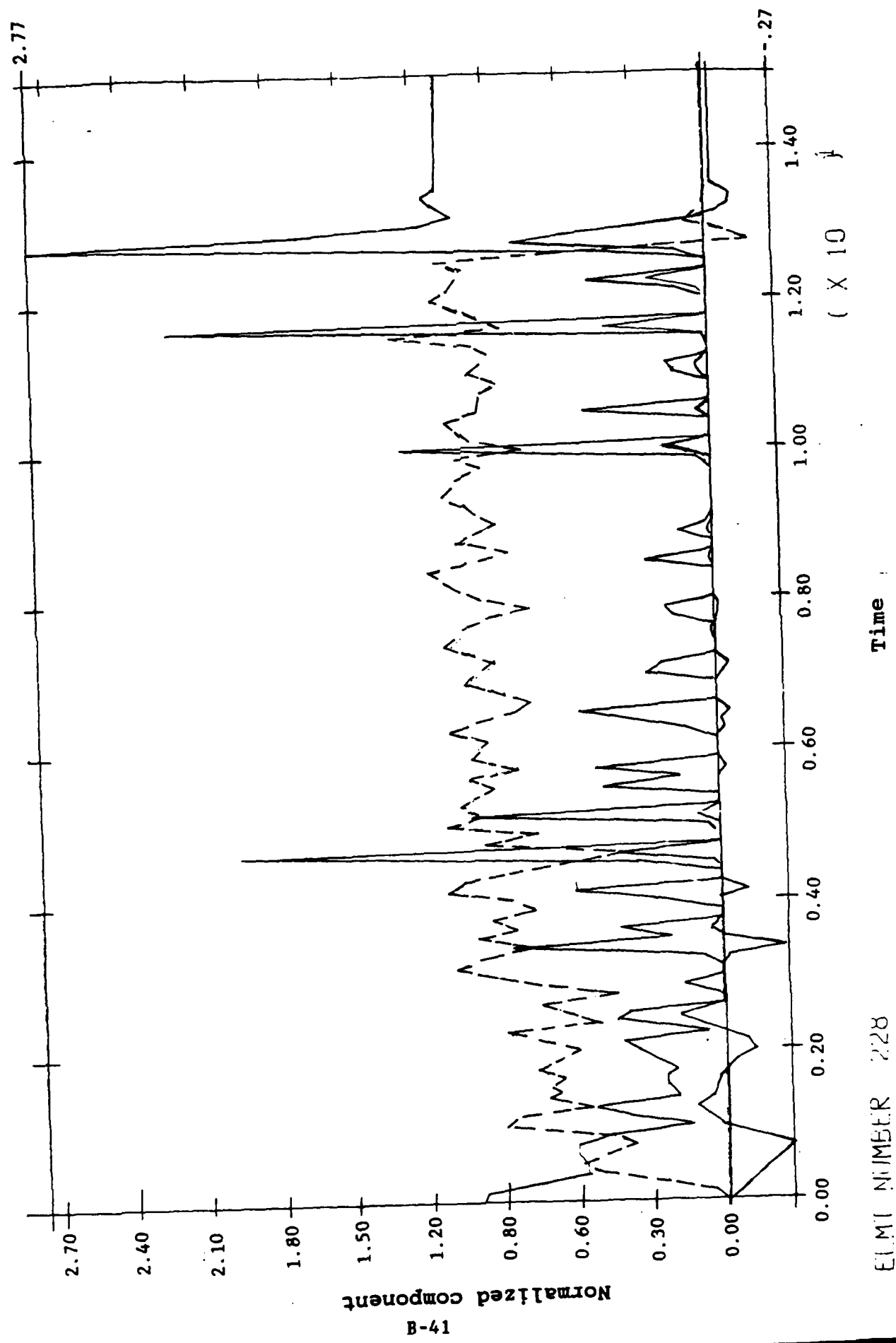


Figure B-10H. Overall stress behavior of soil

UNIVERSITY OF CALIFORNIA, BERKELEY - K - 000000000000

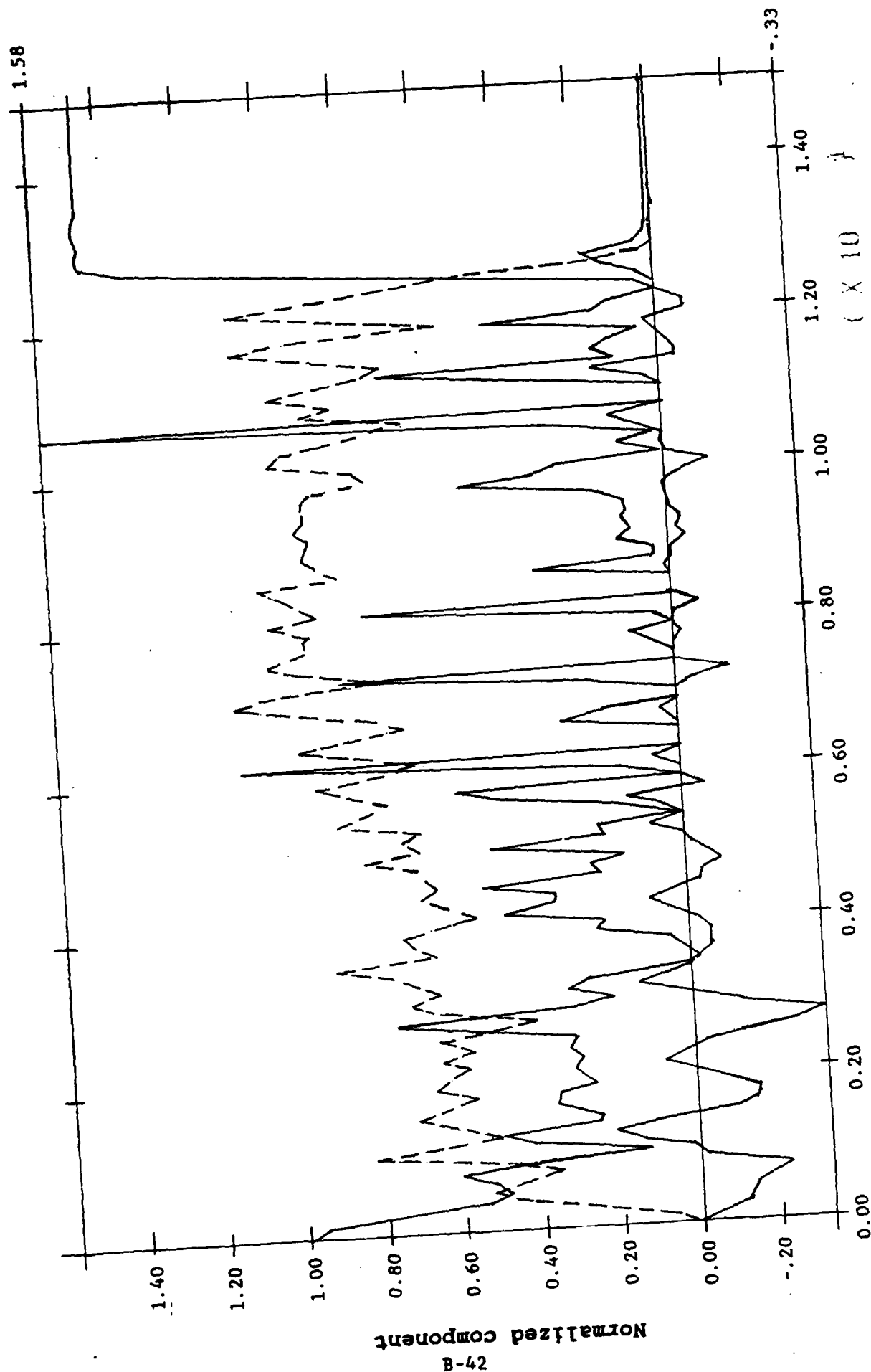


Figure B-101. Overall stress behavior of soil

Appendix C
DRY RETAINING WALL TEST

INTRODUCTION

The test procedures and test results are reported in Reference C-1. Leighton-Buzzard sand was used and was poured dry from a hopper behind the wall. Density was adjusted by altering the rate of flow and height of the drop. The loose backfill case ($D_r = 55$ percent) was selected for this analysis. A reinforced micro-concrete wall model, 175 mm high with a stem thickness of 15 mm was bolted rigidly to the test container with the sand backfill placed behind it. The model was then placed on board a centrifuge and "spun up" to a centrifugal acceleration of 80 gs. The container was then subjected to a sinusoidal input acceleration motion perpendicular to the plane of the wall. The corresponding prototype situation is analyzed hereafter.

Figure C-1 shows the finite element mesh used for the analysis. The backfill is discretized by using 280 elements. The soil parameters are given in Table C-1. The retaining wall is modelled by using 12 linear beam elements with $\rho = 2.76 \times 10^3$ kg/m (mass per unit length), $E = 1.70 \times 10^{10}$ N/m² (Young's modulus), $G = 6.54 \times 10^9$ N/m² (shear modulus), $I = 1.44 \times 10^{-1}$ m⁴ (bending moment of inertia); and $A = 1.20$ m² (cross-section area). The soil and wall subdomains are interfaced by using 14 slide line elements, with $K = 10^{10}$ (penalty parameters). Also, the interface between the wall and the backfill is assumed frictionless.

The bottom boundary is assumed rigid and the side boundary smooth in the vertical direction.

The computed wall crest deflection under gravity load is 4.55 cm, which compares favorably with the measured test value (4.7 cm).

In order to simulate the dynamic test conditions, the same sinusoidal horizontal acceleration was imposed on the bottom boundary nodes and the soil right side boundary, with a maximum acceleration = 0.20 g and a frequency of 0.75 Hz for 16 seconds (12 cycles).

Figure C-2 shows the computed horizontal acceleration time histories at the bottom (Figure C-2(a)) and at the top (Figure C-2(b)) of the wall. Note that as the result of the interaction with the nonlinear soil mass, the computed response at the top of the wall is amplified and exhibits superharmonics (typical of nonlinear systems). Figure C-3(a) shows the computed horizontal displacement at the top of the wall. The amplitude of alternating crest deflection is 3.725 cm which compares most favorably with the recorded amplitude ($0.50 \times 80 = 4$ cm) in the test (Ref C-1).

Figure C-3(b) shows the computed vertical displacement of the top soil element at the interface with the wall. Although sinusoidal in shape, this motion occurs with a much longer period (about 12.5 seconds) than the input horizontal motion (1.33 seconds).

Figure C-4 shows the computed vertical, horizontal, and shear stress time histories, normalized by dividing them by the initial vertical stress, close to the base of the wall (Figure C-4(a), element A in Figure C-1) and at midheight (Figure C-4(b), element B in Figure C-1). At midheight, initially, an active state of stress prevails and $K = 0.40$. As a result of the stress concentration at the corner, initially, $K = 0.675$ at the bottom, closer to a passive state. As a result of the shaking, the lateral stress fluctuates and exhibits a net decrease at the bottom of the wall! ≈ 0.35 after 12 cycles, but stays about the same at midheight.

MODELING ASSUMPTIONS

In general, retaining (contact) wall analysis with a cohesionless (no tension) soil model and a "flexible" wall can be difficult. The problems arise due to the wall yielding outward and the soil, following the wall, and failing (going into tension). Convergence may not be achieved due to time step size, or material stiffness (this is in respect to the contact interface). Solutions to this problem and combinations of the solutions are as follows:

1. Shorten time steps. The smaller step will allow for more iterations over the prior range of wall deformation, and ease the convergence problems.

2. Adjust material stiffness in each layer of element to approximate the actual value in a particular layer. In the general analysis, one stiffness is input and is adjusted by the computed confining stress (through the reference mean stress during gravity initialization) to reflect the material stiffness in any layer. This adjustment when combined with the contact (penalty) problem may cause divergence in the solution. Setting the material stiffness in each layer to actual values will reduce the computational burden.

3. Move the structure "slightly" into the soil body. This forces the contact element to have an "initial displacement" and relieves the zero or tensile stresses in the soil elements. Placement of the structure (wall) inside the soil by the amount of one over the contact element stiffness (one/penalty parameter) is generally sufficient. This then applies a small horizontal force on the soil in the initial iteration. Fluid horizontal degrees of freedom at the soil wall interface must, at this time, be fixed to achieve restraint. The contact elements do not restrain the fluid from horizontal movement, or transmit fluid force. This presents an additional problem, in that, as the back fill begins to liquefy, the wall, permeable or impermeable, does not "feel" the fluid forces, with the exception of momentum transferred through the solid phase. This may or may not be a significant problem but does require investigation, particularly in the area of reflected waves in the fluid.

The free field vertical boundary for the retaining wall problem may be approached from several directions depending on the type of analysis (static or dynamic), or on the boundary conditions present in the test (rigid container walls for model or centrifuge model tests). Several options are described below:

1. Figure C-5(a) shows a retaining wall model with the free field (continuum) modeled as a stable slope. This type of cross section is used in centrifuge model tests by various researchers (Schofield, Scott, Steedman). The static analysis obviously presents little difficulty in this system. The dynamic can prove very simple as well. The free surface should provide very efficient "damping" due to the very low shear modulus in the pressure dependent soil modulus.

2. Figure C-5(b) shows essentially the same soil-structure model, without the free field slope. In this case the free field vertical boundary is controlled by a K_0 pressure loading. This configuration will constrain soil movement in the horizontal direction in the same manner as the stable slope. It carries the advantages of reducing the number of elements in the analysis as well as being applicable to saturated soil problems. The obvious disadvantage is that the boundary may show tendencies to reflect waves in dynamic analysis. This factor may be compensated with the application of damping elements or extension of the horizontal length of the model.

Note the "stable slope" model in Figure C-5(a) can be adapted to saturated dynamic problems as well, but with significant effort necessary to establish the correct pressure loading on the slope for internal hydro static equilibrium.

3. Figure C-5(c) shows the same configuration for the soil-wall model. The "free field" vertical boundary is restrained by a boundary (contact) element. The boundary element differs from the contact element in the "spring" stiffness value. The element will allow deflection to the right and will return the force as specified by the displacement. The stiffness for each element should be derived in a manner which would account for the total elastic stiffness of the element being bounded, such as in the following:

$$K_1 = \frac{2H_1(1+u)}{6} \left(G_1 + 2G_2 \right)$$

where K_1 = Boundary element stiffness at node 1 fig X 6

H_1 = Height of element 1

G_1 = Stiffness of element 1 at node 1

G_2 = Stiffness of element 1 at node 2

G_1 and G_2 may be computed from:

$$G_1 = G_0 \left(\frac{p}{p_1} \right)^N$$

which is defined as the reference mean stress in the DYNAFLOW manual. The moduli relationship is nonlinear with depth, but the approximation of linearity over the range of one element should be adequate. In addition, boundary elements which connect to more than one element should have a stiffness which is the sum of the two adjoining stiffness, i.e., $K_1 = E G_2$ from element 1 & G_1 element reflected waves from both the solid and fluid phases may again pose a problem, but increasing the mesh length and/or applying damping element should improve the behavior in the free field.

PROBLEMS AND FIXES

The retaining wall problem described at the beginning of this appendix encountered many of the difficulties described above. Examination of this data set shows each of the fixes discussed. One major difficulty arose when comparing computed and measured displacements. The actual wall was contrasted of micro-concrete, and would therefore yield in an elasto-plastic manner. Program DYNAFLOW, at that time, could consider only elastic beam elements. This made computation of the plastic crest deflections impossible. The approximate elastic displacements, due to gravity, and the "cyclic" crest deflections were computed with good accuracy. Program DYNAFLOW now incorporates an elasto-plastic beam element. Reanalysis with these elements would provide an interesting analysis and test of the nonlinear element.

REFERENCE

C-1. M.D. Bolton and R.S. Steedman. "Centrifugal testing of micro-concrete retaining walls subjected to base shaking," in Proceedings of Soil Dynamics and Earthquake Engineering Conference, Southampton, U.K., 1982, pp 311-329.

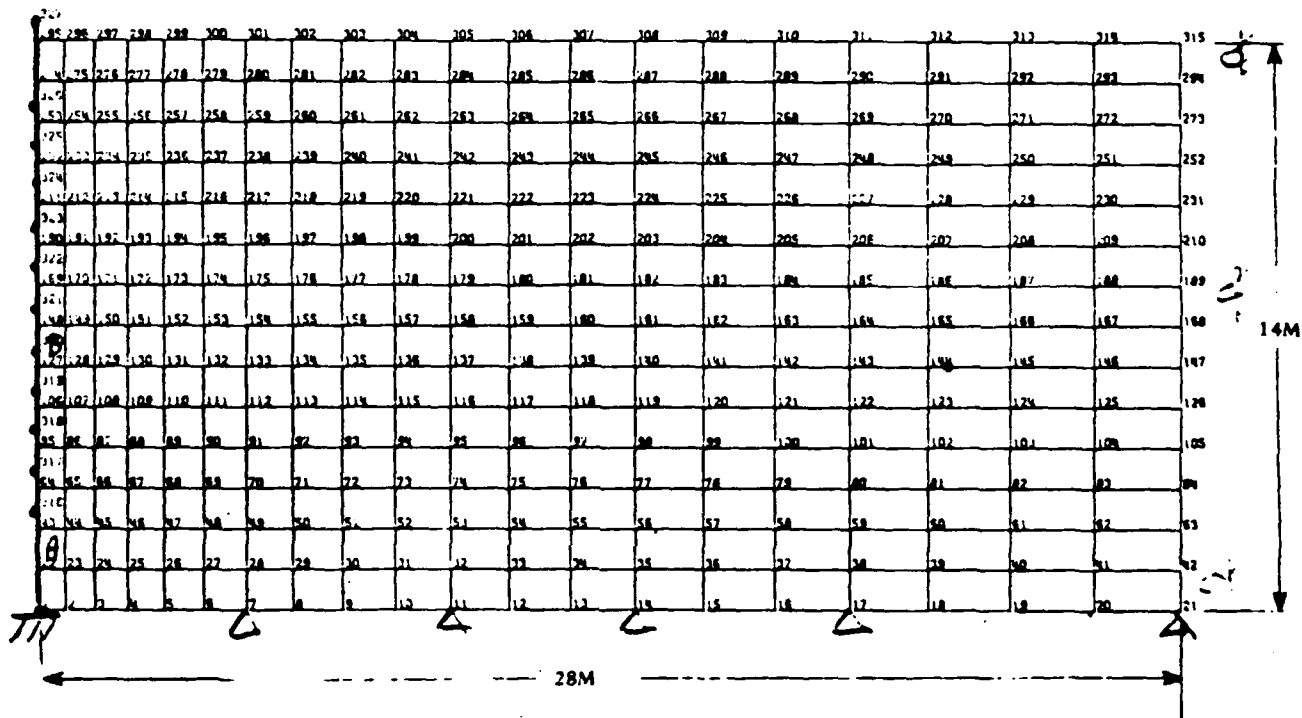


Figure C-1. Undeformed mesh for retaining wall

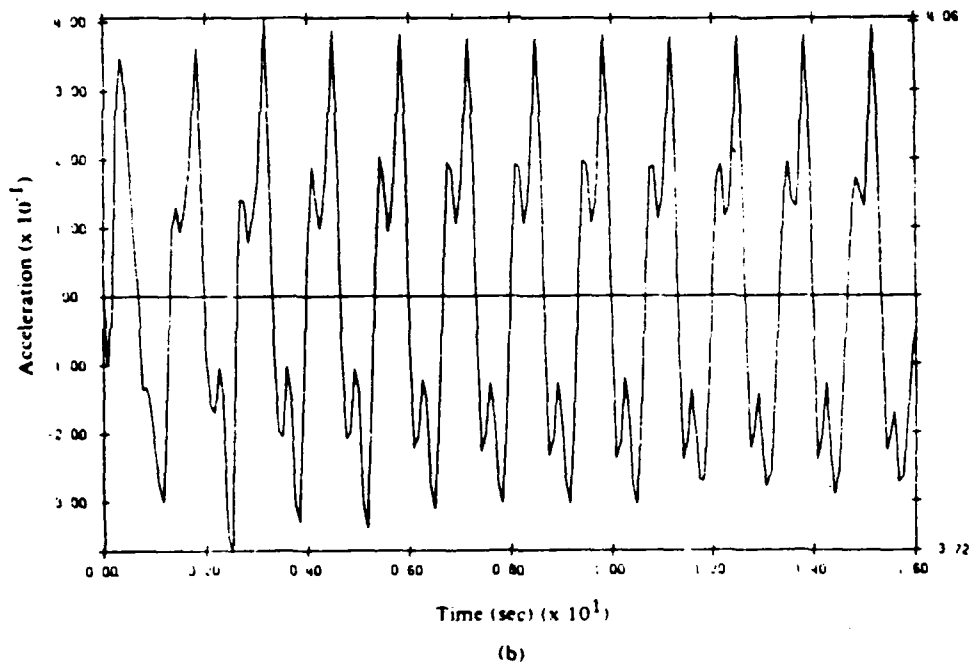
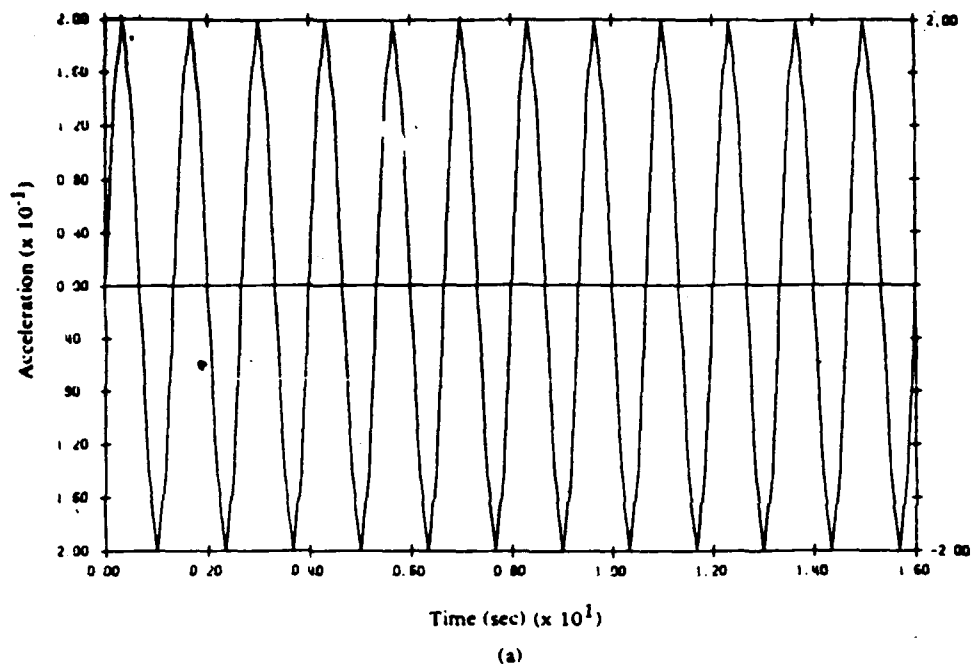


Figure C-2. Input horizontal accelerations and resulting accelerations at top of retaining wall

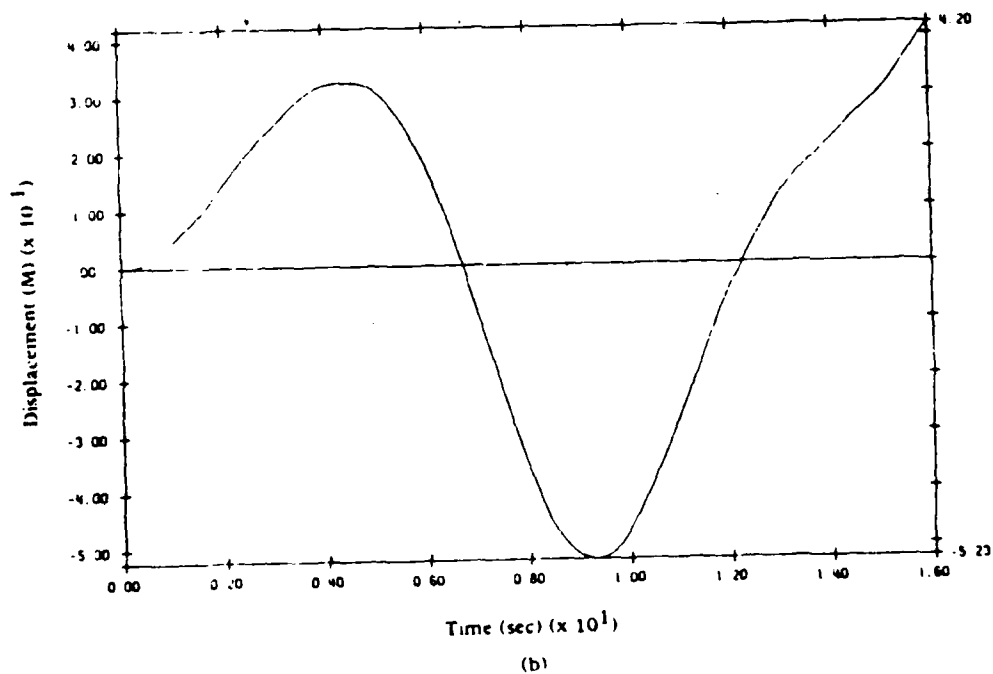
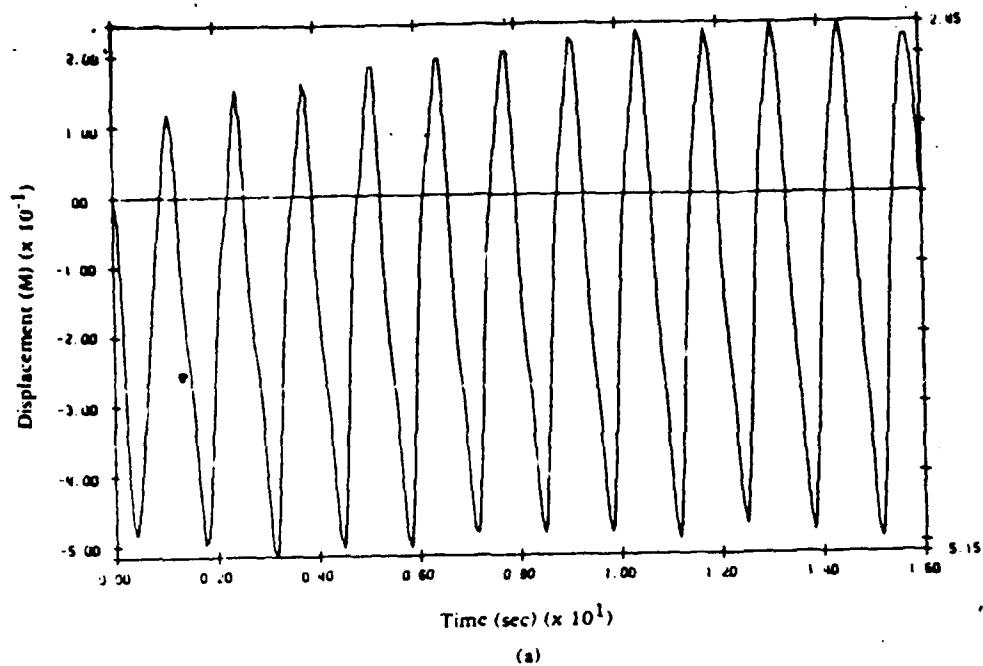


Figure C-3. Horizontal displacements at top of retaining wall and vertical motions in soil-structure contact

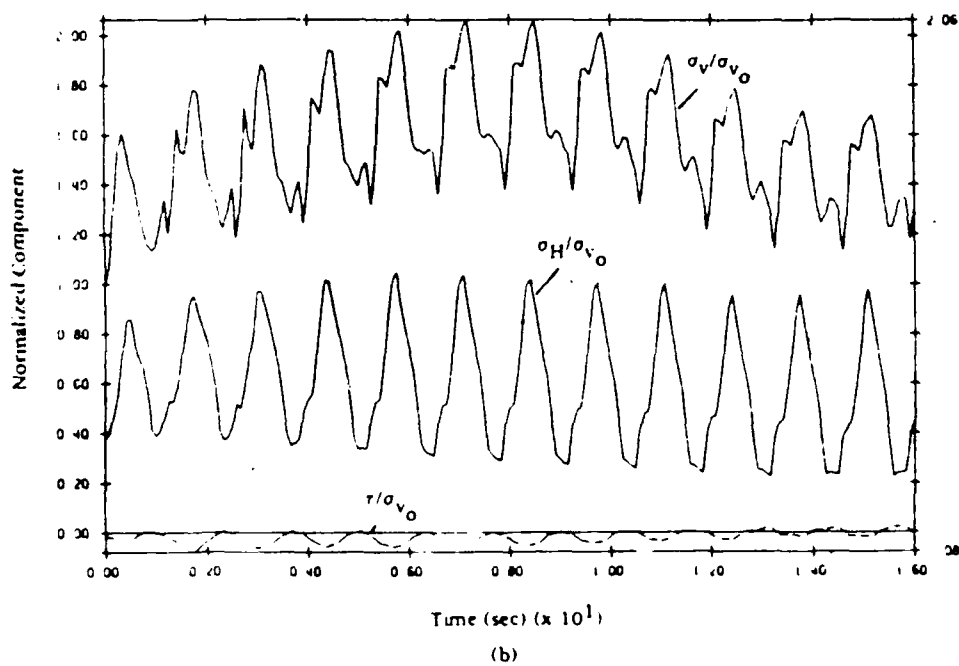
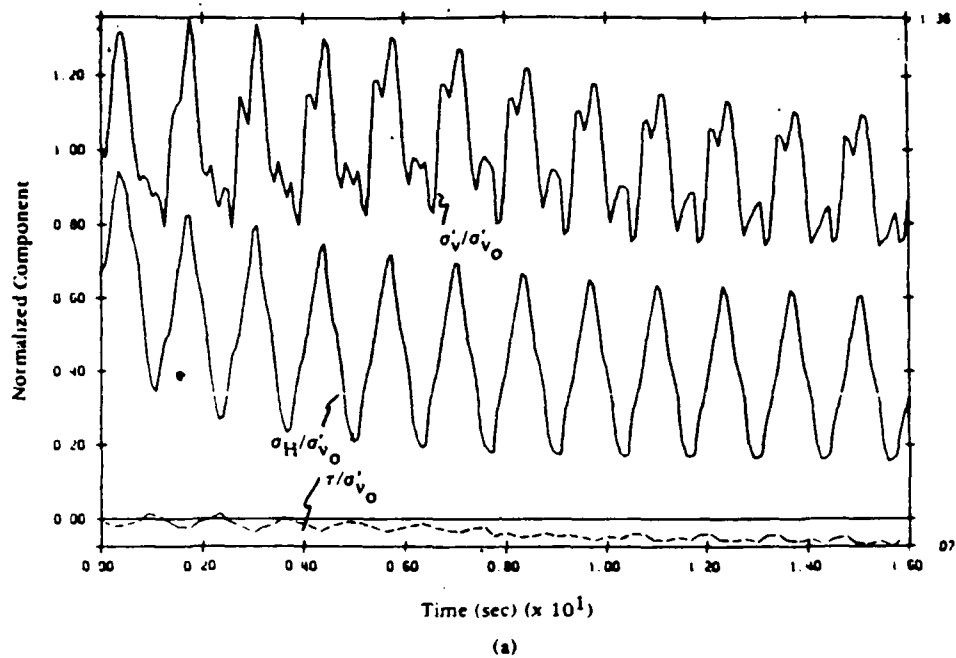


Figure C-4. Normalized vertical, horizontal, and shear stresses

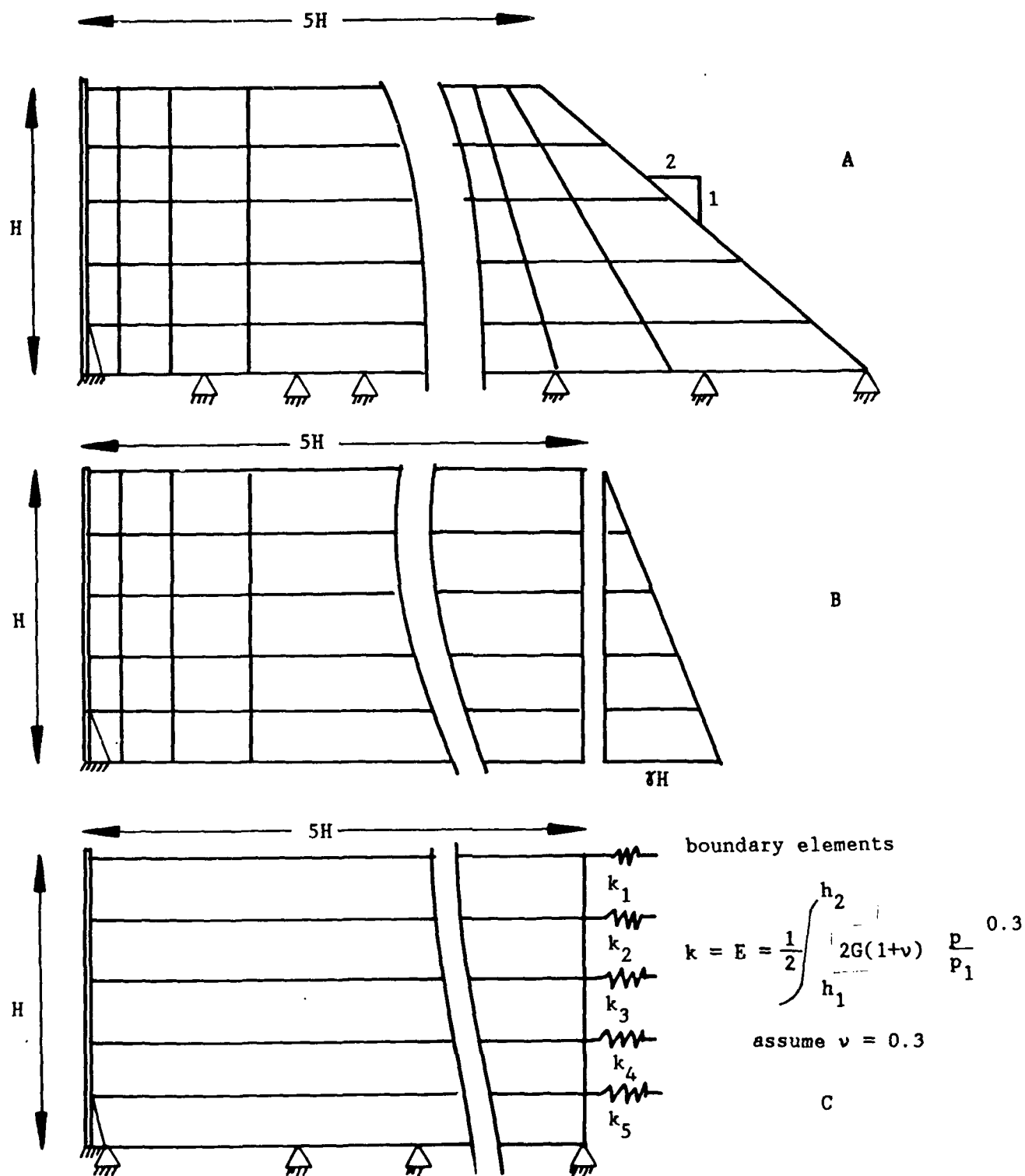


Figure C-5. Retaining wall model

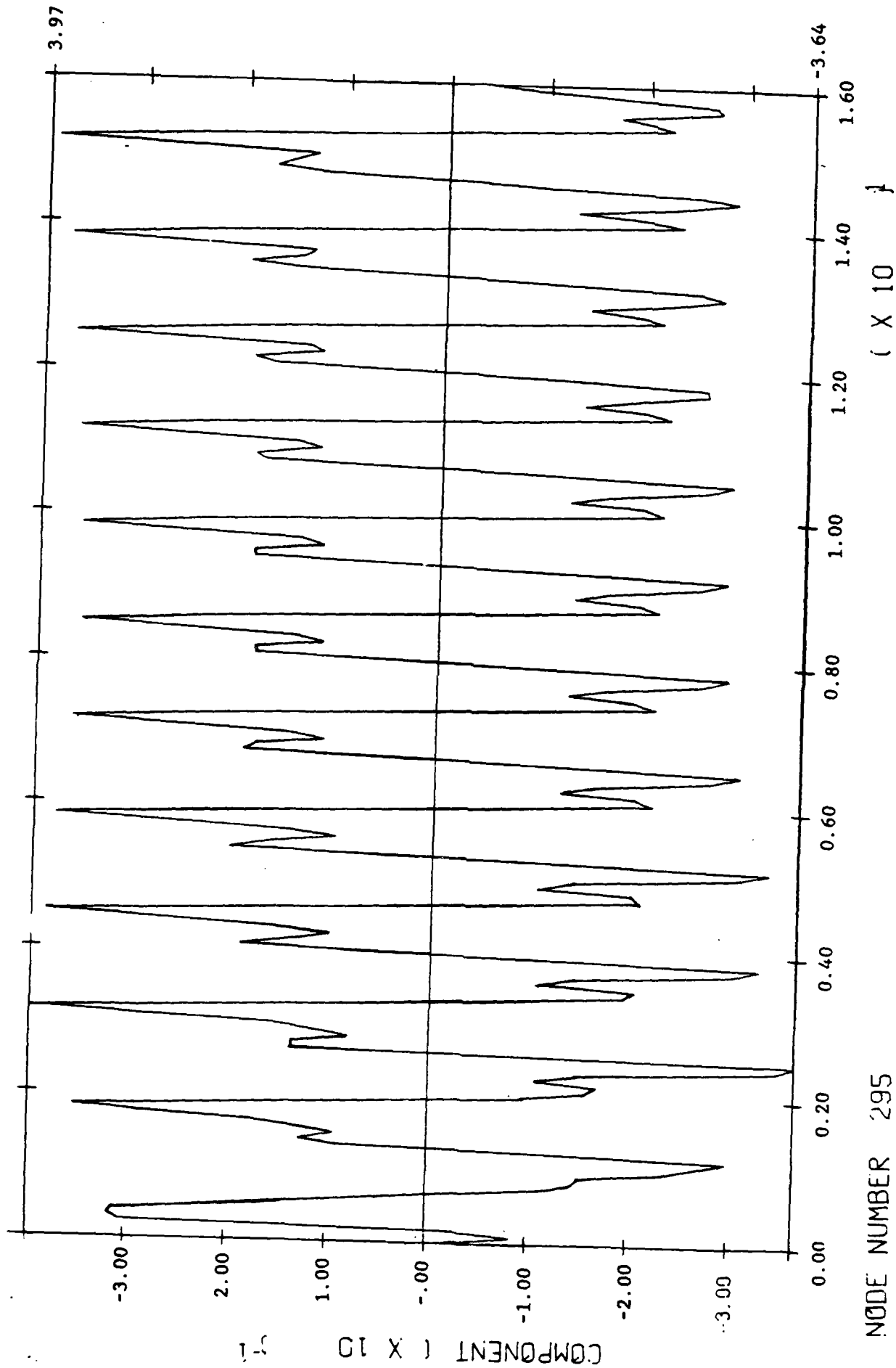
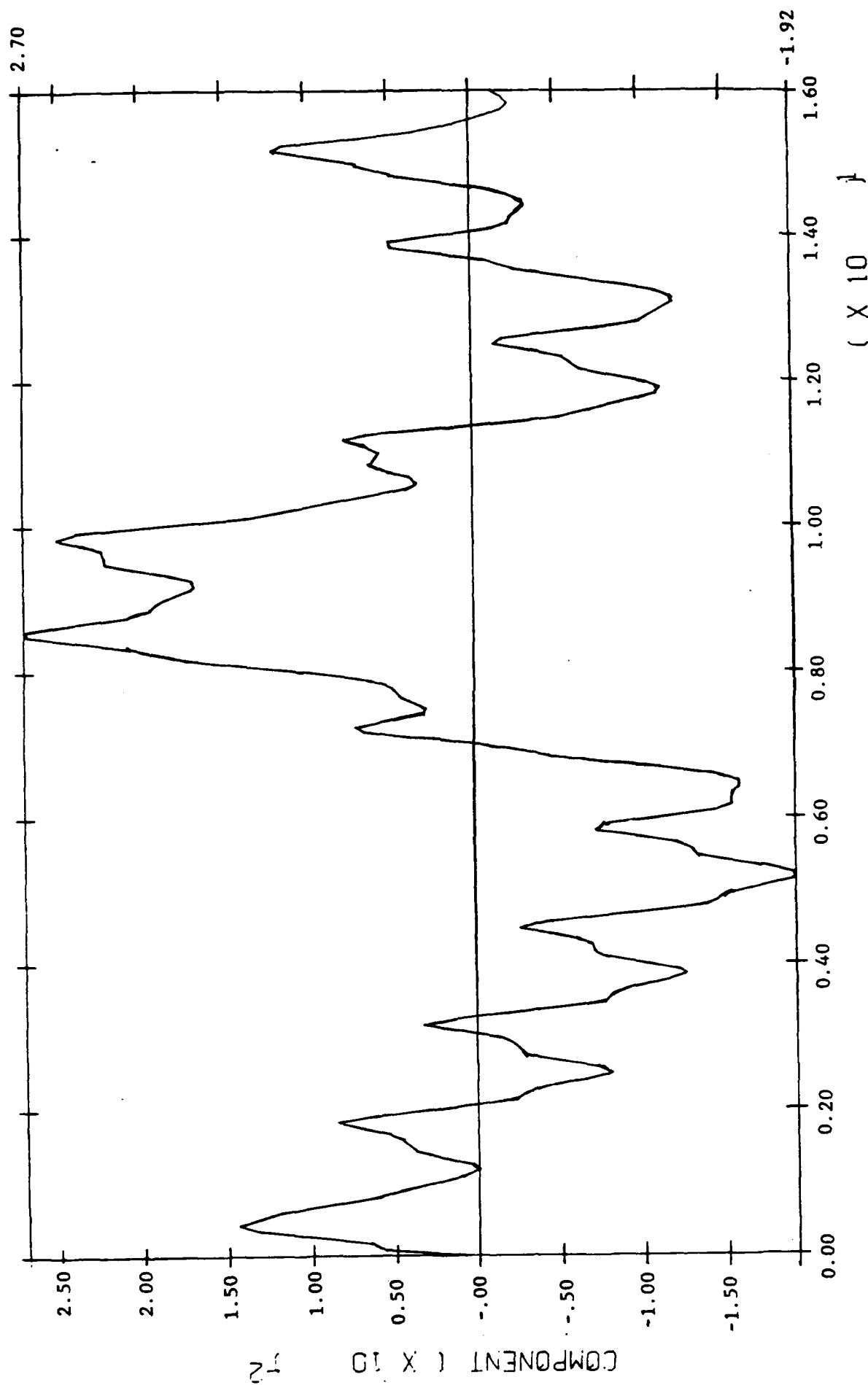


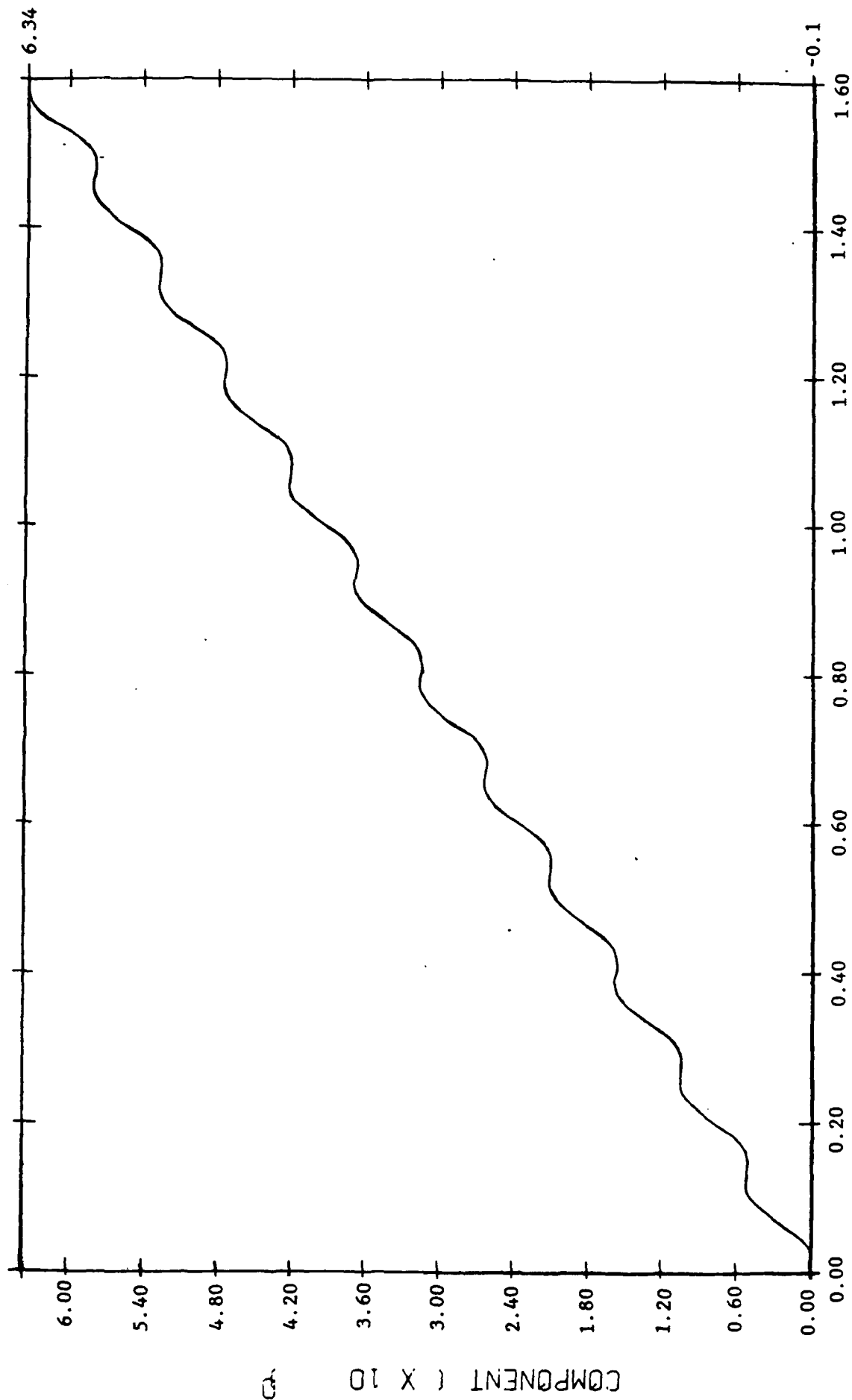
Figure C-6A. Horizontal acceleration



NODE NUMBER 295

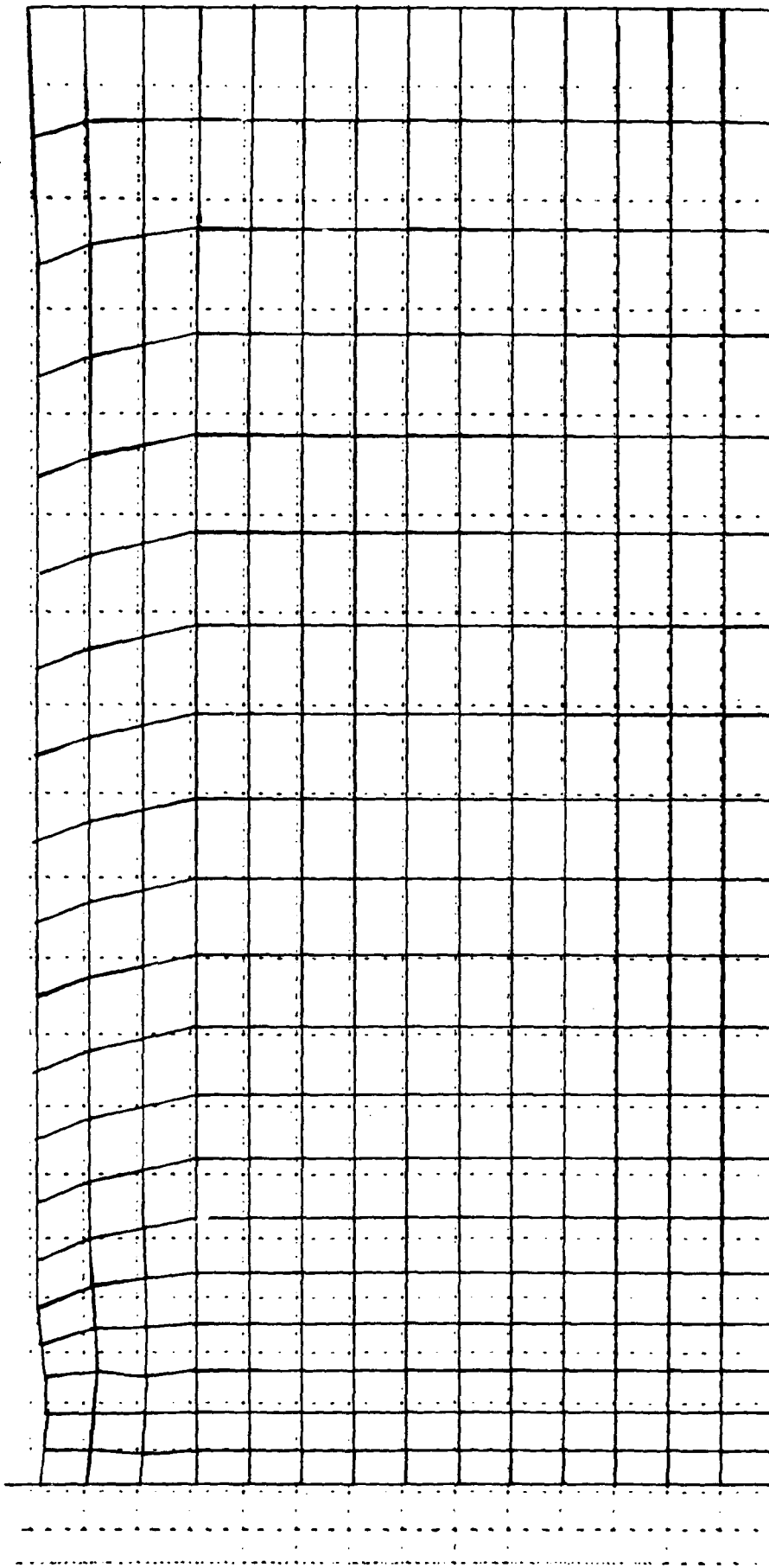
ACCELERATION

Figure C-6B. Vertical acceleration



Node Number 295
Displacement

Figure C-7. Horizontal displacement



DEFORMED MESH

STEP NO. 96

Figure C-8. Deformed mesh for retaining wall

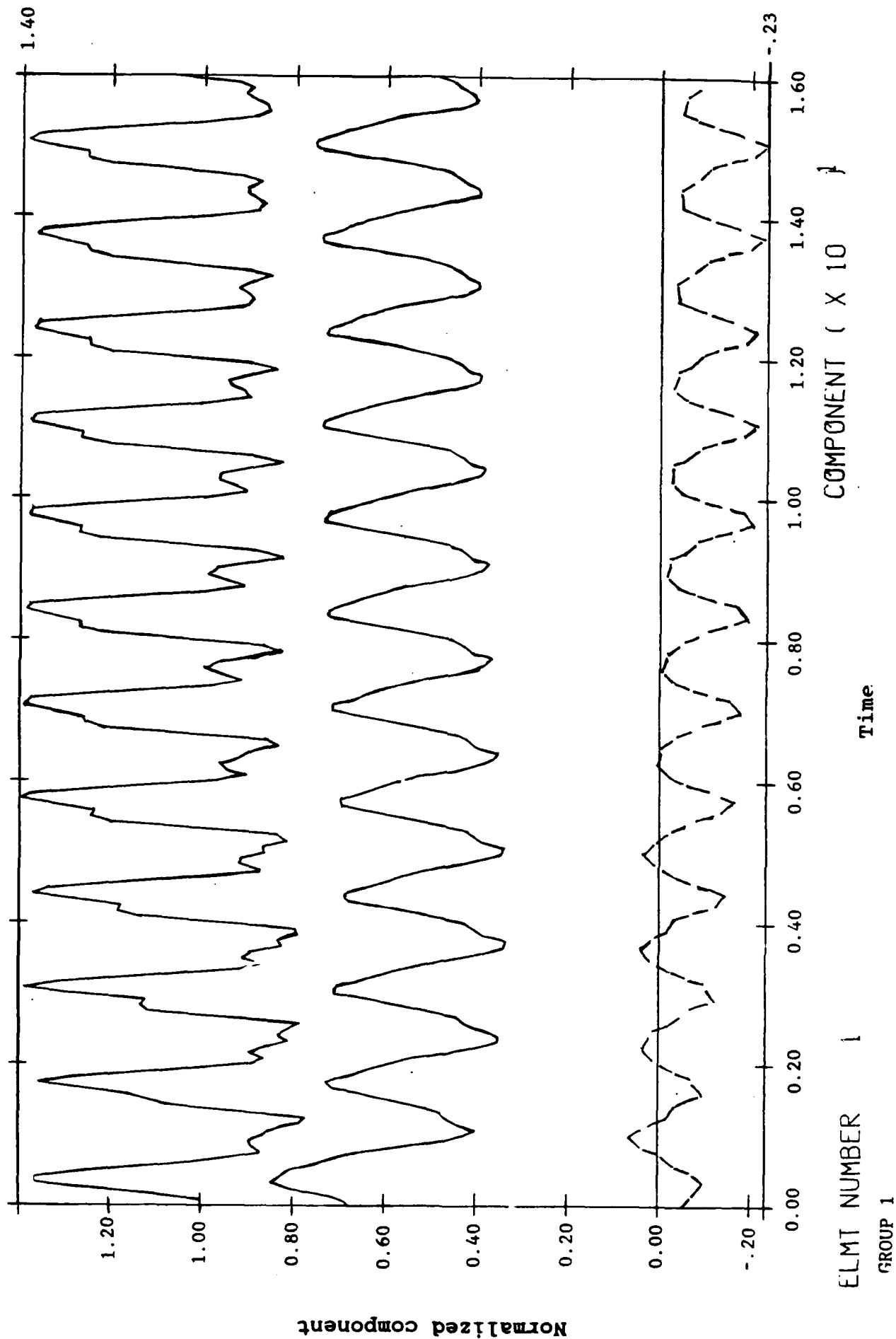


Figure C-9A. Overall stress behavior of soil

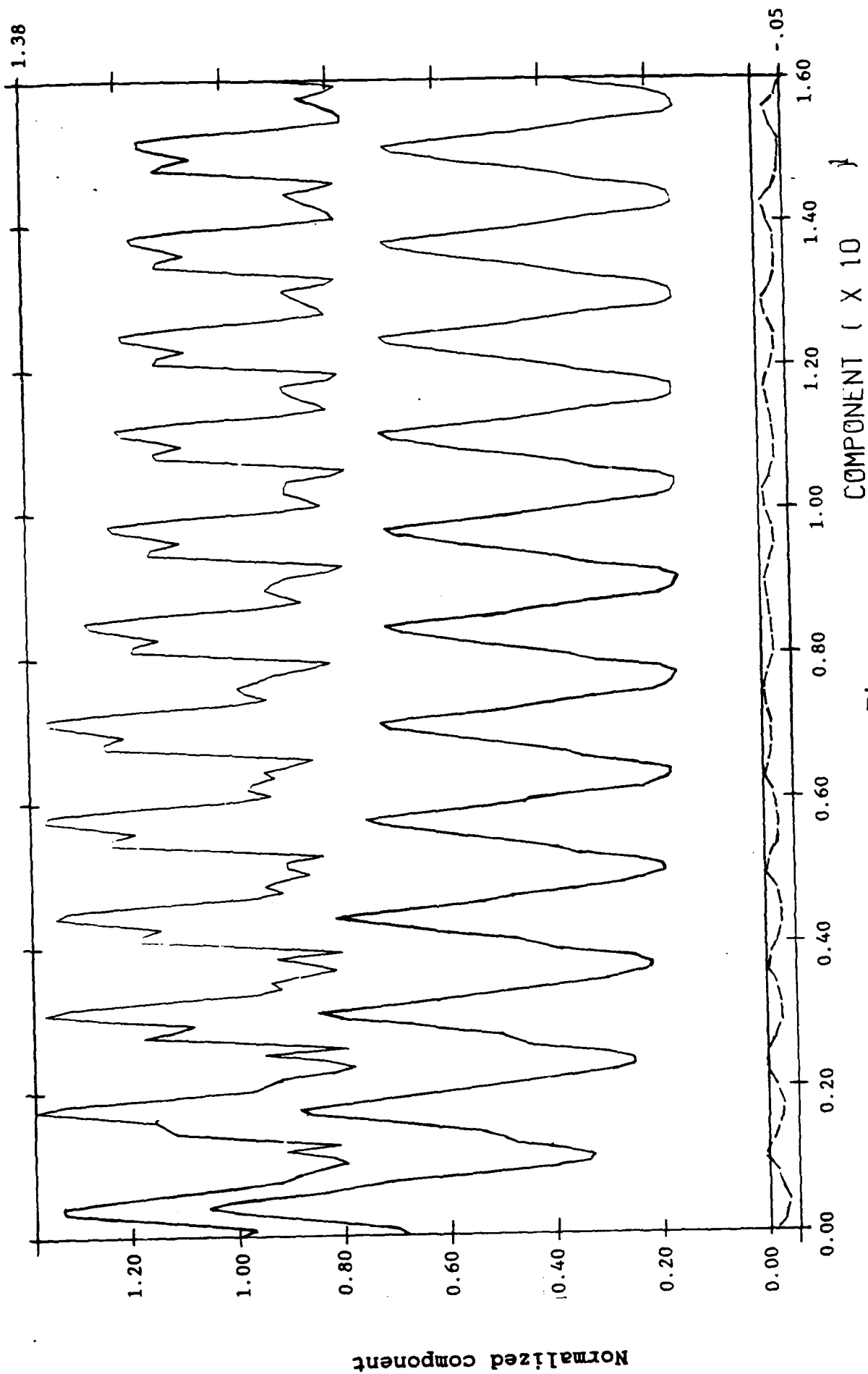


Figure C-9B. Overall stress behavior of soil

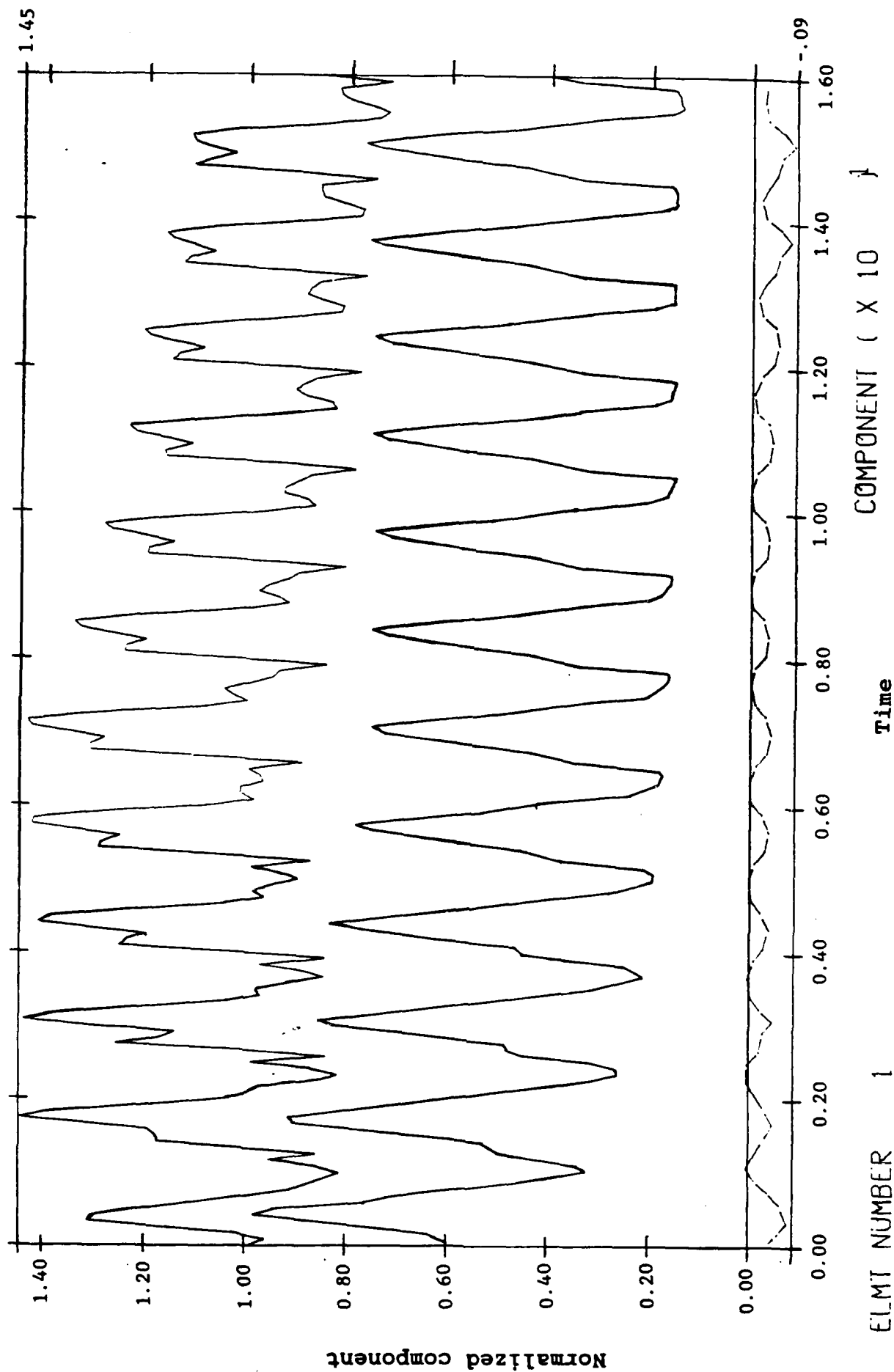
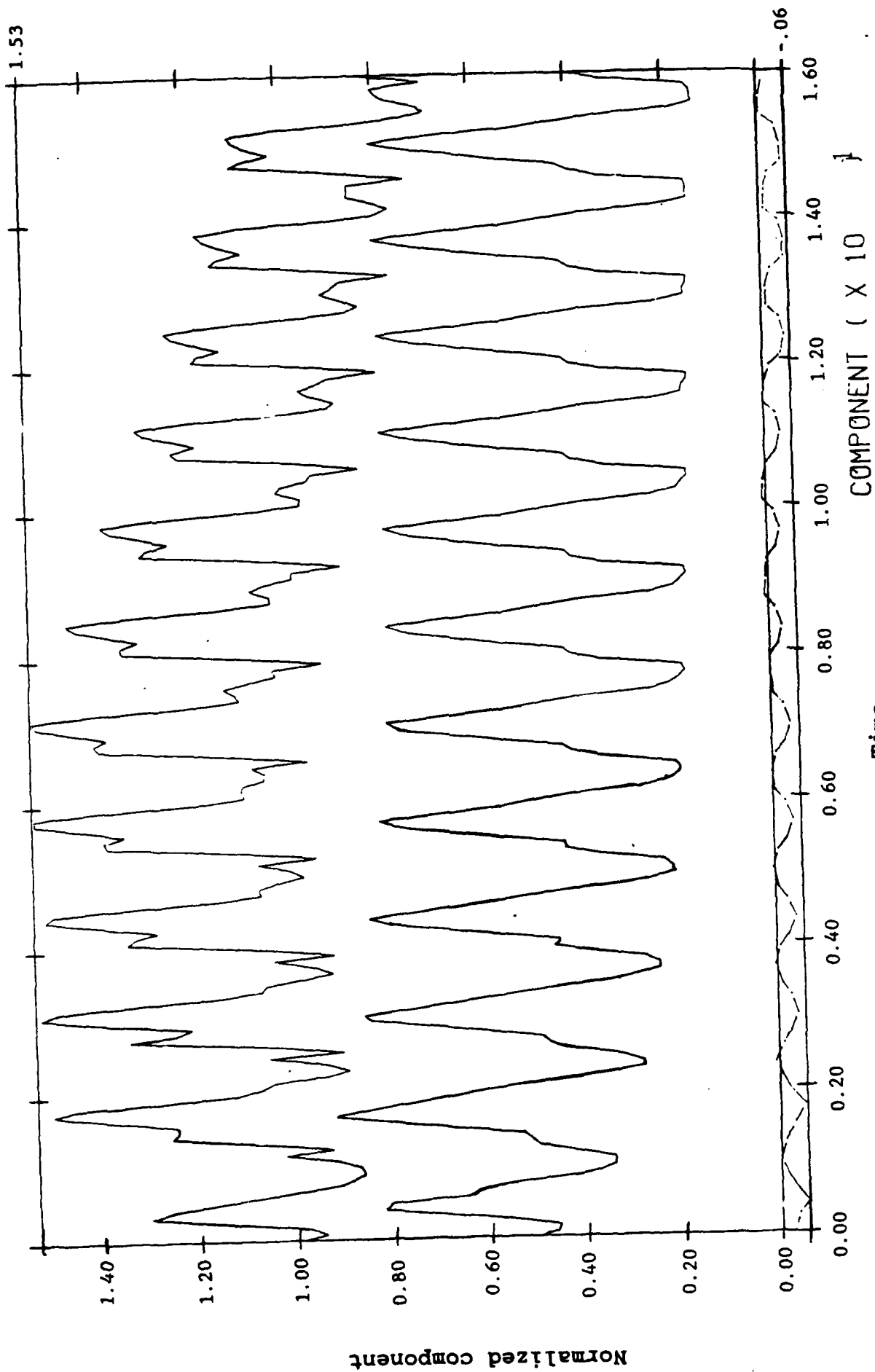


Figure C-9C. Overall stress behavior of soil



ELMT NUMBER 1

GROUP 5

Figure C-9D. Overall stress behavior of soil

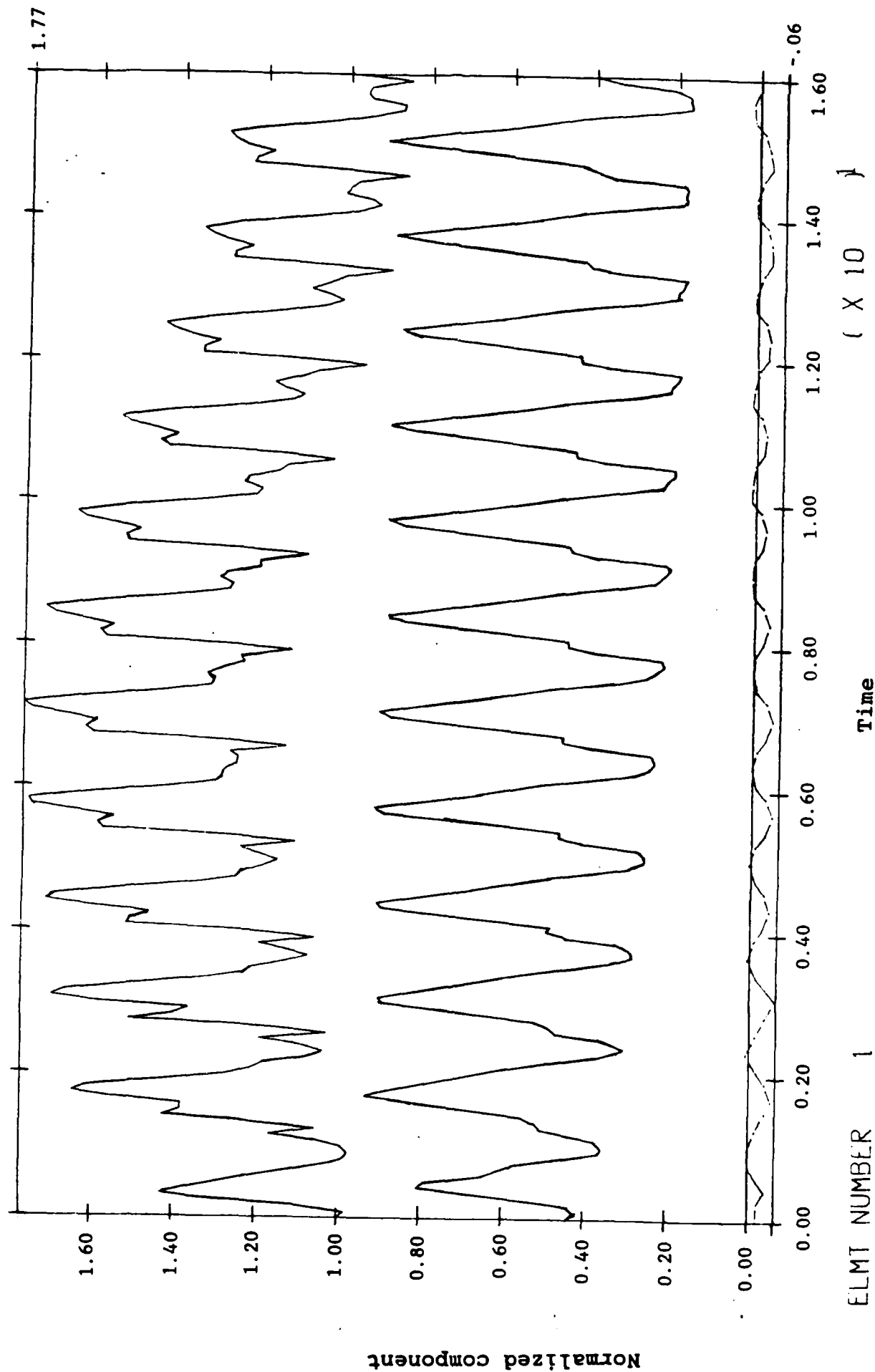


Figure C-9E. Overall stress behavior of soil

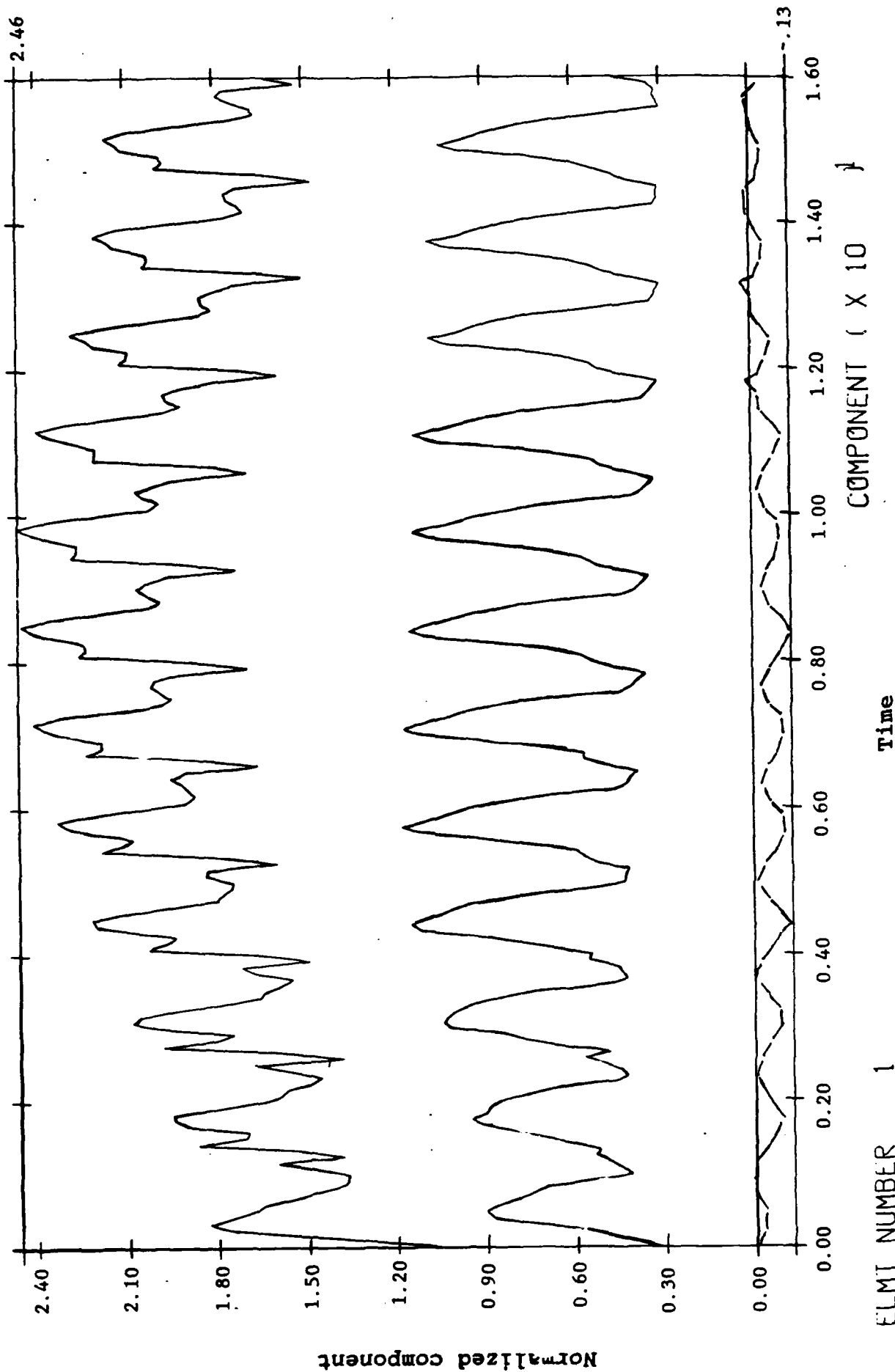


Figure C-9F. Overall stress behavior of soil

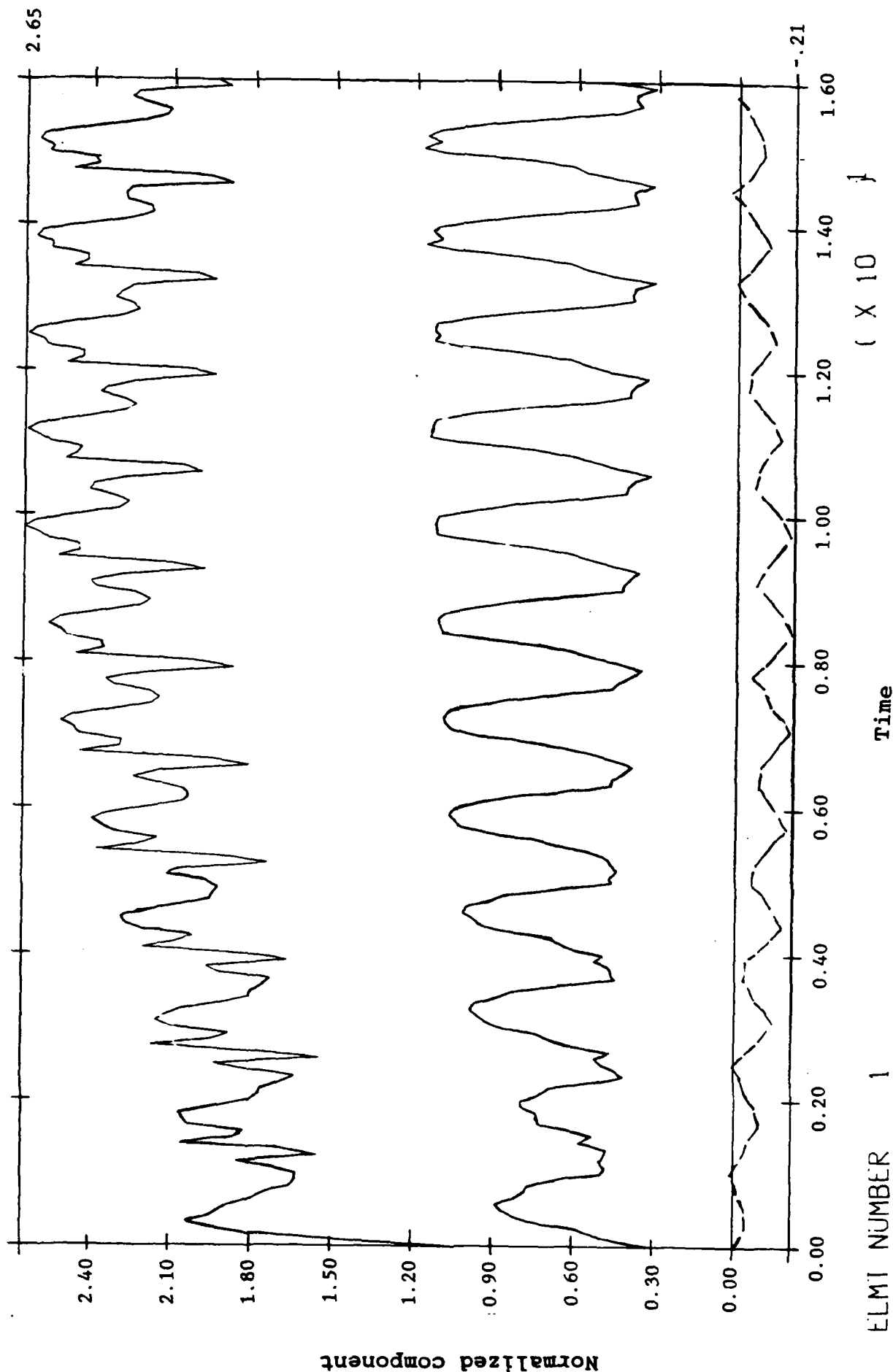


Figure C-9G. Overall stress behavior of soil

GROUP 9

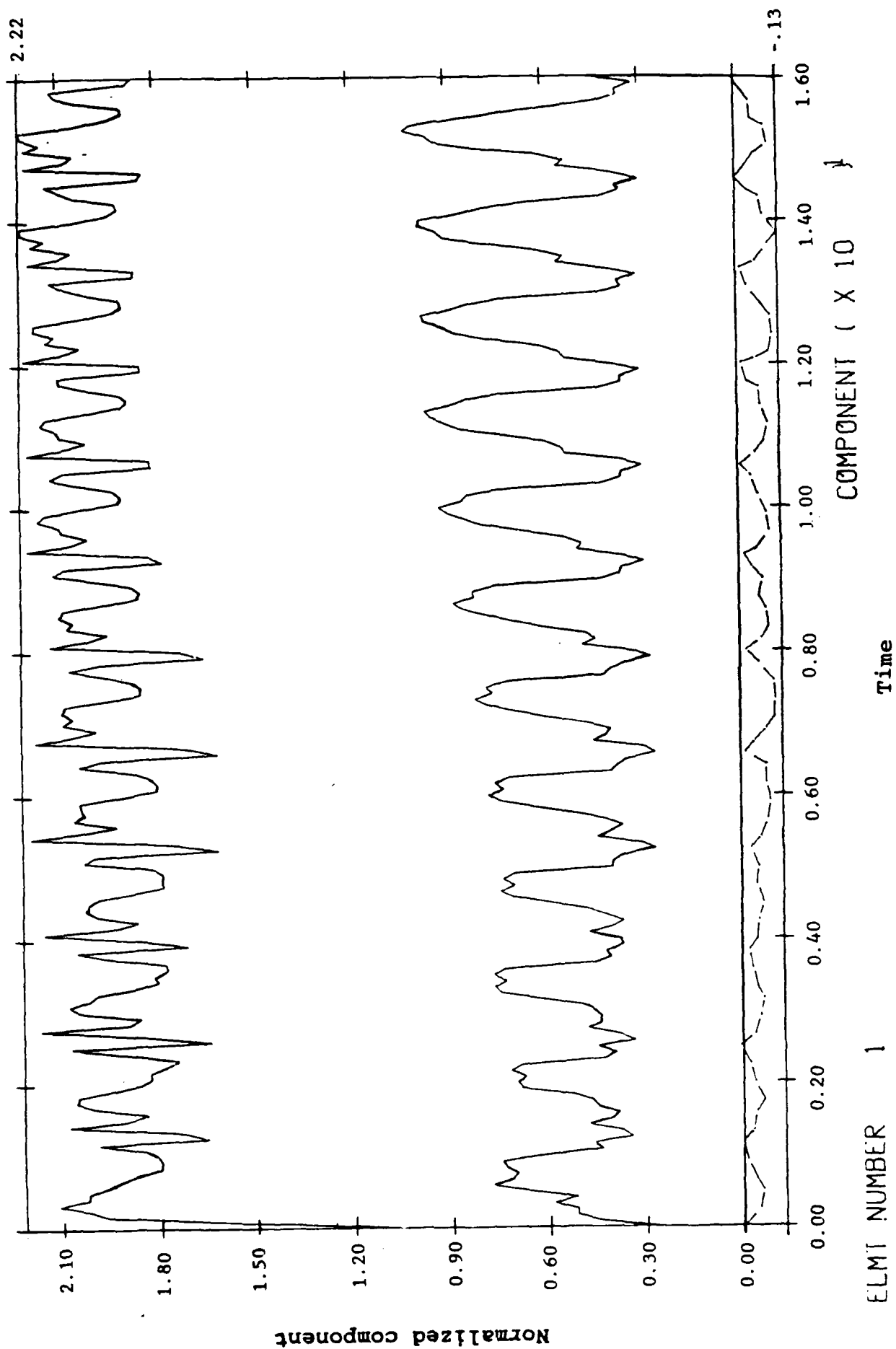


Figure C-9H. Overall stress behavior of soil

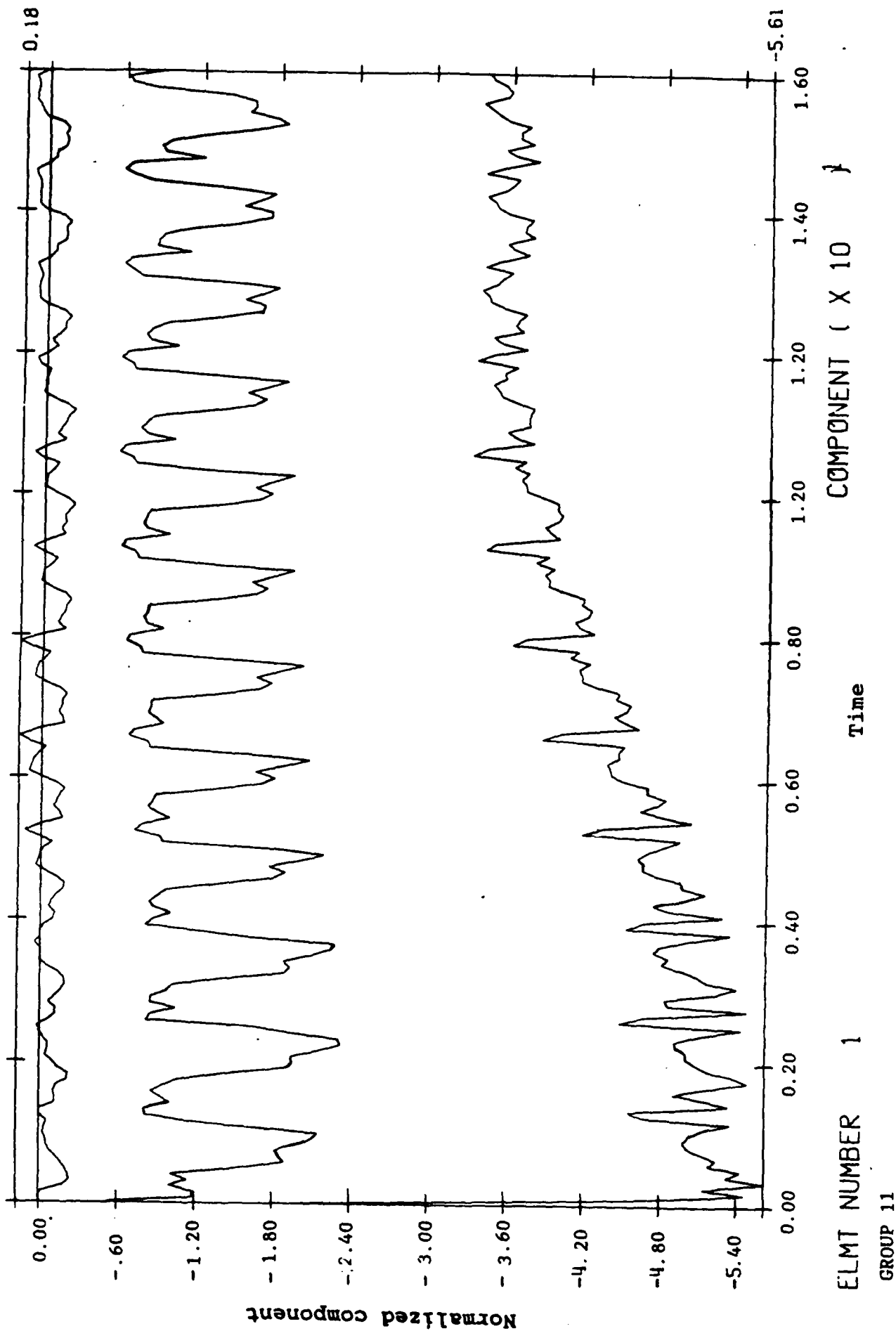


Figure C-9I. Overall stress behavior of soil

[illegible]

Table C-1. Continued

Table C-1. Continued

C-39

Table C-1. Continued

APPENDIX D
STORAGE TANK CONSOLIDATION TEST

INTRODUCTION

The centrifuge model consisted of a storage tank placed over a soft foundation strata. The tank model was constructed of rolled aluminum plate, which formed the walls. The base consisted of a flexible, rubber membrane to approximate the conditions of a prototype tank's flexible base. A cross section of the model package is presented in Figure D-1.

The model was then mounted on a centrifuge and accelerated to 60 gs. The model was maintained at this acceleration for 6.00 seconds to allow for consolidation to take place. Once hydrostatic conditions were reached, the simulation of the tank loading and unloading began (Figure D-1). Pore pressure and surface displacements were recorded through an automated data acquisition system. More detailed information can be found in Reference D-1.

The material model properties for the kaolinite simulation were derived from the undrained triaxial compression and extension tests presented above. The triaxial test data for the extension test was scaled from its original confining pressure to be at the same confining pressure as the compression test required for input to Program MUD. The effect of this scaling on the final solution was minimal.

The material model properties for the layers of Monterey "O" sand were constructed from test data presented above. Modifications were made to the critical stress ratio, parameters to reflect a somewhat higher relative density, which was back calculated from the weight of the sand used in this test. Triaxial test data were not available for the sand used in this test.

The finite element model consisted of 16 sand and 48 clay elements as shown in Figure D-2. The tank loading and unloading was simulated by a uniform pressure distribution over the inner four elements as shown in Figure D-3. To properly initiate the stresses and consolidation characteristics of the model, the problem was started at an initial gravity of zero, and then increased to the required 60 level over a time period of 250 seconds. The model was then maintained at this acceleration level throughout the test. After the appropriate time period for consolidation (6,000 seconds) the loading/unloading simulation began. The loading/unloading simulation consisted of three filling and two releasing steps. The entire trace of the loading is shown in Figure D-4. Each loading increment consisted of a 125-second load step and 1,875 seconds of dissipation to allow for consolidation time.

Because this is a layered system, which is similar to those found in nature, it is important to correctly capture the effects of all of the layers on the system response. The displacement traces shown in Figure D-5 show the instantaneous settlement of the sand. Displacement characterization overall is in good agreement while the actual measurements are acceptable. There was some difficulty in the degree of rebound that the numerical model exhibited. The errors here are caused by the difficulty in determining the correct input parameters for the material model as well as soil deposit inconsistencies in placement and uniformity acknowledged by the original investigators. The pore pressure traces (Figure D-4) are in excellent agreement with those measured during the test. Dissipation is represented with excellent accuracy in all cases demonstrating Program DYNAFLOW's capability in modeling three-dimensional consolidation problems.

MODELING ASSUMPTIONS

The storage tank simulation is an example of modifying the material model to analyze problems involving clay (cohesive soil). Figure D-2 shows the boundary conditions. The analyses should be treated as axisymmetric.

The significant area of difficulty is in the joining of two distinct soil types. This requires careful consideration of the units used to derive the soil model for each soil type and the reference pressure selected for each model, to deliver consistent output units. Soil weight and penalty (fluid moduli) parameters should be considered as well. The computation of reference pressures is shown in the following:

MONTEREY SAND

Soil model derived in units of: kg/cm^2

Desired output units: lb/in^2

Reference Moduli at derived pressure: $800 \text{ kg/cm}^2 (=G)$ 800 kg/cm^2 at 1 kg/cm^2

$$1 \text{ kg/cm}^2 = 2.2 \text{ lb/cm}^2$$

$$2.2 \text{ lb/cm}^2 = 14.19 \text{ lb/in}^2 \text{ P}$$

$$800 \text{ kg/cm}^2 = 11,355 \text{ lbs/in}^2$$

$G \qquad \qquad G_o$

from the equation

$$G = G_o \left(\frac{P}{P_o} \right)^{0.5}$$

$$\frac{11,355}{800} = \left(\frac{14.19}{P_o} \right)^{0.5}$$

$$\frac{(14.19)^2}{14.19} = \frac{1}{P_o}, \quad P_o = \frac{1}{(14.19)} = 0.0671$$

Checking

$$800 \left(\frac{14.19}{0.0671} \right)^{1/2} = 11,355$$

So, when an effective mean confining stress of 14.19 psi (1 kg/cm²) is computed, the moduli used in the solution will be 11,355 psi (800 kg/cm²).

KAOLINITE CLAY

Soil model derived in units of kilo pascals (kPa)

Initial confining stress for soil model: 620 kPa = 90 lb/in²

$$G_r = 1.06 \times 10^4 \text{ kPa} = 1,537 \text{ lb/in}^2$$

$$G = G_o \left(\frac{P}{P_o} \right)^{0.5}$$

$$1537 \text{ lb/in}^2 = 1.06 \times 10^4 \text{ kPa} \left(\frac{90 \text{ lb/in}^2}{P_o} \right)^{0.5}$$

$$\left(\frac{1537 \text{ lb/in}^2}{1.06 \times 10^4 \text{ kPa}} \right)^2 \left(\frac{1}{90 \text{ psi}} \right) = \frac{1}{P_o}$$

$$P_o = 4280.62$$

Checking

$$1.06 \times 10^4 \left(\frac{90}{4280.6} \right)^{0.5} = 1537 \text{ lb/in}^2$$

The units are now in terms of pounds per square inch.

Now to calculate the value for the fluid bulk modulus:

Maximum Effective Stress:

depth of soil is 8 inches.

$$\gamma_{\text{solid}} = 0.0796 \text{ lb/in} \quad \gamma_{\text{fluid}} = 0.036 \text{ lb/in}^3$$

$$n = \text{porosity} = 0.5$$

$$\gamma_{\text{buoyant}} = 0.0796 \times (1 - 0.51) = 0.039 \text{ lb/in}^3$$

$$\text{Gravity} = 60g$$

$$\tau_{\max} = 60g \text{ (in) } (0.039 \text{ lb/in}^3) \\ = 18.72 \text{ psi}$$

Now compute the maximum bulk moduli of the elastic phase:

$$\left(\frac{18.72}{4280.6} \right)^{0.5} 3.53 \times 10^3 = 233.7 \text{ lb/in}^2$$

Now, selection of the fluid bulk modulus

$$B_f \geq 233.7 \text{ lb} \times 10^3 = 2.337 \times 10^5$$

The process should be repeated for the sand as well, and the maximum of the two values used. In general, the fluid bulk can be set to a value of 1×10^{10} without introducing significant error in the analysis. If in doubt, it is always good to check the solution over a range of fluid moduli to see if the answer varies considerably.

PROBLEM AND SOLUTIONS:

The tank consolidation problem was difficult to simulate correctly for several reasons. The major difficulty occurred as a result of poor characterization of the coefficient of consolidation. This factor controls the dissipation of pore pressure, and must be considered along with the material permeability. This topic was discussed in depth in Appendix B. Once the valuator consolidation coefficients were correct, the solution worked quite well.

REFERENCE

D-1. Shen, et al. Centrifuge consolidation study for purposes of plasticity theory validation, University of California, Davis, 1985.

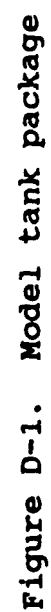
SHEN CLAY FOR TANK CONSOLIDATION PROBLEM

100	1	2	1	0	1	8
11	12	00				
6.00	0.50		0.00		1.00	
1	0.		0		615.0	0.
2		65.0	0.00025		601.9	
3		120.0	0.00050		586.3	
4		170.0	0.00100		536.6	
5		200.0	0.00150		486.7	
6		222.0	0.00200		449.1	
7		237.0	0.00250		424.7	
8		275.0	0.00500		331.7	
9		295.0	0.00750		288.5	
10		301.0	0.01000		210.1	
11		305.0	0.01250		216.7	
1		0.0	0.0		615.0	
2		-60.0	-0.00025		600.5	
3		-115.0	-0.00050		586.7	
4		-170.0	-0.00100		579.0	
5		-220.0	-0.00150		552.3	
6		-245.0	-0.00200		538.0	
7		-270.0	-0.00250		524.0	
8		-320.0	-0.00500		483.7	
9		-350.0	-0.00750		448.0	
10		-375.0	-0.01000		434.7	
11		-390.0	-0.01250		428.0	
12		-392.0	-0.01500		432.0	

Table D-1. MUD input Shen clay

[illegible]

[illegible]



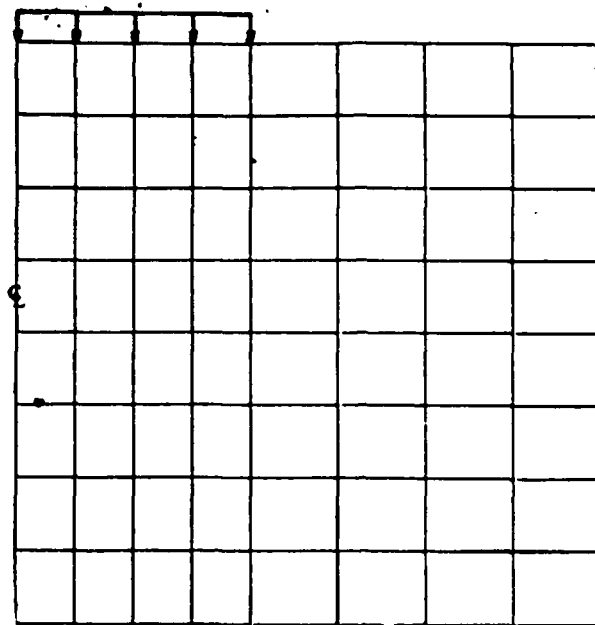


Figure D-2. Undeformed mesh used for model storage tank test

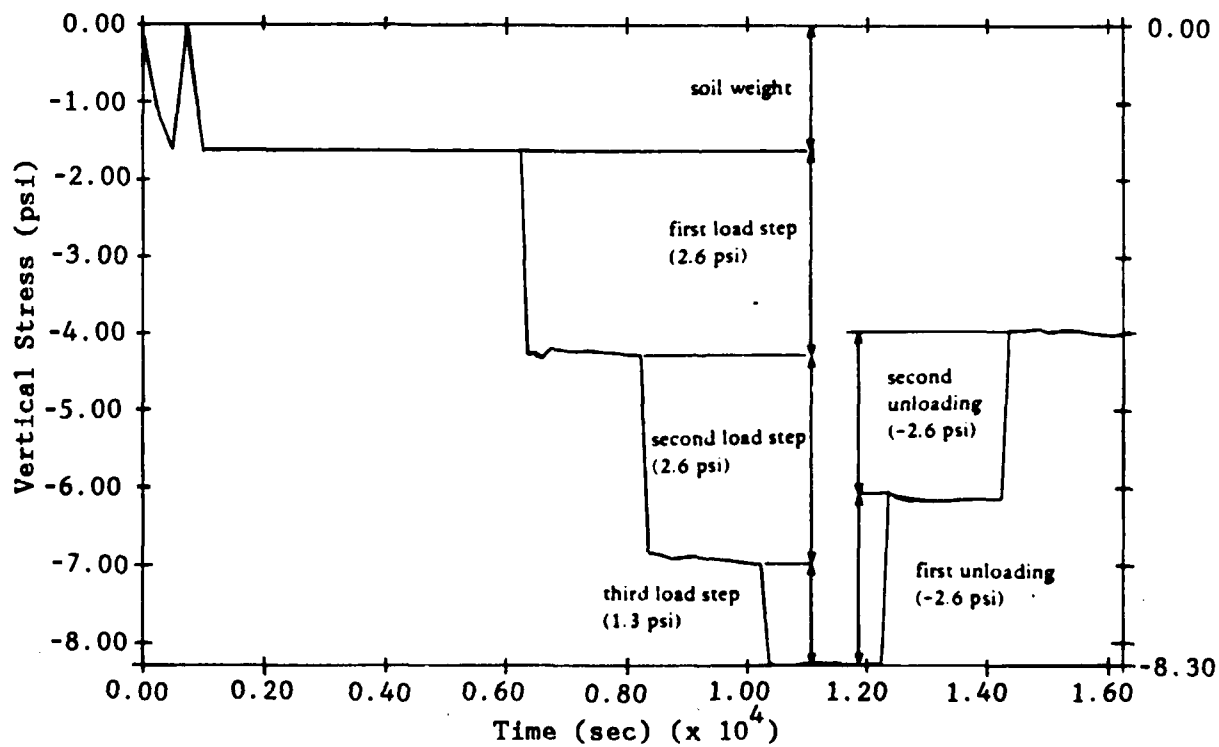


Figure D-3. Pressure loading sequence

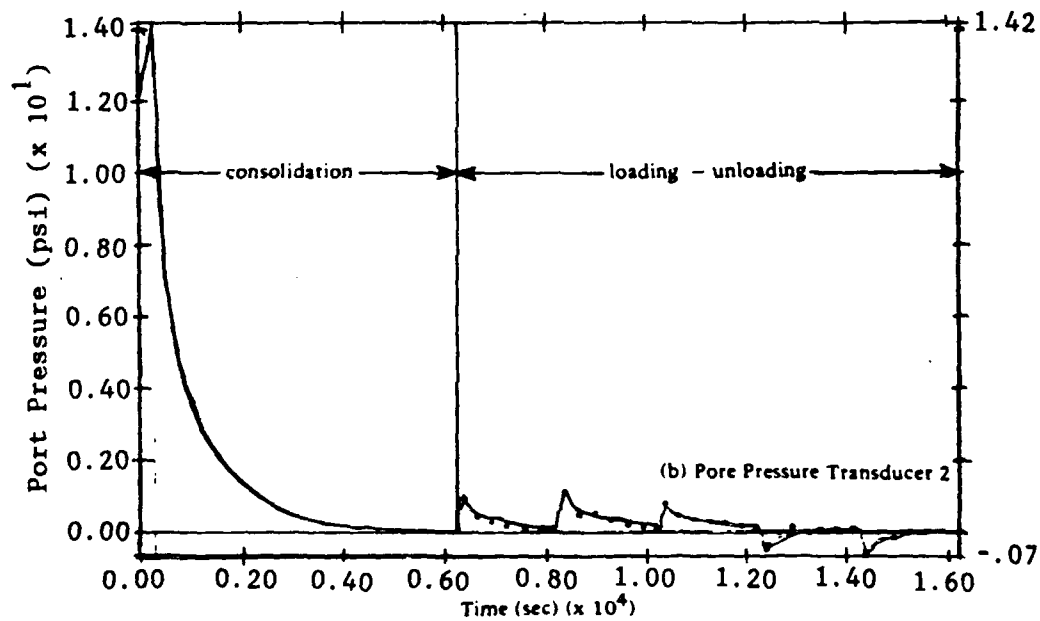
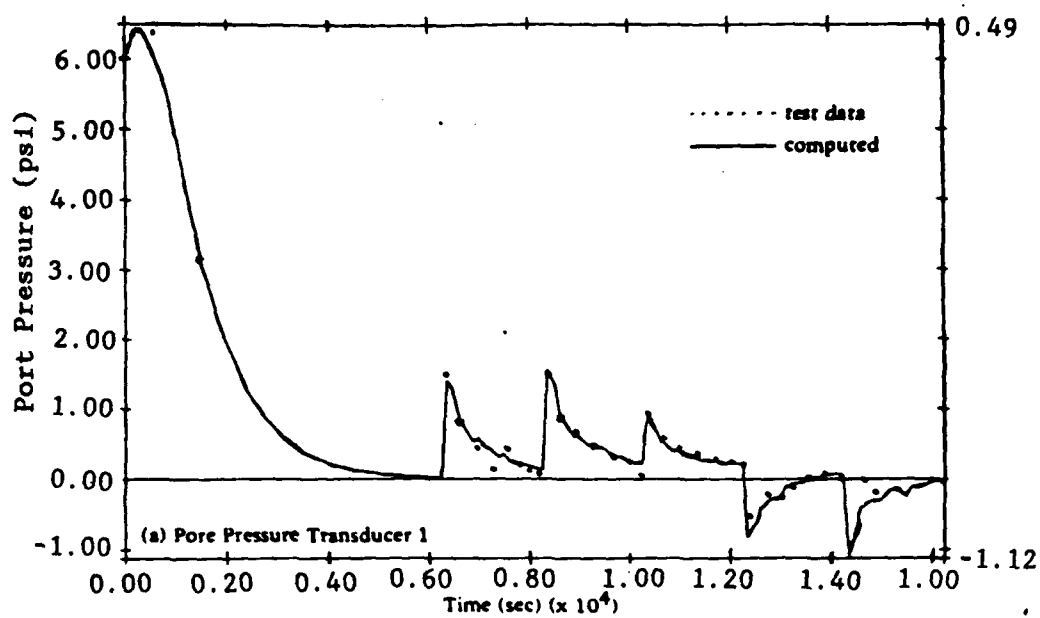


Figure D-4. Pore pressure traces

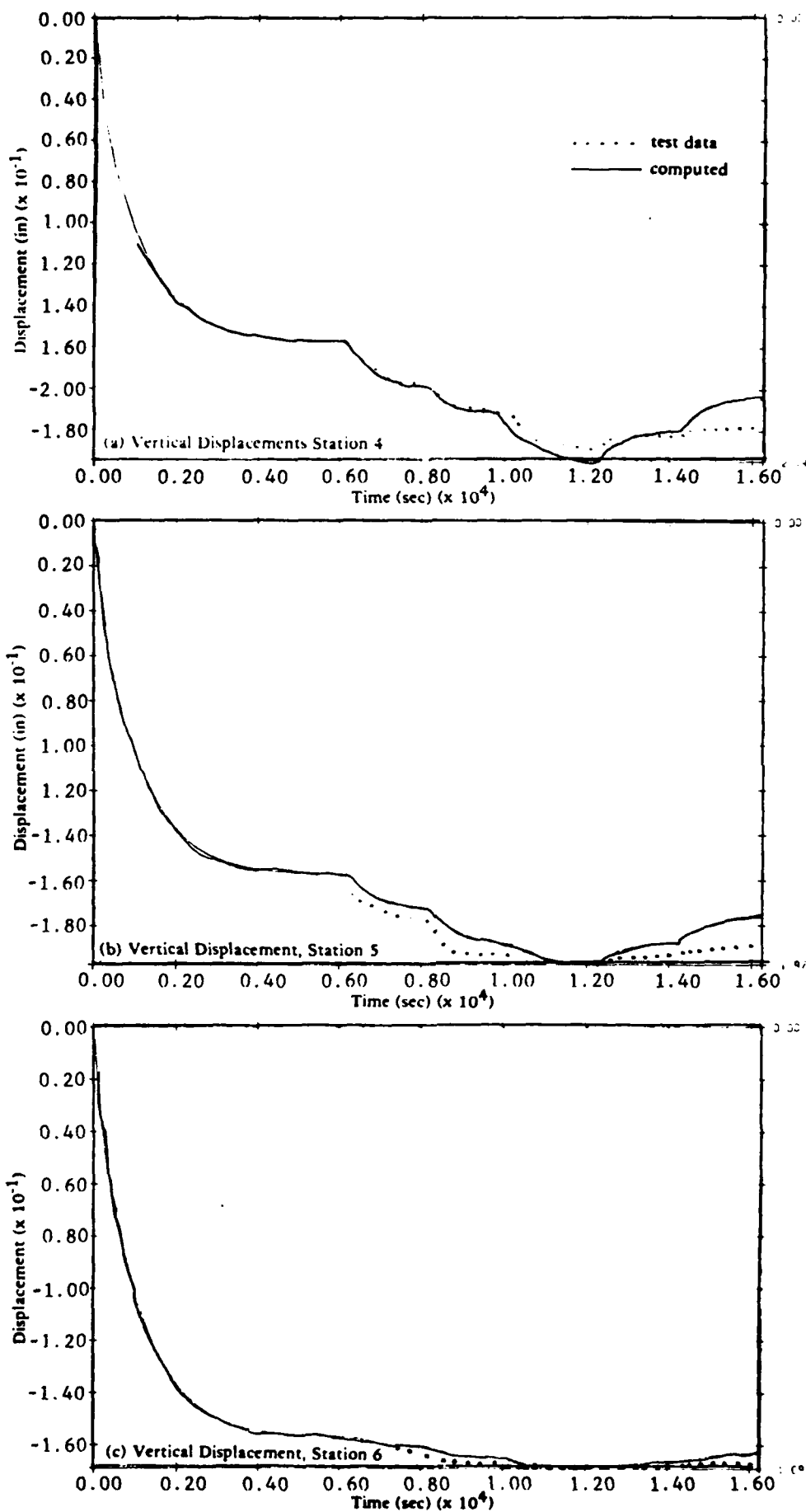


Figure D-5. Free-field displacements

Appendix E
BLAST-INDUCED LIQUEFACTION

INTRODUCTION

Blast-induced soil liquefaction is the result of a compression wave passing through a soil field. The compression wave induces volume changes in the soil skeleton which, in a saturated system, causes a rise in pore fluid pressure. If the wave causes sufficient degradation the effective stress in the soil skeleton will drop to zero, creating a state of initial liquefaction.

Professor Wayne Charlie of the University of Colorado, Fort Collins is doing extensive work in the area of blast-induced liquefaction. The experimental program includes one-dimensional laboratory studies and a planned full-scale field test program.

The laboratory experiments were carried out using a modified Hopkins bar device, which induces a shock-wave into a soil sample. The testing device and procedures are described fully in Reference E-1.

SOIL MODEL DERIVATION

The soil used for the laboratory simulations in Reference E-1 was a Monterey 0/40 sand. Monterey 0/40 is very similar in structure and properties to Monterey 0 sand which has been used in prior analysis of geotechnical centrifuge tests (Ref E-2). Triaxial shear test results for the Monterey 0/40 sand were not available. For this reason, a material model from Reference E-2 was adapted to the cyclic uniaxial test results from Reference E-1. The results of the material model fitting process are shown in Figure E-1. The computed behavior agrees reasonably well with the test results. The computed rebound behavior is somewhat softer than the actual tests.

FINITE ELEMENT SIMULATION

To simplify the modeling of the one-dimensional tests, only the soil was considered. This removed the difficulty of trying to correctly capture the boundary and interface effects.

The soil model was given the same initial conditions that were present in the laboratory tests. The initial effective stress of 172 kPa ($\approx 1.75 \text{ kg/cm}^2$) was created by applying an internal fluid pressure of 310 kPa ($\approx 3.16 \text{ kg/cm}^2$) and a confining stress of 482 kPa (4.91 kg/cm^2).

The finite element model consisted of 20 four-node isoparametric quadrilateral element (Figure E-2). The boundary conditions were assigned to fix nodes 41 and 42 in both the horizontal and vertical direction. The remaining nodes were fixed in the vertical direction and free to translate in the horizontal.

Because of the time scale in the input loading, a purely implicit time stepping algorithm was used in this analysis. The values for the input loading were digitized from pore pressure transducer records from the laboratory test. These values were then applied as point loads to the finite element model.

Numerical simulations are carried out for two tests from a series denoted as "low impact" in Reference E-1. The tests are a series of impacts on a single soil sample. The simulation of the loading required three restarts of the solution to record each "impact" and the reconsolidation at the end of the test. The results of the first impact are shown in Figure E-3. Figure E-4 is the laboratory test record while Figure E-3 shows the computed pore pressure response. The behavior of the computed pore pressure is in excellent agreement with that recorded in the test. Figure E-5 shows the reconsolidation and pore pressure increase recorded after the end of loading. Figure E-6 and E-7 show the second impact test and simulation results, respectively. Again, computed response is in very good agreement with that recorded in the test. The final accumulation of pore pressure at the end of the simulation is somewhat less than the measured pressure.

The results of the simulation show good agreement with the test results. This is a good demonstration of the Princeton University Effective Stress Soil Model's capability on a problem that exhibits a very different stress path than the triaxial shear test.

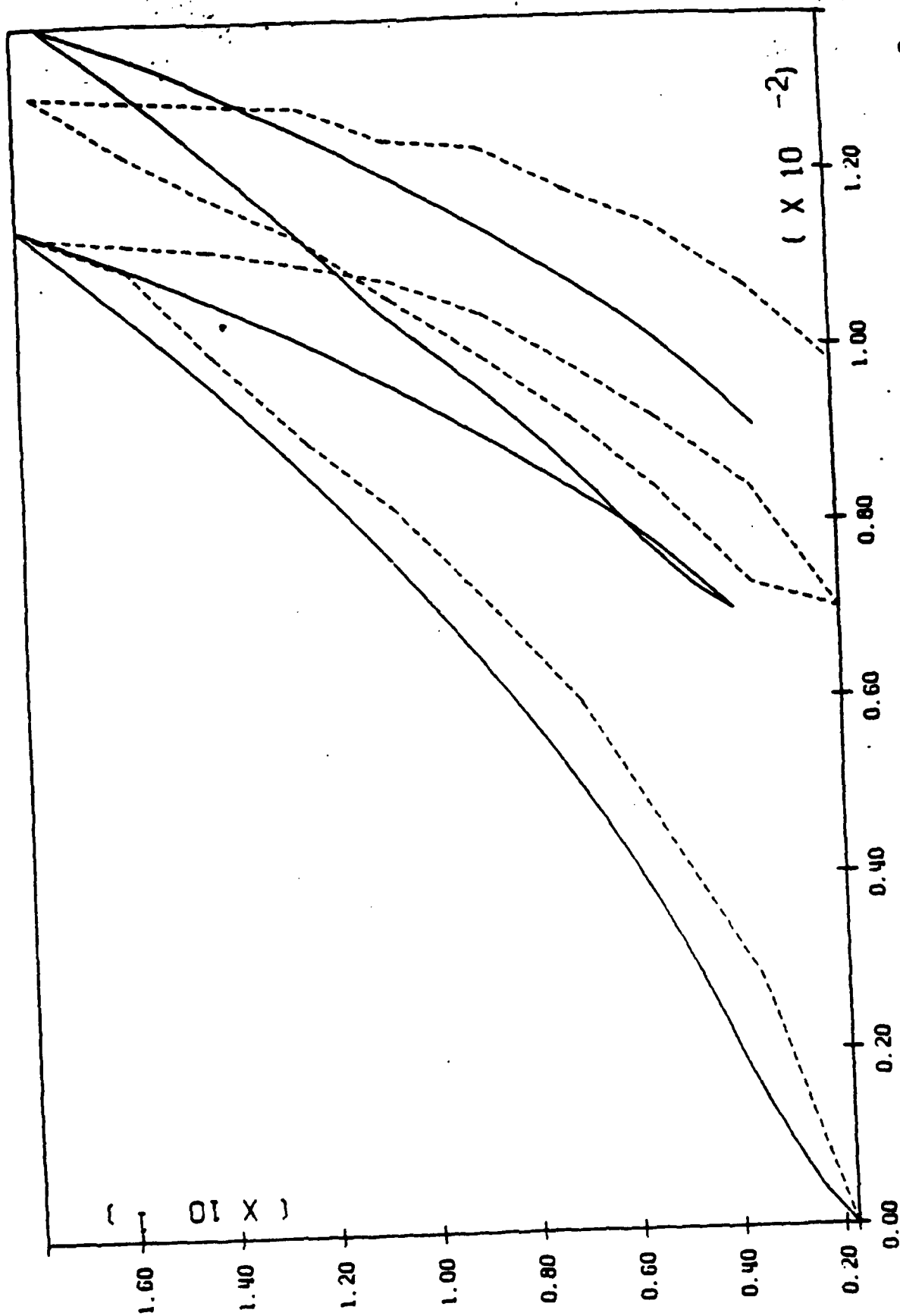
MODELING ASSUMPTIONS

The blast-induced liquefaction simulation involved inducing a prescribed compression wave in the soil sample and tracing the induced pore pressures. The boundary conditions in the problem are shown in Figure E-2. The only question in the analysis involved the effects of the rigid end restraints. The rigid boundary was considered to be reflective. This did not become apparent in the solution. Once the initial load time function and load were complete, the solution was stopped and the acceleration array was cleared. This eliminated any chance of transient "noise" inhibiting the reconsolidation of the specimen Figure E-5. The solution was restarted again to simulate the second (and subsequent) impacts.

REFERENCES

- E-1 Charlie Wayne, et al. Blast-Induced liquefaction potential and transient pore pressure response of saturated sands, Colorado State University, Fort Collins, CO, Oct 1985.
- E-2. Naval Civil Engineering Laboratory. Technical Report R-917: Evaluation and validation of the Princeton University Effective Stress Soil Model, by J.H. Prevost, J.M. Ferritto, and R.J. Slyh. Port Hueneme, CA, Dec 1986.

MONTEREY '0' SAND - DR=40% - SC1,SE1 - CONFINED COMPRESSION SIMULATION



E-4

S22 VS E11- E22
 Figure E-1. Simulated and Measured Cyclic Ko Triaxial Test
 NO. OF EXPERIMENTS 2
 OT NO. 1

NESTART FOR INTERNAL DIFFUSION AND DETERMINATION OF PP INCREASE

1	3	5	7	9	11	13	15	17	19	21	23	25	27	29	31	33	35	37	39	41
2	4	6	8	10	12	14	16	18	20	22	24	26	28	30	32	34	36	38	40	42

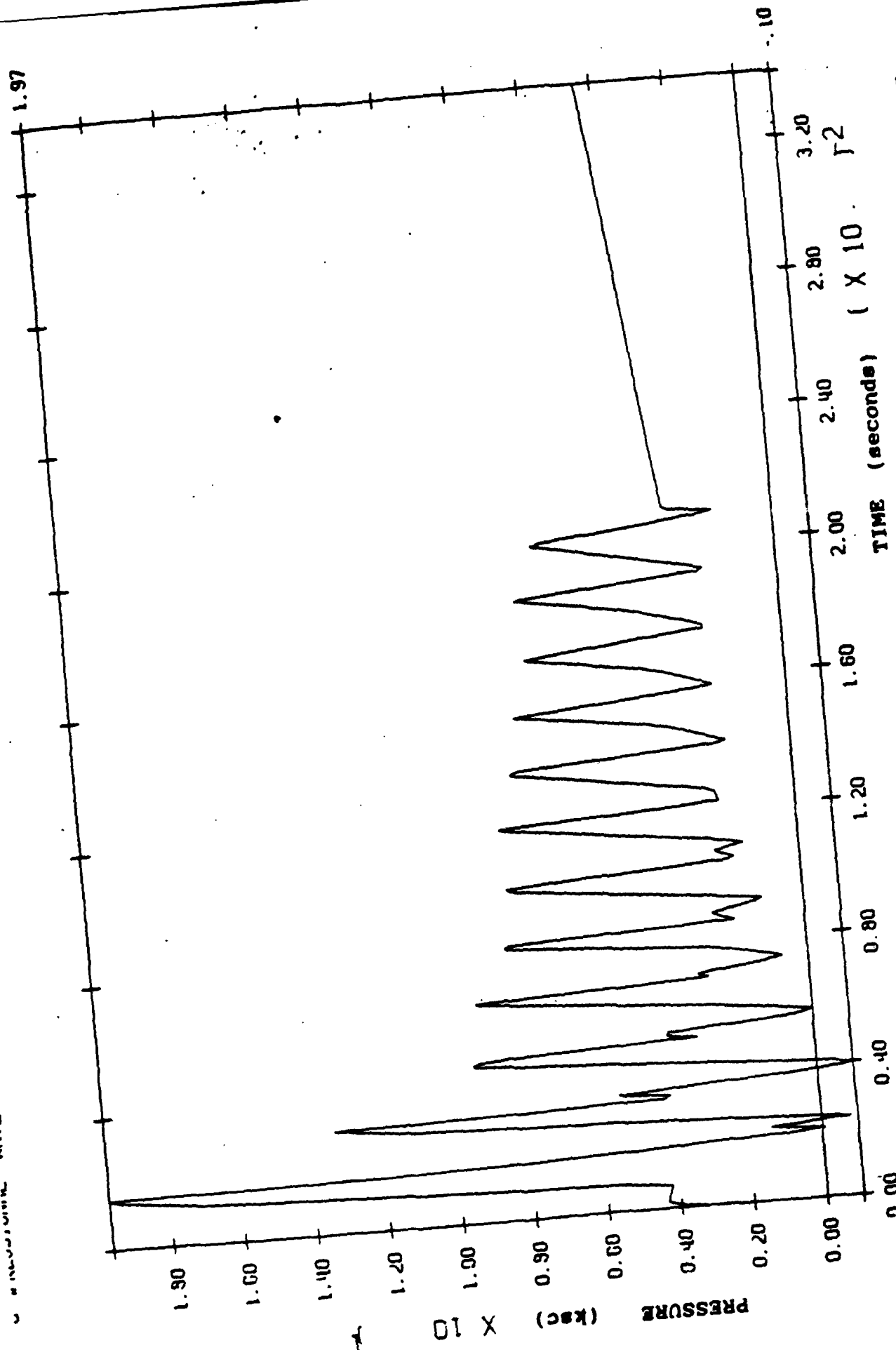
UNDEFORMED MESH

STEP NO. 0

WED. SEP 16 1987 PLOT NO. 1

Figure E-2. Finite Element Mesh, Blast Induced Liquefaction

COMPUTED AND MEASURED PORE PRESSURES, IMPACT 1,



ELMT NUMBER 10 GROUP NBER 1
 CPN NUMBER 15
 Figure E-3. Computed and Measured Pore Pressures, Impact 1,
 Blast Induced Liquefaction
 JT NO. 19

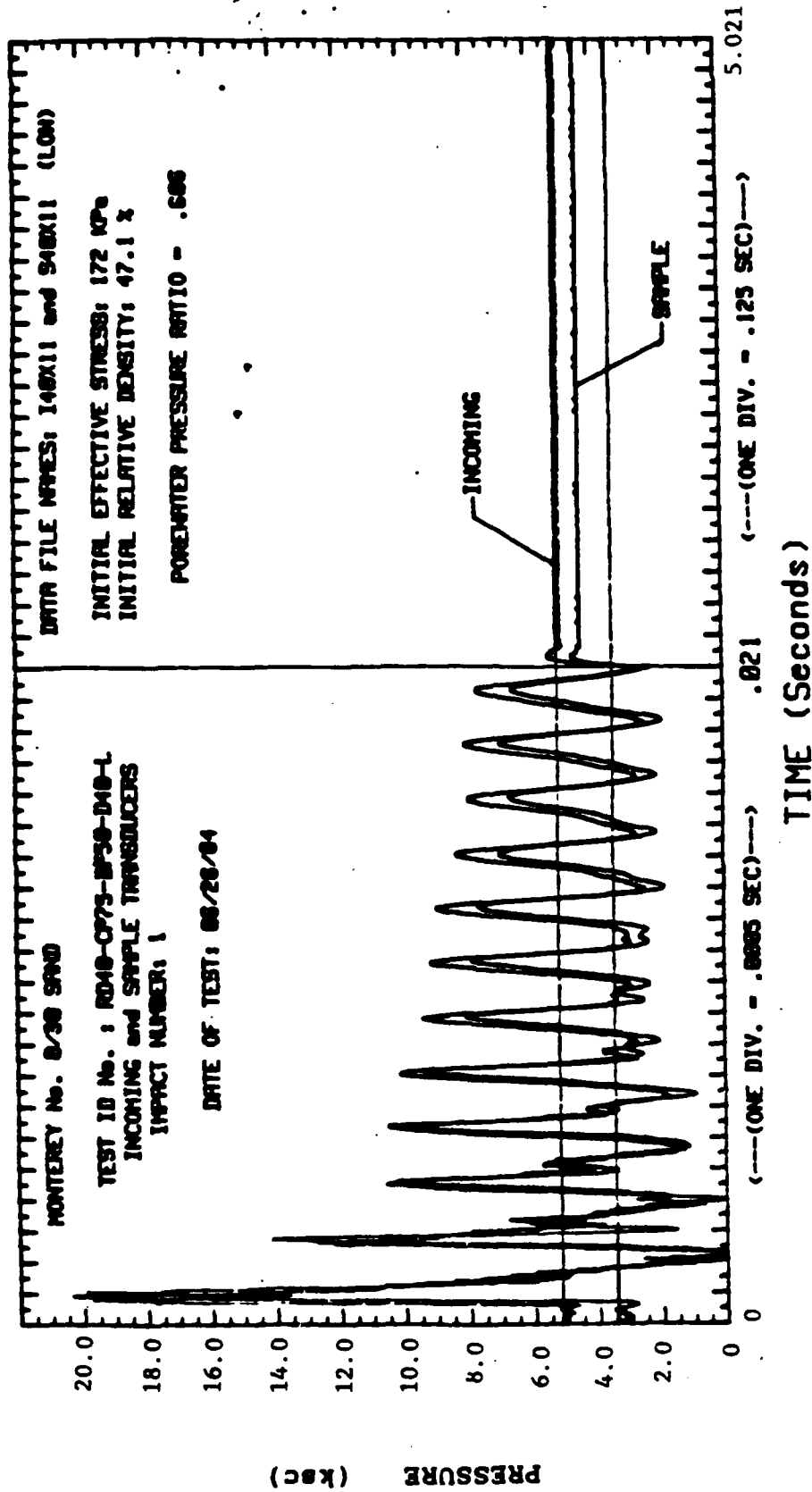
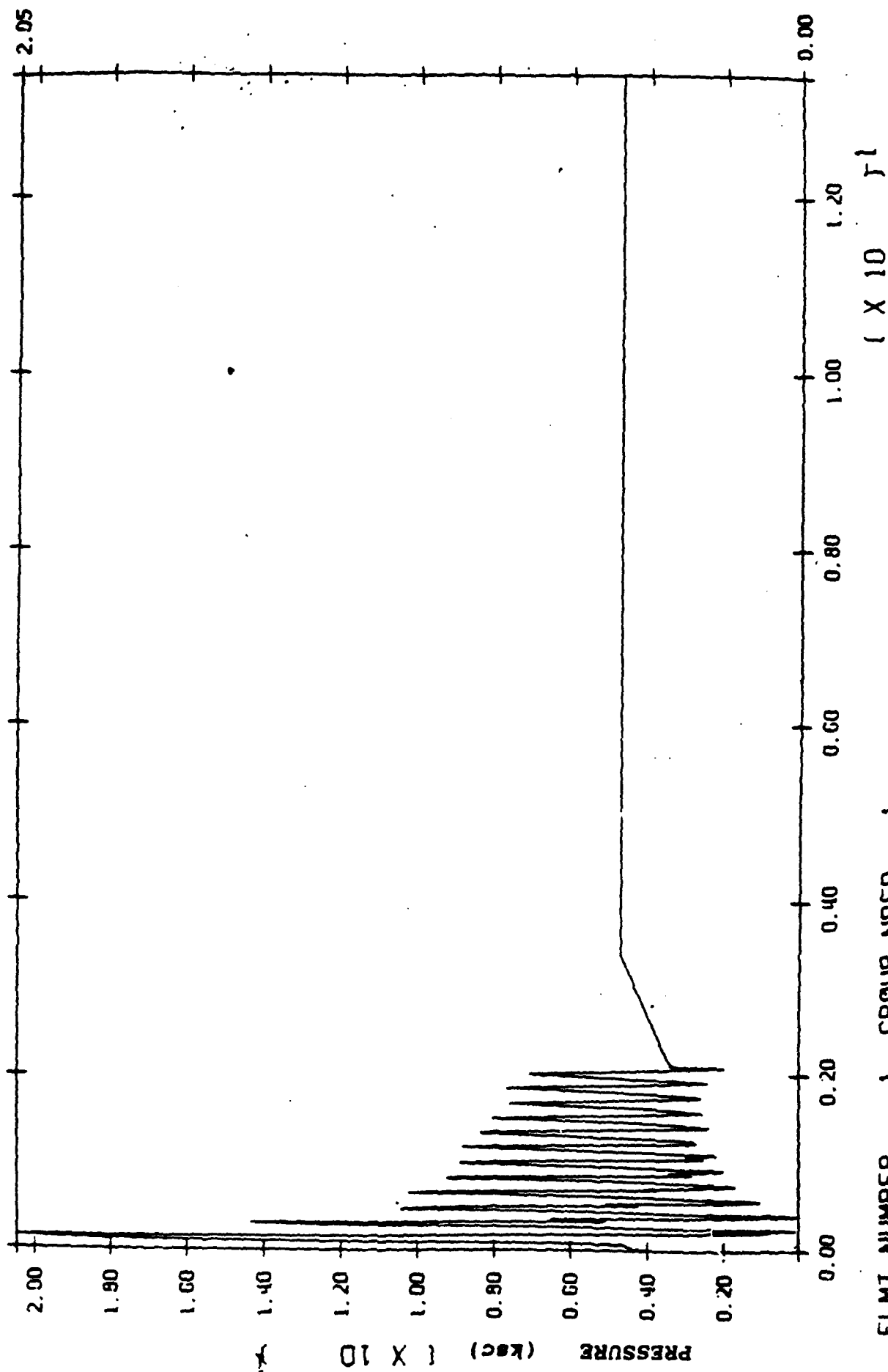


Figure E-4. Computed and Measured Pore Pressures, Impact 1,
Blast Induced Liquefaction

RESTART FOR DIFFUSION AND DETERMINATION OF PP INCREASE



ELMT NUMBER 1 GROUP NBER 1

CPN NUMBER 16 Figure E-5. Re-consolidation of Soil Sample, Impact 1, 16
Blast Induced Liquefaction

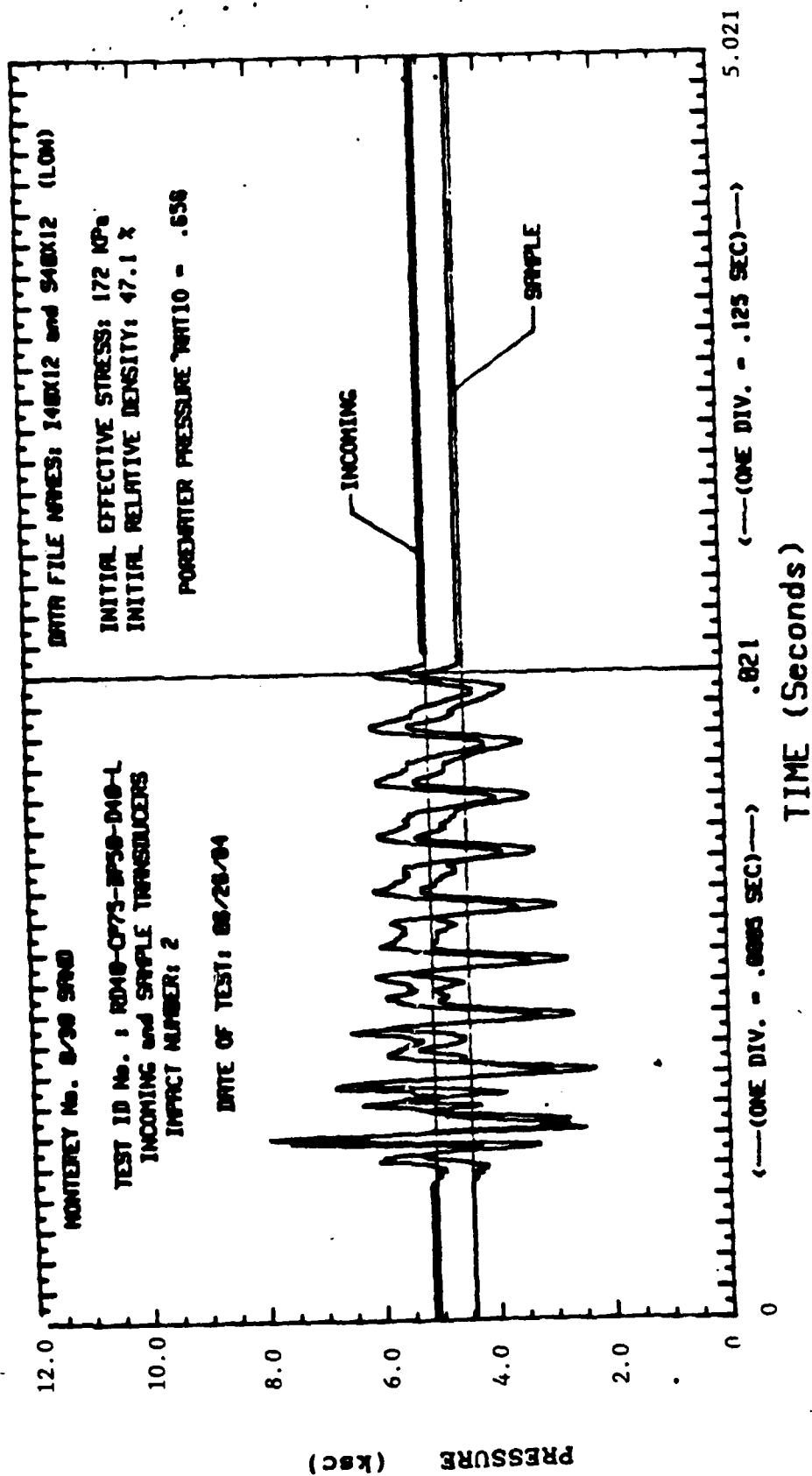


Figure E-7. Computed and Measured Pore Pressures, Impact 2,
Blast Induced Liquefaction

Appendix F
CALTECH CENTRIFUGE TESTS

FINITE ELEMENT SIMULATIONS, CALTECH TESTS

Soil Model Derivation

Drained monotonic triaxial compression and extension tests for the Nevada sand were conducted by The Earth Technology Corporation. Cyclic triaxial and cyclic simple shear tests were also conducted. Data from the monotonic triaxial tests was input to Program MUD to derive the Princeton University Effective Stress Soil Model. The parameters derived from Program Mud are given in Table F-1. The soil model was then used to predict behavior in the monotonic and cyclic tests noted above.

Results for the triaxial compression simulation are shown in Figures F-1(a) and (b). The agreement between computed (solid line) and measured deviatoric stress-strain (dashed line) is very good (Figure F-1(a)). Comparative volumetric strain predictions for the compression test (Figure F-1(b)) are slightly larger than those measured. Results for the triaxial extension test simulation are given in Figures F-2(a) and (b). The data from the triaxial extension test shows an abrupt failure at 12 psi. This behavior was considered to be a testing problem, and the input to Program MUD was extrapolated to exhibit smoothed behavior. The computed (solid line) behavior is therefore stronger than the measured (dashed line, Figure F-2(a)), after the break is the original data. Agreement between measured and computed behavior before the break is very good. The cyclic triaxial test results were given as strain and pore pressure versus number for cycles (Figure F-3). No stress-strain data was recorded. The deviatoric stress versus strain results of the simulated cyclic triaxial test are shown in Figure F-4(a). Figure F-4(b) shows the undrained stress path behavior of the model.

Figure F-3 shows the comparison of measured and simulated behavior for axial strain and pore pressure versus number of cycles.

Figure F-5(a) and (b) show the simulation results for the cyclic simple shear test. Figure F-5(a) shows the simulated shear stress versus shear strain results. Figure F-5(b) shows the simulated stress path results. Figure F-6 shows the measured and simulated results for pore pressure and shear strain versus number of cycles.

Agreement for both cyclic tests was marginal. The primary difficulty encountered was matching the large generation of pore pressure measured in the first cycle in both tests. This factor, when modeled correctly, led to numerical liquefaction in two or three cycles. Figures F-4 and F-5 are therefore representative of a material which qualitatively models the pore pressure generation but does not reflect the cyclic capability of the two tests.

Soil Column Simulation

The finite element model for the soil column described above consisted of 14 isoparametric quadrilateral elements. The finite element mesh is shown in Figure F-7. Each node in the mesh was defined to have two solid and two fluid degrees of freedom. Nodes 1 and 2 were fixed against vertical motion. Horizontal motion for nodes 1 and 2 was defined by the input accelerations from the load time function. Nodes 3 to 30

were linked by assigning the same equation number to each pair of nodes on every layer (i.e., 3 and 4, 5 and 6, etc.). Use of this technique simulates a continuum of material in the horizontal direction and enforces the translation of shear-only waves up the column. Figures F-8a, b, c, and d show computed acceleration response for nodes 1, 10, 20, and 28, respectively. The measured response for the same points is shown in dashed lines. Agreement between computed and measured accelerations is very good up to 0.10 second. The computed acceleration drops to zero at that point due to the liquefied state of the soil near the base. Figure F-9 shows the computed vertical surface accelerations. Figures 10a, b, c, d, and e show the computed pore pressure response for elements 1, 2, 5, 10, and 14. Figure F-10(a), element 1, shows excellent agreement between computed (solid line) and measured pore pressure response (dashed line), up to liquefaction. Figure F-10(b) shows the computed pore pressure behavior one element above the base. The behavior is very similar to that exhibited in element 1. Figures F-10(c) and (d) agree well with the measured behavior.

Simulation of the reconsolidation at the end of shaking is not possible once liquefaction has occurred. Figure F-10(f) shows the results of shaking being stopped before liquefaction occurs, and then allowing reconsolidation to take place. The consolidation behavior (beyond 0.1 seconds) shows good agreement with measured results.

Soil Structure Simulation

The soil-structure simulation was carried out using the mesh shown in Figure F-11. The mesh consists of 136 two-phase and 16 single-phase quadrilateral elements. The boundary conditions at the base of the mesh are fixed against translation in both the horizontal and vertical directions. The vertical boundaries were restrained using the model slaving procedure described above. The vertical interface between the soil and structure were bridged with six frictional contact elements. Figure F-12 shows idealization of the soil-structure interface.

Figures 13(a) and (c) show the input horizontal accelerations along the base of the mesh and the computed accelerations at node 9, respectively. Agreement between the computed and measured response is acceptable. Figures F-14(a) and (b) show the computed horizontal and vertical accelerations on the structure.

Figures 15(a), (b), and (c) show the computed pore pressure for elements 17 and 20 in the free field away from the structure. Agreement between the computed behavior recorded in the soil column tests is very good. Figures F-16(a), (b), and (c) show the computed excess pore pressure histories from directly below the structure (elements 69, 71, and 73). Note the increase in time required to reach the maximum pore pressure compared with that computed in the free field. The agreement between the computed and measured behavior, up to liquefaction, beneath the structure is acceptable.

Figure F-17 shows deformed mesh configurations for 0.05 second. Note the outward "flow" of material from beneath the structure. This behavior is representative of failure modes predicated analytically.

MODELING ASSUMPTIONS

The finite element simulations of the Caltech centrifuge soil structure test described above incorporated contact boundaries. This technique was chosen to simulate the structural settlements with relation to the soil surface. The centrifuge test showed these settlements (1/2 of the exposed structure length) to be significant.

Another modeling technique that would produce good results with respect to accelerations and pore pressures is to treat the soil-structure system as a continuum with no discontinuities. This involves modeling the soil-structure interface in perfect contact, and allowing pore-water migration to occur across that interface, controlled by very low permeability. This technique removes some validity in the behavior very close to the structure, but greatly eases the computational problems. The structure, in this case, is treated as a poro-elastic solid with unit weights for the material selected such that the real structure buoyant weight is modeled correctly.

PROBLEMS AND SOLUTIONS

The behavior of the solution as modeled (with contact interfaces) was extremely difficult to control. The problems arise from the contact element stiffness, and high frequency noise being developed due to these elements. This resulted in a high degree of numerical "resonance" (unreasonably high accelerations) induced into the soil, at the interface. This was "controlled" by increasing the numerical damping in the Newmark's integration procedure. Pore fluid migration at the discontinuity also induced problems. Because the contact element does not restrain the pore fluid, those degrees of freedom had to be "fixed" for the solution to proceed. This fixity seems to produce other difficulties as they are a rigid point in the fluid. Thus, as the accelerations are integrated and displacements are computed for the solid phase, the fluid phase is rigidly restrained. This factor definitely effects the behavior (and validity) of the finite element model. The solution to the problem, without code modification, is to either ignore the effects, or lower the water table. Either choice brings out essentially the same results. It is good to note at this point that the poro-elastic structure does not suffer from either the contract element difficulties or the problems associated with the pore water degrees of freedom being fixed.

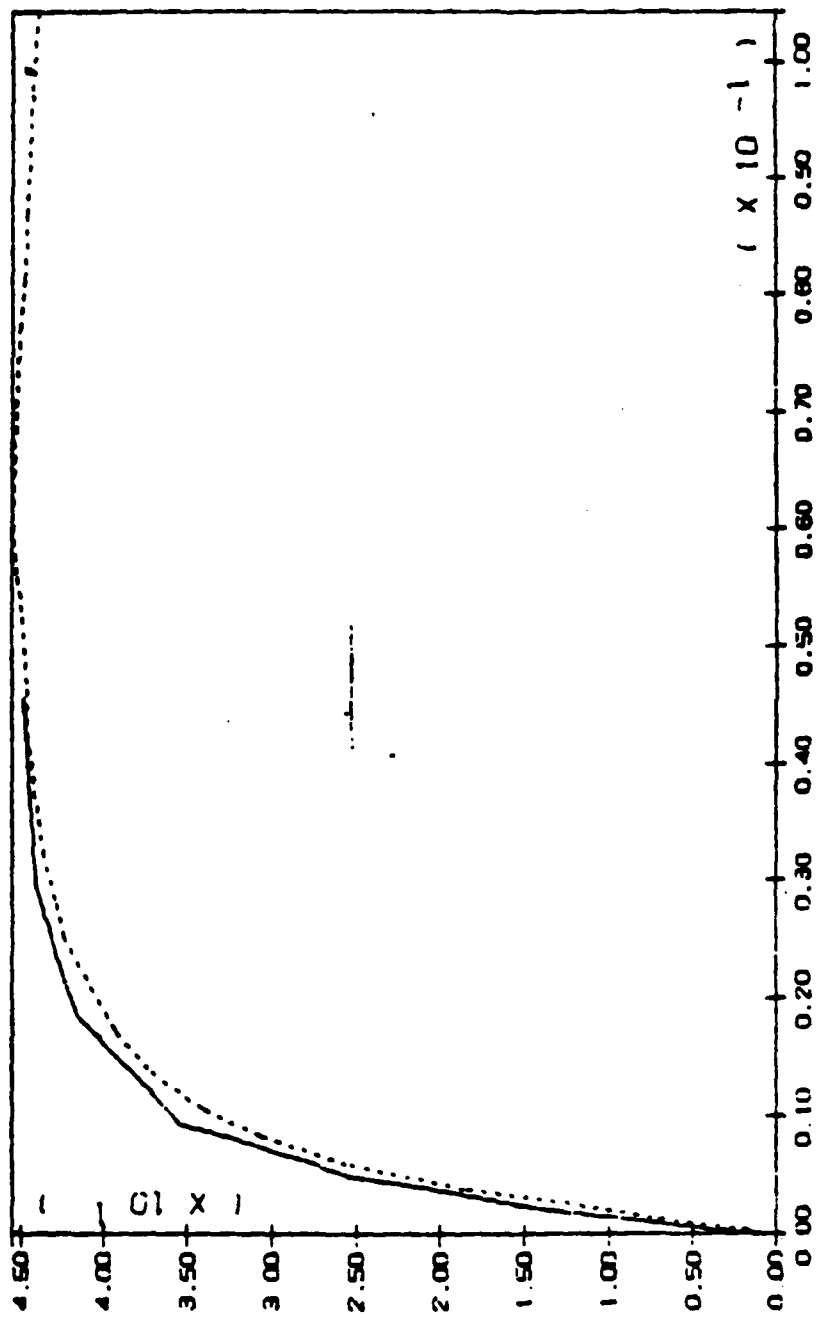
Table F-1. Soil Parameters, Nevada Sand

$\rho_s = 0.0975 \text{ lb/in}^3$	Mass density, solid grains
$\rho_w = 0.0361 \text{ lb/in}^3$	Mass density, fluid
$n = 0.457$	Porosity
$l \leq 0.006 \text{ in/s}$	Friction angle, compression
$\phi_c = 33^\circ$	Friction angle, extension
$\phi_e = 29^\circ$	Elastic shear modulus
$G_i/p_i = 3600 \text{ lb/in}^2$	Elastic bulk modulus
$B_i/p_i = 2400 \text{ lb/in}^2$	Reference pressure
$\eta = 0.5$	Power exponent
$\eta_c = 0.88$	Critical stress ratio, compression
$\eta_e = 0.76$	Critical stress ratio, extension

Resulting Model Parameters				
Yield Surface Number	α Surface Location	m Surface Size	H'_c/p_i Plastic Compression Moduli	H'^1_E/p_i Plastic Extension Moduli
1	0.027	0.15	10000.0	15000.0
2	0.054	0.25	9000.0	14000.0
3	0.158	0.48	8050.0	13080.0
4	0.056	0.55	2674.0	7561.0
5	0.013	0.73	854.0	3064.0
6	0.066	0.93	173.6	800.0
7	0.070	1.29	48.5	256.7
8	0.063	1.42	37.7	207.2
9	0.035	1.48	22.6	125.0

..... PLOTTED BY 100 111 ON 100 (10)
 DO YOU WANT THIS PLOT SENT TO ANALOG PLOTTER ?
 Answer [Y] YES [N] NO

NEVADA SAND DRAINED CELL PRESS = 13.889 AXIAL COMP

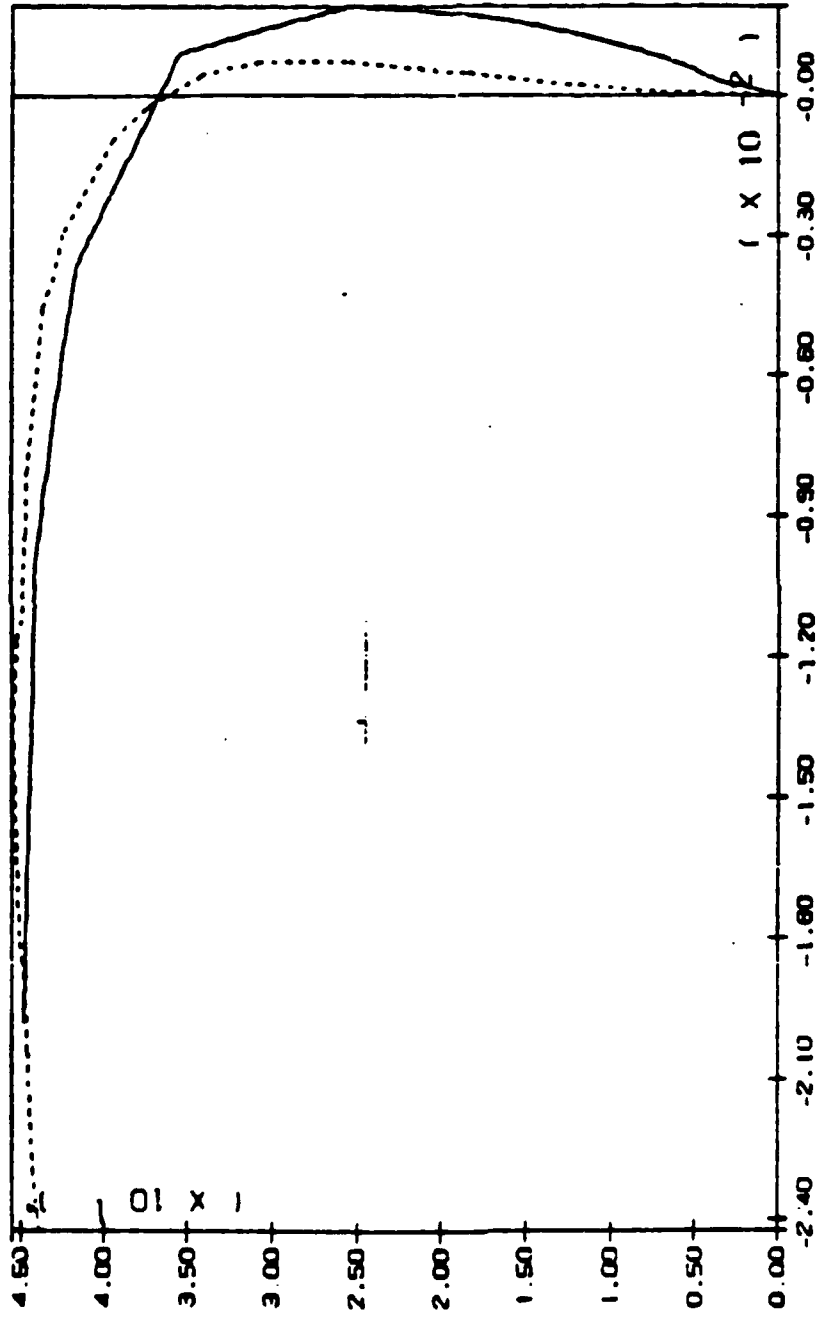


S11 - S22 VS E11 - E22 NO. OF EXPERIMENTS 2
 WED. SEP 16 1987 PLOT NO. 1

Figure F-1A. Drained Triaxial Compression Simulation for the Nevada Sand

..... NUMBER OF VOLS (17) 00 00 000

NEVADA SAND DRAINED CELL PRESS = 13.889 AXIAL COMP



P VS EV

NO. OF EXPERIMENTS 2

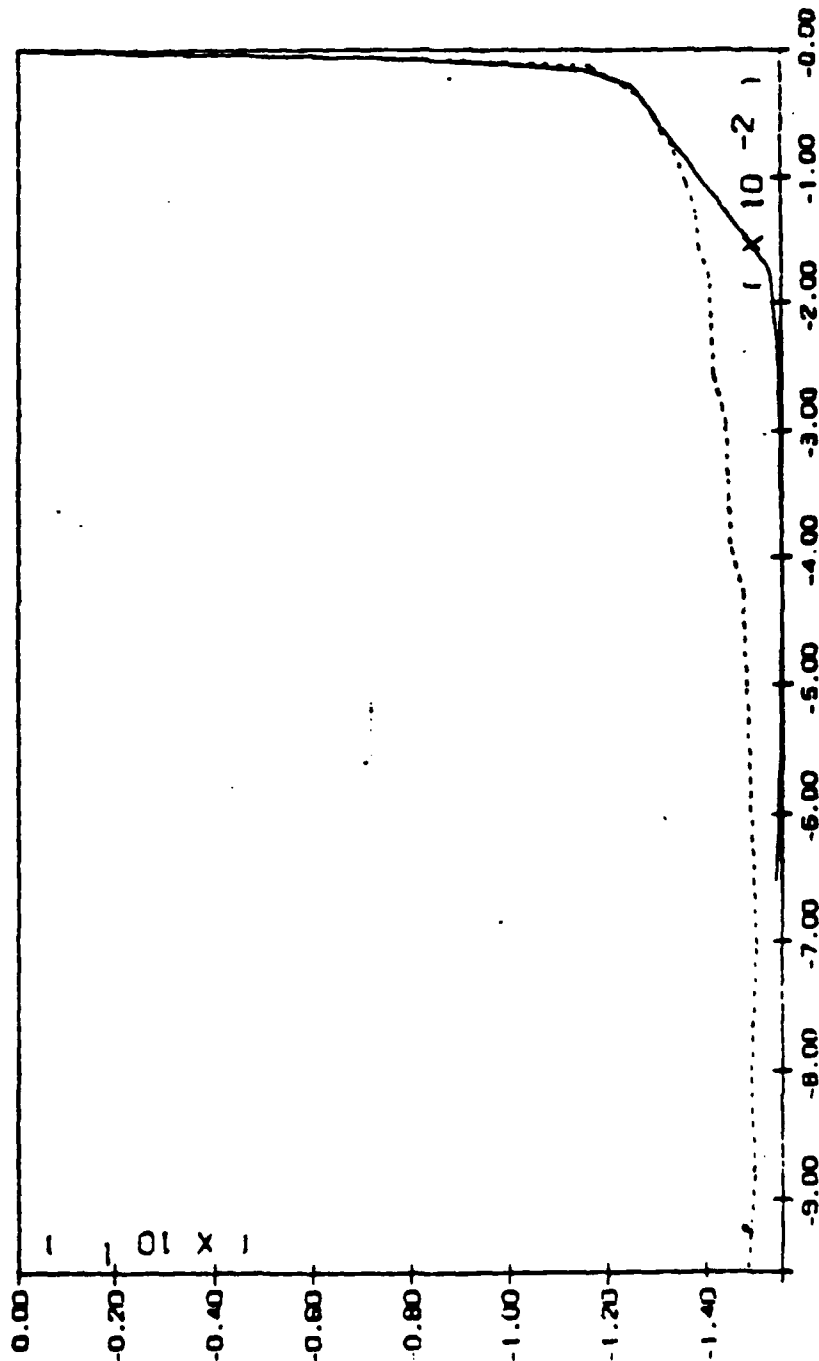
WED. SEP 16 1987 PLOT NO. 3

NO. VOLS. USED 17 VOLS. FILE NO. 00 00 000

Figure F-1B. Drained Triaxial Compression Simulation
for the Nevada Sand

..... Modified by VES 1971 03 10 101

NEVADA SAND DRAINED CELL PRESS = 13 889



S11 - S22 VS E11 - E22

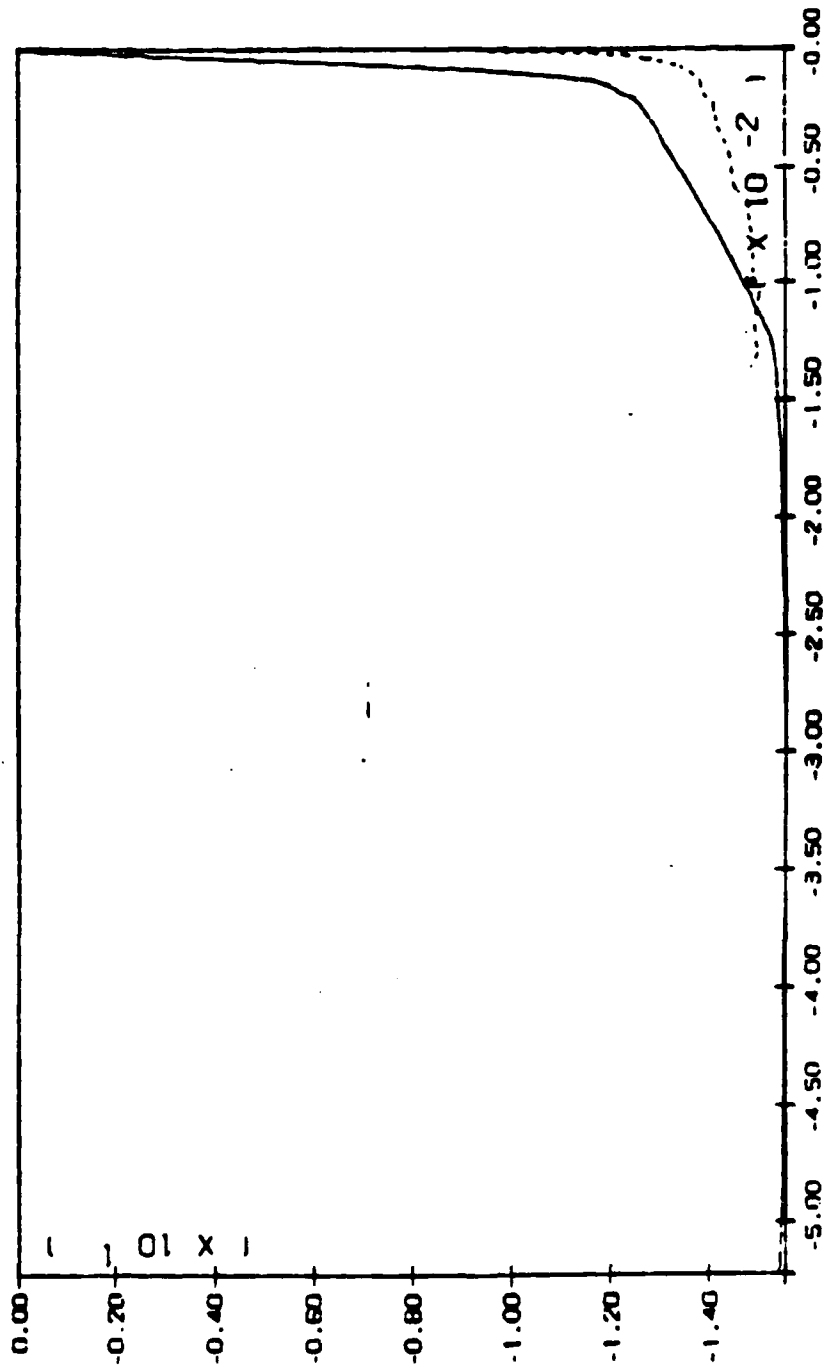
NO. OF EXPERIMENTS 2

WED. SEP 16 1987 PLOT NO. 1

Figure F-2A. Drained Triaxial Extension Simulation for the Nevada Sand

***** GENERATED BY NED (17) 08 08 08 (88)

NEVADA SAND DRAINED CELL PRESS = 13.889



P VS EV

NO. OF EXPERIMENTS 2

WED. SEP 16 1987 PLOT NO. 3

Figure F-2B. Drained Triaxial Extension Simulation for the Nevada Sand

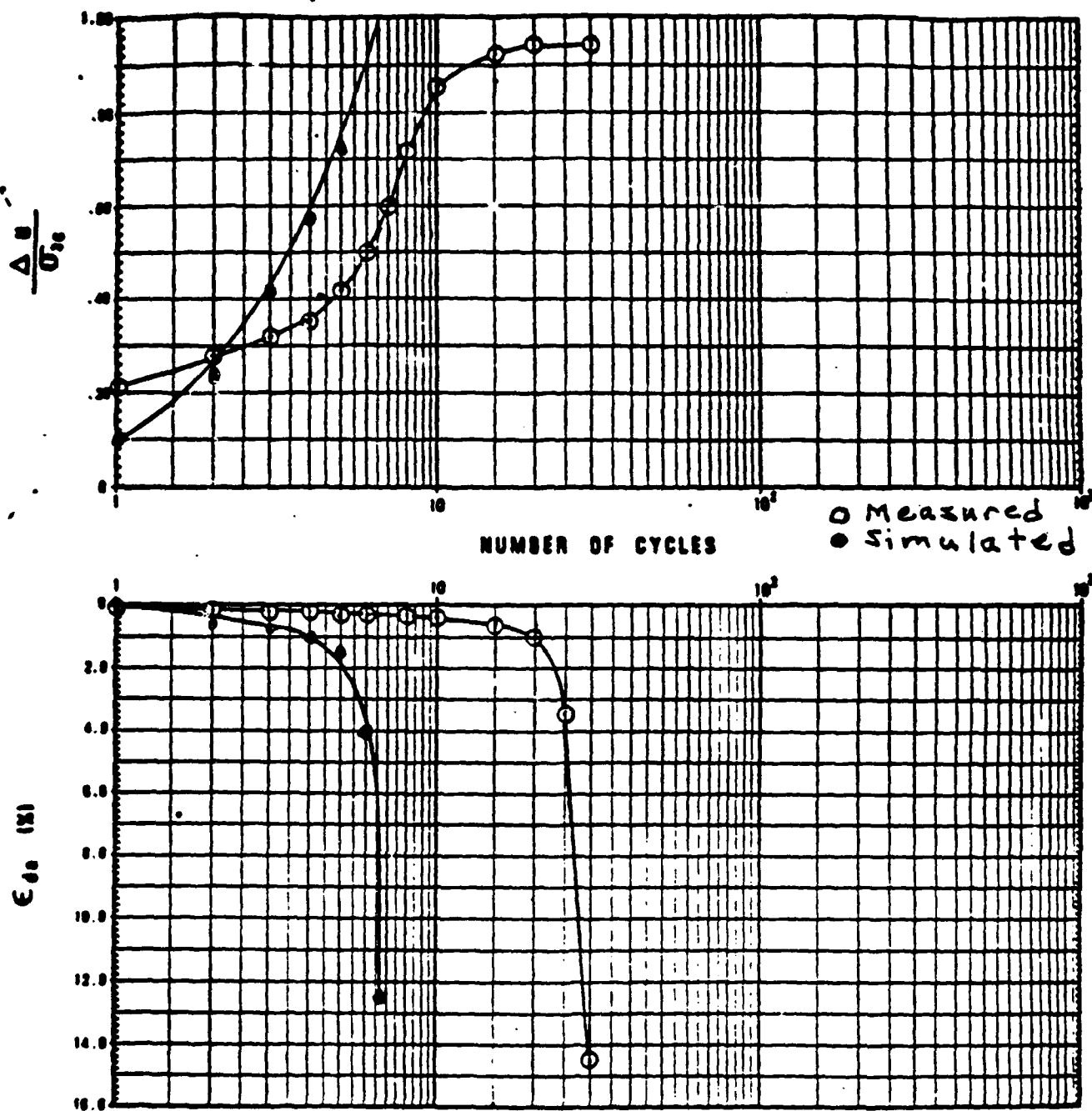
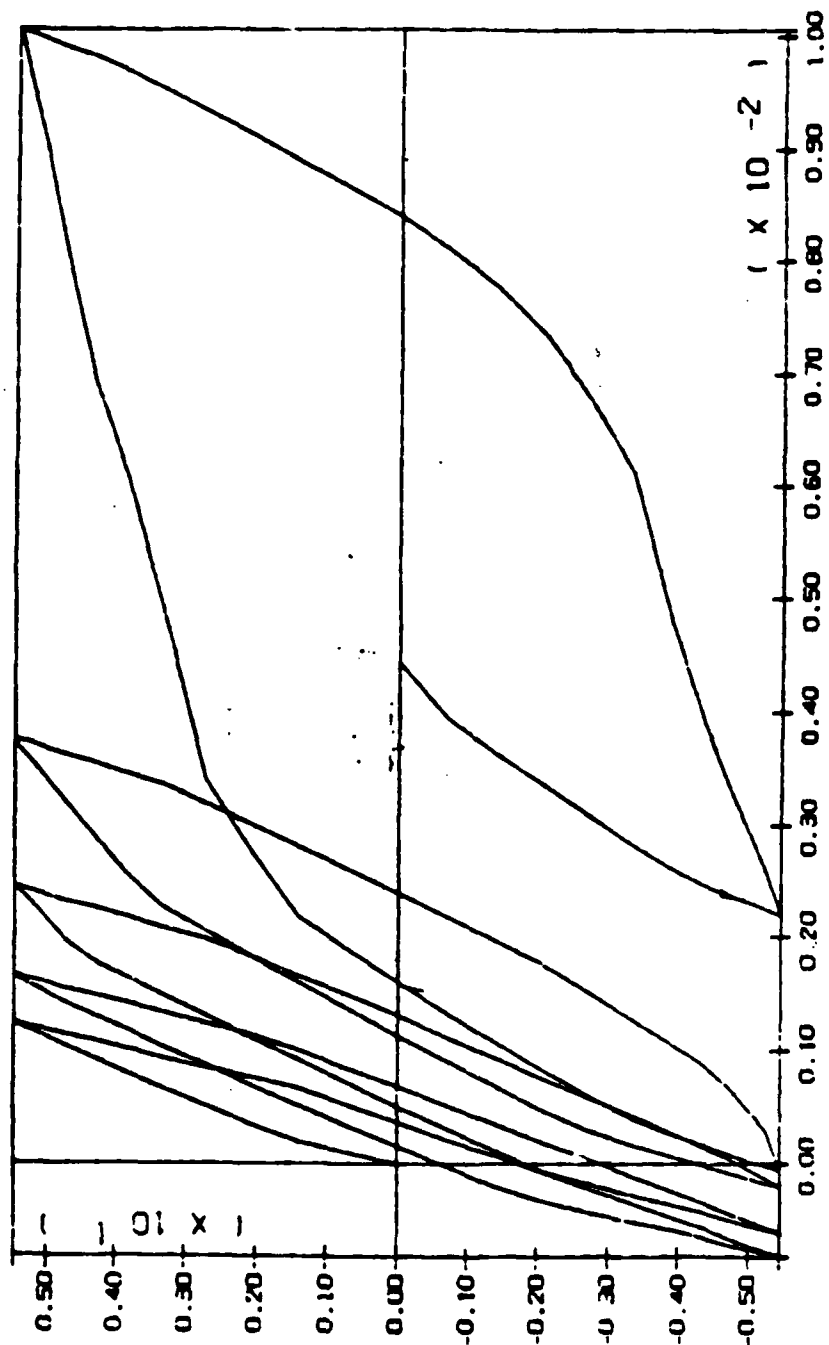


Figure F-3. Simulated and Measured Undrained Cyclic Triaxial Results

***** REVISED BY VLS (V) 08/80 (88)

NEVADA SAND DRAINED CELL PRESS = 13.869



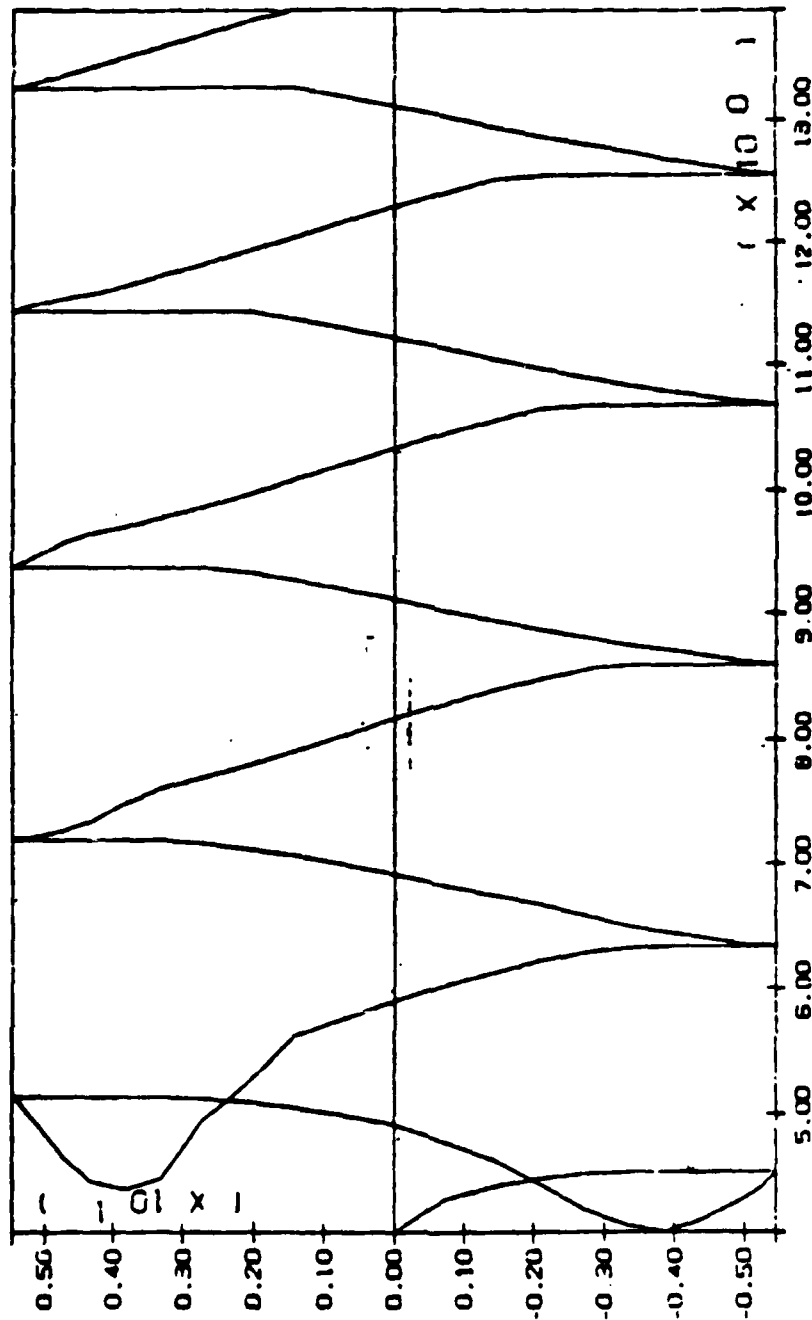
S11 - S22 VS E11 - E22
NO. OF EXPERIMENTS 2
WED. SEP 16 1987 PLOT NO. 1

NO. OF EXPERIMENTS 2

Figure F-4A. Cyclic Undrained Triaxial Simulation

----- GENERATED BY VES (V) ON 08/08/87

NEVADA SAND DRAINED CELL PRESS = 13.889



S11 - S22 VS P
NO. OF EXPERIMENTS 2
WED. SEP 16 1987 PLOT NO. 3

NO. OF EXPERIMENTS 2

Figure F-4B. Cyclic Undrained Triaxial Simulation

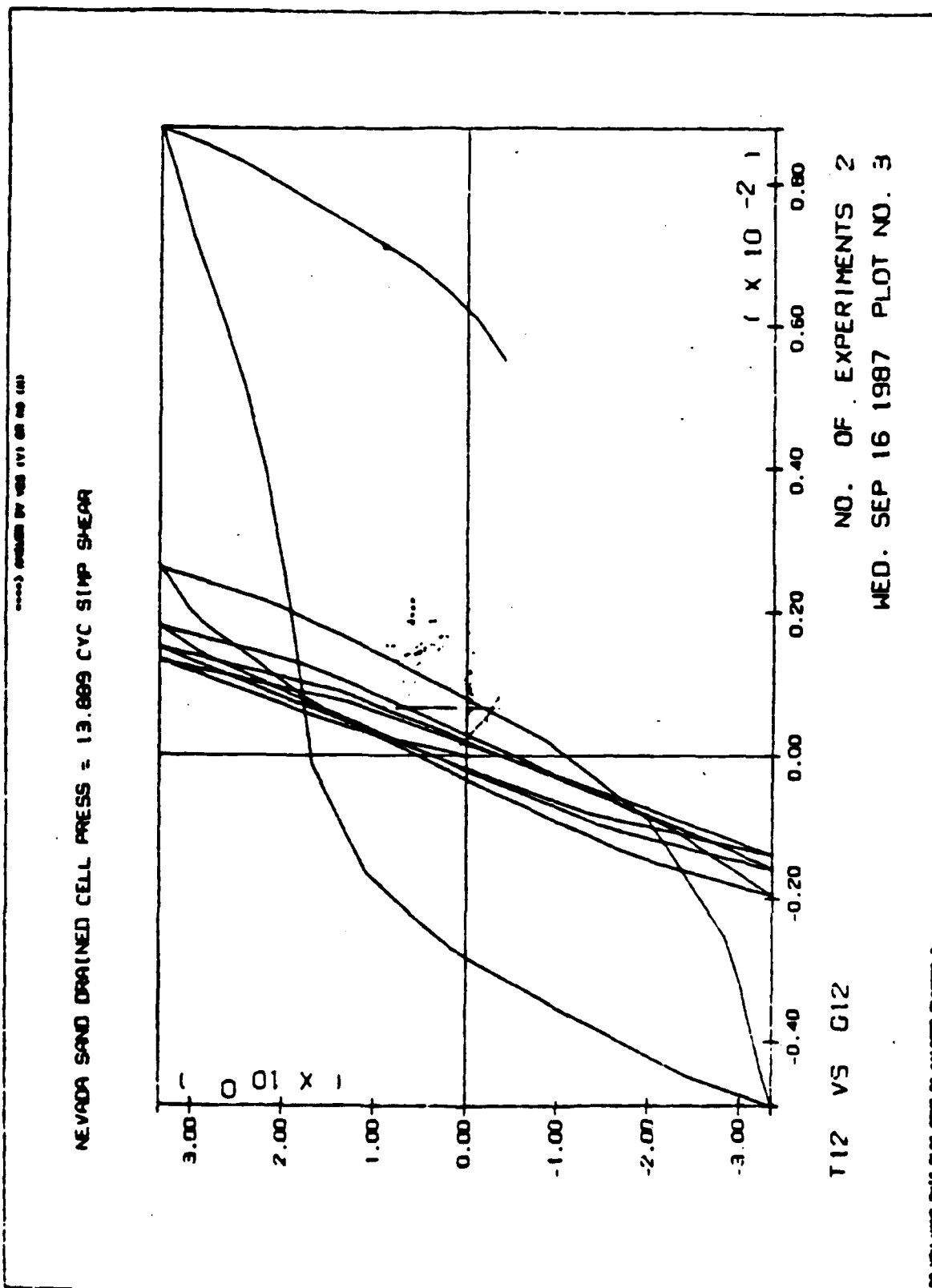
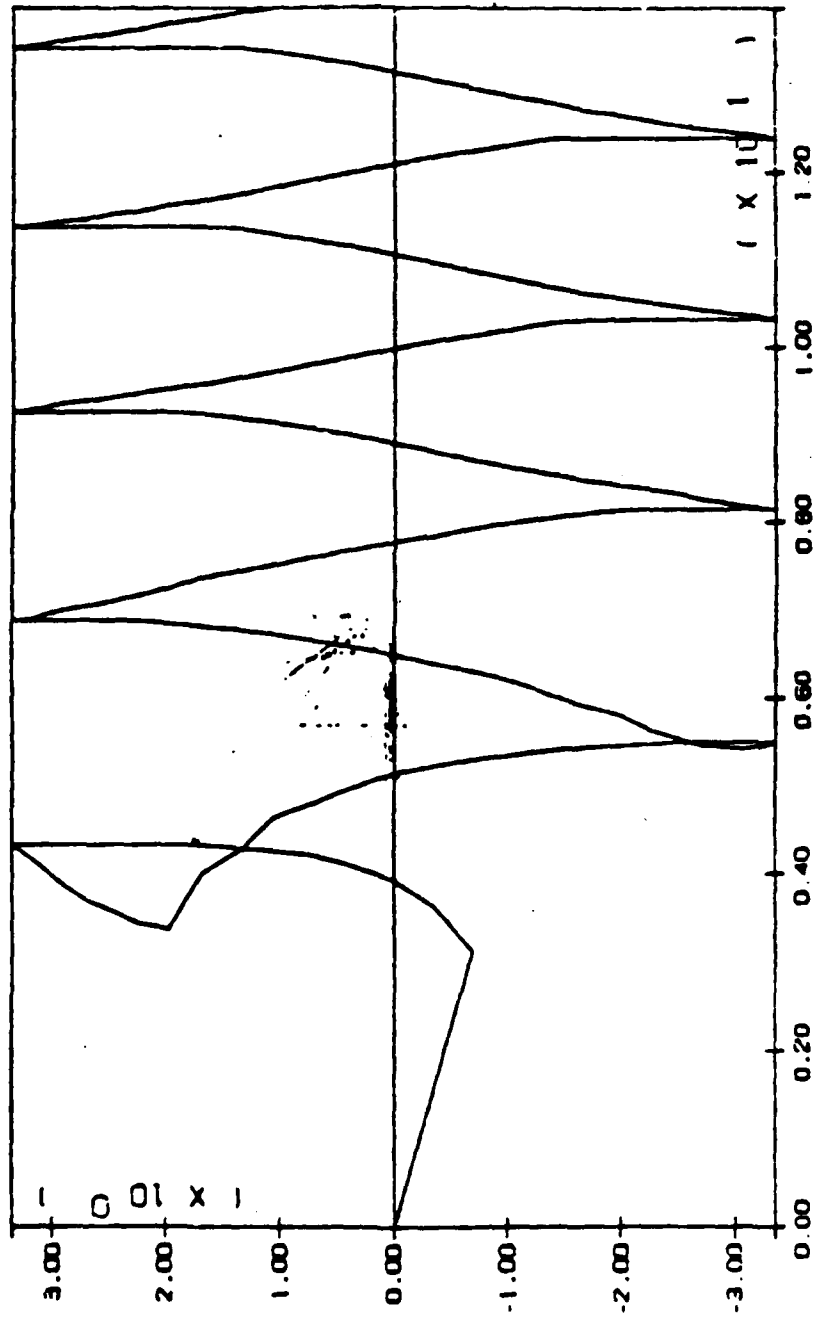


Figure F-5A. Cyclic Undrained Simple Shear Simulation

GRAPHED BY VES (11 08 88)

NEVADA SAND DRAINED CELL PRESS = 13.889 CYC SIMP SHEAR



T12 VS P
NO. OF EXPERIMENTS 2
MED. SEP 16 1987 PLOT NO. 7

Figure F-5B. Cyclic Undrained Simple Shear Simulation

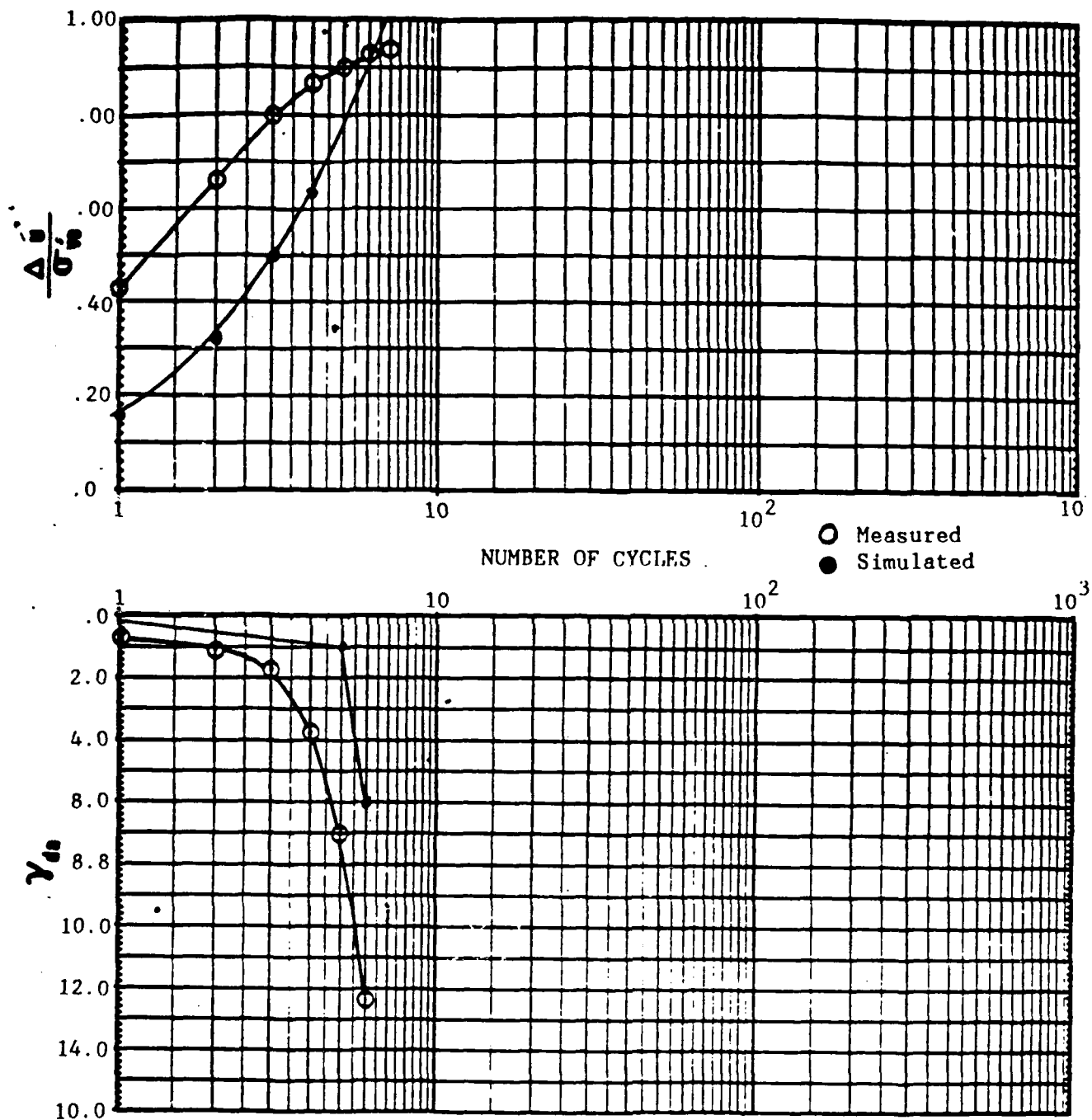


Figure F-6. Simulated and Measured Undrained Cyclic Simple Shear Results

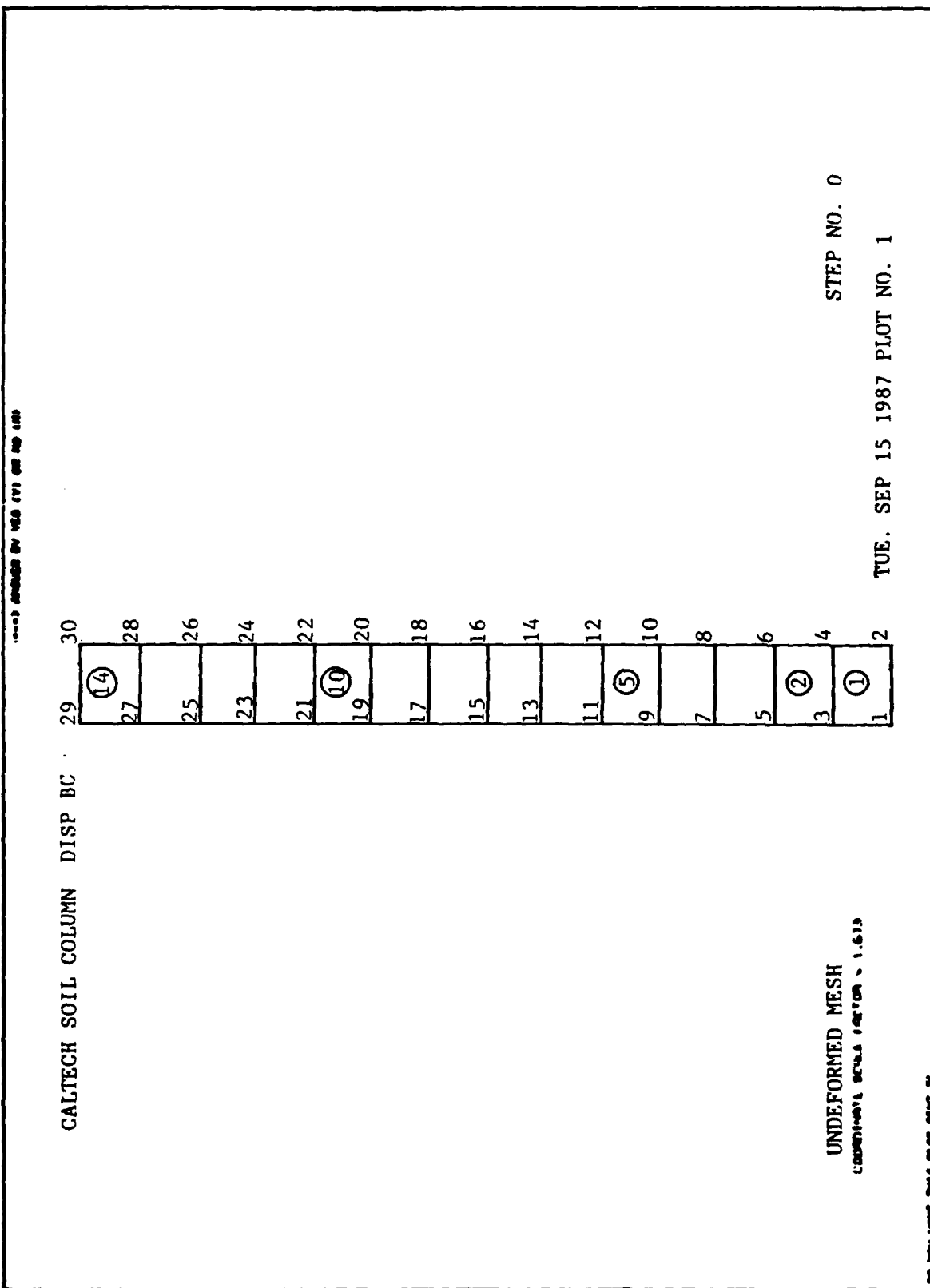


Figure F-7. Finite Element Mesh, Soil Column Simulation

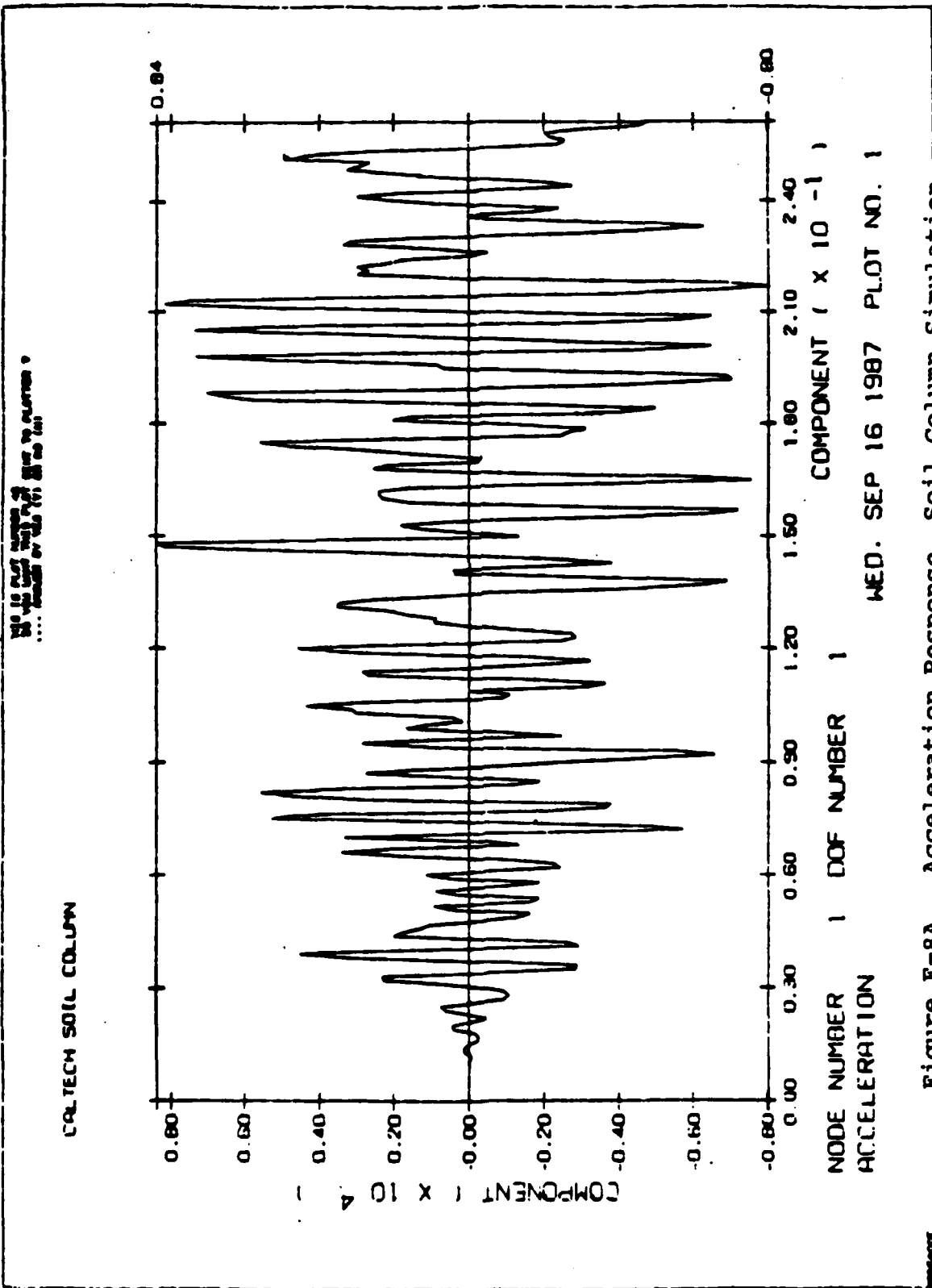


Figure F-8A. Acceleration Response, Soil Column Simulation

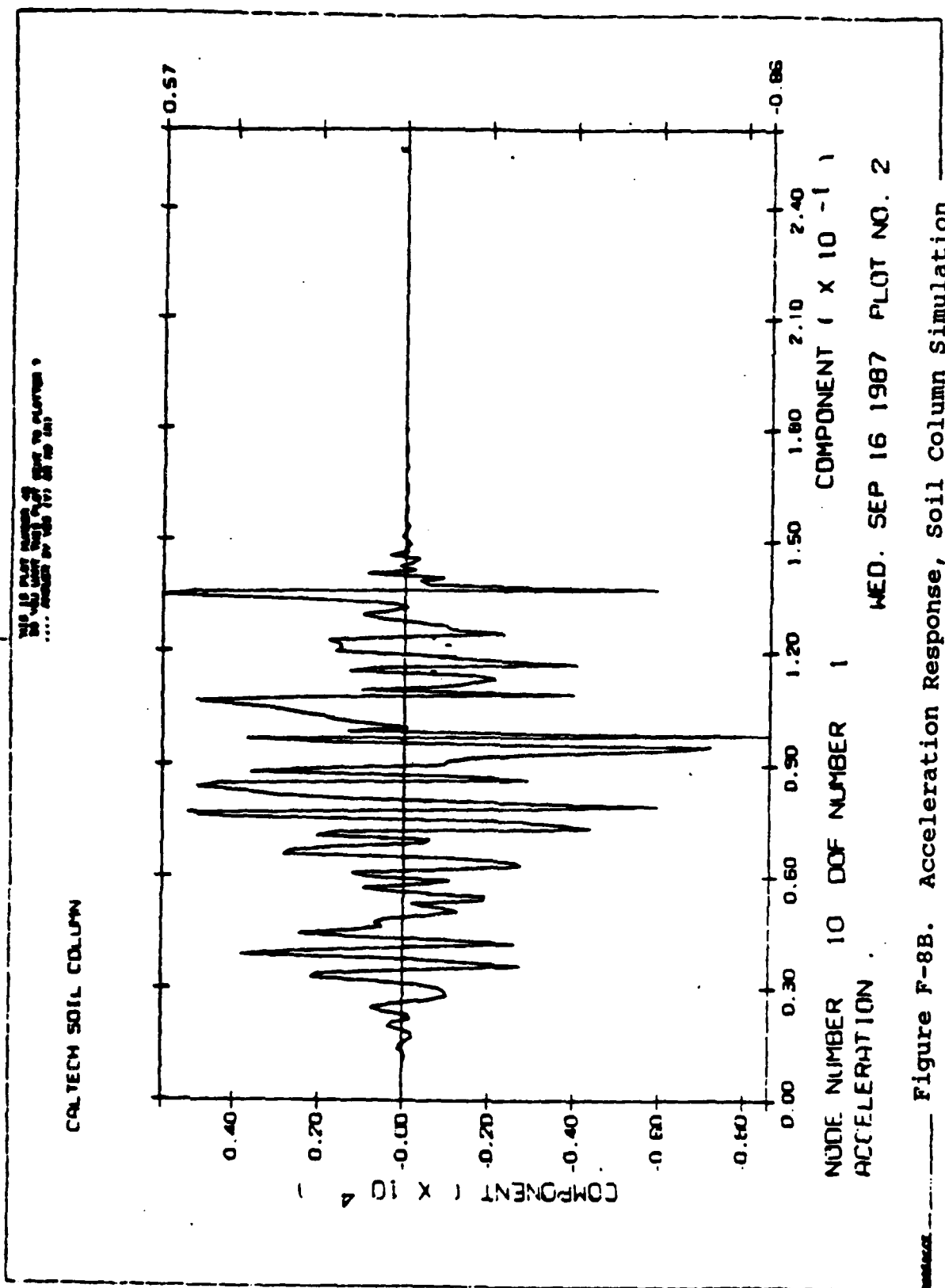


Figure F-8B. Acceleration Response, Soil Column Simulation

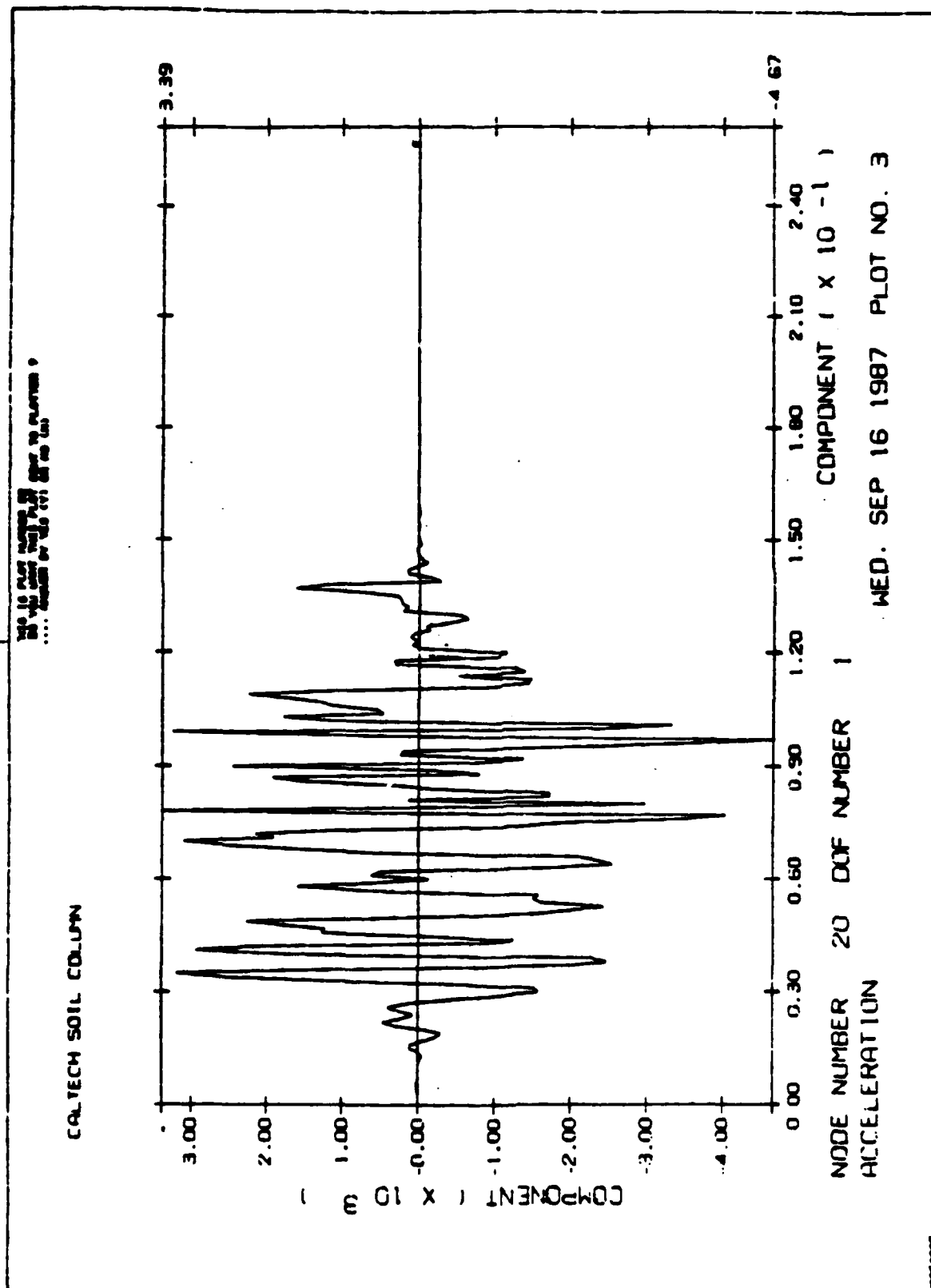


Figure F-8C. Acceleration Response, Soil Column Simulation

THIS IS A PLOT NUMBER 6
 OF THE SOIL COLUMN
 NUMBER OF 100 (100 100 100)

CALTECH SOIL COLUMN

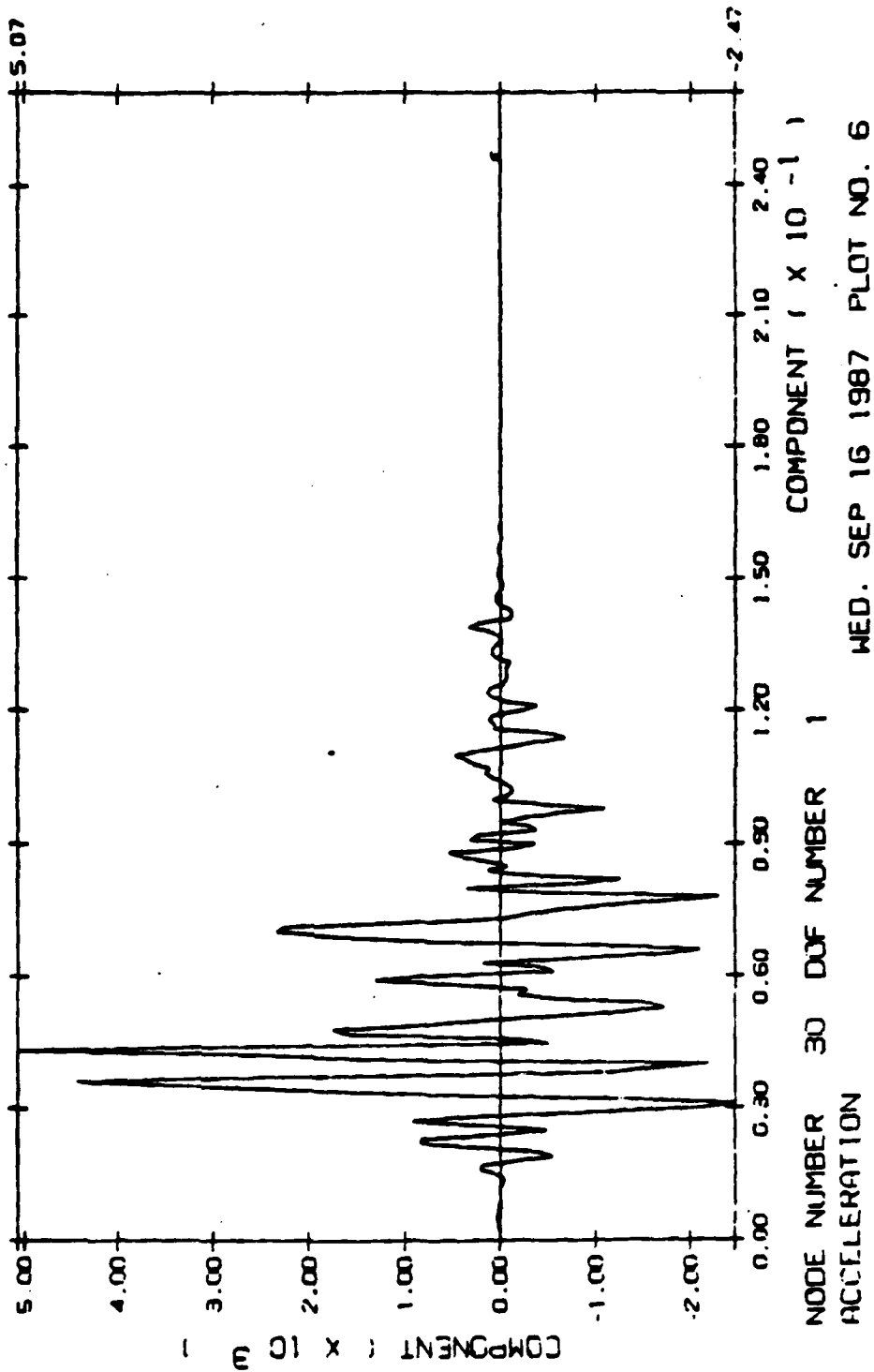


Figure F-8D. Acceleration Response, Soil Column Simulation

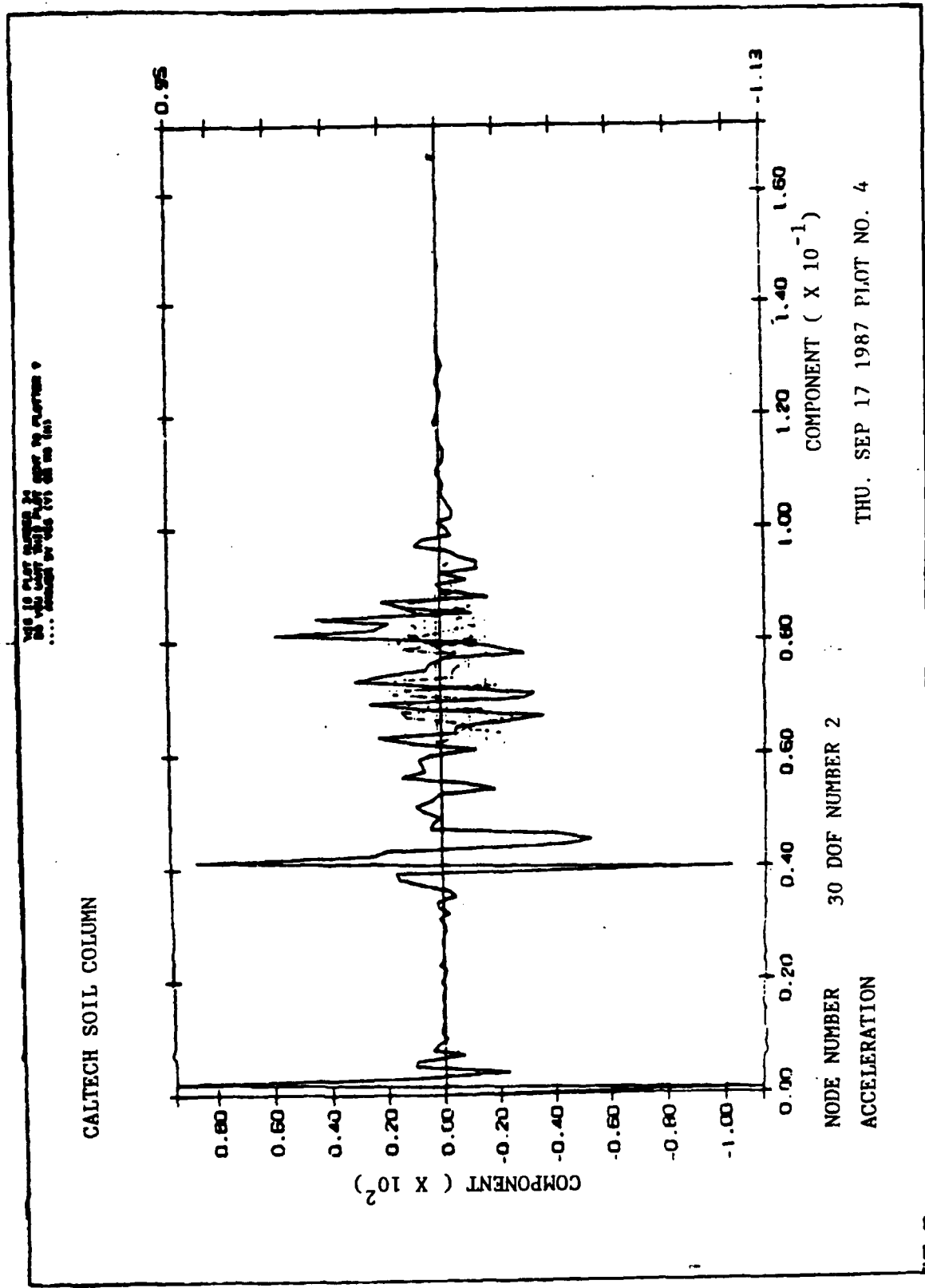


Figure F-9. Acceleration Response, Top of Soil Column

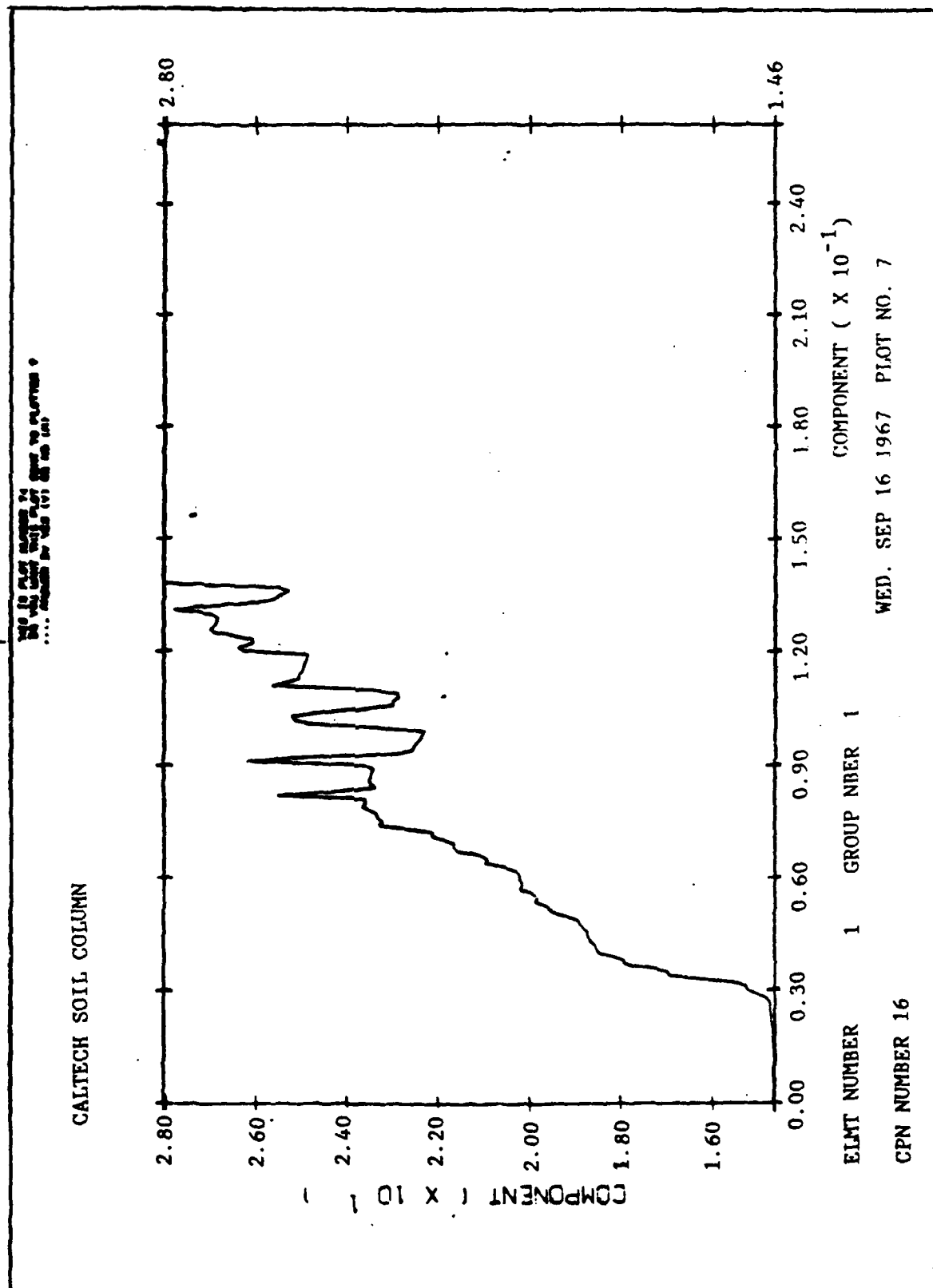


Figure F-10A. Pore Pressure Response, Soil Column Simulation

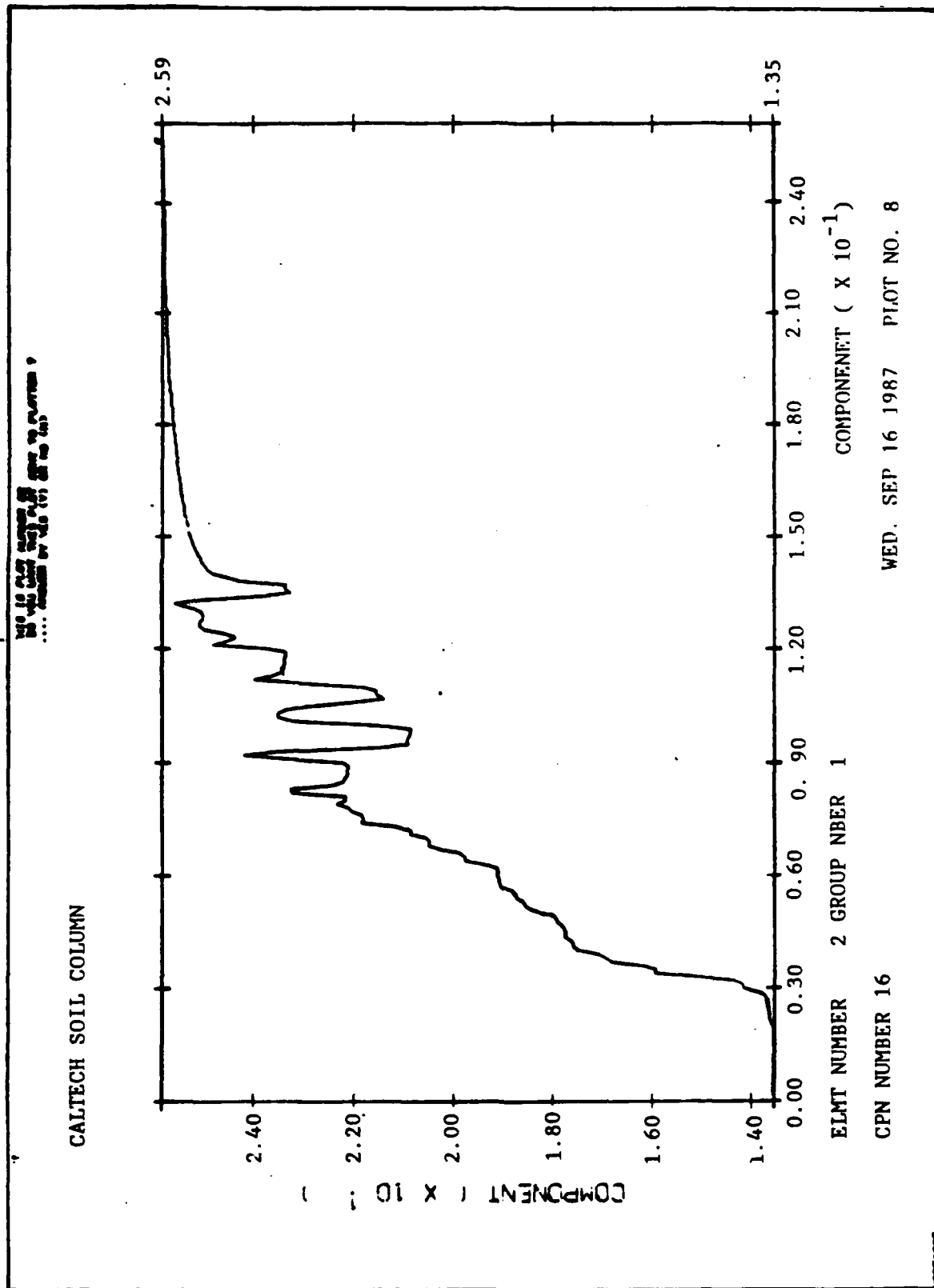


Figure F-10B. Pore Pressure Response, Soil Column Simulation

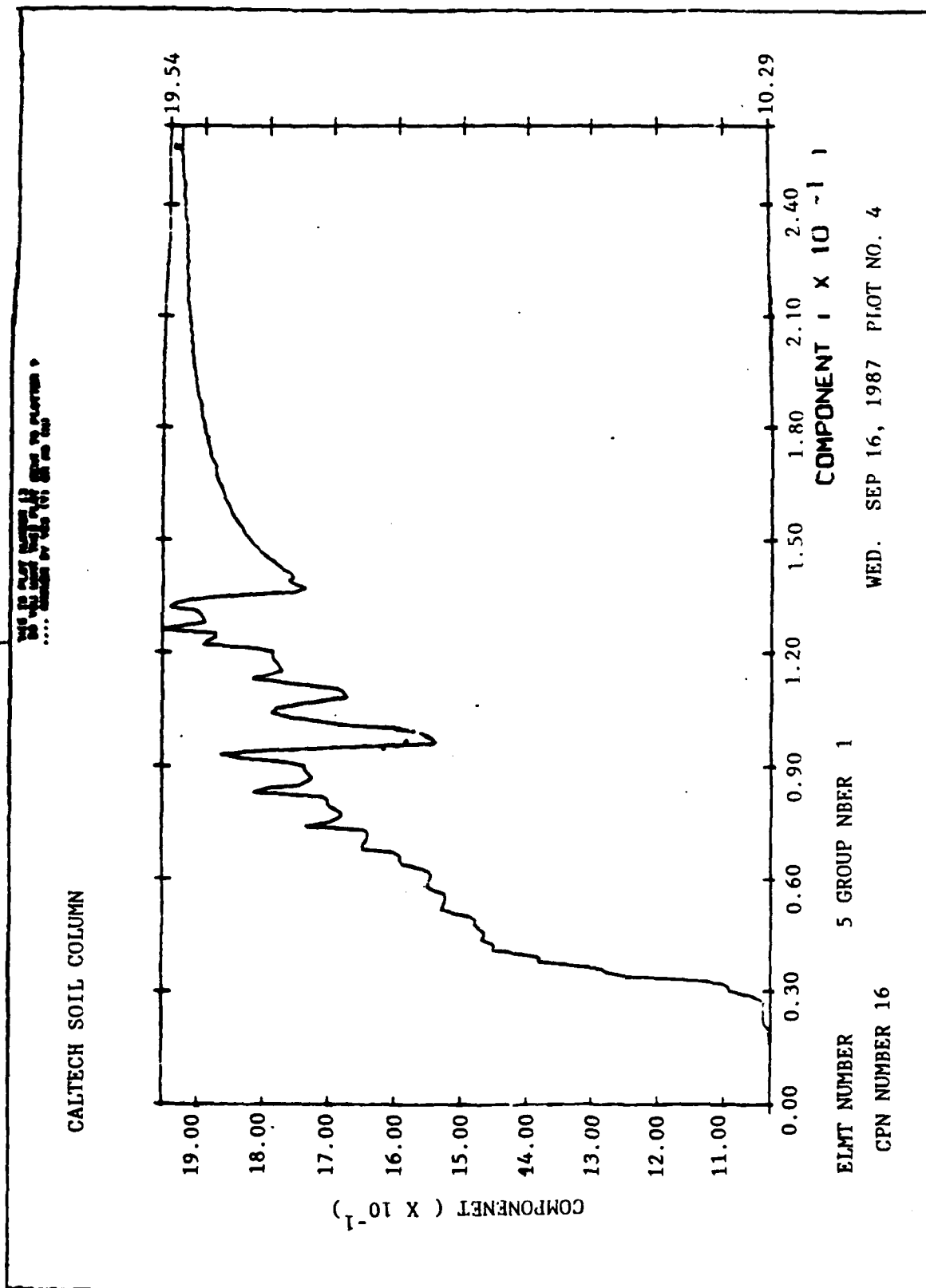


Figure F-10C. Pore Pressure Response, Soil Column Simulation

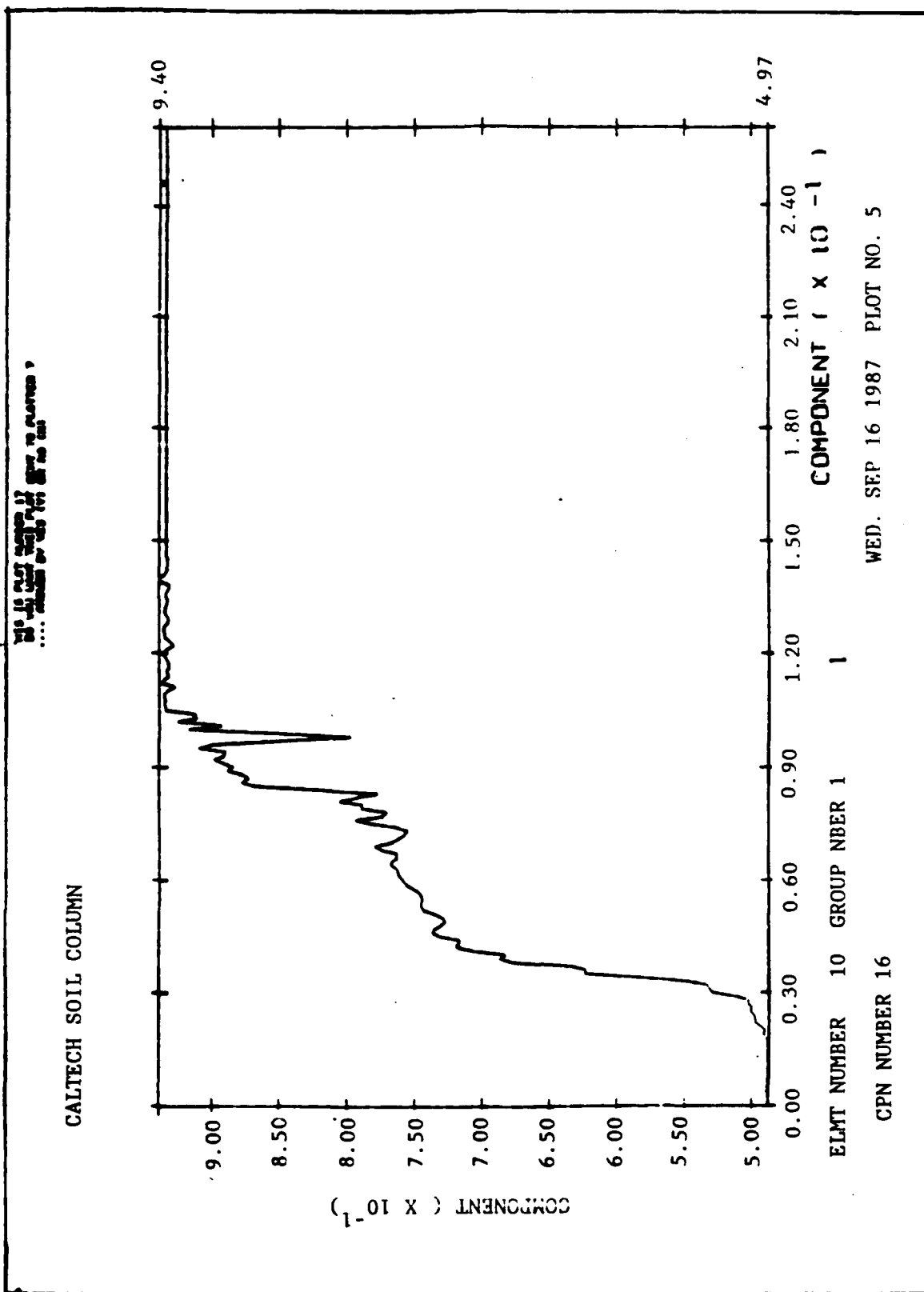


Figure F-10D. Pore Pressure Response, Soil Column Simulation

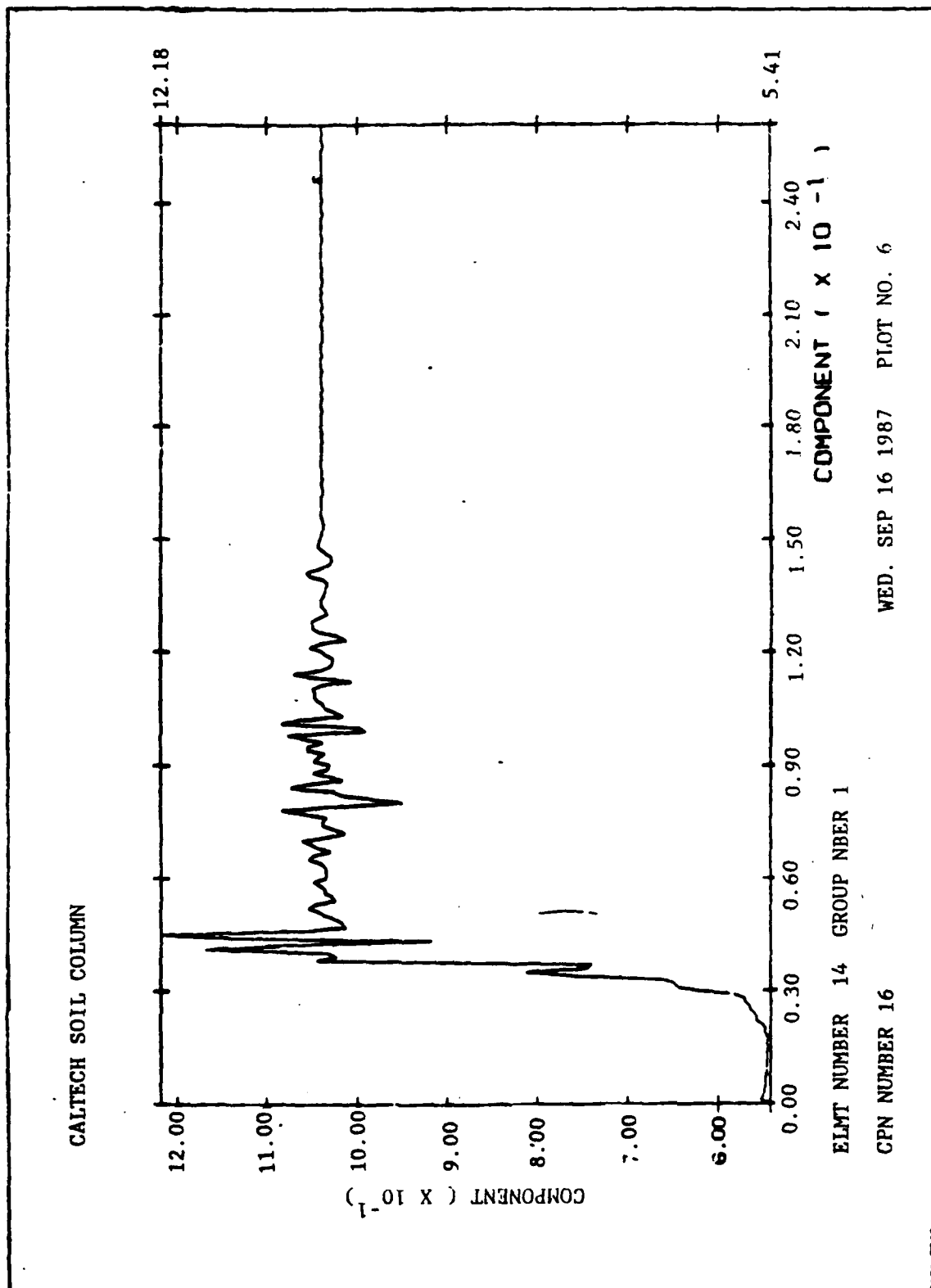
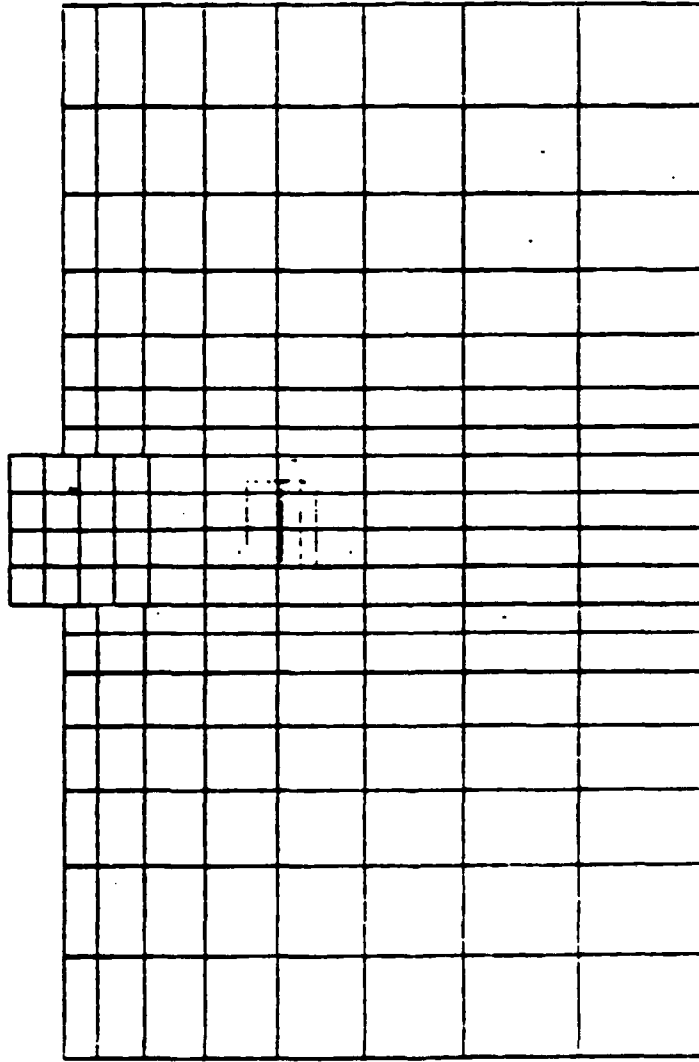


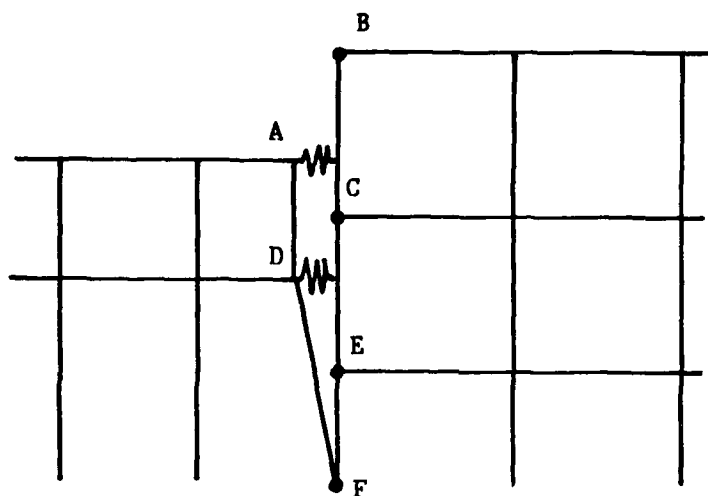
Figure F-10E. Pore Pressure Response, Soil Column Simulation



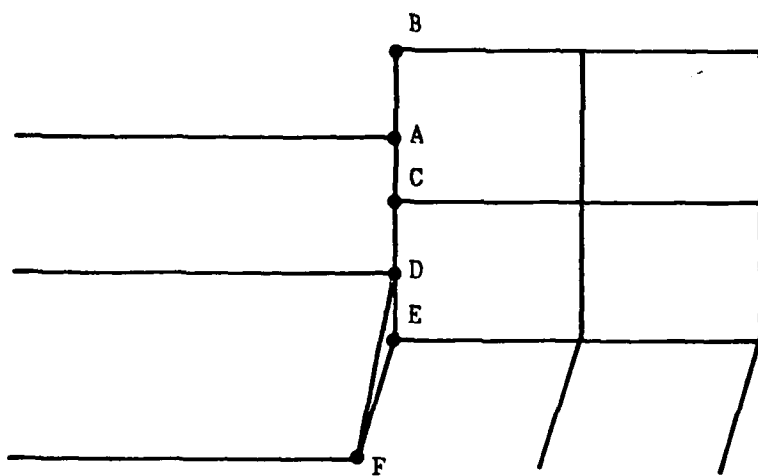
UNDEFORMED MESH

STEP NO. 0
TUE. SEP 15 1987 PLOT NO. 1

Figure F-11. Finite Element Mesh, Soil-Structure Simulation



Idealized element configuration



Typical contact in dynamic configuration

Figure F-12. Idealized Soil-Structure Interface

SOIL STRUCTURE TEST. NEVADA SAND. BEAM MODEL. ACCELERATION BC

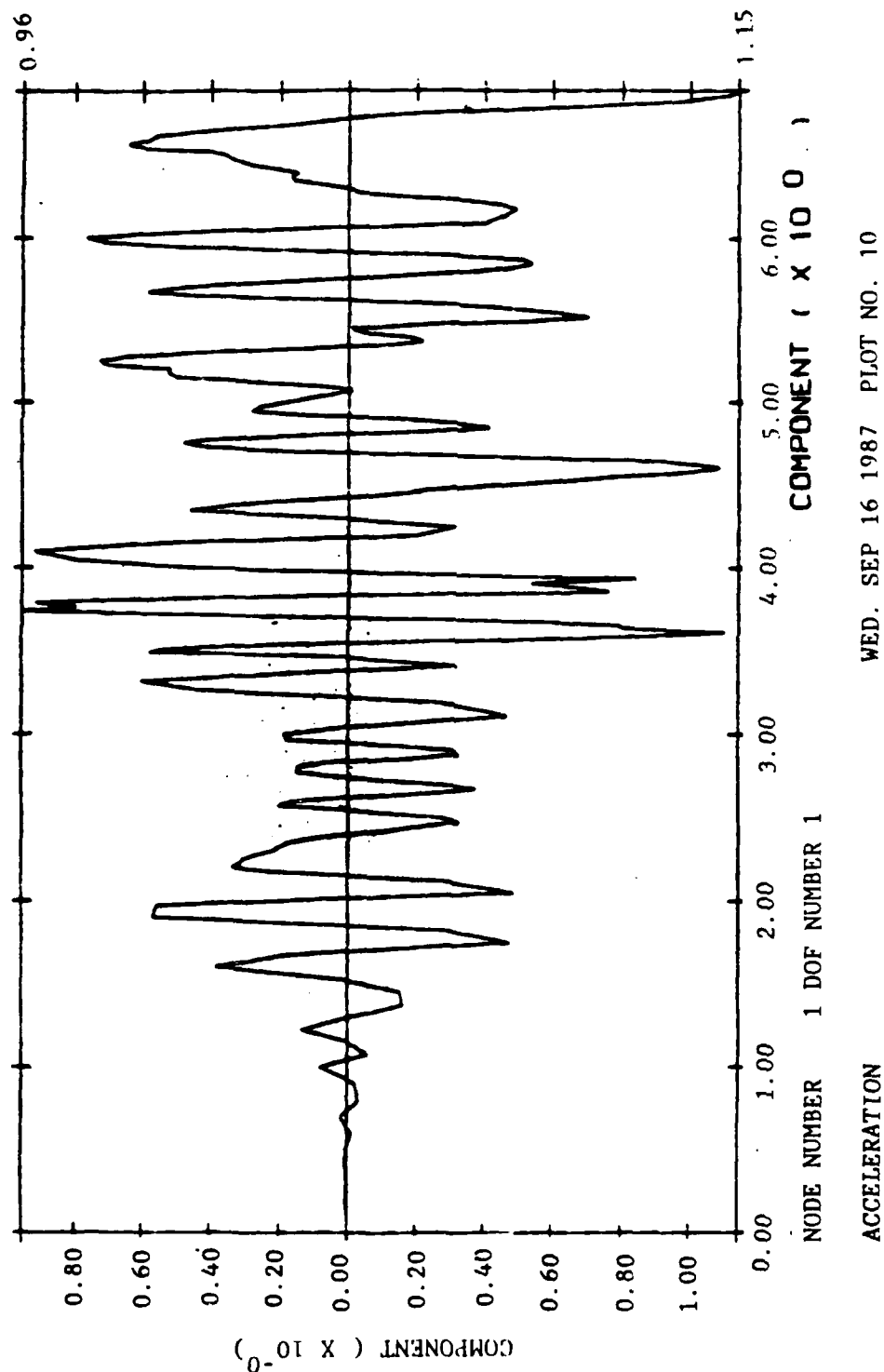
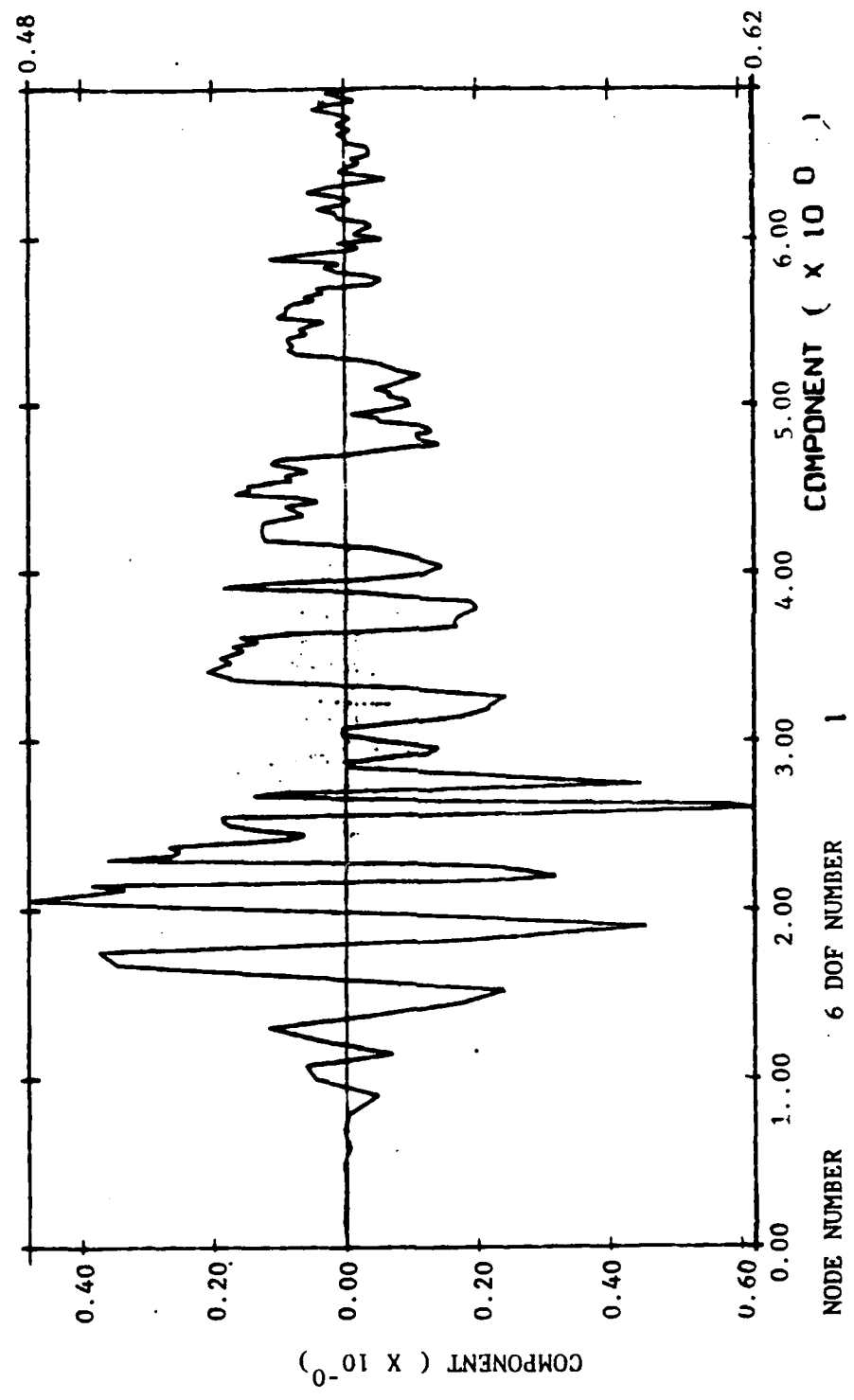


Figure E-13A. Acceleration Response, Soil-Structure Simulation

NO. 13 SEP 16 1987
 ...
 ...

SOIL STRUCTURE TEST. NEVADA SAND. BEAM MODEL. ACCELERATION BC



WED. SEP 16 1987 PLOT NO. 11

Figure F-13B. Acceleration Response, Soil-Structure Simulation

THIS IS PLOT NUMBER 21
 OF 40 PLOTS IN THE SET OF PLOTS
 ... ANALYSIS BY THE 101 20 AND 101

SOIL STRUCTURE TEST. NEVADA SAND. BEAM MODEL. ACCELERATION BC

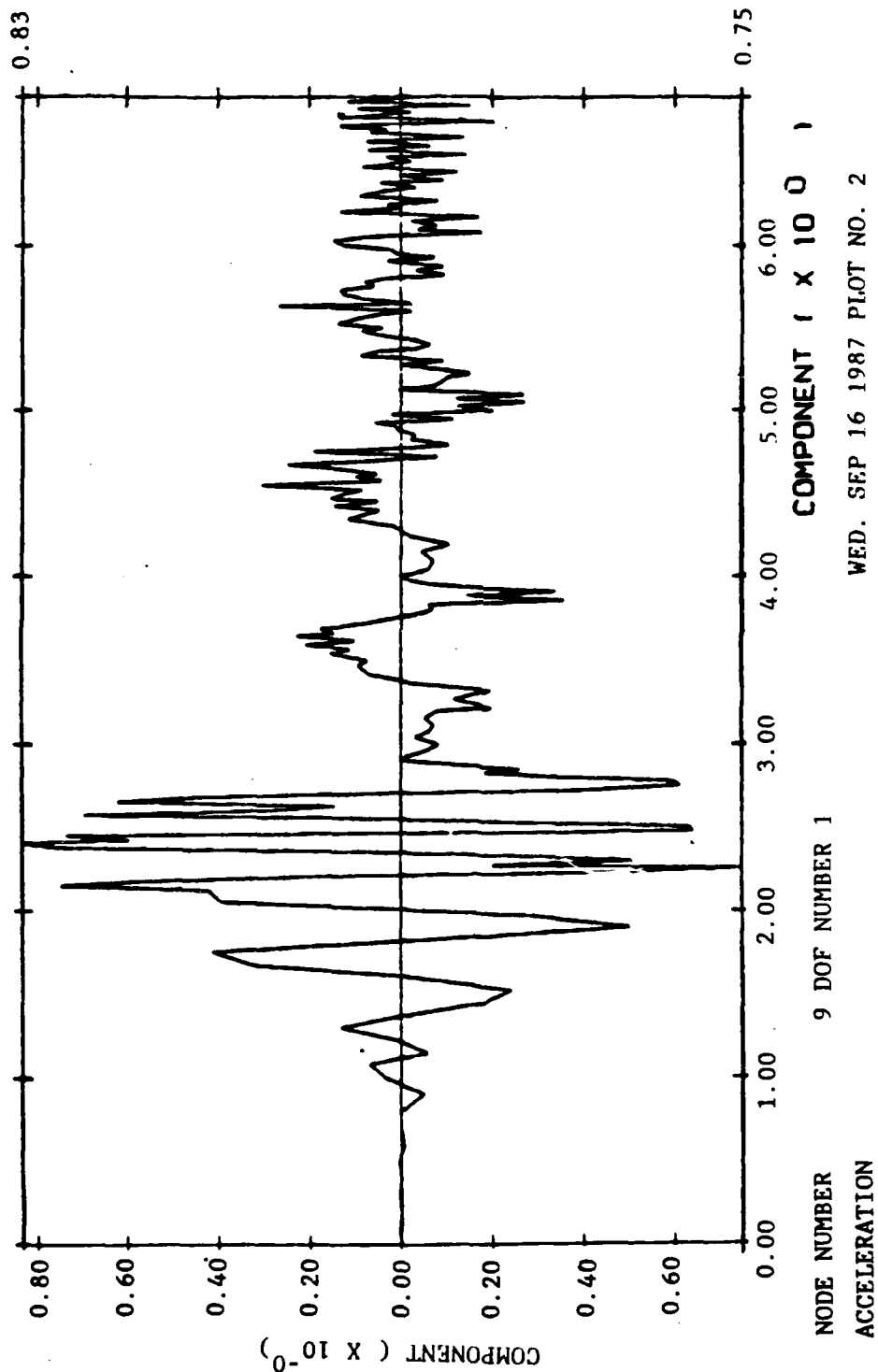
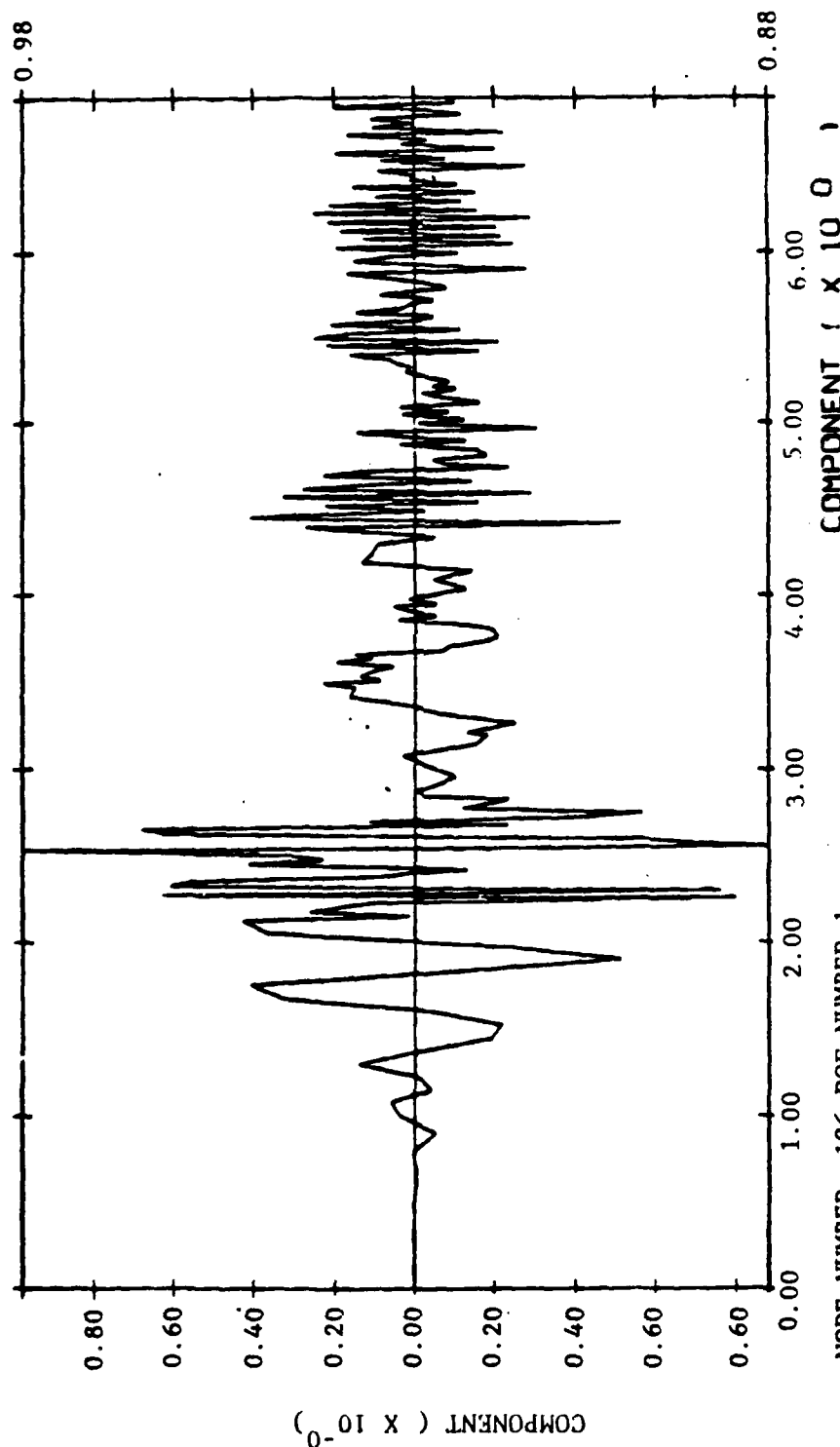


Figure F-13C. Acceleration Response, Soil-Structure Simulation

THIS IS A PLOT OF THE
 SOIL STRUCTURE TEST. BEAM MODEL. ACCELERATION BC
 ...

SOIL STRUCTURE TEST. NEVADA SAND. BEAM MODEL. ACCELERATION BC



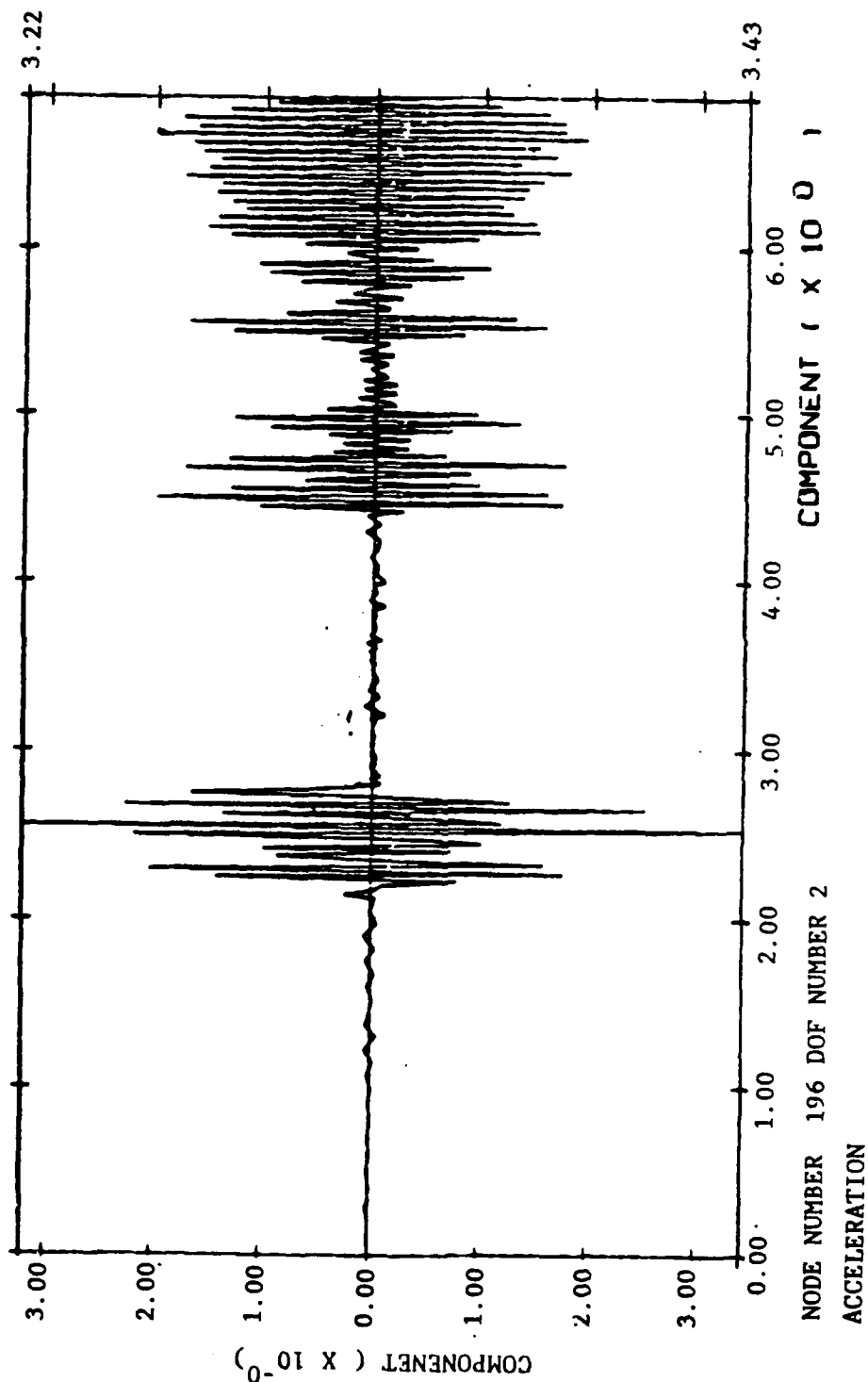
NODE NUMBER 196 DOF NUMBER 1

ACCELERATION

WED. SEP 16 1987 PLOT NO. 5

Figure F-14A. Structure Acceleration Response, Soil-Structure Simulation

SOIL STRUCTURE TEST. NEVADA SAND. BEAM MODEL. ACCELERATION BC



WED. SEP 16 1987 PLOT NO. 19

-Figure F-14B. Structure Acceleration Response, Soil-Structure Simulation

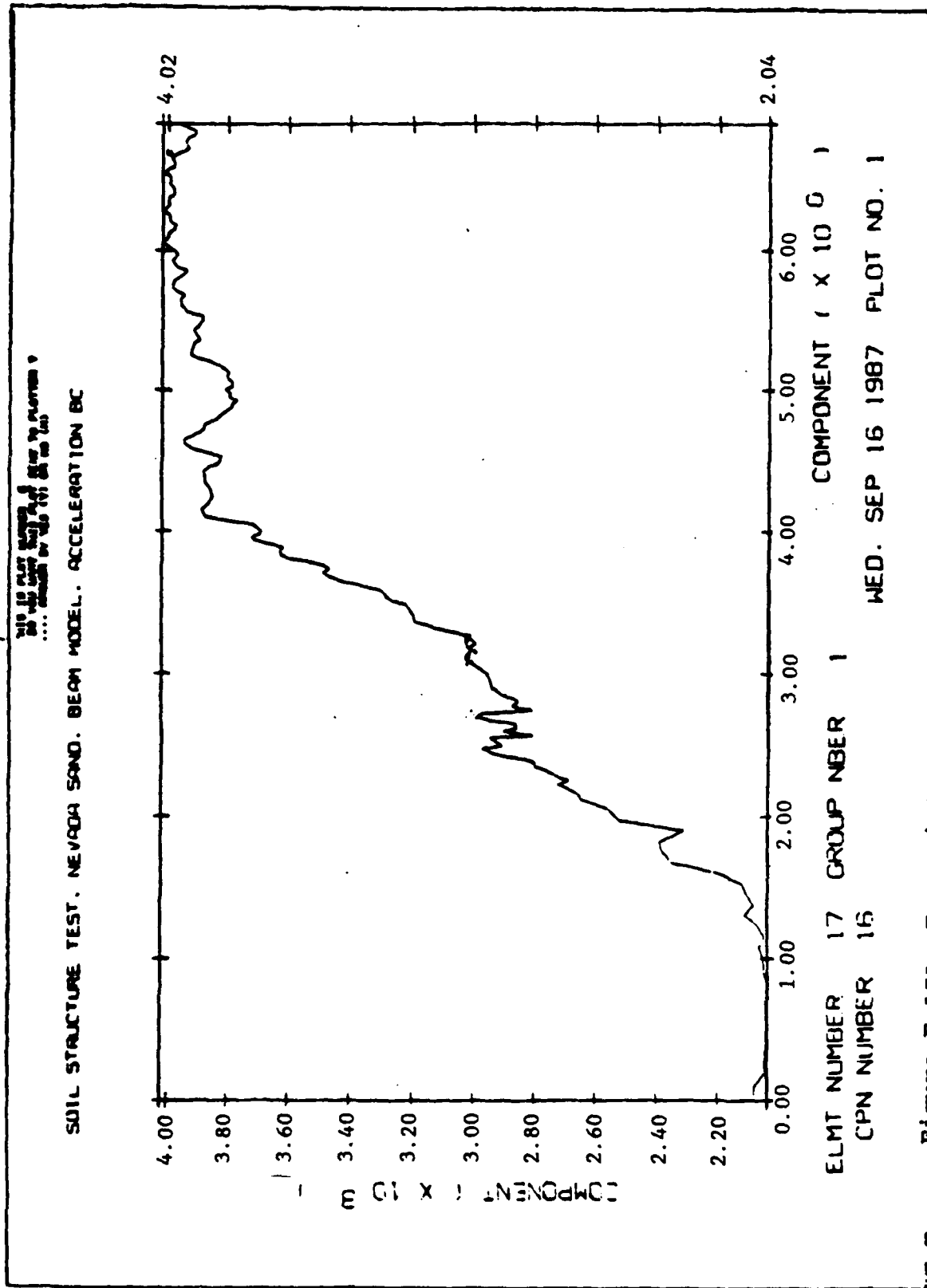


Figure F-15A. Free Field Pore Pressure Response, Soil-Structure

THE 15 DAY PERIOD
 ... WAS USED TO
 ...

SOIL STRUCTURE TEST. NEVADA SAND. BEAM MODEL. ACCELERATION BC

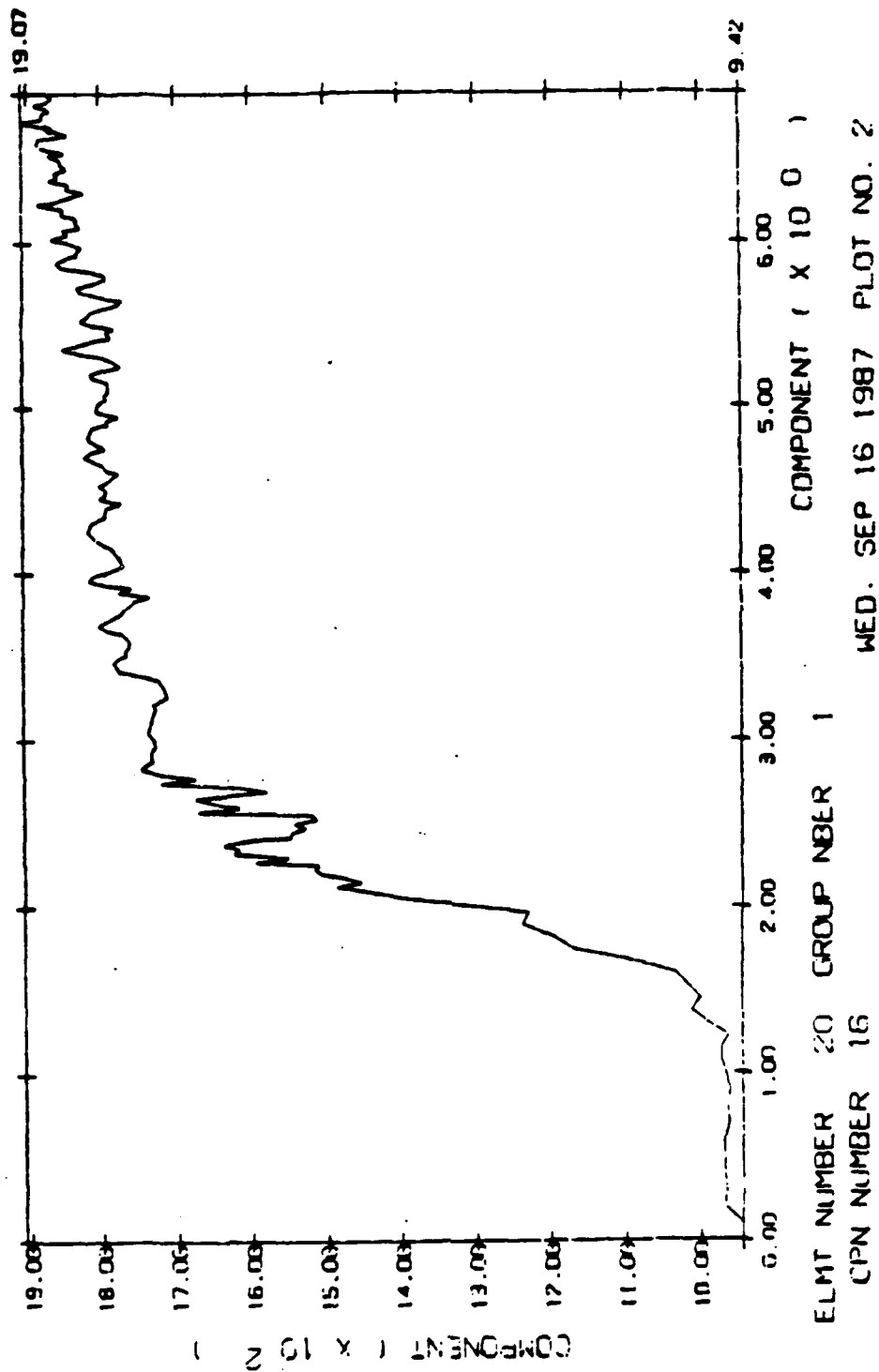


Figure F-15B. Free Field Pore Pressure Response, Soil-Structure

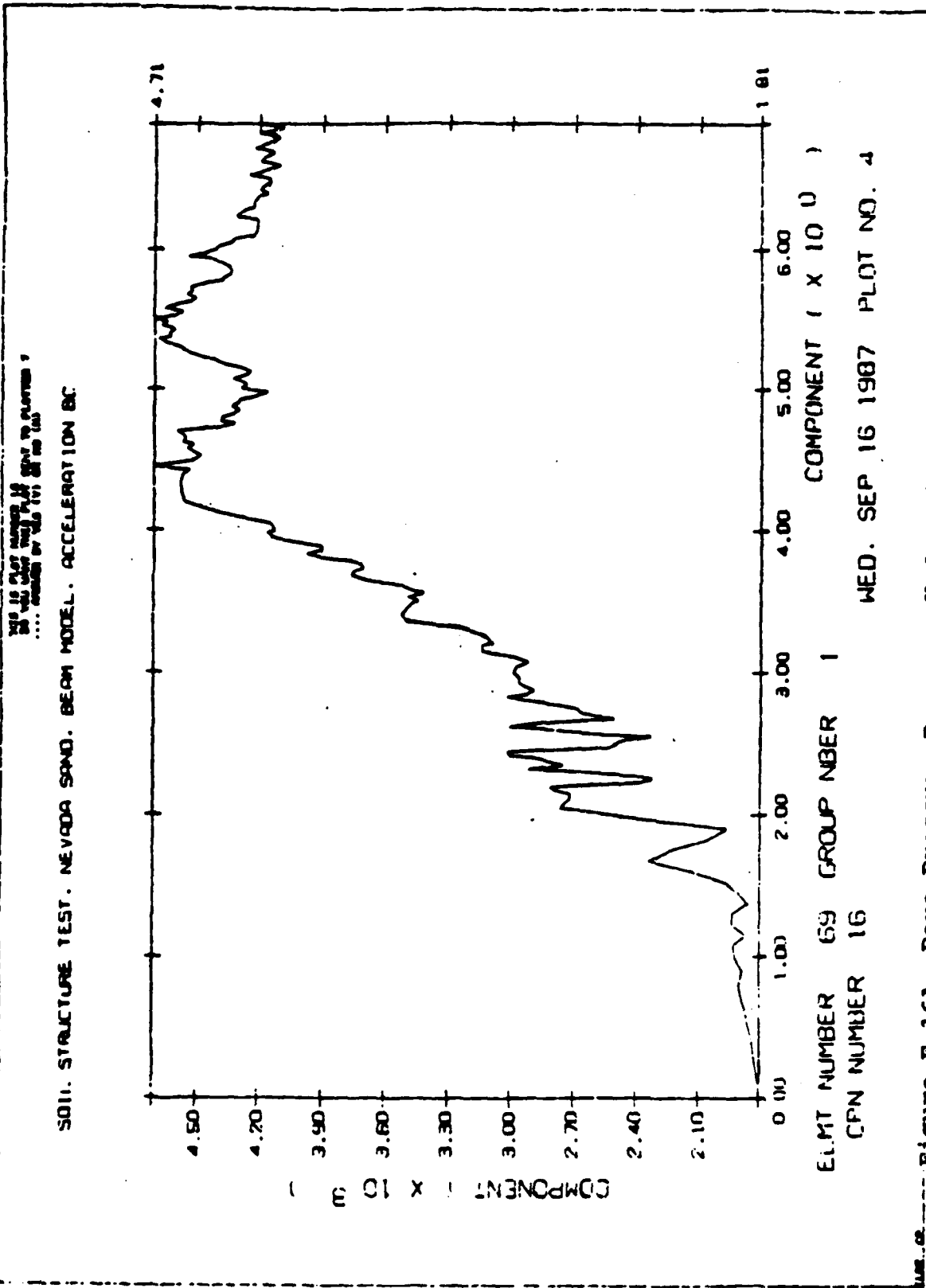


Figure F-16A. Pore Pressure Response Under Structure, Soil-Structure

THIS IS PLOT NUMBER 16
 OF THE PORE PRESSURE RESPONSE

SOIL STRUCTURE TEST. NEVADA SAND. BEAM MODEL. ACCELERATION BC

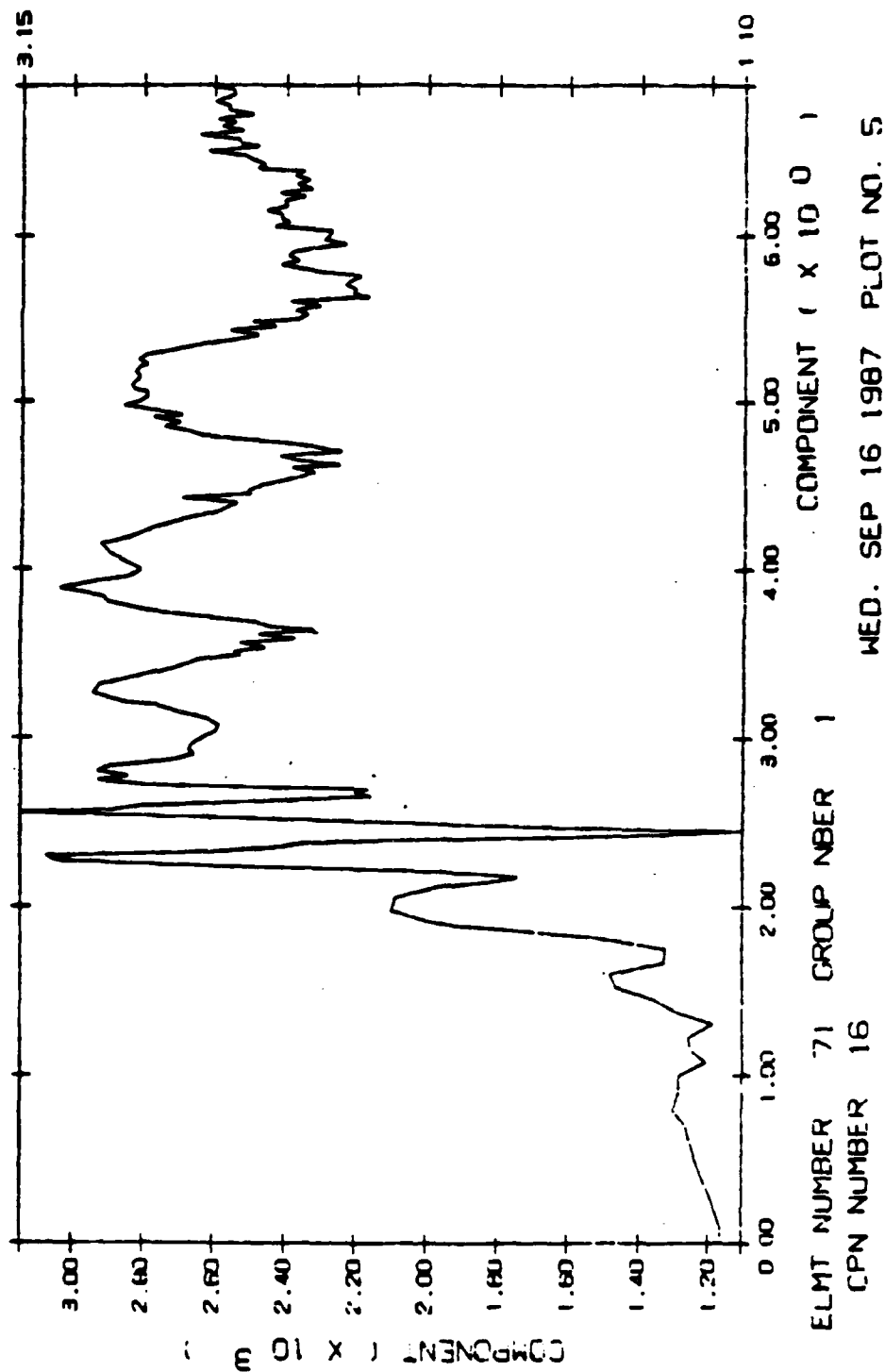


Figure F-16B. Pore Pressure Response Under Structure, Soil-Structure

SOIL STRUCTURE TEST. NEVADA SAND. BEAM MODEL. ACCELERATION BC

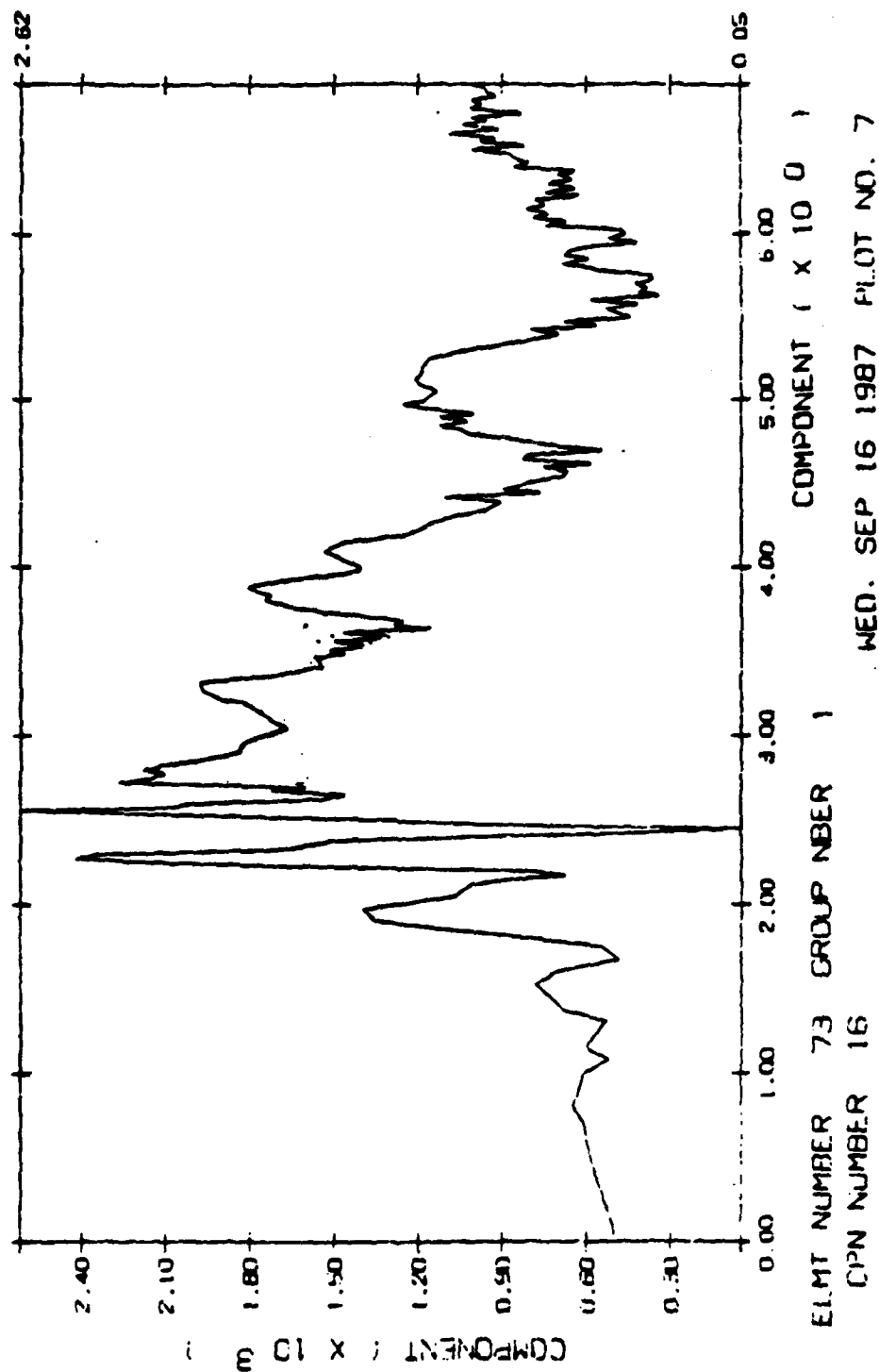
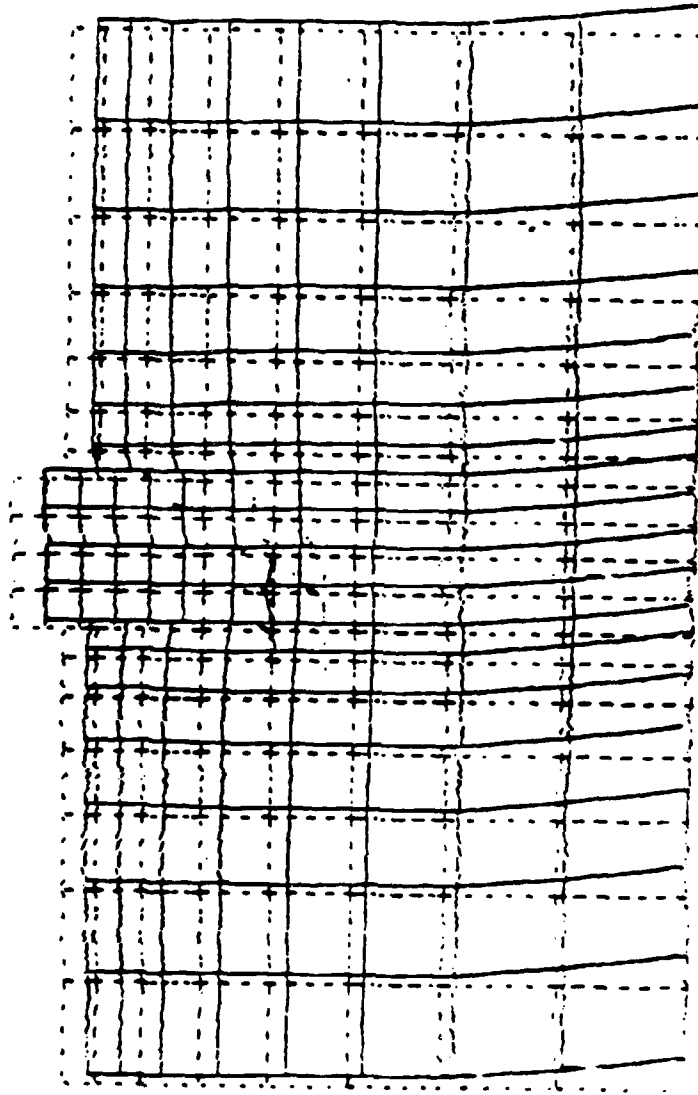


Figure F-16C. Pore Pressure Response Under Structure, Soil-Structure

... continued for 100 ft, 200 ft, 300 ft

SOIL STRUCTURE TEST, NEVADA SAND, BEAM MODEL, ACCELERATION BC



Deformed Mesh

Step No. 200

Plot No. 1

Figure F-17. Deformed Finite Element Mesh, Soil-Structure Simulation

Appendix G

SOIL DATA

The Princeton University Effective Stress Soil Model has been fitted to a number of different soils. The following pages list the input data and derived soil mode for:

- 1) Leighton-Buzzard 120/220 Sand
- 2) Monterey 0 Sand
- 3) Fine Silica Sand
- 4) Meisers Bluff Sand
- 5) Banding Sand
- 6) Kaolinite Clay

The input data required for the material model derivation are:

Deviator (shear) strain
Deviator (shear) strain
Mean effective stress
Volume strain

Modifications to the material model derivation, Program MUD, will allow for determinations of the material model from undrained shear test data, thus volume strain information can be ignored.

M U D : INPUT DATA STRUCTURE

====> CARD 1 (20A4)

TITLE

.... EACH DATA SET BEGINS WITH A TITLE CARD.
TWO BLANK CARDS FOLLOW THE LAST DATA SET

====> CARD 2 (16I5)

CONTROL INFORMATION:

NYS, MODE, IPLOT, IPUNCH, ITEST, ISMTH, MATYP

NYS = NUMBER OF YIELD SURFACES

MODE = EXECUTION MODE
EQ.0; DATA CHECK
EQ.1; EXECUTION

IPLOT = PLOTTING CODE
EQ.0; NO PLOTS
EQ.1; PLOT INPUT DATA
EQ.2; PLOT YIELD SURFACES
EQ.3; PLOT BOTH 1 AND 2 ABOVE

IPUNCH= PUNCH CODE
EQ.0; NO PUNCH OUTPUT
EQ.1; PUNCH OUTPUT FILE

ITEST = DATA SELECTION (FOR PRESSURE NONSENSITIVE MATERIALS)
EQ.0; USE AXIAL COMPRESSION TEST DATA
EQ.1; USE AXIAL EXTENSION TEST DATA

ISMTH = INPUT DATA SMOOTHING SELECTION
EQ.0; NO DATA SMOOTHING
EQ.1; DATA SMOOTHING

MATYP = MATERIAL TYPE

====> CARD 3 (16I5)

NC, NE, NK

NC = NUMBER OF DATA POINTS IN COMPRESSION TEST
NE = NUMBER OF DATA POINTS IN EXTENSION TEST
NK = NUMBER OF DATA POINTS IN CONSOLIDATION TEST

====> CARD 4 (8F10.0)

C, XN, XL, TOL

C = YIELD SURFACES AXIS RATIO (GE.0.0)

EQ.0.0; PRESSURE NONSENSITIVE MATERIAL
NE.0.0; PRESSURE SENSITIVE MATERIAL

XN = POWER EXPONENT (GE.0.0)

XL = VOLUMETRIC EXPONENT (GE.0.0)

TOL = TOLERANCE (GE.0.0 .AND. LE.1.0)
EQ.0.0; SET INTERNALLY EQ.1.0

====> CARD(S) 5 (I5,5X,7F10.0)

AXIAL COMPRESSION TEST RESULTS

N, QC(N), EC(N), PC(N), EVC(N)

.... TERMINATE WITH A BLANK CARD

N = STEP NUMBER
QC(N) = SHEAR STRESS
EC(N) = SHEAR STRAIN
PC(N) = MEAN NORMAL STRESS (EFFECTIVE)
EVC(N) = VOLUMETRIC STRAIN

====> CARD(S) 6 (I5,5X,7F10.0)

AXIAL EXTENSION TEST RESULTS

N, QE(N), EE(N), PE(N), EVE(N)

.... TERMINATE WITH A BLANK CARD

====> CARD(S) 7 (I5,5X,7F10.0)

CONSOLIDATION TEST RESULTS (IF ANY)

N, QK(N), EK(N), PK(N), EVK(N)

.... TERMINATE WITH A BLANK CARD

T E S T A : INPUT DATA STRUCTURE

====> CARD 1 (20A4)

TITLE

.... EACH DATA SET BEGINS WITH A TITLE CARD.
TWO BLANK CARDS FOLLOW THE LAST DATA SET

====> CARD 2 (8I5)

CONTROL INFORMATION:

NSD, MODE, NEXP, NLC, NLS, IPLOT, IP1, ISIG

NSD = NUMBER OF SPACE DIMENSIONS (GE.2 AND LE.3)

MODE = EXECUTION MODE (GE.0)
EQ.0; DATA CHECK
EQ.1; EXECUTION

NEXP = NUMBER OF EXPERIMENTS (GE.1 AND LE.3)

NLC = NUMBER OF LOAD CASES (GE.0)

NLS = NUMBER OF LOAD STEPS (GE.0)
EQ.0; DEFAULT SINUSOIDAL LOAD-TIME FUNCTIONS
GE.1; USER'S PRESCRIBED LOAD-TIME FUNCTIONS

IPLOT = STRESS-STRAIN PLOTS (GE.0)
EQ.0; NO PLOTS
EQ.1; PLOT STRESS-STRAIN RESULTS

IP1 = YIELD SURFACES PLOTS (GE.0)
EQ.0; NO PLOTS
NE.0; PLOT EVERY IP1 STEP

ISIG = INPUT TYPE PARAMETER (GE.0)
EQ.0; INPUT = STRAINS
EQ.1; INPUT = STRESSES

====> CARD(S) 3 (2I5,F10.0)

I, NTS(I), CYCL(I)

I = EXPERIMENT NUMBER (I = 1,.....,NEXP)

NTS(I) = NUMBER OF TIME STEPS (GT.0)

CYCL(I) = NUMBER OF CYCLES (IF NLS.EQ.0)
= TIME STEP (IF NLS.GT.0)

====> CARD(S) 4 (8F10.0) * NLC

LEIGHTON-BUZZARD 120/200 SAND - DR=55% - SC3,SE3 - MODIFIED

100	1	3	1	1	0	6
13	12	00				
1.0000	0.50	0.00	1.00			
1	0.	0.	1.	0.		
2	.1	.000519	1.033	.0001179		
3	.22	.00125	1.07	.00026		
4	.3	.001852	1.1	.0003722		
5	.4	.002592	1.133	.0005143		
6	.483	.0033	1.16	.00063		
7	.847	.00678	1.283	.00156		
8	1.236	.01435	1.41	.0029		
9	1.59	.0263	1.53	.0052		
10	2.06	.0544	1.685	.0074		
11	2.17	.0649	1.73	.00778		
12	2.44	.1072	1.81	.0074		
13	2.59	.15	1.86	.0059		
1	0.	0.	1.	0.		
2	-.044	-.000237	.985	-.00007		
3	-.088	-.000519	.97	-.00007		
4	-.2197	-.00157	.927	-.000148		
5	-.337	-.00298	.888	.000037		
6	-.3815	-.00426	.873	.00048		
7	-.41	-.00538	.86	.00082		
8	-.44	-.00689	.85	.00123		
9	-.51	-.0119	.83	.00245		
10	-.565	-.0209	.81	.0051		
11	-.6	-.0455	.8	.00587		
12	-.643	-.0674	.786	.00623		

LEIGHTON-BUZZARD 120/200 SAND - DR=55% - SC3,SE3 - MODIFIED - DRAINED COMPRESS

LEIGHTON-BUZZARD 120/200 SAND - DR=55% - SC3,SE3 - MODIFIED - DRAINED COMPRESS

3	1	1	1	0	1	0	01	01	13
1	050	0.25							
0.00	-2.45	0.00							
2	8	9							
9.634E+01	1.927E+02	6.423E+01	5.000E-01						
-1.000E+00	-1.000E+00	-1.000E+00	0.0	0.0		0.0			
1.300E+00	8.500E-01	0.0	-1.000E+00	0.0		0.43	0.0		0.0
1	6.582E-02	9.668E+02	1.168E+03	0.0		0.0	0.0		
-1.033E-02	2.066E-02	-1.033E-02	0.0	0.0		0.0			
2	1.430E-01	3.577E+02	4.592E+02	0.0		0.0	0.0		
-2.087E-02	4.174E-02	-2.087E-02	0.0	0.0		0.0			
3	2.659E-01	2.194E+02	3.373E+02	0.0		0.0	0.0		
-3.227E-02	6.454E-02	-3.227E-02	0.0	0.0		0.0			
4	3.267E-01	1.620E+02	2.654E+02	2.113E-01		0.0	0.0		
-2.990E-02	5.979E-02	-2.990E-02	0.0	0.0		0.0			
5	5.016E-01	4.203E+01	8.195E+01	5.593E-01		6.955E-01	0.0		
-5.287E-02	1.057E-01	-5.287E-02	0.0	0.0		0.0			
6	6.380E-01	1.747E+01	4.131E+01	8.488E-01		8.864E-01	0.0		
-7.954E-02	1.591E-01	-7.954E-02	0.0	0.0		0.0			
7	7.612E-01	7.597E+00	2.199E+01	1.086E+00		7.604E-01	0.0		
-9.266E-02	1.853E-01	-9.266E-02	0.0	0.0		0.0			
8	9.023E-01	3.774E+00	1.321E+01	1.233E+00		7.872E-01	0.0		
-1.068E-01	2.135E-01	-1.068E-01	0.0	0.0		0.0			
9	9.930E-01	1.169E+00	4.474E+00	1.295E+00		8.411E-01	0.0		
-1.086E-01	2.172E-01	-1.086E-01	0.0	0.0		0.0			
1	0.	0.	1.	0.					
2	.1	.000519	1.033	.0001179					
3	.22	.00125	1.07	.00026					
4	.3	.001852	1.1	.0003722					
5	.4	.002592	1.133	.0005143					
6	.483	.0033	1.16	.00063					
7	.847	.00678	1.283	.00156					
8	1.236	.01435	1.41	.0029					
9	1.59	.0263	1.53	.0052					
10	2.06	.0544	1.685	.0074					
11	2.17	.0649	1.73	.00778					
12	2.44	.1072	1.81	.0074					
13	2.59	.15	1.86	.0059					

LEIGHTON-BUZZARD 120/200 SAND - DR=55% - SC3,SE3 - MODIFIED - DRAINED EXTENSION

3	1	1	1	0	1	0	01	01	12
1	050	0.25							
0.00	+0.58	0.00							
2	8	9							
9.634E+01	1.927E+02	6.423E+01	5.000E-01						
-1.000E+00	-1.000E+00	-1.000E+00	0.0	0.0		0.0			
1.300E+00	8.500E-01	0.0	-1.000E+00	0.0		0.43	0.0		0.0
1	6.582E-02	9.668E+02	1.168E+03	0.0		0.0	0.0		
-1.033E-02	2.066E-02	-1.033E-02	0.0	0.0		0.0			
2	1.430E-01	3.577E+02	4.592E+02	0.0		0.0	0.0		
-2.087E-02	4.174E-02	-2.087E-02	0.0	0.0		0.0			
3	2.659E-01	2.194E+02	3.373E+02	0.0		0.0	0.0		
-3.227E-02	6.454E-02	-3.227E-02	0.0	0.0		0.0			
4	3.267E-01	1.620E+02	2.654E+02	2.113E-01		0.0	0.0		
-2.990E-02	5.979E-02	-2.990E-02	0.0	0.0		0.0			
5	5.016E-01	4.203E+01	8.195E+01	5.593E-01		6.955E-01	0.0		
-5.287E-02	1.057E-01	-5.287E-02	0.0	0.0		0.0			

LEIGHTON-BUZZARD 120/200 SAND - DR=55% - SC3,SE3 - MODIFIED - DRAINED COMPRESS

6	6.380E-01	1.747E+01	4.131E+01	8.488E-01	8.864E-01	0.0
-7.954E-02	1.591E-01	-7.954E-02	0.0	0.0	0.0	
7	7.612E-01	7.597E+00	2.199E+01	1.086E+00	7.604E-01	0.0
-9.266E-02	1.853E-01	-9.266E-02	0.0	0.0	0.0	
8	9.023E-01	3.774E+00	1.321E+01	1.233E+00	7.872E-01	0.0
-1.068E-01	2.135E-01	-1.068E-01	0.0	0.0	0.0	
9	9.930E-01	1.169E+00	4.474E+00	1.295E+00	8.411E-01	0.0
-1.086E-01	2.172E-01	-1.086E-01	0.0	0.0	0.0	
1	0.	0.	1.	0.		
2	-.044	-.000237	.985	-.00007		
3	-.088	-.000519	.97	-.00007		
4	-.2197	-.00157	.927	-.000148		
5	-.337	-.00298	.888	.000037		
6	-.3815	-.00426	.873	.00048		
7	-.41	-.00538	.86	.00082		
8	-.44	-.00689	.85	.00123		
9	-.51	-.0119	.83	.00245		
10	-.565	-.0209	.81	.0051		
11	-.6	-.0455	.8	.00587		
12	-.643	-.0674	.786	.00623		

MONTEREY 'O' SAND - DR=40% - SC3,SE3 - MODIFIED

MONTEREY 'O' SAND - DR=40% - SC3,SE3 - MODIFIED				
100	1	1	1	0 0 8
13	12	00		
0.0000	0.50	0.00	1.00	
1	0.	0.	1.	0.
2	0.19	0.00085	1.063	0.00019
3	0.425	0.00205	1.142	0.00049
4	0.674	0.00347	1.225	0.00094
5	0.907	0.00579	1.3	0.0015
6	1.153	0.0089	1.384	0.0022
7	1.397	0.0133	1.466	0.0029
8	1.639	0.0193	1.55	0.0037
9	1.816	0.0286	1.61	0.004
10	2.084	0.0431	1.695	0.0043
11	2.29	0.0682	1.762	0.0037
12	2.435	0.11	1.81	0.0011
13	2.544	0.1715	1.85	-0.0032
1	0.	0.	1.	0.
2	-0.059	-0.00035	0.98	0.00004
3	-0.132	-0.00080	0.956	0.00015
4	-0.19	-0.00120	0.936	0.0003
5	-0.25	-0.00145	0.917	0.0006
6	-0.294	-0.00195	0.902	0.001
7	-0.368	-0.00333	0.877	0.00384
8	-0.413	-0.0066	0.862	0.0048
9	-0.444	-0.0107	0.852	0.00485
10	-0.477	-0.0205	0.841	0.00485
11	-0.51	-0.0344	0.83	0.0048
12	-0.55	-0.0561	0.817	0.00475

MATERIAL MODEL FROM PROGRAM MUD

MATERIAL MODEL FROM PROGRAM MUD

MONTEREY 0 SAND

	2	8	8							
	1.118E+02	2.235E+02	7.451E+01	5.000E-01						
	-1.000E+00	-1.000E+00	-1.000E+00	0.000E-01	0.000E-01	0.000E-01	0.000E-01	0.000E-01	0.000E-01	0.000E-01
	7.500E-01	3.000E-01	0.000E-01	-1.000E+00	0.000E-01	0.000E-01	0.000E-01	0.000E-01	0.000E-01	0.000E-01
1	8.937E-02	1.180E+03	1.581E+03	0.000E-01	0.000E-01	0.000E-01	0.000E-01	0.000E-01	0.000E-01	0.000E-01
-2.979E-02	5.958E-02	-2.979E-02	0.000E-01	0.000E-01	0.000E-01	0.000E-01	0.000E-01	0.000E-01	0.000E-01	0.000E-01
2	1.861E-01	5.244E+02	8.136E+02	0.000E-01	0.000E-01	0.000E-01	0.000E-01	0.000E-01	0.000E-01	0.000E-01
-6.203E-02	1.241E-01	-6.203E-02	0.000E-01	0.000E-01	0.000E-01	0.000E-01	0.000E-01	0.000E-01	0.000E-01	0.000E-01
3	4.080E-01	1.169E+02	2.105E+02	3.398E-01	0.000E-01	0.000E-01	0.000E-01	0.000E-01	0.000E-01	0.000E-01
-4.739E-02	9.478E-02	-4.739E-02	0.000E-01	0.000E-01	0.000E-01	0.000E-01	0.000E-01	0.000E-01	0.000E-01	0.000E-01
4	4.977E-01	6.915E+01	1.424E+02	5.958E-01	0.000E-01	0.000E-01	0.000E-01	0.000E-01	0.000E-01	0.000E-01
-6.665E-02	1.333E-01	-6.665E-02	0.000E-01	0.000E-01	0.000E-01	0.000E-01	0.000E-01	0.000E-01	0.000E-01	0.000E-01
5	6.371E-01	2.346E+01	5.776E+01	8.589E-01	0.000E-01	0.000E-01	0.000E-01	0.000E-01	0.000E-01	0.000E-01
-8.814E-02	1.763E-01	-8.814E-02	0.000E-01	0.000E-01	0.000E-01	0.000E-01	0.000E-01	0.000E-01	0.000E-01	0.000E-01
6	8.152E-01	3.137E+00	1.008E+01	1.158E+00	5.913E-01	0.000E-01	0.000E-01	0.000E-01	0.000E-01	0.000E-01
-1.219E-01	2.438E-01	-1.219E-01	0.000E-01	0.000E-01	0.000E-01	0.000E-01	0.000E-01	0.000E-01	0.000E-01	0.000E-01
7	9.091E-01	1.110E+00	4.209E+00	1.270E+00	5.324E-01	0.000E-01	0.000E-01	0.000E-01	0.000E-01	0.000E-01
-1.302E-01	2.604E-01	-1.302E-01	0.000E-01	0.000E-01	0.000E-01	0.000E-01	0.000E-01	0.000E-01	0.000E-01	0.000E-01
8	9.699E-01	5.242E-01	2.174E+00	1.294E+00	5.988E-01	0.000E-01	0.000E-01	0.000E-01	0.000E-01	0.000E-01
-1.251E-01	2.503E-01	-1.251E-01	0.000E-01	0.000E-01	0.000E-01	0.000E-01	0.000E-01	0.000E-01	0.000E-01	0.000E-01

MONTEREY 'O' SAND - DR=40% - SC3,SE3 - MODIFIED - DRAINED COMPRESSION

MONTEREY 'O' SAND - DR=40% - SC3,SE3 - MODIFIED - DRAINED COMPRESSION									
3	1	1	1	0	1	0	1	1	13
1	050	0.25							
0.00		-2.50	0.00						
2	8	8							
1.118E+02	2.235E+02	7.451E+01	5.000E-01						
-1.000E+00	-1.000E+00	-1.000E+00	0.0	0.0	0.0				
1.300E+00	6.000E-01	0.0	-1.000E+00	0.0	0.43	0.0	0.0		0.0
1	8.937E-02	1.181E+03	1.581E+03	0.0	0.0	0.0			
-2.979E-02	5.958E-02	-2.979E-02	0.0	0.0	0.0				
2	1.861E-01	5.244E+02	8.136E+02	0.0	0.0	0.0			
-6.203E-02	1.241E-01	-6.203E-02	0.0	0.0	0.0				
3	4.080E-01	1.169E+02	2.105E+02	3.398E-01	0.0	0.0			
-4.739E-02	9.478E-02	-4.739E-02	0.0	0.0	0.0				
4	4.977E-01	6.915E+01	1.424E+02	5.958E-01	0.0	0.0			
-6.665E-02	1.333E-01	-6.665E-02	0.0	0.0	0.0				
5	6.371E-01	2.346E+01	5.776E+01	8.589E-01	0.0	0.0			
-8.814E-02	1.763E-01	-8.814E-02	0.0	0.0	0.0				
6	8.152E-01	3.137E+00	1.008E+01	1.158E+00	5.913E-01	0.0			
-1.219E-01	2.438E-01	-1.219E-01	0.0	0.0	0.0				
7	9.091E-01	1.110E+00	4.209E+00	1.270E+00	5.324E-01	0.0			
-1.302E-01	2.604E-01	-1.302E-01	0.0	0.0	0.0				
8	9.699E-01	5.242E-01	2.174E+00	1.294E+00	5.988E-01	0.0			
-1.251E-01	2.502E-01	-1.251E-01	0.0	0.0	0.0				
1	0.	0.	1.	0.					
2	0.19	0.00085	1.063	0.00019					
3	0.425	0.00205	1.142	0.00049					
4	0.674	0.00347	1.225	0.00094					
5	0.907	0.00579	1.3	0.0015					
6	1.153	0.0089	1.384	0.0022					
7	1.397	0.0133	1.466	0.0029					
8	1.639	0.0193	1.55	0.0037					
9	1.816	0.0286	1.61	0.004					
10	2.084	0.0431	1.695	0.0043					
11	2.29	0.0682	1.762	0.0037					
12	2.435	0.11	1.81	0.0011					
13	2.544	0.1715	1.85	-0.0032					

MONTEREY 'O' SAND - DR=40% - SC3,SE3 - MODIFIED - DRAINED EXTENSION									
3	1	1	1	0	1	0	1	1	12
1	050	0.25							
0.00		+0.50	0.00						
2	8	8							
1.118E+02	2.235E+02	7.451E+01	5.000E-01						
-1.000E+00	-1.000E+00	-1.000E+00	0.0	0.0	0.0				
1.300E+00	6.000E-01	0.0	-1.000E+00	0.0	0.43	0.0	0.0		0.0
1	8.937E-02	1.181E+03	1.581E+03	0.0	0.0	0.0			
-2.979E-02	5.958E-02	-2.979E-02	0.0	0.0	0.0				
2	1.861E-01	5.244E+02	8.136E+02	0.0	0.0	0.0			
-6.203E-02	1.241E-01	-6.203E-02	0.0	0.0	0.0				
3	4.080E-01	1.169E+02	2.105E+02	3.398E-01	0.0	0.0			
-4.739E-02	9.478E-02	-4.739E-02	0.0	0.0	0.0				
4	4.977E-01	6.915E+01	1.424E+02	5.958E-01	0.0	0.0			
-6.665E-02	1.333E-01	-6.665E-02	0.0	0.0	0.0				
5	6.371E-01	2.346E+01	5.776E+01	8.589E-01	0.0	0.0			
-8.814E-02	1.763E-01	-8.814E-02	0.0	0.0	0.0				
6	8.152E-01	3.137E+00	1.008E+01	1.158E+00	5.913E-01	0.0			
-1.219E-01	2.438E-01	-1.219E-01	0.0	0.0	0.0				

MONTEREY 'O' SAND - DR=40% - SC3,SE3 - MODIFIED - DRAINED COMPRESSION

7	9.091E-01	1.110E+00	4.209E+00	1.270E+00	5.324E-01	0.0
-1.302E-01	2.604E-01	-1.302E-01	0.0	0.0	0.0	
8	9.699E-01	5.242E-01	2.174E+00	1.294E+00	5.988E-01	0.0
-1.251E-01	2.502E-01	-1.251E-01	0.0	0.0	0.0	
1	0.	0.	1.	0.		
2	-0.059	-0.00035	0.98	0.00004		
3	-0.132	-0.00080	0.956	0.00015		
4	-0.19	-0.00120	0.936	0.0003		
5	-0.25	-0.00145	0.917	0.0006		
6	-0.294	-0.00195	0.902	0.001		
7	-0.368	-0.00333	0.877	0.00384		
8	-0.413	-0.0066	0.862	0.0048		
9	-0.444	-0.0107	0.852	0.00485		
10	-0.477	-0.0205	0.841	0.00485		
11	-0.51	-0.0344	0.83	0.0048		
12	-0.55	-0.0561	0.817	0.00475		

NAVY PROJECT - FINE SILICA SAND - RAW DATA

NAVY PROJECT - FINE SILICA SAND - RAW DATA

20	1	0	0	0	0	08
14	11	00				
0.0000	0.50	0.00	1.00			
1	0.00000	0.00000	2.00000	0.00000		
2	0.4950	0.00040	2.16467	0.00028		
3	0.7960	0.00129	2.26533	0.00050		
4	1.00300	.00198	2.33467	.00071		
5	1.83300	.00535	2.61133	.00170		
6	2.58300	.01089	2.86133	.00298		
7	3.31500	.02252	3.10533	.00449		
8	3.73400	.03604	3.24467	.00530		
9	4.09900	.05907	3.36667	.00568		
10	4.36400	.09022	3.45467	.00530		
11	4.55900	.12170	3.52000	.00422		
12	4.74100	.16920	3.58067	.00211		
13	4.81100	.21684	3.60367	-.00032		
14	4.81200	.26446	3.60400	-.00272		
1	0.00000	0.00000	2.00000	0.00000		
2	-.29500	-.00078	1.90168	.00030		
3	-.60500	-.00368	1.79856	.00118		
4	-.88800	-.01106	1.70412	.00358		
5	-1.06800	-.02158	1.64399	.00611		
6	-1.24000	-.04167	1.58663	.00921		
7	-1.36700	-.07365	1.54424	.01143		
8	-1.45000	-.11389	1.51653	.01163		
9	-1.48400	-.14425	1.50547	.01061		
10	-1.50200	-.17425	1.49938	.00887		
11	-1.50500	-.20410	1.49835	.00683		

2 8 7

G-15

MIESER-BLUFF 3.45MPA - CHECK CASE

MIESER-BLUFF 3.45MPA - CHECK CASE

100	1	00	1	0	0	8
20	13					
	0.	.5	0.	1.		
1		0.0000	0.0000	3.450	0.0000	
2		0.2500	0.0007	3.533	0.00005	
3		0.5000	0.0020	3.617	0.0002	
4		1.0000	0.0050	3.783	0.0010	
5		1.7700	0.01	4.040	0.003	
6		3.0000	0.02	4.450	0.005	
7		3.8200	0.03	4.723	0.008	
8		4.6000	0.04	4.983	0.010	
9		5.1400	0.05	5.163	0.012	
10		5.6500	0.06	5.333	0.011	
11		6.0000	0.07	5.450	0.010	
12		6.3800	0.08	5.577	0.010	
13		6.6200	0.09	5.657	0.005	
14		6.9000	0.10	5.750	-0.005	
15		7.4500	0.12	5.933	-0.010	
16		7.9800	0.15	6.110	-0.009	
17		8.4000	0.17	6.250	-0.020	
18		8.7500	0.20	6.367	-0.018	
19		8.8800	0.22	6.410	-0.039	
20		9.0000	0.25	6.450	-0.050	
1		0.0000	0.00000	3.450	0.00000	
2		-0.6200	-0.0020	3.243	0.004	
3		-1.0000	-0.0050	3.117	0.007	
4		-1.3000	-0.007	3.017	0.009	
5		-1.5500	-0.010	2.933	0.011	
6		-1.8000	-0.012	2.850	0.013	
7		-1.9700	-0.015	2.793	0.015	
8		-2.1200	-0.020	2.743	0.017	
9		-2.3000	-0.030	2.683	0.024	
10		-2.4200	-0.040	2.643	0.029	
11		-2.5000	-0.050	2.617	0.036	
12		-2.5600	-0.060	2.597	0.044	
13		-2.6000	-0.070	2.583	0.050	

MIESER-BLUFF 3.45MPA - CHECK CASE

MIESER-BLUFF 3.45MPA - CHECK CASE

2	8	10							
.589E+02	3.179E+02	1.060E+02	5.000E-01						
-3.450E+00	-3.450E+00	-3.450E+00	0.000E-01	0.000E-01	0.000E-01	0.000E-01	0.000E-01	0.000E-01	0.000E-01
7.500E-01	3.000E-01	0.000E-01	-3.450E+00	0.000E-01	0.000E-01	0.000E-01	0.000E-01	0.000E-01	0.000E-01
1	1.255E-01	5.368E+02	6.509E+02	1.973E-02	0.000E-01	0.000E-01	0.000E-01	0.000E-01	0.000E-01
1.826E-02	-3.652E-02	1.826E-02	0.000E-01	0.000E-01	0.000E-01	0.000E-01	0.000E-01	0.000E-01	0.000E-01
2	1.836E-01	2.636E+02	3.350E+02	1.189E-01	0.000E-01	0.000E-01	0.000E-01	0.000E-01	0.000E-01
2.516E-03	-5.032E-03	2.516E-03	0.000E-01	0.000E-01	0.000E-01	0.000E-01	0.000E-01	0.000E-01	0.000E-01
3	3.673E-01	1.445E+02	2.331E+02	4.283E-01	0.000E-01	0.000E-01	0.000E-01	0.000E-01	0.000E-01
-2.363E-02	4.725E-02	-2.363E-02	0.000E-01	0.000E-01	0.000E-01	0.000E-01	0.000E-01	0.000E-01	0.000E-01
4	6.060E-01	6.616E+01	1.379E+02	7.014E-01	0.000E-01	0.000E-01	0.000E-01	0.000E-01	0.000E-01
-2.272E-02	4.544E-02	-2.272E-02	0.000E-01	0.000E-01	0.000E-01	0.000E-01	0.000E-01	0.000E-01	0.000E-01
5	7.744E-01	3.143E+01	8.277E+01	8.875E-01	0.000E-01	0.000E-01	0.000E-01	0.000E-01	0.000E-01
-4.497E-02	8.995E-02	-4.497E-02	0.000E-01	0.000E-01	0.000E-01	0.000E-01	0.000E-01	0.000E-01	0.000E-01
6	9.113E-01	1.101E+01	3.530E+01	8.829E-01	1.353E+00	0.000E-01	0.000E-01	0.000E-01	0.000E-01
-6.290E-02	1.258E-01	-6.290E-02	0.000E-01	0.000E-01	0.000E-01	0.000E-01	0.000E-01	0.000E-01	0.000E-01
7	1.019E+00	6.166E+00	2.416E+01	8.585E-01	4.678E+00	0.000E-01	0.000E-01	0.000E-01	0.000E-01
-8.159E-02	1.632E-01	-8.159E-02	0.000E-01	0.000E-01	0.000E-01	0.000E-01	0.000E-01	0.000E-01	0.000E-01
8	1.109E+00	3.331E+00	1.463E+01	1.013E+00	1.727E+00	0.000E-01	0.000E-01	0.000E-01	0.000E-01
-8.104E-02	1.621E-01	-8.104E-02	0.000E-01	0.000E-01	0.000E-01	0.000E-01	0.000E-01	0.000E-01	0.000E-01
9	1.155E+00	1.708E+00	7.703E+00	1.185E+00	1.948E+00	0.000E-01	0.000E-01	0.000E-01	0.000E-01
-7.325E-02	1.465E-01	-7.325E-02	0.000E-01	0.000E-01	0.000E-01	0.000E-01	0.000E-01	0.000E-01	0.000E-01
10	1.183E+00	1.344E+00	6.170E+00	1.225E+00	2.571E+00	0.000E-01	0.000E-01	0.000E-01	0.000E-01
-6.752E-02	1.350E-01	-6.752E-02	0.000E-01	0.000E-01	0.000E-01	0.000E-01	0.000E-01	0.000E-01	0.000E-01

MIESER-BLUFF MODEL FROM 3.45MPA DRY SAND PREDICTING 3.45MPA UNDRAINED CYCLIC

MIESER-BLUFF MODEL FROM 3.45MPA DRY SAND PREDICTING 3.45MPA UNDRAINED CYCLIC

3	1	1	1	0	1	0	01	1	1
1	300	4.00							
+0.0000	-0.9020			+0.0000					
2	8	10							
1.589E+02	3.179E+02	1.060E+02	5.000E-01						
-3.450E+00	-3.450E+00	-3.450E+00	0.000E-01	0.000E-01	0.000E-01	0.000E-01	0.000E-01	0.000E-01	0.000E-01
1.170E-00	8.000E-01	0.000E-01	-3.450E+00	1.060E+08	0.000E-01	0.000E-01	0.000E-01	0.000E-01	0.000E-01
1	1.255E-01	5.368E+02	6.509E+02	1.973E-02	0.000E-01	0.000E-01	0.000E-01	0.000E-01	0.000E-01
1.826E-02	-3.652E-02	1.826E-02	0.000E-01	0.000E-01	0.000E-01	0.000E-01	0.000E-01	0.000E-01	0.000E-01
2	1.836E-01	2.636E+02	3.350E+02	1.189E-01	0.000E-01	0.000E-01	0.000E-01	0.000E-01	0.000E-01
2.516E-03	-5.032E-03	2.516E-03	0.000E-01	0.000E-01	0.000E-01	0.000E-01	0.000E-01	0.000E-01	0.000E-01
3	3.673E-01	1.445E+02	2.331E+02	4.283E-01	0.000E-01	0.000E-01	0.000E-01	0.000E-01	0.000E-01
-2.363E-02	4.725E-02	-2.363E-02	0.000E-01	0.000E-01	0.000E-01	0.000E-01	0.000E-01	0.000E-01	0.000E-01
4	6.060E-01	6.616E+01	1.379E+02	7.014E-01	0.000E-01	0.000E-01	0.000E-01	0.000E-01	0.000E-01
-2.272E-02	4.544E-02	-2.272E-02	0.000E-01	0.000E-01	0.000E-01	0.000E-01	0.000E-01	0.000E-01	0.000E-01
5	7.744E-01	3.143E+01	8.277E+01	8.875E-01	0.000E-01	0.000E-01	0.000E-01	0.000E-01	0.000E-01
-4.497E-02	8.995E-02	-4.497E-02	0.000E-01	0.000E-01	0.000E-01	0.000E-01	0.000E-01	0.000E-01	0.000E-01
6	9.113E-01	1.101E+01	3.530E+01	8.829E-01	1.353E+00	0.000E-01	0.000E-01	0.000E-01	0.000E-01
-6.290E-02	1.258E-01	-6.290E-02	0.000E-01	0.000E-01	0.000E-01	0.000E-01	0.000E-01	0.000E-01	0.000E-01
7	1.019E+00	6.166E+00	2.416E+01	8.585E-01	4.678E+00	0.000E-01	0.000E-01	0.000E-01	0.000E-01
-8.159E-02	1.632E-01	-8.159E-02	0.000E-01	0.000E-01	0.000E-01	0.000E-01	0.000E-01	0.000E-01	0.000E-01
8	1.109E+00	3.331E+00	1.463E+01	1.013E+00	1.727E+00	0.000E-01	0.000E-01	0.000E-01	0.000E-01
-8.104E-02	1.621E-01	-8.104E-02	0.000E-01	0.000E-01	0.000E-01	0.000E-01	0.000E-01	0.000E-01	0.000E-01
9	1.155E+00	1.708E+00	7.703E+00	1.185E+00	1.948E+00	0.000E-01	0.000E-01	0.000E-01	0.000E-01
-7.325E-02	1.465E-01	-7.325E-02	0.000E-01	0.000E-01	0.000E-01	0.000E-01	0.000E-01	0.000E-01	0.000E-01
10	1.183E+00	1.344E+00	6.170E+00	1.225E+00	2.571E+00	0.000E-01	0.000E-01	0.000E-01	0.000E-01
-6.752E-02	1.350E-01	-6.752E-02	0.000E-01	0.000E-01	0.000E-01	0.000E-01	0.000E-01	0.000E-01	0.000E-01
1	0.0	0.0	0.0	0.000	0.000	0.000	0.000	0.000	0.000

CASTRO BANDING SAND, 4KG, DR=50

CASTRO BANDING SAND, 4KG, DR=50

100	1	1	1	1	0	8
21	21	00				
0.0000	0.50	0.00	1.00			
1	-0.0000	0.0000	-0.0000	0.0000		
2	1.3429	0.0009	0.2285	0.0009		
3	2.0856	0.0018	0.7857	0.0023		
4	2.4572	0.0027	1.1571	0.0036		
5	2.6427	0.0054	1.5287	0.0054		
6	2.8286	0.0077	1.9001	0.0072		
7	3.0144	0.0113	1.9561	0.0113		
8	3.1144	0.0154	2.0856	0.0154		
9	3.3857	0.0194	1.9561	0.0194		
10	3.9429	0.0276	1.9001	0.0276		
11	4.3143	0.0335	1.7142	0.0335		
12	4.6856	0.0384	1.5287	0.0389		
13	5.2428	0.0443	1.1571	0.0448		
14	5.7999	0.0493	0.9715	0.0497		
15	6.1713	0.0552	0.7857	0.0552		
16	6.7285	0.0606	0.5999	0.0606		
17	7.4714	0.0660	0.4144	0.0665		
18	7.8428	0.0719	0.0427	0.0715		
19	8.5858	0.0778	-0.1428	0.0782		
20	9.1430	0.0837	-0.5141	0.0837		
21	9.7001	0.0891	-0.7000	0.0891		
1	0.0000	-0.0000	-0.0000	0.0000		
2	-0.8957	-0.0009	0.2285	0.0009		
3	-1.3911	-0.0018	0.7857	0.0023		
4	-1.6390	-0.0027	1.1571	0.0036		
5	-1.7627	-0.0054	1.5287	0.0054		
6	-1.8867	-0.0077	1.9001	0.0072		
7	-2.0106	-0.0113	1.9001	0.0113		
8	-2.0106	-0.0154	2.0856	0.0154		
9	-2.2583	-0.0194	2.0856	0.0194		
10	-2.6299	-0.0276	1.9001	0.0276		
11	-2.8776	-0.0335	1.7142	0.0335		
12	-3.1253	-0.0384	1.5287	0.0389		
13	-3.4969	-0.0443	1.1571	0.0448		
14	-3.8685	-0.0493	0.9715	0.0497		
15	-4.1163	-0.0552	0.7857	0.0552		
16	-4.4879	-0.0606	0.5999	0.0606		
17	-4.9834	-0.0660	0.4144	0.0665		
18	-5.2311	-0.0719	0.0427	0.0715		
19	-5.7267	-0.0778	-0.1428	0.0782		
20	-6.0984	-0.0837	-0.5141	0.0837		
21	-6.4700	-0.0891	-0.7000	0.0891		

CASTRO BANDING SAND, 4KG, DR=50 UNDRAINED SIMULATION

CASTRO BANDING SAND, 4KG, DR=50 UNDRAINED SIMULATION

3	1	1	0	0	1	0	01	01	01
1	025	0.25							
0.000	-7.506	0.000							
2	8	4							
4.974E+02	9.947E+02	3.316E+02	5.000E-01						
-4.000E+00	-4.000E+00	-4.000E+00	0.000E-01	0.000E-01	0.000E-01	0.000E-01	0.000E-01	0.000E-01	0.000E-01
0.900E+00	3.000E-01	0.000E-01	-4.000E+00	0.000E-01	0.000E-01	0.000E-01	0.000E-01	0.000E-01	0.000E-01
1	2.042E-01	1.232E+03	1.372E+03	3.183E-01	9.012E-02	0.000E-01			
-3.803E-02	7.606E-02	-3.803E-02	0.000E-01	0.000E-01	0.000E-01	0.000E-01			
2	4.432E-01	4.078E+02	6.781E+02	7.215E-01	5.110E-01	0.000E-01			
-2.523E-02	5.046E-02	-2.523E-02	0.000E-01	0.000E-01	0.000E-01	0.000E-01			
3	6.802E-01	7.523E+01	1.303E+02	1.668E+00	1.714E+00	0.000E-01			
3.057E-03	-6.114E-03	3.057E-03	0.000E-01	0.000E-01	0.000E-01	0.000E-01			
4	1.140E+00	2.352E+01	4.872E+01	1.700E-00	1.740E-00	0.000E-01			
4.921E-02	-9.842E-02	4.921E-02	0.000E-01	0.000E-01	0.000E-01	0.000E-01			
1	-0.0000	0.0000	-0.0000	0.0000					
2	1.3429	0.0009	0.2285	0.0009					
3	2.0856	0.0018	0.6757	0.0023					
4	2.4572	0.0027	1.1571	0.0036					
5	2.6427	0.0054	1.5287	0.0054					
6	2.8286	0.0077	1.8401	0.0072					
7	3.0144	0.0113	1.9961	0.0113					
8	3.1144	0.0154	2.1456	0.0154					
9	3.4857	0.0194	1.9561	0.0194					
10	3.9429	0.0276	1.8401	0.0276					
11	4.3143	0.0335	1.7142	0.0335					
12	4.7856	0.0384	1.5287	0.0389					
13	5.1428	0.0443	1.1571	0.0448					
14	5.6999	0.0493	0.9715	0.0497					
15	6.1713	0.0552	0.7857	0.0552					
16	6.6885	0.0606	0.5999	0.0606					
17	7.4714	0.0660	0.4144	0.0665					
18	7.8428	0.0719	0.0427	0.0715					
19	8.5858	0.0778	-0.1428	0.0782					
20	9.1430	0.0837	-0.5141	0.0837					
21	9.7001	0.0891	-0.7000	0.0891					

SHEN CLAY FOR TANK CONSOLIDATION PROBLEM

100	1	3	1	0	1	6
11	9	00				
1.0000	0.50	0.00	1.00			
1	0.	0.	1.	0.		
2	35.0	0.00025	90.0			
3	58.0	0.00050	97.9			
4	88.0	0.00100	104.3			
5	115.0	0.00150	117.3			
6	127.0	0.00200	118.1			
7	137.0	0.00250	120.7			
8	171.0	0.00500	130.7			
9	180.0	0.00750	137.5			
10	181.0	0.01000	139.1			
11	182.0	0.01250	147.4			
1	0.0	0.0	90.0			
2	-17.0	-0.00025	89.7			
3	-32.0	-0.00050	92.7			
4	-57.0	-0.00100	103.0			
5	-85.0	-0.00150	118.3			
6	-102.0	-0.00200	131.0			
7	-117.0	-0.00250	145.0			
8	-167.0	-0.00500	186.7			
9	-187.0	-0.00750	206.0			

SHEN CLAY FOR TANK CONSOLIDATION PROBLEM

2 8 8

1.300E+05 2.600E+05 8.667E+04 5.000E-01
-6.150E+02-6.150E+02-6.150E+02 0.000E-01 0.000E-01 0.000E-01
7.500E-01 3.000E-01 6.000E+00-6.150E+02 0.000E-01 0.000E-01 0.000E-01 0.000E-01
1 7.997E-02 1.566E+06 1.510E+06 1.069E-01 5.301E-02 0.000E-01
-8.987E-03 1.797E-02-8.987E-03 0.000E-01 0.000E-01 0.000E-01
2 2.063E-01 2.012E+05 1.725E+05 2.256E-01 2.337E-01 0.000E-01
1.225E-03-2.449E-03 1.225E-03 0.000E-01 0.000E-01 0.000E-01
3 3.537E-01 1.095E+05 9.793E+04 3.941E-01 4.957E-01 0.000E-01
1.346E-02-2.692E-02 1.346E-02 0.000E-01 0.000E-01 0.000E-01
4 4.253E-01 9.871E+04 6.890E+04 6.158E-01 6.744E-01 0.000E-01
6.446E-03-1.289E-02 6.446E-03 0.000E-01 0.000E-01 0.000E-01
5 5.469E-01 3.432E+04 2.422E+04 1.096E+00 1.148E+00 0.000E-01
4.232E-03-8.464E-03 4.232E-03 0.000E-01 0.000E-01 0.000E-01
6 7.952E-01 2.966E+04 1.213E+04 0.000E-01 0.000E-01 0.000E-01
-6.370E-03 1.274E-02-6.370E-03 0.000E-01 0.000E-01 0.000E-01
7 9.467E-01 9.188E+03 3.453E+03 1.002E+00 8.917E-01 0.000E-01
-1.833E-02 3.666E-02-1.833E-02 0.000E-01 0.000E-01 0.000E-01
8 1.146E+00 3.712E+04-1.306E+03 0.000E-01 0.000E-01 0.000E-01
-8.237E-02 1.647E-01-8.237E-02 0.000E-01 0.000E-01 0.000E-01